Terms and Conditions of Use of Digitised Theses from Trinity College Library Dublin

Copyright statement

All material supplied by Trinity College Library is protected by copyright (under the Copyright and Related Rights Act, 2000 as amended) and other relevant Intellectual Property Rights. By accessing and using a Digitised Thesis from Trinity College Library you acknowledge that all Intellectual Property Rights in any Works supplied are the sole and exclusive property of the copyright and/or other IPR holder. Specific copyright holders may not be explicitly identified. Use of materials from other sources within a thesis should not be construed as a claim over them.

A non-exclusive, non-transferable licence is hereby granted to those using or reproducing, in whole or in part, the material for valid purposes, providing the copyright owners are acknowledged using the normal conventions. Where specific permission to use material is required, this is identified and such permission must be sought from the copyright holder or agency cited.

Liability statement

By using a Digitised Thesis, I accept that Trinity College Dublin bears no legal responsibility for the accuracy, legality or comprehensiveness of materials contained within the thesis, and that Trinity College Dublin accepts no liability for indirect, consequential, or incidental, damages or losses arising from use of the thesis for whatever reason. Information located in a thesis may be subject to specific use constraints, details of which may not be explicitly described. It is the responsibility of potential and actual users to be aware of such constraints and to abide by them. By making use of material from a digitised thesis, you accept these copyright and disclaimer provisions. Where it is brought to the attention of Trinity College Library that there may be a breach of copyright or other restraint, it is the policy to withdraw or take down access to a thesis while the issue is being resolved.

Access Agreement

By using a Digitised Thesis from Trinity College Library you are bound by the following Terms & Conditions. Please read them carefully.

I have read and I understand the following statement: All material supplied via a Digitised Thesis from Trinity College Library is protected by copyright and other intellectual property rights, and duplication or sale of all or part of any of a thesis is not permitted, except that material may be duplicated by you for your research use or for educational purposes in electronic or print form providing the copyright owners are acknowledged using the normal conventions. You must obtain permission for any other use. Electronic or print copies may not be offered, whether for sale or otherwise to anyone. This copy has been supplied on the understanding that it is copyright material and that no quotation from the thesis may be published without proper acknowledgement.

Polymer/clay nanocomposites

A thesis submitted to the University of Dublin in partial fulfilment of the requirements for the degree of

Doctor in Philosophy

Oana-Mihaela Istrate, MSc, BSc Eng

Trinity College Dublin

January 2012

Supervisor

Dr. Biqiong Chen

Declaration

I declare that this thesis has not been submitted as an exercise for a degree at this or any other University and it is entirely my own work.

I agree to deposit this thesis in the University's open access institutional repository or allow the library to do so on my behalf, subject to Irish Copyright Legislation and Trinity College Library conditions of use and acknowledgement.

Oana-Mihaela Istrate

January 2012

Abstract

Polymer/clay nanocomposites are a new class of materials with unique properties that are not shared by the pristine polymers or the conventional composites. These materials may present enhanced mechanical, thermal, barrier and flammability properties which make them ideal for applications in the aeronautic, automotive, constructions and healthcare fields. Typically, polymer/clay nanocomposites may be synthesized by: *in situ* polymerisation, solvent method and melt compounding. Following either one of these methods conventional composites and intercalated and/or exfoliated nanocomposites may be obtained. The overall aim of this thesis was to further understand the impact of clay addition on polymer foams, polymers and polymer blends, which are often found in the recycled stock, and to investigate the mechanical and thermal properties with respect to the structure of clay.

Thermosetting polymer/clay nanocomposite foams with intercalated nanostructures were developed *via in situ* polymerisation. The relative modulus-relative density relationship for low-density polymer/clay nanocomposite foams was described by Gibson-Ashby normalised model and by using other established theories. Thermoplastic polymer/clay nanocomposites were produced by solvent method, using a novel clay which was pre-treated with a blowing agent. The sequential degradation of the blowing agent inside the gallery of clay produced porous highly exfoliated polymer/clay nanocomposites. The structure-property relationship for porous polymer/clay nanocomposites was found to be best described by the Mills-Zhu model.

Polymer/clay micro and nanocomposites were developed by melt mixing compatibilised and noncompatibilised high density polyethylene with organoclay or natural clay. It was observed that in a non-polar polymer matrix, nanocomposites formed only when organoclay was dispersed in the presence of a compatibiliser. Different clays were melt compounded with polystyrene, it was observed that in order to obtain polymer/clay nanocomposites the clay had to be either treated with a cationic surfactant or directly mixed with a non-ionic surfactant.

In order to assess if polymer/clay nanocomposites with enhanced exfoliation could be manufactured *via* melt compounding with blowing agent-treated organoclays two polymer matrices were chosen, polystyrene and polypropylene/maleated polypropylene. The study showed that the dispersion of blowing agent-treated organoclays led to the enhancement of the exfoliation degree in intercalated/exfoliated nanocomposites.

Since the mechanical properties of polymer/clay nanocomposites depend on a number of factors, among which crystallinity and clay exfoliation degree. Nylon 6 was melt compounded with different clays, which yielded different exfoliation degrees. The effect of the clay was assessed by examining the crystallinity and structure of the polymer/clay nanocomposites before and after they were subjected to uniaxial deformation. It was established that the clay obstructed the polymer from reaching a more thermodynamically stable state.

The addition of clay was investigated in compatibilised and noncompatibilised polymer blends. It was observed that the clay located in the low polarity polymer in the noncompatibilised blend and in both polymers and at the interface when the compatibilising agent was added, thus, the clay acted as a reinforcing agent and as a compatibiliser. The structure-property relationship for compatibilised and noncompatibilised polymer blends was developed.

Recycled polystyrene was melt compounded with organoclay or blowing agent treated clay. Similarly, recycled polyethylene was melt mixed, with or without the addition of a compatibiliser, with the previously mentioned clays. The studies showed that in a polystyrene matrix the clay intercalated, whereas the different grades of polyethylene led to conventional composites. Still, the addition of clay enhanced the mechanical properties and facilitated the degradation process which enabled the reuse of recycled material.

In conclusion, the addition of clay to polymer, polymer cellular solids and polymer blends can be beneficial because the clay, upon appropriate treatments, has the ability to improve the mechanical and thermal properties, whilst the degree of exfoliation in a polymer/clay nanocomposite can be improved with the pre-treatment of the organoclay with blowing agents. By performing different mechanical tests it was observed that a ratio of the mass fraction of intercalated nanostructures to that of exfoliated nanostructures equal to unity would result in superior mechanical properties compared to the fully intercalated or fully exfoliated polymer/clay nanocomposites. This work adds a new level of knowledge to polymer/clay nanocomposites by examining the changes in the crystallinity of the polymer matrix and by developing a clay treatment method that has the potential to lead to controlled exfoliation; it also offers a detailed analysis on the toughness of polymer/clay nanocomposites and its effects on the fracture surface. Since it is imperative to know the structure-property relationship in order to attain the desired materials, this work has evaluated this relationship for low and high density polymer/clay nanocomposite foams, for polymer/clay nanocomposites and for polymer blend/clay nanocomposites.

Acknowledgements

I would like to express my deepest gratitude to my supervisor Dr. Biqiong Chen for giving me the chance to study for a PhD and for all the support and encouragement over the last 3 years. Thank you for supervising my work with patience and wisdom.

I would also like to thank Peter O'Reilly for all his help with the mechanical tests. In addition, I would like to thank the students who have helped me over the past three years: Salma Bedair, Chris Jebb, Declan Reidy, Judith Greaney, Eoin Kearney and Valérie Messager. Thank you to Mick Reilly and the technicians in the workshop: Sean, J.J., Gabriel, Alex and Danny, for manufacturing my moulds and notching my samples. I would also like to thank Joan Gillen for helping me whenever it was needed. I would like to thank Athlone Institute of Technology and the people there (Michael Gunning, Clem Higginbotham and Paul Blackie) for facilitating access to use their extruder to blend my materials.

My life in Ireland would have been completely different if it wasn't for the people I have met here, so thank you to my fellow post-grads, to the people that I have met while studying here and to my friends. I would like to give special thanks for support, coffee and laughter to: Thomas, Eoghan, Steve, Alanna, Nathalie, Iratxe, Martin, Darren, Emma, Kevin and Karl.

I would like also to express my gratitude to the Environmental Protection Agency of Ireland through grant number EPA 2008 PhD WRM 4 for their financial support.

Last but definitely not least, I would like to thank my family for their support, encouragement, patience and understanding. Thank you to my parents for loving me and always believing in me. Thank you also to my brother, for being the computer wise that he is.

Table of contents

Nomenclature

DSC – Differential Scanning Calorimetry

DTG – Differential Thermogravimetric Analysis

FT–IR – Fourier Transformed Infrared Spectroscopy

MicroCT – X-Ray Micro-Computed Tomography

PLM – Polarised Light Microscopy

SEM – Scanning Electron Microscopy

TEM – Transmission Electron Microscopy

TGA – Thermal Gravimetric Analysis

XRD – X-ray Diffractometer

ABS – acrylonitrile butadiene styrene

ADC – azodicarboxamide

ADC-Clay – azodicarboxamide treated organoclay Nanomer® I44.P

C30B – Cloisite 30B

Clay – organomodified clay Nanomer® I44.P

Clay(SB) – sodium bicarbonate treated organoclay Cloisite 30B

Clay(ADC) – azodicarboxamide treated organoclay Cloisite 30B

DHTDMAC – bis(hydrogenated tallow alkyl)dimethyl chloride

EtOH – ethanol

ETFE – ethylene tetrafluoroethylene

FEP – fluorinated ethylene propylene

HDPE – high density polyethylene

LDPE – low density polyethylene

LPC – liquid polymer crystal

MDI – methylene diphenyl diisocyanate

MF – melamines

MMT – natural montmorillonite

MMT-AQ – DHTDMAC treated montmorillonite

MMT-P – MMT treated with anionic surfactant

MMT-E – MMT treated with non-ionic surfactant

MMT-gel – MMT suspension in water

NCH – nylon 6/clay hybrid

ODA – octadecylamine

PA – polyamide

PBI – polybenzimidazole

PBT – poly(butylene terephthalate)

PC – polycarbonate

PCL – poly(ε-carpolactone)

PCy – polycyanates

PE – polyethylene

PEEK – polyether ether ketone

PEI – polyethyleneimine

PEgMA – polyethylene grafted maleic anhydride

PET – poly(ethylene terephthalate)

PFA – perfluoroalkoxy

PI – polyimides

PLLA – poly(L-lactide)

PLS – polymer layered silicates

PMMA – poly(methyl methacrylate)

POM – polyoxymethylene

POSS – polyhedral oligomeric sislesquioxanes

PP – polypropylene

PPE – poly(phenylene ethynylene)

PPgMA – polypropylene grafted maleic anhydride

PPS – polyphenylene sulphide

PR – phenolic resins

PS – polystyrene

PSU – polysulfone

PTFE – polytetrafluoroethylene

PU – polyurethane

PVC – poly(vinyl) chloride

R-PE – recycled polyethylene

R-PS – recycled polystyrene

SAN – styrene acrylonitrile

SB – sodium bicarbonate

SB-Clay – sodium bicarbonate treated organoclay Nanomer® I44.P

UF – urea-formaldehydes

UP – unsaturated polyesters

THF – tetrahydrofuran

ZnO – zinc oxide

β – lamellar thickening factor

δ – displacement

η – calibration factor

μ_c – mass fraction of clay

μ_c^0 – mass fraction of clay platelets in the organoclay

μ, λ – Lamé constants

ρ_p – density of polymer

ρ_c – density of clay

ρ_c^0 – density of clay platelets

ρ_f – density of foam

ρ_s – density of solid

ζ – shape factor

υ – Poisson's ratio

υ_c – Poisson's ratio of the clay platelets

υ_p – Poisson's ratio of the polymer

ϕ - volume fraction

ϕ_{conv} – volume fraction of clay in conventional composites

ϕ_c^0 – volume fraction of clay platelets

ϕ_e – volume fraction of exfoliated clay platelets

ϕ_r – volume fraction of reinforcement

ϕ_s – volume fraction of solid contained in the cell edges

χ_c – degree of crystallinity

ω – energy density

a – crack length

a_0 – precrack length

A – specific gallery area

A_T – total specific surface area of the clay platelets

b_0 – original un-cracked ligament

B – sample thickness

C_1 – geometric constant for the cell edges

C_2 – geometric constant for the cell faces

C_3 – energy constant

C_4 – temperature constant

C_5, C_6 – curve-fitting parameters

$d_{(001)}$ – basal spacing

d_1 – basal spacing for the clay

d_2 – basal spacing for the intercalated clay tactoids

f_e – mass fraction of exfoliated nanostructures;

f_i – mass fraction of intercalated nanostructures;

E – Young's modulus

E_s – modulus of solid

E_f – modulus of foam

E_p – modulus of polymer

E_{cp} – modulus of clay platelets

ΔE^* – free energy of activation for transporting a chain segment

F – force

ΔF^* – free energy of formation of a critical size nucleus

G – shear modulus

G_0 – pre-exponential factor

G_1 – spherulitic growth rate

G_p – shear modulus of polymer

G_r – shear modulus of reinforcement

h – thickness of a clay platelet

ΔH_m – melting enthalpy of the sample

ΔH_m^0 – melting enthalpy for the 100% crystalline polymer

K – bulk modulus

k– fraction of absorbed polymer on the clay layer that behaves like clay

k_B – Boltzmann constant

K_g – nucleation parameter

K_1 – linear-elastic stress intensity factor

K_p – bulk modulus of polymer

K_r – bulk modulus of reinforcement

n – displacement

N_{min} – minimum number of clay platelets per stack in a clay tactoid;

N_{max} – maximum number of clay platelets per stack in a clay tactoid;

$\overline{N}$ – average number of clay platelets per stack in a clay tactoid

p_0 – atmospheric pressure, υ_f is Poisson's ratio,

q – arc length

dq – element of arc length along the curve surrounding the tip of the notch

$\mathcal{R}$ – gas constant

R_g – radius of gyration of the polymer chain

s – ratio of intercalated polymer to clay

T – stress

ΔT – degree of supercooling

T_c – crystallisation temperature

T_g – glass transition temperature

T_m – melting temperature

T_m^0 – equilibrium melting point

T^d_{peak} – maximum degradation temperature

U – area under the load displacement curve

U* – transport activation energy

W – sample width

x_1, x_2 – coordinates

List of figures

List of tables

Chapter 1. Introduction

Polymers are macromolecules characterised by the repeat of structural units and high molar mass. They can be linear or branched, i.e., thermoplastic polymers or tridimensional or cross-linked, i.e., thermosetting polymers. Thermoplastic polymers can be amorphous or semicrystalline, thus brittle or ductile materials. Polymers present a myriad of applications (i.e., packaging, construction, automotive, etc.). It has been shown that the addition of a filler (e.g. calcium carbonate, talc and glass fiber) can lead to conventional composites which may show improved properties compared to the pristine polymers. Traditionally polymers were reinforced with micro-sized fillers. In the recent years the incorporation of low concentrations of nanometre-sized fillers has become a crucial strategy to improve and diversify polymer materials. Polymer nanocomposites are a new class of materials that consist of a polymeric matrix containing well-dispersed particles or fillers with at least one of its dimensions at the nanometre scale. A well accepted definition of polymer nanocomposites is that they are composites in which small amounts of nanometre sized fillers are homogenously dispersed in a polymer matrix. They can also be defined as a two phase-system, where at least one dimension of the reinforced filler is on the nanometre scale. As defined, the fillers added to the matrix are very small in quantity, normally less than 10 wt.%, unlike conventional composites where the amount of microfillers can reach up to 50 wt.% of the total materials weight.[1-3]

Clay minerals have been used for a long time as catalysis, absorbents and rheological modifiers in the chemical and coatings industries.[4-6] The use of clays as polymer additive fillers also has an eloquent history with polymer intercalation of montmorillonite being first investigated more than 70 years ago.[7]

In 1987, the researchers at Toyota Laboratories, with their pioneering work, have discovered that clay particles can delaminate and act as more than just an absorbing agent that was well established since 1950,[4, 5] and layered silicates have gained importance as modifiers in improving polymer performance. Using nylon 6 as the polymer matrix and a small quantity of clay (less than 10 wt.%)[2] as the reinforcing agent, it was discovered that this hybrid polymer material possessed unique and significantly improved mechanical and thermal properties compared to the pristine polymer.[8] This led to the first use of this material in the early 1990s as the timing belt cover in automotive cars.[2, 9] Prior to this, articles written on organoclays and polymer/clay composites were almost inexistent;

however, with the new improved material properties came new applications which resulted in an exponential increase in the number of studies on polymer/clay nanocomposites. Today, polymer/clay nanocomposites represent an area with tremendous potential that receives substantial interest from both academia and industry.

Unlike other reinforcing agents (e.g. carbon fibers and carbon nanotubes) that take time to generate, clay is ubiquitous in nature and environmentally friendly. The ability of clay to adsorb different chemicals[4, 5] recommended this material to be used as a reinforcing agent for polymer materials. The most exploited type of clay is montmorillonite, an aluminosilicate mineral with a hydrophilic character. Montmorillonite clays exhibit rich intercalation chemistry mostly due to their excellent capability to absorb hydrophilic (polar) substances. This characteristic makes them prone towards being chemically modified in order to transform them into materials that are compatible with polymers with low-polarity. The typical chemical treatment involves a cation exchange reaction in which the metallic ions that inhabit the clay gallery are exchanged by surfactant molecules, rendering the clay hydrophobic. This process facilitates the dispersion of clay in less hydrophilic polymer matrices.[10, 11]

Polymer/clay nanocomposites can be described as the union of two different components represented by an inorganic nanofiller that is imbedded into an organic matrix at nanoscale level.[12] These new hybrid materials are usually manufactured by: *in situ* polymerisation, solution method or melt compounding. Using any of these methods to mix the monomer/polymer with the clay, conventional composites and intercalated and/or exfoliated nanocomposites can be manufactured (Figure 1.1). In conventional composites the clay is dispersed in the polymer matrix; however, the noncompatibility of the two components prevents the clay from delaminating; thus, the polymer is reinforced by clay particles. In an intercalated nanostructure the polymer penetrates inside the gallery. Although the polymer chains increase the distance between silicate layers, the amount of intercalated polymer is not enough to delaminate the clay platelets; in which case, the reinforcement is made up by clay tactoids, i.e., stacked clay platelets. When the polymer content inside the clay gallery increases ordered exfoliation occurs and past that threshold exfoliated clay platelets can be observed in the polymer matrix. Regardless of the type of exfoliation in the polymer/clay nanocomposite, the reinforcement is represented by single clay platelets.

The constantly evolving interest in this new class of polymer materials springs from the ability of polymer/clay nanocomposites to display superior and even unique properties

compared to the pristine polymers or their conventional polymer counterparts.[8] Typically, in conventional composites, the same degree of property improvement would be attained with the addition of a large quantity of the filler.[2] However, due to the unique ability of clay to disperse as clay tactoids or individual clay platelets and create an unusual high contact surface with the polymer matrix, only very small quantities of clay, typically less than 5 wt.% are necessary.[13] This is because of the superior properties of a clay platelet over a clay particle. Thus, a montmorillonite clay particle is characterised by a Young's modulus of 14 GPa,[14] an aspect ratio of about 10,[15] a density of 2600 $kg \cdot m^{-3}$ and a surface area of 38 $m^2 \cdot g^{-1}$,[16] whereas a clay platelet presents a Young's modulus of 230 GPa,[16] an aspect ratio of about 50-1500,[17] a density of 3100 $kg \cdot m^{-3}$ and a surface area of 760 $m^2 \cdot g^{-1}$.[8, 16] By intercalating/exfoliating the clay platelets, the surface area of the clay platelet becomes more exposed and allows for the stress to which the polymer matrix is subjected to transfer to the clay nanostructure.

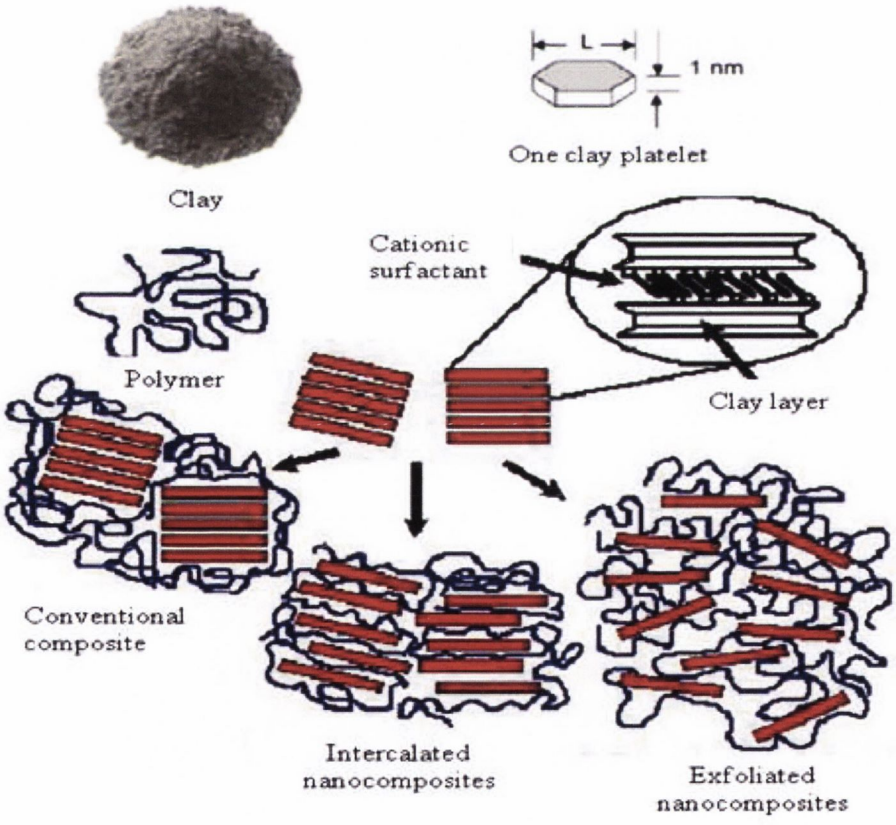

Figure 1.1. The clay mineral may delaminate in single clay platelets. By treating the clay with a cationic surfactant *via* a cation exchange process and sequentially dispersing the organoclay in a polymer matrix: conventional composites and intercalated and exfoliated nanocomposites may be obtained (Modified from reference[18]).

The hydrophilic character of clay determines it to be prone towards polar substances such as epoxy, polyurethane or polyethylene oxide, in which clay may produce intercalated and/or exfoliated structures. However, most of the world's plastic production is represented by thermoplastic polymers (e.g. polyethylene, polypropylene, polystyrene) that are non-polar or characterised by a low polarity. In these polymers, natural clay tends to form large aggregates leading to conventional composites. The typical solution, to using clays in non-polar and low polar polymers, is to add a compatibilising agent and/or to organically modify the clay, making it more compatible to the polymer matrix and able to be dispersed in the material. Over the years a series of approaches have been investigated in the search of achieving enhanced exfoliation. In most of the cases the clay treatment process has proven tedious, economically unviable and environmentally harmful.

So far, the research on polymer/clay nanocomposites has established that the mechanical properties depend on a series of factors, such as the degree of delamination, dispersion and orientation of the clay platelets, the testing temperature in relation to the glass transition temperature, the crystallinity degree and crystalline phase, the interactions between the polymer matrix and the filler, etc. One of the greatest questions in regard to polymer/clay nanocomposites is whether an intercalated nanocomposite is superior to an exfoliated nanocomposite. To the day, there are a number of contradictory theories on this aspect, especially in regard to the toughness of polymer/clay nanocomposites.

Still, the superior properties that have been achieved in some cases with the dispersion of clay platelets in pristine polymers have advised the addition of clay platelets in polymer foams and in polymer blends.

Foams are light materials with a myriad of applications varying from weight-bearing structures to isolations and tissue engineering scaffolds for cell attachment and growth.[19] The dispersion of clay in polymer foams has resulted in changes in the morphology and thermal and mechanical properties. However, so far, the role of the clay in polymer foam is uncertain, and its impact on the mechanical properties has yet not been quantified.

In the past, it has been envisioned that the addition of a third component to an immiscible polymer blend may prove beneficial in reducing the surface tension between the other components. Due to the high surface of the clay platelets, this material seemed the perfect choice; however, its hydrophilic character launched a series of questions in regard to the location and the role of clay in an immiscible polymer blend.

Although the addition of clay has been shown to improve the structure, thermal and mechanical properties of the polymer matrix, there are still a number of questions that need to be answered in regard to the role of the clay and its dispersion, morphology and mobility in the polymer matrix, and the changes that undergo in the polymer matrix. By understanding these factors and the role of the clay in the polymer matrix, products with specific properties can be designed, thus increasing the life-span of plastic materials. Also, the small amount of filler used in polymer/clay nanocomposites makes these materials easier to recycle and reintroduce back on the market.

1.1. Project aim and objectives

This project aims to investigate the effects of clay on the structure, thermal and mechanical properties of polymer/clay nanocomposites and study the fundamental science underpinning the development of this relatively new class of materials. It involves the use of pristine polymers that are often found in the plastic recycled stock and employs the use of natural clay and organomodified clays as nanofillers in order to develop new materials for various applications including plastic recycling. The principal objectives of this project are as follows:

1. Study low-density thermosetting polymer and polymer/clay nanocomposite foams and establish the best mixing sequence to obtain an optimal foam structure characterised by superior mechanical properties. The main goal of this work was to determine a structure-property relationship for low-density polymer/clay nanocomposite foams by using the established theories for conventional cellular materials.

2. Investigate thermoplastic polymer and polymer/clay nanocomposite porous solids manufactured *via* a novel procedure. Typically porous polymer/clay nanocomposites are manufactured by dispersing the clay in the polymer matrix, followed by the addition of the blowing agent. The main purpose of this study was to determine whether this type of clay treatment can lead to exfoliated polymer/clay nanocomposites.

3. Assess whether a natural clay or an organoclay would be more suitable for manufacturing polymer/clay nanocomposites *via* melt compounding. The main objective of this work was to establish the necessity of the

compatibilising agent and to determine the appropriate clay load for optimal mechanical properties.

4. Study the thermal and the mechanical properties of low-polarity amorphous polymer/clay composites and nanocomposites. The main goal of this work was to treat the natural clay with cationic, anionic and non-ionic surfactants and to assess which type of treatment presented the most promising outcome. For comparison the polymer was also mixed with the natural clay and a gel based on the same natural clay.

5. Develop a versatile route to prepare highly exfoliated nanostructures *via* melt processing. The main goal of this work was to develop novel organoclays by pretreating as-received organoclay with blowing agents and study the structure, thermal and mechanical properties of polymer/clay nanocomposites manufactured by dispersing the novel clays into different polymer matrices.

6. Study intercalated/exfoliated polymer/clay nanocomposites with different degrees of exfoliation. The main aim of this project was to assess the changes that undergo in the crystallinity and crystalline structure of the polymer and polymer/clay nanocomposites with exposing the material to unaixial deformation.

7. Investigate the toughness of polymer and polymer/clay nanocomposites using tensile low and high speed test as well as fracture mechanics. The main objective of this work was to assess whether intercalated or exfoliated polymer/clay nanocomposites would present superior toughness as opposed to the other.

8. Study immiscible polymer blend/clay nanocomposites and investigate the effects of clay on structure, thermal and mechanical properties. The main goal of this study was to investigate the role of the clay and to quantify the relationships between the mechanical properties and the amount of reinforcement added.

9. Investigate the structure, thermal and mechanical properties of recycled polymer/clay composites and nanocomposites. The main aim of this work was to study the impact that clay addition had on the recycled polymers and

to establish the potential of using clays to reintroduce the plastic materials back into consumption.

Ultimately, it is hoped that this work would improve the understanding of adding clay platelets to a polymer matrix. It is hoped that this work will establish the most appropriate clay morphology to obtain optimal thermal and mechanical properties. By knowing the factors that control the structure and properties of a polymer/clay nanocomposite better materials with optimal properties can be designed, which will increase the life of polymer based materials and reduce the plastic consumption. It is hoped that the dispersion of clay would help reintroduce recycled materials back on the market and aid the future recycling process, thus increasing the life span of a polymer and reducing the need of pristine polymer manufacturing.

Chapter 2. Literature Review

2.1. Introduction

A composite material is a solid structure with multiple phases, representing a combination of two or more materials with different physical and chemical properties and exhibiting the best qualities of two or more, natural or synthetic, materials in order to create a new material. The evolution of composite materials is presented in Figure 2.1.[20] Contemporary, composite materials are the result of research and innovation of artificial engineering. These novel materials present specific properties and characteristics that sometimes can be different from the properties of the individual constituents.[8] These properties depend on the components, and mainly on the interfacial forces that exist between the components. Composite materials can be used in a wide range of applications which include the fields of construction, marine, aerospace, infrastructure, military, healthcare, etc.

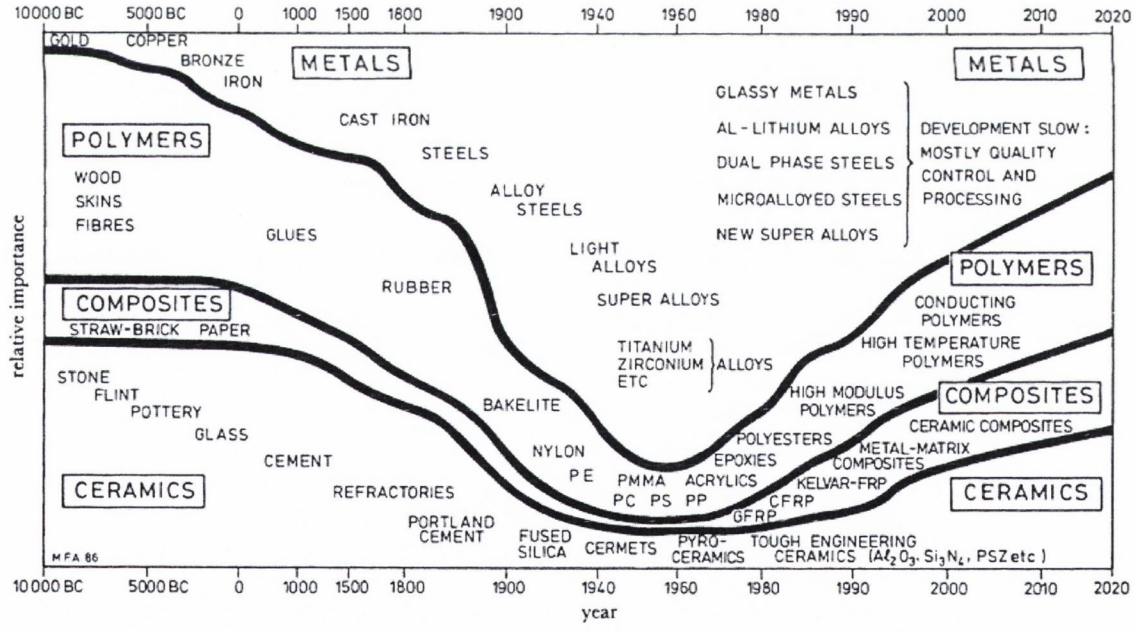

Figure 2.1. Schematic diagram of the evolution of materials from mechanical and civil engineering. The relative importance of four classes of materials (polymers, ceramics, metals and composites) as a function of time (Reproduced from reference[20]).

Polymer composites can be defined as materials that are formed from a macromolecular compound and a reinforcing agent or a filler which once dispersed in the

soft component does not dissolve in it.[21] The macromolecular compound can be a thermosetting or a thermoplastic polymer also known as the polymer matrix. The reinforcing agent can be a filler or a nanofiller of inorganic or organic nature. The polymer matrix offers the bulk properties of the composite materials, while the reinforcement component contributes with additional qualities. In many cases, a composite material is distinguished by the presence of a strong and stiff component embedded in a softer constituent forming the matrix.[21] The most common method to classify the composite materials is based on material matrix or based on reinforcing material structure. This classification denotes the existence of macrocomposites (e.g. steel concrete and glass reinforced polymers), microcomposites (e.g. epoxy resins reinforced with inorganic fillers) and nanocomposites.[22] Nanocomposites can be defined as reinforced polymers for which at least one of the dimensions of the dispersed filler is in the nanometre range.[23, 24] These materials can be hybrid materials of inorganic-organic nature or even organic-organic nature that allow the study of a molecular dimension system.[25] In contrast to the conventional polymer composites, polymer nanocomposites present radical improvements of the mechanical, thermal, conductive, and flammability properties.[2, 26-29]

2.2. Nanocomposites

Nanocomposites have been regarded as part of the nanomaterials family.[30] This new member represents a class of multiphase materials characterised by the dispersion of nanoparticles,[31] nanofibers (for example single or multiwall carbon nanotubes),[32] or intercalation/exfoliation of layered silicates within a polymer matrix.[8] Depending on the type of filler used, the nanodomains can constrain the polymer chains or enhance the toughening efficiency of the polymer nanocomposites.[33] Because of their nanometre sizes, filler dispersion nanocomposites can exhibit remarkably improved properties when compared to the pure polymers or their traditional composites.[8, 23, 34, 35]

The changes observed in the properties of polymer-inorganic nanocomposites are due to the mixing and binding of two different phases: the inorganic phase provides the high-performance thermal and mechanical properties, while the organic phase contributes to the processing and adhesive properties.[36] From a mechanical point of view, the most interesting nanofillers are those with a high aspect ratio (average length/diameter or thickness ratio), including layers (nanoclays and layered double hydroxyls) and fibrous materials (cellulosic nanofibers, carbon nanotubes and metal oxide nanotubes etc.).[22]

Among these nanofillers, nanoclays have attracted a great share of the attention because of their low cost, ready availability, eco-friendly nature, good swelling properties, and nonisometric structure derived from a high aspect ratio, which can maximise the reinforcing effect in terms of mechanical, thermal, and barrier properties.[23] The properties of polymer/clay nanocomposites largely depend on their nanoscale structure, which includes the dispersion of the silicate layers, the interaction between the polymer molecules and the silicate surface, the influence of inorganic layers on the polymer conformation and morphology, the compatibility between the organic and inorganic components and the way in which they are prepared.[8, 32, 37, 38]

2.3. Polymer matrix

Polymers molecules have high molar masses and are composed of a large number of repeating units. There are both naturally occurring and synthetic polymers. Typically, polymers may exhibit a linear, branched or cross-linked topology. The linear and branched polymers, also known as thermoplastic polymers, may be reprocessed by heating or dissolution in a suitable solvent. The cross-linked polymers involve a tri-dimensional network and are also known as thermosetting polymers which cannot be reshaped without permanent degradation of the chemical bonds.

2.3.1. Thermosetting polymers

The thermosetting polymers are the result of curing or cross-linking a resin with a solid, semi-solid or liquid organic reactive intermediate material, also known as the curing agent. This process can take place at room temperature or at elevated temperature and leads, *via* an irreversible chemical reaction known as polymerisation or cure, to the formation a high molecular weight, tri-dimensional product.[39]

The thermosetting polymers can be arranged in an arbitrary order according to their performances and consumption level in the following classification (Figure 2.2):[40]

- old materials of modest properties: urea-formaldehydes (UF);
- thermosetting polymers with good thermal behaviour: phenolic resins (PR) and melamines (MF);
- thermosetting polymers with the most uses for their general qualities: unsaturated polyesters and polyurethanes (PU);

- thermosetting polymers with a broad range of properties (used for high tech composites): epoxy;
- flexibility and heat resistance, physiologically harmless thermosetting silicones;
- thermosetting polymers with high-tech uses, limited distribution: polyimides (PI);
- thermosetting polymers with highly targeted uses and very limited distribution: polycyanates (PCy).

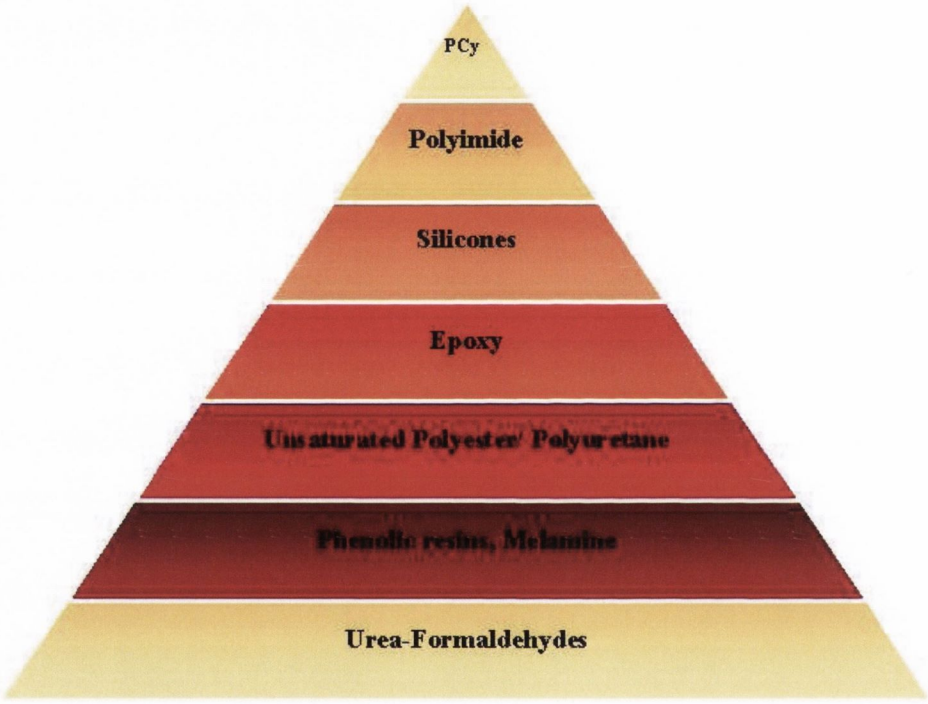

Figure 2.2. Arbitrary classification of commonly used thermosetting polymers (Modified from reference[40]).

2.3.2. Thermoplastic polymers

Thermoplastic polymers possess good resistance to chemical substances[40] and their mechanical properties are strongly dependent on the temperature and applied strain rate.[21] An arbitrary order of the main families of thermoplastics according to their performances and consumption level is the following classification (Figure 2.3):[40]

- commodity thermoplastics: polyethylene (PE), polypropylene (PP), poly(vinyl chloride) (PVC), polystyrene (PS) and polyphenylene ether (PPE);

- copolymers with more specific applications: acrylonitrile butadiene styrene (ABS) and styrene acrylonitrile (SAN);
- engineering thermoplastics: polyamide (PA), polycarbonate (PC), poly(methyl methacrylate) (PMMA), polyoxymethylene (POM), poly(phenylene ethynylene) (PPE), poly(ethylene terephthalate) (PET) and poly(butylene terephthalate) (PBT), etc.;
- engineering thermoplastics with more specific performances: polysulfone (PSU), polyethyleneimine (PEI) and polyphenylene sulphide (PPS), etc.;
- thermoplastic polymers with high-tech uses, limited consumption: ethylene tetrafluoroethylene (ETFE) and polyether ether ketone (PEEK);
- thermoplastic polymers with high-tech uses, more limited consumption: liquid polymer crystal (LPC), polytetrafluoroethylene (PTFE), perfluoroalkoxy (PFA), fluorinated ethylene propylene (FEP) and polyimide (PI);
- thermoplastic polymers with highly targeted uses and very restricted consumption: polybenzimidazole (PBI).

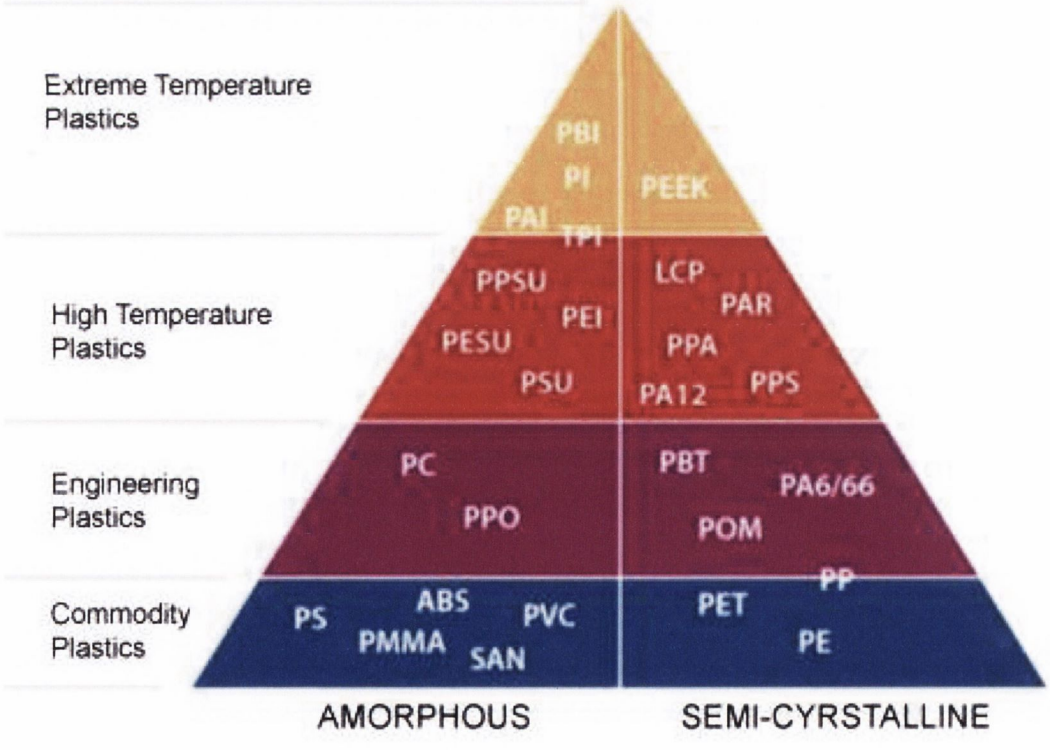

Figure 2.3. Arbitrary classification of amorphous and semicrystalline thermoplastic polymers (Reproduced from reference[41]).

2.4. Reinforcing agents

Reinforcing materials play a multitude of roles when it comes to them being used as part of composite materials; the most important ones are those of reducing the costs of the composites and modifying the physical and mechanical properties of the final product.[10, 32, 42, 43] Some of the properties that can be modified by adding reinforcing agents are: stiffness, tensile strength, hardness, abrasion resistance, dimensional stability, heat resistance, fire resistance, optical properties or, if the polymers' insulating properties are not desired, electrical conductivity.[31]

2.4.1. Fillers

Inorganic fillers, with micrometer range dimensions (e.g. calcium carbonate, glass fibers and talc) have been used to improve the mechanical properties of the polymers.[9, 42, 44] Usually the content of fillers in a conventional composite material is between 20 and 40 wt.%, and, in some polymers, can exceed 50 wt.%; however, the interaction between the polymer matrix and the filler is limited.[2]

2.4.2. Nanofillers

In the case of nanofillers, the content of filler in a polymer composite material is typically lower than 10 wt.% due to their high aspect ratio[45] displayed by the nano-reinforcing agent. It was also found that the nanocomposites exhibited the best properties at a nanofiller load of about 5 wt.% [13] and in the case of PMMA with a 0.5 wt.% organoclay (i.e., Cloisite® 20A) content, the mechanical properties were found to increase significantly.[46] Typically, the density of the filler is higher than the density of the polymer matrix, thus, conventional composites present higher density than their polymer counterparts. However, the use of small filler contents in polymer/clay nanocomposites renders lighter materials that can be easily recycled, making this new class of materials a necessity in a world with limited resources.

There are a number of factors that affect the interaction between nanofillers and polymer matrix; among which filler volume (weight) fraction, degree of dispersion, the filler geometry and orientation, etc. Nanofillers are classified by their geometry in three categories (Figure 2.4):

- particles (carbon black, silica nanoparticle, polyhedral oligomeric sislesquioxanes) with a tri-dimensional nanosize distribution;[32, 35]
- fibrous materials (carbon nanotubes or whiskers) with a two-dimensional distribution;[32, 47]
- layered (organo-silicates or graphene) represented by single layers with one dimensional nanosize, having a nanometre thickness and a high aspect ratio with a platelet like structure.[48, 49]

The most common nanofillers are carbon nanotubes, layered silicates or graphene due to their very high aspect ratio,[49] which can be over 1000 sometimes.[9] Clay minerals are potential nanoscale additives because they are comprised of silicate layers in which the fundamental unit is a 1 nm thick planar structure and they have the ability to undergo cation-exchange reactions[50, 51] and intercalate with various organic molecules, which results in increased distance between the silicate layers[12] and possible complete intercalation and/or exfoliation in a polymer matrix.

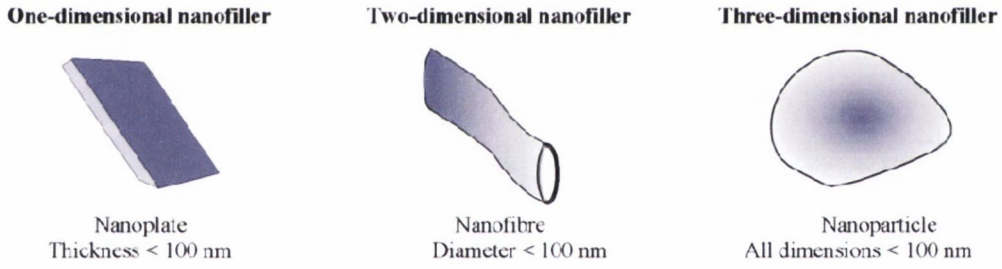

Figure 2.4. Nano-objects used for nanocomposites, as defined in ISO/TS27687 (2009).

2.4.2.1. Clays (layered silicates)

Clays are usually classified by their structure in: allophone, kaolinite, halloysite, smectite, illite, chlorite, vermiculite, attapulgite–palygorskite–sepiolite and mixed layered minerals.[52] These layered silicate clay minerals are characterised by the presence of certain groups of hydrous aluminium, magnesium, iron silicates and may contain sodium, calcium, potassium, and other ions.[53] The atomic structure of clay minerals, illustrated for smectites (i.e., montmorillonite) in Figure 2.5, consists of two basic units, an octahedral layer and a tetrahedral layer. The octahedral layer is comprised of closely packed oxygens and hydroxyls in which aluminium, iron and magnesium atoms are arranged in octahedral coordination.[54] In the tetrahedral layer the silicon atom is positioned at equal distances

from the four oxygen atoms; this forms the SiO_4 group that once linked with other similar groups leads to a hexagonal network of repeating units of Si_4O_{10}.[55] The space between the 2:1 and 1:1 layers is occupied by water molecules and cations.

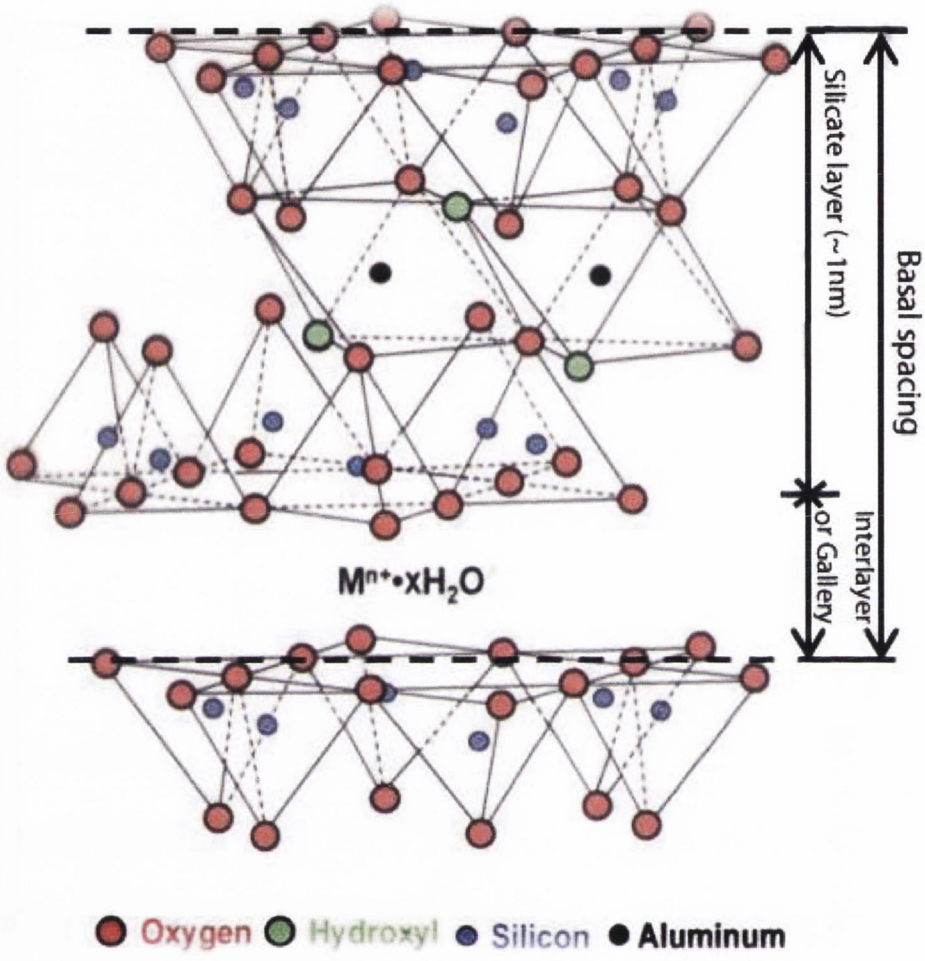

Figure 2.5. Unit structure of a layered silicate (Reproduced from reference[9]).

The natural clays can be divided into two main classes: expanding (e.g. smectites and vermiculite) and non-expanding (e.g. kaolinites).[56] The class of smectites and the class of vermiculites are also known as the class of 2:1 silicates[32] because the clays are formed of two tetrahedral sheets bonded with an octahedral sheet. Whereas, the class of the kaolinites is the class 1:1 silicates characterised by the presence of an octahedral sheet and a tetrahedral sheet (Table 2.1). In the class of smectites one can find in nature, according to Murry,[54] the following silicates: sodium montmorillonite, calcium montmorillonite, nontronite (iron montmorillonite), saponite (magnesium montmorillonite), beidelite (aluminium montmorillonite) and hectorite (lithium montmorillonite).

Table 2.1. General chemical formulas of different clay groups.[57]

Clay Group	Chemical formula
Kaolines (Kaolinite)	$[Si_4]Al_4O_{10}(OH)_8 \cdot nH_2O$, n = 0 or 4
Smectite (e.g. MMT)	$M_x[Si_8]Al_{3.2}Fe_{0.2}Mg_{0.6}O_{20}(OH)_4$
Vermiculite	$M_x[Si_7Al]Al_{3.2}Fe_{0.5}Mg_{0.5}O_{20}(OH)_4$
Ilite (hydrous micas)	$M_x[Si_{6.8}Al_{1.2}]Al_3Fe_{0.25}Mg_{0.75}O_{20}(OH)_4$
Chlorite	$(Al(OH)_{2.55})_4[Si_{6.8}Al_{1.2}]Al_{3.4}Mg_{0.6}O_{20}(OH)_4$

Some of the clays, i.e., montmorillonite (MMT-used as a generic term for the montmorillonites), saponite and hectorite, from the smectites class present excellent intercalation abilities,[12] whilst the class of vermiculites is characterised by the ability to expand at elevated temperatures.[9] Compared to other nanofillers, layered silicates are the materials of choice for creating polymer nanocomposites because they are ubiquitous in nature,[58] can be obtained in a mineralogical pure form at low costs, can intercalate polymer into their galley and can delaminate into single clay platelets. The quality of clay is mostly evaluated by the cation exchange capacity (CEC), which refers to the reaction properties of the MMTs, representing the number of exchangeable cations that a mineral can adsorb, and being characterised by values between 66 and 123 meq.·(100 g)$^{-1}$.[59] The characteristics of some of the most used clays are presented in Table 2.2.

The chemistry of the smectites class is governed by: a substantial cation exchange capacity (~100 meq·(100 g)$^{-1}$ for hectorite), reactive edges on individual clay platelets, an ability to interact with a wide range of natural and synthetic organic compounds, a large effective surface area for absorption of organic compounds and strong, local electric fields in the interlayer region between platelets.[12] One of the most important characteristics of the layered silicates used as fillers for polymer/clay nanocomposites is their structure, characterised by the basal plane spacing, comprised of the silicate layer and the interlayer (Figure 2.3).[9] The intralayer in the case of the smectite clays has the following theoretical formula $(OH)_4Si_8Al_4O_{20} \cdot nH_2O$; however, there is considerable substitution in the octahedral sheet and some in the tetrahedral sheet.[54]

Table 2.2. Characteristics of clay groups.[57]

Layer Structure	Clay Group	Layer Charge x-1.0 / e	Basal Spacing / nm	CEC/ meq.·(100 g)$^{-1}$
1:1	Kaolines (Kaolinite)	<0.01	0.714	1-10
2:1	Smectite (e.g. MMT)	0.5-1.2	1.24-1.7	80-120
	Vermiculite	1.2-1.8	0.93-1.4	120-150
	Ilite (hydrous micas)	1.4-2.0	1.0	~30
2:1 with hydroxide	Chlorite	Variable	1.4	10-40

Okada and Usuki[2] ranked the effect of different clays based on the mechanical properties of a nylon 6/clay nanocomposites with 5 wt.% reinforcing agent, as follows: montmorillonite>mica>sapronite>hectorite. Montmorillonites also exhibit a very rich intercalation chemistry, which has the advantage of allowing them to be chemically modified and of transforming them into materials that are compatible with organic polymers in order to disperse them on a nanometre level.[10, 11]

Montmorillonite is the clay mineral of choice for polymer/clay nanocomposites due to its favourable enthalpy of mixing[60] and its high cation exchange capacity which leads to a small amount of ionic interactions holding the layers together[61] making it easy for the surfactants, monomers and polymers to intercalate themselves between the layers. The industrial applications of this smectite depend mainly on the treatment technology, chemical composition and crystal structure.[36] Sodium montmorillonite was characterised by Vanorio et al.[14] as having a bulk density of 2 g·cm^{-3}, a grain density of 2.3 g·cm^{-3} and a Young's modulus of 14 GPa. The value for Young's modulus is smaller compared the values obtained for analogous minerals like pyrophyllite and muscovite mica which have values in the range of 49-81 GPa that have been attributed to bigger interlayer distances.[16]

On a molecular level, montmorillonite can be described as a hydrous aluminosilicate clay mineral, being depicted as an aluminium octahedron sandwiched between two layers of silicon tetrahedron. The structure is held together with the help of weak dipolar or van der Waals forces and electrostatic forces. This facilitates the intercalation of water or organic molecules in the basal spacing and leads to the expansion of the crystal lattice.[62] In

the pristine form the excess in negative charges that montmorillonite possesses is balanced by cations (Li^+, Na^+, Ca^{2+}), as can be observed in Figure 2.5, making it miscible with hydrophilic polymers.[60] Each layered silicate sheet had a theoretical stiffness of 230 GPa,[16] is approximately 1 nm thick,[63] possesses a lateral dimension that varies from 30 nm to several microns or longer, an aspect ratio of about 50-1500,[17] and a surface area of 760 $m^2 \cdot g^{-1}$.[35] Compared to clay particles (stacks or clusters of layers) that have an aggregate specific gravity of 2.6,[63] the silicate layers have a specific gravity of 3.1.[63] This indicates their ability to expand their volume once they are dispersed in a hydrophilic solvent.

Typically, montmorillonite occurs in two main varieties: sodium montmorillonite characterised by a high swelling capacity in water and calcium montmorillonite with a low swelling capacity.[64] The calcium montmorillonite has a basal space of 1.42 nm and the layer charge deficiency is balanced by the interlayer calcium cation and two water layers (0.42-0.45 nm), while sodium montmorillonite has a basal space of 1.22 nm and the charge deficiency is balanced by sodium ions and one water layer (0.25 nm).[54] The most important property of montmorillonite is adsorption which is emphasized by the cation exchange in the interlayer space.[64]

2.4.3. Clay treatments

Polymer/clay nanocomposites can be synthesised in a number of ways, but typically an organic treatment (e.g. cation exchange) is needed to ensure compatibility between a hydrophobic polymer and the hydrophilic clay.[31] The clay compatibilisation is based on organoclay technology that was first developed by Jordan[4, 5, 65] in the 1950s and in which the clay is treated so that it becomes compatible with hydrophobic materials,[66] such as polyolefins and waxes. The necessity of the treatment springs from the highly polar ionic surface of the clay minerals that make the clay incompatible with most of the polymers (i.e., poly(methyl methacrylate) and polystyrene) and the presence of the forces that hold the structure together, which need to be overcome in order to achieve the dispersion of single silicate layers.[12, 67] However, the compatibility and the dispensability of the clay also depend on the polymer and its properties, especially the nature of the molecule, the chain length and the packing density.[7] Typically, the hydrophilic character of the natural clay can be altered *via* cation exchange, covalent bonding or adsorption of molecules.[68]

The most commonly used organic treatment is ion exchange with alkyl ammonium salts[51] which are attracted by electrostatic forces between the negative smectite layers and

the ions inside the gallery.[69] As a result the clay becomes organophilic and its miscibility and dispersion in organic solvents are improved.[70] The nature of the alkylammonium salt (cationic surfactant) used to form organoclay depends on the nature of the polymer matrix in which the clay will be dispersed.[71] For example, for polar polymers alkyl benzyl dimethylammonim or alkyl hydroxyethylammonium halides may be used according to de Pavia et al.[72] The role of the alkylammonium cations is to lower the surface energy of the inorganic nanofiller, to improve the wetting abilities of the polymer matrix and to increase the basal spacing.[73] The ion exchange reaction (showed schematically in Figure 2.6) has two major consequences: the gap between the clay sheets is widened which makes it easier for the polymer chains to enter the basal space and the surface properties of each single sheet are changed from hydrophilic to hydrophobic as mentioned above.[74]

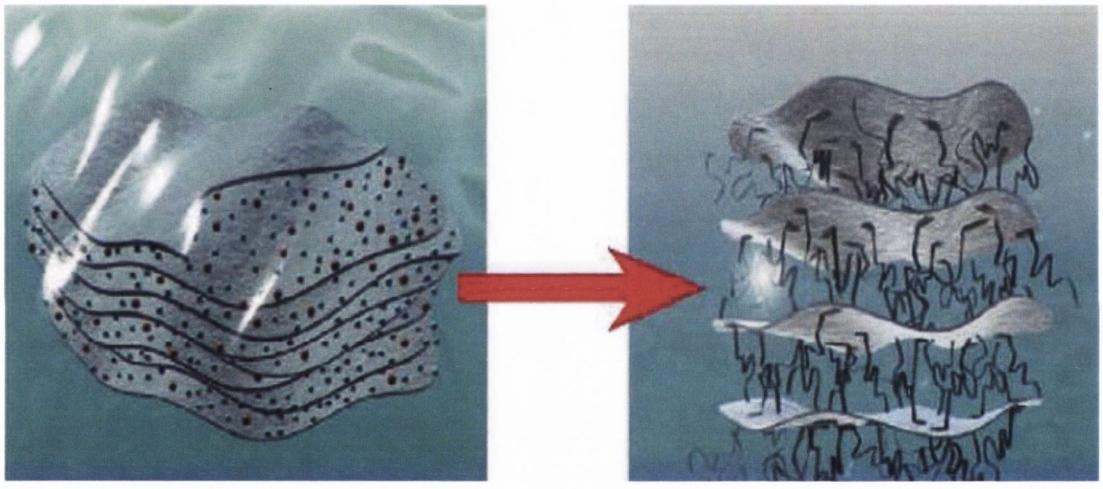

Figure 2.6. Schematic picture of an ion-exchange reaction. The inorganic, relatively small (sodium) ions are exchanged against more voluminous organic onium cations (Reproduced from reference[7]).

The basal space of the clay is increased by the addition of surfactants that are characterised by the presence of a cationic polar group (that is hydrophilic) and a large organic group (of at least C_{12}), that will provide a better interaction between the clay and the polymer.[75] At low interlayer packing densities, the chains and the surfactant are characterised by a disordered monolayer arrangement; however, the chains have the tendency of adopting more extended conformations as the packing density increases.[7]

The expandable nature of montmorillonite,[76] makes this clay an ideal nanofiller for polymer/clay nanocomposites. The ion exchange helps push the layers apart, so that the

polymer can enter the gallery and create intercalated and/or exfoliated clay structures. The intercalated nanocomposites are characterised by an increased basal plane spacing [77] and a well maintained order of the layered silicates.[78] However, when the clay layers are completely pushed apart to create a disordered array, the composite is considered to be 'exfoliated'.[8] The cation exchange process involves the reaction between a layered MMT and a quaternary ammonia salt (Figure 2.7).[36]

$$RN^{+}H_3 \cdot X + \text{Na-MMT} \rightarrow \text{R-}N^{+}H_3 \cdot X + Na^{+}$$

|

MMT

Organo-montmorillonite

Figure 2.7. Cation exchange dispersion reactions (In the formula, R=HOOCAr (Ar= 1,4 – phenylene), $HOCH_2CH_2$, $CH_3(CH_2)_{15}N(CH_3)_2$ or $CH_3(CH_2)_{11}$ and X = Cl-, H_2PO^{4-} or $H2PO^{3-}$, Reproduced from reference[36]).

Unlike cation exchange, chemical bonding is based on the grafting of functional polymers on the surface of clay minerals. With the formation of covalent bonds between the reactive surface groups and the organic species the clay becomes hydrophobic. This process can be applied only on 2:1 clay minerals that possesses the silanol and alumino groups on the edge of the surface and have the ability to react with the organic agent by grafting reactions.[79] According to Liu[80] the chemical bonding can be accomplished by one-step and two-step grafting methods.

Figure 2.8. General mechanism for one-step grafting reactions, characterised by condensation of functional polymers, where X – surface group; Y – organic species and Z – organo-modified part of the clay (Reproduced from reference[80]).

The one step grafting method is characterised by condensation of the functionalised polymers with reactive groups on a solid substrate, as shown in Figure 2.8. Some of the

approaches considered so far are the use of polycations[81] that will be absorbed on the clay surface or the use of cationic polymers, like polyethyleneimine.[82]

Two-step grafting (Figure 2.9) is depicted by the covalent attachment of a macromonomer or a macroinitiator on a solid surface, followed by chain growth. The pre-treatment is necessary to increase the number of silanol groups and it is usually achieved by treating the clay with acid[83] which removes the octahedral cations leaving behind two Si-OH groups.

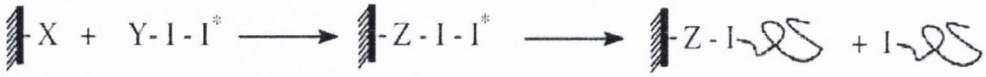

Figure 2.9. General mechanism for two-step grafting reactions, represented by the covalent attachment of a macronitiator, followed by chain growth, where X – surface group; Y – I - I* - macroinitiator; Z – I - I* - organo-modified part of the clay containing an initiator group and Z – I - organo-modified part of the clay containing a polymer (Reproduced from reference[80]).

Clays have always been used as adsorbents to control chemical spills and to protect the environment, due to their expandable nature and adsorption/absorption capabilities. The gallery expansion may be described as follows: when water molecules come in contact with the montmorillonite unit they enter into the interlayer gallery and cluster around the interlayer cations like sodium, magnesium, iron, etc, and at the same time partially charged oxygen atoms covalently bond with the surface oxygen that exists in the clay gallery, leading to the expansion of the interlayer.[27] Appling the same mechanisms it has been observed that basal space of clay increases[84] when organic substances are absorbed between the silicate layers. The surface modification of clay minerals with polymers by physical absorption is controlled by chemical interactions such as hydrogen bonding, ion-dipole interactions,[80] co-ordination bonds, acid base reactions, charge transfer and van der Waals forces.[72]

In some clays (e.g. montmorillonites) the number of hydroxyl groups is limited to the edges of the particle. Since a small number of organic molecules can be covalently linked,[83] an increase in the amount of organic molecules presented into the gallery is attributed to the absorption forces.

To the day, the most used clay treatment is cation-exchange; a large number of montmorillonite clays treated with different surfactants are currently commercially available.

2.5. Polymer/clay nanocomposites

In 1987 the first polymer/clay nanocomposites were created at Toyota Central R&D Labs.[2, 85] This new concept generated a ripple effect that expanded the field of polymer composite science including preparation, structures and interfaces. These relatively new materials opened the doors to a series of new applications in a multitude of fields such as construction, automotive, marine, aerospace, healthcare, and electric and food industries.

The first nanocomposite was based on in-reactor processing of ε-caprolactam and montmorillonite that was previously treated by ion exchange with the hydrochloride salt of aminolauric acid (12-aminodecanoic acid).[2] The nylon 6/montmorillonite composites developed by the Toyota Group had a very small amount of layered silicate, less than 10 wt.%,[86] and were characterised by enhanced thermal and mechanical properties.[87] However, the in-reactor process proved tedious and the only use was the timing belt cover in Toyota Camry.[2, 88] The interest in polymer/clay nanocomposites reached a new level when Giannelis et al.[60] found that these materials can be obtained by melt mixing, making this approach environmentally safe and easy to use.

Typically, the manufacturing process of polymer/clay nanocomposites involves two stages: transformation of the clay into an organoclay and blending the modified clay into the monomer or polymer matrix.[89] The properties of the nanoclay filled polymeric systems are found to be superior[90] compared to the properties of the pristine polymers and even to the properties of the systems reinforced with microsized particles, such as talc, glass fibers and glass beads. The improvements observed in the case of nanocomposites depend mainly on the degree of dispersion of the clay particles in the polymeric matrix.[91]

2.5.1. Synthesis

There are a multitude of methods that can be used to obtain polymer/clay nanocomposites; among these the following can be enumerated: *in situ* polymerisation, solution intercalation, melt processing, co-vulcanization, solid-state intercalation, emulsion and supercritical CO_2 methods.[8] The most important methods are: *in situ* polymerisation,

solution casting and melt intercalation which typically result in intercalated and intercalated/exfoliated nanocomposites.[8, 92, 93] The manufacturing of nanocomposites involves either the intercalation of a suitable monomer followed by the expansion of the interlayer *via* subsequent polymerisation,[94] the intercalation of a polymer from solution or the intercalation of a polymer melt. Although the nanocomposites obtained through *in situ* polymerisation are more likely to result in exfoliation, the most viable method for producing nanocomposites at an industrial level is the melt intercalation method, which is environmentally friendly and presents commercial feasibility.[70, 95]

Regardless of the method used, the main requirement is the compatibility between the polymers and the clays which can be achieved by the use of organoclays and compatibilisers.[32] The clays are modified with surfactants that create an interface between the clay and the polymer. In order to achieve the intercalation of the polymer into the galleries of clay the selection of the appropriate organoclay is required; nevertheless, in many cases the use of compatibilisers (maleic-anhydride and hydroxyl functional groups) is also necessary to intercalate the non-polar polymers. The compatibilisation agent of two intrinsically noncompatible components should have parts which react thermodynamically stable and easy with both components. Surfactants fulfil only partially these requirements, because although their ionic part interacts in a favourable way with the surface of clay, the long alkyl tail can exhibit limited compatibility with the polymer chain. This issue may be solved with the use of 'macro-surfactants', like block or grafted copolymers[74] and assuring the compatibility between the maleated oligomer and the polymer matrix.[96]

The use of compatibilisers plays a much bigger part in creating nanocomposites, for example, the use of maleic anhydride grafted polyethylene does not only have the ability to promote the exfoliation of clay and to create good interfaces[97, 98] between clay and polyethylene, but it also toughens the polymer matrix, according to Moraweic et al.[99] The nature of the polyolefin grafting the polymer is very important as Garcia-Lopez et al.[100] demonstrated by investigating the differences between using a maleic anhydride grafted polypropylene (PPgMA) and diethyl maleated grafted polypropylene.

2.5.1.1. *In situ* polymerisation

The *in situ* polymerisation technique for obtaining polymer/clay nanocomposites is based on the polymerisation method typically used to synthesise any polymer. This technique is based on the addition of a clay suspension in a liquid monomer or a monomer

solution followed by dispersive mixing, in the presence of an initiator and at high temperatures where appropriate.[8] Step by step *in situ* polymerisation (Figure 2.10) can be described as follows: the clay is modified, usually by ion exchange, so it becomes hydrophobic; the functionalised clay is then dispersed in the monomer solution,[34] the monomer is absorbed into the galleries of the layered silicate, creating a larger basal space and allowing the polymerisation to take place within the intercalated sheets. The polymerisation process is initiated either by heat or radiation, by diffusion of a suitable initiator, or by a catalyst fixed through cationic exchange inside the gallery before the clay is swelled by the monomer.[9, 88, 101] Polymer/clay nanocomposites have also been synthesised by an array of in *situ* polymerisation methods, such as: ring opening polymerisation, conventional free radical polymerisation, cationic polymerisation and living anionic polymerisation; however, by using this method limited structural and molecular weight control is achieved.[102]

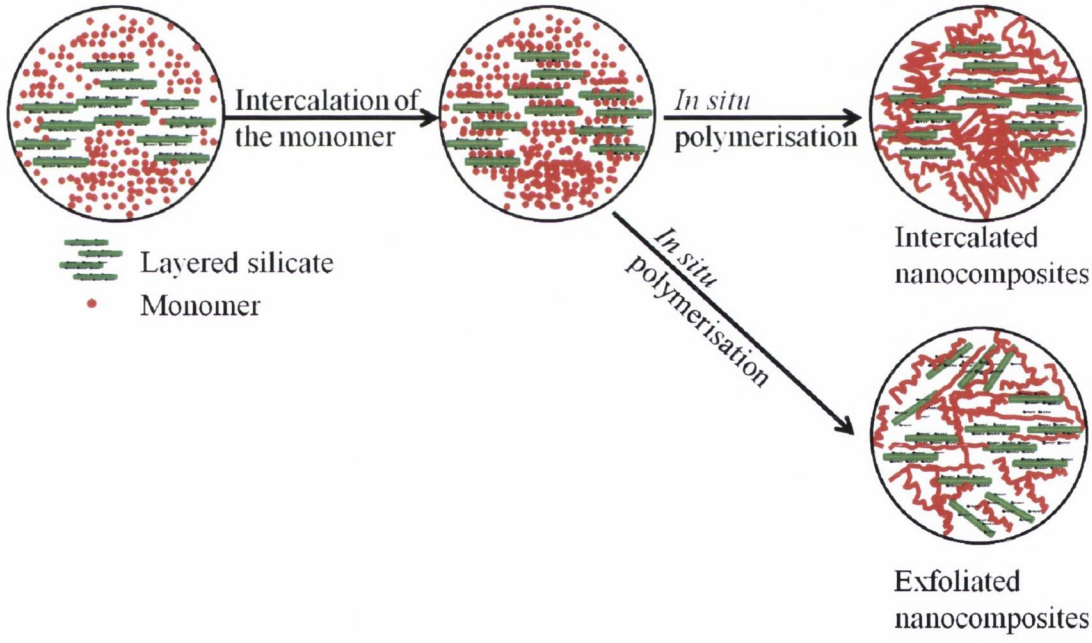

Figure 2.10. Schematic representation of polymer layered silicate obtained by *in situ* polymerisation.

One of the advantages of using *in situ* polymerisation is the tethering effect, which appears due to the modification of the surface of clay, making it easier for the polymeric chains to link to the layered silicate surface; this aspect was observed for nylon 6 when the surface of clay was modified with 12-aminododecanoic acid (ADA).[35] The most applied process, according to Akat et al.[102] is *in situ* conventional free radical polymerisation

because of its simplicity (it does not require any additional catalyst, such as inorganic salts), applicability to a wide range of monomers without any specific structural selectivity and the advantage of having the chain growth take place between the silicate layers, which leads to the exfoliation of clay and to the formation of nanocomposites.

The *in situ* intercalative polymerisation has been applied for polymerisation in suspension, in solution, in bulk, in emulsion or in microemulsion, making it possible to obtain almost any type of polymer/clay nanocomposites. This method has been successfully applied for polymer/clay nanocomposites with montmorillonite and different polymer matrices, such as: nylon 6,[103] nylon 12,[50] PMMA,[101] PP[104, 105] and PET,[106] etc. Although it is a widely applied technique, *in situ* polymerisation is defined as a time and cost consuming preparation route in which exfoliation is not always thermodynamically possible because the clay platelets may re-aggregate during subsequent processing steps and it can only be used by the resin manufacturer that can dedicate an entire line of production to realise this process.[7]

2.5.1.2. Solution intercalation

The preparation of nanocomposites *via* solution-blending methods is not considered to be the most practical method because it involves the use of environmentally unfriendly solvents.[107] Nevertheless, by using a solvent, individual clay platelets may become more mobile as the solvent offers an environment for the rearrangement of reactive sites into a variety of patterns.[12]

The solution intercalation process is based on a solvent system in which the polymer or monomer is soluble and the silicate layers are swellable.[87] This process (Figure 2.11) can be described by the following steps: the organoclay is swollen in a solvent (such as: water, chloroform or toluene) while the polymer is also dissolved in the same solvent or two solvents that dissolve one into the other; the two solutions are then mixed together and if necessary heated at an appropriate temperature so that the polymer, with the help of the solvent, intercalates between the silicate layers.[7, 9, 88, 108] When the process is considered to be complete the solvent is removed by evaporation or by precipitation in a non-solvent.[107] Although this method is acknowledged to be very unfriendly towards the environment, it has a major advantage, that of synthesising nanocomposites based on polymers with low, such as poly(methyl methacrylate), or even zero polarity.[88]

Thermodynamically the driving force for solution intercalation is the entropy gained by desorption of solvent molecules,[87] which allows the polymer chains to diffuse between the layers of the filler[109] and is partially compensated by the decrease entropy that the confined, intercalated polymer chains possess.[110] In this procedure it is expected for the entropy driven intercalation to occur even in the absence of the enthalpy gain due to favourable interactions between the macromolecules and the surface of the clay layers.[107]

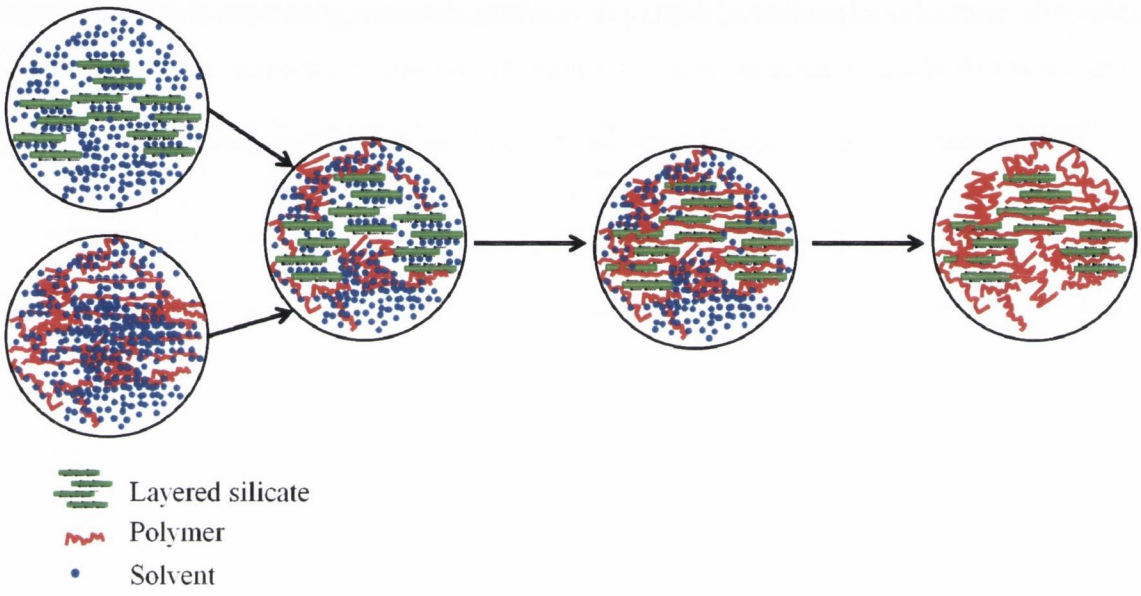

Figure 2.11. Schematic representation of polymer layered silicate obtained by intercalation from solution.

One of the most important factors of the solution intercalation method is the nature of the solvent, as it was proven by Aranda and Ruiz-Hitzky[111] who intercalated poly(ethylene oxide) into montmorillonite in the presence of different solvents, showing that the polarity of the solvent represents a crucial factor in the intercalation of the polymer into the galleries of clay. This method has been applied mainly for water-soluble polymers,[39] such as: poly(ethylene oxide), poly(vinyl alcohol), poly(acrylic acid), poly(N-vinyl pyrrolidone), poly(ethylene vinyl alcohol). However, it has also been applied for water insoluble polymers, such as: poly(ε-caprolactone)(PCL)/clay[112] in chloroform as a co-solvent of water, and high-density polyethylene (HDPE) with xylene and benzonitrile.[113]

2.5.1.3. Melt intercalation

This method is convenient and useful from an industrial point of view because it does not employ the use of organic solvents and it can be easily combined with conventional polymer processes, such as extrusion and injection moulding.[70, 114] Another advantage is that the structure of the nanocomposite can be altered by changing the melt blending conditions.[115] The disadvantages[116] presented by this method are related to the processing difficulties and product quality; the high temperatures and prolonged exposure can lead to molecular degradation, while the insufficient wetting between the high viscous polymers and fillers may result in inhomogeneous dispersion of the latter.

The layered silicate is mixed with the polymer in the molten state as observed in Figure 2.12. If the layered surfaces are compatible enough with the chosen polymer, the clay aggregates will be dispersed in the polymer matrix. During the melt mixing process, shear forces are produced which may delaminate the silicate stack and even peel the clay platelets from the stack one at a time while allowing the macromolecules to diffuse between the silicate layers.[117] The properties of the materials obtained through melt intercalation are highly dependent on the mixing speed of the extruder. A lower speed is recommended for the improvement of the mechanical properties[71] due to the low throughput, low rotation time and an increase in the residence time inside the extruder which allows more time for the polymer to intercalate between the clay layers.

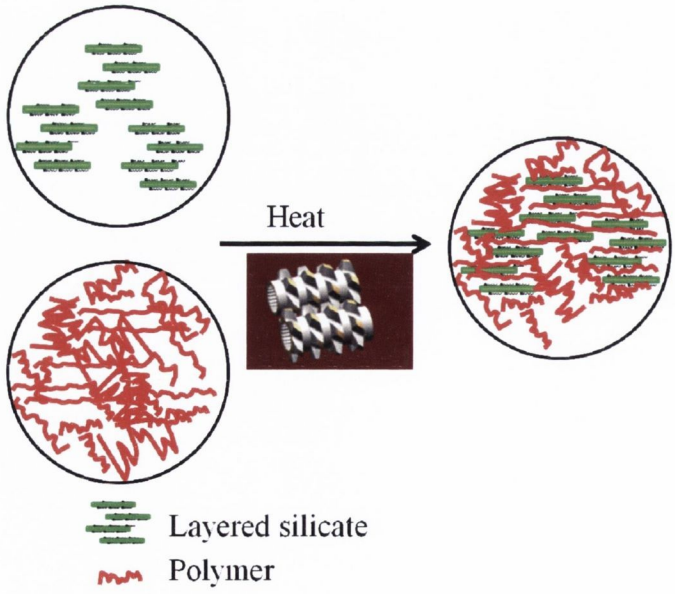

Figure 2.12. Schematic representation of polymer layered silicate obtained by direct polymer melt intercalation.

This process has been analysed and it has been observed that from a thermodynamic point of view intercalation is favourable for higher molecular weight molecules, while from a kinetic point of view, high molecular weight chains will take longer to intercalate.[110] A very important factor of the mixing process is enthalpy,[88] which can be classified into two components: non-polar interactions that are generally unfavourable and arise from interactions between the polymer chains and the surfactant aliphatic (non-polar) chains and polar interactions which originate from the Lewis acid/Lewis base character of the layered polar silicates interacting with polymeric chains. The thermodynamics of this process has been studied by Vaia and Giannelis[110] by using a lattice-based mean field theory, which showed that the outcome of polymer intercalation is determined by interplay of entropic and enthalpic factors. They showed that kinetically the process is influenced by the temperature used for melt intercalation and by the increase in the interaction between the polymer and the organo-layered silicate, which led to a reduction in the diffusivity level and an improvement in the monomeric friction coefficient that the polymer exhibits in the interlayer space. By confining the polymer chains inside the basal space of the silicate layers, a decrease of the overall entropy of the macromolecular chains is observed.[118] This entropic deficiency can be compensated by an increase in conformational freedom of the tethered alkyl surfactant chains as the inorganic layers separate.[119] Because it is less likely that a small increase in the gallery spacing of the layer silicates will lead to a strong influence of the total entropy charge, it has been concluded[88] that intercalation may be partially driven by the changes in total enthalpy.[70] It can also be stated that the equilibrium nature of polymer/organoclay nanocomposites is strongly related to the nature of the polymer (polar or non-polar), the charge density of the layered silicate, the chain length and structure of the surfactant molecules.[32]

2.5.2. Morphology

The dispersion of layer silicates into a polymer matrix results in the formation of three major types of morphologies: conventional composites and nanocomposites which can be intercalated and/or exfoliated (Figure 2.13).[12, 117] The conventional composites can be described as a phase-separated composite in which the polymer matrix and the inorganic filler are immiscible[78] and the clay tactoids are dispersed simply as a segregated phase resulting in poor mechanical properties.[120] The intercalated and exfoliated

morphologies correspond to the dispersion on a nanometre scale of the layered silicates within a continuous polymer matrix.[121] The type of composite that forms when a layered silicate is dispersed in polymer matrix depends on the nature of the components used,[9] which include the polymer matrix, layered silicate and surfactant; and it also depends on the behaviour of the polymers in the gallery and on the macroscopic behaviour of the clay particles in the mixture.[70, 122]

Intercalated nanocomposites are characterised by well-ordered multilayer structures[12] in which the *d-spacing* increases as polymer chains or monomer molecules diffuse into the clay galleries.[91] To facilitate the intercalation process, the clay particles are treated with organic modifiers that increase the space between the silicate layers to 2-3 nm [12] so that the polymer chain can ease into the gallery. In an intercalated state, the clay layers remain parallel to each other, and a new intensity peak in wide-angle X-ray diffraction (WAXD) patterns characterises the increased *d*-spacing.[91]

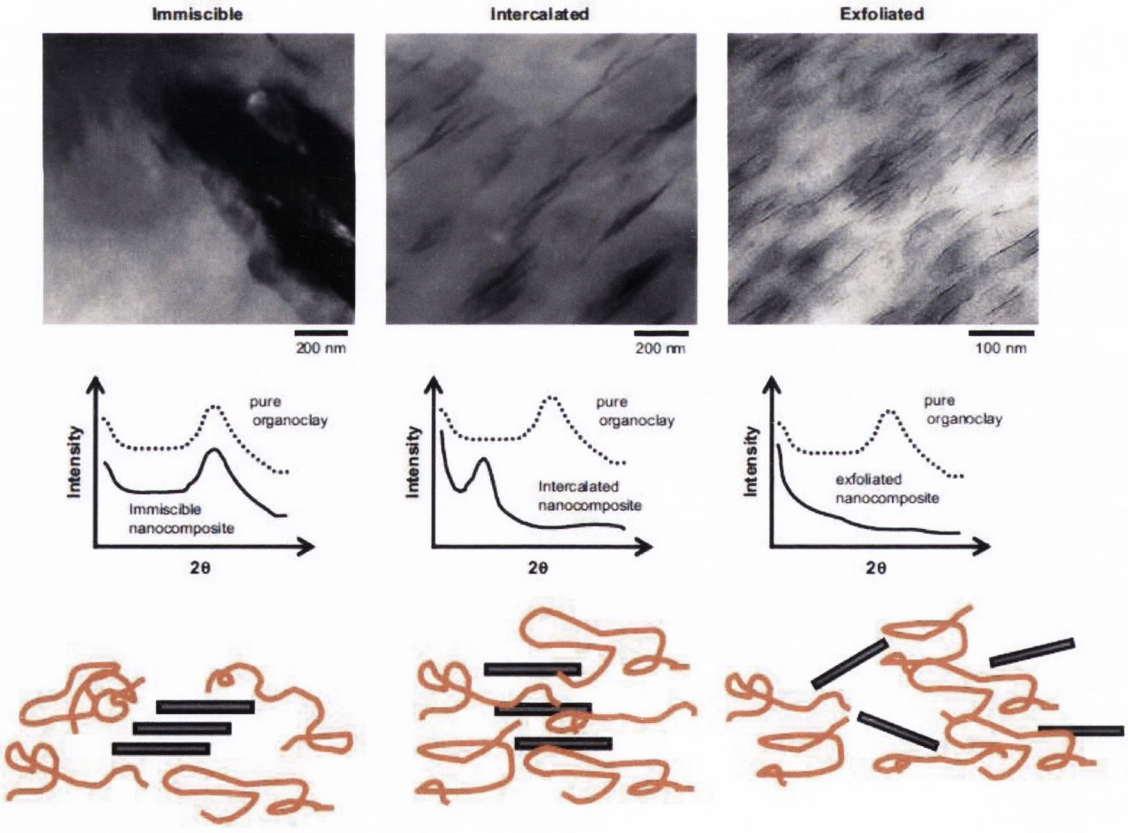

Figure 2.13. Illustration of different states of dispersion of organoclays in polymers with corresponding XRD and TEM results (Reproduced from reference[117]).

Exfoliated nanocomposites are also referred to as delaminated composites due to the complete separation of the crystal structure of clay in individual clay layers in the polymer matrix.[27] The delaminated nanocomposite structures result when the individual layers are no longer close enough to interact with the gallery cations of the adjacent layers, a case in which the interlayer spacing can be equal to the order of gyration of the polymer; therefore, the silicate layers may be considered well dispersed in the polymer.[12] Some of the authors[55, 123] consider that there are two types of exfoliation that appear in a nanocomposite: ordered and disordered. These considerations are based on the distance between the silicate layers, which can be assessed *via* X-ray diffraction (XRD) and transmission electron microscopy (TEM), as observed in Figure 2.13.[8, 77, 117] An exfoliated nanocomposite is considered to be ordered when one can still observe the silicate layers as being stacked one in top of the other, and is considered to be disordered when the entropy value is high and the silicate layers are no longer stacked, but individually dispersed in the polymeric matrix.[12, 91] In layered silicate nanocomposite systems, a fully exfoliated system is characterised by the absence of intensity peaks in WAXD pattern which is equivalent to the absence of the basal plane spacing, i.e., $d_{(001)}$.[8, 91, 124] This type of structure is thought to have the ability to tolerate higher stresses on all sides of the material.[125]

For a thermosetting polymer matrix, i.e., epoxy, it has been stated by Daniel et al.[76] that the degree of exfoliation depends on the rate of curing and on the sequence of gelation between the layers (intragallery) and outside the clay particles (extragallery). Thus, if the resin between the layers cures faster than the outside resin, and reaches full cure before gelation of the outside resin, the clay will be exfoliated. On the other hand, for thermoplastic polymers, Swain and Isayev[126] have stated that "an intercalated structure is obtained when the polymer matrix and the clay do not have sufficient attractive interactions, while an exfoliated structure is observed when they have strong attractive interactions." Thus, polar polymers are characterised by a high degree of exfoliation because the polar group allows the clay to easily disperse in the polar matrix whereas non-polar polymers, i.e., polyolefin, present a smaller degree of exfoliation in the polymer matrix.[95, 97] As a result in order for non-polar polymers to present a higher degree of exfoliation they have to be modified[107] with maleic anhydride, for example, in the case of PP and PE, so they would be more compatible with the organoclays. Therefore, the affinity between the polymer matrix and the clay represents a key factor in attaining intercalated and/or exfoliated polymer/clay nanocomposites.

2.5.3. Properties

Nanocomposites, like any other materials, can be characterised by mechanical, electrical and gas barrier properties, flame resistance and thermal stability, etc.[127] Due to the fact that composite materials are heterogeneous systems,[42] they are also characterised by the properties of the components, their composition and structure, interfacial interactions between the matrix and the filler[121] and processing methods.[32] However, there are a number of factors that influence the above mentioned properties, such as: the aspect ratio of the filler,[128] volume fraction of the reinforcement,[39] the effects of polymer immobilisation by adsorption on clay surfaces, the polymer/clay interaction,[129] changes in the crystallinity of the polymer[130] and mobility of the clay platelets,[8] etc.

The vast majority of conventional composites (immiscible systems) are characterised by weak interactions between the two phases, polymer matrix and filler, leading to no significant improvements in the mechanical and thermal properties.[75] It is believed that the size of the clay particles is similar to the size of the polymer molecules enabling an intimate mixing between the two species and that the conformation of the polymer chain changes due to the confinement between the silicate layers.[131] As a result, the addition of clay is characterised by a larger surface (interface) area per volume[63] than the polymer matrix. This leads to the formation of nanocomposite materials that may be endowed with new and unexpected properties.[8] That being said, polymer nanomaterials are characterised by improvements in more than one area. Nevertheless, the reasons for the enhanced properties are multiple and far from being fully understood.

2.5.3.1. Mechanical properties

The mechanical properties are dictated by the structure of the nanocomposites[8, 132] which is directly dependent on the dispersion and the degree of intercalation and/or exfoliation of the clay platelets in the polymer matrix, and indirectly dependent on the thermal diffusion of the polymer molecules in the galleries of clay and on the mechanical shearing action.[32] The quantity of filler is also a very important factor,[39] unlike in the case of composite materials when substantial amounts of modifier are required to improve the mechanical properties,[133] in the case nanocomposites small low filler concentrations are necessary in order to achieve similar or superior properties compared to the neat polymer or composite counterpart (Figure 2.14).[3, 132]

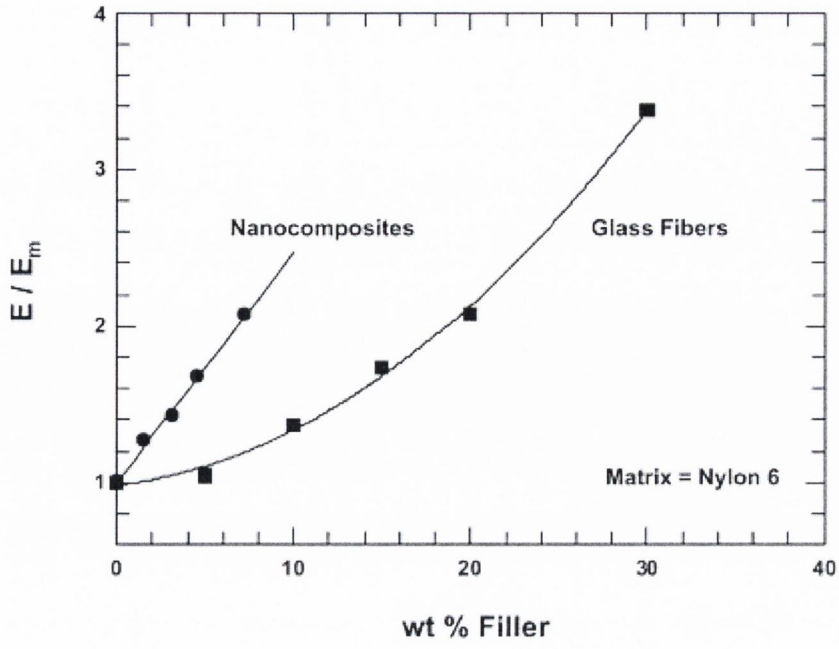

Figure 2.14. Comparison of the reinforcement of nylon 6 by organically modified montmorillonite (nanocomposites) and glass fibers. Nanocomposite filler concentration is based on the wt.% inorganic montmorillonite, since the aluminosilicate is the reinforcing component (Reproduced from reference[3]).

2.5.3.1.1. Fracture mechanics (theory)

Fracture mechanics allows for the study of crack propagation within solid materials. In pristine polymers the fracture mechanism can be influenced by molecular orientation and manufacturing methods, whilst in composite materials the nature of the reinforcing material presents another influential factor.[134, 135] In nanocomposites, the toughness is considered to be influenced by four main factors: (1) the temperature at which the mechanical tests are being performed as opposed to the glass transition temperature of the polymer matrix, (2) the degree of dispersion of the nanofiller particles inside the polymer matrix, (3) the mobility of the filler, which includes the delamination and the re-orientation of the filler, and (4) the potential changes in morphology and intrinsic properties of the polymer matrix which occur with the addition of clay.[8, 136-138] Still, it is hard to assess the type of nanostructure that would be most suitable in order to attain superior toughness in a polymer/clay nanocomposite compared to its neat polymer counterpart. There are a number of cases in which an intercalated polymer/clay nanocomposite is characterised by a higher toughness than an exfoliated polymer/clay nanocomposite.[135, 139] However, there are also

cases in which an exfoliated polymer/clay nanocomposite was found to present superior toughness compared to the intercalated nanocomposite.[136]

In an attempt to explain the changes that undergo in an intercalated polymer/clay nanocomposite, manufactured *via* injection moulding, Kim et al.[17] uniaxially deformed nylon 6/clay nanocomposites. They have established that the triumph of an intercalated nanostructure over an exfoliated nanostructure, in this case, was due to the orientation of the clay tactoids in the flow direction, thus in the testing direction. They have also demonstrated that there are three possibilities of tactoid orientation (Figure 2.15) which lead to different responses: (1) the perpendicular orientation of the layers that leads to splitting of the layers in the middle region (a); (2) the angled orientation that leads to an opening phenomenon in which open bundles of intercalated tactoids are formed (b); (3) the parallel orientation that leads to slipping a phenomenon (c).

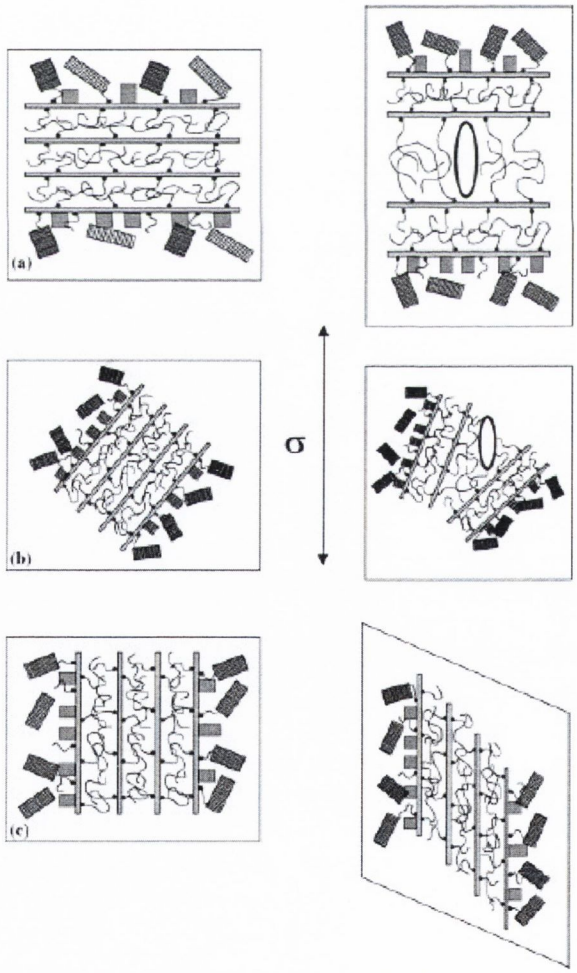

Figure 2.15. Schematic deformation processes in the intercalated nanomorphology system: (a) splitting, (b) open bundles and (c) slipping (Reproduced from reference[17]).

On the other hand, the changes that undergo in a fully exfoliated polymer/clay nanocomposite are far from understood. Cotterell et al.[140] have hypothesised that the well exfoliated clay platelets may delaminate from the polymer matrix (i.e., PP), under constrained yield stress, when the delamination or the splitting energy is lower than 1 $J \cdot m^{-2}$. However, Lim et al.[141] have suggested that the presence of single clay platelets may induce a constrain effect on the surrounding polymer chains (i.e., nylon 6) thus lowering the toughness of the polymer/clay nanocomposite compared to its pristine polymer counterpart.

Toughness, a key property of polymer systems,[142] has been defined as the energy absorbed during fracturing, which can be ductile or brittle, depending on the amount of deformation that precedes it.[143] The toughness of a material may be measured *via* low speed mechanical tests, e.g. tensile testing, or *via* high speed mechanical tests, i.e., impact tests. In a tension test the energy per volume to cause the failure is the area under the strain–stress curve, representing the toughness in a tensile test and being known as tensile energy at break or strain energy.[143] Charpy and Izod impact tests are high speed impact tests, in which the toughness is expressed as the absorbed energy during fracture per area. Although, these tests are commonly used, especially in industry; on the scientifically research level, they do not provide force-displacement signals, associated with data collection, and may be misleading when used for low toughness systems.[134, 135, 140]

In the case of composite and nanocomposite materials, the high speed of the test may prevent the filler from acting to its full potential, a low speed test being more indicative of the performance of the material.[135] The toughness of polymer and polymer/clay nanocomposites can be characterised using fracture mechanics principles. Depending on the ductility of the material, the toughness of a material can be quantified using the J-integral approach (for not too ductile fractures) or the essential work of fracture principles (for a very ductile fracture growth).[144]

The toughness of polymeric materials is often characterised by the J-integral concept established by Rice,[145, 146] which states that the difference between the external work and the change of the internal potential energy within the area surrounded by an integration line (Figure 2.16) can be expressed by a mathematical expression[147] (Equation 2.1) of a line or a path that encloses the crack front from one crack surface to the other and represents the energy release rate for a non–linear elastic solid.[148]

$$J = \int_{\Gamma} \omega dx_2 - \int_{\Gamma} T \frac{dn}{dx_1} dq \qquad (2.1)$$

where ω represents the energy density, T is the stress, n is displacement, q represents the arc length, x_1 and x_2 are the coordinates and dq is an element of arc length along the curve surrounding the tip of the notch, Γ.[145, 146]

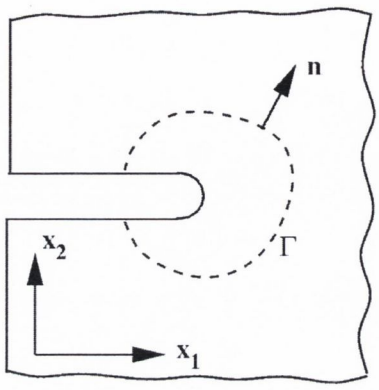

Figure 2.16. Model for crack growth under J controlled conditions (Reproduced from reference[143]).

Usually J–integral is used to characterise the local strain–stress field around the crack front by creating a J–R curve (plotting J versus the crack extension in the region of J–controlled growth).[149] Unlike other crack evaluation methods, the J-integral method is path independent, the crack having the same value regardless of its direction.[145, 146] In calculating the potential energy an initial crack is introduced, which is in accordance with the general theorem stated by Griffin[150] in 1921, as follows: "In an elastic solid body deformed by specified forces applied at its surface, the sum of the potential energy of the applied forces and the strain energy of the body is diminished or unaltered by the introduction of a crack whose surfaces are traction-free." Thus, the crack extension is the sum of the changes in strain energy, kinetic energy and inelastic energy and surface energy.[145]

The J-integral is calculated using Equation 2.2:[148]

$$J = \eta \frac{U}{B(W-a_0)} \tag{2.2}$$

where U represents the area under the load displacement curve, a_0 is the length of the precrack and W and B are the width and thickness of the sample. The calibration factor (η) represents a direct correlation between the toughness of the material and the geometry of the specimen used. η is equal to 2 for the single edge notched beam specimen (SENB), while for compact tension specimens (CT)

$$\eta = 2 + 0.522\frac{b_0}{W} \tag{2.3}$$

where b_0 represents the original un-cracked ligament, i.e., the distance from the original crack front to the back edge of the specimen. Since the value for the J-integral is calculated as a function of the area under the load-extension curve, for an elastic-plastic body, J is the sum of both elastic (J_{el}) and plastic (J_{pl}) contributions (Equation 2.4):[151]

$$J = J_{el} + J_{pl} \tag{2.4}$$

In order to assess the impact that the presence of clay has on the relative contributions, i.e., the plastic work converted to heat and the rate of internal heat generation, which can be measured by assuming that the only source of heating comes from plastic deformation,[152, 153] the J integral may be calculated according to Equation 2.5.[154] However, not all the plastic work is converted to heat.[152, 153] Previous studies have shown that in a metal approximately 0.9 of the plastic work is converted to heat whereas the remaining energy is converted to latent heat and directly influences the properties of the material.[155, 156] Similarly, during the deformation of polymers (i.e., bisphenol A polycarbonate) at low strain rates (i.e., 0.18-1.8 min^{-1}) 0.5 to 0.8 of the mechanical work converted to heat and dissipated, whereas the rest was stored as internal energy.[157]

$$J = J_{el} + J_{pl} = \frac{K^2(1-\nu_p^2)}{E} + \frac{\eta U^{pl}}{B(W-a_0)} \tag{2.5}$$

For small scale yielding and assuming that we are dealing with a sharp notch in an isotropic material and omitting the stress that occurs at the crack tip, the stress intensity factor (K_I) may be determine using linear-elastic fracture mechanics[146] according to ISO 7448-3:2005. Thus,

$$K_I = \frac{F}{BW^{1.5}}\left[\frac{3\left(\frac{a_0}{W}\right)^{0.5}\left(1.99-\left(\frac{a_0}{W}\right)\left(1-\frac{a_0}{W}\right)\left(2.15-3.93\frac{a_0}{W}+2.7\left(\frac{a_0}{W}\right)^2\right)\right)}{2\left(1+2\frac{a_0}{W}\right)\left(1-\frac{a_0}{W}\right)^{3/2}}\right] \tag{2.6}$$

for the SENB specimens and

$$K_I = \frac{F}{BW^{0.5}}\left[\frac{\left(2+\frac{a_0}{W}\right)\left(0.886+4.64\left(\frac{a_0}{W}\right)-13.32\left(\frac{a_0}{W}\right)^2+14.72\left(\frac{a_0}{W}\right)^3-5.6\left(\frac{a_0}{W}\right)^4\right)}{\left(1-\frac{a_0}{W}\right)^{3/2}}\right] \tag{2.7}$$

for the CT specimens. Here F is the applied force. The J-integral concept yields a J-Δa curve that represents the strain-stress field around the crack front.[149]

The toughness of polymer materials can be determined *via* the multiple specimen technique (i.e., loading several specimens to different displacements) or the single specimen technique (i.e., monitoring the crack growth during loading-unloading cycles performed on a single specimen).[147] Unlike the multiple specimen technique that requires for several identical specimens to be loaded to obtain different amounts of crack growth, the single specimen technique uses a single specimen, is time efficient and eliminates the questions about the time effects of polymer processing and the stable crack growth.[158] Also, while the multi-specimen test technique allows for the crack to be measured at the end of the test, the single specimen technique requires a crack monitoring system. The single-specimen test method may be performed either by using the elastic unloading compliance method or the electrical resistance method.[159] The former is characterised by the use of a gauge in order to monitor the displacement, enlists periodic unloadings during the test and calculates the Δa as a function of the slope of the unload line. The latter is characterised by the use of an electrical potential crack monitoring system and measures the potential drop in the uncracked ligament, thus the electrical sensitivity of the specimen is measured and correlated with the crack length during the test. A relatively new method involves the use of video equipment to measure the crack growth.[47, 159-161] Unlike the previously mentioned methods, the single specimen technique with a video monitoring system does not involve the unloading of the specimen or the *in situ* measurement of the crack growth.[159] In the case of polymers, loading-unloading methods are avoided due to the viscoelastic nature of the material.[154]

Improving the toughness of semicrystalline polymers has represented a challenge and over the years a number of approaches have been tested. To the day, the methods that were found to be most successful in improving the toughness of polymers are the addition of soft fillers, e.g. rubber,[162, 163] hard fillers, e.g. calcium carbonate,[140, 164, 165] carbon nanotubes[47] or clay platelets,[166] or a mixture of the two.[138, 167, 168] Studies on the fracture toughness of polymeric materials have shown that composites often present a decrease in toughness with the addition of inorganic filler.[140] Since in a polymer/clay nanocomposite the material that deforms is the polymer matrix, the changes in the toughness of the material may be a consequence of: the manufacturing process used to obtain the new materials (i.e., exposing the materials to high temperatures followed by cooling to room temperature)[169] or to the incompatibility between the polymer matrix and the inorganic filler (i.e., diminished bond strength due to the hydrophilic nature of the inorganic filler).[170] In order for a filler to improve the toughness of a polymer, it has to fulfil three main

requirements: 1) the critical interparticle distance, which is expected to lower the local plastic resistance thus increasing the macroscopic ductility;[162, 163, 165] 2) regular filler dispersion in order to avoid the occurrence of crack-initiating large agglomerates;[138, 165] and 3) the occurrence of matrix-plastic debonding in order to allow unhindered deformation around the particles.[165, 171, 172]

2.5.3.1.2. Elastic modulus – volume fraction relationships

In classical composite theory the structure-property relationship can be assessed by considering the volume fraction of the filler, since the volume fraction is directly correlated to the weight fraction (Equation 2.8). As opposed to conventional composites, nanocomposites are characterised by an increase in the volume of the clay reinforcement due to intercalation or exfoliation processes that is responsible for the substantial enhancement of the properties.[173]

The volume fraction of clay dispersed in a polymer matrix depends on the type of structure that the clay platelets present inside the polymer, i.e., conventional, intercalate or exfoliated or a combination of the two. To better assess the variation in the elastic modulus and the clay content, for conventional composites, the volume of clay needs to be taken into consideration.

$$\frac{1}{\phi_{conv}} = 1 + \frac{1-\mu_c}{\mu_c}\frac{\rho_c}{\rho_p} \tag{2.8}$$

where: μ_c is the mass fraction of clay; ρ represents the density for which the subscripts c and p stand for the clay platelets and polymer.

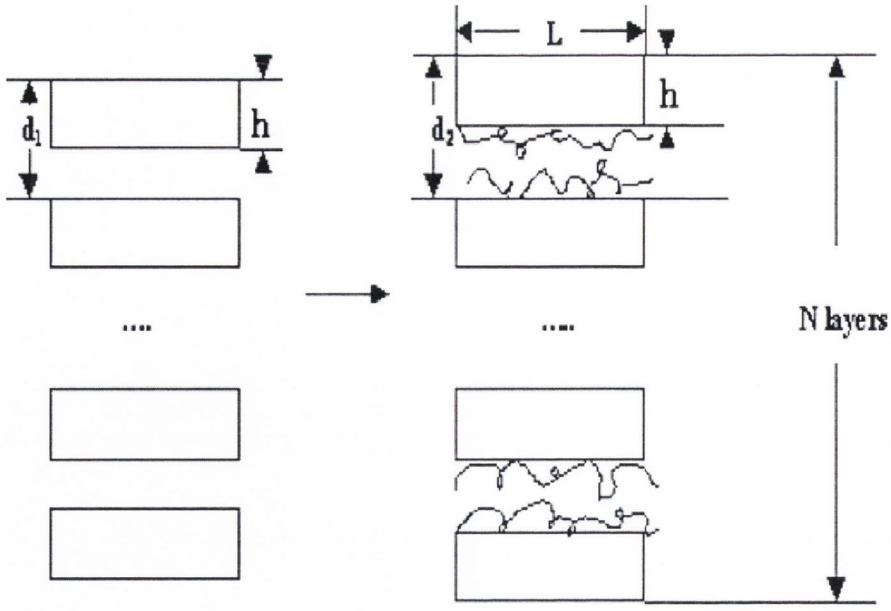

Figure 2.17. Schematic diagram of intercalation for the reinforcement (Reproduce from reference[122]).

In intercalated polymer/clay nanocomposites, the intercalated tactoids act as a reinforcing agents[16] which as can be observed in Figure 2.17 and are characterised by a sandwich type of structure with the polymer being confined between the silicate layers. For the intercalated nanostructures presented in the polymer/clay nanocomposite the elastic modulus of the reinforcement may be calculated by considering a sandwich-type composite in which the polymer chains exhibit a porous structure.[122, 174] Due to the small amount of surfactant (approximately 10% of the volume) existing inside the clay gallery of an organoclay and the close value of the density of the surfactant and polymer, the density and the modulus of the surfactant are considered to be equivalent to the density and modulus of the intercalated polymer.[122] In order to estimate the elastic modulus of the interlayer porous material the Gibson-Ashby model for open cells (Equation 2.9)[175] is used.

$$E_f = C_1 E_p (\frac{\rho_f}{\rho_p})^2 \tag{2.9}$$

where E represents the modulus for which the subscripts p and f refer to the fully dense solid and foam and ρ_f represents the density of the foam, calculated according to Equation 2.10. C_1 is a geometrical constant that approximates to the value of unity.[175]

$$\rho_f = \frac{(1-\mu_c^0+s)\mu_c}{(d_2-h)A} \tag{2.10}$$

where μ_c^0 is the mass fraction of clay platelets in the organoclay; s is the ratio of intercalated polymer to clay (i.e., 0.18);[122] d_2 is the basal spacing for the intercalated clay tactoids; h is the thickness of a clay platelet (i.e., 0.98 nm)[122] and A is the specific gallery area (i.e., 310 $m^2 \cdot g^{-1}$).[122]

The volume fraction of clay platelets (ϕ_c^0) in the intercalated clay tactoids is calculated with Equation 2.11 for untreated clay and with Equation 2.12 for organoclay.

$$\phi_c^0 = \frac{hN}{d_2(N-1)+h} \tag{2.11}$$

$$\phi_c^{0'} = \frac{d_1'(N-1)+h}{d_2(N-1)+h} \tag{2.12}$$

where N represents the average number of clay platelets per stack, d_1 is the basal spacing of the untreated clay and d_1' is the basal spacing of the organoclay.

Thus, the volume fraction of polymer in the tactoids is calculated according to the formula $\phi_p = 1 - \phi_c^0$. Using these parameters, the elastic modulus of the clay tactoids is determinate, according to the Christensen's model (Equation 2.13)[122, 174] for a sandwich structure in which platelet and polymer layers alternate.[174]

$$E_r = \phi_c^0 E_{cp} + \phi_p E_f + \frac{\phi_c^0 \phi_p E_{cp} E_f (\upsilon_c - \upsilon_p)^2}{[\phi_c^0 E_{cp}(1-\upsilon_p^2) + \phi_p E_f (1-\upsilon_c^2)]} \tag{2.13}$$

where E_{cp} is the elastic modulus of clay platelets (i.e., 230 GPa),[16] υ_c is the Poisson's ratio of the clay platelets (i.e., 0.28)[122] and υ_p is the Poisson's ratio of the polymer. Often, the third term of Equation 2.13 is very low compared to the previous two terms, thus its impact is limited. The volume fraction of reinforcement in intercalated polymer/clay nanocomposites is calculated according to the type of clay.[122] For natural clay the volume fraction of reinforcement is calculated according to Equation 2.14.

$$\frac{1}{\phi_c} = 1 + \frac{1-\mu_c(1+s)}{\rho_p d_2 \mu_c A} \tag{2.14}$$

For organoclay, the volume fraction of reinforcement is determined *via* Equation 2.15.

$$\frac{1}{\phi_c'} = 1 + \frac{\rho_c(1-\mu_c-\mu_c\mu_c^0 s)[d_1(N-1)+h]}{\mu_c \rho_p [d_2(N-1)+h]} \tag{2.15}$$

Unlike for intercalated nanostructures, in exfoliated polymer/clay nanocomposites the reinforcement is represented by single clay platelets on which polymer chains are adsorbed. The volume fraction of exfoliated clay platelets is calculated according to Equation 2.16.

$$\phi_e = \frac{\mu_c \mu_c{}^0 \rho}{\rho_c^0}\left(1 + kR_g A_T \rho_c^0\right) \tag{2.16}$$

where k is the fraction of absorbed polymer on the clay layer that behaves like clay (i.e., 0.2);[122] A_T is the total specific surface area of the clay platelets (i.e., 658 $m^2 \cdot g^{-1}$).[122] ρ_c^0 represents the density of the clay platelets (i.e., 3100 $kg \cdot m^{-3}$)[122] and R_g is the radius of gyration of the polymer.

The most commonly used theoretical models are the Mori-Tanaka model,[176, 177] the Halpin-Tsai model,[15, 178] the lower bounds of the Hashin–Shtrikman model[179] and the Christensen model.[122, 179-181]

The theoretical elastic modulus (E) determined from the Mori-Tanaka model,[176, 177] may be calculated according to Equation 2.17:

$$\frac{E}{E_p} = \frac{1}{1 + \frac{\phi_r\left[-2\upsilon_p A_3 + (1-\upsilon_p)A_4 + (1+\upsilon_p)A_5 A_0\right]}{2A_0}} \tag{2.17}$$

where E_p is the modulus of the pristine polymer matrix, υ_p is the Poisson's ratio of the polymer matrix, is $\phi_r$the volume fraction of reinforcement clay tactoids or clay platelets and A_0, A_3, A_4 and A_5 are Mori-Tanaka coefficients calculated according to Appendix I.[177]

When using the Haplin-Tsai model[15, 178] to predict the modulus of the composite, the following equations are used:

$$\frac{E}{E_p} = \frac{1 + \zeta\eta\phi_r}{1 - \eta\phi_r} \tag{2.18}$$

where ζ is the shape factor and

$$\eta = \frac{\frac{E_r}{E_p} - 1}{\frac{E_r}{E_p} + \zeta} \tag{2.19}$$

where E_r represents the elastic modulus of the reinforcement.

According to the Haplin-Tsai model the shape factor should be 2w/t, where w/t represents the aspect ratio of the filler; however, van Es has made a correction to the original model recommending that a shape factor of 2w/3t should be used, 2w/t being too high for most fillers.[131] This recommendation is based on the fact that at a shape factor of 2w/3t, the stiffness of an unidirectional platelet reinforced composite determined from the Halpin-Tsai model[15, 178] coincides with the theoretical modulus predicted *via* the Mori-Tanaka model.[176, 177]

Due to the small amount of reinforcement used, the structure-property relationships can be described by the lower bounds of the Hashin–Shtrikman model.[179] The equations used are:

$$K = K_{\mathrm{p}} + \frac{(K_{\mathrm{r}} - K_{\mathrm{p}})\phi_r}{1 + (K_{\mathrm{r}} - K_{\mathrm{p}})(1 - \phi_r)/(K_{\mathrm{p}} + \frac{4}{3}G_{\mathrm{p}})} \tag{2.20}$$

$$G = G_{\mathrm{p}} + \frac{(G_{\mathrm{r}} - G_{\mathrm{p}})\phi_r}{1 + (G_{\mathrm{r}} - G_{\mathrm{p}})(1 - \phi_r)/(G_{\mathrm{p}} + G_{\mathrm{p}}\frac{(9K_{\mathrm{p}} + 8G_{\mathrm{p}})}{6(K_{\mathrm{p}} + 2G_{\mathrm{p}})})} \tag{2.21}$$

where K and G represent the bulk and the shear moduli for which the subscripts *p* and *r* refer to the polymer matrix and the reinforcement. For polymer the bulk and shear moduli are determined according to the following equations:

$$K_p = \frac{E_p}{3(1 - 2\upsilon_{\mathrm{p}})} \tag{2.22}$$

$$G_p = \frac{E_p}{2(1 + \upsilon_{\mathrm{p}})} \tag{2.23}$$

Similarly, the bulk and shear moduli for the reinforcement may be calculated.

Young's modulus for the composite material was calculated using the following formula:

$$E = \frac{9KG}{(3K + G)} \tag{2.24}$$

2.5.3.1.3. Mechanical properties of nanocomposites (overview)

The mechanical properties of polymer nanocomposite have shown that the addition of a small amount of nanofiller can improve the mechanical properties of the polymer matrix.[8, 25, 44, 63, 136, 182] These improvements are due to the superior mechanical properties that the nanofillers display as opposed to their polymer counterpart.

The flexural and tensile strength were found to decrease by approximately 10% when 30% $CaCO_3$ are added to a HDPE matrix while the impact strength increased by 25%.[183] Polyethylene is a non-polar polymer[184] making it very difficult to obtain polymer/clay nanocomposites due to the difference in the polar character of the pristine clay and polymer matrix. When a Brazilian montmorillonite was used to reinforced high density polyethylene by Araujo et al.[75] Young's modulus, yield strength and elongation at break were found to slightly increase for organomodified clays, while the impact strength reduced with the addition of clays. The use of pristine nanosilica as a reinforcing agent for HDPE, by Barus et al.[121] led to improved stiffness, yield strength and fracture toughness. These enhancements were not obtained when modified silica was used. For 4 wt.% organoclay (i.e., Cloisite® 15A) added to HDPE[185] Young's modulus was found to increase from 1.2 GPa to 1.4 GPa, while the elongation at break and impact strength decreased by 75% and 15%, respectively. The addition of a 4 wt.% dimethyl dialkyl ammonium modified clay[186] resulted in a 21% increase elastic modulus, while the yield stress remained constant due to weak interactions between the clay and the polymer matrix, which were confirmed by the 55% decrease in elongation at break.

Yuan et al.[131] reported that the dispersion of 4 wt.% organoclay (i.e., Nanomer® I44.P) in a polypropylene matrix led to enhanced Young's moduli, yield strength and toughness by 54%, 15% and 25%, measured at room temperature. They also showed that although the yield strength was enhanced by the addition of 4 wt.% organoclay into a thermoplastic polyolefin matrix, the impact strength maintained at approximately 10 $kJ \cdot m^{-2}$ in the 20-40 °C temperature range.[131] Sharma et al.[71] reported that the mechanical properties of polypropylene were improved with the addition of 3 wt.% nanoclay (i.e., octadecylamide treated natural clay); the tensile modulus increased compared to pristine polymer by 36.5% when clay treated with p-aminobenzoic acid was added and only by 22.8% when untreated clay was used. For the same clay and quantity a 21.9% increase in the tensile strength was also observed. The addition of a compatibilising agent (i.e., PPgMA) further increased the tensile strength to 48.8%. With the addition of a

compatibilising agent the stress from the polymer matrix was transferred more effectively to the silicate layers, leading to even higher values of Young's modulus.[60]

The use of a compatibilising agent has to be kept to 5-10 wt.% for PPgMA in PP/PPgMA/I.30T materials, according to Garcia-Lopez et al.[187] An increase in the maleated content added to the materials resulted in decrease shear force during processing. A similar observation was made for PE nanocomposites by Yuan et al.,[188] whom suggested that the PEgMA quantity should be kept close to the quantity of filler used (i.e., $CaCO_3$). Recently, Kim et al.[189] showed that the addition of equal quantities of PPgMA and organoclay (i.e., dimethyl, dehydrogenated tallow-MMT) into a PP matrix gave rise to optimum mechanical and thermal properties. By having equal quantities of compatibilising agent and nanocalcium carbonate (5 wt.%), Yuan et al.,[188] observed that Young's modulus increased by 25% and the elongation at break decreased by 30%, while by doubling the compatibilising agent content the elastic modulus was marginally improved by and the elongation at break decreased by another 85%. The increase in compatibilising agent reduced the toughness of the material by decreasing the energy absorbed. In most of the cases the impact strength decreases with the addition of clay; however, when the clay was modified with dioctadecyl-dimethylammonium chloride by Zhao et al.[190] a 10% increase was observed when 0.05 wt.% organoclay added. When testing the impact strength in the temperature range of -40 °C and 70 °C for a 4 wt.% organoclay content,[129, 131, 186] it was discovered that for the same clay the toughness response varied with the polarity of the polymer used.

For a HDPE matrix[186] the toughness had values of approximately 10 $kJ \cdot m^{-2}$ even at -40 □C, while a polypropylene matrix led to improvements in toughness at positive temperatures and kept it constant at negative values,[131] as depicted in Figure 2.18. The improvements observed were attributed to the increase in the inter-gallery space, better dispersion and the strong interaction between the clay and polymer matrixes.[129] Morawiec et al.[99] discovered that the use of an organomodified clay to reinforce LDPE resulted in the decrease of the elongation at break, regardless of the use of a compatibilising agent; however, the elastic modulus was found to increase with the addition of organoclay and to decrease by over 6% when LDPE/PEgMA=87:13 (w/w) were mixed.

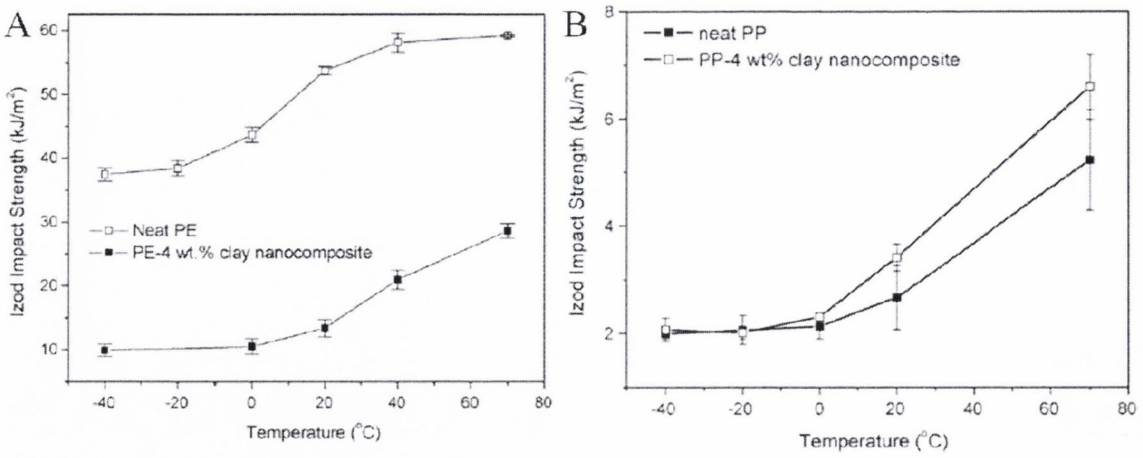

Figure 2.18. Izod impact strength for A. neat PE and 4 wt.% clay-reinforced PE nanocomposite and B. neat PP and 4 wt.% clay-reinforced PP nanocomposite as a function of temperature (Reproduced from reference[191]).

Dispersing 4.2 wt.% Cloisite® 30B, *via* melt compounding, in nylon 6, Fornes et al.[192] obtained a 60% increase in Young's modulus and a 29% improvement in yield strength; however, the elongation at break was found to decrease by up to 88%. By using 3.2 wt.% Cloisite® 30B, the modulus and yield strength of nylon 6 were found to improve by 52% and 25%, whilst for a 6.5 wt.% clay content the modulus and yield strength improved by 89% and 35%.[138] Regardless of the clay content, the elongation at break and impact strength decreased, compared to pristine nylon 6, by 68-91% and 22-29%.[138] Similar variations have been observed when 4.5 wt.% montmorillonite was treated with dimethyl bis(hydrogenated-tallow) ammonium (i.e., Cloisite® 20A);[192] the modulus and strength increasing by 57% and 26%, whilst the elongation at break diminished by 78% compared to pristine nylon 6.

Ray et al.[193] discovered that the flexural modulus increased by 26% when polylactide (PLLA) was reinforced with 4 wt.% organically modified synthetic fluorine mica. Compared to the flexural properties of PLLA/clay nanocomposites at 4 wt.% clay load, the flexural modulus and the flexural strength the nadir and the zenith at a clay load of 7 wt.%.[194] Chen and Evans[180] observed that a content of 4.2 wt.% organoclay (Bentone®105) platelets increased the tensile strength, Young's modulus and elongation at break of PCL by 88%, 23% and 216%, respectively, the addition of clay resulting in polymeric materials with superior mechanical properties. Ludueña et al.[195] found that the stiffness of a cast poly(ε-caprolactone) (PCL) film, with intercalated and exfoliated structures, was enhanced by 47% compared to the pristine polymer film. By subsequently

incorporating a chemical blowing agent into PCL with 5 wt.% organoclay (i.e., Nanolin® DK2), the porous solid presented a 60% increase in compressive modulus compared to the pristine porous polymer. The dispersion of 1 wt.% clay (i.e., MMT) in a PU foam reduced the cell diameter by 20%, whilst enhancing the compressive modulus by 20%.[196]

The mechanical properties of thermosetting materials reinforced with clay have been found to improve with the addition of montmorillonite. The dispersion of 5 wt.% clay in the case of epoxy-clay nanocomposites[197] led to a 25% increase in the storage modulus, whilst the addition of 21.5 wt.% organoclay into polyurethane enhanced the storage modulus by 350%.[137] When 5 wt.% tallow modified clay (Cloisite® 30B) was added to polyurethane the compressive strength and the compressive modulus were increased by 650% and 780%, respectively.[198] The reinforcing of polyurethane foam with 1 wt.% MMT led to improvements in tensile, flexural and compressive responses.[90] The tensile modulus was increased by 69.3%, while the compressive and flexural moduli were enhanced by 20.4% and 29.7%, respectively. Saha et al.[90] also observed that tensile, flexural and compressive strength increased by 20%, 31.3% and, respectively, 37.8%, while the yield strength increased from 2.7 MPa for the pristine polyurethane foam to 3.9 MPa for the natural clay reinforced foam.

2.5.3.1.4. Toughness (contradictory theories)

So far, it has not been established if complete exfoliation or complete intercalation may improve the toughness of a polymer/clay nanocomposite. There are a number of cases in which an intercalated nanocomposite is characterised by a higher toughness than an exfoliated nanocomposite.[135, 139] However, there are also cases in which an exfoliated polymer/clay nanocomposite was found to present superior toughness compared to the intercalated nanocomposite.[136]

Depending on the polymer matrix and type of clay, complete exfoliation has been found to give contradictory results. Zilg et al.[199] reported a low toughness/stiffness balance in fully exfoliated hectorite in an epoxy matrix compared to intercalated mica or bentonite in the same polymer matrix. Yu et al.[200] observed an insignificant decrease in the toughness of well exfoliated nylon 66/MMT with the augmentation of the clay load. However, Dasari et al.[201] reported that well exfoliated clay platelets in nylon 66 led to a 62% reduction in impact strength of the nanocomposite material compared to its pristine polymer counterpart. Analysing the difference between the intercalated and exfoliated

polymer/clay nanocomposites with a nylon 6 matrix, Dasari et al.[139] observed that the intercalated nanocomposites (with 10 wt.% organoclay, Cloisite® 15A) presented an impact strength 30% higher than the exfoliated nanocomposites (with 10 wt.% organoclay, Cloisite® 93A). Chen and Evans[135] found that in an intercalated PS/clay nanocomposite with 4 wt.% clay platelets (i.e., Bentone® 111), the impact strength marginally decreased compared to the pristine polystyrene, whilst the tensile strain energy was found to increase by up to 120%. They have also noted that the dispersion of the same amount of organoclay in ABS resulted in highly exfoliated polymer/clay nanocomposites characterised by a 90% decrease in the impact strength and a 61% reduction on the tensile energy at break.

Since in most of the cases the nanocomposite material presents intercalated and exfoliated nanostructures, it is expected for the toughness of polymer/clay nanocomposites to be influenced by the degree of intercalation. Due to the contradictory results obtained using intercalated and exfoliated nanostructures it has been suggested that a partial exfoliated nanocomposite may be better than a fully exfoliated nanocomposite.[141, 202] This suggestion has been made based on data from polymer/elastomer/clay nanocomposites (i.e., nylon 6/maleic anhydride grafted polyethylene-octane elastomer/organoclay and nylon 6/maleic anhydride grafted styrene–ethylene–butylene–styrene /organoclay).[141, 202]

2.5.3.2. Barrier properties

Barrier properties appear as a response to the movement of the silicate layers,[203] which gives rise to new applications that can be divided into two categories: engineering (barrier properties) and biodegradability.[8] Sinha Ray et al.[193, 204] discovered that the dispersion of different amounts of organoclay in PLLA led to polymer/clay nanocomposites with better biodegradability than the pristine polymer. The quality of nanocomposites, from the barrier properties point of view, relies on the degree of exfoliation. Exfoliated nanocomposites present a "tortuous pathway"[194] created by the delamination of the clay layers and that has the ability to retard the transport of diffusing species like different gases[2] and water vapours.[66] By using a small quantity of nanoclay[205] the permeability of a film may be reduced by 50-500 times.[73] The incorporation of impermeable nanoparticles into a polymer forces the permeating molecules to move around them in a random walk,[7] making the material impermeable for liquids and gases (Figure 2.19).[206]

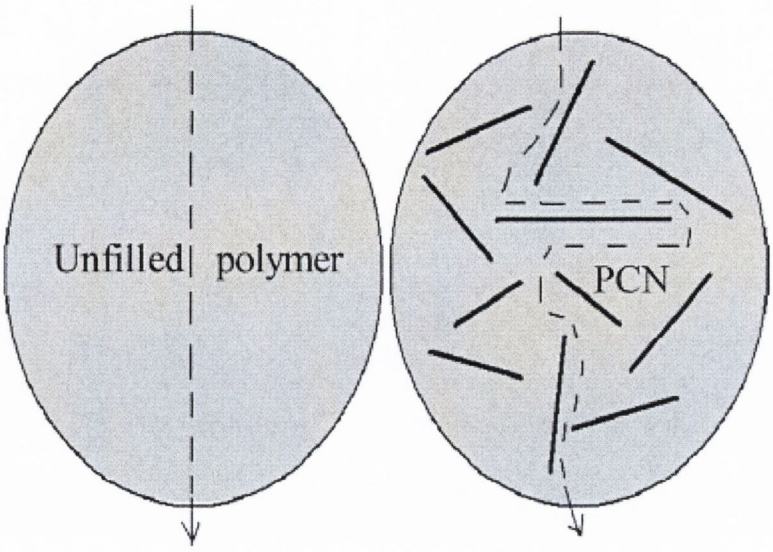

Figure 2.19. Proposed model for the "torturous path" in an exfoliated polymer/clay nanocomposite (Reproduced from reference[9]).

The factors that determine the gas permeability of a material are: the degree of crystallinity, the compactness of the structure, the polarity of the polymer matrix, the interface created between the polymer matrix and the filler and the clay content.[98, 206-208] The degree of crystallinity was found to increase when nylon 6 was reinforced with montmorillonite, which resulted in decrease in crystalline permeation, enhancing the barrier properties.[209] The polarity of the polymer and the interface that forms between the polymer and the clay play a key role in the barrier properties. If the polymer is polar, like poly(ε-caprolactone),[207] by reinforcing it with montmorillonite a compact structure forms on the surface of the silicate layers narrowing the permeation pathways. A poor interface between the clay and polymer matrix can lead to a decrease in the barrier properties. Another factor that has to be taken into account when creating polymer/clay nanocomposites is the clay loading. For a clay loading of 5 wt.% organoclay (i.e., Cloisite® 20A), the oxygen permeability of ethylene vinyl acetate (EVA) is reduced by 50% while for a higher clay loading the barrier properties levelled off.[98]

By adding unmodified clay (i.e., sodium montmorillonite) to an epoxy matrix Osman et al.[124] discovered that the oxygen permeability improved by 20%; however, when modified clay was used it led to the formation of a poor interface between the clay layers and the polymer matrix that resulted into a higher transmission rate.

Although polyolefin present high gas permeability, making them ideal to be used for bottles and containers, their limited oxygen barrier[73] render them inappropriate to be used for packaging products that require a long shelf life. The simple addition of clay into non-polar polymers may not generate significant improvements due to the small interactions that occur between the two species. Even when the clay is modified and some compatibilisers are used, the barrier properties of polyolefins present a series of challenges, such as the inability of an isotropic polymer phase to wet and bond with an anisotropic organoclay surface.[66] However, some increases in the saturation uptake level have been observed and attributed to the clustering and transport phenomena.[7] Analysing different types of polyethylene, Zhong et al.[98] discovered that HDPE has the highest gas permeability and that with the addition of maleic anhydride grafted polyethylene the permeability of the gas increased. This enhancement was attributed to changes in the polarity of the polyethylene. By improving the polarity the interactions between polyethylene and non polar oxygen were weaken. For LDPE the gas permeability was increased by 24% when 7 wt.% MMT content was added to the pristine polymer.[95] However, if the use of a compatibilising agent was employed the oxygen barriers were found to decrease by 25% for LDPE with 5 wt.% low density PEgMA, while for HDPE with an equal content of PEgMA the oxygen permeability was three times higher than the one of pristine HDPE.[98] The barrier properties of HDPE can be improved by creating a blend that will take into consideration the permeability toward water vapour that HDPE has and the oxygen permeability that nylon 66 has, creating a new material with excellent barrier properties.[210] In the case of polypropylene the dispersion of 4 wt.% montmorillonite generated a 50% reduction in permeability to liquids and gases.[60] When 2 wt.% montmorillonite treated with polyethylene glycol was added to a polypropylene matrix the oxygen permeability was reduced compared to the neat polymer.[205]

2.5.3.3. Thermal Stability

Thermal degradation of polymers represents a limitation to their applicability resulting in significant changes in the initially specified properties. The parameters that control the thermal stability of polymer/clay nanocomposites are the intrinsic thermal resistance of the polymer matrix, the nature and content of the compatibilising agent used (if appropriate), the nanofiller content, the chemical properties of the surfactant and the interaction between the polymer matrix-surfactant-clay layers, polymer confinement between the silicate layers, etc.[127, 211, 212] There are two stages of degradation for pristine

montmorillonite (dehydration, between 100 and 400 °C, and dehydroxylation, between 500 and 1000 °C) and four stages for organomodified montmorillonite (decomposition of absorbed water and gases, below 180 °C; decomposition of organic substances, from 200 to 500 °C; dehydroxylation of aluminosilicates, from 500 to 700 °C; and oxidation of carbonaceous residue, between 700 and 1000 °C).[213] The general outcomes of exposing a polymer to high temperatures are: changes in molecular weight (and molecular weight distribution) which result in property changes (i.e., reduced ductility, colour changes, cracking and reduction in all other desirable physical properties).[90] The changes in molecular weight imply a polymer degradation phenomenon which can occur *via* chain scission.[214] Chain scission can lead to the formation of primary or secondary radicals that facilitate the depolymerisation process.[215, 216]

As discussed before, the clay layers are characterised by a good barrier action which improves the thermal stability of the polymer/clay nanocomposites; however, if the clay used is organomodified with alkylammonium than this can decompose at 240 °C [184, 217] and the products can act as catalysers[218, 219] to the polymer matrix. The thermal stability of a nanocomposite reinforced with an organomodified clay was characterised by taking into consideration the impact of the organoclay as having two opposing functions: the barrier effect (which improves the thermal stability) and catalysis effect towards the degradation of the polymer (which would decrease the thermal stability).[190] The former implies the existence of a chemical bond between the clay and the polymer,[220] and although it has been implied that this effect only manifests on the surface of the material, recent studies show that this effect is important throughout the polymer matrix.[221] The latter implies the degradation of the surfactant and the degradation of the polymer chains which result in products that facilitate further degradation of the polymer matrix.[222]

In the case of unmodified clay the improvement in thermal degradation can be lower than 10 °C, while with the addition of the same amount of modified clay (3 wt.%), the degradation temperature may increase by 35-50 °C.[71] In some cases the dispersion of 5 wt.% untreated clay (i.e., Cloisite® Na) marginally increased the peak degradation temperature of nylon 6, whilst by melt compounding the nylon 6 with 5 wt.% quaternary ammonium cation exchanged clay (i.e., SCPX® 2004) the peak degradation temperature decreased by close to 10 °C, due to the presence of the organomodifier.[223] Tang et al.,[211] discovered that polymer/clay nanocomposites presented, in most of the cases, higher peak degradation temperatures, compared to the microcomposites; this was attributed to the ablative reassembling ability of the clay platelets to create a protective surface.

2.5.3.4. Flame retardancy

Flame retardation is a technique that normally involves the addition of certain chemicals into the polymeric structure that will result in a decrease of the flammability of the polymer. Flame retardants commonly used include: melamine, phosphorous compounds, graphite and intumescent and non-intumescent solutions.[224, 225] The most used flame retardants are intumescent solutions that have the ability to swell the material in which they are incorporated when exposed to heat, increasing its volume while decreasing its density and creating a light char on the surface of the material, char which is a poor conductor of heat and which will protect the material.[225, 226] An intumescent flame retardant is an environmental, halogen free additive, made of three basic components: an acid source (e.g. ammonium polyphosphate), a carbonization compound (e.g. polyol) and a blowing agent (melamine phosphate).[226] Although these products are environmentally safe, they present a series of disadvantages, such as decrease in the physical and mechanical properties[12] of the material in which they were inserted.

Nanofilled polymer composites are characterised by increased heat resistance and decreased flammability.[7, 51] The low flammability can be described as an ablative behaviour,[121] upon being exposed to heat the polymer degrades and forms a protective surface layer, characterised by the presence of the filler, which has isolating properties, creating a mass transport barrier.[227] The thermostability of polymer/clay nanocomposites increased with the addition of a small quantity of clay. Although the addition of clay led to increases in flame retardancy, for nanocomposites to comply with the current standards of fire reduction they have to be combined with conventional flame retardants.[228]

The addition of PEgMA to a HDPE/organoclay (i.e., Cloisite® 20A) system creates an interface and reduces the burning rate by 10-15% compared to the neat polymer, at clay loadings lower than 1 wt.%, this indicated an increase in flame retardancy.[114] An even higher increase was observed in the case polypropylene with PPgMA and 4 wt.% organomodified clay, the flame retardancy was improved by up to 75% compared to the pristine polymer matrix.[60] The improvements observed in the flame retardancy were attributed to the formation of a physical barrier, visible in the char that forms when polymer/clay nanocomposites are burned and that acts as a barrier to mass and heat transfer.[227]

2.6. Polymer blend/clay nanocomposites

The interest in polymer blends is constantly increasing because they confer the manufacturer the ability to tailor the final properties of the material by combining two or more polymers that have different properties resulting in multiphase systems with enhanced performances.[229] However, the simple mixing of two polymers will most likely not result in a useful material, because most of the polymer blends are classified as immiscible.

The process of compatibilising two polymers can be achieved by the addition of a third component or by an *in situ* chemical reaction between the two components.[230] In some of the cases the compatibilising agent can be maleated polypropylene or block copolymers. The thermodynamics of adding a third component into a polymer blend can be summarised by considering the Gibbs free energy of the third component (S) and the two polymers (A and B):[231, 232]

$$\Delta G_m = \Delta G_{AS} + \Delta G_{BS} - \Delta G_{AB} \qquad (2.25)$$

In Equation 2.25 the interacting pairs are identified in the subscripts of the free energy. The system is considered thermodynamically stable when ΔG_m<0, thus for a miscible system ($|\Delta G_{AS} + \Delta G_{BS}| > |\Delta G_{AB}|$), whilst for an immiscible system $\Delta G_{AB} > 0$ and $\Delta G_{AS}, \Delta G_{BS} < 0$. $\Delta G_{AS}, \Delta G_{BS}$ represent free energies of interaction of the components with the surface, ΔG_{AB} is the free energy of mixing and ΔG_m represents the free energy of the entire system.[232]

The addition of a third component is the easiest method that can be applied to obtain a compatibilised polymeric blend. The role of the compatibiliser is to: optimize the interfacial tension of the two components, to stabilise the morphology of the blend and to improve the performance of the material by increasing the adhesion between the phases in solid state.[233] Polymer blends are characterised by a high degree of immiscibility and when the clay is added; it has the tendency to migrate towards the component that has the highest polarity.

The insertion of organoclay in polymer blends significantly changes the structure, typically decreasing the size of the dispersed phase.[234] The reduction in particle size with the addition of clay has been attributed by Sinha Ray et al.[231] to the increase in the viscosity of the blend and to the possibility of dispersing the clay in the interfacial region, transforming the clay into a compatibiliser. They have concluded that there are three

possible mechanisms of organoclay compatibilisation: the addition of an organic modifier that is miscible in both components, *via* solid-melt adsorption which leads to free energy gains and change in the interfacial tension of the two phases and the shift of the interphase.

Hua et al.[235] observed that montmorillonite modified with octadecyl ammonium acted as a compatibilising agent in blends of nylon 6 with 10 wt.% PP, improving the tensile modulus and strength. Replacing the PP with HDPE, in a HDPE/nylon 6 (75/25) blend, the tensile properties were found to decrease compared to the ones presented by the neat polymers due to poor stress transfer across the interface and the non-homogeneity of the sample on a microscopic level; however, the addition of 4.8 wt.% Cloisite® 15A located the clay in the more polar nylon 6 phase improving the modulus and the tensile strength by over 50% compared to the neat polymer blend.[229]

Polystyrene and polypropylene are two of the most used polymers, and by mixing them together an immiscible polymeric blend is formed, which is characterised by a semicrystalline phase (PP) and an amorphous one (PS).[236] For a PS/PP (20/80) blend, the particle size decreases from 8 μm to 1 μm with the addition of 5 wt.% organoclay (Cloisite® 20A),[231] whilst the TEM revealed that the clay tactoids were located at the interface of the two components increasing the Young's modulus by 14% and the elongation at break from 1.5 mm to 4.4 mm. By substituting the PP with PPgMA, Ray et al.[231] observed that in the PS/PPgMA (20:80) blend with 5 wt.% organoclay (i.e., Cloisite® 20A), the clay had exfoliated in the PPgMA matrix and due to the high amount of compatibilising present in the system, the exfoliated clay layers surrounded the PS domains; this material presented a significant increase in Young's modulus and a substantial decrease in the elongation at break, compared to the neat polymer blend. This suggested that in this case, the clay does not act as a compatibilising agent. In a separate study, the addition of 4 wt.% organoclay (octadecyl trimetyl ammonium modified MMT)[237] to PS/PP blend (20:80), resulted in PS chains intercalated inside the clay galleries. The addition of a compatibilising agent, i.e., PPgMA, located the clay only in the modified PP phase in which it was homogeneously dispersed.

Whether the clay acts as a compatibiliser is still uncertain. The addition of organoclay to a polystyrene/poly(ethyl methacrylate) reduced the domain size resulting in a good dispersion; however, this outcome may be a result of the high surfactant content used to modify the clay or of the increased viscosity of the polymer blend/clay nanocomposites.[238] The polymer system used to disperse the clay, the presence of an additional compatibiliser and last but not least the location of the clay and the degree of

exfoliation are all factors that may influence the role of the clay in an immiscible polymer blend.

2.7. Polymer/clay nanocomposite foams

Foams can be described as the dispersion of a gas in a liquid which once solidified consist of individual cells (pores) and walls that form a skeletal structure.[239] These materials present an array of applications varying from weight-bearing structures to isolations and tissue engineering scaffolds for cell attachment and growth.[19] Foams can be classified according to density, pore size, nature of cells and rigidity of the material formed upon solidification. Since the mechanical and thermal properties of foams depend mainly on the relative density (the density of the foam divided by the density of the solid, ρ_f/ρ_s), which also dictates the porosity of foams,[240] foams can be divided into low-density foams ($\rho_f/\rho_s<0.1$)[241] and structural foams ($0.4<\rho_f/\rho_s<0.8$)[242] or porous solids ($0.3<\rho_f/\rho_s$).[243] According to the cell size, polymer foams can be classified into the following categories: macrocellular (>100 μm), microcellular (1-100 μm), ultramicrocellular (0.1-1 μm) and nanocellular (0.1-100 nm).[19] Looking at the nature of the cells formed, the foams can be divided into open and closed cell foams, whilst according to the rigidity of the skeletal structure, the foams can be considered to be rigid or flexible.

A number of conventional polymers, such as low density polyethylene,[244, 245] polypropylene,[246] polystyrene (PS),[247] poly(vinyl chloride)[248] and poly(ethylene terephthalate),[249] and biodegradable polymers such as PCL[250, 251] and PLLA,[252] have been foamed using different chemical[253-255] or physical[244, 245, 247, 250] blowing agents for various applications.[246, 256] Since the addition of clay has proven to improve the thermal and mechanical properties of non-cellular polymers, a wide range of polymer/clay nanocomposite foams have been developed and investigated, including for example: PP/clay,[246] PE-clay,[257] PMMA/clay,[46] PS/clay,[258] PC/clay,[259] PU/clay,[196, 256, 260-263] PLLA/clay[264] and PCL/clay[265] nanocomposite foams. It was found that the presence of clay in a foam or a porous solid often reduced the cell size and increased the cell density due to the ability of clay to act as a nucleation agent.[260, 266, 267] In some cases the presence of clay produced lighter materials with superior mechanical properties.[196, 251, 260, 262]

The characterisation of linear elastic properties[268] of foams as a function of relative density can be depicted by the general empirical formula (Equation 2.26):[269]

$$\frac{foam\ property}{solid\ property} = C(\frac{\rho_f}{\rho_p})^n \quad (2.26)$$

where C is property of the polymer matrix which includes all the geometric constants of proportionality,[240] n represents the deformation mode of the struts that make up the foam,[269] e.g. tensile or compressive,[268] and is characterised by values between 1 and 4 [270] and ρ is the density, for which the subscripts s and f refer to the solid and the foam structures, respectively. C and n present a complex dependence on the microstructure of the foam including the cell type (e.g. open or closed), geometrical arrangement of cells,[269] cell size[271] and angle of intersection. Substituting the property and n in Equation 2.26 with Young's modulus and 2 lead to:

$$\frac{E_f}{E_s} = C_1(\frac{\rho_f}{\rho_p})^2 \quad (2.27)$$

where E_f and E_s are the Young's moduli of the foam and the fully dense solid that makes up the strut respectively, and C_1 is a function of strut porosity.[240]

For closed-cell foams the variation in the relative modulus with the relative density is described by the sum of three contributions (Equation 2.28): cell-edge bending, compression of the cell fluid and membrane stretching,[240]

$$\frac{E_f}{E_s} = C_1\phi_s^2(\frac{\rho_f}{\rho_p})^2 + C_2(1-\phi_s)\frac{\rho_f}{\rho_p} + \frac{p_0(1-\upsilon)}{E_s(1-\frac{\rho_f}{\rho_p})} \quad (2.28)$$

where p_0 is the atmospheric pressure, υ is Poisson's ratio, ϕ_s is the volume fraction of solid contained in the cell edges and C_1 and C_2 are geometric constants for the cell edges and the cell faces, respectively.

2.8. Recycled polymeric materials

Advanced technology in petrochemical-based polymers has brought many benefits to mankind. However, it becomes more evident that the ecosystem is considerably disturbed and damaged as a result of the non-degradable plastic materials being used especially for disposable items. The environmental impact of persistent plastic waste is causing global concerns, and alternative disposal methods are limited. Incineration of the plastic waste always produces a large amount of carbon dioxide and toxic gases contributing to global warming and pollution. Furthermore, satisfactory landfill sites are limited, and the

petroleum resources are finite and becoming scarce. For these reasons there is an urgent need to develop renewable source-based, environmentally friendly plastic materials, especially in short-term packaging and disposable applications, that would not involve the use of toxic components in their manufacture and could allow for the materials to be composted into naturally occurring degradation products.[194]

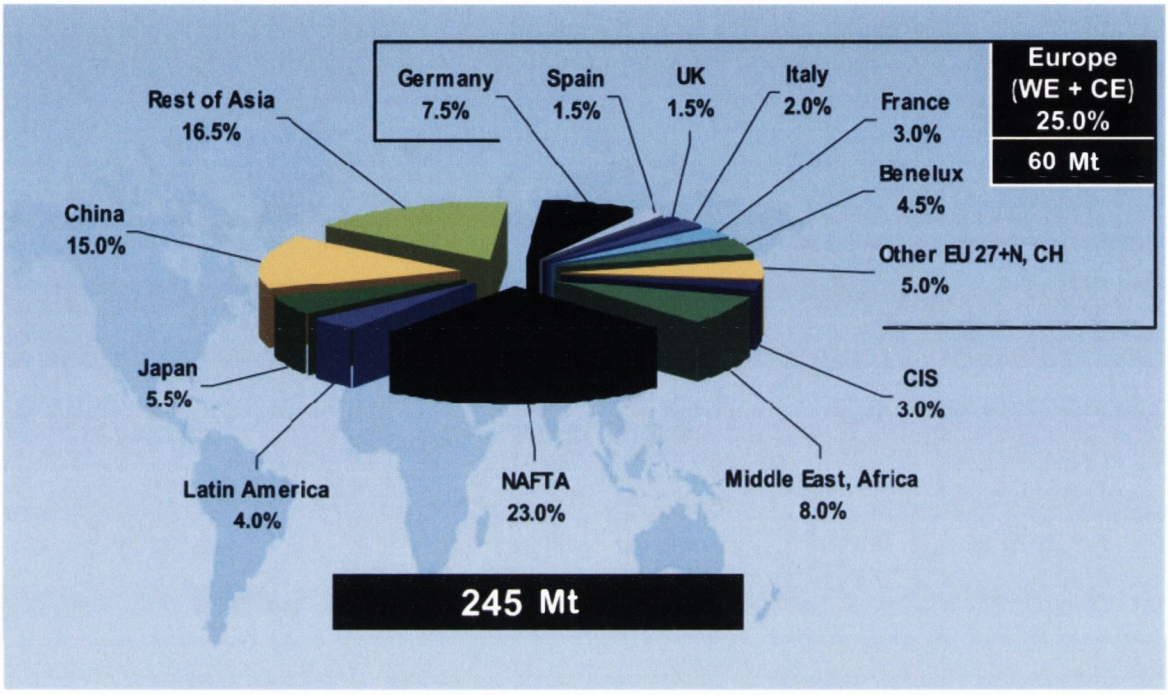

Figure 2.20. World plastic production 2008 by country and region (Reproduced from reference[272]).

In 2008 the world plastic production was of 245 Mt, from which Europe accounted for 25% with 60 Mt produced (Figure 2.20).[272] Over 170 million tonnes of plastics which are made from valuable resources and are not fully recyclable,[273] are used globally each year. However, because of the import/export of products, today's issues are caused not only how much plastic is produced, but how much plastic is demanded. In 2008 the demand of plastics in Europe was of 48.5 Mt,[272] with 38 Mt being represented by thermoplastics alone.[272] Most of the thermoplastic demand (Figure 2.21) is represented by high-volume plastics (i.e., PE, PP, PVC, PS and PET) which account for 75% of Europe's plastic demand with the packaging industry using 38%,[272] a demand that increases daily. The exponential increase in the plastic production, the demand and the limited resources and disposal sites have prompted the search for new low cost, eco-friendly recycling methods with higher barrier properties.[206]

Recycling represents the optimal solution for reusing the plastic materials. In Europe 21.3% of the plastics are recycled.[272] This includes mechanical recycling characterised by the use of physical means to produce plastic pellets from waste and feedstock recycling characterised by the use of chemical means to crack and depolymerise plastic waste.[274]

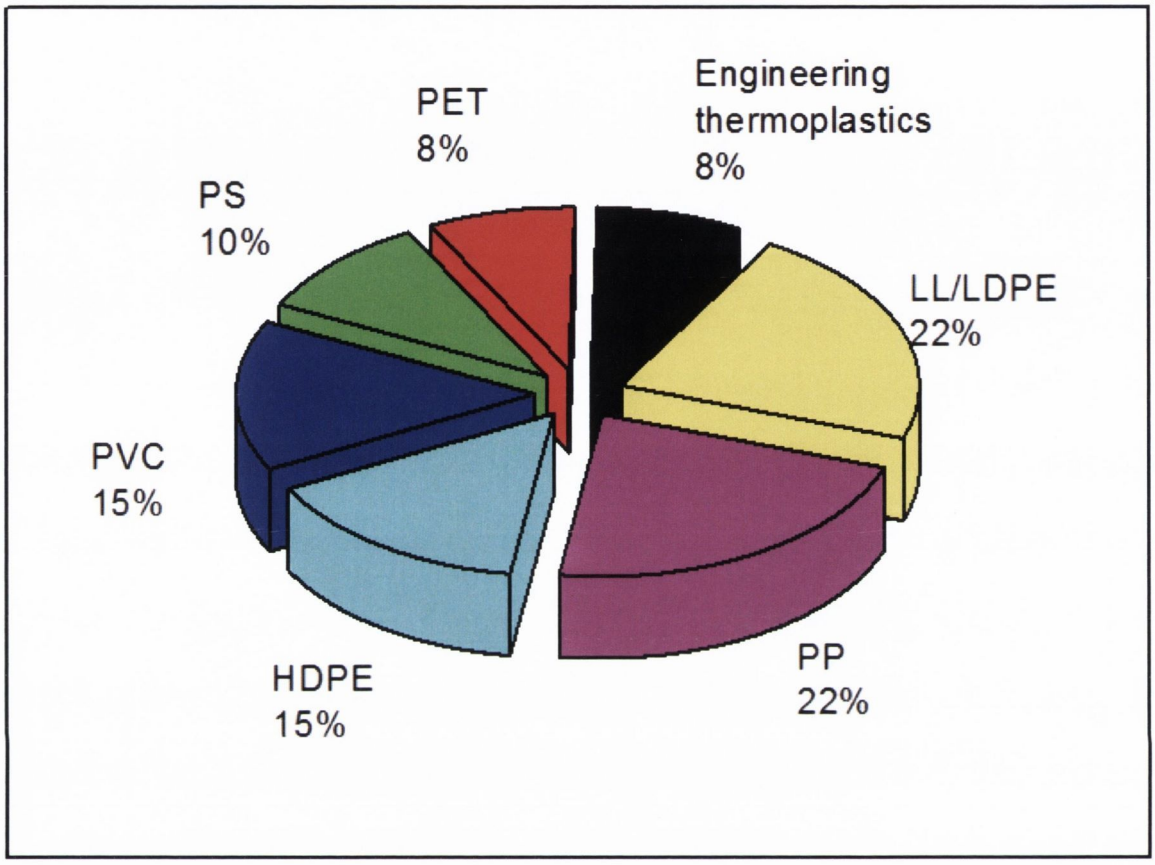

Figure 2.21. The thermoplastic demand in Europe (2008) categorised by thermoplastic polymer type (Modified from reference[275]).

The plastic recycled stock is represented by commodity polymers (PE, PP, PVC, PS) and engineering plastics (PC, PET, polyamides). Some of the plastic wastes are collected together making the separation process a tedious work. Thus, management, dismantling, identification and separation of the mixed plastics are mandatory steps.[274] Other problems include the presence of contaminants and hazardous substances and the thermo- and/or photo-oxidative degradation that the polymers may suffer.[276]

Mechanical recycling has been identified by Karlsson and Vilaplana[274] as the most suitable method to recover the polymeric material from the recycled plastic stock. This process involves the following steps: separation, washing, grinding, remelting and processing polymer waste. The resulting plastic is characterised by inferior mechanical

properties due to the changes that the polymer suffers during previous processing steps, such as molecular damage caused by chain scission, crosslinking or formation of double bonds, natural aging, heat and/or light deteriorations.[276]

The recycled material may be used along pristine polymers in order to reduce costs[277] or by employing the use of additives in order to restore some of the original properties of the polymeric material. Some of the additives considered are stabilisers and clays. Stabilisers have been used to improve the mechanical and thermal stability of the recycled stock.[276] The addition of clay[278] or talc[279] was also found to enhance the mechanical and thermal properties of the recycled materials. The use of clay increases the ability to recycle these materials. The recycling character for nylon 6/clay nanocomposites, for example, is similar to the one of pristine nylon 6. This allowed the reuse of the materials for at least 6 times without the occurrence of any deterioration in the properties.[2]

The limited resources and the constant demand of plastic materials make the reuse of recycled plastics a fundamental issue. By adding different stabilisers during the mechanical recycling process the structure and the properties of the polymers may be damaged. The simple addition of clay prevents this aspect and also allows for the clay to create an interface between different grades of plastics that are mixed and mechanically recycled at once. This simple method eliminates the need to break the recycled stock into very specific types and grades of polymers; it eliminates the necessity of using only clean plastics and expands the versatility of the recycled materials.

2.9. Summary

The papers reviewed depict different methods to obtain property enhancements in polymer/clay nanocomposites with intercalated and/or exfoliated nanostructures. They point out that the structure and thermal and mechanical properties of the polymer/clay nanocomposites are closely related to the degree of exfoliation, degree of dispersion, degree of crystallinity and the compatibility between the polymer matrix and the natural or organomodified clay. Although, so far the effect of clay on the crystallinity degree of a semicrystalline polymer had been investigated, the effect of clay on the crystallinity degree once the polymer has been uniaxially deformed have not been fully taken into account.

Compared to pristine solid polymers, the mechanical properties of foamed and porous polymers are typically found to decrease. Over the years the addition of clay into polymers has led to nanocomposite materials with superior mechanical and thermal

properties. Thus, clay has been inserted into foamed polymers in an attempted to improve their properties. However, so far, the porosity of cellular solids has not been successfully controlled, nor has the structure-property relationship in foamed polymer/clay nanocomposites been investigated.

One of the greatest challenges in properly describing the mechanical properties of polymer and polymer/clay nanocomposites is fracture toughness. Typically, the toughness of a material is investigated *via* impact testing, and rarely as the energy absorbed by a material before failure. To the day, the investigations in the toughness of polymer/clay nanocomposites at low testing speeds are limited and the orientation of the polymer chains and, where applicable, the orientation of the reinforcing agent has not been properly investigated. The contradictory theories regarding the toughness of intercalated or exfoliated polymer/clay nanocomposites have prompted the question if an intercalated/exfoliated nanocomposite would be superior to the two limiting cases. However, so far, this has been has not been studied.

The impact of clay addition to immiscible polymer blends has been previously considered; however, the location of clay represents one of the major questions of polymer blend/clay nanocomposites. Although intensive research has been performed on immiscible polymer blends, the structure-property relationship has not yet been considered. This aspect represents a key factor in facilitating the reuse of recycled polymers, which due to the presence of different polymer grades in the recycled stock may act as an immiscible polymer blend.

The worldwide increasing polymer demand, the limited resources and disposable landfills make the use of recycled polymers a necessity. Typically the recycled materials present decreased mechanical properties; thus, the insertion of a filler is of critical interest.

Chapter 3. Relative modulus-relative density relationships in low density polymer-clay nanocomposite foams

3.1. Introduction

Since they were first reported in 1987,[2] polymer/clay nanocomposites have presented an unusual interest due to their unique properties.[8] These new materials are the result of dispersing inorganic clay fillers with dimensions in the nanometre range into a polymer matrix.[280] Polymer/clay nanocomposites often exhibit superior or distinct properties from the ones possessed by the pristine polymers or the conventional composites, which can be mainly attributed to the large interfacial surface area between the organic and inorganic phases and the intrinsic properties of clay platelets and tactoids.[8, 136, 281] For best property enhancements, the content of clay fillers is typically kept under 10 wt.% [282] due to its high aspect ratio and small size,[283] in comparison with up to 50 wt.% for a conventional reinforcing agent such as carbon black or calcium carbonate, in a thermosetting polymer matrix.[2]

Foams present an array of applications varying from weight-bearing structures to isolations and tissue engineering scaffolds for cell attachment and growth.[19] The mechanical and thermal properties of foams depend mainly on the relative density (the density of the foam divided by the density of the solid), which also dictates the porosity of foams.[240] A number of polymers, such as polyurethane, polystyrene, polycarbonate and polyethylene, have been foamed using different chemical compositions and different processing conditions[239] in order to obtain foams for sound, vibration and heat insulation, impact resistance and light weight applications.[246, 256]

The linear elastic properties[268] of foams can be described as a function of relative density by the general empirical formula (Equation 2.26). One of the most important properties of foams is Young's modulus for which an array of models considering different cell geometries,[284] cell regularities,[285] relative densities and material deformation mechanisms have been developed and selected models based on Equation 2.26 are presented in Table 3.1.[240, 270, 286-296]

Table 3.1.Summary of selected models from the literature for open and closed cells

Cell type	Geometrical constant (C)	Density exponent (n)	Reference
Open	1	2	Gibson and Ashby[240]
Open	0.376	1.29	Roberts and Garboczi[270]
Open	0.535	1.81	Roberts and Garboczi[270]
Open	4.2	3.15	Roberts and Garboczi[270]
Open	0.3	2	Hagiwara and Green[270, 295]
Open	90	2	McCullough et al.[290]
Open	68	1	McCullough et al.[290]
Open	1.05	2.54	Liu et al.[291]
Open	0.167	1	Thomas and Gent[287, 293]
Open	0.88	2	Choi and Lakes[294]
Open	0.7	2	Dement'ev and Tarakonov[294, 296]
Closed	0.33	1	Renz and Ehrenstein[286, 288]
Closed	0.0598	1.066	Mills and Zhu[289]
Closed	0.0807	1.155	Mills and Zhu[289]
Closed	0.977	1.627	Mills and Zhu[289]
Closed	0.64	1.4	Roberts and Garboczi[292]
Closed	0.76	1.7	Roberts and Garboczi[292]

The deformation suffered by the pristine foam is strongly dependent on the cell type; in most of the cases, the values for density exponent lie between 1 and 2 for closed cells,[286, 288, 289, 292] while for open cells the values lie between 1 and 4.[240, 270, 287, 290, 291, 293-296] The different values of n reflect the change in the dominant deformation mechanism.[297] According to Gibson and Ashby,[240] the variation of the relative Young's modulus with the relative density for open cells is best described by a deformation value of 2 (Equation 2.9), value which accounts for the bending and the stretching of the cells[285] and relates the relative density of the cells with the thickness and the length of the cells.[240] For closed-cell

cellular solids the variation in the relative modulus with the relative density is the result of three contributions: cell-edge bending, compression of the cell fluid and membrane stretching,[240] represented in Equation 2.28.

The addition of clay improves the specific compressive modulus (the ratio of modulus to density) of a polymer foam and in some cases the compressive modulus without considering the density.[260, 262] This enhancements are due to the nucleating effect of the clay that reduces the density of the polymer foam, decreases the cell size and increases the cell density.[260, 266] Saha et al.[196] discovered that the cell diameter of a PU foam decreased by 20% with the addition of 1 wt.% clay, whilst the compressive modulus increased by 20%. Thirumal et al.[262] reported a 30% decrease in the density of a PU foam with the addition of 4.3 wt.% organoclay. Liu et al.[265] showed that at low clay loads, clay may provide nucleation sites for PCL foams that led to smaller cells and thinner cell walls; however, a clay content of over 10 wt.% caused an increase in the cell thickness and cell size.[267]

Despite the significant development in polymer/clay nanocomposite foams, the structure-property correlations of this new class of foams are yet to be well understood and their relative modulus-relative density relationships were not adequately addressed in the literature. The main goal of this work was to determine the relationship between relative modulus and relative density for low-density polymer/clay nanocomposite foams by using the established theories for conventional cellular materials as reviewed above. PU was selected for this study because of its wide applications,[19, 260, 261] easy processing[260, 298] and high polarity which allows it to form nanocomposites with natural clays[299, 300] and to provide idealised polymer-clay systems without involvement of an organic surfactant. A typical commercial formula for the preparation of rigid PU foams, described as the mixing of a polyol with a diisocyanate, was adopted. PU-natural clay nanocomposite foams containing different clay amounts were prepared by varying the mixing sequence of the polyol, diisocyanate and natural clay. The structures of the foams were investigated by using X-Ray Diffraction (XRD), Scanning Electron Microscopy (SEM), X-Ray Micro-Computed Tomography (Micro-CT) and the modulus was obtained from compression testing.

3.2. Experimental

3.2.1. Materials

A liquid-polyol blend with a density of 1090 $kg \cdot m^{-3}$ and a viscosity of 735 mPa·s (Bayer VP.PU 29HB74, denoted as polyol) and a liquid mixture of diphenylmethane-4,4'-diisocianate with an N=C=O content of 30.5-32.5 wt.%, a density of 1230 $kg \cdot m^{-3}$ and a viscosity of 160-240 mPa·s (Desmodur 44V20L, denoted as MDI) were kindly supplied by Bayer Materials Science (Germany). Natural sodium montmorillonite clay (325 mesh) was generously supplied by Bentonite Performance Materials LLC (Wyoming Plant, South Dakota, USA). The inorganic content of the clay was determined as 88.6% by Loss on Ignition by heating the clay from room temperature to 600 °C at a rate of 10 $°C \cdot min^{-1}$ with a dwell of 600 s at 600 °C in a Eurotherm 2416CG furnace (Lenton Thermal Designs LTD). The chemical composition of the clay was analyzed to be SiO_2, 64.12 wt.%; Al_2O_3, 18.92 wt.%; Fe_2O_3, 3.78 wt.%; MgO, 2.29 wt.%; Na_2O, 1.88 wt.%; CaO, 1.19 wt.%; K_2O, 0.44 wt.%; and TiO_2, 0.13 wt.% by using an Panalytical Axios X-Ray Fluorescence Spectrometer according to ISO 12677 method at CERAM (Stoke-on-Trent, United Kingdom). All the materials were used as received.

3.2.2. Preparation of polyurethane-clay nanocomposite foams

PU-clay foams were prepared by *in situ* polymerisation with reference to the method supplied by the manufacturer for preparing the pristine PU foam. The pristine PU foam was prepared by mixing 30 g of polyol with an equal amount of MDI in a rectangular container (20 cm x 11 cm x 3 cm) for 10 s at room temperature. PU-clay nanocomposite foams containing different clay contents were prepared using three mixing sequences. In the first sequence 30 g of polyol, 30 g of MDI and a pre-weighed amount of clay were mixed simultaneously for 10 s in the rectangular container, denoted as polyol/MDI/clay. In the second sequence 30 g of polyol were mixed with the clay for approximately 120 s and then 30 g of MDI were added and mixed for 10 s, denoted as polyol/clay + MDI. In the third sequence 30 g of MDI were mixed with the clay for approximately 120 s and then 30 g of polyol were added and mixed for a further 10 s, denoted as MDI/clay + polyol. Following mixing, each of the foams was kept in the container at room temperature for approximately 600 s to grow and stabilize before it was removed for preparation of test specimens. In all the three methods, two amounts of clay platelets, i.e., 4 wt.% and 8 wt.%,

were used. The material compositions and mixing methods of the samples are summarised in Table 3.2.

Table 3.2. Material compositions and mixing sequences of PU and PU-clay nanocomposite foams

Sample ID	Mixing sequence	Content of clay platelets / wt.%
PU	polyol/MDI	-
M14	polyol/MDI/clay	4
M18		8
M24	polyol/clay + MDI	4
M28		8
M34	MDI/clay + polyol	4
M38		8

3.2.3. Structural characterisation and mechanical testing

XRD was carried out on a Phillips PW1720 X-Ray Diffractometre with a $CuK\alpha_1$ (λ=0.15406 nm) anode tube at the standard conditions of 40 kV and 20 mA. The samples were tested from 2° to 10°, 2θ angle, at a step size of 0.02° and duration of 2.5 seconds per step. Powder samples grounded from the foams were used.

SEM was performed on a Tescan Mira Variable Pressure Field Emission Scanning Electron Microscope and a Zeiss Ultra Scanning Electron Microscope. The images were taken at a voltage of 5.0 kV (Tescan) and 6.0 kV (Zeiss) and analysed with the ImageJ software to characterise the cell diameter. The cell size was measured for an array of cells, considering only the cells that appear to be fully and well defined inside the SEM image. The average value for 20 cells with a confidence level of 95% was reported. Prior to being analysed the samples were mounted on stubs and their surface was gold (Tescan) or platinum (Zeiss) coated.

Micro-CT was run on a Scanco Micro-CT 40 (Scanco Medical AG, Switzerland) at the standard resolution (acquisition: 250 projections per 180° with 1024 samples each, an

energy of 55 kVp and a current of 145 μA). The micrographs were realised using a predefined threshold that was found to give the most accurate interpretation of the image throughout the whole scan in order to assess the structure and porosity of the foams. The threshold was adjusted after the values for sigma and support parameters were set. These parameters were used to identify the struts and the pores present in the structure, whereas the threshold was modified in order to observe the fine details of the porous structure. The value of the threshold used was set as to attain the most detailed scan of each of the slices throughout the entire structure, regardless of the material analysed. The densities of the foams were determined by measuring the weights and volumes of five prismatic specimens for each type of foam, using a balance and a calliper.

Compressive tests were carried out on an Instron 1011 universal testing machine with a load cell of 500 N and at a rate of 10 $mm \cdot min^{-1}$. Testing was arbitrarily terminated at the deformation of 50% according to ASTM C365-05. Four surface grounded prismatic specimens (25.4 mm x 25.4 mm x 12.7 mm) were tested for each type of foam. The mean and standard deviation values reported represent a confidence level of 95%. Statistical significance was assessed by a Two-tailed, Type II 't' test with a criterion that the probability of a difference in means due to chance should be less than 0.05.

3.3. Results and discussion

3.3.1. Structure

Figure 3.1 shows the X-ray diffraction patterns of natural clay and polyurethane-clay nanocomposite foams obtained from different mixing sequences and at different clay loadings. Natural montmorillonite displayed a peak at $2\theta \approx 7.1°$ corresponding to a $d_{(001)}$ of 1.24 nm. By mixing the clay, polyol and MDI simultaneously (mixing sequence 1), $d_{(001)}$ increased to 1.85 nm regardless of the clay content which is similar to the values obtained for the natural clay intercalated with poly(ethylene glycol)s and glycerol.[130, 301, 302] The increase in $d_{(001)}$, as also found by Cao et al.[260] and Harikrishnan et al.,[261] suggested the presence of an intercalated structure in the nanocomposite. Natural montmorillonite is a hydrophilic clay that presents approximately 6 wt.% water molecules between the layers.[303] Intercalation of the polyol into clay galleries was mainly driven by the entropic change associated with the loss of these water molecules from the galleries.[304] Similar *d*-spacings and peak shapes were obtained for mixing sequence 2 (i.e., polyol/clay + MDI), suggesting that the nanostructures formed were similar for these two mixing sequences.

Change of the clay content from 4 wt.% to 8 wt.% increased the peak intensity indicating the presence of more intercalated clay tactoids in the latter.

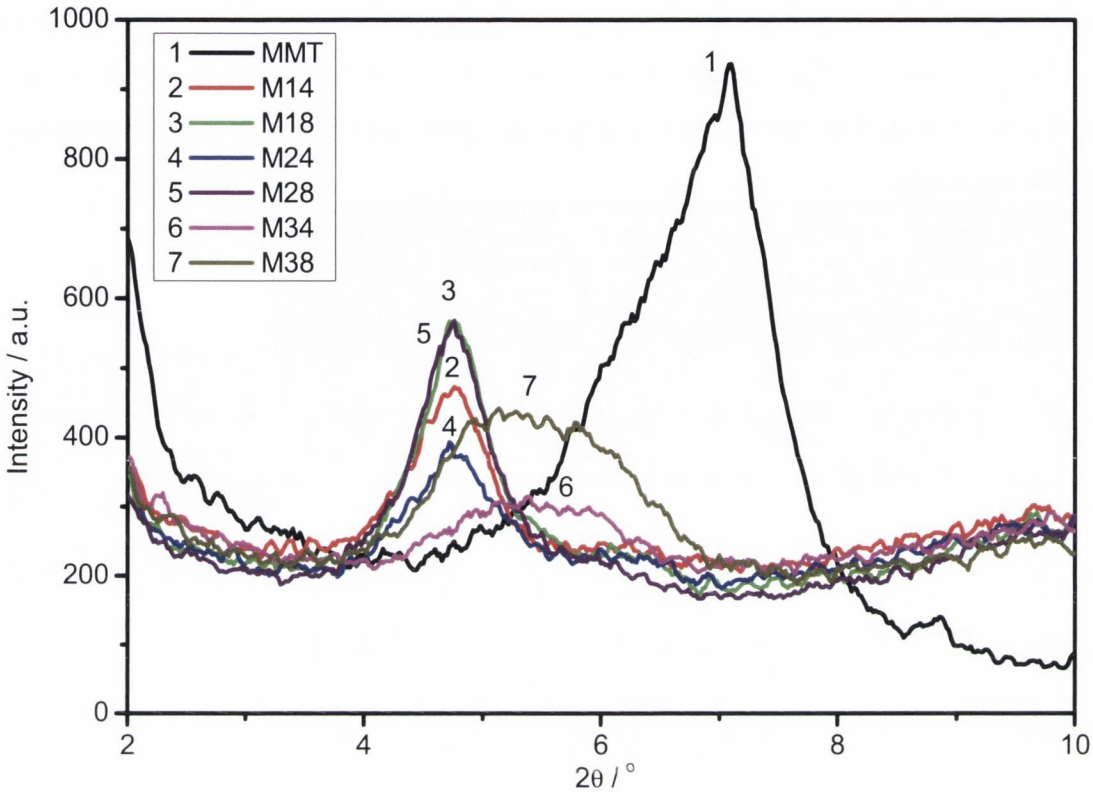

Figure 3.1. XRD profiles of natural clay and polyurethane-clay nanocomposite foams. MMT, i.e., pristine natural clay, represents the control sample. By dispersing natural clay in polyurethane, the polymer intercalates between two consecutive silicate layers, thus shifting the 2θ angle towards lower values.

Compared to the first two mixing sequences, the *(001)* peak of the clay shifted to a higher 2θ value and became broader for mixing sequence 3, implying that the $d_{(001)}$ was reduced and that the clay layers become less ordered in the nanocomposite.[305, 306] It is known that the reaction between an isocyanate and water produces an amine and carbon dioxide (Figure 3.2). By reacting the water present inside the clay galleries[307] with the MDI an amine was formed, minimizing the degree of intercalation of the polyol in the later stage,[8, 308] but at the same time CO_2 was also produced, presumably causing some clay layers to lose their ordered structures and perhaps to expand their layer spacing slightly further. Regardless of the clay content, a value of 1.61 nm was obtained. This value was close to the ones reported for the amine-intercalated natural clay, being 1.4 – 1.5 nm,[308, 309]

confirming the formation and presence of the amine in clay galleries. Such amine may adopt a monolayer conformation in the galleries[309] in contrast to the bilayer conformation adopted by the polyol,[8] leading to a smaller *d-spacing* in M34 and M38 (Curves 6 and 7) compared to that from the first two mixing sequences (Curves 2-5). The fact that the first two mixing sequences led to similar nanostructures in the nanocomposites which were however different from the one produced from the third mixing sequence, implied that the natural clay preferred to intercalate the polyol as opposed to the MDI under a competitive absorption process.

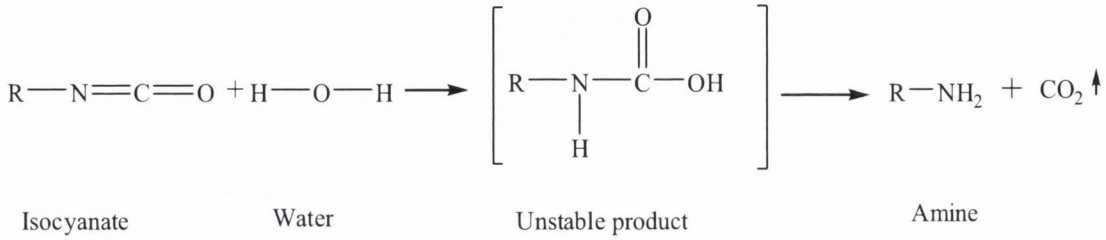

Figure 3.2. Reaction between an isocyanate and water.

From the representative SEM images given in Figure 3.3 it can be observed that the PU foam presented a structure of mostly closed cells with a cell diameter of approximately 760 μm. Additions of clay substantially reduced the cell size and increased the number of cells observed in the same image size, which is in accordance with the previous findings[196, 260, 262, 310] on the ability of clay platelets to act as nucleating agents during the foaming process. The results from quantitative analysis of 20 cells with a confidence level of 95% using the ImageJ software showed that in the presence of clay the cell diameter of the PU foam decreased by 41-67% for 4 wt.% clay content (Table 3.3, Column 1). The cell diameter was found to increase with the augmentation of the clay content for the first two mixing sequences; however, it remained 32-49% lower compared to the value for the pristine PU foam. These comparisons were statistically significant as determined by a Two-tailed Type II 't' test with $p<0.05$.

Changes of the cell diameter of the polymer foam arise from two competing effects of the clay: the nucleation effect[196, 260] which decreased the cell diameter and the blowing effect[311] which increased the cell diameter. The former depended on the interfacial surface area between the polymer and the clay and hence the degree of clay dispersion in the polymer. The latter was due to the presence of water in clay galleries. Both were related to the clay content. Reductions of the cell diameter by the clay (Figure 3.3 and Table 3.3)

suggested that the nucleation effect was dominant in all cases. An increase in the clay content led to a growing amount of water available in the clay galleries which either directly acted as the blowing agent for foaming in the first two mixing sequences or reacted with the intercalating MDI to produce CO_2 in the third mixing sequence. The increase in the cell diameter with clay content augmentation implied that the blowing effect had a greater impact compared to the nucleation effect in these cases.

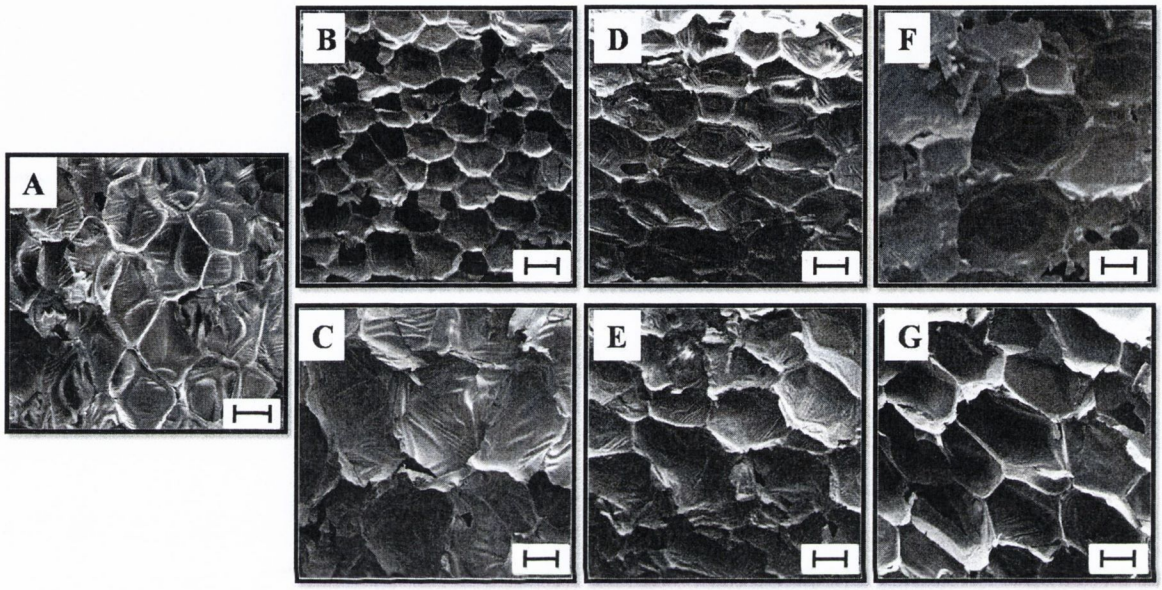

Figure 3.3. Representative SEM images of (A) PU foam (Scale bar: 500 μm) and (B-G) PU-clay nanocomposite foams (Scale bar: 200 μm): B. M14; C. M18; D. M24; E. M28; F. M34; and G. M38.

The effects of clay addition, clay content and mixing sequence on the cell size are confirmed by Micro-CT images, presented in Figure 3.4. Reconstruction of tridimensional images showed that the foams have uniform cell size throughout the sample (e.g. Figures 3.4A2 and 3.4E2). Since clay decreased the cell diameter, the uniform reduced cell size indicated that clay was well dispersed in PU, agreeing with the XRD results which suggested intercalation of PU into clay. However, the cells, which were found to be mostly closed in the SEM micrographs (Figure 3.3), appeared to be opened in the Micro-CT scans. This is because most of the solid material is drawn by the surface tension towards the cell edges during the foaming process[312] so the cell faces are too thin for the Micro-CT to detect at the pre-set threshold.

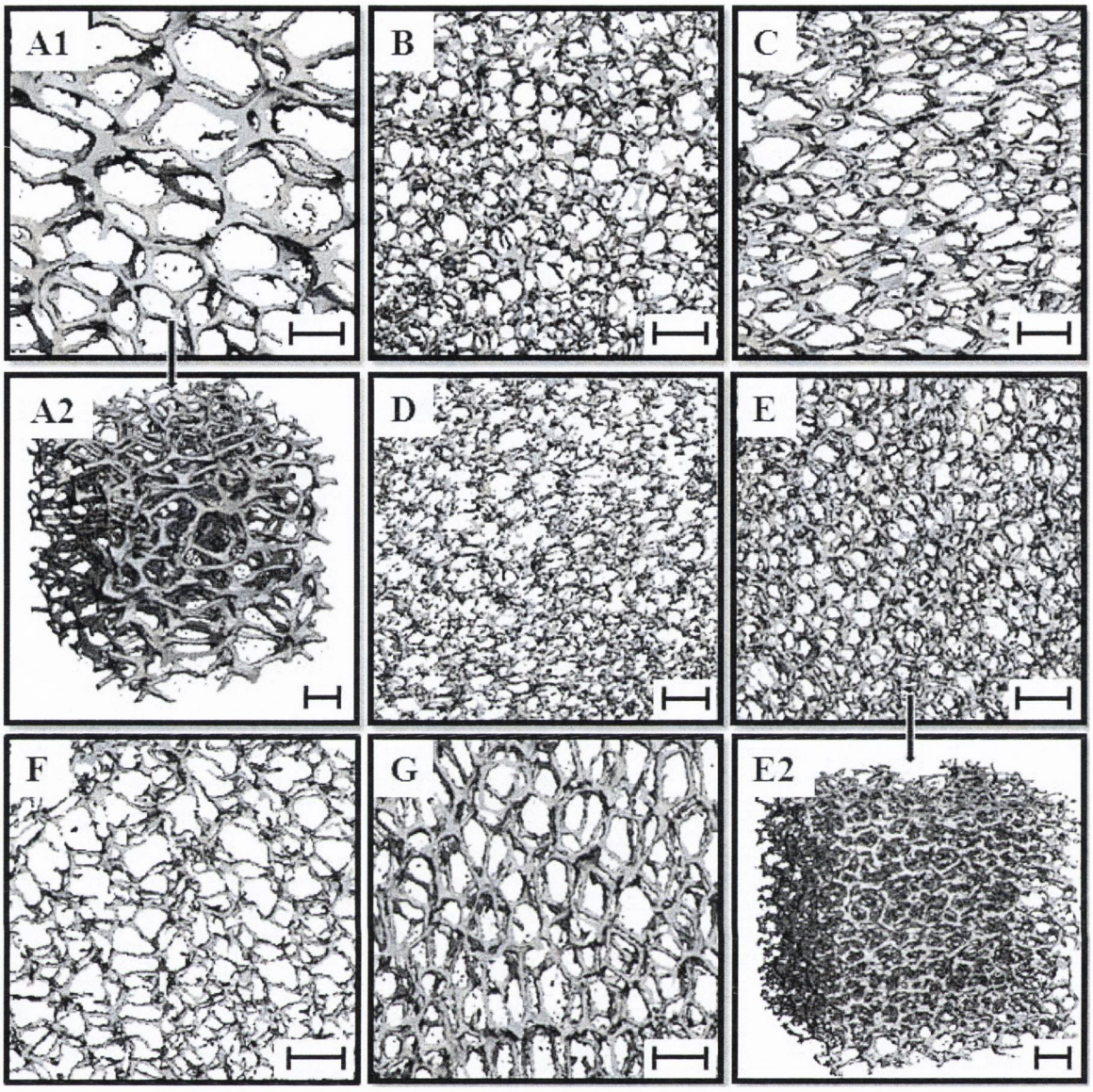

Figure 3.4. Micro-CT scans of (A1) PU foam and (B-G) PU-clay nanocomposite foams: B. M14; C. M18; D. M24; E1. M28; F. M34; and G. M38 and 3D reconstructions of A2. PU and E2. M28 foams (Scale bar: 500 μm).

The densities of the PU and PU-clay nanocomposite foams and solids as well as the porosities of the foams are given in Table 3.3, Columns 2-5. The density of the PU-clay nanocomposite foams decreased compared to the density of the pristine foam, with statistical significance for the higher amount of clay present in mixing sequences 1 and 2 and for 4 wt.% clay content present in mixing method 3, and statistical insignificance for the remaining foams. The reduction in the density of nanocomposite foams confirmed the nucleation effect of the clay as discussed above. The densities of non-cellular PU-clay nanocomposites, ρ_s, (Column 3, Table 3.3) were calculated according to Equation 3.1, taking into account that both the clay and the polymer change their volumes during

nanocomposite formation due to intercalation of some polymer molecules into clay galleries. [120]

$$\rho_s = \frac{\mu_{cp} - \mu_c + \mu_c \mu_{cp}}{\frac{\mu_c d_2}{\rho_{cp} d_1} + \frac{\mu_{cp} - \mu_c - s\mu_c}{\rho_p}} \tag{3.1}$$

where ρ_p is the density of the polymer, i.e., PU in this case which is 1200 kg·m^{-3},[240] and ρ_c is the density of natural clay platelets, i.e., 3100 kg·m^{-3}.[120] d_1 and d_2 are the basal plane spacing of natural clay and the clay intercalated with the polymer, s is the saturated ratio of the intercalating polymer to the clay (i.e., 0.18 g polymer per g of clay)[122] and μ_{cp} is the mass fraction of the inorganic content in natural clay determined from the Loss on Ignition analysis, i.e., 0.886, while μ_c is the mass fraction of clay platelets in the composite, i.e., 0.04 or 0.08, in this work. Additions of clay slightly increase the density of the PU solid.

Table 3.3. Cell diameters, densities and porosities of PU and PU-clay nanocomposite foams.

Sample	Cell diameter / mm	Foam density / kg·m^{-3}	Solid density/ kg·m^{-3}	Porosity[a] / %	Porosity[b] / %
PU	0.76±0.10	48±9	1200 [c]	96	97
M14	0.25±0.02	41±4	1230	97	98
M18	0.52±0.12	37±5	1262	97	98
M24	0.33±0.03	38±4	1230	97	98
M28	0.39±0.05	36±4	1261	97	98
M34	0.45±0.11	38±3	1234	97	97
M38	0.48±0.03	39±5	1271	97	98

[a]Calculated from the densities of the foams and solids presented in Columns 2 and 3; [b]Calculated from Micro-CT results; [c]From literature.[240]

The porosities given in the fourth column of Table 3.3 were calculated from the densities of the foam and its corresponding solid, i.e., $1 - \rho_f/\rho_s$. The as-prepared PU foam was highly porous with a porosity of 96%, and the presence of clay only provided marginal increases in the porosity because of the high starting value. These porosities were in excellent agreement with those obtained from Micro-CT by reconstructing the three-dimensional images of the foam samples (Column 5). The negligible difference of approximately 1% was attributed to the thin cell faces and probably some cell edges that were undetectable with the pre-set threshold. Since $\rho_f/\rho_s < 0.05$, the PU-clay nanocomposite foams can be classified as 'low-density foams'.[313]

3.3.2. Mechanical properties

The compressive moduli for the PU and PU-clay nanocomposite foams determined from the compressive testing data are given in Figure 3.5. Compared to pristine PU foam, the compressive modulus for simultaneous mixing of the three components (M14 and M18) was found to increase with the clay addition by close to 30%, whilst the mixing of 4 wt.% clay with the MDI or polyol followed by the addition of the other component was found to decrease with the clay addition. The variations observed in these materials were without statistical significance compared to the pristine PU foam. The mixing of 8 wt.% clay with polyol followed by the addition of MDI (M28) led to a statistically significant increase of modulus by 35% as opposed to the pristine PU foam and by 69% compared to M38 where a different mixing sequence was adopted and a larger cell size was found. These results are different from the ones reported for PU/vermiculite foams containing between 1.2 wt.% and 3.7 wt.% clay in which the compressive moduli were found to be greater in mixing sequence 3 than for mixing sequence 2.[314] Besides cell size, the densities of the foam and its corresponding solid, the modulus of the corresponding solid, the geometric information of the cells in the foam and the deformation mechanism of the foam also affect the compressive modulus of the foam.

To eliminate the effect of foam density, specific compressive modulus of the foams was calculated and the results are also presented in Figure 3.5. For mixing sequences 1 and 2, the augmentation of the clay content was found to increase the specific modulus by up to 81% for M28. However, when the clay was first mixed with the MDI the specific compressive modulus was found to be similar to the one of pristine PU, regardless of the

clay content. This confirms that the variation of the compressive modulus depends on the clay content and mixing sequence.

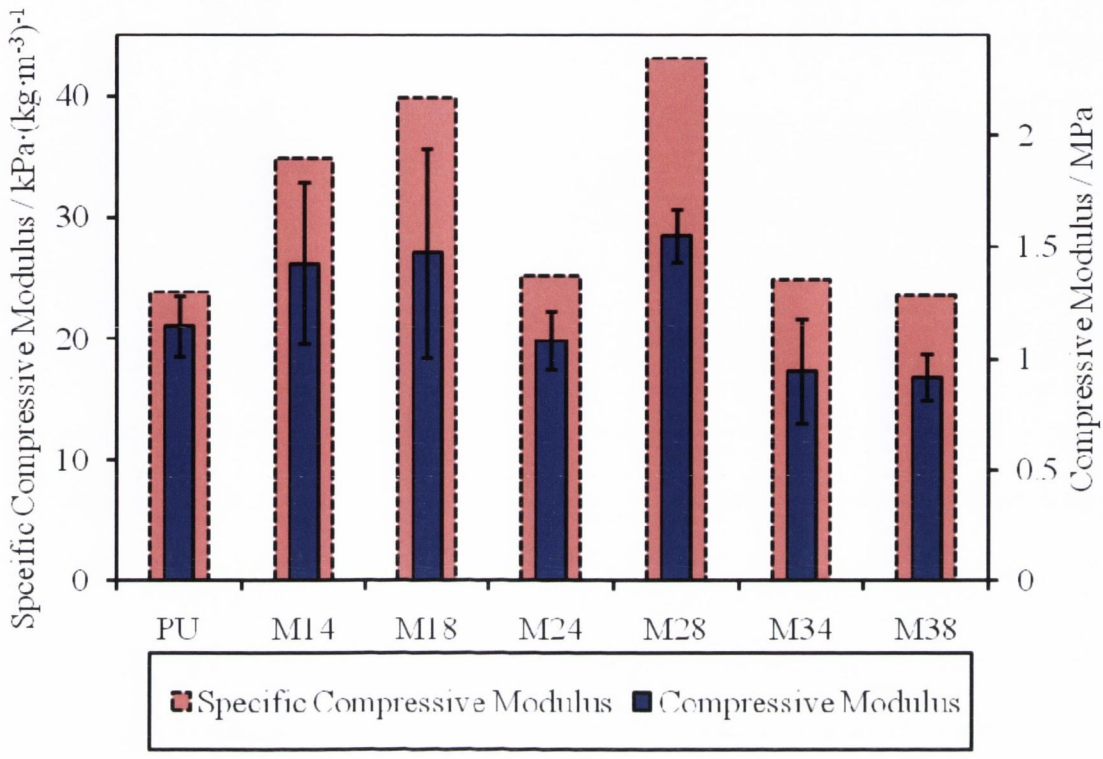

Figure 3.5. Compressive modulus and specific compressive modulus of PU and PU-clay nanocomposite foams (error bars represent the standard deviation for compressive modulus).

To study the effects of densities of foam and solid, the modulus of solid on the modulus of foam, the geometric information of cells and the deformation mechanism of foams, the relationships between relative modulus and relative density of foams should be established. All the theoretical models for the relative modulus-relative density relationships of foams represented by Equation 2.9 and Table 3.1 were tested to investigate if they work for these nanocomposite foams. The moduli of the foams and the densities for the foams and solids were taken from Tables 3.3 and Figure 3.5. The moduli for nanocomposite solids were calculated by employing the Halpin-Tsai model[178] (Equations 2.18-2.19) with the van Es correction.[15] The modulus of the reinforcement was calculated by considering the clay tactoids as a sandwich structure.[122, 174] In order to evaluate the modulus of the clay tactoids it was considered that unfilled rigid PU solid was characterised by a modulus of 1600 MPa [240] and a Poisson's ratio of 0.33 [315] and that the

clay platelets presented a modulus of 230 GPa [16] and a Poisson's ratio of 0.28.[122] Because the nanocomposites reinforced the PU matrix by intercalated clay tactoids, clay reinforcement refers to intercalated clay tactoids. Thus, the effective volume fraction, ϕ_c, was calculated using Equation 2.13, which is substantially greater than the nominal volume fraction of the clay particles.[122]

Among all the models presented in Table 3.1, the ones developed by Dement'ev and Tarakonov (C_1=0.7 in Equation 2.9)[294, 296] and Choi and Lakes (C_1=0.88 in Equation 2.9)[294] best fit the experimental data despite that they are open-cell models, while the rest do not give reasonable predictions. The correlation between the experimental data for the PU/clay nanocomposite foams and the theoretical values predicted using these two models is given in Figure 3.6 which shows reasonably good agreement. It is noted that both models were developed based on conventional polyester-based PU foams with 97% porosity, same as the value for the nanocomposite foams studied in this work. The good correlation indicates that the relative modulus-relative density relationship for polymer foams is applicable to nanocomposite foams provided the porosities are similar.

As previously discussed, the PU and PU/clay nanocomposite foams are low density closed-cell materials with most of the material located within the cell walls. The fact that the above two models best fit the experimental data also suggests that the low density closed-cell foams can be considered as open cells, agreeing with the previous findings for general cellular solids that most of the load is carried by the cell edges in this type of foams[313] and the low density closed cells tend to behave as open cells.[312]

Among the remaining models presented in Table 3.1, the original Gibson-Ashby model for open cells, where $C_1 = 1$ and $n = 2$ for Equation 2.8, assumes a two dimensional continuous structure in which the cell edges meet at a 90° angle, have square cross sections and the vertices link three edges.[240, 286] However, as it can be observed from the SEM and Micro-CT images, the cells present hexagonal cross sections, a different angle at which the edges meet and a higher nodal connectivity, which may explain the fact that this model is inadequate to predict the values for the pristine PU foam and PU-clay nanocomposite foams. In contrast, the tetrakaidecahedron cell shape observed for these foams is the same as the shape found in the foams studied for both the Dement'ev-Tarakonov[294, 296] and the Choi-Lakes[294] models, noting that such tetrakaidecahedron shape is commonly found for polymer foams, for example other PU-clay foams,[262] PCL-clay foams[251] and PP-clay foams.[246]

In the normalised Gibson-Ashby model[286] for open cells, C_1 is the coefficient used for the normalisation of the Young's modulus of the foam, namely $C_1 = (E_f^p/E_s^p)(\rho_s^p/\rho_f^p)^2$ where the superscript p refers to the pristine polymer. Inserting the normalisation coefficient into Equation 2.8 results Equation 3.2, in which the coefficient is equal to 0.45 in this work. The theoretical values predicted using this normalised model are also presented in Figure 3.6, showing good agreement with the experimental data and in general confirming that an open-cell model may be used for studying low-density nanocomposite foams.

$$\frac{E_f}{E_s} = \frac{E_f^p}{E_s^p}\left(\frac{\rho_s^p}{\rho_f^p}\right)^2\left(\frac{\rho_f}{\rho_s}\right)^2 \tag{3.2}$$

The Gibson-Ashby model for closed-cell foams given in Equation 2.26 was also considered for prediction of the relative modulus of nanocomposite foams. Because the contribution of the cell fluid is minimal,[240] Equation 2.26 can be reduced to Equation 3.3.

$$\frac{E_f}{E_s} = C_1\phi_s^2\left(\frac{\rho_f}{\rho_s}\right)^2 + C_2(1-\phi_s)\frac{\rho_f}{\rho_s} \tag{3.3}$$

In order to determine the volume fraction of solid (ϕ_s) contained in the edges of the cells, a relative volume of the cell faces to the cell edges of 0.1 [313] (characteristic for rigid polyurethane foams) was used, which led to a ϕ_s value of 0.94.[240, 313] As previously introduced, C_1 is the geometric constant for the cell struts so it is the same as the constant for the open cells, i.e., 0.45. Inserting these two values and the moduli and densities for the pristine PU foam and solid into Equation 3.3, C_2 was determined as 0.03. Like the previous three models, the theoretical values predicted using Equation 3.3 are given in Figure 3.6. It is seen that this additional curve almost overlaps with the curve for the normalised open-cell model, further confirming that the open-cell model is a simplified version of the closed-cell model and low density closed-cell foams can indeed be considered as open-cell foams.

To validate the applicability of the normalised Gibson-Ashby model for low-density polymer/clay nanocomposite foams, gelatine/sepiolite nanocomposite foams were developed by Frydrych et al.[316] It was found that the normalised model presented the most accurate description of the experimental data, showing good approximations for the entire range of investigated porosities (i.e., 96-98%). Using a porosity range of 97-98%, Liu et al.[317] reinforced the applicability of the normalised Gibson-Ashby model. They have found

that for nanofibrous bacterial cellulose/chitosan scaffolds the relative density-relative modulus relationship was predicted reasonably well by the previously mentioned model. Thus, it can be stated that the normalised Gibson-Ashby model may be used to predict the relative density-relative modulus relationship in polymer nanocomposite foams with high porosity (i.e., 96-98%).

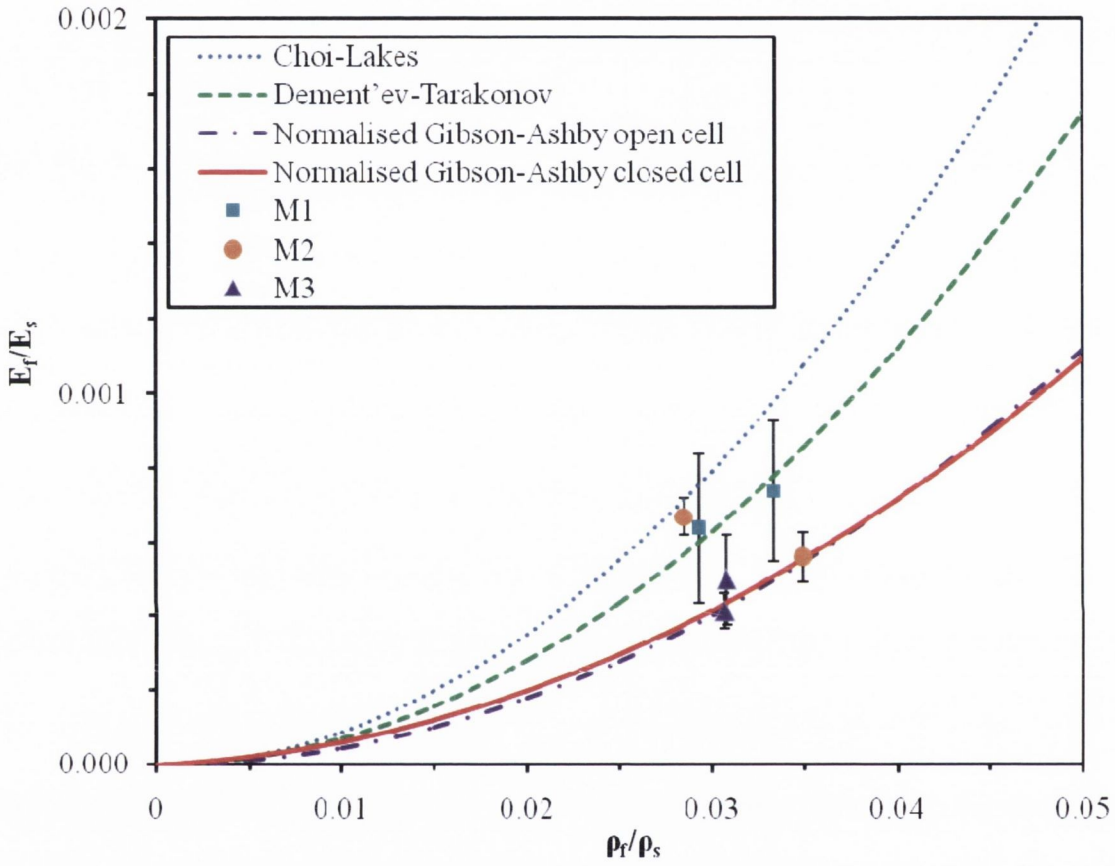

Figure 3.6. Theoretical and experimental data of relative Young's modulus versus relative density for PU-clay nanocomposite foams showing they are in good agreement.

As shown in Figure 3.6, the theoretical relative moduli predicted using all the above-discussed four models appear to be reasonably close to the experimental data. In contrast, other models presented in Table 3.1 give values markedly deviated from the experimental results. These imply the normalised Gibson-Ashby models for open cells and closed cells work reasonably well for low-density nanocomposite foams ( ). In the case of high-porosity PU-clay nanocomposite foams, the C_1 in is approximately 0.45-0.88. These results further suggest that the established models for

conventional cellular solids can be applied to polymer nanocomposite foams provided that all the parameters in the models are correctly calculated.

3.4. Conclusions

PU-natural clay nanocomposites containing different clay contents were prepared with different mixing sequences and used for the study of relative modulus-relative density relationships in a relatively new class of foam materials, i.e., polymer/clay nanocomposite foams. It is found that the addition of clay decreases the cell size and density of the polymer foam, acting as a nucleation agent as previously reported by others, and the increase of clay content leads to a greater cell size which is the result of the blowing effect from the growing amount of water present in the clay galleries. The uniform cell structures with varying cell sizes in the PU-clay foams observed using SEM and Micro-CT, together with the shifts of the *(001)* peak for the clay detected by XRD, confirm the formation of polymer/clay nanocomposites. The nanocomposite foam prepared by mixing the polyol blend with 8 wt.% natural clay followed by the addition of diisocyanate provides an increase in the specific compressive modulus of the PU foam by 81%. This enhancement is attributable to the strong interactions between the polymer and the clay due to formation of hydrogen bonds and nanostructures, the large specific surface area and high stiffness of clay, and the small cell size that occurs due to the nucleation effect of clay.

Modelling the relative modulus versus relative density for the low density nanocomposite foams (with a porosity higher than 95%) finds that their relationship can be reasonably predicted by the classical Gibson-Ashby models for open-cell and closed-cell foams provided the modulus of the starting polymer foam is normalised to obtain the correct geometric constants and the modulus and density of the nanocomposite solids contained in the cells are properly calculated. In the case of high-porosity PU-clay nanocomposite foams, the geometric constant of foam C_1 in $E_f/E_s = C_1(\rho_f/\rho_s)^2$ was determined to be approximately 0.45-0.88.

Chapter 4. Porous exfoliated poly(ε-caprolactone)/clay nanocomposites: preparation, structure and properties

4.1. Introduction

Past years have marked a turning point in polymer foaming, some of the commodity plastics, known for their biochemical endurance, being replaced by biodegradable polymers, e.g. poly(ε-caprolactone) (PCL), poly(lactic acid) (PLLA) and poly(glycolic acid). Possessing the ability to degrade upon bioactive environment exposure into small molecules, e.g. water, CO_2 and biomass,[318] these polymers may represent a possible solution to the growing waste problem that the world is facing.[319] Lately, biodegradable polymers have been used for a series of packaging and biomedical applications, e.g. drug delivery systems, bioabsorbable surgical sutures, tissue engineering scaffolds and temporary internal fixation of a variety of tissue damages.[320, 321]

Compared to traditional cellular polymers, porous biodegradable polymers often present low stiffness, brittleness and/or high gas permeability.[322] Recent research shows that strength, stiffness, thermal stability and barrier properties of biopolymers can be greatly improved with the addition of a small amount of nanoclay.[7, 180, 195]

Since clay is ubiquitous in nature, environmentally friendly and biocompatible,[323] using it as nanofiller for biodegradable and biocompatible porous polymers results in the formation of green and biomedical nanocomposites with enhanced properties.[321] This relatively new class of materials represents a viable alternative to conventional porous polymers used for packaging and biomedical applications.

The previous research on porous polymer/clay nanocomposites, including biopolymer-based foams, was mainly concerned with the materials manufactured by mixing the polymer, clay and blowing agent (physical, e.g. CO_2, N_2 or a combination of both[250] or chemical, e.g. azodicarboxamide (ADC), sodium bicarbonate (SB) or zinc carbonate)[255] simultaneously,[254] with the blowing agent playing the sole role of creating bubbles. The hypothesis of this work was that by pre-incorporating a chemical blowing agent into the clay galleries and expanding the clay galleries during bubble formation, the blowing agent will attain a secondary role, that of enhancing the exfoliation degree. Since it is considered advantageous to obtain fully exfoliated polymer/clay nanocomposites, it is expected that the resultant porous materials will have better properties as opposed to existing porous nanocomposites with comparable material compositions. Semicrystalline PCL was selected as the matrix because of its ductility, biocompatibility and wide range of

biomedical applications such as drug delivery systems, wound dressings and sutures and bio-resorbable implants.[320, 322, 324, 325] Sodium bicarbonate and azodicarboxamide, known for their low toxicity and progressive gas yield,[253] were chosen as blowing agents. The structures were investigated by X-ray Diffraction (XRD), Transmission Electron Microscopy (TEM) and X-Ray Micro Computed Tomography (Micro-CT), thermal properties and crystallinities were studied by Thermal Gravimetric Analysis (TGA) and Differential Scanning Calorimetry (DSC) and mechanical properties were obtained from compression testing.

4.2. Experimental section

4.2.1. Materials

Poly(ε-caprolactone), $\overline{M}_n$=70,000-90,000, was purchased from Sigma-Aldrich (Ireland). A commercially available organoclay, Cloisite® 30B (C30B), that is, a methyl, tallow, bis-2-hydroxyethyl, quaternary ammonium modified montmorillonite, was generously supplied by Southern Clay Products Inc. (Texas, USA). The cation exchange capacity was 90 meq./100g clay, the density was 1980 $kg \cdot m^{-3}$ and the inorganic content was 70%. Reagent-grade sodium bicarbonate, $NaHCO_3$ and azodicarboxamide, $C_2H_4O_2N_4$, were purchased from Sigma-Aldrich (Ireland). Due to the high decomposition temperature[255] of azodicarboxamide, zinc oxide, ZnO (Analytical grade) from Sigma-Aldrich was used to activate the blowing agent and reduce the decomposition time.[326] Tetrahydrofuran (THF) was used as a solvent. All materials were used as received.

4.2.2. Clay treatment

C30B was pre-treated with two chemical blowing agents, namely sodium bicarbonate and azodicarboxamide/zinc oxide to give the SB- and ADC-treated clays. In both cases, 6.5 g of C30B were first dispersed overnight, under constant stirring, in 325 mL of THF:H_2O=1:1 (v/v) to produce a clay suspension. For the SB-treated clay, a 2.5 wt.% (w/w) solution of SB in distilled water was added to the clay suspension. For the ADC-treated clay, the clay suspension was mixed with a 5 wt.% (w/w) solution of ADC:ZnO=1:1 (w/w) in distilled water. In order to achieve a good dispersion of ADC and ZnO in water, the solution was ultrasonicated for 1 h before being added to the organoclay

suspension. The treated-clay suspensions were kept under constant stirring for ca. 24 h and dried in an oven for 8 h at 80 °C, followed by being grounded into fine powders.

4.2.3. Preparation of porous PCL/clay nanocomposites

Porous PCL-treated clay nanocomposites were obtained in two steps, preparation of solid nanocomposites and thermal degradation of the blowing agent to create pores. In the first step, polymer/clay nanocomposites with 5.8 wt.% blowing agent-treated organoclay were prepared following the procedure described below. First, the blowing agent-treated organoclay was dispersed in THF to obtain a 3 wt.% clay dispersion. Separately, PCL was dissolved in the same solvent to create a 10 wt.% solution. Then, the clay dispersion was mixed with the PCL solution at predetermined volumes at room temperature for 2 h on a magnetic stirring plate and ultrasonicated for 1 h. Finally, the resulting mixture was cast and dried at room temperature in a fume cupboard to obtain the solid nanocomposite.

In the second step, the nanocomposites were compression moulded in a cylindrical mould on a hot plate at 150 °C for 1 h. The mould was then covered and inserted in an oven for 1 h at 190 °C for SB-treated clay and at 210 °C for ADC-treated clay, temperatures which were predetermined, from the TGA results, as the optimal foaming conditions for both blowing agents. Porous PCL samples without clays were prepared following a protocol similar to the one described above. However, in these cases 30 min. at a temperature of 115 °C on the hot plate were sufficient, while the oven temperatures were lowered to 170 °C and 190 °C for SB and ADC, respectively.

4.2.4. Characterisation

XRD was carried out on a Phillips PW1720 X-Ray Diffractometre with a $CuK_{\alpha 1}$ (λ=0.15406 nm) anode tube at the standard conditions of 40 kV and 20 mA. Clay powders and thin discs of nanocomposites before and after foaming were tested from 2° to 10°, 2θ angle, at a step size of 0.02° and duration of 2.5 seconds per step.

TEM was performed on a TECNAI G2 20 twin electron microscope for porous polymer/clay nanocomposites and on a JEOL JEM-2010 for non-porous polymer/clay nanocomposites at 200 kV accelerating voltage. The specimens were sectioned using a Reichert-Jug 'Ultracut' or a NOVA ultramicrotome equipped with a diamond knife. The sections (~100 nm in thickness) were collected in a trough filled with water and placed on

a 200 mesh copper grid for porous solids and 400 mesh titanium grids for non-porous samples.

FT-IR spectra were realised on a FT-NIR instrument (Perkin Elmer Spectrum One NTS) equipped with ATR Sampling Accessory. The samples were run from 650 cm^{-1} to 4000 cm^{-1} at a resolution of 2 cm^{-1}.

TGA was performed on a Perkin Elmer Pyrus 1 TGA equipped with an ultra-micro balance with a sensitivity of 0.1 μg, under air flow (20 $mL \cdot min^{-1}$), from 100 °C to 650 °C at a heating rate of 10 $°C \cdot min^{-1}$.

DSC was carried out on a Perkin Elmer Diamond DSC at a scan rate of 20 $°C \cdot min^{-1}$. The crystallinity of the porous and non-porous polymer/clay nanocomposites was calculated, using Equation 4.1 [251, 327] and considering the melting enthalpy of the sample (ΔH_m) from the second heat scan in order to eliminate the effects of the heating history.

$$\chi_c(\%) = \frac{\Delta H_{\mathrm{m}}}{\mu_p \cdot \Delta H_{\mathrm{m}}{}^{0}} \cdot 100 \qquad (4.1)$$

where μ_p is the weight fraction of PCL in the nanocomposite sample and $\Delta H_m{}^0$ is the melting enthalpy for the 100% crystalline PCL, i.e., 136 $J \cdot g^{-1}$. [328]

Micro-CT was run on a Scanco Micro-CT 40 Scanner (Scanco Medical AG) at the standard resolution (acquisition: 250 projections per 180° with 1024 samples each, an energy of 55 kVp and a current of 145 μA). The micrographs were realised using a predefined threshold that was found to give the most accurate interpretation (as defined in Chapter 3) of the image throughout the whole scan in order to assess the structure and porosity. The Image J software was used to analyse the pore size. For each micrograph, a substantial number of pores were measured and the mean and standard deviation normalised for 20 pores with a 95% confidence level are presented.

Compressive tests were carried out on an Instron 8501 universal testing machine with a load of 100 kN at a rate of 1 $mm \cdot min^{-1}$. Testing was arbitrarily terminated at the deformation of 60% according to ASTM C365-05. Five surface-ground cylindrical specimens with a diameter of 19 mm and a height of approximately 10 mm were tested for each type of the porous solids. The mean and standard deviation values reported present a confidence level of 95%. Statistical significance was assessed by a Two-tailed, Type II 't' test with a criterion that the probability of a difference in means due to chance is less than 0.05. The bulk density of the porous solids was calculated as the ratio of the weight to the

volume of each sample. The diameter and height of each cylindrical specimen were measured with a Vernier calliper in at least three points, while the weight was measured on an analytical balance. Five specimens were weighed and measured for each of the porous solids considered. The mean and standard deviation values reported present a confidence level of 95%.

4.3. Results and discussion

4.3.1. Structure

Figure 4.1 shows the X-ray diffraction patterns of the organoclay, the blowing agent-treated organoclays and the PCL/treated organoclay nanocomposites, before and after foaming. The untreated organoclay (Curve 1) presented a peak at $2\theta = 4.8°$, corresponding to a basal plane spacing, $d_{(001)}$, of 1.85 nm. By modifying the clay with the blowing agents, $d_{(001)}$ remained the same for azodicarboxamide (Figure 4.1A, Curve 2), while for sodium bicarbonate it slightly decreased (Figure 4.1B, Curve 5) probably due to removal of some surfactant molecules or impurities from the galleries. As the molecular sizes of the blowing agents are smaller than the one of the surfactant, their entrance, if available, may not increase the gallery spacing. To further characterise the structures of the treated organoclays, FT-IR was used and the results are shown in Figure 4.2. When the organic blowing agent was used to modify the organoclay, the position of the Si-O stretching band[329] in the organoclay (Curve 1) shifted from 1004 cm^{-1} to 1010 cm^{-1} in the ADC-treated clay (Curve 5) due to hydrogen bonding with the carbonyl groups present in ADC.[330]

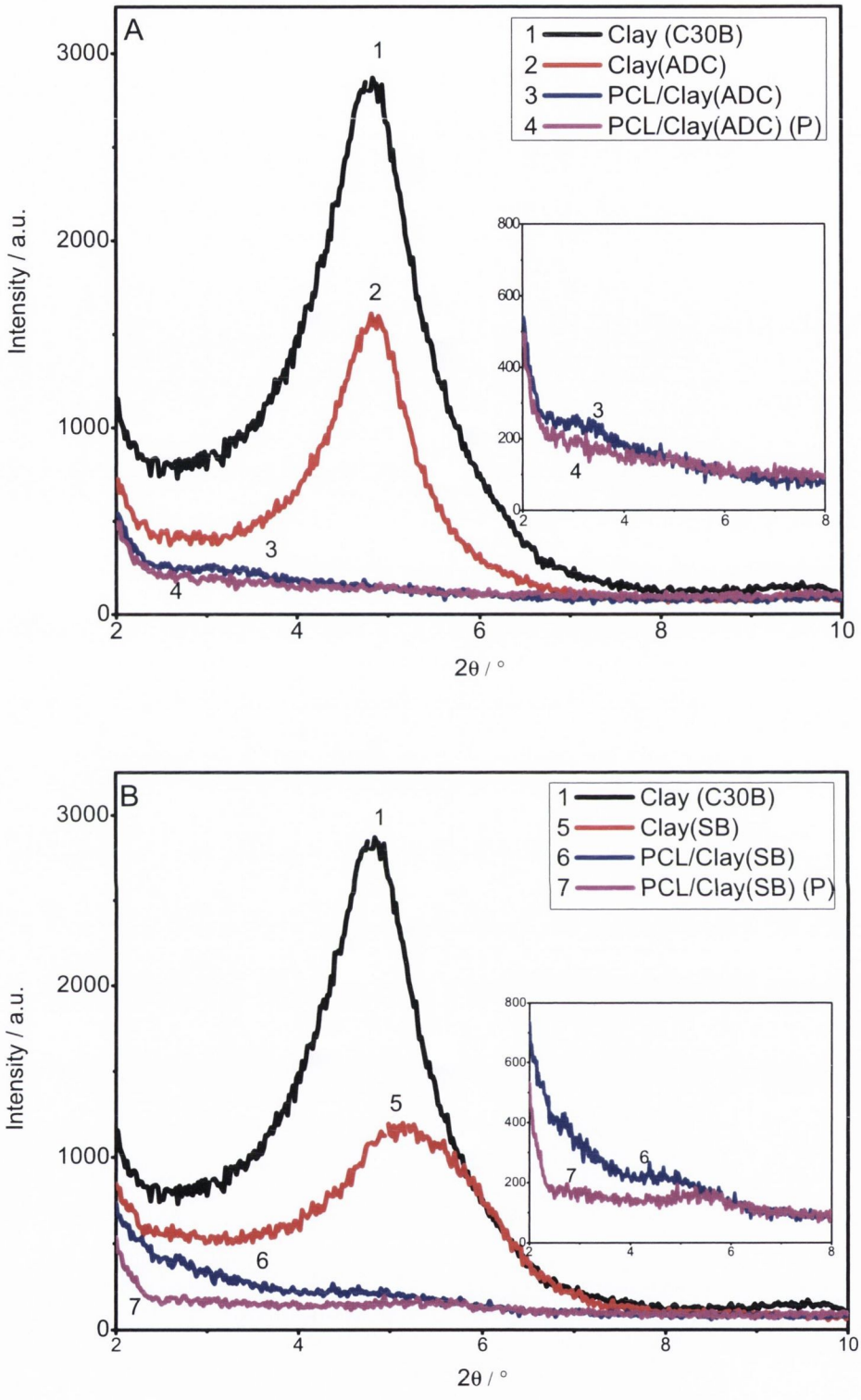

Figure 4.1. XRD traces for clays and nanocomposites. 1. Clay (C30B), 2. Clay(ADC), 3. PCL/Clay(ADC), 4. PCL/Clay(ADC) (P), 5. Clay(SB), 6. PCL/Clay(SB), and 7. PCL/Clay(SB) (P).

Although the XRD spectrum does not present a shift toward a lower 2θ angle, the FT-IR results might indicate a change inside the clay gallery suggesting that the ADC molecules could have entered the gallery, resulting in strong interactions with the clay. This postulation was supported by the shifts that occurred in the water bands present inside the clay gallery (Curve 1). The band at 3429 cm^{-1}, characteristic to stretching of the interlayer water,[331, 332] shifted to 3150 cm^{-1} (Curve 5). The shift was due to hydrogen bonding between the water molecules and stretching of the N-H bonds in the ADC molecules. Similar changes were observed when SB was used to treat the organoclay, with the two peaks designated to the interlayer water at 1639 cm^{-1} and 3429 cm^{-1} [331, 332] shifting to 1684 cm^{-1} and 3459 cm^{-1} (Curve 3). The changes in the absorption peaks observed *via* FT-IR indicated that the clay treatment has been successful and that in both cases the blowing agents have entered the gallery of clay.

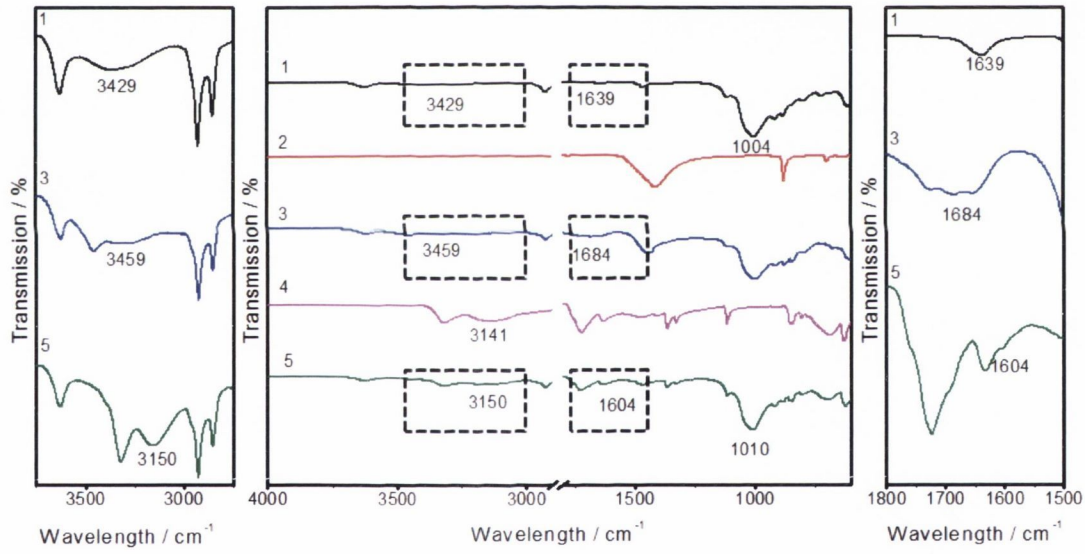

Figure 4.2. FT-IR spectra for treated organoclays and related materials: 1. C30B, 2. SB, 3. Clay(SB), 4. ADC and 5. Clay(ADC).

For the blowing agent-treated organoclays dispersed into PCL, the $d_{(001)}$ peaks presented in the treated organoclays were found to shift toward smaller 2θ values and/or diminish their intensity considerably (Figure 4.1, Curve 1 versus Curve 3 or 6) suggesting the co-existence of intercalated and exfoliated structures, which was subsequently confirmed from the TEM results. Upon foaming, the intensity of the peaks was further diminished (Figure 4.1, insets), initially indicating an increase in the exfoliation degree.[8] Figure 4.3 shows the TEM images of PCL/treated clay nanocomposites before and after

foaming. As can be observed from Figures 4.3A, the clay layers appeared mainly as intercalated tactoids with occasional exfoliated single clay platelets before foaming. The intercalated structures were found to have between 2 and 7 layers with an average of 4 clay platelets per stack (determinate from over 10 stacks, with a 95% confidence interval). The few exfoliated clay platelets were either ordered (Figure 4.3A, inset) or disordered. Partially intercalated and partially exfoliated clay platelets in PCL/clay nanocomposites have been previously reported by Liu et al.[251] for 5 wt.% DK2 (a montmorillonite modified by methyl tallow bis-2-hydroxyethyl ammonium, the surfactant being the same as for C30B) and Ludueña et al.[195] for 2.5, 5 and 7.5 wt.% C30B.

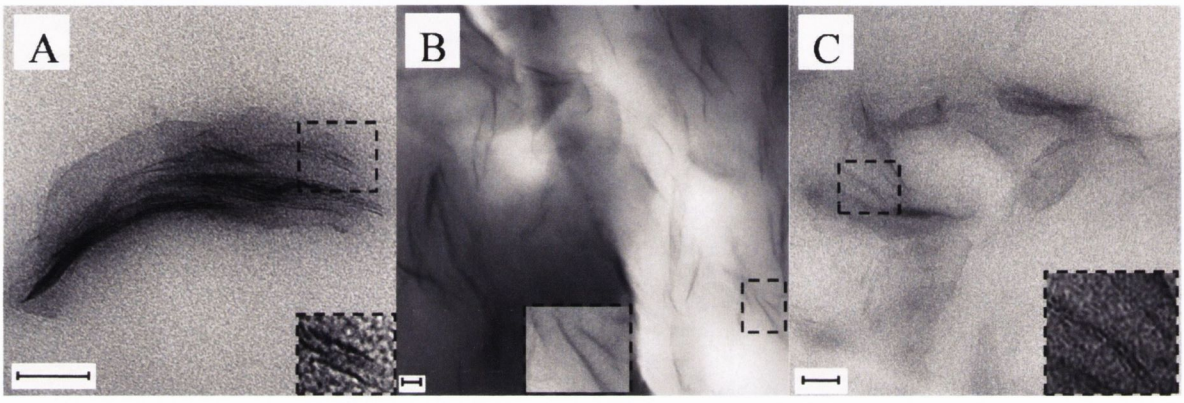

Figure 4.3. TEM images of: A. PCL/Clay(SB) nanocomposite, B. porous PCL/Clay(SB) nanocomposite and C. porous PCL/Clay(ADC) nanocomposite (Scale bar: 100 nm for the main figure and 25 nm for the insets).

Analysing the structures that occurred in porous PCL/blowing agent-treated clay nanocomposites (Figures 4.3B and 4.3C), it was confirmed that the enhancement in the exfoliation degree is dependent on the blowing agent used to treat the clay. The insertion of inorganic blowing agent molecules inside the clay gallery resulted in well dispersed clay platelets with ordered and disordered full exfoliation (Figure 4.3B, inset). Ordered exfoliated and single delaminated clay layers were also observed when organic blowing agent molecules were used to treat the clay. However, in this case 40% of nanostructures were found to be intercalated structures with an average of 2 layers per stack and a basal spacing of 2.9 nm (Figure 4.3C, inset), with the remaining 60% being fully exfoliated. Nevertheless, these results revealed that in both cases the exfoliation and dispersion of clay platelets were improved remarkably after the blowing agent was degraded in the clay galleries.

The type of blowing agent used influenced the amount of gas dispersed and the viscosity of the melt.[250, 255] The inorganic blowing agent produced, upon degradation (Figure 4.4), non-polar carbon dioxide (CO_2) and water molecules that were released inside the clay gallery. Combining the high solubility of CO_2 in water and the polar nature of the water molecules,[333] the degradation product presented a high affinity for the hydrophilic clay platelets and a high diffusivity in the polymer[19] which led to the occurrence of fully exfoliated porous polymer/clay nanocomposites. The non-polar nitrogen molecules (N_2) that the organic blowing agent yielded upon decomposition (Figure 4.4) resulted in intercalated/exfoliated nanocomposites.

$$2\ NaHCO_3 \longrightarrow Na_2CO_3 + CO_2\ (g) + H_2O\ (g)$$

$$C_2H_4O_2N_4 \longrightarrow N_2\ (g) + CO\ (g) + CO_2\ (g) + NH_3\ (g)$$

Figure 4.4. Thermal decomposition of blowing agents.

The process of obtaining highly exfoliated porous polymer/clay nanocomposites was summarized in Figure 4.5. Firstly, the organoclay was treated with an inorganic blowing agent. This allowed the small blowing agent molecules to enter the clay gallery mainly due to hydrogen interactions between the blowing agent and the interlayer water. Secondly, the treated clay was dispersed in the polymer matrix *via* the solution method. This step permitted PCL chains to penetrate inside the clay gallery which resulted in mostly intercalated and minor exfoliated nanocomposite structures (Figure 4.3A). Finally, the PCL/blowing agent-treated clay nanocomposites were exposed to higher temperatures which degraded the blowing agent according to Figure 4.4. The production of gas inside the clay gallery expanded the basal spacing further, leading to fully exfoliated porous nanocomposites in the case of using SB as the blowing agent and highly dispersed porous nanocomposites when ADC was used instead of SB.

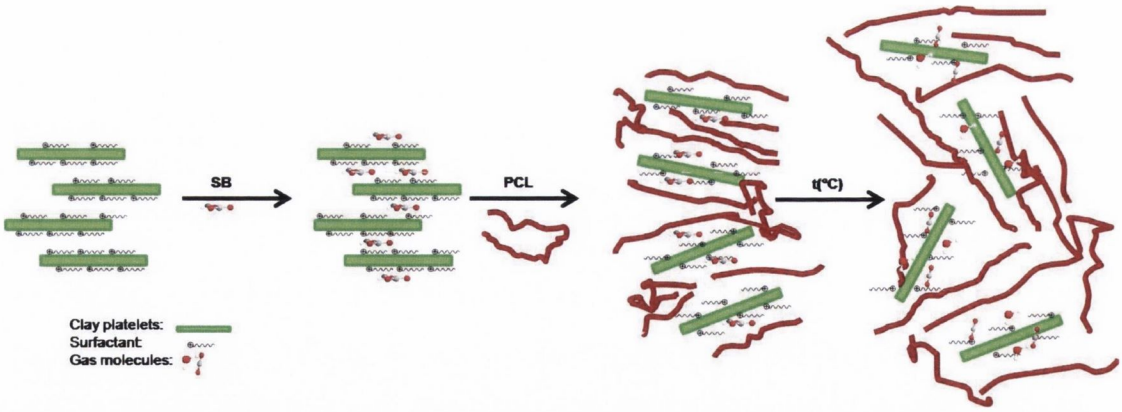

Figure 4.5. Exfoliation process in porous PCL/blowing agent-treated organoclay nanocomposites.

The effects of the treated organoclays on the microstructure of the porous PCL were investigated. The structure, presented in Micro-CT scans (Figure 4.6), appeared to be irregular in the absence of clay (Figure 4.6A and 4.6B1), throughout the entire sample (Figure 4.6B2). The pore dimensions of the porous solids were characterised by a wide range of values due to the high number of gas molecules produced.[253] By adding the blowing agent-treated organoclays, relatively uniform structures were formed and observed in section (Figure 4.6D1 versus Figure 4.6B1) and throughout the entire specimen (Figure 4.6D2). The clay-filled porous solids presented 39% and 46% reductions in pore size, with statistical significance, for SB and ADC (Table 4.1, Column 2). These changes may be attributed to the ability of clay to act as a nucleating agent[251] and presumably to create a barrier effect,[334] inhibiting cell growth[324] and demonstrating that clay plays an essential role in controlling the cellular structure.[251]

The density of the porous PCL/clay nanocomposites (ρ_f, Table 4.1, Column 3) increased, by up to 40%, compared to their respective polymer counterparts. The density of solid polymer/clay nanocomposites (ρ_s, Table 4.1, Column 4) was calculated according to the equations presented in Appendix II and considering that the clay platelets were fully exfoliated when the inorganic blowing agent was used to treat the organoclay as it was observed from the TEM images (Figure 4.3B) and intercalated/exfoliated in the case with the organic blowing agent according to the TEM images (Figure 4.3C). For these calculations, values of 1980 $kg \cdot m^{-3}$, 3100 $kg \cdot m^{-3}$ and 1140 $kg \cdot m^{-3}$ [122] were used as the densities of organoclay, clay platelets and PCL. The amount of surfactant adsorbed on the surface of the clay platelets was not considered in the solid density calculation because the difference in the densities of the surfactant and of the polymer was too small to have an impact on the solid density.[335] The solid density of the polymer-blowing agent systems was

taken as the density of the solid PCL, i.e., 1140 $kg \cdot m^{-3}$, due to the insignificant amount of the residual blowing agent present in the systems (~1.5 wt.%). The porosities presented in Column 5 were calculated from the densities of the porous materials and their corresponding solid densities, i.e., $1-\rho_f/\rho_s$.

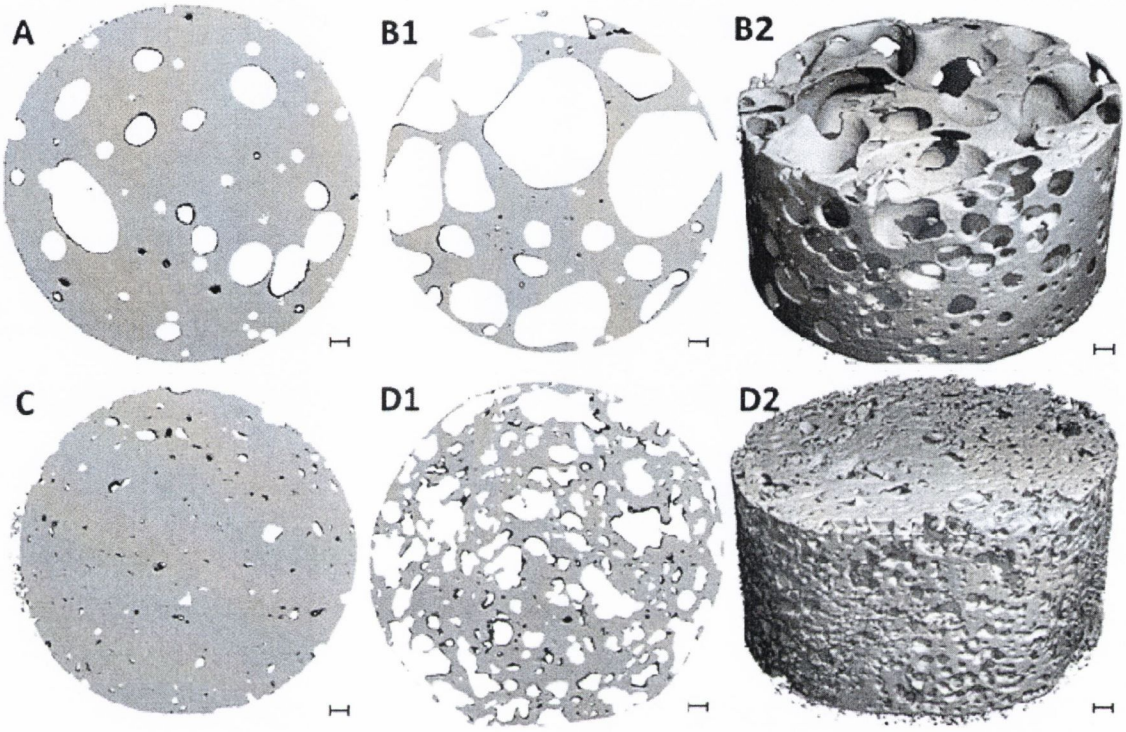

Figure 4.6. Micro-CT scans for porous solids: A) PCL(SB) (P), B) PCL(ADC) (P), C) PCL/Clay(SB) (P), and D) PCL/Clay(ADC) (P) (Scale bar: 1 mm).

As can also be observed from Table 4.1, the porosity and pore size of the porous materials varied with the blowing agent used. The porous PCL obtained with ADC showed a pore size and porosity 212% and 178% higher than the porous PCL(SB). This is a consequence of lower gas yield and poorer blowing efficiency that the inorganic blowing agent, SB, has in contrast to the organic blowing agent,[254] and the high solubility that the CO_2 produced by SB has compared to the N_2 produced by ADC (Figure 4.4).[250] The relative densities (ρ_f/ρ_s) were found to be 0.74 for PCL/Clay(SB) (P) and 0.45 for PCL/Clay(ADC) (P). Since they are higher than 0.1, the materials cannot be considered as low-density foams, but structural foams ($0.4<\rho_f/\rho_s<0.8$)[336] or porous solids ($0.3<\rho_f/\rho_s$).[175]

Table 4.1. Pore sizes, densities and porosities of porous PCL and PCL/clay nanocomposites

Sample ID	Material	Pore size/ mm	Foam density/ $kg \cdot m^{-3}$	Solid density/ $kg \cdot m^{-3}$	Porosity[b] / %
PCL(SB) (P)	PCL foamed with SB	0.57±0.20	851±30	1140 [a]	23.6
PCL/Clay (SB) (P)	PCL/SB treated clay nanocomposites, foamed	0.35±0.07	882±130	1189	25.8
PCL(ADC) (P)	PCL foamed with ADC	1.78±1.12	392±170	1140 [a]	65.6
PCL/Clay (ADC) (P)	PCL/ADC treated clay nanocomposites, foamed	0.96±0.10	549±11	1229	55.3

[a]From literature;[337] [b]Calculated from densities of foams and solids presented in Columns 2 and 3.

4.3.2. Crystallinity and thermal properties

The crystallinity and thermal properties of non-porous and porous polymers and polymer/clay nanocomposites were affected by the addition of clay and the type of blowing agent used. Table 4.2 shows that the crystallisation temperature (Column 1) of PCL increased by 10.1 °C by the addition of SB-treated clay. The variations in the crystallinity with the addition of clay can be accounted for by two factors: nucleation that increases crystallinity and reduction in the flexibility of polymer molecular chains that impedes rearrangement of macromolecular chains into ordered crystalline structures and hence reduces crystallinity. Both factors are related to clay dispersion and content. In PCL/Clay(SB), the degree of crystallinity (Column 2) increased from 43.9% in PCL(SB) to 49.7% which may be attributed to a more prominent nucleating effect of clay on crystallisation.[251] However, when ADC was used to treat the clay, the crystallisation temperature and crystallinity remained almost unchanged with the inclusion of clay, due to equal impacts of the two effects. After foaming, the porous PCL(SB) presented similar changes in the crystallisation temperature and the crystallinity with the presence of clay to

the cases in its counterpart before foaming. Again not the same effects were observed for the porous PCL(ADC). The use of organic blowing agent with an activator to treat the organoclay led to a slight decrease in the crystallisation temperature and the crystallinity. The higher crystallinity in the porous PCL/Clay(SB) and lower crystallinity in the porous PCL/Clay(ADC) compared to their respective porous PCL suggest that the nucleation effect prevails in the former whereas chain stiffening effect dominates in the latter.

Table 4.2. DSC results of PCL and PCL/clay nanocomposites before and after foaming

Material	Before foaming		After foaming	
	T_c / °C	χ_c / %	T_c / °C	χ_c / %
PCL(SB)	20.5	43.9	28.8	37.0
PCL/Clay(SB)	30.6	49.7	34.3	42.7
PCL(ADC)	26.8	49.0	30.3	43.7
PCL/Clay(ADC)	26.1	49.0	28.0	41.0

The thermal degradation behaviours for PCL/treated clay nanocomposites before and after foaming were analysed by TGA. From the derivative thermogravimetric (DTG) curves (Figure 4.7) it can be observed that before foaming (Figure 4.7A) the presence of clay platelets increased the degradation temperature (i.e., the peak temperature observed) from 363 °C in PCL(SB) to 397 °C in PCL/Clay(SB), and from 390 °C in PCL(ADC) to 400 °C in PCL/Clay(ADC). The enhancements in the degradation temperature with the clay addition were due to strong bonding between the polymer and the clay. The higher degradation temperature recorded for PCL(ADC) compared to PCL(SB) may be ascribed to the presence of the ZnO molecule that prevents degradation. A similar variation was observed by Liufu et al.[338] for polyacrylate/ZnO composites where the addition of 14.3 wt.% ZnO particles increased the degradation temperature of the polymer from 370 °C to 385 °C. The degradation temperatures for the porous materials (Figure 4.7B) appeared to present slightly lower values compared to the non-porous materials presumably because of the degradation of clay surfactants. However, similar to the nanocomposites before foaming the addition of clay enhanced the degradation temperatures of the porous PCL from 355 °C to 396 °C for porous PCL/Clay(SB) and from 380 °C to 387 °C for porous

PCL/Clay(ADC), confirming improvements in thermal properties with the incorporation of clay.

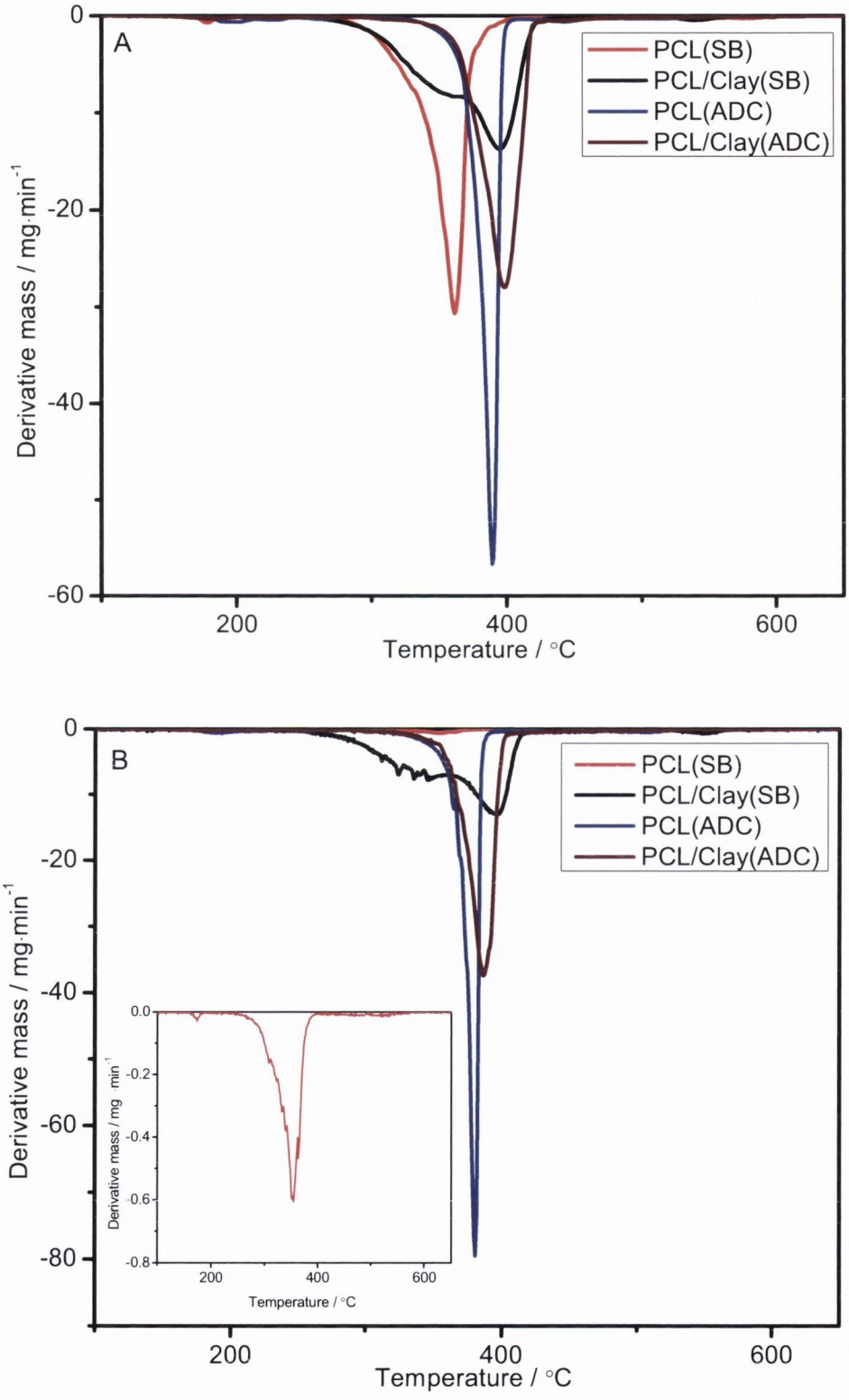

Figure 4.7. DTG curves of PCL and PCL/clay nanocomposites (A) before and (B) after foaming.

4.3.3. Mechanical properties

The compressive moduli and compressive stresses at 10% strain were determined *via* compressive testing performed on the foaming direction for porous PCL and PCL/clay nanocomposites and the results are presented in Table 4.3. The addition of clay exhibited a statistically significant increase in the modulus and stress of the porous polymer by 152% and 177% for ADC, which stems from the strong and stiff clay reinforcing filler, the strong interactions between the polymer and the clay and the reduced degree of crystallinity, porosity and pore size. For SB as the blowing agent, the incorporation of clay increased the compressive stress of the porous PCL by 84% whilst maintaining a similar modulus. The effects of treated organoclays on the mechanical properties of porous PCL are further discussed by eliminating the effects of porosity (density) and plotting the relative modulus-relative density relationships for the porous nanocomposites. The blowing agent used also influenced the compressive properties: the modulus of the porous PCL diminished from 109.8 MPa for sodium bicarbonate to 17.1 MPa for azodicarboxamide due to different porosities and pore sizes formed.

Table 4.3.Compressive properties of porous PCL and PCL/clay nanocomposites

Material	Compressive modulus / MPa	Compressive stress at 10% strain / MPa
PCL(SB) (P)	109.8±31.8	4.3±1.3
PCL/Clay(SB) (P)	92.0±32.7	7.9±4.4
PCL(ADC) (P)	17.1±4.9	1.3±0.4
PCL/Clay(ADC) (P)	43.1±3.3	3.6±0.1

In order to eliminate the effect of density, the specific compressive stress (the ratio of stress to density) and specific modulus (the ratio of modulus to density) were calculated and the results are depicted in Figure 4.8. For ADC-treated organoclay, the specific modulus and specific compressive stress at 10% strain of the porous polymer were found to present statistically significant enhancements of 73% and 69% with the presence of clay. The addition of SB-treated clay exhibited an increase of 72% in the specific compressive

strength. Thus, the improvements observed in the mechanical properties of porous PCL/clay nanocomposites are attributable to the good dispersion of the strong and stiff clay platelets inside the polymer matrix and the smaller pore size.

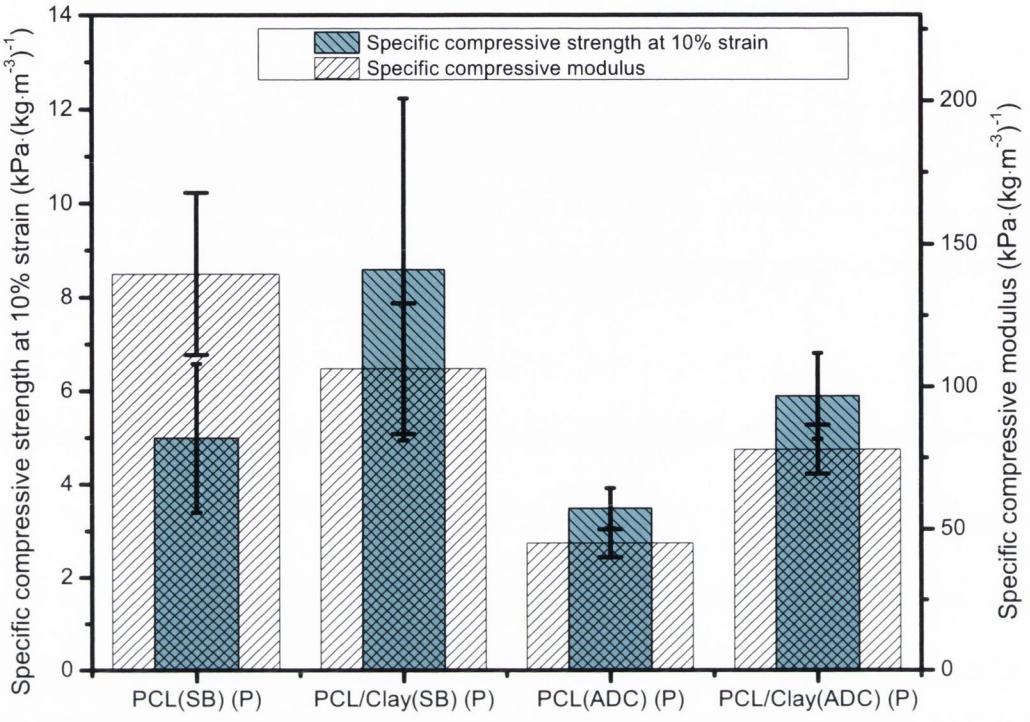

Figure 4.8. Specific compressive modulus and specific compressive stress at 10% strain of porous PCL (The bars represent averages of five measurements; the error bars represent ± one standard deviation).

An enhancement in the compressive modulus of porous PCL/clay nanocomposites was previously reported by Liu et al.[251] who found that by premixing PCL with 5 wt.% DK2 (3.5 wt.% clay platelets)[339] followed by the addition of ADC the modulus of the porous PCL increased by approximately 60%, while the specific compressive modulus presented an increase of close to 10%. At 5.8 wt.% ADC-treated clay (i.e., 2.2 wt.% clay platelets-calculated according to the equations presented in Appendix II), we discovered that by pre-treating the organoclay (C30B containing the same surfactant as that of DK2) with the blowing agent, the compressive modulus increased by 152%, while the specific compressive modulus was enhanced by 69%, compared to the pristine porous PCL(ADC). This showed that pre-treating the clay with the blowing agent led to porous PCL/clay

nanocomposites characterised by a higher degree of exfoliation and a greater decrement in pore size (46% versus 43%),[251] which resulted in superior mechanical properties.

To examine the effect of foam and solid densities and the compressive modulus of the solid materials on the compressive modulus of porous materials, the relative moduli of the porous PCL/clay nanocomposites (compressive modulus for porous material or foam/compressive modulus for solid, E_f/E_s) were determined. A number of closed-cell models, based on Equation 2.26 [175] and transformed to Equation 4.2 for elastic moduli, were tested.

$$\frac{E_f}{E_s} = C_1 (\frac{\rho_f}{\rho_p})^n \tag{4.2}$$

where C_1 is a geometrical constant and n deformation suffered by porous solid.

The moduli for the solid nanocomposites were calculated according to the Mori-Tanaka model[176, 177] and considering a compressive modulus for solid PCL of 324 MPa[340] and a modulus for clay platelets of 230 GPa.[16] The modulus for the solid polymer/clay nanocomposite with fully exfoliated clay platelets that occurred in PCL/Clay(SB) (P) was calculated to be 1360 MPa using the Mori-Tanaka model[176, 177] (Appendix I and Appendix II). An aspect ratio of the reinforcing filler of 75, determined by measuring over 25 clay platelets in the TEM images and considering a 95% confidence interval, and an effective volume fraction of the reinforcing filler,[122] i.e., the exfoliated clay platelets with a fraction of adsorbed polymer molecules behaving like the solid, of 0.06, were used for such calculation.

The modulus for the solid intercalated/exfoliated nanocomposite that occurred in PCL/Clay(ADC) (P) was determined by considering that the nanomaterial included two nanocomposite systems, i.e., intercalated and exfoliated. The intercalated nanosystem was assumed to occur in 25% of the polymer matrix with the exfoliated one distributing in the rest of the matrix, on the basis that the ratio of the number of intercalated platelets to the total number of clay platelets in the nanocomposite was 0.4 and that two platelets made up one intercalated tactoid. The modulus of the solid exfoliated nanocomposite was calculated, according to the Mori-Tanaka model[176, 177] with the application of the effective volume fraction, to be 878 MPa. The modulus of the solid intercalated nanocomposite was determined, using the Mori-Tanaka model[176, 177] and considering the intercalated clay tactoid as the reinforcing filler, as 444 MPa. Using the rule of mixtures, the modulus of the solid intercalated/exfoliated nanocomposite was determined as 769 MPa. Details of these calculations are available in the Appendix II.

By inserting the values of relative density and solid moduli calculated above into Equation 4.2 where C_1 and n differ with various models for closed cells,[289, 292, 341-343] it was found the Mills-Zhu model,[289] described by Equation 4.3, gives the best predictions for the experimental data and was therefore presented in Figure 4.9. Other models tested[288, 289, 292, 341-343] gave unreasonable predictions of the experimental data. The Mills-Zhu model was developed based on Clutton and Rice's data[344] for LDPE and only underestimated the experimental data by 16% for PCL/Clay(SB) (P) and by 43% for PCL/Clay(ADC) (P).

$$\frac{E_f}{E_s} = 0.0807\left(\frac{\rho_f}{\rho_p}\right)^{1.155} \tag{4.3}$$

The predicted results from the normalised Gibson-Ashby model[175, 336, 345] described by Equation 3.3 and used to depict the relative density-relative modulus relationship in low-density polymer/clay nanocomposite foams were also presented in Figure 4.9.

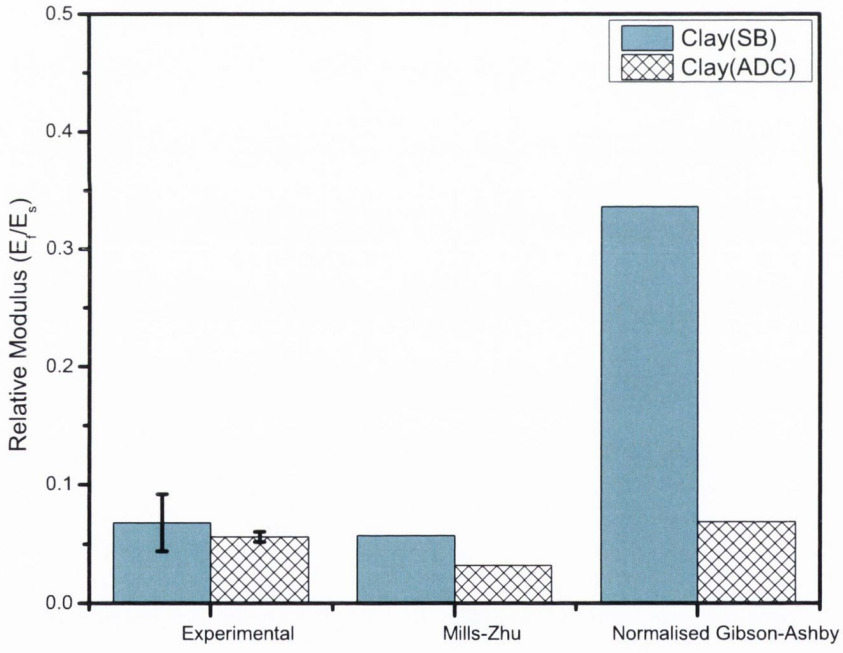

Figure 4.9. Experimental and theoretical data of relative Young's modulus for porous PCL/clay nanocomposites.

For the normalised Gibson-Ashby model[175, 336, 345] the volume fraction of the solid contained in the foam was estimated from the foam and solid densities for each porous material (Table 4.1).[346] This model presented different variations for the treated clays, highly overestimating the experimental datum for PCL/Clay(SB) (P) while only

overestimating the experimental modulus of PCL/Clay(ADC) (P) by 22%. These variations are due to the fact that in porous solids with a porosity lower than 70%,[173] the solid is located both in the edges and in the faces of cells and not mostly in the cell edges as it is expected for low-density foams, with a porosity higher than 95%.[241] As a result, porosity along with cell structure constitutes a key factor in governing the relative density-relative modulus relationships for foams.[175, 336] Thus, it was confirmed that the normalised Gibson-Ashby model that was developed for low-density polymer/clay nanocomposite foams in the previous Chapter may only be applied for foams with porosity higher than 95%.

Overall, the reasonably good agreement between the experimental data and the theoretical values predicted using the Mills-Zhu model[289] suggests that this model can be used to design the mechanical properties of the porous nanocomposites.

4.4. Conclusions

Highly exfoliated porous PCL/clay nanocomposites were prepared using a novel method by inserting the blowing agent into the galleries of an organoclay before nanocomposite formation to render the blowing agent dual roles in the foaming process, i.e., formation of bubbles and facilitation of clay exfoliation. Sodium bicarbonate and azodicarboxamide were used as the blowing agents and their entrance into clay galleries was confirmed by FT-IR. The insertion of the blowing agent into clay galleries prior to foaming improved the exfoliation degree of clay in PCL substantially, as characterised using XRD and TEM, resulting in fully exfoliated PCL/Clay(SB) and highly dispersed PCL/Clay(ADC) porous solids. The addition of clay controlled the nucleation and cell growth, decreasing the pore size by 39-46% and leading to the occurrence of more uniform cell structures.

Thermal analysis results showed that for sodium bicarbonate the crystallinity of the porous PCL increased from 37% to 42.7% due to the nucleating effect of the exfoliated clay platelets, while the degradation temperature increased by 41 °C. Although very small amounts of clay platelets were used, i.e., 2.2 wt.% and 2.9 wt.%; the compressive modulus and stress at 10% strain of the porous polymer were found to increase by up to 152% and 177%, respectively. Eliminating the effect of the density, the specific compressive modulus remained up to 73% higher than that of the porous PCL, while the specific compressive stress at 10% strain improved by up to 69%. The relative density-relative modulus relationship was found to be best described by the Mills-Zhu model for closed cell

structures. These biocompatible porous solids are expected to find applications in biodegradable packaging and carriers of drugs, chemicals and medical and diagnostic devices.

Chapter 5. Structure, thermal and mechanical properties of HDPE/clay micro- and nanocomposites

5.1. Introduction

High density polyethylene is one of the most used polymers. This polymer has become a constant presence in our lives being used in a myriad of areas from packaging materials to pipes, toys and patio furniture to automobile fuel tanks. Polyethylene is characterised by a non-polar character which inhibits the ability of clay to absorb and/or adsorb. In this case, organomodification of the clay surface may not be enough, so in order to achieve the best possible properties in a non-polar polymer/clay composite material, the addition of a compatibilising agent is often necessary. Typically for HDPE, maleated-polyethylene (PEgMA) is used to lower the highly non-polar character of the matrix;[98] however, maleated styrene–ethylene–butylene–styrene (MA-SEBS) has also been used.[185]

The most optimum method to obtain composites and nanocomposites is melt intercalation because it does not involve the use of solvent like solution dispersion does, making this approach environmentally safe, nor does it involve the need to create a specialised production line as is the case of *in situ* polymerisation. For the highly non-polar polymers, e.g. polyethylene, the tedious polymerisation process (i.e., in reactor process involving high temperatures and catalysts or the use of solvents in a slurry process)[347-349] and the restricted solubility (in highly toxic organic solvents, i.e., xylene) make melt compounding the only viable solution to mass produce polymer/clay nanocomposites. Melt intercalation is characterised by the direct mixing of a layered silicate with a polymer in molten state and the intercalation of the polymer between the layers of the silicate.[88] This method is easily adaptable to existing processes like roll-milling, extrusion and moulding.[70]

Previous studies on HDPE had shown that the addition of clay may lead to conventional microcomposites or nanocomposites, depending on the surfactant used to treat the natural clay and compatibiliser.[190] Regardless of the type of clay (i.e., (N-γ-trimethoxylsilanepropyl)octadecyldimethylammonium chloride treated natural clay or dioctadecyldimethylammoinum chloride treated natural clay), the flexural modulus of the material increased with the amount of clay used as the reinforcing agent, whilst the dispersion of (N-γ-trimethoxylsilanepropyl)octadecyldimethylammonium chloride treated natural clay embrittled the HDPE matrix and decreased the impact strength of the

polymer/clay nanocomposites.[190] The dispersion of 3 wt.% esthearildimethylammonium chloride-treated montmorillonite in HDPE was found to slightly increase the tensile modulus while the impact strength was reduced by 23%.[75] Similarly, the dispersion of 4 wt.% organoclay (i.e., Cloisite® 15A) in HDPE led to a 17% increase in the tensile modulus and a 15% reduction in the impact strength.[185]

The current project aims at assessing the type and the optimal amount of clay that is necessary to disperse in a non-polar polymer (i.e., HDPE). The effect of clay addition was assessed by dispersing natural clay (i.e., montmorillonite, MMT) and an organomodified clay (Clay) in HDPE. In order to facilitate the dispersion of clay and ensure intercalation, a compatibilising agent (i.e., PEgMA) was added. The effect of clay type, content and compatibility with the polymer matrix were structurally investigated *via* X-ray Diffraction. The thermal properties of the compatibilised and noncompatibilised polymer and polymer/clay systems were investigated *via* thermogravimetric analysis (i.e., TGA), whilst the mechanical properties were tested *via* tensile and impact testing. The impact fractured surface of the specimens was investigated *via* scanning electron microscopy.

5.2. Experimental Section

5.2.1. Materials

High density polyethylene produced by Dow Plastics (DOW HDPE, Grade: 25055E) was purchased from Resinex (United Kingdom). The HDPE presented a density of 953 $kg \cdot m^{-3}$.[350] The compatibilising agent polyethylene-grafted-maleic anhydride (PEgMA) was purchased from Sigma Aldrich. The maleated compatibiliser presented a density of 925 $kg \cdot m^{-3}$ (manufacturer's data). Natural sodium montmorillonite clay (325 mesh) was generously supplied by Bentonite Performance Minerals LLC (Wyoming Plant, South Dakota, USA). The Clay, i.e., Nanomer® I44.P, a dimethyl dihydrogenated tallow ammonium chloride (2M2HTA) modified montmorillonite, from Nanocor Corporation (Illinois, USA) was kindly supplied by Nordmann, Rassmann GmbH (Hamburg, Germany). The silicate layers content of the clays were determined *via* Loss on Ignition[351] to be 88.6% for MMT and 60% for Clay, whilst the densities were determined at 30 °C on a Micromeritics AccuPyc 1330 pycnometer to be 2616 $kg \cdot m^{-3}$ for MMT and 1605 $kg \cdot m^{-3}$ for Clay. The chemical composition of the MMT was analysed to be SiO_2, 64.12 wt.%; Al_2O_3, 18.92 wt.%; Fe_2O_3, 3.78 wt.%; MgO, 2.29 wt.%; Na_2O, 1.88 wt.%; CaO, 1.19 wt.%; K_2O, 0.44 wt.%; and TiO_2, 0.13 wt.% by using a Panalytical Axios X-Ray

Fluorescence Spectrometer according to ISO 12677 method at CERAM (Stoke-on-Trent, UK).[345] All materials were used as received.

5.2.2. Nanocomposite manufacturing and sample preparation

High density polyethylene and compatibilised HDPE (HDPE/PEgMA=90/10, w/w) with 4 wt.% or 8 wt.% clay platelets content were melt compounded on a twin screw extruder at 150, 160, 165 and 170 °C from hopper to die. The materials were passed at 200 rpm. After cooling in water, the extrudates were pelletized. In order to obtain the specimens for the tensile and impact testing, a bench top injection moulder (Ray Ran model 2 Test Sample Injection Moulding Apparatus, UK) was used at a barrel temperature of 175 °C, a tool temperature of 55 °C and a pressure of 0.55 MPa.

5.2.3. Characterisation

XRD was carried out on a Phillips PW1720 X-Ray Diffractometer with a $CuK_{\alpha 1}$ (λ = 0.15406 nm) anode tube at the standard conditions of 40 kV and 20 mA. The samples were tested from 2° to 10°, 2θ angle, at a step size of 0.02° and a duration of 2.5 seconds per step. Solid samples were used.

SEM imaging was performed on tensile tested surfaces using a Tescan MIra Variable Pressure Field Emission Scanning Electron Microscope at a voltage of 5.0 kV. Prior to being analysed the samples were mounted on stubs and their surface was gold coated.

TGA measurements were performed on a Perkin Elmer Pyrus 1 TGA under nitrogen flow (20 $mL \cdot min^{-1}$), from 30 °C to 650 °C at a heating rate of 10 $°C \cdot min^{-1}$.

The tensile tests were run on an Instron 8501, in accordance with ISO 527-1:1996 Standard, at a load range of 1000 N, and an extensometer with a gauge length of 25 mm. The testing speed was set at 2 $mm \cdot min^{-1}$ up until 8% strain (before yielding) was achieved, moment at which the extensometer was removed and the speed was increased to 50 $mm \cdot min^{-1}$. Four dog bone specimens (Type 1BA) were tested for each of the materials. Impact tests were run according to standard ISO 179:1997 at room temperature on a Charpy impact tester, JinJian XJJD-5, at a speed of 2.9 $m \cdot s^{-1}$ and using a hammer of 0.5 J. Four specimens (80 mm x 10 mm x 4 mm, length x width x thickness) were tested for each batch of materials. Prior to being tested the impact specimens were notched with a type A notch, using a cutter and a milling machine. The mean and standard deviation values

reported for the mechanical tests represent a confidence level of 95%. Statistical significance was assessed by a Two-tailed, Type II 't' test with a chance probability lower than 0.05.

5.3. Results and Discussion

5.3.1. Structure

As observed from Figure 5.1A the dispersion of natural clay in compatibilised and noncompatibilised HDPE does not produce any well defined *(001)* diffraction peaks. The lack of peaks in this area may be attributed to the formation of either highly exfoliated nanostructures or conventional composites, or it may be due to the orientation of the solid disk sample.[8] The highly non-polar character of the HDPE and the strong hydrophilic behaviour of MMT suggested that it was more likely that conventional composites had formed.[119] By dispersing 4 wt.% or 8 wt.% organomodified clay in noncompatibilised HDPE, the *(001)* diffraction peaks were visible (Figure 5.1B). However, these peaks do not present any shifts which would indicate again the formation of conventional composites. The formation of conventional composites in HDPE has been previously reported in literature.[190] This phenomenon has been attributed to the presence of polar hydroxyl groups on the edges of the clay layers and to the highly non-polar character of the polymer matrix.[119, 352] The incompatibility between the polar groups and the non-polar polymer results in repulsion forces between the two species. Thus, clay agglomerates form inside the polymer matrix.

The addition of 4 wt.% Clay in HDPE/PEgMA shifted the *(001)* peak from 3.3° to 2.9°, corresponding to an increase in basal spacing, $d_{(001)}$, from 2.7 nm to 3 nm. Such an increase indicated the formation of an intercalated nanocomposite. The successful generation of nanostructures with the addition of a compatibilising agent was in accordance with the previously reported results and attributed to the compatibilising effect of the PEgMA.[353, 354]

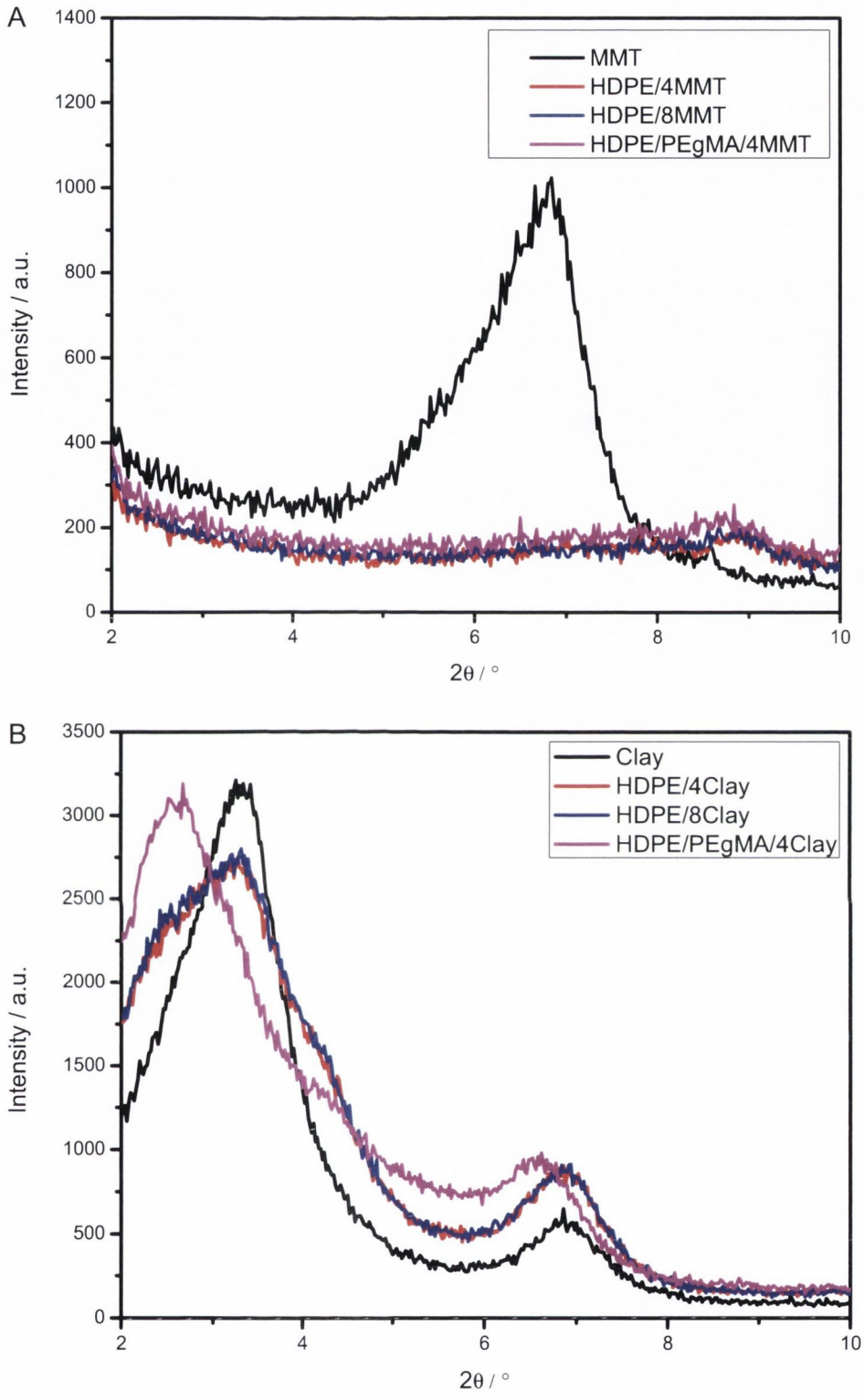

Figure 5.1. XRD diagrams for HDPE: (A) montmorillonite (MMT) and montmorillonite reinforced HDPE and (B) organoclay (Clay) and organoclay reinforced HDPE.

5.3.2. Thermogravimetric analysis

In order to evaluate the effect of the dispersion of natural clay and organoclay in compatibilised and noncompatibilised high density polyethylene polymeric systems, thermogravimetric analysis was performed. Figure 5.2 presents the differential thermogravimetric (DTG) curves that were used to assess the peak degradation temperature (T_d^{peak}) of pristine polymer and compatibilised and noncompatibilised polymer/clay composites and nanocomposites. It is well known that the addition of clay to a polymer system may induce the formation of two distinct effects: catalyst and barrier.[190, 218, 219] The former emerges due to the incompatibility between the clay and the polymer matrix and surfactant degradation where an organoclay is used, whilst the later occurs due to excellent dispersion of the clay which results in strong bonding between the clay and the polymer.[75, 227, 355, 356]

From Figure 5.2 it may be observed that as opposed to the pristine polymer (exhibiting a T_d^{peak} of 491 °C), the addition of clay shifted the peak degradation temperature towards lower values, regardless of the type of clay used or of the presence of PEgMA. This implied that the catalyst effect of the clay was more prominent than the barrier effect of the clay. The catalyst effect exhibited by MMT can be attributed to the agglomeration of clay particles and incompatibility between the filler and the polymer matrix. Similarly, the dispersion of Clay in HDPE presented a catalyst effect due to the agglomeration of clay particles and Hoffman decomposition of the surfactant.[190, 357] The presence of the barrier effect was visible only in the intercalated nanocomposite, where the T_d^{peak} increased from 466 °C in HDPE/PEgMA to 480 °C in HDPE/PEgMA/4Clay. Thus, the presence of a compatibiliser and the dispersion of organoclay resulted in intercalated nanostructures with improved interactions between the clay and polymer matrix which facilitated the barrier effect of the Clay. These findings are in good agreement with the previously reported literature.[190]

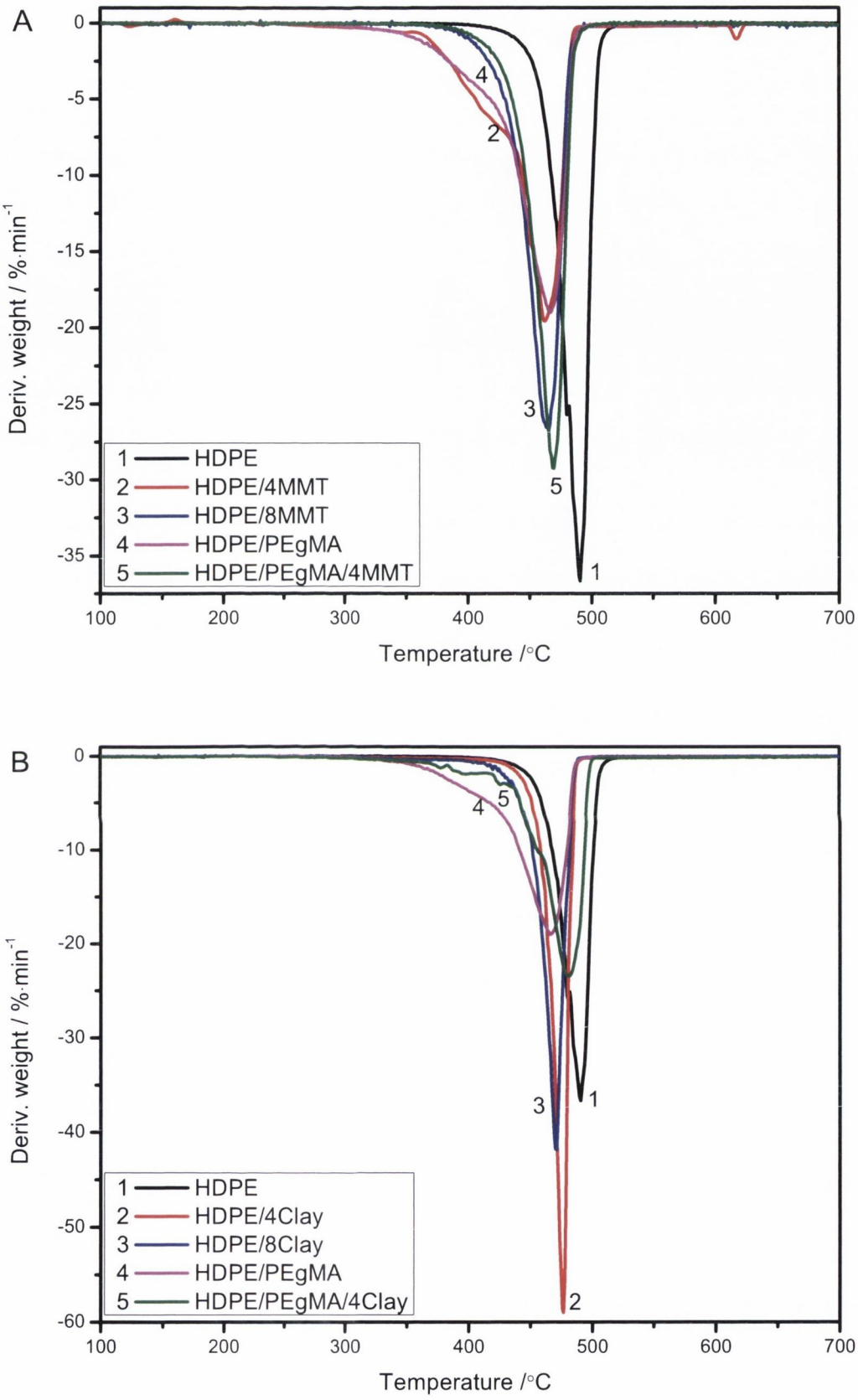

Figure 5.2. Differential thermogravimetric curves for pristine HDPE and HDPE/PEgMA and compatibilised and noncompatibilised HDPE/clay nanocomposites.

5.3.3. Mechanical properties

The dispersion of 4 wt.% or 8 wt.% natural clay (i.e., MMT) in HDPE resulted in 9-11% statistically significant increase in the Young's moduli (Figure 5.3). Using the same polymer matrix, the dispersion of organoclay led to statistically insignificant enhancements in the elastic moduli. The dispersion of Clay in the compatibilised HDPE resulted in a similar statistically significant enhancement of the Young's moduli compared to the HDPE/PEgMA system, whilst the elastic modulus of HDPE/PEgMA/4MMT remained similar to the one of the polymer matrix. Thus, the presence of a compatibilising agent in a highly non-polar polymer matrix improved the stiffness as opposed to the HDPE/PEgMA system and presumably owing to the dispersion of organoclay and the formation of intercalated nanostructures. The improvement in the Young's modulus exhibited by the microcomposites and nanocomposites as opposed to the neat polymers was due to the presence of the clay particles and clay platelets which are characterised by higher moduli than the polymer.

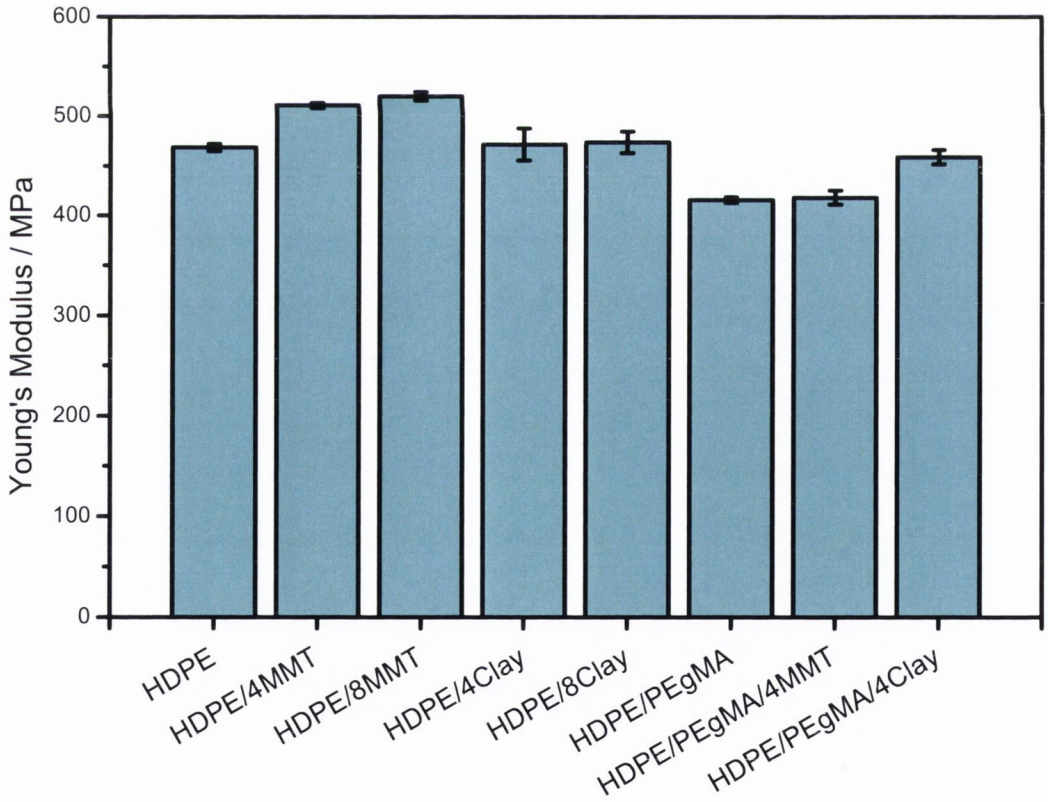

Figure 5.3. Young's modulus for neat polymer, compatibilised polymer, compatibilised and noncompatibilised polymer/clay systems (The bars represent averages of four measurements; the error bars represent ± one standard deviation).

The toughness of the neat polymer materials and polymer/clay composites and nanocomposites was investigated *via* Charpy impact testing and the results were depicted in Figure 5.4. The presence of natural clay or organoclay led to 18-40% statistically significant reductions in the impact strength. Although for the HDPE/MMT system the toughness does not present significant variations with the augmentation of the clay content, the use of an organoclay led to a 14% reduction in the impact strength of the polymer/clay microcomposites with the increase in the clay load for 4 wt.% to 8 wt.%. This suggested that the 4 wt.% clay content is optimal for reinforcing polymer/clay materials, which is in good agreement with the previous literature observations.[13]

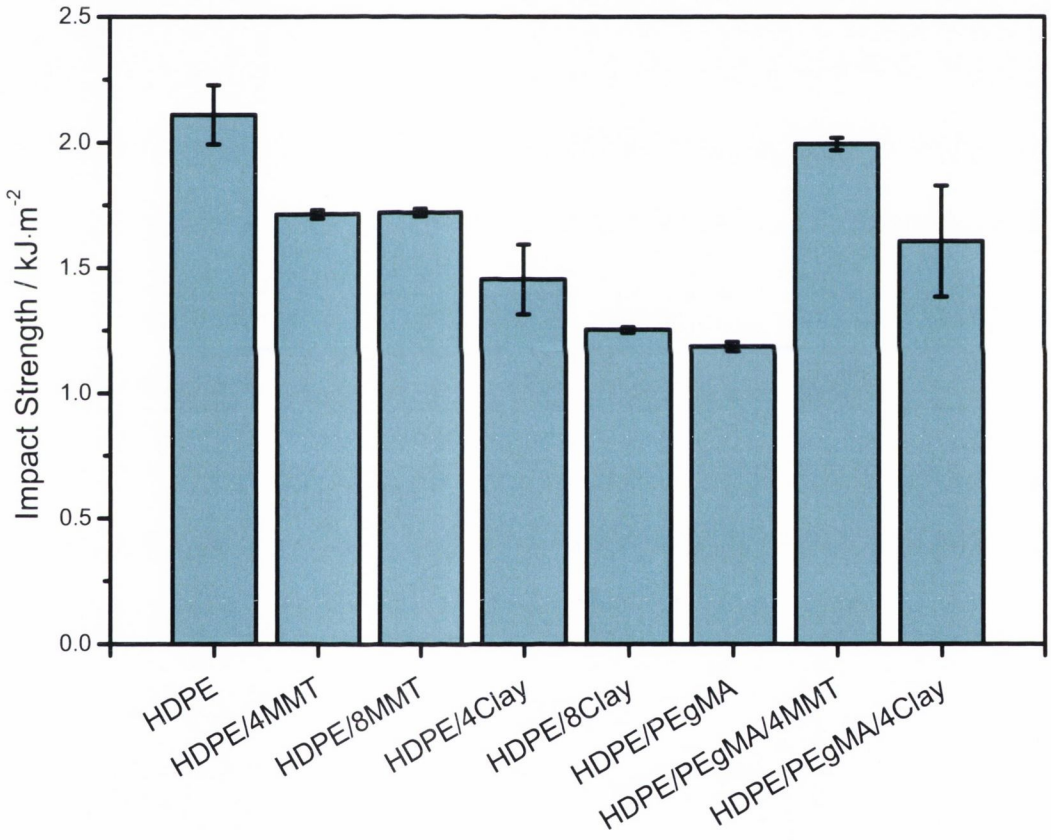

Figure 5.4. Impact strength for neat polymer, compatibilised polymer, compatibilised and noncompatibilised polymer/clay systems (The bars represent averages of four measurements; the error bars represent ± one standard deviation).

The impact strength of HDPE/PEgMA/4MMT and HDPE/PEgMA/4Clay decreased, without statistical significance, as opposed to pristine HDPE. Comparing the impact strength of the compatibilised polymer/clay composite systems with HDPE/PEgMA, the

toughness of the materials increased with statistical significance by 35-68%. This demonstrated the necessity of using a compatibilising agent when dispersing organoclay clay in the non-polar polymer matrix. These results are different from the previously reported impact strength data for HDPE compatibilised with 10 wt.% maleated styrene–ethylene–butylene–styrene system,[185] where the addition of 4 wt.% organoclay (i.e., Cloisite® 15A) produced intercalated nanocomposites and led to a 44% decrease in the impact strength compared to the HDPE/MA-SEBS.

5.3.4. Surface analysis

In order to clarify the variations observed in the mechanical properties the impact fractured surfaces of the considered polymer systems were analysed *via* SEM (Figure 5.5). The fractured surface of pristine HDPE presented a vein-type pattern with small fibrils (Figure 5.5A), whilst the addition of the maleated component led to a slightly smoother surface, which implied a faster breaking (Figure 5.5B). These results are in good agreement with the impact strength determined *via* Charpy impact test (Figure 5.4).

The dispersion of natural clay in noncompatibilised HDPE led to the formation of fractured surfaces in which clay agglomerations and dislocations (Figure 5.5C and Figure 5.5E) were encountered. The clay agglomerates presented a size of approximately 5 μm in HDPE/4MMT and increased their dimensions with the augmentation of the clay load (approximately 7 μm). HDPE/Clay composites presented slightly more uniform fracture surfaces and well defined fibrils (Figure 5.5D and 5.5F), which corresponded to better dispersion of the clay particles.[358] Still, even in this a case few agglomerates were observed; however, their dimensions (approximately 1.5 μm) remained unchanged after the augmentation of the clay load. Typically, the presence of fibrils may imply a lower crack propagation speed, whereas, the agglomeration of clay may alter the crack propagation path, thus increasing the amount of energy adsorbed during the fast fracturing process. The presence of the maleated component resulted in homogeneous fracture surfaces with vein-type pattern and terraced aspect (Figure 5.5G) and fibrils (Figure 5.5H). The terraced aspect, combined with the vein-type pattern and the fibrils observed for the HDPE/PEgMA/Clay compared to HDPE/PEgMA which showed a smoother surface, are in good agreement with the enhancements observed in the impact strength (Figure 5.4). This again emphasised the necessity of using a maleated component as a compatibilising agent in order to facilitate the dispersion of clay in a highly non-polar polymer matrix.

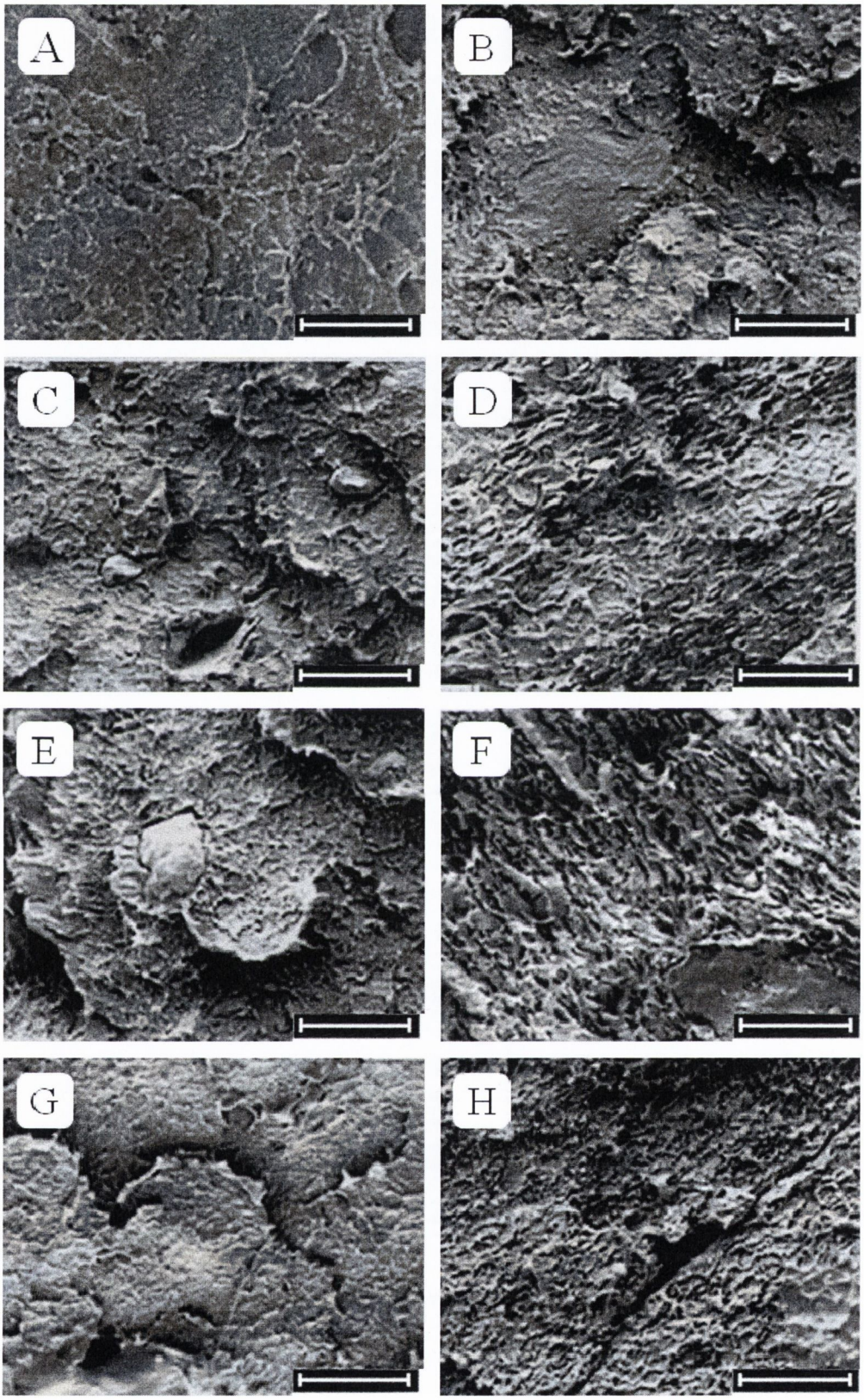

Figure 5.5. SEM images of impact fracture surfaces: A. HDPE, B. HDPE/PEgMA, C. HDPE/4MMT, D. HDPE/4Clay, E. HDPE/8MMT, F. HDPE/8Clay G. HDPE/PEgMA/4MMT and H. HDPE/PEgMA/4Clay (Scale bar: 10 μm).

5.3.5. Elastic modulus-volume fraction relationships

The changes in the modulus of polymer/clay composites and nanocomposites with the addition of clay in polymer matrices are of great significance for the fundamental scientific understanding and design of engineering materials. To better assess the variation in the elastic modulus and the clay content, the volume fraction of clay was taken into consideration. As it was revealed from the XRD traces (Figure 5.1), the dispersion of MMT in compatibilised and noncompatibilised HDPE and the dispersion of organoclay in noncompatibilised HDPE resulted in conventional composites, whilst the dispersion of Clay in compatibilised HDPE led to intercalated polymer/clay nanocomposites. The structure-property relationship for microcomposites and nanocomposites was characterised by considering two classical composite material theories: the Halpin-Tsai[15, 178] equations and the lower bounds of the Hashin–Shtrikman model.[359]

Case 1. Conventional composites. The highly non-polar character of HDPE obstructed the delamination of the clay particles, which resulted in the formation of conventional composites, regardless of the type of clay dispersed. Also, the dispersion of natural clay in HDPE/PEgMA resulted in conventional composites, due to the hydrophilic character of the natural clay, the highly non-polar polymer matrix and the limited amount of maleic anhydride that was available in the system. For the conventional polymer/clay composite the volume fraction of reinforcing agent was calculated according to Equation 2.8.[122] The volume fractions of clay particles in the composite were determined to be: 0.018 and 0.039 for 4 wt.% and 8 wt.% clay platelets in MMT dispersed and 0.044 and 0.097 for 4 wt.% and 8 wt.% clay platelets in Clay dispersed. The volume fraction of clay particles in HDPE/PEgMA/4MMT was calculated according to Equation 2.8 [122] to be 0.018.

By inserting the volume fractions in the Halpin-Tsai model[178] with the van Es correction[15] and the lower bound of the Hashin-Shtrikman model[359] the theoretical moduli for HDPE/clay composites were calculated. The modulus of natural clay particles was taken as 14 GPa,[16] whilst the modulus of organoclay particles was determined[122, 174, 175, 360, 361] to be 82.8 GPa. The Poisson's ratio was taken as 0.28 [122] for clay and 0.45 [350] for HDPE and HDPE/PEgMA. For HDPE and HDPE/PEgMA the elastic modulus was taken from Figure 5.3. The experimental and theoretical elastic moduli are displayed in Figure 5.6. The pronounced variations in the elastic moduli presented by the theoretical values

compared to the experimental data are a consequence of the limited exposure of the clay particles. Thus, the models do not account fully for the uneven distribution of clay particles in the polymer matrix and/or for the formation of clay agglomerates which were observed *via* SEM (Figure 5.5). However, the experimental data for the conventional composite models were found to agree reasonably well with theoretical values from the lower bound of the Hashin-Shtrikman model,[359] presenting an accuracy of up to 77-99%.

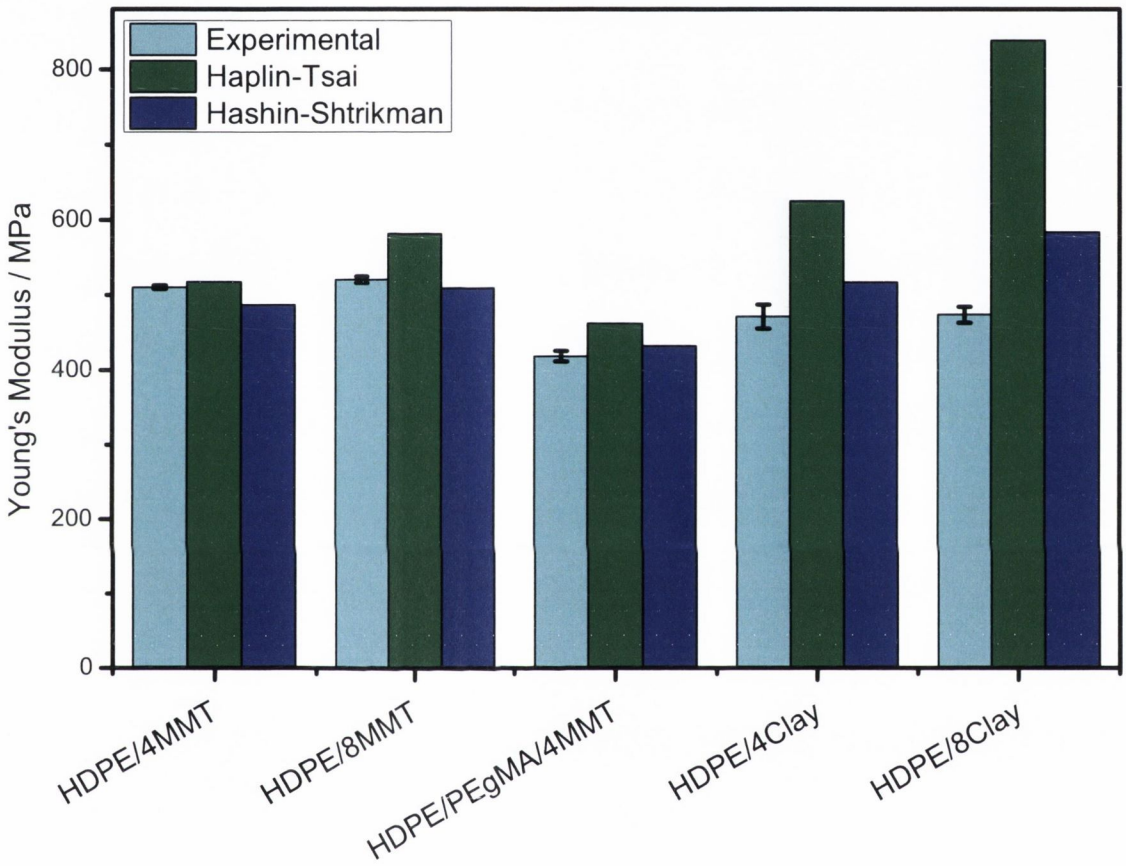

Figure 5.6. Experimental and theoretical elastic moduli for compatibilised and noncompatibilised HDPE/clay composites (The bars for the experimental results represent averages of four measurements; the error bars represent ± one standard deviation).

Case 2. Intercalated nanocomposites. The dispersion of organoclay in the presence of the compatibilising agent led to the formation of intercalated polymer/clay nanocomposites. In this case, the reinforcement was represented by clay tactoids. In order to calculate the elastic modulus of the reinforcement, the intercalated tactoids were considered as a sandwich-type composite in which the surfactant and the polymer

molecules presented as a porous structure in the gallery.[122] The volume fraction of reinforcement was calculated to be 0.049 according to Equation 2.15 and considering that a large number of clay platelets made up the clay tactoid which represented the reinforcement. The modulus of the clay tactoid was calculated to be 75 GPa, according to literature[122, 174, 362] and by considering an elastic modulus of the clay platelets of 230 GPa.[16] By inserting the volume fraction of the reinforcement in the Halpin-Tsai model[178] with the van Es correction[15] and the lower bound of the Hashin-Shtrikman model[359] the theoretical moduli for HDPE/PEgMA/Clay nanocomposites were calculated and the results were depicted in Figure 5.7.

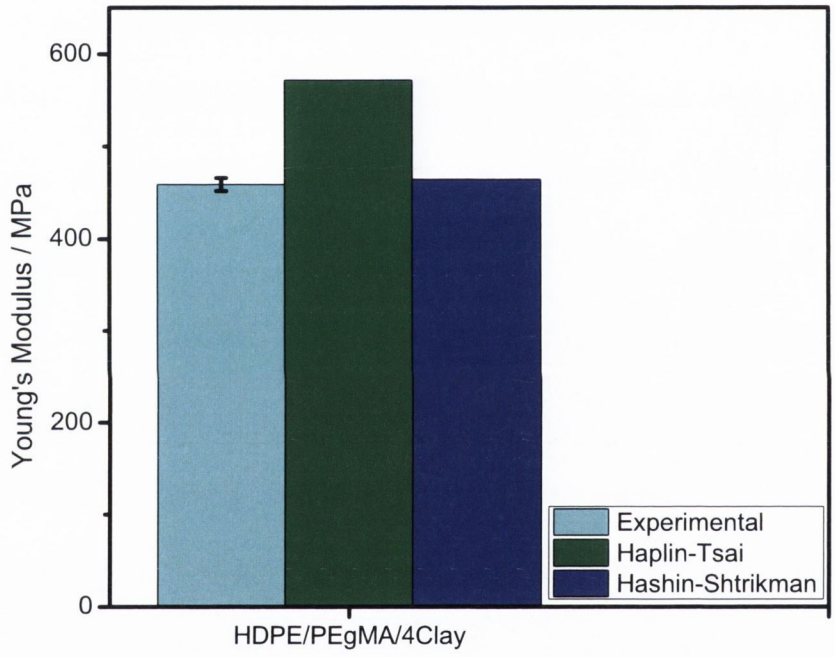

Figure 5.7. Experimental and theoretical elastic moduli for HDPE/PEgMA/Clay nanocomposites (The bar for the experimental result represents the average of four measurements; the error bar represents ± one standard deviation).

The experimental moduli for HDPE/PEgMA/Clay nanocomposites was best described by the lower bound of the Hashin-Shtrikman model,[359] presenting a 99% accuracy. The good agreement of the Hashin-Shtrikman model[359] with the experimental datum attested once again to the necessity of considering the effective volume fraction of the reinforcement in nanocomposites.

5.4. Conclusions

Polymer/clay microcomposites and nanocomposites were prepared by melt compounding natural clay or organoclay with compatibilised and noncompatibilised high density polyethylene. The presence of natural clay in compatibilised and noncompatibilised HDPE and the dispersion of clay in noncompatibilised HDPE led to conventional composites. Compared to pristine HDPE, the microcomposite materials exhibited reduced peak degradation temperature due to the presence of agglomerates and/or the degradation of the surfactant. However, the polymer/clay nanocomposites obtained by dispersing organoclay in a compatibilised HDPE matrix, presented increased peak degradation temperature due to strong bonding between the clay tactoids and the maleated polyethylene present in HDPE.

The stiffness of the HDPE/MMT microcomposites increased with the augmentation of the clay content, whilst it remained relatively unchanged when organoclay was dispersed. However, the toughness of the HDPE/Clay microcomposites decreased when the clay content was increased from 4 wt.% to 8 wt.%. This indicated that 4 wt.% represented the optimal clay load. The dispersion of 4 wt.% natural clay or organoclay in compatibilised HDPE resulted in up to 10% stiffness enhancement and up to 68% toughness improvement compared to HDPE/PEgMA. The structure-property relationship was described by the lower bound of the Hashin-Shtrikman model for the microcomposites (with 77-99% accuracy) and the nanocomposite (with 99% accuracy).

The formation of intercalated polymer/clay nanocomposites and the improvements in the thermal and the mechanical properties showed the importance of using compatibilising agents and organomodified clay for highly non-polar polymer matrices, such as HDPE.

Chapter 6. Preparation of polystyrene/clay composites of different morphologies cationic, anionic or non-ionic surfactants

6.1. Introduction

Polystyrene is a commodity plastic that is a constant presence in our lives, from food containers to CD cases to refrigerators and air conditioners. Depending on the tacticity that the polystyrene polymer chain adopts, there are three main types of polystyrene: isotactic, syndiotactic and atactic (Figure 6.1). Polystyrene is manufactured *via* free radical polymerisation for atactic polystyrene or *via* transition metal catalysed polymerisation (e.g. Ziegler-Natta catalyser) for isotactic and syndiotactic polystyrene.[363] The atactic polystyrene is an amorphous polymer that is considered a glassy thermoplastic commodity polymer and has been on the market since 1925. Unlike atactic polystyrene, isotactic and syndiotactic polystyrenes are semicrystalline polymers that emerged on the market in the last 50 years. Since most of the market is covered by atactic polystyrene, the amorphous character of this polymer make it an unique candidate for fundamental studies without considering the effect of the clay on the polymer crystallinity.[136, 364] However, the low-polarity of this polymer matrix obstructs the dispersion and the separation of the hydrophilic natural clay into individual clay layers.[365, 366] Using different natural clays or organoclays and synthesis methods, polystyrene/clay conventional composites and nanocomposites with intercalated or exfoliated nanostructures have been reported in the literature and were recently comprised in a detailed review.[56] To the day, the manufacturing of polystyrene/clay nanocomposites typically involves the organomodification of natural clay *via* cation exchange[367] or the insertion of a monomer inside the basal spacing of the clay.

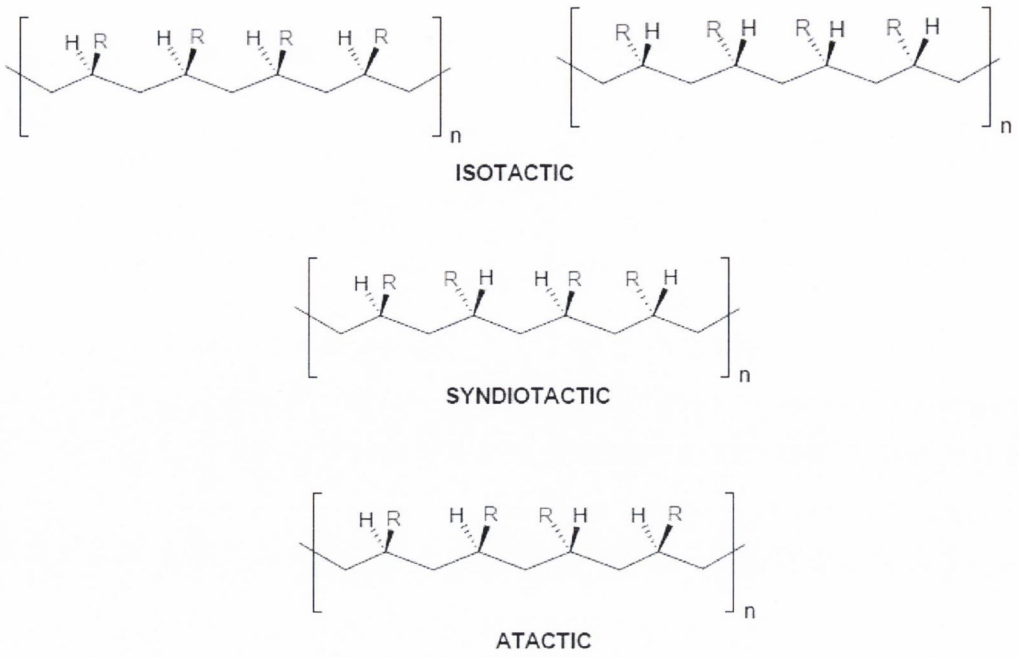

Figure 6.1. Types of tacticity of polystyrene (R= Phenyl ring).

There are a myriad of organoclays available on the market, but is there such one that is most appropriate for a PS matrix? Is there a facile method of obtaining PS/clay nanocomposites with superior mechanical and thermal properties? To address these issues three surfactants have been chosen: a typically anionic surfactant based on phosphate ester, a cationic surfactant with an ammonium compound and a non-ionic surfactant based on nonylphenol. These are all common types of surfactants that were selected for the high hydrophobic character. A surfactant is characterised by a hydrophilic and a hydrophobic part, which makes this chemical species a potential candidate for the treatment for natural clay and for obtaining polymer/clay nanocomposites. Although there are a number of studies on different surfactants, a systematic study where cationic, anionic and non-ionic surfactants have been used to treat a natural clay for preparation and investigation of polymer/clay nanocomposites is missing. The aim of this project was to investigate the most appropriate surfactant and treatment approaches to obtain polymer/clay nanocomposites. In this regard, three distinct methods were used to disperse the clay: 1) dispersion of natural clay in water in order to create a slurry, 2) organomodification of the natural clay with cationic or anionic surfactants and 3) simultaneous melt compound mixing of the polymer and the clay in the presence of a non-ionic surfactant. For comparison reasons, polymer/natural clay microcomposites were also prepared. The structure and thermal and mechanical properties were assessed for the polymer/clay conventional composites and nanocomposites. The structural characterisation was performed *via* X-ray diffraction and transmission electron microscopy. The thermal

properties were investigated *via* thermogravimetric analysis, whilst the mechanical properties were tested *via* tensile and impact testing. The impact fractured surface of the specimens was investigated *via* scanning electron microscopy.

6.2. Experimental Section

6.2.1. Materials

Polystyrene (DOW STYRON, Grade: 634), from DOW Plastics with a density of 1050 $kg \cdot m^{-3}$, was purchased from RESINEX (UK). Natural sodium montmorillonite clay (325 mesh) was generously supplied by Bentonite Performance Materials LLC (Wyoming Plant, South Dakota, USA). The inorganic content of the clay (CEC 105 meq per 100g) was determined as 88.6%.[345] The chemical composition of the clay was described in Chapter 3. Surfactants: bis(hydrogenated tallow alkyl) dimethyl ammonium compound, nonylphenol ethoxylate and a mixture of phosphate esters in alcohol ethoxylate were generously supplied by Akzo Nobel Surface Chemistry (Stenungsund, Sweden). The quaternary ammonium compound, Arquad 2HT-75 (DHTDMAC), with the general formula $[R\text{-}N(CH_3)_2\text{-}R]^+Cl^-$ where R represents the tallow, is a cationic surfactant. Arquad 2HT-75 is a tallow based chloride in an isopropanol-water mixture with M_w=573.5 and a density of 880 $kg \cdot m^{-3}$. The mixture of mono- and diphosphate esters based on alcohol ethoxylate in acid form, Phospholan PE 169, is an anionic surfactant with a density of 1040 $kg \cdot m^{-3}$. The nonylphenol ethoxylate, Ethylan HA, is a non-ionic surfactant with a density of 1064 $kg \cdot m^{-3}$. All the materials were used as received.

6.2.2. Clay treatment

Montmorillonite solutions were prepared by dispersing clay platelets in distilled water at 80 °C for three hours in order to obtain 2.5% solutions of clay. The solutions were then sonicated, at room temperature, using a probe ultrasonicator UP 200S (power 200 W frequency 24 kHz) from Hielscher Ultrasonics GmbH (Germany) for 45 minutes in order to obtain montmorillonite gels (denoted as MMT-gel).

MMT modified with bis(hydrogenated tallow alkyl)dimethyl ammonium compound (denoted as MMT-AQ) was obtained by first creating a MMT solution and a surfactant solution. MMT (1 wt.%) was dispersed in distilled water at 80 °C for 6.5 hours. A 5%

solution of quaternary ammonium compound in distilled water was prepared by mixing the surfactant at 40 °C for 3.2 hours. After the MMT solution was cooled, the surfactant mixture was added, under constant stirring. The mixture was kept under constant stirring at 40 °C for 3.2 hours and then ultrasonicated for 1.6 hours. A flocculated solution was obtained which was left to settle in the fume cupboard for 36 hours. The solution was then filtrated on a Bruckner funnel coupled with a vacuum pump. The clay paste was put in a Petri dish and dried in the oven at 80 °C for 6 hours. The dried bis(hydrogenated tallow alkyl) dimethyl chloride-treated montmorillonite was then grinded and kept in a desiccator until use.

In order to obtain the MMT modified with Phospholan (MMT-P) three steps were necessary. First the anionic surfactant was dissolved in ethanol, under constant stirring at room temperature, for 1 hour. Simultaneously, MMT was dispersed in distilled water (1:30, w:w) at room temperature for 1 hour. The surfactant solution was then added to the MMT solution and the mixture was stirred for 5 hours at room temperature and subsequently ultrasonicated for 90 minutes. The solution was left to settle at room temperature in the fume cupboard overnight and then washed with distilled water. The supernatant was then decanted and the modified clay was transferred to a Petri dish and heated in the oven for 6 hours at 60 °C. The dried phospholan-treated montmorillonite was grinded into a fine powder and kept in a desiccator until use.

6.2.3. Preparation of polymer/clay nanocomposites

Polystyrene with 4 wt.% or 8 wt.% clay platelets of MMT (denoted as PS/4MMT and PS/8MMT), MMT-gels (denoted as PS/4MMT-gel and PS/8MMT-gel) or MMT-AQ (denoted as PS/4MMT-AQ and PS/8MMT-AQ) and 4 wt.% clay platelets MMT-P (denoted as PS/4MMT-P) were prepared on a Prism twin screw extruder (UK) with 16 mm diameter screws and a length to diameter ratio of 25. The operating temperature of the extruder was maintained at 160, 165, 175, and 180 °C from hopper to die. The screw speed was preset at 200 rpm. Polystyrene with 4 wt.% clay platelets of MMT was directly mixed with 5.3 wt.% Ethylan HA Powder (MMT-E), in the previously mentioned conditions, the resulting materials was denoted as PS/4MMT-E. In order to assure that the materials have been properly mixed PS with MMT-AQ, MMT-E and MMT-P were passed through the extruder a second time, using the same processing conditions.

6.2.4. Characterisation

X-ray Diffraction was carried out on a Phillips PW1720 X-Ray Diffractometre with a $CuK\alpha_1$ (λ=0.15406 nm) anode tube at the standard conditions of 40 kV and 20 mA. The samples were tested from 2° to 10°, 2θ angle, at a step size of 0.02° and duration of 2.5 seconds per step. Powder samples were used.

Transmission Electron Microscopy was performed on a TECNAI G2 20 Twin electron microscope at 200 kV. The specimens were ultramicrotomed using a Reichert–Jug 'Ultracut' equipped with a diamond knife. The sections (~100 nm in thickness) were collected in a trough filled with water and placed on a 200 mesh copper grid.

Fourier Transformed Infrared Spectroscopy spectra were performed on a FT-NIR instrument (Perkin Elmer Spectrum One NTS) equipped with ATR Sampling Accessory. The samples were run from 650 cm^{-1} to 4000 cm^{-1} at a resolution of 2 cm^{-1}.

Scanning Electron Microscopy imaging on tensile fractured surfaces was performed using a Zeiss Ultra Scanning Electron Microscope at a voltage of 5.0 kV. Prior to being analysed the samples were mounted on stubs and their surface was gold or platinum coated.

Thermal Gravimetric Analysis was performed on a Perkin Elmer Pyrus 1 TGA equipped with an ultra-micro balance with a sensitivity of 0.1 µg, under nitrogen flow (20 $mL \cdot min^{-1}$), from 100 °C to 650 °C at a heating rate of 10 $°C \cdot min^{-1}$.

Tensile and impact specimens were obtained with a bench-top injection moulder (Ray Ran model 2 Test Sample Injection Moulding Apparatus, UK) which was used at a barrel temperature of 210 °C, a tool temperature of 55 °C and a pressure of 0.76 MPa. The tensile tests were carried, at room temperature, on a Zwick Z005 machine according to ISO 527:1993. The tests were performed using a 2.5 kN load cell and a cross head speed of 1 $mm \cdot min^{-1}$. Six dog bone specimens (Type M-II) were tested for each of the materials. Impact tests were run according to standard ISO 179:1997 at room temperature on a Charpy impact tester (JinJian XJJD-5, China) at a speed of 2.9 $m \cdot s^{-1}$ and using a hammer of 0.5 J. Six specimens (80 mm x 10 mm x 4 mm, length x width x thickness) were tested for each batch of materials. Prior to being tested the impact specimens were notched with a type A notch, using a 45° cutter and a milling machine. The mean and standard deviation values reported for the mechanical tests represent a confidence level of 95%. Statistical significance was assessed by a Two-tailed, Type II 't' test with a criterion that the probability of a difference in means due to chance is less than 0.05.

6.3. Results and Discussion

6.3.1. Structure

As observed from Figure 6.2, natural clay, MMT presented a well defined peak at a 2θ value of 7.1°, which corresponded to a basal spacing, $d_{(001)}$, of 1.2 nm. By treating the clay with an anionic surfactant, i.e., diphosphate ester, the *(001)* diffraction peak shifted to a lower 2θ value of 5°. Thus, the basal spacing, $d_{(001)}$, increased from 1.2 nm to 1.8 nm, which suggested that the surfactant had intercalated inside the gallery of the natural clay. Similarly, by treating the clay with a cationic surfactant, i.e., quaternary ammonium compound, the *(001)* peak of the natural clay shifted to a 2θ value of 3.2°, corresponding to a $d_{(001)}$ value of 2.8 nm. This also suggested that the surfactant had intercalated inside the clay gallery. The higher increase in the basal spacing of the natural clay when the cationic surfactant was used instead of the anionic surfactant indicated that the natural clay had a higher affinity for the former than for the latter surfactant, which is in good agreement with the previous literature findings.[125]

In order to confirm that the cationic and the anionic surfactants have penetrated inside the gallery of clay, FT-IR analysis was performed (Figure 6.2). By modifying the MMT, the Si-O-Si stretching band[368, 369] in the natural clay shifted from 996 cm^{-1} in neat MMT to 1009 cm^{-1} in MMT-P and to 1010 cm^{-1} in MMT-AQ. These positive shifts were due to hydrogen bonding between the Si-O of the clay and the carbonyl groups of surfactants.[370] This suggested that the silanol absorption band has modified and that the cationic and anionic surfactants had intercalated inside the clay gallery.[329, 371] This is in good agreement with the negative shift in the 2θ observed *via* XRD (Figure 6.2) which indicated the enhancement of the basal spacing.

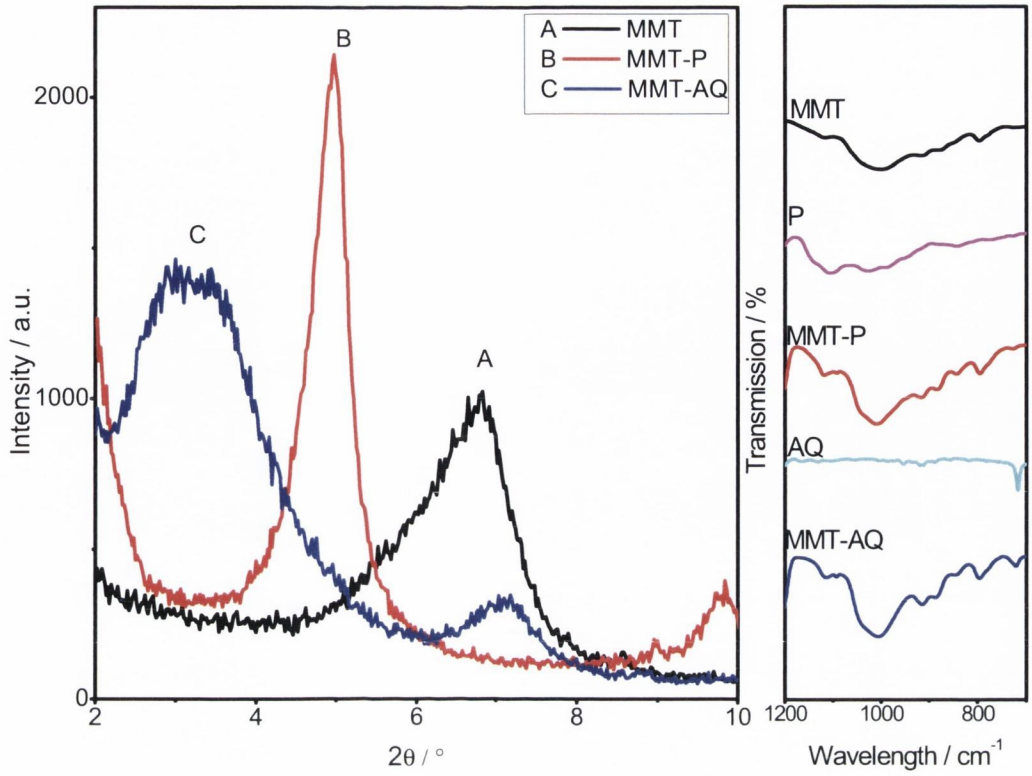

Figure 6.2. XRD (left) and FT-IR (right) profiles of natural clay: A. MMT and organoclays: B. MMT-P and C. MMT-AQ. P and AQ from the FT-IR spectra denote the diphosphate ester anionic surfactant and quaternary ammonium cationic surfactant, respectively.

The structure of clay in PS was evaluated *via* XRD (Figure 6.3). As observed from Figure 6.3A, by dispersing a cationic surfactant-treated clay in the low-polarity PS matrix, the *(001)* diffraction peak exhibited by the treated clay at 3.2° (Figure 6.2, Curve C) disappeared in PS/4MMT-AQ (Curve 1) and shifted to 2.7° in PS/8MMT-AQ (Curve 2). Since the augmentation of the clay content presented a shift in the *(001)* peak towards a lower 2θ value which implied the presence of intercalated nanostructures, it is reasonable to assume that PS/4MMT-AQ presented exfoliated or intercalated/exfoliated nanostructures. To clarify the type of structure, TEM imaging was performed and will be sequentially discussed. The dispersion of an anionic surfactant-treated MMT in PS led to an insignificant shift in the 2θ peak, which indicated the formation of conventional composites (Figure 6.3, Curve 3). Since no additional increase was observed, it may be possible that the clay platelets with surfactant intercalated inside the gallery did not allow the polymer to penetrate inside. The direct mixing of the non-ionic surfactant with PS shifted the *(001)* peak of the MMT from a 2θ value of 7.1° to 5° (Figure 6.3, Curve 4).

This indicated that the shear forces produced during the extrusion process facilitated the intercalation of the non-ionic surfactant and may have also allowed the entrance of the low-polarity polymer inside the gallery.

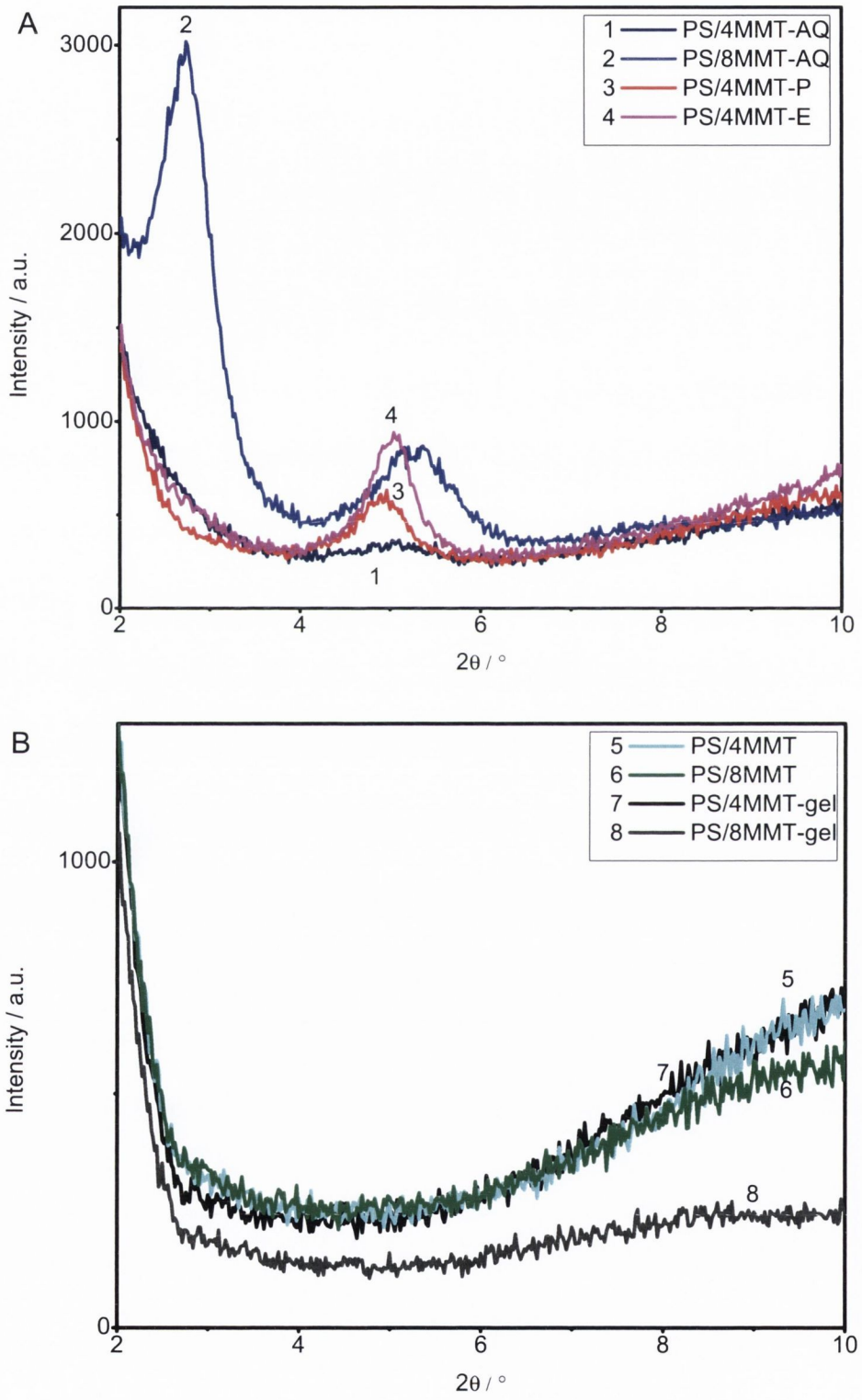

Figure 6.3. XRD profiles of: A. PS/treated-natural clay and B. PS/natural clay composites and nanocomposites.

In order to establish the contribution of the surfactants in the PS/MMT systems, PS/MMT and PS/MMT-gel, with 4 and 8 wt.% clay platelets, were also XRD analysed and the results were depicted in Figure 6.3B. As observed the dispersion of MMT or MMT-gel does not present any *(001)* diffraction peaks. This suggested the possibility of obtaining fully exfoliated nanostructures or the disappearance of the *(001)* peak might arise from uneven distribution of the low-content clay. Taking into consideration that the slurry process used to manufacture PS/MMT-gel has proven successfully in nanocomposite formation for other polymers,[28, 29] the type of composite structure formed was investigated further *via* TEM.

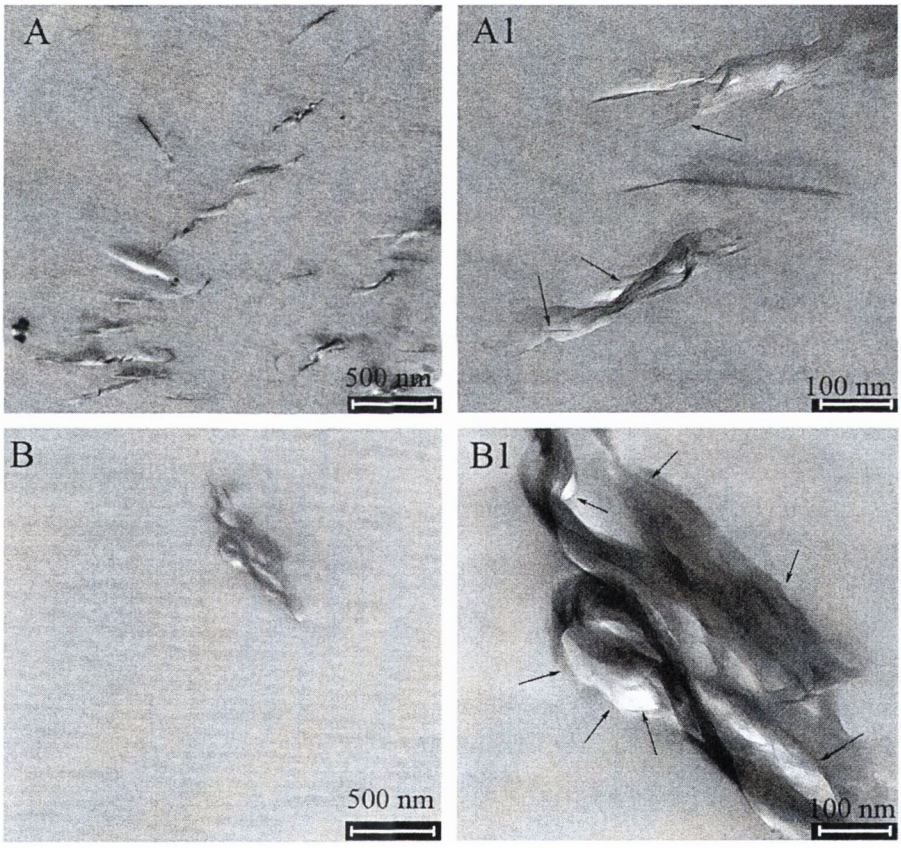

Figure 6.4. Low and high magnification TEM images of A. PS/4MMT-AQ nanocomposites (the arrows indicate single clay platelets) and B. PS/4MMT-gel composites (the arrows indicate intercalated clay tactoids).

The high and low magnification TEM images for polystyrene/DHTDMAC-treated montmorillonite nanocomposite exhibited intercalated and exfoliated nanostructures (Figure 6.4A and Figure 6.4A1). The higher magnification image presented

intercalated/exfoliated nanostructures; however, most of the nanostructures presented as intercalated tactoids (Figure 6.4A1, the arrows indicated single clay platelets). The low magnification image for PS/4MMT-gel (Figure 6.4B) showed an isolated clay tactoid which suggested sporadic dispersion of the filler. Although previous studies on nylon 6 have gone as far as suggesting full exfoliation of the clay platelets,[28, 29] the dispersion of 4 wt.% MMT-gel in PS led to mostly conventional composites and a few clay tactoids (indicated by arrows in Figure 6.4B1). Even though the clay platelets were exfoliated in water before processing the water slurry method was not viable for a low polarity polymer such as PS. This indicated that this type of nanocomposite manufacturing would only work for hydrophilic polymer matrices. Using a low polarity polymer matrix such as PS polymer/clay nanocomposites may be obtained when the clay has been cation exchanged. Thus, the dispersion of cationic surfactant-treated natural clay in PS resulted in mostly intercalated polymer/clay nanocomposites, while an anionic treatment applied to the clay resulted in conventional composites.

6.3.2. Thermal analysis

In order to evaluate the effect of natural/modified clay addition in polystyrene and the influence of different surfactants on the polymeric systems, thermogravimetric analyses were performed. The differential thermogravimetric (DTG) curves that were used to assess the peak degradation temperature (T_d^{peak}) were depicted in Figure 6.5. The dispersion of clay in a polymer matrix may induce two opposing effects: barrier and catalyst.[190, 218, 219] The latter is induced by the degradation of the surfactant, whilst the former is related to the strong interaction between the clay and the polymer matrix.[190, 357] As observed from Figures 6.5A and 6.5B the DTG curves for PS/clay composites and nanocomposites presented two degradation peaks, a first less prominent peak and a well defined second peak which was used to establish the peak degradations temperature. The presence of the first peak may be attributed to the degradation of the surfactant which induced a catalyst effect on the polymer matrix. The dispersion of organomodified MMT (i.e., MMT-AQ and MMT-P) showed a strong hindrance effect, even in the conventional composite PS/4MMT-P. Thus, the peak degradation temperature was enhanced by up to 28 °C as opposed to pristine PS (i.e., 424 °C), regardless of the of amount of clay dispersed or type of structure formed. The increase in the degradation temperature of the PS/organoclay nanocomposites has been previously reported in literature[214] and attributed to the excellent dispersion of the clay tactoids. A similar effect was observed when the clay was simultaneously mixed with

the polymer matrix and the nonylphenol ethoxylate surfactant. However, in this case, the T_d^{peak} increased by only 11 °C compared to neat PS while the second peak presented a shoulder.

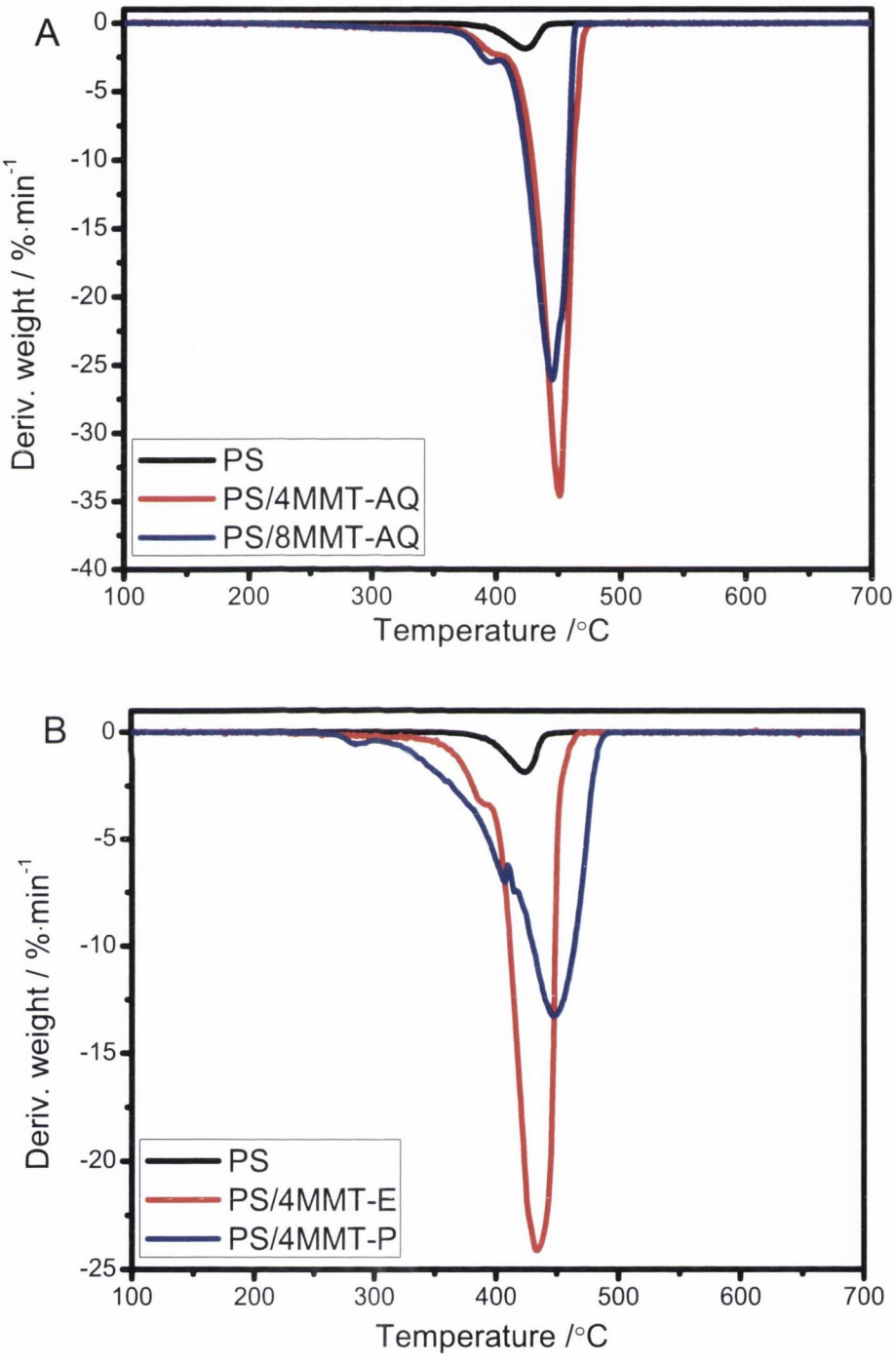

Figure 6.5. Differential thermogravimetric for pristine PS and A) PS/MMT-AQ, B) PS/MMT-E and PS/MMT-P, C) PS/MMT-gel and D) PS/MMT.

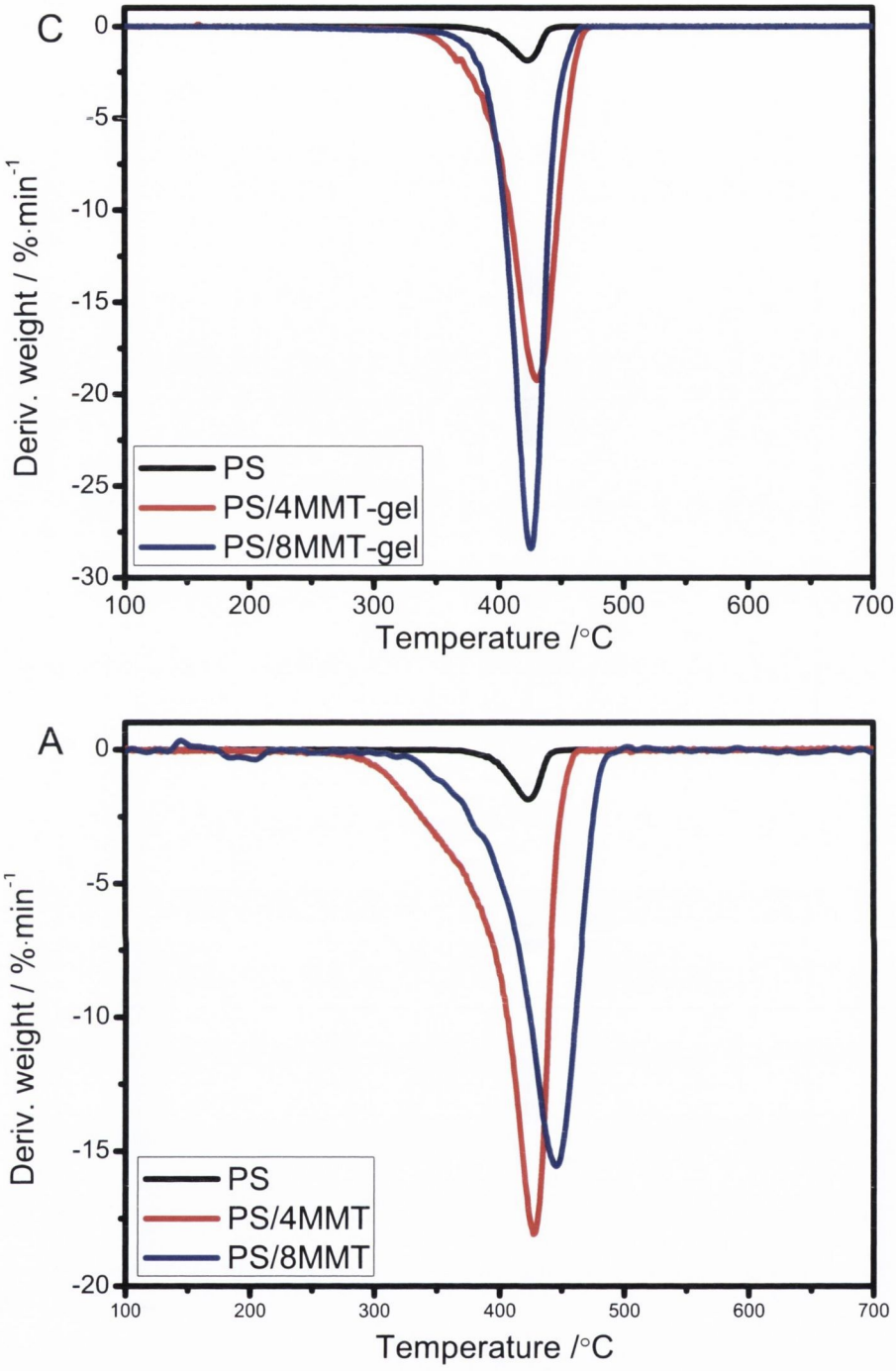

Figure 6.5. (Continued)

The thermogravimetric behaviours of PS/MMT and PS/MMT-gel were also analysed. In this case, the increase in the T_d^{peak} was marginal for 4 wt.% which implied that the catalyst effect induced by the formation of agglomerates and the barrier effect induced by strong bonding between the species were equally strong.[190, 372] However, the augmentation of the clay content enhanced the peak degradation temperature in PS/MMT

(Figure 6.5D). The increase in the residual water content induced a catalyst effect that slightly decreased the peak degradation temperature of the PS/8MMT-gel (Figure 6.5C) compared to PS/4MMT-gel. Regardless of the clay treatment applied to the MMT the thermal stability of the polymer/clay micro- and nanocomposites was improved compared to pristine PS, which is in agreement with the previously literature reports.[214]

6.3.3. Mechanical properties

The mechanical properties of PS and PS/clay composites and nanocomposites have been investigated *via* tensile and impact tests. The tensile strain-stress curves are displayed in Figure 6.6. The PS/8MMT-AQ nanocomposite presented the highest Young's moduli, whilst PS/4MMT-gel presented an almost ductile behaviour. Although the elongation at break of PS/4MMT-gel was superior to PS and PS/clay composites and nanocomposites, the ultimate tensile strength exhibited by the neat PS was higher than the values for PS/clay composites and nanocomposites, regardless of the clay type and content. The tensile properties of the materials were summarised in Table 6.1.

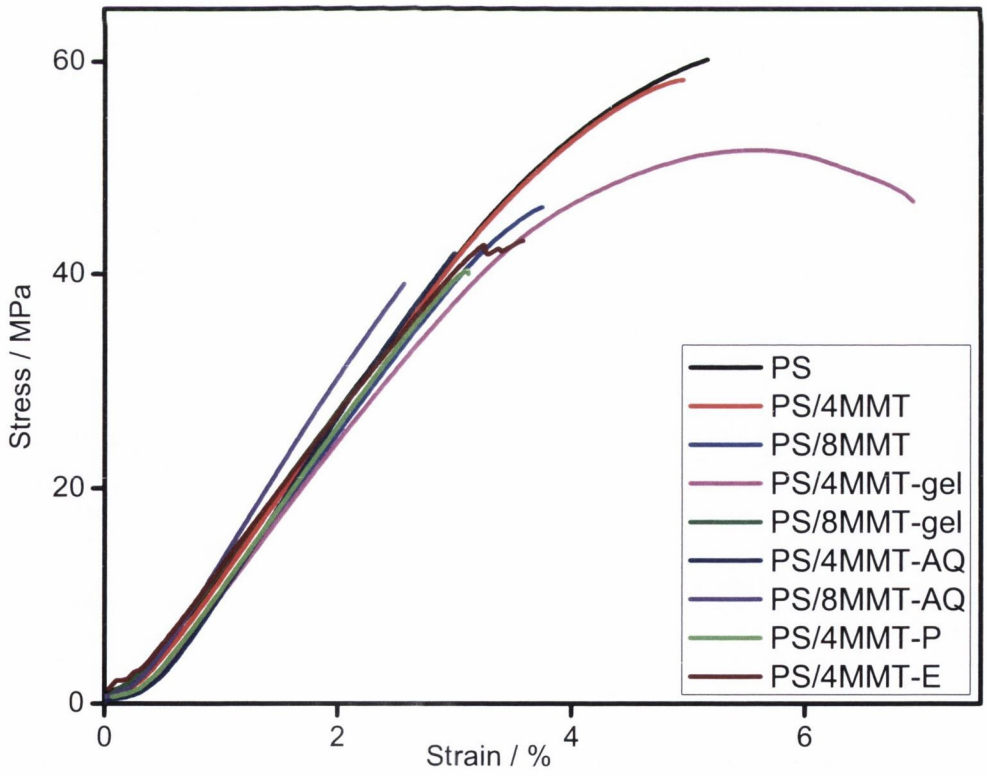

Figure 6.6. Strain-stress curves for PS and PS/clay composites and nanocomposites.

The Young's modulus of polymer/clay nanocomposites (Table 6.1, Column 1) was enhanced by up to 17%, with statistical significance, compared to neat PS and increased with the augmentation of the clay content. Replacing the cationic surfactant with the anionic component the elastic modulus of PS marginally increased, without statistical significance.

Table 6.1. Tensile properties of PS/clay micro- and nanocomposites[a,b]

Material	Young's Modulus / MPa	Ultimate Tensile Strength / MPa	Elongation at break / %
PS	1310(±11)	59.2(±0.9)	5.1(±0.1)
PS/4MMT	1343(±14)	55.3(±4.5)	4.5(±0.4)
PS/8MMT	1361(±3)	46.3(±0.9)	3.7(±0.2)
PS/4MMT-gel	1317(±15)	52.3(±1.0)	6.5(±0.3)
PS/8MMT-gel	1353(±15)	38.6(±1.8)	3.0(±0.2)
PS/4MMT-AQ	1456(±32)	39.5(±0.3)	2.8(±0.1)
PS/8MMT-AQ	1536(±46)	40.7(±0.3)	2.7(±0.1)
PS/4MMT-P	1385(±46)	40.5(±0.9)	3.3(±0.2)
PS/4MMT-E	1306(±71)	42.6(±2.5)	3.5(±0.4)

[a]Five specimens were tested for each material; [b]The values in parenthesis represent the standard deviation.

Compared to pristine PS, the ultimate tensile strength of the polymer/clay micro- and nanocomposites (Table 6.1, Column 2) decreased by 7-34%. Typically a reduction in the tensile strength would indicate low interactions between the clay and the polymer, i.e., poor dispersion or plasticisation effect of the surfactant or even the degradation of the surfactant during processing. In the present study the reduction in the tensile strength can be a consequence of the enhanced brittle effect that the presence of clay may induce and also an indication of plastic deformation in PS/4MMT. Similar to the ultimate tensile stress, the elongation at break (Table 6.1, Column 3) was reduced for most of the composites by 13-48% compared to the neat PS. Interestingly, the PS/4MMT-gel composite showed a 29% improvement in the elongation at break. This enhancement can

be attributed to the sporadic dispersion of clay tactoids and microcomposites in the PS matrix (Figure 6.4B and 6.4B1), which is due to the highly hydrophilic character of the clay in the MMT-gel that promoted the intercalation of water molecules between the clay layers. Although the fast evaporation of the water molecules during the melt compounding process collapsed the gallery and led to clay agglomerations, in some cases the clay layers allowed for the intercalation of the polymer chains. Upon subjecting this mostly conventional polymer/clay composite to slow (i.e., 1 $mm \cdot min^{-1}$) uniaxial deformation, it is possible that the microcomposite structures unfolded into neatly stacked clay layers, whilst the polymer chains were being straightened and then slightly elongated. So, it may be hypothesized that a layered structure had formed between the straightened and slightly elongated polymer chains and the stacked clay layers. The reduction in the stress, observed in Figure 6.6 for PS/4MMT, can be attributed to the breaking of the brittle polymer chains.

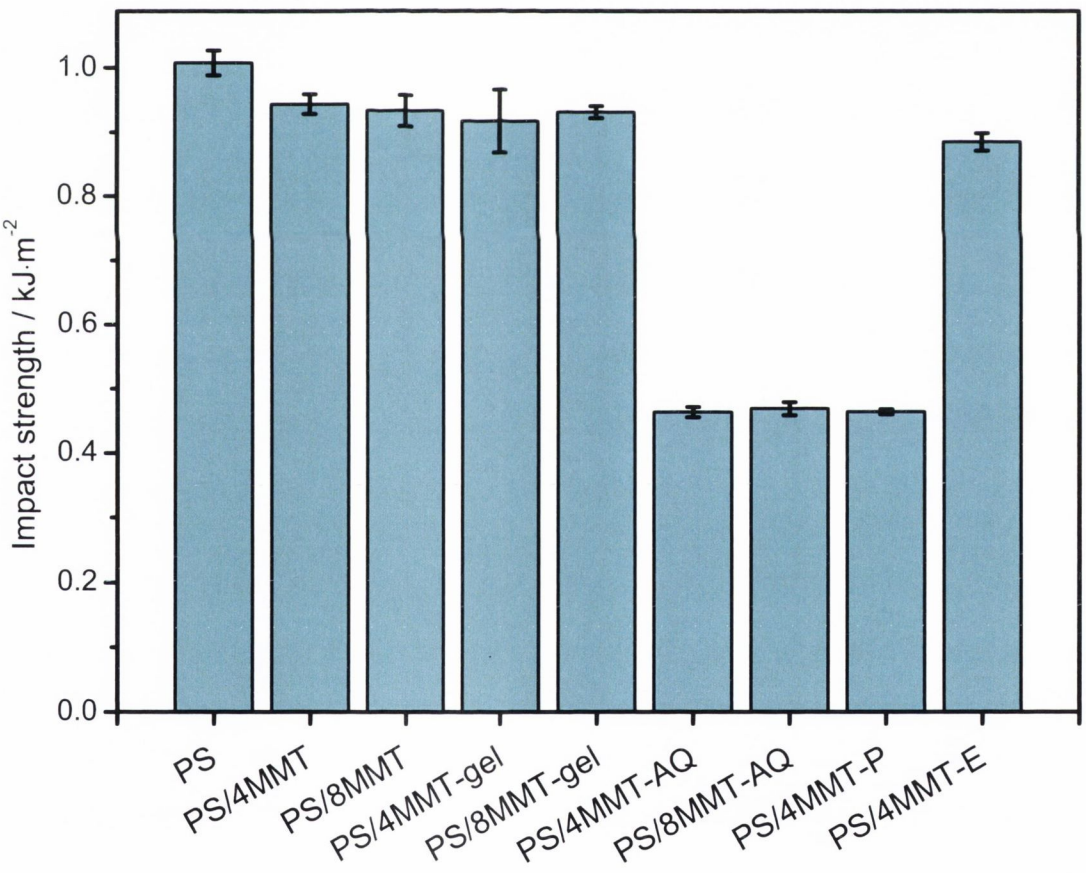

Figure 6.7. Impact strength of neat PS and PS/clay micro- and nanocomposites. The bars for the experimental results represent averages of six measurements; the error bars represent ± one standard deviation.

The toughness of the materials determined *via* Charpy impact test was summarised in Figure 6.7. The impact strength of PS/clay micro- and nanocomposites was found to decrease by 6-54% compared to neat PS. The dispersion of cationic or anionic surfactant-treated natural clay in PS led to massive reductions in the toughness of the polymer/clay micro- and nanocomposites. However, the dispersion of MMT or MMT-gel in the PS matrix or the simultaneous mixing of the non-ionic surfactant with the MMT and the polymer matrix led to a marginal depreciation of 6-12% compared to neat PS. The weaker mechanical and thermal properties obtained for polymer/anionic or non-ionic surfactant-treated natural clay are in good agreement with the literary observations.[373]

As observed from Table 6.1 and Figure 6.7, the dispersion of a MMT-gel solution with 4 wt.% clay tactoids in a brittle low-polarity hydrophobic PS matrix resulted in a material that exhibited ductility. Although compared to the pristine PS the stiffness and the toughness determined *via* Charpy impact test presented by the PS/4MMT-gel displayed similar values, the increased ductility and marginal reduction in the ultimate tensile strength indicated that the material presented an increase in the energy at break. This suggested that this method that has been previously used for nylon 6 [22,23] can be implemented for the dispersion of natural clay in low-polarity hydrophobic polymers. Thus, the use of this virtually simple method of dispersing the clay can lead to superior materials.

6.3.4. Surface analysis

To clarify the changes in the mechanical properties of the neat PS and PS/clay composites, the impact fractured surface was analysed *via* SEM (Figure 6.8). The impacted surface of pristine PS was smooth with few occasional fibrils and a slightly terraced aspect (Figure 6.8A).The dispersion of MMT in the PS matrix resulted in rougher fractured surfaces (Figure 6.8B and 6.8C), which would indicate that a higher amount of energy might have been absorbed during the fracture surface.[135] The dispersion of MMT-gel led to a relatively flat surface with slight rugosity, which showed a terraced aspect with the increase in the clay content (Figure 6.8D vs. Figure 6.8E). The MMT-AQ presented a relatively flat surface with small "fish-slips" (Figure 6.8G and Figure 6.8H). By treating the MMT with an anionic surfactant and dispersing it in PS, a surface with a more terraced aspect was observed (Figure 6.8F). The dispersion of neat MMT in PS and the melt compounding of PS with MMT and non-ionic surfactant produced rough layered impact

surfaces. Unlike PS/MMT-AQ nanocomposites, the PS/MMT showed better defined terraces (Figure 6.8G and Figure 6.8H). The presence of the non-ionic surfactant reduced the layered aspect and led to a slightly more uniform surface (Figure 6.8I), similar to PS (Figure 6.8A), explaining the similar impact strength of PS/MMT-E and PS observed in Figure 6.7.

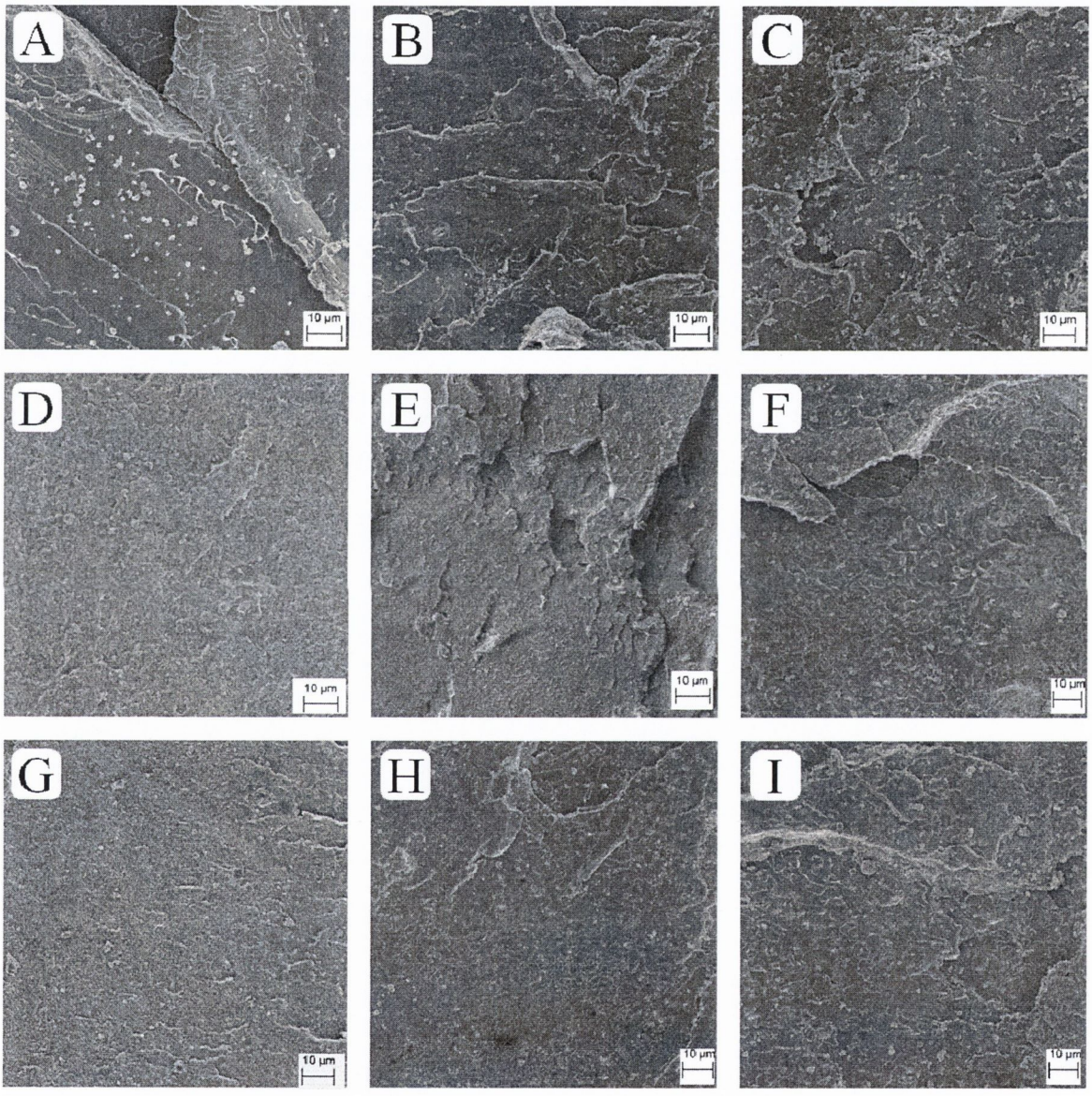

Figure 6.8. SEM images of A) PS, B) PS/4MMT, C) PS/8MMT, D) PS/4MMT-gel, E) PS/8MMT-gel, F) PS/4MMT-P, G) PS/4MMT-AQ, H) PS/8MMT-AQ and I) PS/4MMT-E.

6.4. Conclusions

Polymer/clay micro- and nanocomposites were manufactured *via* melt processing on a twin screw extruder. Natural clay, pre-treated MMT with cationic or anionic surfactants, simultaneously melt mixed MMT with a non-ionic surfactant or MMT slurry were dispersed in a PS matrix. The cationic surfactant-treated MMT and the simultaneously melt mixed MMT and non-ionic surfactant led to polymer/clay nanocomposites, whereas, the rest of the systems presented conventional composites.

The presence of the MMT and cationic or anionic surfactant-treated MMT in PS increased the peak degradation temperature by over 20 °C, due to strong bonding between the clay and the polymer. However, the dispersion of MMT-gel in PS presented little variations in the peak degradation temperature.

The tensile properties of the polymer/clay micro- and nanocomposites showed improved Young's moduli and elongation at break compared to the pristine PS. The dispersion of cationic surfactant-treated MMT in PS led to 11-17% enhancements in elastic moduli, which increased with the augmentation of the clay content. Typically, the addition of clay to PS led to a more brittle behaviour reducing the elongation at break and the impact strength. However, the dispersion of 4 wt.% MMT-gel to PS increased the elongation at break by 27%.

The thermal and mechanical properties suggested that the treatment of natural clay with a cationic surfactant and the melt mixing of the PS with MMT and a non-ionic surfactant are the optimal approaches for the low polarity polymer. From the structure and the thermal properties the two materials appear to be similar; however, PS/4MMT-AQ exhibited increased stiffness at the expense of toughness, whilst PS/4MMT-E presented a marginal decrease in toughness. The direct mixing of the non-ionic surfactant with PS and MMT represented the optimal choice. The use of MMT-gel for PS showed promise and a clay content of 4 wt.% proved ideal for the polymer/clay system. Typically, PS presents a brittle behaviour; however, using this simple process, the amorphous polymer/MMT-gel composite exhibited a ductile character. This finding proves that this accessible method can be applied for low-polarity polymers.

Chapter 7. A facile method for improving clay exfoliation in polymer nanocomposites

7.1. Introduction

Since their discovery polymer/clay nanocomposites[2, 85] have received significant attention, expanding the field of polymer composite science in the aspects of preparation, structures and interfaces, and resulting in a series of new applications in construction, automotive, marine, aerospace, healthcare, electric and packaging industries, etc. The reasons for the prolific usage of polymer/clay nanocomposites lie primarily in the fact that this new class of materials is often characterised by superior and even distinctive properties compared to their polymer or conventional composite counterparts.[8, 90, 374-377] The enhanced properties depend mainly on the morphology of the nanocomposites and the degree of dispersion of the clay in the polymeric matrix.[91, 375]

The morphology of clay in polymer nanocomposites plays a crucial role in influencing the mechanical and thermal properties.[139, 378-380] For example, Chen et al.[381, 382] showed that the highly exfoliated poly(L-lactide) (PLLA)/clay nanocomposite containing 5 wt.% epoxy-modified organoclay exhibited a tensile modulus, a tensile strength and an elongation at break 69%, 26% and 9% higher than the original values for neat PLLA and 37%, 30% and 67% higher than the values for the mostly intercalated PLLA nanocomposites with the same amount of un-modified organoclay. Shi et al.[380] revealed that the storage moduli of the exfoliated ethylene vinyl acetate copolymer (EVA)/clay nanocomposites were 17-79% higher than the values of the intercalated nanocomposites at comparable clay loads (i.e., 1-5 wt.%) and the thermal degradation temperature was also higher at a 2 wt.% clay content in the former.

To achieve superior mechanical and thermal properties such as mechanical strength, stiffness and thermal stability, it is considered advantageous for clay to exfoliate in the polymer matrix. Exfoliation exposes the large specific surface area of single clay platelets, i.e., 760 $m^2 \cdot g^{-1}$,[12] to maximize the interactions between the clay and the polymer, and makes use of the high stiffness of clay platelets, i.e., ~230 GPa,[16] which is remarkably higher than that of natural clay particles, i.e., about 6.2-14 GPa.[14, 16, 383]

However, to obtain nanocomposites with full or enhanced clay exfoliation is not a straightforward task. Over the years a series of approaches have been tested. Most of the successful methods involved complex processes of polymerisation and/or the use of

advanced surfactants for clay treatments.[380-382, 384, 385] For instance, Wang et al.[384] synthesized exfoliated polystyrene/organoclay nanocomposites by free radical polymerisation of styrene with 2 wt.% 2-(dimethylamino) ethyl-triphenylphonium bromide cation exchanged montmorillonite. Gilman et al.[385] manufactured exfoliated nylon 6/montmorillonite nanocomposites by melt compounding *via* the use of 1,2-dimethyl-3-hexadecylimidazolium as the surfactant. Shi et al.[380] produced mostly exfoliated EVA/clay nanocomposites *via* a solvent intercalation method by using a Master batch of poly(vinyl acetate)/silicate nanocomposite prepared by copolymerising vinyl acetate and 2-(acryloxyethyl) trimethyl ammonium chloride which was subsequently mixed with montmorillonite.

Melt compounding is the most cost-effective and environmentally friendly method to produce polymer/clay nanocomposites at the industrial level. The goal of this work was to develop a versatile route to facilitate clay exfoliation during melt processing in order to obtain nanocomposites with enhanced exfoliation degrees and improved properties. This was done by introducing a conventional blowing agent inside the galleries of clay and expanding the galleries upon degradation of the blowing agent during melt processing. A low-polarity polymer, polystyrene and a non-polar polymer, polypropylene with an organic compatibiliser, namely maleic anhydride grafted polypropylene (PPgMA), were used as polymer matrices, to which blowing agent-treated organoclays were added as the reinforcing filler. PS and PP were selected as the matrices because of their wide range of applications in particular for uses in commodity products. Two common low-cost and low-toxic blowing agents, namely sodium bicarbonate (SB) and azodicarboxamide (ADC) were selected as the blowing agents for the treatment of commercial organoclay. PP without the compatibiliser was also mixed with the blowing agent-treated organoclay to produce conventional composites for comparison. The untreated organoclay was studied as a control. It was demonstrated that the presence of the blowing agent in clay galleries had indeed enhanced the exfoliation degree of clay in polymer nanocomposites and hence their mechanical and thermal properties.

7.2. Experimental Section

7.2.1. Materials

Polypropylene (SABIC PP, Grade: 500P), from SABIC (Saudi Basic Industries Corporation) with a density of 905 $kg \cdot m^{-3}$, and polystyrene (DOW STYRON, Grade: 634),

from DOW Plastics with a density of 1050 $kg \cdot m^{-3}$, were purchased from RESINEX (UK). Organoclay, Nanomer® I44.P, a dimethyl dihydrogenated tallow ammonium chloride modified montmorillonite, from Nanocor Corporation was kindly supplied by Nordmann, Rassmann GmbH (Hamburg, Germany). This organoclay (denoted as Clay) is characterised by a density of 1605 $kg \cdot m^{-3}$ and an organic content of 40% established by performing Loss on Ignition test.[351] As a compatibilising agent PPgMA with 8–10 wt.% maleic anhydride composition and a density of 934 $kg \cdot m^{-3}$ was purchased from Sigma Aldrich. Reagent-grade sodium bicarbonate ($NaHCO_3$) and azodicarboxamide ($C_2H_4O_2N_4$) were purchased from Sigma-Aldrich, and each acted as the blowing agent. Due to the high decomposition temperature of ADC,[386] zinc oxide (analytical grade) from Sigma-Aldrich was used to activate the blowing agent and reduce the decomposition time.[326] Tetrahydrofuran (THF) from Hazmat (Ireland) was used as a solvent. All materials were used as received.

7.2.2. Clay treatment

The commercial organoclay was pre-treated with two common chemical blowing agents, namely SB and ADC/zinc oxide to give the SB- and ADC-treated clays, following a procedure described in our previous work for a different clay.[371] Briefly, a 2.5 wt.% clay suspension in a THF solution was mixed at room temperature for 48 hours with a 10 wt.% SB solution or a 5 wt.% ADC and zinc oxide solution. Following a standstill period, the supernatant of the solution was decanted and the treated clay was washed repeatedly with distilled water before being dried at room temperature overnight in a fume cupboard and then heated in an oven at 60 °C for 24 h. The dried clay was subsequently ground into fine powders and the clay platelets content was assessed by performing Loss on Ignition tests, to be 30% for SB-Clay and 21% for ADC-Clay. The densities for SB-Clay and ADC-Clay were determined, using a Micromeritics AccuPyc 1330 pycnometer, to be 1660 $kg \cdot m^{-3}$ and 2246 $kg \cdot m^{-3}$, respectively.

7.2.3. Preparation of polymer/clay nanocomposites

Compatibilised PP (PP/PPgMA=90/10, w/w) and PS with 4 wt.% clay platelets of the untreated and treated organoclays were prepared on a twin screw extruder containing screws with a diameter of 16 mm and a length to diameter ratio of 25. The operating temperature of the extruder was maintained at 160, 165, 175, and 180 °C for the four

processing zones from hopper to die. The screw speed was set at 200 rpm. In order to assure that the materials have been sufficiently mixed and that the blowing agents have been degraded to a greater extent, the cooled and pelletised extrudates were passed through the extruder two more times at a screw speed of 100 rpm and a die temperature of 180 °C for polymer/Clay and polymer/SB-Clay or 200 °C for polymer/ADC-Clay nanocomposites. To ensure that the blowing agents were fully degraded the materials were heated in a convection oven for 10 minutes at 210 °C and then ground.

7.2.4. Characterisation

XRD was carried out on a Phillips PW1720 X-Ray Diffractometre with a $CuK\alpha_1$ (λ=0.15406 nm) anode tube at the standard conditions of 40 kV and 20 mA. The samples were tested from 2° to 10°, 2θ angle, at a step size of 0.02° and a duration of 2.5 seconds per step. Powder samples were used.

TEM was performed on a TECNAI G2 20 Twin electron microscope at 200 kV accelerating voltage. The specimens were ultramicrotomed using a Reichert–Jug 'Ultracut' equipped with a diamond knife. The sections (~100 nm in thickness) were collected in a trough filled with water and then placed on a 200 mesh copper grid.

Fourier Transformed Infrared Spectroscopy (FT-IR) spectra were realised on a FT-NIR instrument (Perkin Elmer Spectrum One NTS) equipped with ATR Sampling Accessory. The samples were run from 550 cm^{-1} to 4000 cm^{-1} at a resolution of 2 cm^{-1}.

SEM imaging on tensile fractured surfaces was performed using a Zeiss Ultra Scanning Electron Microscope at a voltage of 5.0 kV. Prior to being analysed the samples were mounted on stubs and their surface were platinum coated.

DSC was carried out on a Perkin Elmer Diamond DSC at a scan rate of 10 °C·min^{-1} in nitrogen atmosphere. In order to eliminate the effects of the heating history of the material, the glass transition temperature (T_g) was taken from the second heat scan.

TGA was performed under nitrogen flow (20 mL·min^{-1}) on a Perkin Elmer Pyrus 1 TGA equipped with an ultra-micro balance with a sensitivity of 0.1 µg, from 100 °C to 650 °C at a heating rate of 10 °C·min^{-1}.

The tensile tests were carried out, at room temperature, on a Zwick Z005 machine (Germany) according to ISO 527:1993. The tests were performed using a 5 kN load cell and a cross head speed of 2 mm·min^{-1}. Five dog bone specimens (50 mm x 5 mm x 1 mm,

length x width x thickness) were tested for each of the materials. The tensile specimens were prepared by compression moulding on a hot press. The ground materials were placed in a tensile mould and heated at 210 °C for 15 minutes after which they were pressed into the mould by applying a pressure of 5.1 MPa for 10 seconds. The mean and standard deviation values reported for the mechanical tests represent a confidence level of 95%. Statistical significance was assessed by a Two-tailed, Type II 't' test with $p<0.05$.

7.3. Results and Discussion

7.3.1. Structure

From the XRD diagrams presented in Figure 7.1, it can be observed that the untreated organoclay (Curve 1) exhibited a broad diffraction peak at a 2θ value of 3.3°, corresponding to a basal spacing, $d_{(001)}$, of 2.7 nm. The blowing agent-treated organoclays (Curve 2 and Curve 3) presented a *(001)* peak that shifted towards higher 2θ values probably due to removal of some surfactant molecules or impurities from the galleries.[371] Since compared to the surfactant, the molecular sizes of the blowing agents were smaller, the intercalation of the latter into the gallery may not result in an increase in the basal spacing.[371] To clarify this, FT-IR was used (Figure 7.1, inset). By treating the clay with blowing agents the position of the Si-O-Si stretching band[368, 369] in the organoclay (Curve 1) shifted from 1009 cm^{-1} to 1015 cm^{-1} for the SB-Clay (Curve 2) and to 1022 cm^{-1} for the ADC-Clay (Curve 3). These positive shifts were due to hydrogen bonding between the Si-O of the clay and the carbonyl groups of ADC and SB.[370] This suggested that the silanol adsorption band has modified and that the blowing agents had intercalated inside the clay gallery.[329, 371] These results are similar to those for another organoclay, Cloisite® 30B, which also showed that the blowing agents had intercalated inside the gallery spacing of the organoclay, without increasing it.[371]

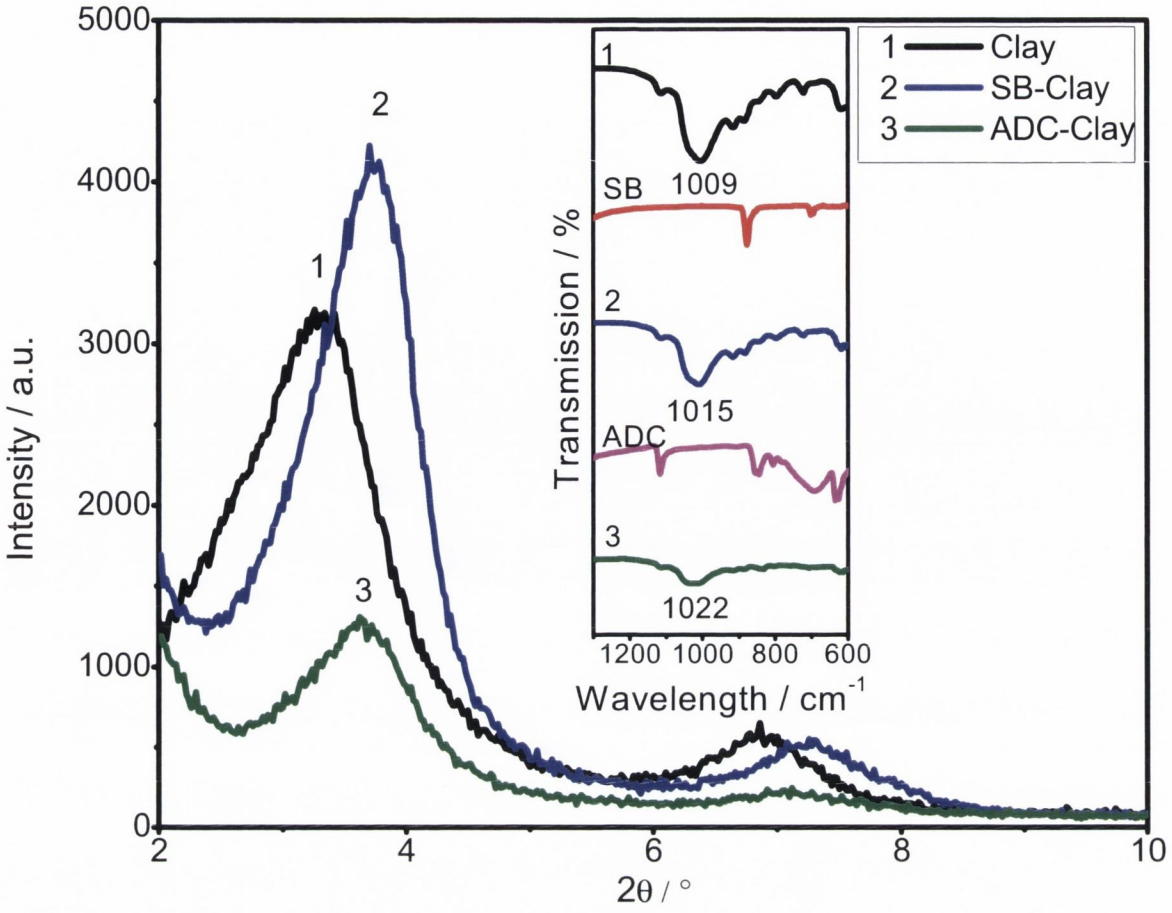

Figure 7.1. XRD profiles of as-received and blowing agent-treated organoclays. Inset: FT-IR spectra for the clays and blowing agents (SB and ADC).

By dispersing as-received organoclay or SB-treated organoclay in PS, the *(001)* clay diffraction peaks at 2θ values of 3.3° and 3.7° shifted to a 2θ value of 2.6° (Figure 7.2A, Curves A1). This corresponded to a basal spacing of 3.4 nm and suggested the formation of a polymer/clay nanocomposite in which intercalated clay tactoids were present. The less prominent peak that PS/SB-Clay exhibited compared to PS/Clay suggested that less ordered crystalline structures were formed and that the exfoliation degree had increased.[98] When the ADC-treated organoclay was dispersed in the PS matrix the *(001)* peak disappeared (Figure 7.2A, Curve A3); however, a small reminiscence of the *(002)* diffraction peak was still visible. This indicated that the exfoliation degree of the clay was further increased and a small fraction of intercalated structures were still presented in the nanocomposite. In either case, incorporation of the blowing agent facilitated the exfoliation of clay in PS.

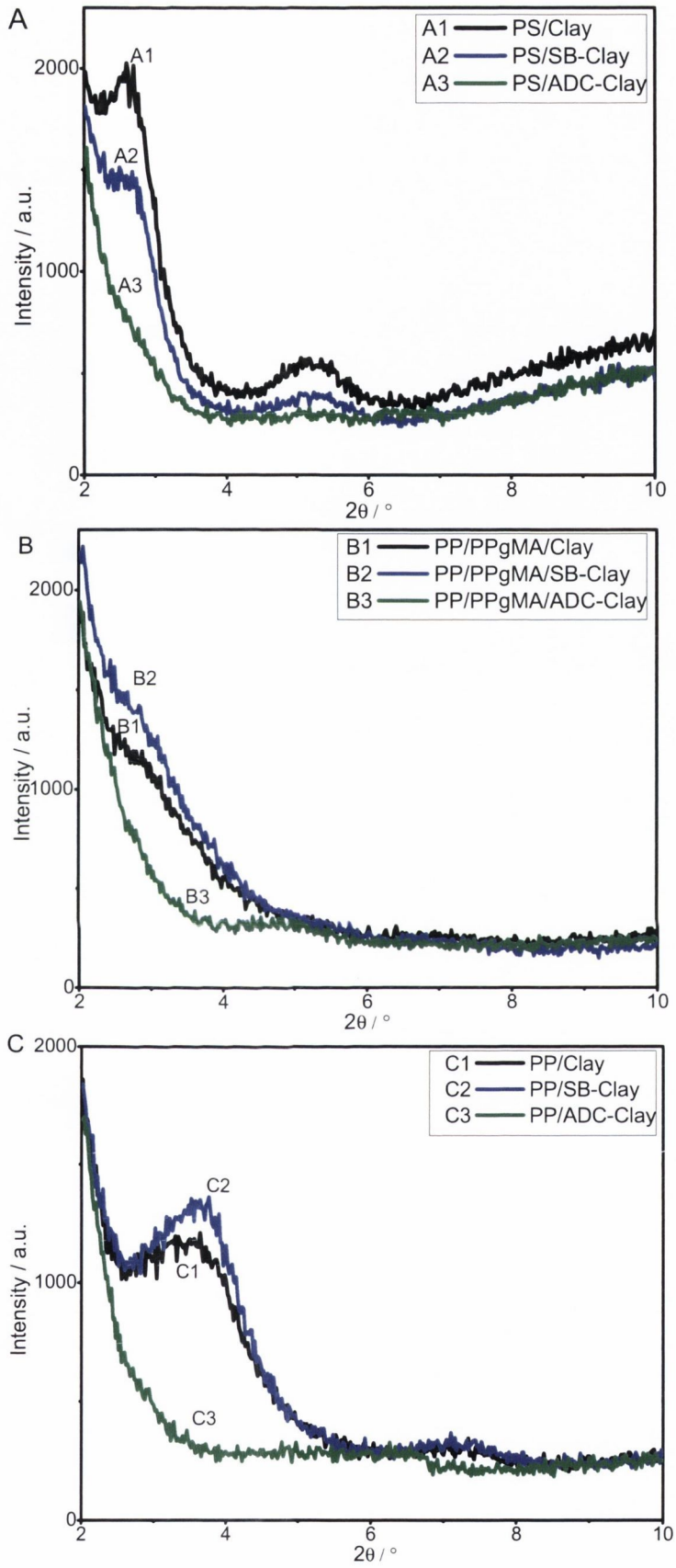

Figure 7.2. XRD profiles of A) PS/clay, B) PP/PPgMA/clay nanocomposites and C) PP/clay composites.

The dispersion of organoclay in PP/PPgMA led to an XRD trace (Figure 7.2B, curve B1) that presented a small *(001)* peak at a 2θ value of 2.9°, corresponding to a basal spacing of 3.0 nm. However, with the additions of the blowing agent-treated organoclays the *(001)* peaks disappeared (Figure 7.2B, curves B2 and B3), again suggesting that pre-treatments of the organoclay resulted in increased exfoliation degrees. Similar to the case with PS/ADC-Clay, the *(002)* peaks were visible (at a 2θ value of 5°) in the traces for PP/PPgMA/SB-Clay and PP/PPgMA/ADC-Clay, implying these nanocomposites still had some intercalated structures. PP/PPgMA/ADC-Clay exhibited a more distinctive *(002)* peak than PP/PPgMA/SB-Clay, demonstrating a higher degree of intercalation or a lower degree of exfoliation in the former.

By dispersing as-received or SB-treated organoclay in the non-polar polymer matrix, i.e., PP, without the organic compatibiliser, the *(001)* peaks of the organoclays maintained nearly the same positions (Figure 7.2C, Curves C1 and C2) as for the clays (Figure 7.1, Curves 1 and 2). This indicated that the addition of the clays to the noncompatibilised PP led to the formation of conventional composites owing to the incompatibility of the non-polar PP and the organoclay. In contrast, the dispersion of ADC-treated organoclay in PP did not give a *(001)* diffraction peak but a small diffraction peak at around 5°. This result seemed to suggest the material presented highly exfoliated nanostructures like in the previous cases, noting that there was no orientation effect from the powdered samples. Based on the incompatibility of the PP and the organoclay it was expected that the treatment of the organoclay with ADC would still lead to a conventional composite and disappearance of the *(001)* peak might arise from uneven distribution of the low-content clay particles. To verify the results derived from XRD, TEM was performed and the results were discussed below.

The dispersion of blowing agent-treated organoclays in PS and PP/PPgMA showed enhanced exfoliation compared to PS/Clay and PP/PPgMA/Clay nanocomposites (Figure 7.3 and summarised in Table 7.1). The PS/ADC-Clay nanocomposites presented a marginal improvement in the exfoliation degree compared to PS/SB-Clay; however, the remaining intercalated nanostructures were characterised by a slightly higher average number of clay platelets per stack. Although on average the number of clay platelets per stack was enhanced, on maximum cases it decreased from 13 (for SB-Clay, Table 7.1, Column 2) and to 7 (for ADC-Clay, Table 7.1, Column 3). This suggested that ADC had a better ability to delaminate the clay layers due to a higher amount of gas produced during degradation of the blowing agent.[254]

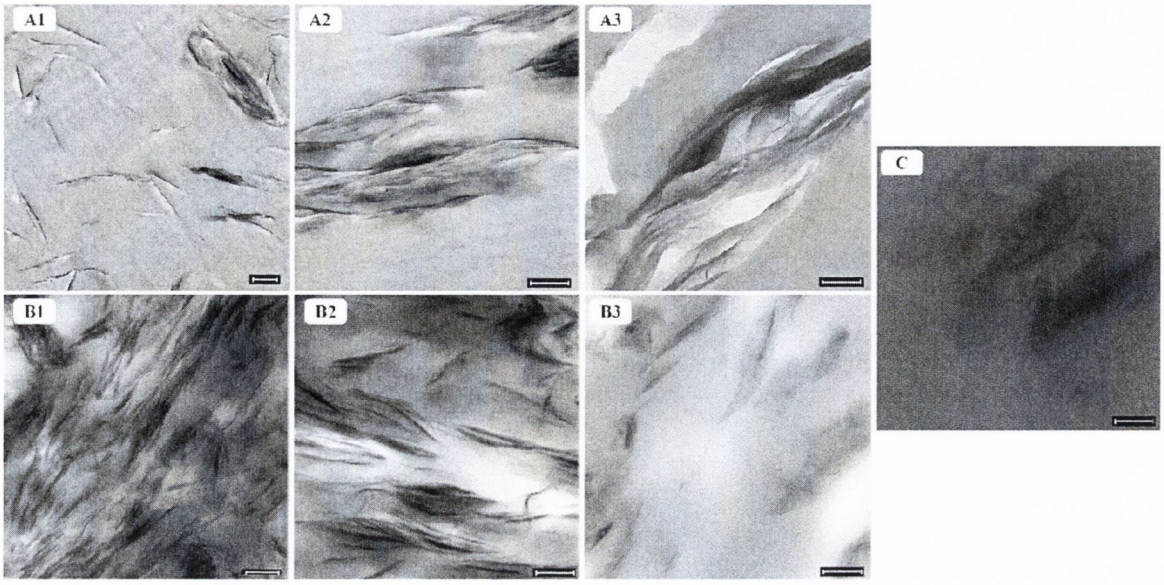

Figure 7.3. Representative TEM images: A1. PS/Clay, A2. PS/SB-Clay and A3. PS/ADC-Clay; B1 PP/PPgMA/Clay, B2. PP/PPgMA/SB-Clay and B3. PP/PPgMA/ADC-Clay; and C. PP/ADC-Clay. The thin well defined dark lines represent single clay platelets and indicate exfoliation, whereas the neatly stacked dark lines represent clay tactoids and indicate intercalation (Scale bar: 200 nm).

For the PP/PPgMA/blowing agent-treated organoclay nanocomposites it was observed that the enhanced exfoliation degree led to a lower average of clay platelets per stack in the remaining intercalated nanostructures (Column 5 vs. Column 6). The highest exfoliation degree was achieved by SB-Clay dispersion in the polymer matrix (Table 7.1, Column 5). Unlike when PS represented the matrix, in PP/PPgMA the number of clay platelets, on maximum cases, did not present radical changes. This was a consequence of the highly un-friendly environment created by the major component, i.e., PP. Thus, the pressure created inside the gallery was not sufficient to overcome the repulsive forces that existed between PP and clay. For the non-polar polypropylene the formation of conventional composites implied by the XRD curves (Figure 7.2C) was confirmed *via* TEM (Figure 7.3C, representative TEM image of PP/ADC-Clay). Large clay agglomerates were seen in the image due to incompatibility of clay and PP.

Table 7.1. TEM results for polymer/clay nanocomposites

Nanocomposite Structure	PS/ Clay[a]	PS/ SB-Clay[a]	PS/ ADC-Clay[b]	PP/ PPgMA/ Clay[a]	PP/ PPgMA/ SB-Clay[a]	PP/ PPgMA/ ADC-Clay[a]
f_e	0.36	0.50	0.56	0.42	0.61	0.50
f_i	0.64	0.50	0.44	0.58	0.39	0.50
N_{min}	2	2	2	2	2	2
N_{max}	16	13	7	6	7	8
$\bar{N}$	3.1	4.1	4.6	2.9	2.4	2.9

[a]Estimated from over 100 nanostructures; [b]Estimated from 25 nanostructures; f_e – mass fraction of exfoliated nanostructures; and f_i – mass fraction of intercalated nanostructures; N_{min} – minimum number of clay platelets per stack in a clay tactoid; N_{max} – maximum number of clay platelets per stack in a clay tactoid; and $\bar{N}$ – average number of clay platelets per stack in a clay tactoid.

The process of obtaining intercalated/exfoliated nanostructures in low-polarity PS and compatibilised PP was summarised in Figure 7.4. Firstly, the organoclay was treated with a blowing agent. This allowed the small blowing agent molecules to penetrate inside the gallery of clay without increasing the basal spacing (Figure 7.1). Secondly, the blowing agent-treated organoclay was mixed with the polymer on a twin screw extruder. During the melt-compounding process the clay dispersed in the polymer matrix while the blowing agent degraded inside the gallery, yielding gas molecules.[371] As the amount of gas increased the clay platelets were pushed apart with the assistance of the shear force during compounding. Repetitive mixing on the twin screw extruder further degraded the blowing agent and separated the clay platelets. This exfoliation mechanism was confirmed by TEM.

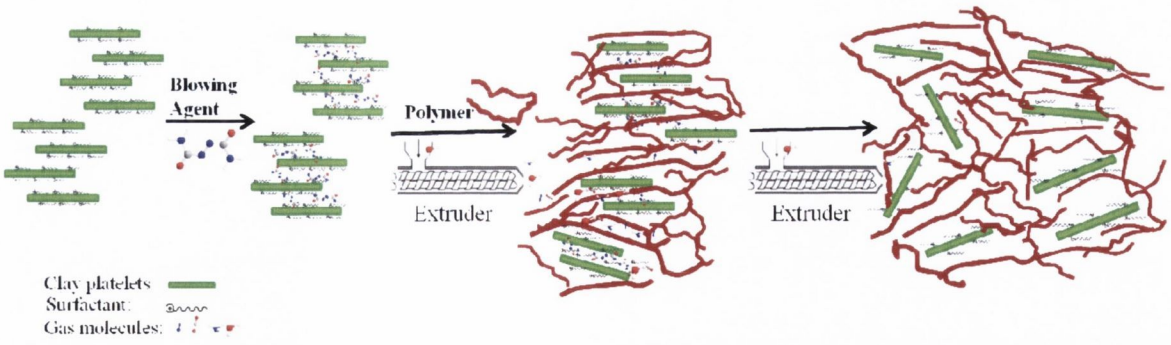

Figure 7.4. Intercalation/exfoliation process in PS/ or PP/PPgMA/blowing agent-treated organoclay nanocomposites.

The dispersion of SB-Clay in a low-polarity polymer (i.e., PS) resulted in the splitting of the clay platelets (indicated by arrows in Figure 7.5A) and ultimately led to a higher exfoliation degree than the PS/Clay nanocomposites (Figure 7.3B vs. Figure 7.3A). Similarly, the dispersion of ADC-Clay in PS or PP/PPgMA enhanced the exfoliation degree compared to as-received clay by generating bubbles within clay layers due to the degradation of ADC (Figure 7.5B).

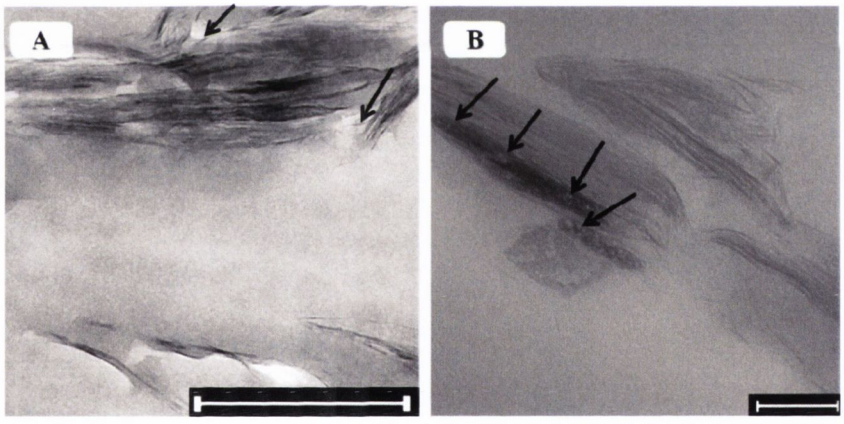

Figure 7.5. TEM images for A. PS/SB-Clay and B. PP/PPgMA/ADC-Clay nanocomposites (Scale bar: 100 nm). The arrows indicate bubble formation between clay layers or splitting of clay layers.

7.3.2. Thermal analysis

The glass transition temperatures, T_g, of the polymers and nanocomposites were measured at the midpoints of the corresponding glass transition regions (Appendix III). The glass transition of polymer/clay nanocomposites depends on the degree of dispersion of the clay, the polymer-filler interactions, the degree of exfoliation and the confinement of

the polymer molecules inside the galley of clay, as well as on the presence and exposure of the surfactant molecules that may induce a plasticisation effect.[387-390] Regardless of the type of clay, the addition of filler to the polymer matrix produced slight reductions in the glass transition temperatures (Table 7.2, Column 1). The dispersion of the as-received organoclay in PS slightly decreased the T_g due to the formation of mostly intercalated nanostructures and weak interactions between the filler and the polymer matrix.[387] The presence of the polymer inside the gallery exposed some of the surfactant which induced a plasticisation effect. By replacing the as-received organoclay with SB-treated organoclay, the T_g further depreciated due to the presence of the polymer and SB molecules in the gallery which resulted in the supplementary exposure of the surfactant and enhanced plasticisation effect.[389, 390] The increase observed in T_g of the PS/ADC-Clay system compared to PS/Clay and PS/SB-Clay nanocomposites comes from the enhanced exfoliation which induced a slow relaxation process.[387]

Similar to PS, the dispersion of as-received clay in PP/PPgMA slightly decreased the T_g. This was due to the exposure of the surfactant which induced a plasticisation effect.[389, 390] The increased exfoliation degree and the presence of the compatibilising agent in PP/PPgMA/blowing agent-treated organoclay nanocomposites facilitated the exposure of the surfactant which induced a plasticisation effect, but on the other hand, exfoliation also induced an increases in T_g because of the strong adsorption of polymer molecules onto its surface.[387-390] Thus, in this case we are dealing with two opposite effects. The decrease observed in the T_g indicated that the plasticisation effect was superior to the slow relaxation dynamics induced by exfoliation.[388-390] However, in the absence of the compatibilising agent, the T_g of PP/clay nanocomposites presented little variation compared to that of the pristine polymer.[390]

The maximum degradation temperatures (T^d_{peak}, measured as the peak temperature on the differential thermogravimetric curves, Appendix III) for PS/clay and for PP/PPgMA/clay nanocomposites were enhanced, regardless of the clay type. For PS/ADC-Clay nanocomposites the peak degradation temperature increased by close to 37 °C compared to the pristine polymer, which is attributable to the strong bonding between the polymer and clay that originated from the good dispersion of clay in the polymer matrix. This is in agreement with the findings of Jang and Wilkie.[214] A similar improvement was observed for PP/PPgMA/SB-Clay and PP/PPgMA/ADC-Clay nanocomposites, where in contrast to the pristine polymer and the polymer/organoclay nanocomposite, the peak degradation temperature increased by over 46 °C and 32 °C, respectively. These significant

enhancements again are due to the excellent dispersion and increased exfoliation of the clay platelets from the blowing agent-treated clays (Figure 7. 3) which led to the strong bonding between the clay and the polymer matrix. The PP/clay conventional composites presented small reductions in the peak degradation temperature, compared to the pristine polymer because of the presence of the surfactant inside the gallery. The absence of enhancements in the T^{d}_{peak}, of the conventional composites, compared to the significant improvements observed in nanocomposites, demonstrated the superiority of the latter over the former, and proved once again that the excellent dispersion of the filler into the polymer matrix is highly important.

Table 7.2. DSC and TGA results for polymers and polymer/clay nanocomposites

Material	T_g/ °C	T^{d}_{peak} / °C
PS	101.3	427.4
PS/Clay	99.5	457.7
PS/SB-Clay	98.6	452.0
PS/ADC-Clay	100.7	464.1
PP/PPgMA	-15.5	438.6
PP/PPgMA/Clay	-16.6	452.9
PP/PPgMA/SB-Clay	-17.9	485.2
PP/PPgMA/ADC-Clay	-17.2	484.2
PP	-19.9	457.9
PP/Clay	-17.8	444.8
PP/SB-Clay	-19.7	451.6
PP/ADC-Clay	-18.2	453.1

7.3.3. Mechanical properties

The tensile testing results of the polymers with and without the additions of clays (Appendix III) are summarized in Table 7.3. The inclusion of sodium bicarbonate as the blowing agent improved the tensile modulus, strength, elongation at break and energy at break simultaneously for both PS and PP/PPgMA. In most nanocomposites, Young's

modulus of the polymer increased with the clay addition and it increased further when the clay was pre-treated with a blowing agent. By dispersing SB-Clay into PS the Young's modulus increased, with statistical significance, from 1.65 GPa in neat PS and 1.72 GPa in PS/Clay nanocomposite to 2.01 GPa in PS/SB-Clay nanocomposite. Similarly, the modulus of the compatibilised PP was enhanced from 0.83 GPa in PP/PPgMA and 0.93 GPa in PP/PPgMA/Clay nanocomposite to 0.98 GPa in PP/PPgMA/SB-Clay nanocomposite. The fact that the polymer/SB-Clay nanocomposites with the enhanced exfoliation degrees exhibited a superior modulus can be attributed to the higher modulus exhibited by the exfoliated single clay layers than that of the intercalated clay tactoids and to the greater interfacial regions where a higher amount of polymer molecules are adsorbed onto the clay surface. The addition of the untreated or treated organoclay also led to small increases in the modulus of the noncompatibilised PP owing to the higher modulus of clay particles than that of the matrix.

Likewise, the ultimate tensile strength and the elongation at break were also found to generally improve in polymer/blowing agent-treated organoclay nanocomposites. The dispersion of SB-Clay into PS increased, with statistical significance, the ultimate tensile strength by 40% and the elongation at break by 11%. By reinforcing the PP/PPgMA with the same clay, a 52%, statistically significant enhancement in the ultimate tensile strength, together with a 204% increase in the elongation at break, were observed. As previously described, the increased exfoliation degree offered greater interfacial regions and stronger interactions in the nanocomposites, allowing more effective stress transfer from the polymer to the clay. In contrast, the conventional PP/clay composites exhibited statistically significant reductions in the ultimate tensile strengths and depreciations in the elongation at break as opposed to the neat PP.

The changes in the Young's modulus, ultimate tensile strength and elongation at break were best reflected by the energy at break, calculated as the area under the tensile strain-stress curve (Appendix III) and representing the integral of total work performed. As opposed to PS and PS/Clay nanocomposite, the energy at break of PS/SB-Clay nanocomposite increased from 226 $kJ \cdot m^{-3}$ and 74 $kJ \cdot m^{-3}$ to 251 $kJ \cdot m^{-3}$. The increases achieved for the PP/PPgMA were more remarkable: the energy at break increased from 81 $kJ \cdot m^{-3}$ in PP/PPgMA and 158 $kJ \cdot m^{-3}$ in PP/PPgMA/Clay nanocomposite to 246 $kJ \cdot m^{-3}$ in PP/PPgMA/SB-Clay nanocomposite. The improvement of toughness was largely due to the good dispersion of the clay in the matrix and the mobility of clay during testing such as orientation of clay layers towards the testing direction and delamination of clay layers from intercalated tactoids.[136, 139] However, regardless of the type of clay dispersed, the energy at

break of the PP/clay conventional composites was found to be dramatically lower that the original value of neat PP because of the poor dispersion of clay particles.

Table 7.3. Tensile properties for polymer and polymer/clay nanocomposites[a,b]

Material	Young's Modulus / MPa	Ultimate Tensile Strength / MPa	Elongation at break / %	Energy at break / $kJ \cdot m^{-3}$
PS	1653(±46)	23(±1)	1.48(±0.14)	226(±60)
PS/Clay	1721(±62)	17(±2)	1.13(±0.06)	74(±25)
PS/SB-Clay	2013(±50)	32(±1)	1.69(±0.22)	251(±38)
PS/ADC-Clay	1585(±13)	20(±2)	1.36(±0.13)	166(±31)
PP/PPgMA	832(±50)	12(±2)	1.19(±0.20)	81(±49)
PP/PPgMA/Clay	927(±20)	13(±2)	1.56(±0.43)	158(±33)
PP/PPgMA/SB-Clay	983(±20)	18(±1)	2.67(±0.05)	246(±37)
PP/PPgMA/ADC-Clay	957(±5)	14(±2)	1.54(±0.40)	190(±118)
PP	899(±34)	28(±1)	8.12(±0.97)	1239(±141)
PP/Clay	1074(±13)	19(±2)	2.32(±0.83)	320(±40)
PP/SB-Clay	1011(±42)	13(±2)	1.55(±0.24)	142(±52)
PP/ADC-Clay	1006(±10)	14(±1)	1.61(±0.14)	117(±18)

[a]Five specimens were tested for each material; [b]The values in parenthesis represent the standard deviation.

The simultaneous enhancements on the stiffness, strength, ductility and toughness of the polymer by the addition of the sodium bicarbonate-treated organoclay demonstrated that the exfoliation approach *via* the use of a common non-toxic blowing agent was feasible and had a very positive influence on the mechanical properties without compromising one to the other. However, Table 7.3 also showed that polymer/ADC-Clay nanocomposites exhibited mechanical properties inferior to those of polymer/SB-Clay. As stated in the experimental section, during the extrusion process the temperature at the die was enhanced to 200 °C in the last two processing steps of the polymer/clay

nanocomposites manufactured with ADC-Clay in order to facilitate the degradation of the blowing agent. This could have also further degraded the clay surfactant, which would have deteriorated the interactions between the phases and hence the mechanical properties. Nevertheless in the case of PP/PPgMA, ADC-Clay still provided more improvements on the mechanical properties than as-received organoclay.

The effect of clay addition into PS, PP/PPgMA and PP was observed *via* SEM, by analysing the centre of the fracture surface of the tensile specimens (Figure 7.6). The tensile broken pristine PS was characterised by a craze-like brittle appearance (Figure 7.6A, inset). The addition of organoclay (Figure 7.6A1) and ADC-Clay (Figure 7.6A3) resulted in rougher tensile break elongated surfaces with smooth domains (insets), characteristic to rapid fracture areas.[131] When SB-Clay was added to PS (Figure 7.6A2), the tensile surface presented a rougher appearance and the slight occurrence of fibrils (inset), which was in good agreement with the enhancements observed in the tensile elongation and energy at break of the material.

By incorporating 10 wt.% PPgMA into PP the tensile break elongated surface presented smooth areas (Figure 7.6B, inset) and vein-type patterns. The addition of clay into the PP/PPgMA resulted in rougher areas, characterised by microvoids and ligaments that, once stretched, deformed covering the microvoids (Figures 7.6B1, 7.6B2 and 7.6B3, insets). The increased roughness of the tensile broken PP/PPgMA/clay nanocomposites compared to pristine PP/PPgMA was in good agreement with the enhancements observed in the energy at break. Compared to PS/Clay and PP/PPgMA/Clay nanocomposites, PS/SB-Clay and PP/PPgMA/SB-Clay nanocomposite presented a rougher "terrace" aspect which can be attributed to the enhanced exfoliation degree of clay and excellent dispersion of clay platelets and clay tactoids. The changes in the aspect of the tensile fracture surface of PS/SB-Clay and PP/PPgMA/SB-Clay were in accordance with the improvement observed in the tensile properties.

The pristine PP was characterised by a vein-type pattern (Figure 7.6C). The addition of organoclay and SB-Clay led to smoother venation and slight fibrillar aspect (Figure 7.6C1 and 7.6C2). In the presence of ADC-Clay, PP presented a fibrillar aspect with localised vein-type pattern (Figure 7.6C and 7.6C3, insets). This pattern has been previously observed by Yuan and Misra[131] and attributed to the tearing of the amorphous part of PP.

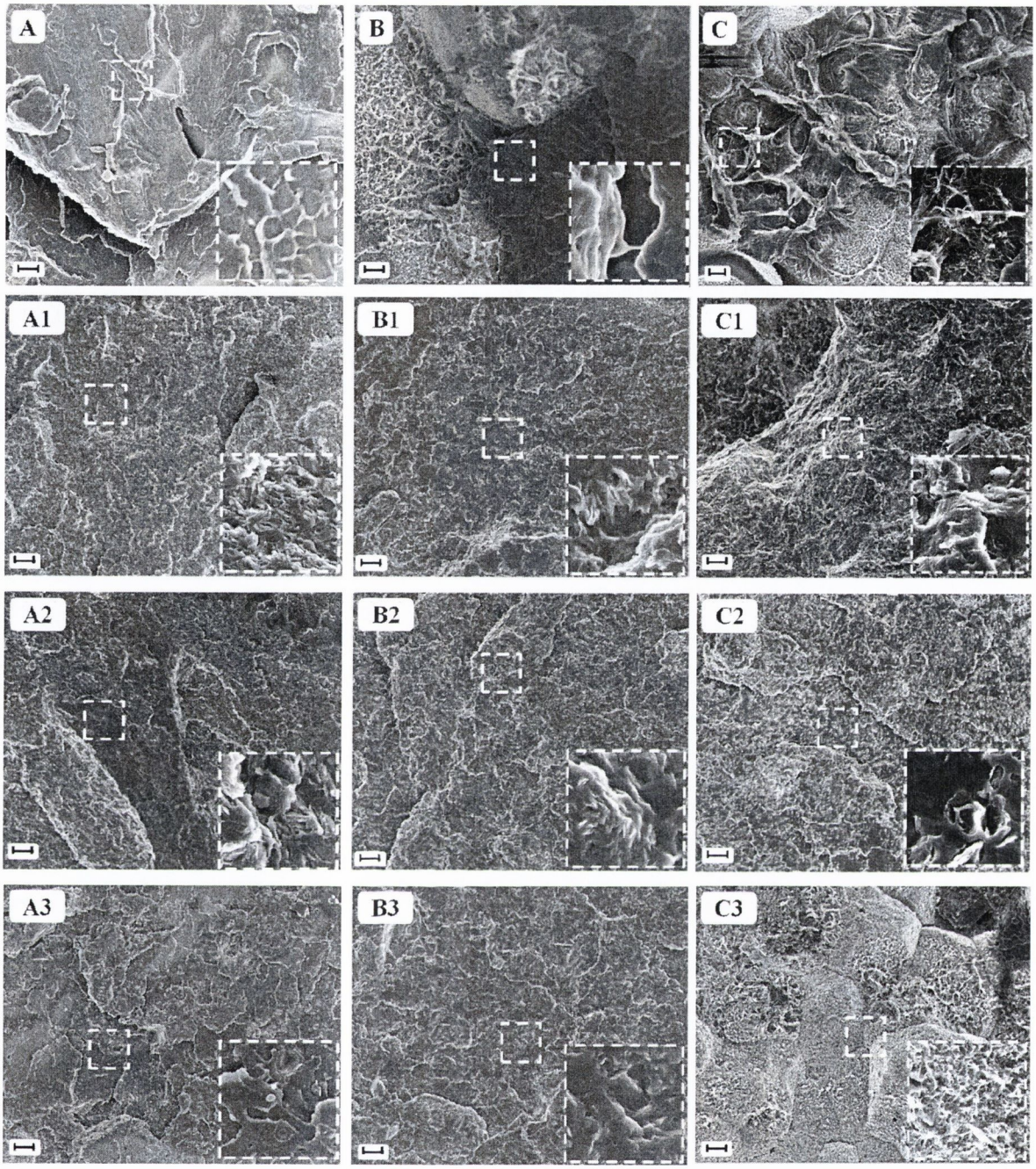

Figure 7.6. SEM images: A. PS, A1. PS/Clay, A2. PS/SB-Clay and A3. PS/ADC-Clay; B. PP/PPgMA, B1. PP/PPgMA/Clay, B2. PP/PPgMA/SB-Clay and B3. PP/PPgMA/ADC-Clay; C. PP, C1. PP/Clay, C2. PP/SB-Clay and C3. PP/ADC-Clay. (Scale bars for the main figures: 10 μm; and for the insets: 1 μm).

Although compared to polymer/as-received organoclay nanocomposites, the polymer/blowing agent-treated nanocomposites presented enhanced exfoliation; complete exfoliation has not been achieved. This is a consequence of the short extrusion time (i.e., approximately 1 minute). The improvements observed in the exfoliation degree indicated

that the pre-treatment of organoclay with blowing agents is a promising procedure that can lead, with increased mixing time, to fully exfoliated nanocomposites.

The effect that full exfoliation would have on the toughness of polymer/clay nanocomposites represents one of the most debated aspects of this field. Dasari et al.[44] observed that by dispersing 10 wt.% clay (i.e., Cloisite® 15A) in a nylon 6 matrix, the highly intercalated nanocomposites presented an impact strength 30% higher than the fully exfoliated polymer/clay nanocomposites obtained with the same amount of clay (i.e., Cloisite® 93A). Chen and Evans[135] reported that the addition of 4 wt.% clay platelets (i.e., Bentone® 111) in PS resulted in mostly intercalate polymer/clay nanocomposites which presented, compared to the pristine polymer counterpart, an insignificant decrease in the impact strength and 117% increase in the tensile energy at break. They have also noted that the dispersion of the same amount of organoclay in acrylonitrile-butadiene-styrene resulted in highly exfoliated polymer/clay nanocomposites which presented a 90% decrease in the impact strength and a 61% reduction on the tensile energy at break. On the other hand, Meng et al.[391] observed that the dispersion of 3 wt.% organoclay (i.e., Cloisite® 30B) in bismaleimide resulted in exfoliated polymer/clay nanocomposites with an impact strength 136% higher than the toughness of the pristine polymer. Basara et al.[379] reported that by dispersing 0.5 wt.% organoclay (i.e., Cloisite® 30B) in epoxy, exfoliated polymer/clay nanocomposites were obtained. These materials presented an impact strength 137% higher than the neat polymer, whilst by using the same amount of clay (i.e., Cloisite® Na^+), intercalated polymer/clay nanocomposites were formed which enhanced the impact strength by only 72%, compared to the neat polymer. The current project revealed that randomly orientated intercalated/exfoliated polymer/clay nanocomposites with a high exfoliation degree presented better stiffness and toughness. Thus, the higher degree of exfoliation does lead to improved toughness in polymer/clay nanocomposites; however, a certain degree of intercalation is also necessary. This finding is in excellent agreement with the hypothesis lunched by González et al.[202] and Lim et al.[141] who studied ternary nanocomposites (i.e., nylon 6/rubber/clay) and suggested that a partially exfoliated polymer/clay nanocomposite may be tougher than a fully exfoliated nanocomposite.

The polymer/clay nanocomposites presented superior thermal and mechanical properties compared to conventional composites and their polymer counterparts. Unlike in the case of conventional composites where the stiffness improvement was achieved at the expense of the toughness, polymer/clay nanocomposites showed enhanced stiffness and toughness. This demonstrated once again the superiority of nanocomposite materials over

conventional materials. Still, it is important to reiterate that the stiffness and toughness of polymer/clay nanocomposites depend on the polymer matrix, type of clay, processing and specimens manufacturing conditions and testing method.

7.3.4. Quantitative analysis of the composite and the nanocomposite moduli

The variations in the modulus with the addition of filler in a polymer matrix are of great significance for the fundamental scientific understanding and the design of engineering materials. The structural analysis discussed above revealed that the dispersion of clay in polypropylene resulted in the formation of conventional composites, whilst in polystyrene and compatibilised polypropylene it resulted in intercalated/exfoliated nanostructures. Since in these nanocomposites the degree of exfoliation varied according to the type of clay used, it is fundamentally important to assess the changes in the stiffness of each material in terms of their structure. Thus, the effective volume fraction of the reinforcement[122] was separately determined for each of the cases. For the structure-property relationship three classical composite material theories were considered: Mori-Tanaka model,[176, 177] Halpin-Tsai model[178] and the lower bound of the Hashin-Shtrikman model.[359]

Case 1. Conventional composites. The highly non-polar character of PP obstructed the delamination of the clay platelets. So, in this case the reinforcement was represented by clay microparticles. For the conventional binary polymer/clay composite the volume fraction of reinforcing agent was calculated according to Equation 2.8.[122] The volume fractions of clay particles inside PP were determined to be: 0.042 for Clay, 0.090 for SB-Clay and 0.110 for ADC-Clay.

By inserting the volume fractions in the Mori-Tanaka model[176, 177] for randomly orientated particles,[392] the Halpin-Tsai model[178] with the van Es correction[15] and the lower bound of the Hashin-Shtrikman model[359] the theoretical moduli for PP/clay composites were calculated. The modulus of the organoclay particles was estimated according to literature[122, 174, 175, 360, 361] and considering that the modulus and the Poisson's ratio of the clay platelets are 230 GPa and 0.28.[122] The elastic modulus of the organoclay particles was found to be 82.8 GPa. For PP the elastic modulus was taken from Table 7.3, whilst the Poisson's ratio was considered to be 0.36.[393] The experimental and theoretical elastic moduli are displayed in Figure 7.7. All the theoretical values produced by conventional composite models were found to agree reasonably well with the experimental data,

presenting an accuracy of 88-99%. However, as can be observed from Figure 7.7., the models predict a reverse trend compared to the experimental data due to the possible occurrence of clay agglomerates and uneven distribution, which are not properly accounted by the experimental models.

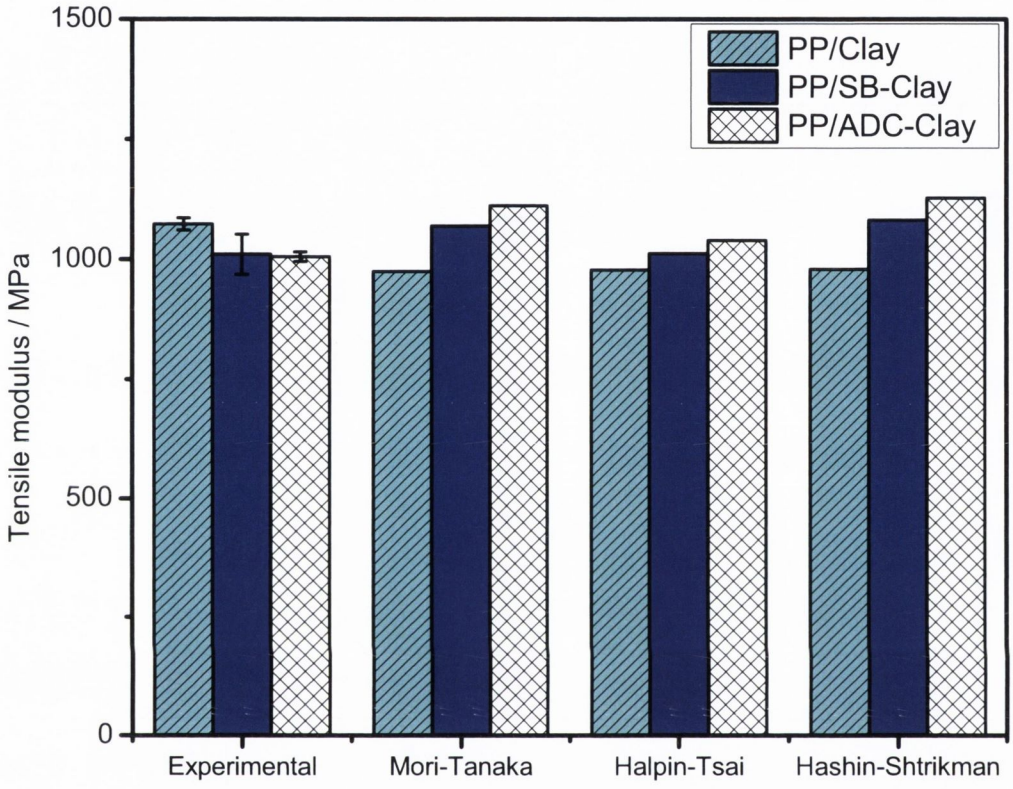

Figure 7.7. Experimental and theoretical elastic moduli of PP/clay conventional composites.

Case 2. Intercalated/exfoliated nanocomposites. An intercalated/exfoliated polymer/clay nanocomposite is considered to be made up of an intercalated nanocomposite and an exfoliated nanocomposite. Unlike clay particles reinforced PP/clay composite, the reinforcement in nanocomposites was represented by clay tactoids in the intercalated nanocomposite and single clay platelets in the exfoliated nanocomposite. The volume fraction of the intercalated nanocomposite (ϕ_p) in the final nanocomposite was assigned by $(f_i/\overline{N})/((f_i/\overline{N}) + (f_e/1))$, where the f_i, f_e and $\overline{N}$ represented the mass fraction of intercalated and exfoliated nanostructures and the average number of clay platelets per stack and were taken from Table 7.1 for each of the nanocomposites. This equation assumes that the intercalated/exfoliated polymer/clay nanocomposite was made up by a

fully intercalated nanocomposite and a fully exfoliated nanocomposite. This equation represents the ratio between the volume of intercalated clay tactoids in the fully intercalated polymer/clay nanocomposite and the volume fraction of intercalated and exfoliated nanostructures in the entire polymer/clay nanocomposite. Thus, the volume fraction of the intercalated nanocomposite in the final nanocomposite was estimated to be 0.33, whilst the volume fraction of the exfoliated nanocomposite in the final nanocomposite, taken as $1 - \phi_p$, was found to be 0.67.

For the intercalated nanostructures presented in the polymer/clay nanocomposite the elastic modulus of the reinforcement was calculated by considering a sandwich-type composite in which the polymer chains exhibited a porous structure, based on the Gibson-Ashby[175] and the Christiansen's models,[122, 174] and according to calculation procedures presented in our previous work.[351] Due to the small amount of surfactant inside the clay gallery and the insignificant amount of blowing agent residue that may remain inside the clay gallery upon high temperature exposure, the density and the modulus of these components were considered to be equivalent to the density and modulus of the intercalated polymer. The modulus was determined by considering that the clay platelets presented an elastic modulus of 230 GPa [16] and a Poisson's ratio of 0.28,[122] whilst the PS was considered to have a Poisson's ratio of 0.33.[394] The elastic modulus of the intercalated clay tactoids present in the PS matrix was calculated to be 86 GPa.[122, 174, 175, 351]

The effective volume fraction of the intercalated clay tactoids (ϕ_i), representing the reinforcement in the intercalated PS/Clay nanocomposite was determined according to Equation 7.1.[122]

$$\phi_i = \frac{\rho \mu_c f_i [d_2(\bar{N}-1)+h]}{\phi_p \rho_c [d_1(\bar{N}-1)+h]} \tag{7.1}$$

where d_1 is the basal spacing of the organoclay (i.e., 2.7 nm), d_2 is the basal spacing for the intercalated clay tactoids (i.e., 3.4 nm), h is the thickness of a clay platelet, i.e., 0.98 nm;[122] ρ is the density of the PS/Clay nanocomposite considered as 1077 kg·m^{-3}. Thus, ϕ_i was found to be 0.108.

Inserting the above values into composite theories the elastic moduli for the PS/Clay intercalated nanocomposite, E_i, were estimated to be 2339 MPa *via* Mori-Tanaka model,[176, 177, 392] 2791 MPa *via* Halpin-Tsai model[15, 178] and 2047 MPa *via* the lower bound of the Hashin-Shtrikman model.[359]

For the exfoliated nanostructures presented in the PS/Clay nanocomposite, the volume fraction of single clay platelets was determined according to Equation 7.2.[122] ϕ_e was found to be 0.064.

$$\phi_e = \frac{\mu_c \mu_c{}^0 \rho(1-f_i)}{\rho_{cp}(1-\phi_p)}(1 + kR_g A_T \rho_{cp}) \quad (7.2)$$

where $\mu_c{}^0$ is the mass fraction of clay platelets in the organoclay; k is the fraction of absorbed polymer on the clay layer that behaves like clay (i.e., 0.2);[122] A_T is the total specific surface area of the clay platelets (i.e., A_T = 658 $m^2 \cdot g^{-1}$).[122] ρ_{cp} represents the density of clay platelets (i.e., 3100 $kg \cdot m^{-3}$).[122] R_g is the radius of gyration, taken from literature as 13.40 nm for PS.[395]

Using the composite theories for the exfoliated nanocomposite present in the PS/Clay nanocomposite the elastic moduli, E_c, were estimated to be 3628 MPa from the Mori-Tanaka model,[176, 177, 392] 5909 MPa from the Halpin-Tsai model[15, 178] and 1884 MPa from the lower bound of the Hashin-Shtrikman model.[359]

In order to calculate the theoretical elastic moduli (E) for the intercalated/exfoliated PS/Clay nanocomposite, the elastic moduli for the intercalated nanocomposite (E_i) and exfoliated nanocomposite (E_c), estimated from the previously mentioned models, were inserted in the rule of mixtures formula (Equation 7.3).[396]

$$E = \phi_p E_i + (1 - \phi_p) E_e \quad (7.3)$$

From Equation 7.3, the elastic modulus of PS/Clay nanocomposite was calculated to be 3209 MPa for the Mori-Tanaka model,[176, 177, 392] 4893 MPa for the Halpin-Tsai model[15, 178] and 1937 MPa for the lower bound of the Hashin-Shtrikman model.[359] These results are depicted in Figure 7.8.

Similar to PS/Clay nanocomposite, volume fraction of the intercalated nanocomposite in the final nanocomposite was determined to be 0.20. From Equation 7.1 and Equation 7.2 the volume fractions of intercalated and exfoliated nanostructures were determined to be 0.360 and 0.075, respectively. The elastic modulus of the intercalated clay tactoids present in the PS matrix was calculated to be 80 GPa.[122, 174, 175, 351] Using the same classical composite material theories, i.e., Mori-Tanaka model,[176, 177] Halpin-Tsai model[15, 178] and the lower bound of the Hashin-Shtrikman model,[359] the elastic moduli for intercalated polymer/clay nanocomposites were calculated to be 4519 MPa, 6647 MPa and 3443 MPa, whilst for exfoliated polymer/clay nanocomposites the moduli were found to be

3945 MPa, 6659 MPa and 1926 MPa, respectively. Thus, the elastic moduli for each of the classical composite material theories were calculated using Equation 7.3 and the results are depicted in Figure 7.8.

For PS/ADC-Clay nanocomposite the ratio of polymer in the intercalated nanocomposite was found to be 0.13. Using Equation 7.1 and Equation 7.2, the volume fractions of intercalated and exfoliated nanostructures in the intercalated nanocomposite and in the exfoliated nanocomposite were determined to be 0.606 and 0.096. The elastic modulus of the intercalated clay tactoids present in the PS matrix was found to be 71 GPa.[122, 174, 175, 351] The elastic moduli for the intercalated and exfoliated nanocomposites were calculated using the previously mentioned classical composite material theories. Using Equation 7.3, the elastic moduli for the intercalated/exfoliated nanocomposite (Figure 7.8) were found to be 5058 MPa for the Mori-Tanaka model,[176, 177, 392] 8822 MPa for the Halpin-Tsai model[15, 178] and 2547 MPa for the lower bound of the Hashin-Shtrikman model.[359]

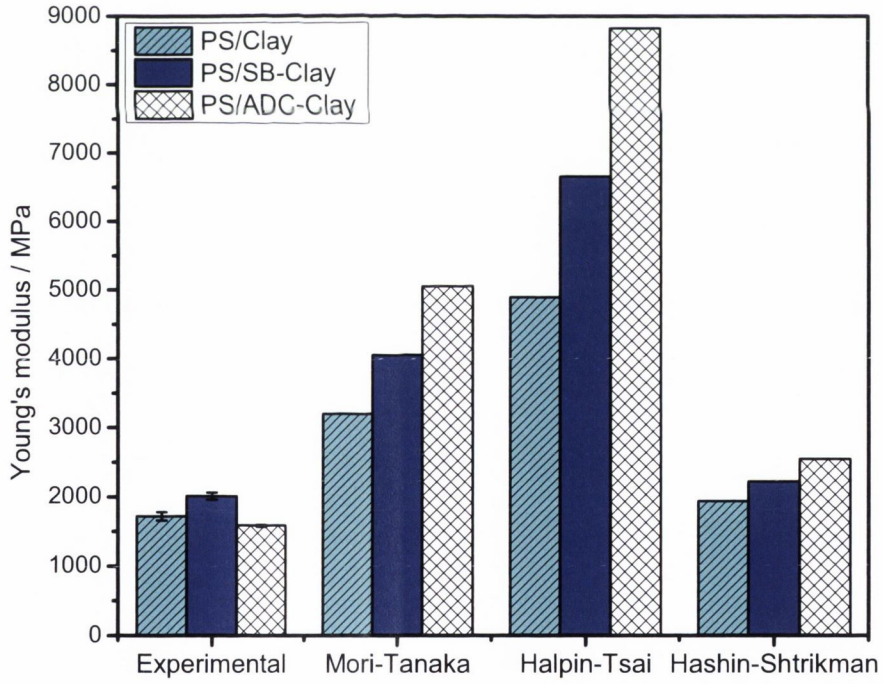

Figure 7.8. Experimental and theoretical elastic moduli of PS/clay nanocomposites.

The Halpin-Tsai[15, 178] and the Mori-Tanaka[176, 177, 392] models overestimated the experimental data by doubling the values for PS/Clay, PS/SB-Clay and PS/ADC-Clay. In comparison, the lower bound of the Hashin-Shtrikman model[359] only overestimated the

experimental moduli for PS/Clay, PS/SB-Clay and PS/ADC-Clay nanocomposites by 13%, 10% and 61%, providing the most accurate prediction of the experimental data. Still, typically the lower bound of the Hashin-Shtrikman model[359] is supposed to be lower than the experimental value. The fact that this model assumes macroscopically homogeneity[397] and does not take into account the changes that might have occurred in the polymer matrix when being subjected to the high processing temperatures are factors that can be responsible for the discrepancies between the theoretical and experimental data. The higher modulus predicted for PS/ADC-Clay nanocomposites suggested that indeed the mechanical properties should have increased with the enhancement of the exfoliation degree. However, the lack of a compatibilising agent and the limited mixing time obstructed the delamination of the clay platelets inside the low-polarity polymer matrix.

The elastic moduli for the intercalated/exfoliated PP/PPgMA/clay nanocomposites were calculated following the method described above for the intercalated/exfoliated PS/clay nanocomposites. Due to the highly non-polar character of PP, it was considered that only the PPgMA adsorbed on the clay platelets, thus the radius of gyration was calculated to be 3.95 nm for PPgMA.[371, 398] As previously, the volume fraction of the intercalated nanocomposite in the final PP/PPgMA/Clay nanocomposite was assigned to be 0.34. Using Equation 7.2 and Equation 7.3 the volume fractions of intercalated (ϕ_i) and exfoliated (ϕ_e) nanostructures were determined to be 0.083 and 0.022, respectively. The modulus of the intercalated clay tactoids present in the PP/PPgMA matrix was calculated to be 104 GPa.[122, 174, 175, 351] The elastic moduli for the PP/PPgMA/Clay intercalated nanocomposite, E_i, were estimated to be 1103 MPa *via* Mori-Tanaka model,[176, 177, 392] 1300 MPa *via* Halpin-Tsai model[15, 178] and 983 MPa *via* the lower bound of the Hashin-Shtrikman model,[359] whilst the elastic moduli for the PP/PPgMA/Clay exfoliated nanocomposite, E_e, were determined from the previously mentioned models to be 1232 MPa, 1673 MPa and 871 MPa, respectively. The elastic moduli for the PP/PPgMA/Clay nanocomposites calculated from Equation 7.3 for the classical composite material theories utilised were depicted in Figure 7.9.

Similar to PP/PPgMA/Clay nanocomposite, the ratio of polymer in the intercalated PP/PPgMA/SB-Clay nanocomposite was considered to be 0.22. The volume fractions of intercalated and exfoliated reinforcement were calculated, from Equation 7.1 and Equation 7.2, to be 0.247 and 0.032. The elastic modulus of the intercalated clay tactoids present in the PP/PPgMA matrix was found to be 84 GPa.[122, 174, 175, 351] Inserting these fractions in the classical composite theories, the elastic moduli of intercalated PP/PPgMA/SB-Clay

nanocomposites (E_i) were determined to be 1744 MPa for the Mori-Tanaka model,[176, 177, 392] 2471 MPa for Halpin-Tsai model[15, 178] and 1371 MPa for the lower bound of the Hashin-Shtrikman model,[359] whilst the elastic moduli of exfoliated PP/PPgMA/SB-clay nanocomposites (E_e) were found to be 1390 MPa for the Mori-Tanaka model,[176, 177, 392] 2033 MPa for Halpin-Tsai model[15, 178] and 887 MPa for the lower bound of the Hashin-Shtrikman model.[359] The elastic moduli of intercalated/exfoliated PP/PPgMA/SB-Clay nanocomposite were calculated according to Equation 7.3 for each of the classical composite theories considered. The results are depicted in Figure 7.9.

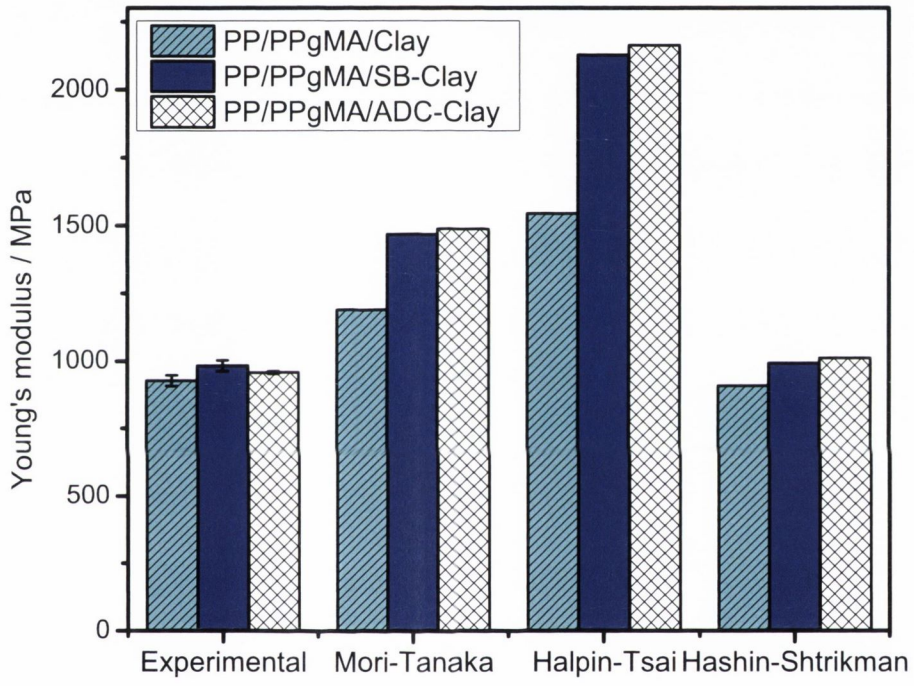

Figure 7.9. Experimental and theoretical elastic moduli of PP/PPgMA/clay nanocomposites.

Using the same procedure, the volume fraction of the intercalated nanocomposite in the final PP/PPgMA/ADC-Clay nanocomposite was determined to be 0.26. From Equation 7.1 and Equation 7.2, the volume fractions of reinforcement were found to be 0.245 for the intercalated PP/PPgMA/ADC-Clay nanocomposite and 0.032 for the exfoliated polymer/clay nanocomposite. The elastic modulus of the intercalated clay tactoids present in the intercalated PP/PPgMA/ADC-Clay nanocomposite was determined to be 104 GPa.[122, 174, 175, 351] Using these values the elastic moduli for the intercalated and exfoliated polymer/clay nanocomposite were calculated *via* Mori-Tanaka model,[176, 177, 392] Halpin-

Tsai model[15, 178] and the lower bound of the Hashin-Shtrikman model.[359] Inserting these values in Equation 7.3, the elastic moduli for PP/PPgMA/ADC-Clay nanocomposite were determined to be 1488 MPa for the Mori-Tanaka model,[176, 177, 392] 2163 MPa for the Halpin-Tsai model[15, 178] and 1011 MPa for the lower bound of the Hashin-Shtrikman model.[359] Again, the results are presented in Figure 7.9.

The values predicted for the PP/PPgMA/clay nanocomposites *via* the Halpin-Tsai[15, 178] model appeared to overestimate the experimental values by 67% for Clay and doubled the experimental values for SB-Clay and ADC-Clay. However, the theoretical values estimated by the Mori-Tanaka model[176, 177, 392] and the lower bound of the Hashin-Shtrikman model[359] presented an accuracy of up to 98% for PP/PPgMA/Clay, 99% for PP/PPgMA/SB-Clay and 94% for PP/PPgMA/ADC-Clay, with the lower bound of the Hashin-Shtrikman model[359] displaying the most accurate prediction of the experimental data (Figure 7.9). The agreement between the Mori-Tanaka model[176, 177, 392] and the Hashin-Shtrikman model[359] has been previously acknowledged[399, 400] and attributed to excellent dispersion and low fractions of filler used.[181, 401] The excellent prediction, of the experimental data, offered by the lower bound of the Hashin-Shtrikman model[359] has been attributed to the dispersion of low volume fractions of reinforcement, characterised by a higher modulus than the matrix.[122, 180, 397, 402]

7.4. Conclusions

Polymer/clay nanocomposites with as-received organoclay or blowing agent-treated organoclay were manufactured by melt compounding the clays with polystyrene or maleated propylene compatibilised polypropylene. The dispersion of the clays in PS and PP/PPgMA led to the formation of intercalated/exfoliated polymer/clay nanocomposites. The degree of exfoliation and specific surface area of the clay platelets was directly dependent on the blowing agent used to treat the clay and indirectly dependent on the polymer matrix in which the clay was dispersed. The type of blowing agent used to treat the clay appeared to be of crucial importance. The ADC-Clay has shown to aid the exfoliation while maintaining a constantly small number of clay platelets per stack. On the other hand, the SB-treated organoclay increased exfoliation and improved delamination. These reflected in the glass transition temperature which slightly diminished due to increased relaxation time of the polymer present inside the clay gallery. The peak

degradation temperature was enhanced with the dispersion of clay by up to 37 °C for PS and by 46 °C for PP/PPgMA.

The mechanical properties presented statistical significant enhancements in the Young's modulus and the ultimate tensile strength, which increased, with the dispersion of SB-Clay, by 22% and 40% for PS and 18% and 52% for PP/PPgMA. These improvements were reflected in the energy at break which increased, compared to the polymer counterpart, by up to 205% in PP/PPgMA/clay nanocomposites. The superiority of blowing agent-treated organoclay over the as received organoclay was ratified by the paramount mechanical properties that the polymer/blowing agent-treated organoclay nanocomposites exhibited over the polymer/as-received organoclay nanocomposites. Thus, the ultimate tensile strength and the elongation at break were found to increase by 89% and 49% in PS/SB-Clay nanocomposite and by 39% and 71% in PP/PPgMA/SB-Clay nanocomposite compared to PS/Clay and PP/PPgMA/Clay nanocomposites. The structure-property relationship for the intercalated/exfoliated nanocomposites was found to be best described by the lower bound of the Hashin-Shtrikman model.

Chapter 8. Changes in crystallinity and crystalline structure in nylon 6/clay nanocomposites

8.1. Introduction

Clay reinforced polymer composites have been a part of our lives for over two decades; however, it was Richard Feynman's, 1959, visionary declaration that "There's plenty of room at the bottom"[403] which motivated the quest for micromaterials and sequentially fuelled the search for nanomaterials. In 1987,[2] the prophecy came true, when the researchers at Toyota Central R&D Labs discovered that the dispersion of a small amount of clay into polyamide 6 created a hybrid material with unique properties. This opened the door to the polymer/clay nanocomposite technology, subsequently leading to the first industrial use of this material as the timing belt cover in automotive cars.[9] Today, polymer/clay nanocomposites, present an increasing interest in both the academia and the industries; this class of materials being often characterised by better and/or unique properties compared to pristine polymers or conventional composites.[8]

The first fully exfoliated polymer/clay nanocomposites have been obtained by *in situ* incorporation of ε-caprolatam with cation exchanged clay (i.e., montmorillonite treated with hydrochloride salt of aminolauric acid).[2, 12] Nylon 6 is a high performance, low cost, thermoplastic polymer that can be amorphous or semicrystalline. Due to its excellent chemical resistance and mechanical properties,[404, 405] this polymer presents a myriad of applications from fibers and engineering plastics to packaging and automotive industry to healthcare and apparel.[406-408]

The semicrystalline polymer, polyamide 6, exhibits four crystalline structures: α, β, δ and γ.[408] The α-phase is a stable monoclinic structure with fully extended nylon chains,[409] in which the amide linkage and methylene units are situated in the same plane (Figure 8.1).[410] Thus, hydrogen bonds form between adjacent anti-parallel orientated nylon 6 chains and create sheets of hydrogen-bonded chains.[411] The γ-phase emerges when hydrogen-bonds form between parallel nylon 6 chains. Due to the strong hydrogen bonding ability that polyamides present, the bonds formed under γ crystallisation require the amide linkage to twist by 60° in order to maximise the number of hydrogen-bonds.[410] Initially, the γ-form was believed to be monoclinic.[409] However, the zigzag chain packing resembles a hexagonal structure which deemed the γ-phase to be considered as pseudo-hexagonal.[411] Research has shown that the β-phase is an intermediate phase between the α-form and the

γ-form.[412] In 2002, Li and Goddard,[408] have discovered that nylon 6 presented a forth crystalline phase, denoted as δ-form, which is an intermediate phase between β-phase and γ-phase. Therefore, it was conceded that polyamide 6 displayed only two original crystalline phases, i.e., α-phase and γ-phase.[409] Typically, the α-phase is considered to be more thermodynamically stable than the γ-phase, with the γ-phase converting to α-phase upon the application of stress at room temperature, melting followed by re-crystallisation or annealing in a saturated-stream atmosphere.[408, 409] However, this transformation implies the break of hydrogen bonds, the formation of new hydrogen bonds and the change in conformation from parallel chains to anti-parallel chains.

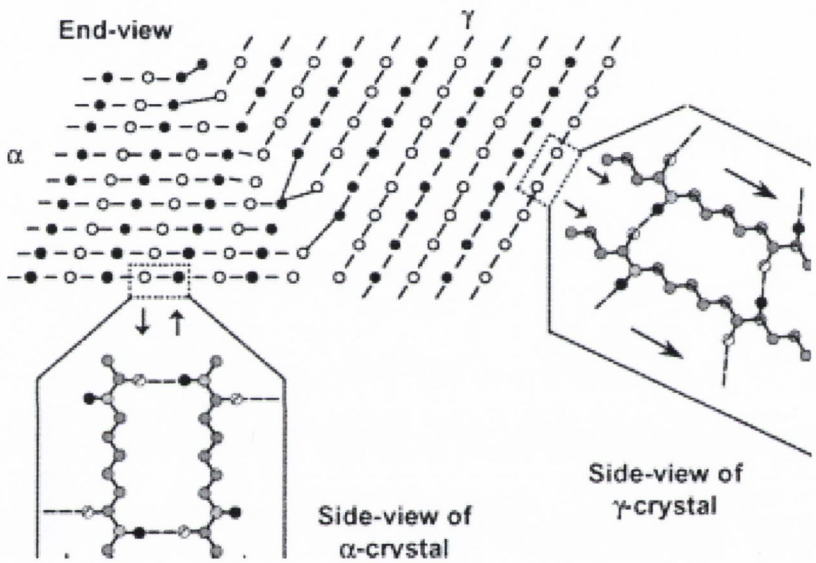

Figure 8.1. Schematic illustration of hydrogen bonding within α and γ crystalline forms of nylon 6 as seen from end and side-view of each crystal. Closed and open circles represent chain axes projecting out of and into the page, respectively. Hydrogen bonds between polyamide chains are represented by dash lines (Reproduced from reference[410]).

The impact of crystallisation temperature and time have been widely analysed and it has been observed that the α-phase was favoured by the slow cooling from molten state or crystallisation at high temperatures, whilst the formation of γ-phase was promoted by low crystallisation temperatures or high cooling rates.[405, 409] Fornes and Paul[410] have studied the impact of injection moulding on the specimens manufactured from pristine polyamide 6 or nylon 6/clay nanocomposites. They have concluded that due to fast cooling the exterior of the specimen was characterised exclusively by γ-form crystallisation, whilst the interior of the specimen displayed both basic crystalline structures.

8.1.1. Crystallisation kinetics

The crystallisation process involves nucleation and growth of polymer crystals.[413] In order to explain these processes, kinetic growth theories have been established. Considering both the nucleation and the diffusive transport phenomena, the Turnbull-Fisher expression (Equation 8.1) relates the crystallisation temperature (T_c) with the primary crystallisation rate (G_1).[414]

$$\ln G_1 = \ln G_0 - \frac{\Delta E^*}{k_B \cdot T_c} - \frac{\Delta F^*}{k_B \cdot T_c} \tag{8.1}$$

where G_1 is the spherulitic growth rate, G_0 is a pre-exponential factor, k_B is Boltzmann constant, ΔE^* is the free energy of activation for transporting a chain segment and ΔF^* is the free energy of formation of a critical size nucleus.[415]

The most common method to analyse the spherules growth rate is the Lauritzen-Hoffman equation (Equation 8.2).[416] This equation analyses the linear growth rate (at high degrees of supercooling, i.e., $\Delta T = T_m^0 - T_c$, where T_m^0 represents the equilibrium melting point)[417] as a function of the deposition of the secondary nuclei and the rate of lateral surface growth.[418]

$$\ln G_1 + \frac{U^*}{\mathcal{R} \cdot (T_c - T_\infty)} = \ln G_0 - \frac{K_g}{T_c \cdot f \cdot \Delta T} \tag{8.2}$$

where U^* is the transport activation energy (Equation 8.3), T_∞ is the hypothetical temperature (i.e., $T_\infty = T_g - 30$) bellow which there is no viscous flow and K_g is a nucleation parameter.[417, 419] $\mathcal{R}$ is the gas constant and f is a correction factor that characterises the variation in the bulk melting enthalpy per volume unit with temperature, i.e., $f = 2 \cdot T_c/(T_m^0 + T_c)$.[419]

The transport activation energy refers to the necessary energy for the crystallised units to be transported across the melt/solid interface.[420] This energy can be calculated with the Williams-Landel-Ferry relation (Equation 8.3):[419, 421]

$$U^* = \frac{C_3 \cdot T_c}{C_4 + T_c - T_g} \tag{8.3}$$

where C_3 and C_4 are constants with the values of 17.3 kJ·mol^{-1} and 51.6 K.[420]

During the growth process of the spherulites the polymer chains fold back and forth arranging themselves into crystal lamellas,[422] characterised by a thickness that is expressed by Hoffman and Weeks equation.[423] This equation introduces a lamellar thickening factor (β) which correlates with the equilibrium melting temperature according to Equation 8.4.[419] This factor represents the ratio between the mature crystal and the initial crystal.[417]

$$\beta = \frac{T_c}{2(T_m^0 - T_m)} \tag{8.4}$$

As the researchers from Toyota have demonstrated, the addition of a small amount of nanofiller can enhance the mechanical properties of this semicrystalline material.[2, 209, 404, 405, 424] To date, the most fundamental studies on polymer/clay nanocomposites use nylon 6 as the base polymer due to its polar character[425] and ability to assist the dispersion of clay without the use of a compatibilising agent.[173] Still, this does not guaranty that, regardless of the type of clay used, fully exfoliated polymer/clay nanocomposites structures will be attained. Using a nylon 6 matrix, other clays and different preparation methods, researchers have reported conventional composites, intercalated and/or exfoliated nanocomposites.[2, 385, 426] The degrees of exfoliation and dispersion of the clay platelets represent key factors in controlling the morphology, structure and mechanical properties of the polymer/clay nanocomposites. This project aims at analysing the changes in the crystalline structure of polymer and polymer/clay nanocomposites before and after subjecting the materials to uniaxial deformation. It also takes into consideration the effect of the clay platelets and how they influence the crystallinity of the system, the changes that take place in the crystalline morphology and crystallinity degree. Since the mechanical and thermal properties of polymer/clay nanocomposites are related to the nanostructure of the materials, intercalated/exfoliated morphologies with different degrees of exfoliation were analysed during the course of the study. The morphology of the materials was investigated *via* X-ray diffraction and transmission electron microscopy, whilst the thermal properties and crystallinity were evaluated by performing thermogravimetric analysis and differential scanning calorimetry. The uniaxial deformation was achieved by performing tensile tests on injection moulded materials. The morphology and crystalline structure of the elongated materials were analysed *via* scanning electron microscopy, TEM and DSC.

8.2. Experimental Section

8.2.1. Materials

The semicrystalline polymer, polyamide 6 (DSM Akulon®, Grade: K222D) from DSM (Netherlands), was purchased from Resinex (UK).Three types of clays were used: natural montmorillonite (MMT), organoclay (Clay) and a blowing agent-treated organoclay (ADC-Clay) that was described in the previous Chapter. Natural sodium montmorillonite clay (325 mesh) was generously supplied by Bentonite Performance Minerals LLC (Wyoming Plant, South Dakota, USA). The Clay, i.e., Nanomer® I44.P, a dimethyl dihydrogenated tallow ammonium chloride (2M2HTA) modified montmorillonite, from Nanocor Corporation (Illinois, USA) was kindly supplied by Nordmann, Rassmann GmbH (Hamburg, Germany). The organoclay was treated with a well known organic blowing agent, azodicarboxamide (ADC) in the presence of zinc oxide, which were both purchased form Sigma-Aldrich Ireland Ltd. (Dublin, Ireland). The clay treatment has been previously discussed in Chapter 7. The clay platelets content was determined for all the clays by Loss on Ignition[345, 351] to be 88.6% for MMT, 60% for Clay and 21% for ADC-Clay. The chemical composition of the MMT was analysed to be SiO_2, 64.12 wt.%; Al_2O_3, 18.92 wt.%; Fe_2O_3, 3.78 wt.%; MgO, 2.29 wt.%; Na_2O, 1.88 wt.%; CaO, 1.19 wt.%; K_2O, 0.44 wt.%; and TiO_2, 0.13 wt.% by using a Panalytical Axios X-Ray Fluorescence Spectrometer according to ISO 12677 method at CERAM (Stoke-on-Trent, UK).[345] Prior to being used the clays were dried in a normal convection oven at 90 °C for 6 hours. The clay densities were determined from five measurements of a dried sample performed at 30 °C on a Micromeritics AccuPyc 1330 pycnometer to be 2616 $kg \cdot m^{-3}$ for MMT, 1605 $kg \cdot m^{-3}$ for Clay and 2242 $kg \cdot m^{-3}$ for ADC-Clay.

8.2.2. Nanocomposite manufacturing and sample preparation

Polymer/clay nanocomposites with 4 wt.% clay platelets content were melt compounded on a twin screw extruder at 180, 188, 210 and 240 °C from hopper to die. The materials were passed three times: first at 200 rpm and then twice at 100 rpm to allow the degradation of the blowing agent present in ADC-Clay. After cooling in water, the extrudates were pelletized. In order to obtain the specimens for the tensile, impact and fracture testing, a bench top injection moulder (Ray Ran model 2 Test Sample Injection Moulding Apparatus, UK) was used at a barrel temperature of 232 °C, a tool temperature of 65 °C and a pressure of 0.76 MPa.

8.2.3. Characterisation

XRD was carried out on a Phillips PW1720 X-Ray Diffractometer with a $CuK_{\alpha 1}$ (λ = 0.15406 nm) anode tube at the standard conditions of 40 kV and 20 mA. The samples were tested from 2° to 10°, 2θ angle, at a step size of 0.02° and a duration of 2.5 seconds per step. Powdered samples were used to characterise the clays, whilst hot pressed disc samples were used for the polymer/clay nanocomposites due to the apparent ductility of the materials.

TEM was performed on a TECNAI G2 20 twin electron microscope at 200 kV accelerating voltage. The specimens were ultrathin-sectioned using a Reichert-Jug 'Ultracut' ultramicrotome equipped with a diamond knife. The sections (~100 nm in thickness) were collected in a trough filled with water and placed on a 200 mesh copper grid.

SEM imaging was performed on tensile fractured surfaces using a Tescan MIra Variable Pressure Field Emission Scanning Electron Microscope at a voltage of 5.0 kV. Prior to being analysed the samples were mounted on stubs and their surface was gold coated.

TGA measurements were performed on a Perkin Elmer Pyrus 1 TGA under nitrogen flow (20 $mL \cdot min^{-1}$), from 30 °C to 650 °C at a heating rate of 10 $°C \cdot min^{-1}$.

DSC was carried out on a Perkin Elmer Diamond DSC at a scan rate of 10 $°C \cdot min^{-1}$. The crystallinity (χ_c) of polymer/clay nanocomposites was calculated, using Equation 4.1.[251, 327] The melting enthalpy for the 100% crystalline nylon 6 was taken from literature as 190 $J \cdot g^{-1}$.[427] In order to eliminate the effects of the heating history of the material, the glass transition temperature (T_g) was taken from the second heat scan. For the neat polymer and the polymer/clay nanocomposites the middle section of injection moulded specimens were analysed before and after tensile testing. The amount of crystalline phase was identified from the second heat scans by determining the area under each of the peaks and analysing the percentage observed under Gaussian deconvolution method[428, 429] (Figure 8.2).

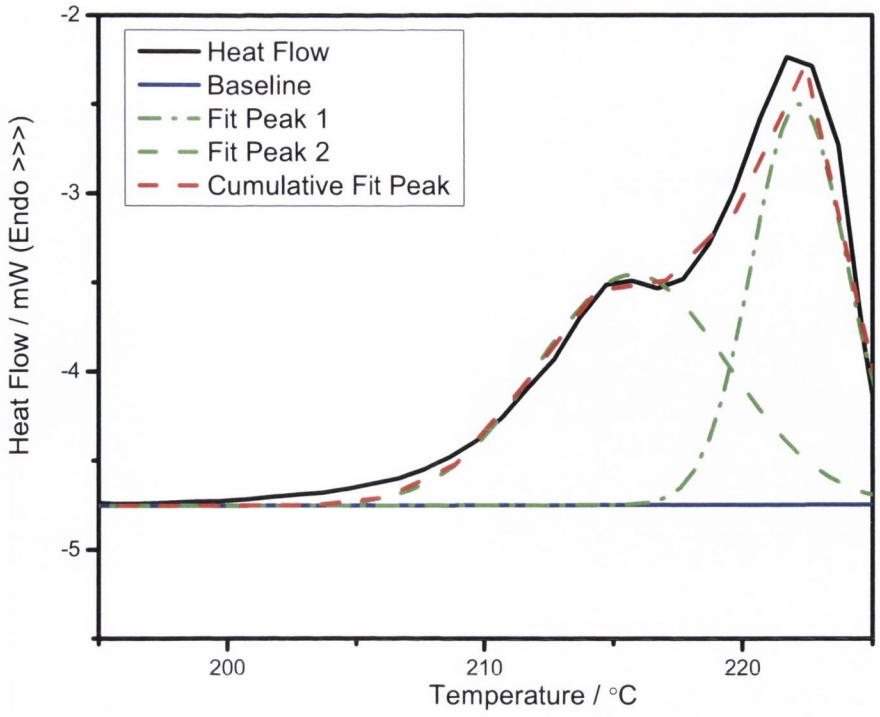

Figure 8.2. Example of Gaussian deconvolution method used to establish the percentage of each of the crystalline phases formed in the pristine polymer and polymer/clay nanocomposites.

Tensile tests were carried, at room temperature, on a Zwick Z005 machine according to ISO 527:1993. The tests were performed using a 2.5 kN load cell and a cross head speed of 10 mm·min^{-1}. Five dog-bone specimens (Type 1BA) were tested for each of the materials. The mean and standard deviation values reported for the mechanical tests represent a confidence level of 95%. Statistical significance was assessed by a Two-tailed, Type II 't' test with a probability lower than 0.05.

8.3. Results and Discussion

8.3.1. Structure

From the XRD diagrams in Figure 8.3 it can be observed that the natural clay exhibited a broad diffraction peak at a 2θ value of 7.1°(Curve 1), corresponding to a basal spacing, $d_{(001)}$, of 1.2 nm. By intercalating the 2M2HTA in the basal spacing of the montmorillonite, the as-received organoclay presented a well pronounced *(001)* diffraction peak at a 2θ value of 3.3°, corresponding to a $d_{(001)}$, of 2.7 nm (Curve 2). Treating the organoclay with a blowing agent shifted the diffraction peak to a slightly higher 2θ value

(Curve 3). This marginal decrease was probably due to the removal of some surfactant molecules or impurities from the galleries. The blowing agent molecules can intercalate inside the basal spacing without actually increasing the distance between the clay platelets, as it was previously discussed in Chapter 4 and in Chapter 7.

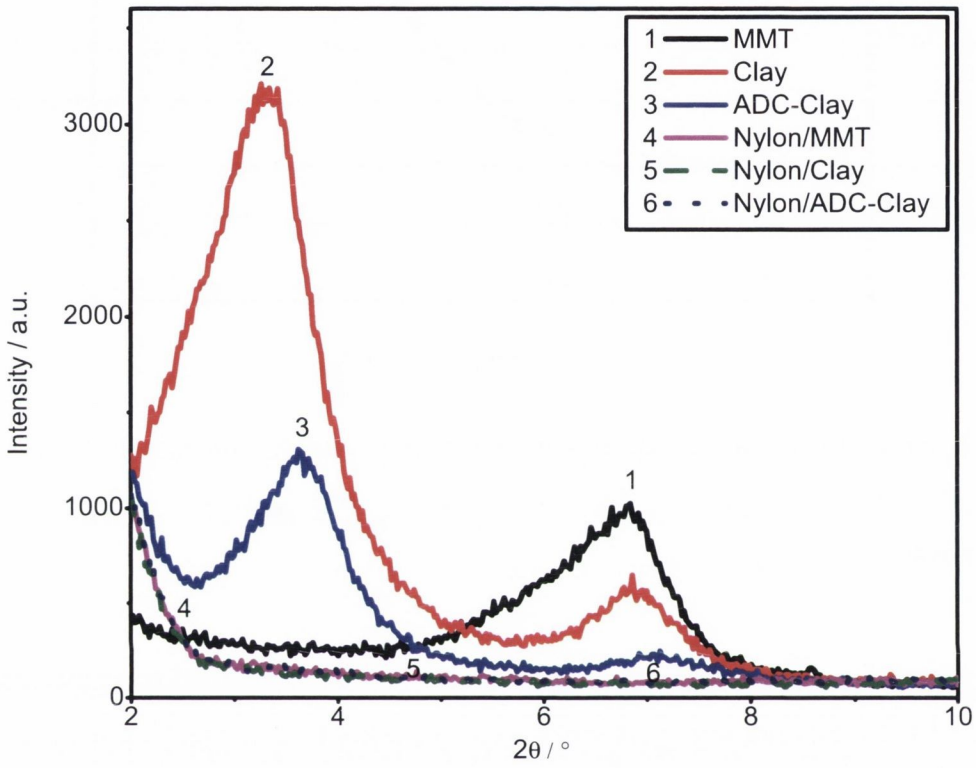

Figure 8.3. XRD profiles of: 1. natural clay (MMT), 2. organoclay (Clay), 3. blowing agent-treated organoclay (ADC-Clay), 4. nylon/MMT, 5. nylon/Clay and 6. nylon/ADC-Clay.

As observed from Figure 8.3, Curves 4-6, the XRD analysis did not detect any significant peaks on the nylon/clay nanocomposite traces. The absence of peaks may be due to the formation of microcomposites, the occurrence of highly exfoliated polymer/clay nanocomposites or the orientation effect of the sample due to the use of a disc specimen.[8] This will be sequentially discussed from the TEM images.

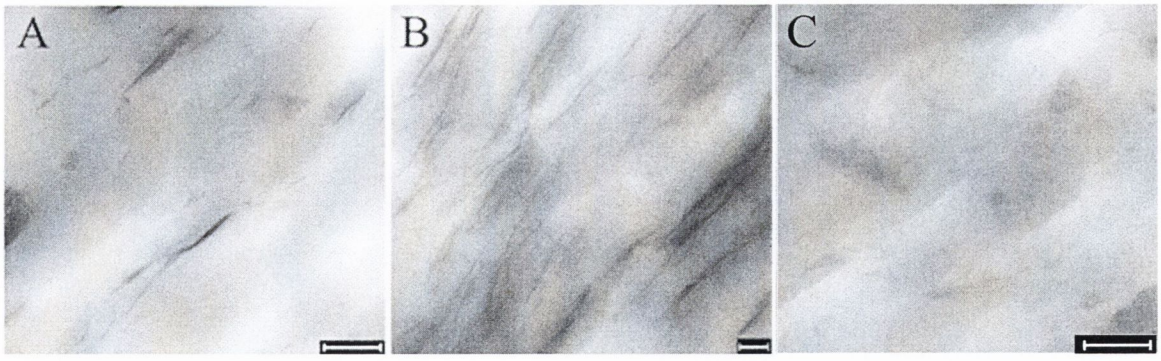

Figure 8.4. TEM images: A) Nylon/MMT, B) Nylon/Clay and C) Nylon/ADC-Clay (Scale bars: 200 nm).

The TEM images revealed that the dispersion of different clays with equal amounts of silicate layers in a nylon 6 polymer matrix led to intercalated/exfoliated polymer/clay nanocomposites in all cases. As shown in Figure 8.4 the dispersion of clay platelets and clay tactoids in the mid section of the specimen (orthogonal to the direction of the flow direction) were orientated in the flow direction, which is in accordance with the previous studies.[424] The clay tactoids and clay platelets appeared to orient in the same direction, at a lower exfoliation degree (Figures 8.4A and 8.4B) and presented a more random orientation, at a higher exfoliation degree (Figure 8.4C). The dispersion of natural montmorillonite resulted in a more sporadic dispersion of clay tactoids and clay platelets (Figure 8.4A), whilst the dispersion of an as-received organoclay or a blowing agent-treated organoclay led to the formation of homogeneous materials (Figures 8.4B and 8.4C). The intercalated/exfoliated nanostructures are summarised in Table 8.1.

Compared to nylon/MMT nanocomposites (Table 1, Column 1), the fraction of intercalated clay tactoids reduced in nylon/Clay nanocomposites (Table 1, Column 2) due to the presence of the surfactant inside the gallery of clay. The dispersion of blowing agent-treated organoclay (Table 1, Column 3) enhanced the ability of clay platelets to delaminate which increased the exfoliation degree. Thus, the degree of exfoliation was influenced by the type of clay mixed in the nylon matrix. Similar to the previous work on PS and PP/PPgMA, the degree of exfoliation attained when ADC-Clay was dispersed into the polymer matrix had increased compared to when the commercially available clay was dispersed into the same polymer. This demonstrates that treating the as-received clay with a blowing agent represents a promising technique that has the potential of leading to fully exfoliated polymer/clay nanocomposites.

Table 8.1.TEM results for nylon/clay nanocomposites

Nanocomposites / Structure	Nylon/MMT[a]	Nylon/Clay[b]	Nylon/ADC-Clay[b]
f_e	0.42	0.52	0.84
f_i	0.58	0.48	0.16
N_{min}	2	2	2
N_{max}	6	7	4
$\overline{N}$	2.6	2.5	2.2

[a]Estimated from over 85 nanostructures; [b]Estimated from over 150 nanostructures; f_e – mass fraction of exfoliated nanostructures; f_i – mass fraction of intercalated nanostructures; N_{min} – minimum number of clay platelets per stack in a clay tactoid; N_{max} – maximum number of clay platelets per stack in a clay tactoid; $\overline{N}$ – average number of clay platelets per stack in a clay tactoid.

8.3.2. Crystalline structure and crystallinity

As observed from Figure 8.5 pristine nylon 6 presented two distinct peaks at 216 °C and 222 °C. Correlative studies between XRD and DSC have established that the peak at 216 °C corresponded to the γ-phase; whist the second peak was associated with the more thermodynamically stable α-phase.[407, 409] The formation of the peak at 216 °C has been attributed to the crystallisation process that some nylon 6 polymer chains may undergo when heated. Thus, imperfect crystals may attempt to perfect their structure in order to reach a more thermodynamically stable state. Zheng et al.[430] explained the phenomenon by assuming that some nylon chains did not crystallise during the cooling process, but once heated they began the crystallisation process, thus the heat released during the reorganisation process counteracted with the heat absorbed during the melting process. By applying the Gaussian deconvolution method[428, 429] (not shown in Figure 8.5) it was determined that the crystallinity degree of the γ-phase was 23%, whilst the crystallinity degree of the α-phase was 19%. The dispersion of MMT and Clay in nylon 6 resulted in a shift in the melting temperature peaks. The peak corresponding to the γ-phase became more prominent and presented a crystallinity degree of 24% for MMT and 25% for Clay, whilst the contribution of the α-phase decreased to a crystallinity degree of 7% for MMT and 5% for Clay.

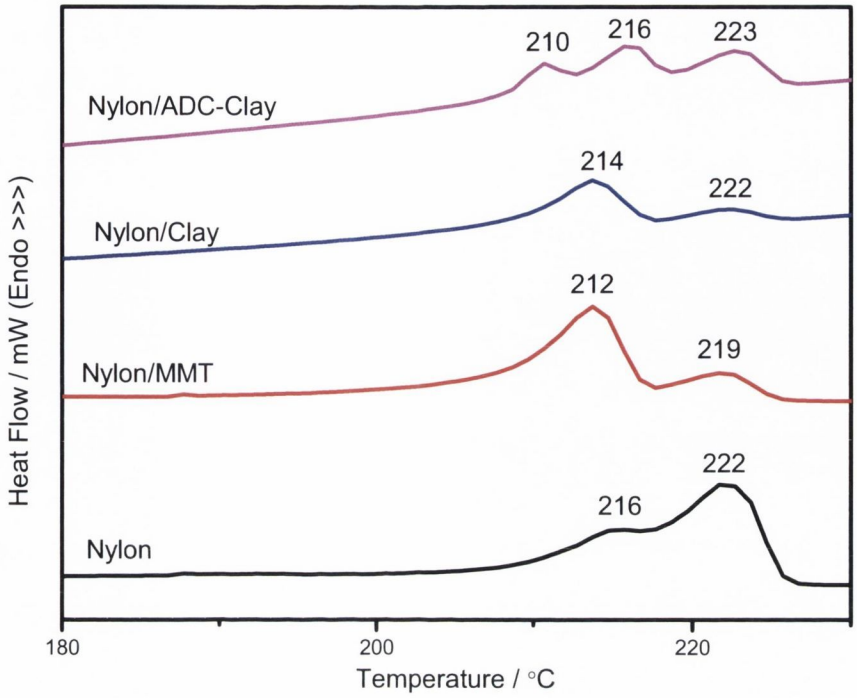

Figure 8.5. DSC second heating scan before tensile testing of pristine polymer and polymer/clay nanocomposites (Gaussian deconvolution method not shown here).

The DSC trace for the nylon/ADC-Clay nanocomposite presented three distinctive melting temperature peaks at 210, 216 and 223 °C representing a crystallinity degree of 18, 9 and 5%, respectively. The proximity of the first two temperature peaks suggested that the polymer crystallised as γ-phase, whilst the latter peak represented the α-phase. The occurrence of two distinct peaks for the less thermodynamically stable phase indicated that the dispersion of blowing agent-treated organoclay has altered the crystalline structure of the polymer. This change can be attributed to the increased degree of exfoliation which created more interfaces between the clay platelets and the polymer and hindered the formation of thermodynamically stable hydrogen bonds. The occurrence of three temperature peaks was previously reported by Zheng et al.[430] who studied the crystalline structure of nylon 6 reinforced with micro and nano ZnO. They have attributed the formation of the middle peak to the spherulitic growth or rearrangement of the polymer chains, by running XRD tests at the temperatures afferent to each of the peaks. However, when running the DSC test at a constant heating rate (i.e., 10 °C·min^{-1}), the third peak was encountered only when nano-sized ZnO was dispersed into the nylon 6 matrix. Thus, it can be hypothesised that in our case the delamination of the clay particles into single clay

platelets increased the number of interfaces and/or the presence of the ZnO particles may favoured the formation of γ-crystallites. The reduction of the α-phase with the dispersion of clay has been previously encountered[405] and ascribed to the presence of the silicate layers which once dispersed into the nylon 6 matrix promoted heterogeneous nucleation of the γ-phase.[412]

The DSC traces for the heating curve of the tensile tested pristine polymer and polymer/clay nanocomposites (Figure 8.6A) showed that after the polymer was subjected to external stresses the elongated materials presented three peaks each, except for nylon/Clay nanocomposites which exhibited only two melting peaks. Similar to the DSC heating traces registered before the samples were elongated (Figure 8.5), the first two peaks were attributed to the γ-phase and the last one, at 223 °C was attributed to the α-phase. The γ-phase peaks were encountered at 210 and 215 °C for nylon/MMT and nylon/ADC-Clay nanocomposites. Although the pristine polymer presented a peak at 216 °C, the first peak was encountered at 192 °C. The less prominent peak exhibited by tensile tested pristine nylon (Figure 8.6B) suggested that this peak represented probably β- and/or δ-phase crystallites, that are intermediate phases between the γ and α.[408] Comparing the DSC trace for the elongated nylon/MMT nanocomposite (Figure 8.6A, Curve 2) with the DSC trace of the un-stressed material (Figure 8.5, Curve 2) it was observed that the higher melting temperature, corresponding to the α-phase crystallinity, remained almost unchanged. However, the peak situated at a lower temperature and corresponding to the γ-phase crystallites split into two peaks at 211 °C and at 214 °C. The occurrence of the second peak may be due to the delamination of the silicate layers which created additional surfaces that acted as nucleation centres and promoted γ-phase formation.[410, 412] The tensile tested nylon/Clay and nylon/ADC-Clay presented quite similar DSC traces to the non-elongated materials.

Analysing the ratio of the α-phase vs. the γ-phase (from the Gaussian deconvolution method, not shown in Figure 8.6) for nylon/ADC-Clay nanocomposite, it was observed that the contribution of each phase stayed relatively the same. In this case, the well dispersed clay platelets presented a limited elongation (Table 8.4, Column 3). Thus, hydrogen bonds were straighten but the system did not provide enough energy for the bounds to break and rearrange into a more stable conformation.[408] However, analysing the crystallinity degree of α and γ-phase radical changes were observed due to the necessity of polymer chains to reach a more thermodynamically stable state. Nylon/Clay nanocomposite presented a decrease in the α-phase crystallinity degree from 5% to 2%,

whilst the γ-phase crystallinity degree was enhanced from 25% to 32%. These changes were attributed to the uniform dispersion of intercalated/exfoliated clay platelets which promoted γ-phase crystallisation. This is in accordance with the previous findings reported in literature, as mentioned above.[430]

Typically after subjecting the pristine nylon to external stresses at room temperature the γ-phase crystallites should change into α-phase crystallites;[408, 409] however, in the presence of clay the γ-phase crystallinity degree increased. During the deformation process the polymer chains are exposed by the external stresses and the polymer lamellas exhibit a slip phenomenon as indicated by Zhou and Wilkes.[431] The sliding of the lamellas causes the breaking of the hydrogen bonds as well as the delamination of the clay tactoids. The polymer chains attempt to reach a more thermodynamically stable state; however, the presence of the clay and its delamination hindered the formation of the hydrogen bonds further and promoted the formation of the less thermodynamically stable bonds. This can be a consequence of the larger distance between polymer lamellas that the γ-phase crystallites present as opposed to α-phase crystallites. Zhao et al.[405] measured the distances between polymer lamellas in α-phase and in γ-phase, and obtained 0.801 nm and 0.933 nm for the cases. Since the thickness of a silicate layer is of 0.98 nm,[122] it can be assumed that in some cases the polymer lamellas and the single clay platelets may create a layered structure. Indeed, Katoh and Okamoto[432] found that nylon 6 formed lamellas on the surface of MMT particles which resulted in a sandwich structure between the polymer chains and the clay platelet.

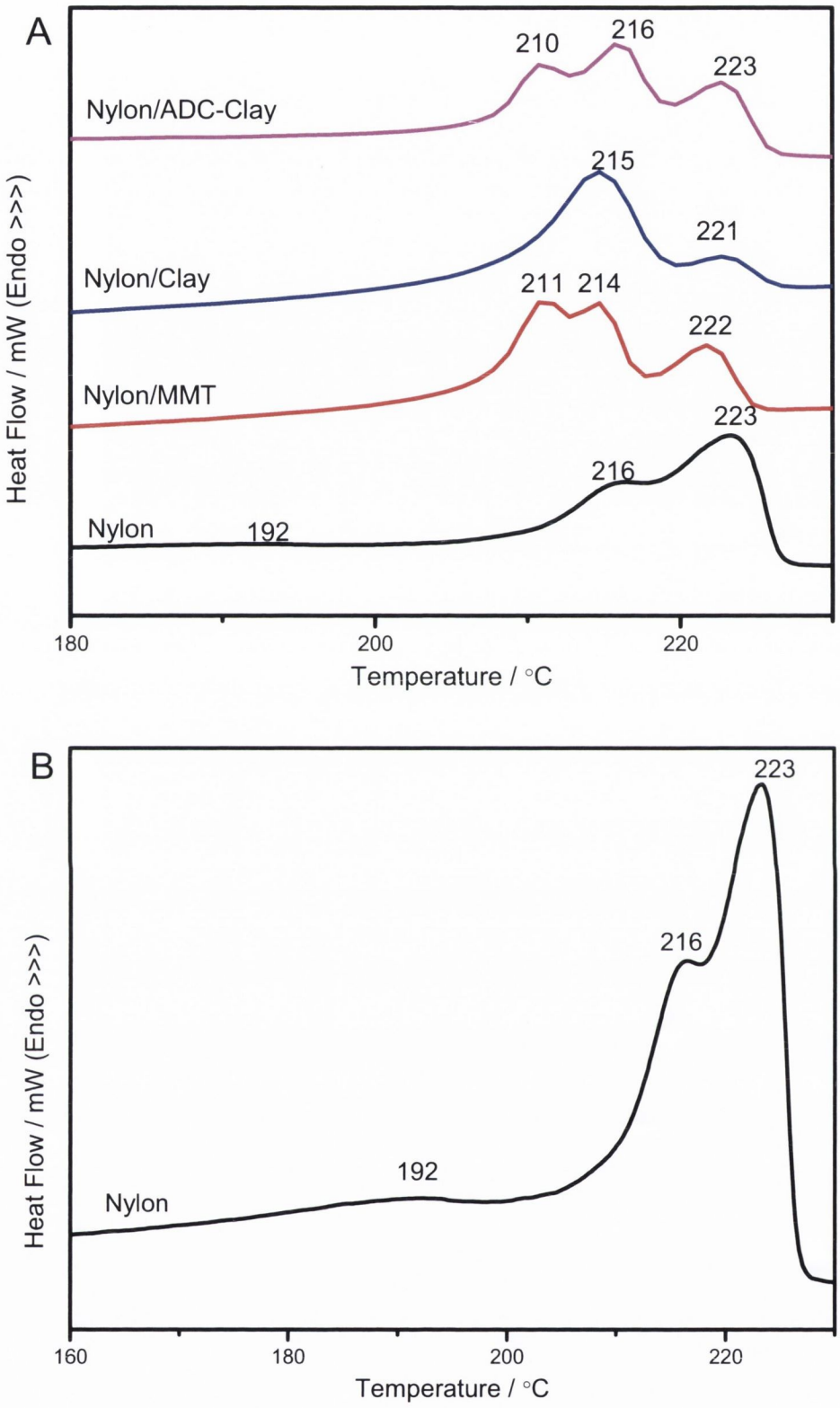

Figure 8.6. DSC second heating scan after tensile testing of A. pristine polymer and polymer/clay nanocomposites and B. heating scan for pristine polymer after uniaxial deformation demonstrating the existence of three peaks at 192, 216 and 223 °C (Gaussian deconvolution method not shown here).

The glass transition temperature was measured at the midpoints of the corresponding glass transition regions. As observed from Table 8.2, Column 1, T_g of the polymer/clay nanocomposites presented insignificant variations compared to the glass transition of the neat polymer. By dispersing clay in nylon 6, the crystallisation temperatures (T_c - measured as the temperature at which the peak on the cooling curve was recorded, Table 8.2, Column 2) was enhanced, whilst the melting temperatures (T_m - measured as the temperature at which the peak on the heating curve was recorded, Table 8.2, Column 3) diminished, regardless of the type of clay. The enhancement in T_c occurred due to the heterogeneous nucleation effect that clay induced in the polymer matrix, which was previously reported in literature.[223, 410] The nucleation effect of the clay led to a reduction in the crystallite size,[223] which reflected in diminished crystallinity degree (Table 8.2, Column 4). The clay prevented the development of large crystalline domains. This diminished the degree of crystallinity of the polymer/clay nanocomposites compared to the neat polymer. Fornes and Paul[410] have studied the dispersion of natural and organoclay (i.e., Cloisite® Na and Cloisite® 30B) in nylon 6 and attributed the reduction in the degree of crystallinity of the polymer/clay nanocomposites, compared to neat polymer, to the presence of clay which obstructed the polymer chains from arranging into crystalline lamellas. The results are in good agreement with their observations and suggest that the chain stiffening effect suppressed the nucleation effect.

Table 8.2. DSC results for polymer and polymer/clay nanocomposites prelevated from tensile specimens before mechanical testing

Material	T_g / °C	T_c / °C	T_m / °C	χ_c / %
Nylon	49	190	222	42
Nylon/MMT	48	197	212	31
Nylon/Clay	51	199	214	30
Nylon/ADC-Clay	50	195	216	32

The thermal and the crystalline properties of the pristine and polymer/clay nanocomposites, after uniaxial deformation have been assessed *via* DSC and the results are presented in Table 8. 3. As can be observed from Table 8.2 and Table 8.3, the glass transition temperature (Column 1), the crystallisation temperature (Column 2) and the

melting temperature (Column 3) afferent to the pristine nylon and nylon/clay nanocomposites did not change after the samples have been subjected to a high stress at room temperature, i.e., lower than the T_g of nylon.

However, comparing the crystallinity of the samples before (Table 8.2, Column 4) and after (Table 8.3, Column 4) subjecting the materials to uniaxial strains it was observed that for pristine nylon the degree of crystallinity decreased, whilst polymer/clay nanocomposites showed a higher degree of crystallinity. The pristine nylon presented a decrease in the crystallinity degree from 42% to 38% when the polymer was subjected to tensile deformation. The apparent lower crystallinity occurred due to the breaking of the bonds, since the sample analysed was acquired from the rupture point. During the tensile test the bonds elongated and the crystallinity increased, due to neat packing of the polymer chains. However, at the breaking point the polymer chains presented enhanced entropy due to the presence of broken chains, and thus slightly lower crystallinity, which is in agreement with the previous literature findings.[433] Nylon/MMT and nylon/Clay nanocomposites presented similar increases in the crystallinity degree which was in good agreement with the similar elongations at break (Table 8.3, Column 3) encountered during the tensile test. However, nylon/ADC-Clay nanocomposite presented a significant increase in the crystallinity degree from 32% to 55% and only minimal elongation at break. This again attested to the fact that in this case the polymer chains straightened and ruptured with minimal elongation of the polymer chains. The increase in crystallinity of the polymer/clay nanocomposites after the samples have been tensile tested was attributed to the good dispersion of the clay platelets. When the polymer chains were straightened and stretched, the clay platelets induced friction forces and created additional surfaces that further aligned the polymer chains and aided the formation of a compact crystalline structure, this is in accordance with the previous findings reported in literature.[434]

The glass transition temperature of the deformed polymer/clay nanocomposites presented some changes as opposed to the T_g of the elongated neat polymer (Table 8.3, Column 2). Upon subjecting the material to elongation the packing density between the polymer chains inside the gallery increased[435] which led to a lower T_g of nylon/MMT nanocomposite compared to pristine nylon. However, this decrease did not occur in the glass transition temperature of the nylon/Clay nanocomposites; in fact, the T_g maintained a very close value to the glass transition temperature of the neat polymer. The lack of change in this case can be attributed to the formation of intercalated and exfoliated nanostructures and to the plasticisation effect of the surfactant[390] which compensated each other. The

polymer presented within the intercalated clay tactoids exhibited a faster relaxation rate, whilst the polymer adsorbed on the exfoliated clay platelets presented a slow relaxation rate.[387, 435] Because the surface of the clay that comes in contact with the polymer matrix is higher in the exfoliated nanocomposite than in the intercalated nanocomposite, it would be expected for the T_g to increase; however, the subsequent exposure of the surfactant that took place with the intercalation/exfoliation effect, induced a plasticisation phenomenon that decreased the T_g. Nylon/ADC-Clay nanocomposites presented exfoliated clay platelets with random orientation (Figure 8.5C); this obstructed the elongation of the polymer chains, whilst increasing the content of nylon adsorbed on the clay platelets. The dense packing density of polymer chains presented a reduction in the relaxation time, thus increasing the glass transition temperature.[387] In this case the superior exfoliation degree exhibited by the ADC-Clay dispersed in the nylon matrix overcame the plasticisation effect of the exposed surfactant.

Table 8.3. DSC results for polymer and polymer/clay nanocomposites prelevated from tensile specimens after mechanical testing

Material	T_g / °C	T_c / °C	T_m / °C	χ_c / %
Nylon	49	190	223	38
Nylon/MMT	46	195	211	35
Nylon/Clay	50	198	215	34
Nylon/ADC-Clay	53	194	216	55

Similar to the crystallinity degree assessed before the samples were uniaxially deformed the crystallinity of nylon/MMT and nylon/Clay nanocomposites decreased compared to pristine nylon. This reduction showed that even when the polymer chains were well elongated, or even broken, the presence of clay obstructed the formation of hydrogen bonds. However, the crystallinity degree of nylon/ADC-Clay nanocomposites increased compared to pristine nylon, after the application of a uniaxial strain, from 38% to 55%. In this case, the presence of well dispersed clay layers enhanced the crystallinity by increasing the amount of polymer adsorbed on the surface of individual clay platelets which was correlated with the higher T_g value. The higher crystallinity encountered for nylon/ADC-Clay nanocomposite compared to nylon/MMT and nylon/Clay

nanocomposites can be attributed to the straightening and minimal elongation of the polymer chains of the former compared to the latter nanocomposites.

Although the exposure of pristine nylon 6 to external stresses transformed the γ-phase crystallites into the more thermodynamically stable α-crystallites by passing through β and δ-phases, the presence of clay platelets promoted the formation of γ-phase and even obstructed the rearrangement of the polymer chains in order to reach a more stable configuration. To assess the ability of semicrystalline nylon 6 to transport crystallisable segments to the melt/solid interface, before and after being subjected to tensile testing, the transport activation energy was calculated according to the Williams-Landel-Ferry relation (Equation 8.3).[419, 421] The results are depicted in Figure 8.7.

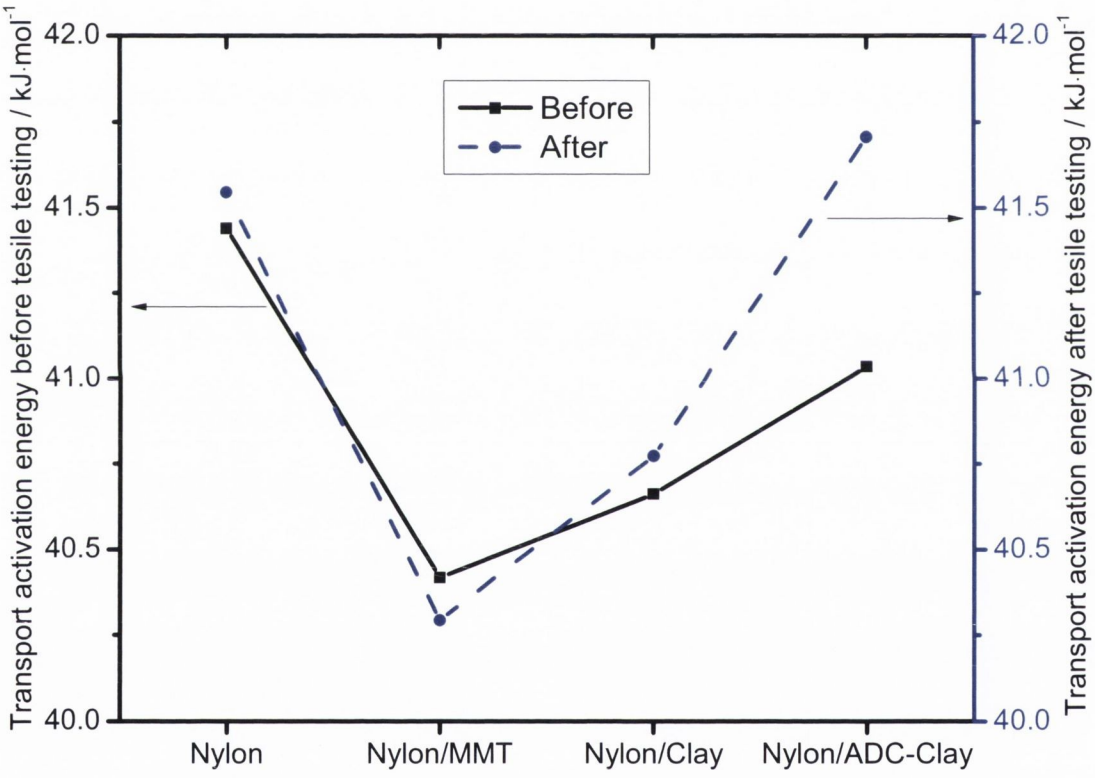

Figure 8.7. Transport activation energy of semicrystalline nylon 6 in pristine polymer and polymer/clay nanocomposites, before and after tensile deformation.

The transport activation energy decreased with the addition of clay, which can be attributed to the presence of clay tactoids and clay platelets that obstructed the formation of hydrogen bonds. This was in good agreement with the reductions observed in the crystallinity of the polymer/clay nanocomposites compared to the crystallinity degree of

the pristine polymer (Table 8.2, Column 4). In most of the cases the transport energy increased after the polymer chains were subjected to external stresses. These improvements were a consequence of reducing the distance between the polymer lamellas. However, the transport energy of the polymer chains from nylon/MMT nanocomposite presented a slight decrease after the elongation process. This may be attributable to the presence of mostly intercalated tactoids that can obstruct the rearrangement of the polymer chains. This will be further discussed from the lamellar thickness factor.

The increase in the exfoliation degree created more nucleation centres which marginally improved the transport energy. By subjecting the material to external stresses the transport energy further improved due to the reduction in the distance between the polymer sheets and the delamination of the clay tactoids which introduced additional nucleation centres. These changes were best reflected in the increase in the crystallinity degree of the polymer in nylon/ADC-Clay compared to the crystallinity degree of the same material before the uniaxial test.

In order to assess the impact of the changes that occurred in the crystalline phase formation after subjecting the neat polymer and the semicrystalline matrix of the polymer/clay nanocomposites to external stresses, the lamellar thickness factor was calculated according to the Hoffman–Weeks expression (Equation 8.4).[423] The percent changes in the lamellar thickness with regard to the before and after β-factors of each crystalline phase are depicted in Figure 8.8. Since the polymer is the only one that deforms during bulk mechanical tests and crystallises during melting and crystallisation processes, it was assumed that the equilibrium melting temperature was the same for neat polymer and polymer matrix, before and after elongation. As observed from the DSC diagrams there are two crystalline phases that are present in the neat polymer and in the polymer matrix, thus according to the work of Ho and Wei[428] the equilibrium meting temperature was considered to be 226.1 °C for the γ-phase and 231.4 °C for the α-phase.

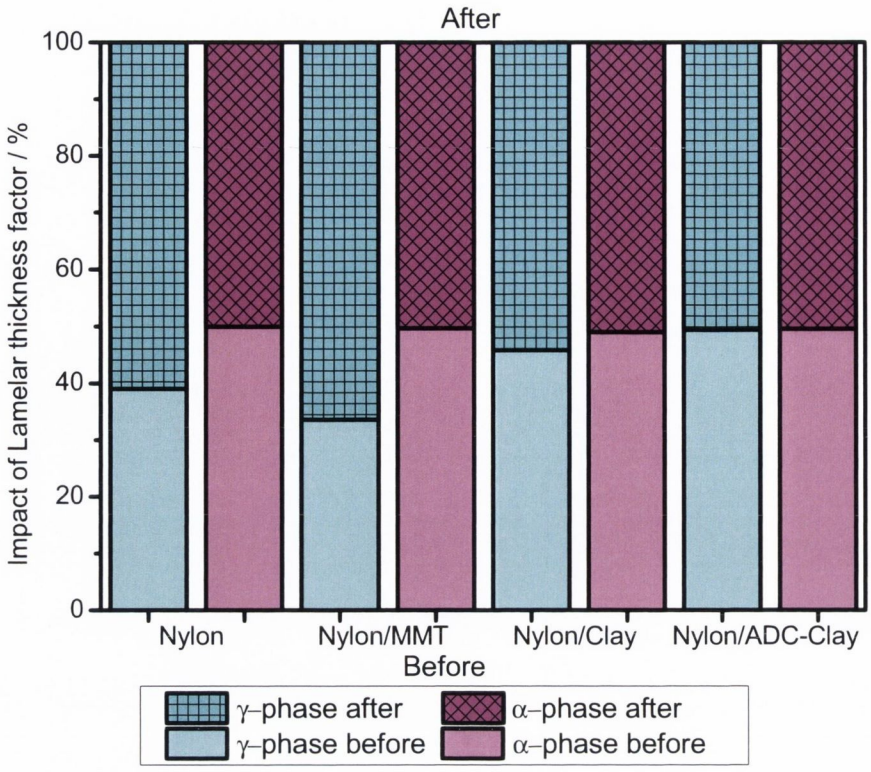

Figure 8.8. Impact of lamellar thickness in α and γ crystalline phase, before and after tensile elongation.

As can be observed from Figure 8.8 the lamellar thickening factor for the lamellas in the γ-phase increased after the neat polymer was subjected to external stresses. In calculating the impact of the lamellar thickness factor of pristine nylon 6, before and after the material was subjected to uniaxial deformations, the peak at 192 °C, which occurred after elongation, was considered to represent γ-phase crystallisation. Figure 8.6 implied that γ-phase crystallisation was favoured after uniaxial deformation. However, it is well known that upon subjecting a pristine polymer to external stresses, the polymer chain attempts to rearrange from γ-phase to α-phase conformation.[408, 409] Thus, it was confirmed that approximately 30% of the polymer had crystallised as β and/or δ-phase.

The presence of clay in the nylon 6 matrices facilitated the increase in the lamellar thickness factor after the polymer was subjected to uniaxial deformation due to the lower thickness of the γ-phase crystals compared to α-phase crystals.[405] Similar to the transfer activation energy, the impact of the lamellar thickness factor on the γ-phase crystallisation after uniaxial deformation decreased with the improvement in the exfoliation degree, whilst the lamellar thickness factor on the α-phase crystallisation presented marginal

variation. Thus, the presence of well dispersed highly exfoliated clay platelets stabilised the crystalline phases before and after uniaxial deformation.

8.3.3. Mechanical properties

The dispersion of clay into nylon 6 led to 53-65% statistically significant enhancements in the Young's moduli (Table 8.4, Column 1). These improvements were due to the presence of the clay platelets that are characterised by a higher modulus than the polymers. Compared to the dispersion of unmodified MMT, the presence of Clay or ADC-Clay in the nylon 6 was characterised by statistically significant enhancements in the stiffness of the material. These differences are directly related to the degree of dispersion, as it can be observed from Figure 8.4, the Nylon/Clay and the Nylon/ADC-Clay nanocomposites are characterised by a more homogeneous structure than the Nylon/MMT nanocomposite. Also, in an intercalated material the reinforcement is represented by clay tactoids with polymer intercalated between the silicate layers, whereas in an exfoliated polymer/clay nanocomposite the reinforcing unit is directly the clay platelet.

Table 8.4. Mechanical properties of nylon and nylon/clay nanocomposites[a,b]

Material	Young's Modulus / MPa	Tensile Strength / MPa	Elongation at break / %	Energy at break / $MJ \cdot m^{-3}$
Nylon	1033(±215)	34.8(±1.1)	219(±20)	21.5(±9.3)
Nylon/MMT	1577(±43)	55.9(±2.4)	16(±2)	33.0(±0.2)
Nylon/Clay	1707(±23)	60.6(±0.2)	11(±1)	33.6(±0.7)
Nylon/ADC-Clay	1694(±3)	62.2(±1.6)	6(±1)	17.9(±3.9)

[a]Five specimens were tested for each material; [b]The values in parenthesis represent the standard deviation.

Similar to the modulus, the dispersion of clay into nylon resulted in 61-79% statistically significant enhancements in the tensile strength (Table 8.4, Column 2) compared to pristine nylon 6. By improving the dispersion of clay platelets and clay tactoids the strength of the nanocomposite materials improved with statistical significance

by up to 11% (nylon/Clay or nylon/ADC-Clay vs. nylon/MMT nanocomposites). These enhancements in the tensile modulus and tensile strength have been previously encountered and attributed to the excellent dispersion of clay platelets and clay tactoids and to the effective transfer of the load from the polymer matrix to the nanofiller.[8, 180]

The energy at break was used to establish the impact that the addition of clay had on the toughness of the polymer matrix, this took into account the ability of clay platelets to improve the strength and stiffness of the material, as well as the effect of the clay platelets on the crystalline structure of the polymer matrix. As observed from Table 8.4, Column 4 the use of MMT or Clay resulted in up to 53% enhancements in the energy at break, whereas, the dispersion of ADC-Clay led to 17% statistically insignificant reduction in the energy absorbed at break. The toughness of the polymer/clay nanocomposites was found to statistically significantly diminish with the decrease in the number of clay platelets stacked in the clay tactoids. This suggested that in nylon 6 nanocomposites it is necessary to have intercalated nanostructures present in order to facilitate the delamination of the silicate layers, thus allowing for more of the energy to be transferred from the polymer matrix to the clay platelet. The higher energy at break absorbed by the polymer/clay nanocomposites with a larger intercalated factor may be also attributed to the increase distance that the hydrogen-bond sheets need to travel once they are subjected to a stress.[408] An increase in the exfoliation degree led to the embrittelment of the material and the obstruction of the straightening of the polymer chains. These findings are in good agreement with the observations made by Dasari et al.[44] who established that for a nylon 6 matrix a higher intercalation degree is preferred over a higher exfoliation degree. The previous work showed that highly exfoliated polymer/clay nanocomposites exhibited superior toughness compared to neat polymer and mostly intercalated polymer/clay nanocomposites. However, it should be noted that the superior exfoliation degrees observed for PS and PP/PPgMA with the dispersion of SB-Clay or ADC-Clay ranged between 50% and 61% as it was observed in Chapter 7. Thus, the exfoliation degree of 52% exhibited by the nylon/Clay nanocomposites fits the previous range. However, the 42% exfoliated nanostructures presented by the nylon/MMT nanocomposite (Table 8.1) suggested the need of higher exfoliation. Since the differences in toughness and exfoliation degree between the two nanocomposite systems are not extreme, it can be concluded from the tensile test that a ratio between the mass of intercalated nanostructures and the mass of exfoliated nanostructures close to unity can lead to polymer/clay nanocomposite systems with superior toughness.

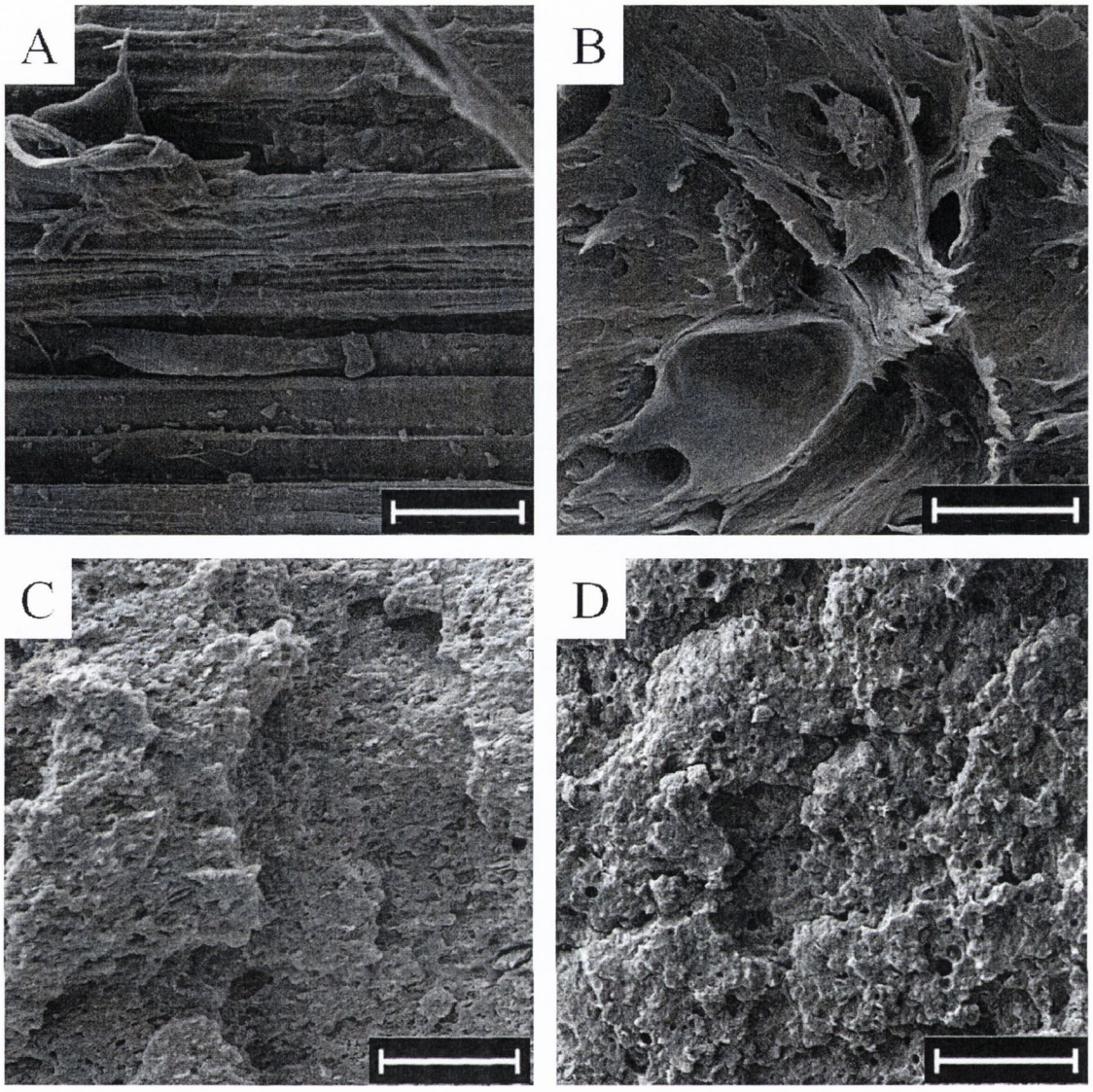

Figure 8.9. SEM images for the tensile fractured surfaces A) tensile elongated nylon fibers; and the tensile surface of B) nylon/MMT, C) nylon/Clay and D) nylon/ADC-Clay nanocomposites (Scale bar: 10 μm).

The effect of clay addition in semicrystalline nylon 6 was observed by SEM analysing the tensile broken specimens (Figure 8.9). The pristine nylon presented a fibrous aspect characterised by well elongated polymer fibers (Figure 8.9A). In some areas the breaking and the friction that occurred during the elongation process introduced small fibrils on the long stretched polymer fibers. These small fibrils may be due to the breaking of the hydrogen chains in the attempt to rearrange from γ-phase crystallisation to α-phase crystallisation. In nylon/MMT nanocomposite, the inability of the polymer chains to transport crystallisable segments to the melt/solid interface and the increased γ-phase lamellar thickness prevented the polymer from elongating throughout the entire tensile surface (Figure 8.9B). Thus, the tensile fractured surface presented areas where the

polymer chains appeared to be elongated yet prematurely broken, and areas where thick crystalline domains caused dislocations. In nylon/Clay nanocomposites, the increase in the exfoliation degree past 50% led to surfaces characterised by a terraced aspect in which small fibrils and microvoids were observed (Figure 8.9C). The formation of microvoids has been previously reported in literature and attributed to debonding of the clay platelets from the polymer matrix or delamination.[17, 436, 437] The surface of the tensile tested nylon/ADC-Clay nanocomposite presented an almost brittle aspect, characterised by the sporadic occurrence of small fibrils (Figure 8.9D). This is in good agreement with the increase in the crystallinity degree observed after the elongation process (Table 8.3, Column 5). The presence of well dispersed highly exfoliated clay platelets acted as nucleation and growth centres even before the specimens were subjected to tensile testing (Figure 8.10). However, during the elongation process the ability of crystallisable segments to order increased (Figure 8.9). Thus, the rearrangement of hydrogen bonds from one configuration to another was obstructed.

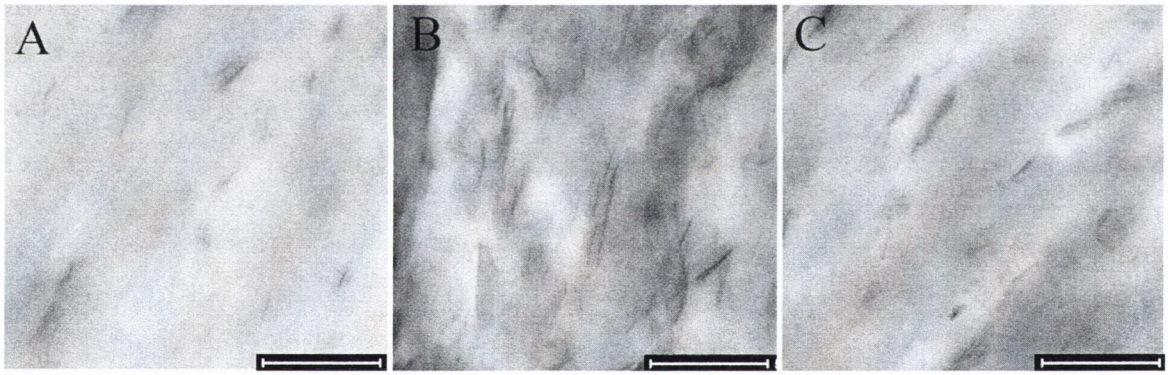

Figure 8.10. TEM images after uniaxial deformation: A) Nylon/MMT, B) Nylon/Clay and C) Nylon/ADC-Clay (Scale bar: 500 nm).

The TEM imaging of the tensile tested polymer/clay nanocomposites showed that during the uniaxial deformation process the clay tactoids became more orientated and in some cases delaminated into single clay platelets, regardless of the type of clay used (Figure 8.10, exemplified in Figure 8.11 for Nylon/Clay nanocomposites). The delamination process observed was in accordance with the observations made by Kim et al.[17] for clay tactoids (in a nylon 6 matrix) orientated in the direction of the applied load. The TEM images suggested that although delamination occurred, the well dispersed clay platelets and the polymer matrix did not debond. These findings are in agreement with the previously reported literature.[437] This ratified the hypothesis proposed for the changes in

crystallinity and the formation of a layered structure between the silicate layers and the crystallite lamellas. Thus, the microvoids observed in the SEM images may be attributed to the presence of clay which obstructed the formation of new hydrogen bonds and forced the formation of γ-phase crystallites in some cases.

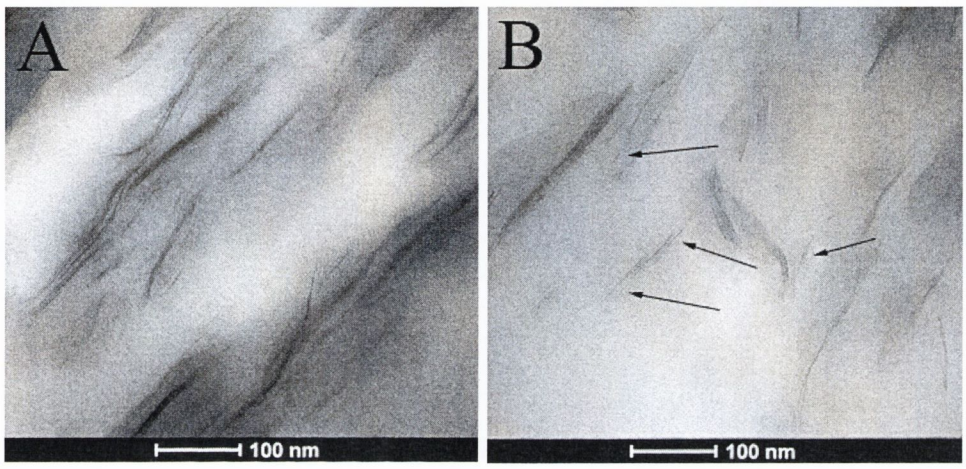

Figure 8.11. TEM images of Nylon/Clay nanocomposite A) before and B) after the tensile test; the arrows indicate delamination of clay tactoids into single clay platelets. As can be observed from the exemplificative TEM images after the test was performed the clay platelets and clay tactoids increase their orientation.

The mobility of the clay platelets, the delamination of the polymer lamellas and the formation of new hydrogen bonds can be observed in Figure 8.11B, where although the orientation was increased there are a few clay tactoids that were orientated transversal to the flow.[424] This can be explained by the breaking of the hydrogen bonds and the rotation that the polymer chains experience during the uniaxial deformation process. Thus, the polymer chains attempted to reach a more thermodynamically stable state, the α-phase crystallinity, and began to rotate; however, the presence of the clay platelets obstructed this move and forced the polymer chains to crystallise in a less thermodynamically stable state, i.e., γ-phase. This led to an incomplete reorientation of the polymer lamellas and of the clay platelets in this case.

8.3.4. Thermogravimetric analysis

In order to evaluate the effect of dispersing different types of clay (with different exfoliation degrees) in a nylon matrix, thermogravimetric analysis (TGA) was performed.

Figure 8.12 presents the differential thermogravimetric (DTG) curves that were used to assess the peak degradation temperature of the pristine polymer and polymer/clay nanocomposites. The dispersion of clay platelets inside a polymer matrix can lead to two distinct effects: barrier and catalyst.[190, 218, 219] In the former the clay platelets may increase the thermal stability of the material, whilst in the latter the surfactant or even the clay platelets may act as catalysers and reduce the thermal stability of the polymer/clay nanocomposites.[190] Nylon/Clay nanocomposites presented an insignificant decrease in the peak degradation temperature which suggested the presence of both effects with equal intensities. Thus, the effect of the excellent dispersed clay platelets in nylon was cancelled by the degradation of the surfactant. Although no surfactant was present in the nylon/MMT nanocomposites, a catalytic effect was induced by the presence of the clay platelets and the hydroscopic character of clay and nylon 6.

The increased exfoliation degree presented by the clay platelets in nylon/ADC-Clay nanocomposites and the overexposure of the surfactant hindered the barrier effect of the clay platelets.[223] However, the differential thermogravimetric curve for the dispersion of ADC-Clay in nylon 6 presented a secondary, less pronounced, peak at 540 °C. This is a consequence of the excellent dispersion of clay platelets and the high exfoliation degree achieved with the use of blowing agent-treated clay. The degradation of the blowing agent inside the gallery exposed the surfactant which induced the Hoffman degradation of the alkyl ammonium and catalysed the degradation of the polymer matrix; phenomena which has been previously reported in literature.[357] However, the exposure of the surfactant and the excellent dispersion of clay platelets allowed for the nylon to be adsorbed on the surface of the silicate layers, as it has previously been reported.[432] Since this effect was not observed when ADC-Clay was dispersed in PS or PP/PPgMA, it can be concluded that the occurrence of a second peak in the degradation of nylon 6/ADC-Clay nanocomposite was due to the degradation of the adsorbed polymer. These findings are in good agreement with the literature reports which suggested that the exfoliation degree cannot be used to predict the thermal stability of polymer/clay nanocomposites.[212, 356]

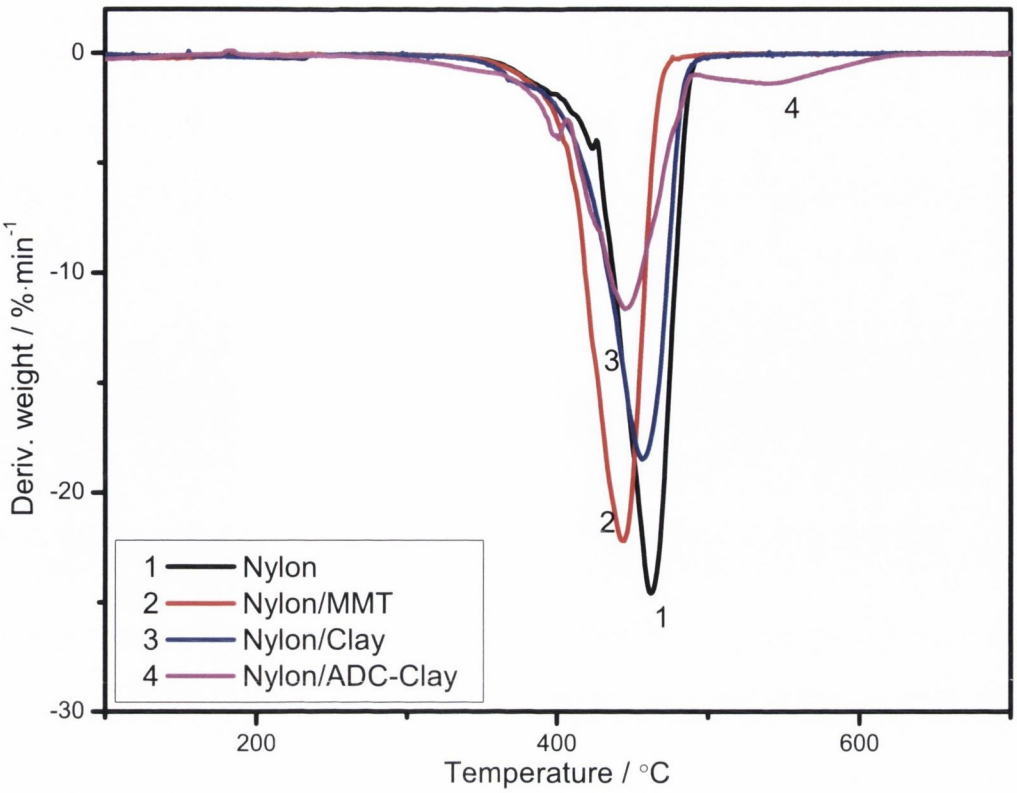

Figure 8.12. Differential thermogravimetric for pristine nylon and nylon/clay nanocomposites.

8.4. Conclusions

Intercalated/exfoliated polymer/clay nanocomposites with different exfoliation degrees have been obtained by dispersing natural clay, organoclay or blowing agent-treated organoclay into a nylon matrix. The thermal analysis showed that the presence of clay tactoids and clay platelets into the nylon matrix was more prone to exhibiting a catalyst effect, which slightly decreased the peak degradation temperature.

Although the mechanical properties of the intercalated/exfoliated nanocomposites appeared to be superior to the properties of the neat nylon, the elongation at break decreased regardless of the exfoliation degree. Still, the presence of clay increased the Young's moduli by 53-65% compared to the neat polymer, whilst the energy at break was enhanced by up to 53%. The exfoliation degree of the clay platelets in the polymer matrix was best reflected by the tensile strength which increased, with statistical significance, by up to 79% compared to the neat material and by up to 11% in nylon/ADC-Clay compared to nylon/MMT nanocomposites.

The thermal and crystallinity analysis showed that the addition of clay increased the crystallisation temperature, whilst decreasing the melting temperature and the crystallisation degree. After subjecting the material to uniaxial stresses, the crystallinity degree of the neat polymer decreased, due to the break of the hydrogen bonds. However, the presence of clay, which initially obstructed the formation of hydrogen-bonds, led to a slight increase in the crystallinity degree of the nanocomposite materials, when the fractions of intercalated and exfoliated nanostructures were similar. An increase in the exfoliation degree resulted in a material that once uniaxially deformed presented superior crystallinity, due to the straightening of the polymer chains and tight packing.

During the elongation process the intercalated clay tactoids delaminate and introduced additional nucleation centres. Although nanovoids were not observed, on a microscopic level, microvoids were encountered. This suggested that the polymer had adsorbed on the clay surface and upon uniaxial deformation it did not debond. However, uniaxial deformation in the presence of clay obstructed the formation of new hydrogen bonds, thus leading to amorphous tearing and microvoid formation.

Chapter 9. On the toughness of polymer/clay nanocomposites

9.1. Introduction

Polymer/clay nanocomposites represent a relatively new class of materials characterised by superior and/or unique properties compared to their neat polymeric counterparts. Although the research on this class of materials started more than two decades ago, there are still a number of questions that need to be elucidated, among which the toughness of polymer/clay nanocomposites stands out. This intricate property, becomes more complex when clay platelets are dispersed in the polymer matrix.[136]

Unlike simpler mechanical properties (i.e., modulus, strength or elongation at break); toughness has proven to be a challenge in terms of characterisation. Typically the toughness of a material can be evaluated from a tensile test, an impact test (i.e., Charpy or Izod impact tests) or a fracture toughness test (i.e., J-integral or essential work of fracture). In a tension test the toughness is represented by the energy per volume to cause the failure, that is the area under the strain–stress curve, also known as tensile energy at break or strain energy.[143] In industry, the Charpy and/or Izod impact tests are the most common methods of evaluating the toughness of a material. However, the high speed of the tests leaves a number of questions regarding the role of the filler. The fracture toughness tests relate the crack growth with the energy absorbed. The J-integral test has been used for the characterisation of fracture toughness of polymer and polymer nanocomposites.[140, 438] This test is suitable for not too ductile systems, represents a natural expression of linear elastic fracture mechanics and deals with a physical crack extension (regardless of the crack length).[161]

Previous studies performed on polymers and polymer/clay nanocomposites have revealed that there are cases in which both the stiffness and the toughness of a polymer/clay nanocomposite are superior to the pristine polymer.[135] However, there are also cases in which the stiffness or the toughness had improved at the expense of the other.[139, 168, 437] Typically, the dispersion of clay in a polymer matrix enhances the modulus and reduces the toughness. This has been explained (for an amorphous polymer) by the presence of clay that may embrittle the polymer, the test temperature in relation to the glass temperature of the material, type of nanocomposite and orientation of the clay platelets

etc.[136, 140] However, for a crystalline polymer, factors like crystallinity degree and crystalline morphology have to be also considered.

The toughness of polymers and polymer/clay nanocomposites is evaluated in most of the cases by Charpy/Izod impact test and only in a few cases the tensile energy at break is considered. This leaves a gap in the toughness assessment of polymer/clay nanocomposites, and sequentially the capability of clay platelets and their polymer intercalations. At the moment there are a number of contradictory results on the degree of exfoliation and its impact on the toughness of the materials (Section 2.5.3.1.4). It has been hypothesised that an intercalated/exfoliated polymer/clay nanocomposite may present better properties.[141, 202] However, this presumption raises another question: What is the optimal ratio between the mass fraction of intercalated and exfoliated nanostructures in a polymer/clay nanocomposite, necessary to achieve superior mechanical properties? The current study aims to answer this question and to elucidate the polymer-clay interactions in regard to the type of test used to assess the toughness, the orientation of the clay platelets and polymer lamellas. For this purpose three clays (i.e., natural clay, commercially available organoclay and blowing agent-treated organoclay) were selected and dispersed into a nylon 6 matrix.

These polymer/clay nanocomposites have been investigated in the previous Chapter and found to render intercalated/exfoliated nanostructures, with an exfoliation degree that varied from 42% in nylon/MMT to 52% nylon/Clay to 84% in nylon/ADC-Clay (Section 8.3.1). The toughness of nylon 6 and nylon 6/clay nanocomposites has been studied by evaluating the energy at break from tensile tests, the toughness strength obtained by performing Charpy impact tests and the fracture resistance characterised *via* J-integral tests. The J-integral test has been performed using the single specimen technique with a video monitoring system. In order to analyse the effect of specimen geometry and specimen orientation two specimen configurations were chosen: single edge notched beam and compact tension. The effects of polymer chain and clay platelet orientation were observed by considering two orientations for the compact tension specimens, i.e., longitudinal and transversal. The effects of polymer deformation were evaluated *via* scanning electron microscopy for all the geometries. The role of the clay in the toughness process was evaluated *via* transmission electron microscopy.

9.2. Experimental Section

9.2.1. Materials

The semicrystalline polymer, polyamide 6 (DSM Akulon®, Grade: K222D) from DSM (Netherlands), was purchased from Resinex (UK). Three types of clays were considered: natural montmorillonite (MMT), organoclay (Clay) and a blowing agent treated organoclay (ADC-Clay). Natural sodium montmorillonite clay (325 mesh) was generously supplied by Bentonite Performance Materials LLC (Wyoming Plant, South Dakota, USA). The Clay, i.e., Nanomer® I44.P, a dimethyl dihydrogenated tallow ammonium chloride (2M2HTA) modified montmorillonite, from Nanocor Corporation (Illinois, USA) was kindly supplied by Nordmann, Rassmann GmbH (Hamburg, Germany). The organoclay was treated with a well known organic blowing agent, azodicarboxamide (ADC) in the presence of zinc oxide (ZnO), which were purchased form Sigma-Aldrich Ireland Ltd. (Dublin, Ireland). The clay treatment follows the procedure described in Chapter 7.

The manufacturing of polymer/clay nanocomposites was presented in Chapter 8. There it was shown that the dispersion of MMT, Clay or ADC-Clay into nylon 6 led to the formation of intercalated/exfoliated polymer/clay nanocomposites. It has also been previously observed that the type of clay used controlled the degree of delamination and the dispersion of clay platelets and clay tactoids.

9.2.2. Preparation of polymer and polymer/clay nanocomposites samples

Polymer and polymer/clay nanocomposites with 4 wt.% clay platelets were moulded into tensile specimens as described in the previous Chapter. Using the same conditions impact specimens and fracture testing specimens were moulded.

9.2.3. Characterisation

Impact tests were performed according to standard ISO 179:1997 at room temperature on a Charpy impact tester (JinJian XJJD-5, China) at a speed of 2.9 $m \cdot s^{-1}$ and using a hammer of 0.5 J. Eight specimens (80 mm x 10 mm x 4 mm, length x width x thickness) were tested for each batch of materials. Prior to being tested the impact specimens were notched with a type A notch, using a cutter and a milling machine. Tensile

tests were carried on a Zwick Z005 machine (according to ISO 527:1993), using a 2.5 kN load cell and a cross head speed of 10 mm·min^{-1}. Five dog bone specimens (Type 1BA) were tested for each of the materials. The mean and standard deviation values reported for the mechanical tests represent a confidence level of 95%. Statistical significance was assessed by a Two-tailed, Type II 't' test, with a criterion that the probability is less than 0.05.

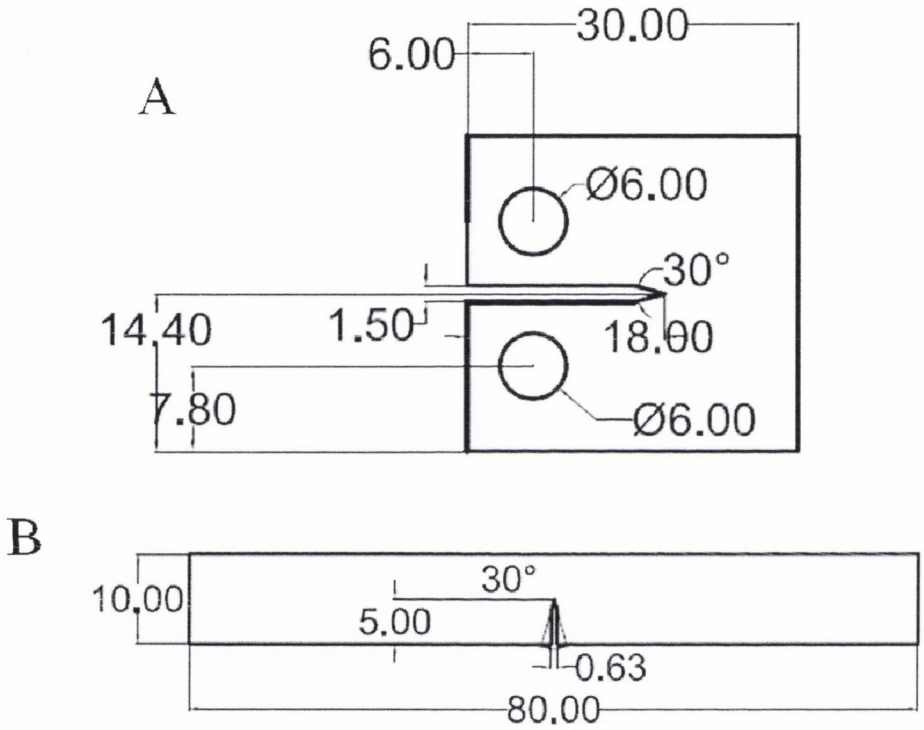

Figure 9.1. Geometry and dimensions of A) compact tension specimen and B) single-edge notched beam specimen (dimensions in mm).

The fracture toughness J-integral tests were performed, at room temperature, on a Zwick Z005 machine using a 2.5 kN load cell and a cross head speed of 0.5 mm·min^{-1} in accordance with ASTM D6068-96 (2002). The geometries of the compact tension (CT) and single-edge notched beam (SENB) specimens are provided in Figure 9.1. The SENB specimens were tested using a three point bending set up with a support span of 40 mm, according to ASTM D6068-96 (2002). The toughness was measured using a single specimen technique and a crack monitoring system. The set-ups for the toughness test are presented in Figure 9.2. In order to allow for the crack monitoring system to record the

crack propagation, the tests were performed using a step function with 0.5 mm per step and a step duration of 60 seconds with a waiting time between the steps of 10 seconds.

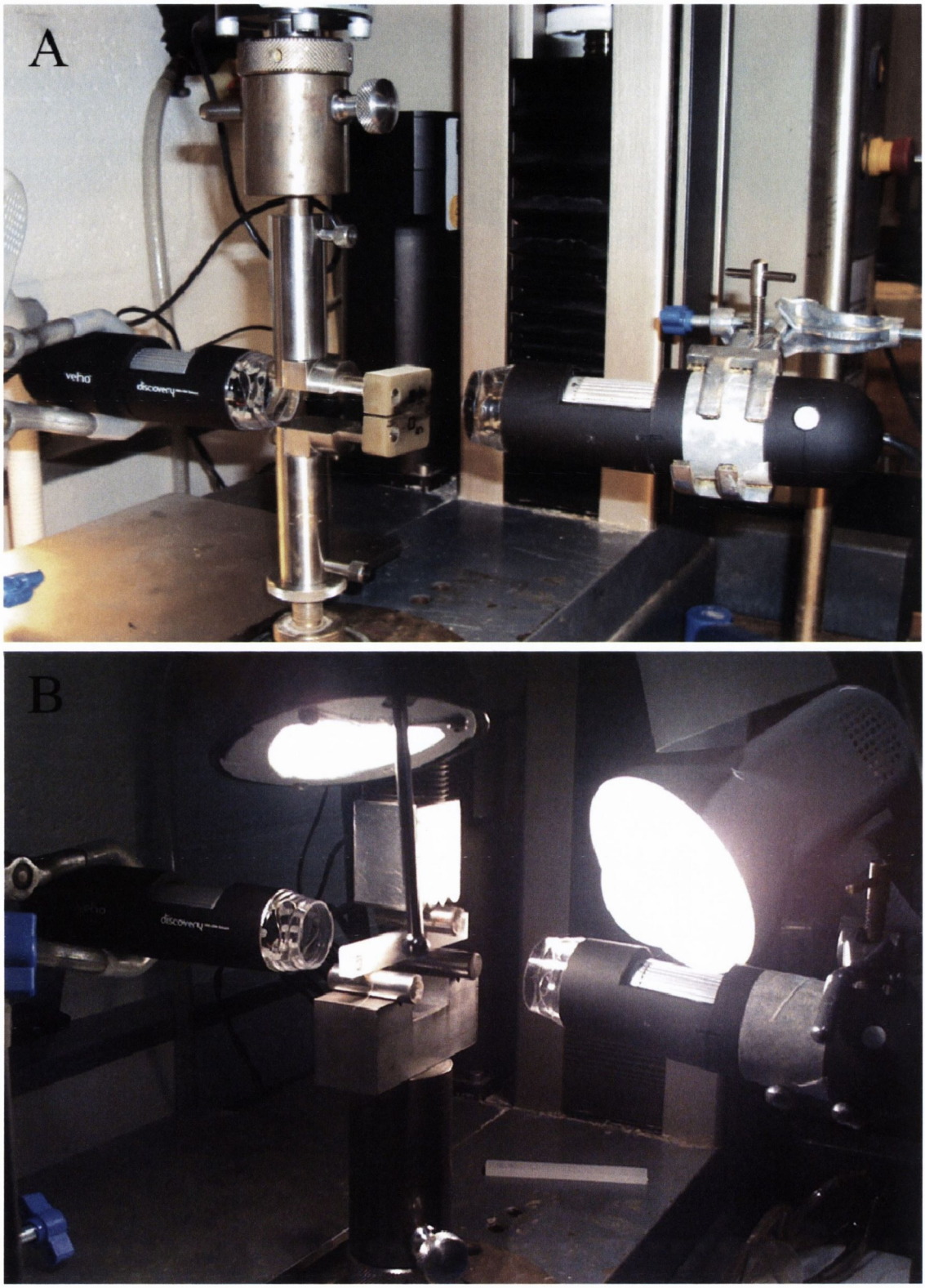

Figure 9.2. Fracture toughness tests set-up for (A) compact tension and (B) single edge notched beam specimen with crack monitoring system.

Prior to being tested the CT and SENB specimens were notched with an envelope type notch according to ISO 7448-3 (2005) (Figure 9.1), using a notching tool and then pre-cracked according to ASTM 6068-96 (2002) to give the original crack length between 50% and 65% of the width. The initial crack was created by tapping with a razor blade according to ASTM D6068-96 (2002) on an INSTRON 8501 using a crack monitoring system to ensure that the crack was accurate (Figure 9.3). The razor crack represented more than 5% of the total original crack length. All the specimens were conditioned in a vacuum oven overnight at 40 °C and then kept in a desiccator for at least 12 hours before testing.

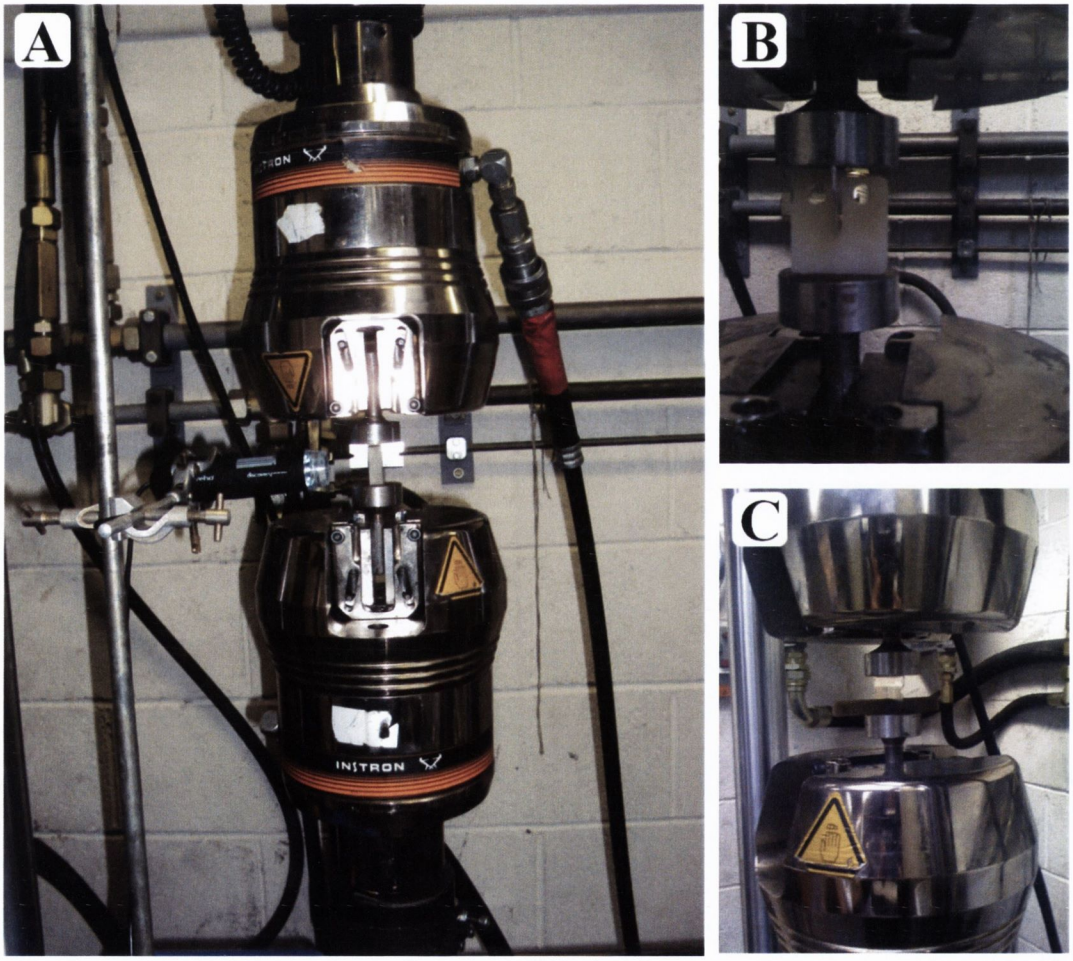

Figure 9.3. Initial crack developed with a razor blade A) general set-up with crack monitoring system, when B) compact tension specimen and C) single edge notched beam specimen while being notched with a razor blade.

TEM was performed on a TECNAI G2 20 twin electron microscope at 200 kV accelerating voltage. The specimens were ultrathin-sectioned using a Reichert-Jug 'Ultracut' ultramicrotome equipped with a diamond knife. The sections (~100 nm in thickness) were collected in a trough filled with water and placed on a 200 mesh copper grid. Sections from un-tested polymer/clay nanocomposites and sections acquired from the crack front and the tip of the crack of the fracture tested (SENB) specimens were analysed (Figure 9.4).

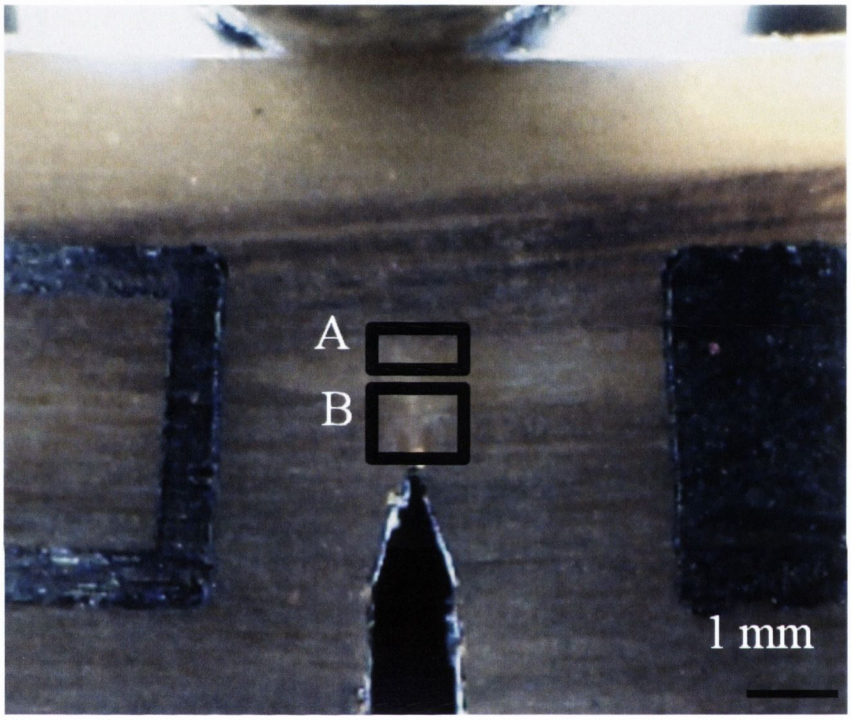

Figure 9.4. The location of the TEM samples that were acquired from SENB polymer/clay nanocomposite specimens: A) crack tip and B) inside the crack front.

SEM imaging was performed on fracture tested surfaces using a Tescan MIra Variable Pressure Field Emission Scanning Electron Microscope at a voltage of 5.0 kV. Prior to being analysed the samples were mounted on stubs and their surface was gold coated. The surfaces of impact tested, fractured tested single edge notch beams and compact tension specimens tested longitudinally or transversally compared to the injection flow were analysed.

9.3. Results and discussion

9.3.1. Mechanical properties

The toughness of polymer and polymer/clay nanocomposites was first evaluated from the energy at break obtained by performing tensile tests and from the impact strength determined by performing Charpy impact tests. The results from the low-speed tensile tests (i.e., 10 $mm \cdot min^{-1}$) and from the high speed impact tests (i.e., 2.9 $m \cdot s^{-1}$) were depicted in Figure 9.5. The toughness of the material determined as the area under the strain-stress curve[136, 439] of a tensile test was found to increase by over 50% with the dispersion of MMT or Clay in the nylon matrix. As described in Chapter 8 the crystallinity degree of the pristine nylon and nylon/MMT and nylon/Clay nanocomposites stayed relatively the same when the materials were subjected to external deformation. The relative constant crystallinity eliminated this factor and, as it was previously discussed in Chapter 8, the increase in toughness was due to the presence of clay platelets which delaminated when subjected to external stresses, to the mobility of the clay platelets and to the mobility and rearrangement of the polymer lamellas. The other mechanical properties presented in the previous Chapter also suggested that the clay was well dispersed and that the stress from the polymer matrix was efficiently transferred to the nanofiller. Although the exfoliation degree increased in nylon/ADC-Clay nanocomposite, the material exhibited an insignificant decrease in the energy at break. This may be a consequence of the random orientation of the clay platelets which obstructed the rearrangement of the hydrogen bonds, as well as the formation of new crystalline lamellas. As it was previously discussed in Chapter 8, nylon/ADC-Clay nanocomposite exhibited a substantial enhancement in the crystallinity degree (Figure 8.3 and summarised in Table 8.2 and Figure 8.4 and summarised in Table 8.3); nevertheless, the ratio between α- and γ-phase crystallites remained relatively constant after the material was subjected to external stresses. Thus, minimal changes in the mobility of the filler and the mobility of the lamellas were displayed by this polymer/clay nanocomposite.

The toughness characterisation of neat polymer and polymer/clay nanocomposites by higher speed impact tests showed that the presence of clay platelets embrittled the polymer matrix, regardless of the exfoliation degree. This is in good agreement with the previous studies.[140] As discussed in the Chapter 8, the presence of clay created weak areas in the polymer matrix by obstructing the formation of hydrogen bonds. However, as opposed to nylon/MMT and nylon/ADC-Clay nanocomposites, the excellent dispersion of clay

platelets and clay tactoids in nylon/Clay nanocomposite resulted in 67-97% statistically significant improvements in impact strength. It has previously been reported in literature[139] that the nylon/clay intercalated nanocomposite (90/10, w/w) presented an impact strength 30% higher than the nylon/clay exfoliated nanocomposite (90/10, w/w). The superior toughness of the intercalated nanocomposite over the exfoliate nanocomposite was attributed to the formation of microvoids due to the delamination of the clay platelets. However, in this case we find that an intercalated/exfoliate nylon/Clay nanocomposite with medium exfoliation presented better toughness than mostly intercalated (nylon/MMT) or mostly exfoliated (nylon/ADC-Clay) nanocomposites.

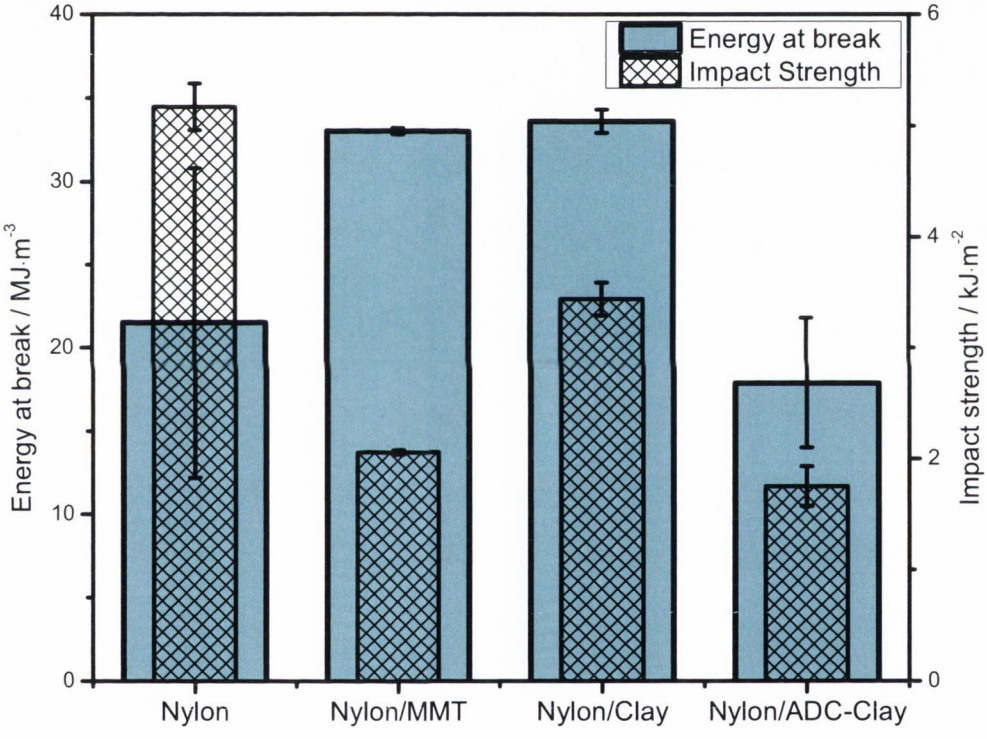

Figure 9.5. Toughness of neat polymer and polymer/clay nanocomposites evaluated as the energy at break (determined by performing low speed tensile tests which were described in Chapter 8) and the impact strength (observed in high speed Charpy impact tests). The bars represent averages of five measurements for the energy at break and eight measurements for the impact strength, whilst the error bars represent ± one standard deviation.

As observed from Figure 9.5, the nylon/Clay nanocomposite presented optimal enhancements in the energy at break and the impact strength as opposed to the other polymer/clay nanocomposites studied. The superior properties exhibited by nylon/Clay

nanocomposite compared to nylon/MMT nanocomposite suggested that the degree of exfoliation in an intercalated/exfoliated nanocomposite has to be controlled. A higher exfoliation degree resulted in a higher crystallinity degree after uniaxial elongation, which embrittled the material. As previously discussed the dispersion of 4 wt.% clay platelets of as-received organoclay in nylon enhanced the energy at break by over 50%, whilst the impact strength decreased by over 30%. Using the same amount of clay platelets Chen and Evans[135] reported that by dispensing organoclay (i.e., Bentone® 111) in PS a highly intercalated polymer/clay nanocomposite was obtained, which presented a substantial increase in the energy at break (over 100%) and no change in the impact strength. However, dispensing the same amount of clay in ABS led to highly exfoliated ABS/clay nanocomposites which exhibited, compared to neat ABS, a tensile energy at break 61% lower and a substantial decrease in the impact strength. As previously discussed in Chapter 8, nylon/Clay nanocomposites was an intercalated/exfoliated nanocomposite with a ratio of intercalated mass fraction to exfoliated mass fraction close to unity, which positioned this material between the literature reported findings[135] for tensile energy at break and impact strength. Thus, it is expected for the enhancements in the tensile energy at break to be superior to the changes in the impact strength that a polymer/clay nanocomposite exhibited as opposed to its polymer counterpart. In the current project the changes in the tensile energy at break and impact strength presented different variations with the degree of exfoliation, which prompted the necessity of more tests to evaluate the toughness of the materials.

9.3.2. J-integral

The fracture toughness of polymers and polymer/clay nanocomposites was evaluated *via* the J-integral method. Although the nylon 6 in used is a semicrystalline material, the high crystallinity degree that the pristine polymer matrix displayed (i.e., 42%), made the material behave almost like a brittle polymer, in accordance with the previous literature findings.[440, 441] Therefore, the investigations on the toughness of neat nylon and nylon/clay nanocomposites (which presented a decrease in the impact resistance of the nanocomposite compared to the pristine material, Figure 9.5) were limited to the elastic factor of the J-integral expression (Equation 2.5). In order to calculate the elastic contribution it was assumed that the material was isotropic, presented small scale yielding and a sharp notch.[146] Thus, for elastic materials, local stresses and deformations that emerged at the

crack tip are a function of the applied loads and geometry expressed solely through the stress intensity factor, K_I.[145]

The fit of the power-law curves (R-curves,[159] i.e., $J = C_5 \Delta a^{C_6}$, where C_5 and C_6 are curve-fitting parameters[437] and C_6 is less than 1, according to ASTM D 6068-96 (2002)) was relatively good, regardless of specimen geometry, with few exceptions (i.e., longitudinally tested nylon/MMT nanocomposite CT specimens and transversally tested nylon/Clay nanocomposite CT specimens; in these cases a number of specimens were analysed and in every case the C_6 curve-fitting parameter[437] was found to be higher than 1).

The correlation coefficients (i.e., R^2), summarised in Table 9.1, were found to be between 0.8596 and 0.9548 for SENB specimens, for which the curves with the data points are presented in Figure 9.6. For CT specimens the correlation coefficients were found to be between 0.8302 and 0.9402 for longitudinal testing (Figure 9.7) and between 0.7514 and 0.9488 for transversal testing (Figure 9.8). Although there is no literature regarding the power-law coefficients for polymer/clay nanocomposites, the current data agrees reasonably well with the correlation coefficient determined for ABS. Bernal et al.[442] performed J-integral fracture toughness tests on ABS, using SENB specimens and monotonic loading, and obtained a correlation coefficient for the power-law of 0.91. Narisawa and Takemori[443] used the J-integral fracture test, with loading-unloading cycles, to assess the fracture toughness of ABS and their power-law fit presented a correlation coefficient of 0.99.[442]

Table 9.1. Curve fitting parameters for pristine polymer and polymer/clay nanocomposites with different exfoliation degrees

Material	R^2_{SENB}	$R^2_{CT(L)}$	$R^2_{CT(T)}$
Nylon	0.9548	0.8653	0.7514
Nylon/MMT	0.9053	0.9402	0.9407
Nylon/Clay	0.8972	0.9377	0.9264
Nylon/ADC-Clay	0.8596	0.8302	0.9488

Analysing the power-law fit resistance curves for SENB polymer and polymer/clay nanocomposites specimens (Figure 9.6), it was observed that the dispersion of clay platelets in the nylon matrix resulted in materials characterised by a higher toughness. The

well dispersed clay platelets prevented the crack from propagating. Although initially the nylon/MMT nanocomposite presented a higher resistance to crack propagation, after the crack propagated beyond 0.05 mm, the J-integral was facilitated in the detriment of the crack propagation processes. This phenomenon has also been observed by Labour et al.[444] for PP/$CaCO_3$ systems. The intersection of the power-law fit resistance curves suggested that a higher exfoliation degree displayed by this polymer/clay nanocomposite can prevent the crack propagation process more efficiently than in a polymer/clay nanocomposite in which the exfoliation degree is lower than 50%. This can be explained by the dispersion of clay platelets and clay tactoids in the polymer matrix, which can obstruct the crack propagation process. However, as the exfoliation degree increased the crack initiation became easier. The shift in the crack initiation may be attributed to the delamination of the clay platelets which will be discussed later from the TEM images.

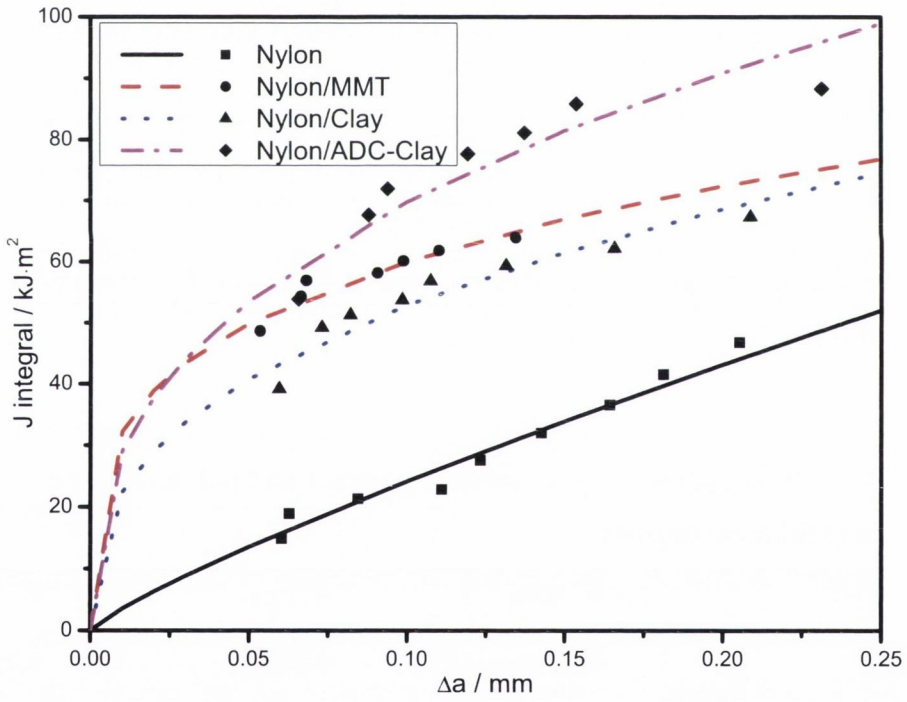

Figure 9.6. J integral values and power-law fit resistance curves for SENB polymer and polymer/clay nanocomposites specimens.

The longitudinally tested compact tension specimens (Figure 9.7) showed that the dispersion of Clay and ADC-Clay in the nylon matrix facilitated the crack initiation process while obstructing the crack propagation. In the early stages of the crack propagation process the nylon/MMT facilitated crack growth in the detriment of the crack initiation process. However, the crossing of the nylon and nylon/MMT nanocomposite

curves at a crack length of 0.22 mm (indicated by an arrow in Figure 9.7) suggested that the crack initiation process became more accessible, whilst the crack propagation became more arduous. The improvement in the crack initiation process past a certain crack length suggested that the clay tactoids may have delaminated during the crack propagation process. This led to an increase of the surface of the clay platelets that came in contact with the polymer matrix, which facilitated the transfer of the load from the polymer to the clay platelets and obstructed the crack path.

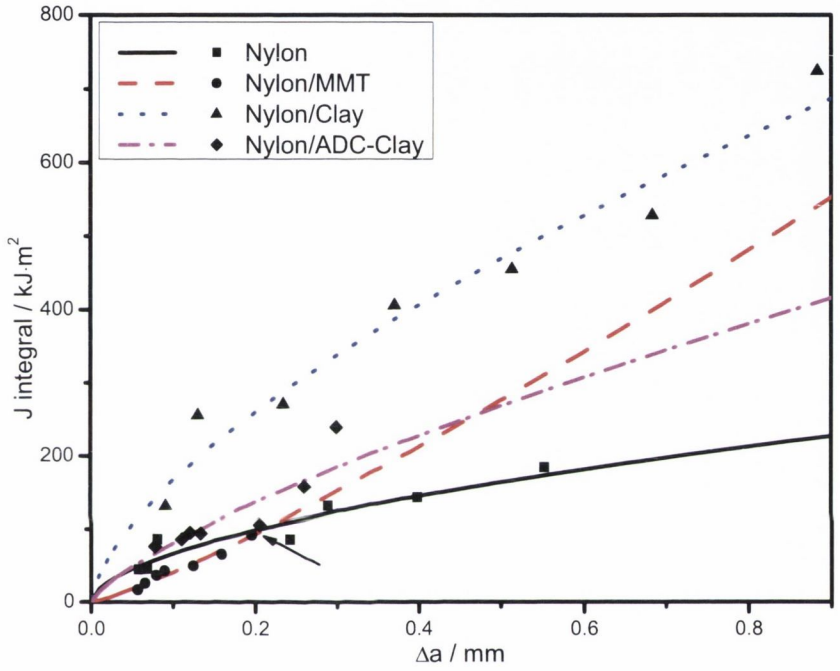

Figure 9.7. J-integral values and power-law fit resistance curves for longitudinally tested CT polymer and polymer/clay nanocomposites specimens.

As observed from Figure 9.8, the evaluation of the fracture toughness transversally tested nylon compact tension specimens presented a close to linear increase in the crack initiation process with the crack propagation. This suggested that the transversal testing, i.e., opening of the crack in the injection moulding direction, was highly obstructed, which may be due to the presence of hydrogen bonds. The nylon 6 presents two major crystalline phases (i.e., α and γ-phase) that are dictated by the connection formed between the amide and methylene units situated on different polymer chains.[408-411] During the injection moulding process the polymer chains orientated in the flow direction and during the cooling of the specimens hydrogen bonds were formed between the polymer lamellas. Thus, the transversal testing implied the breaking of bonds which facilitated the crack

initiation in the detriment of crack propagation.[444] Compared to neat nylon, the polymer/clay nanocomposites appeared to promote crack propagation, whilst hindering the crack initiation process. This pungent obstruction of the crack initiation process can be attributed to the presence of the clay platelets, which in this case facilitated the crack growth process.

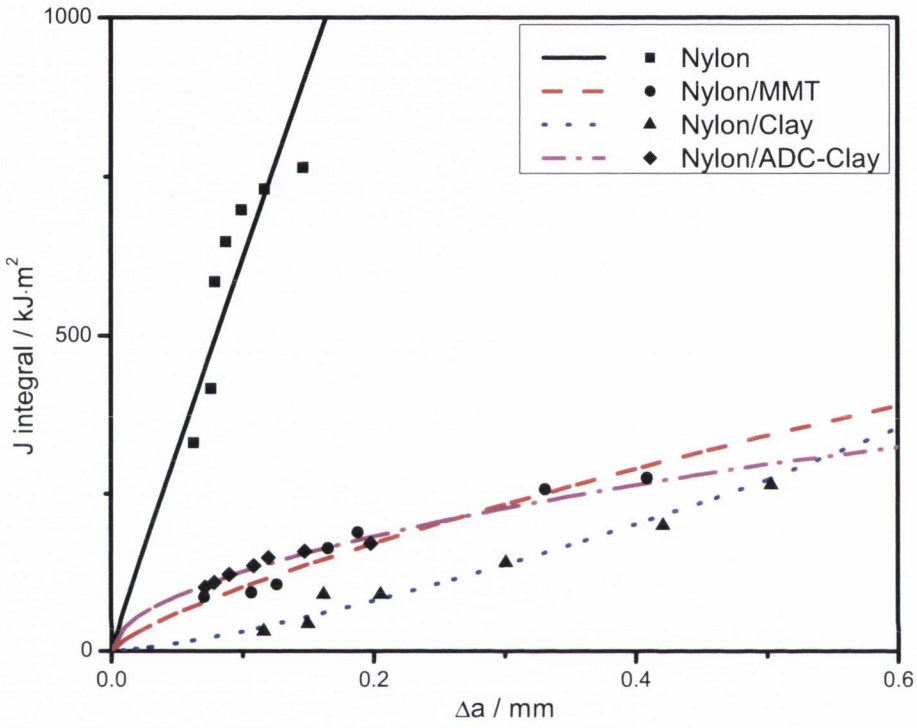

Figure 9.8. J-integral values and power-law fit resistance curves for transversally tested compact tension specimens of polymer and polymer/clay nanocomposites.

Analysing the SENB and the longitudinally tested CT specimens (Figure 9.6 vs. Figure 9.7) it was observed that the parallel orientation of the clay platelets and clay tactoids obstructed the crack propagation process. However, in a SENB specimen the higher exfoliation degree (nylon/ADC-Clay nanocomposite) provided the higher toughness, whilst in a CT specimen a medium exfoliation degree (nylon/Clay nanocomposite) displayed the best fracture toughness resistance. In order to assess if the geometry of the specimens tested influenced the variations observed in the power-law regression curves, Figure 9.6 and Figure 9.7 the power-law equations were linearised and their linear slopes were determined. Comparing the slopes for SENB specimens with the slopes for longitudinally tested CT specimens it was observed that they presented

statistically significant differences. Thus, the geometry of the fractured specimens influences the fracture toughness of the nanocomposite materials.

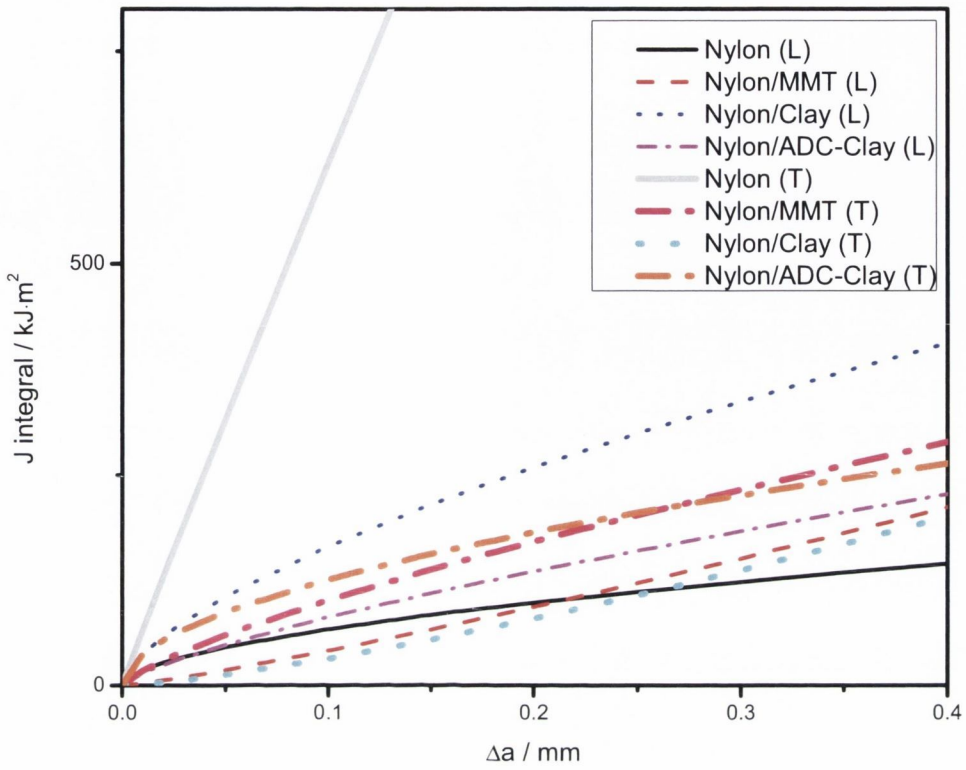

Figure 9.9. Power-law fit resistance curves for longitudinally (L) and transversally (T) tested compact tension specimens of polymer and polymer/clay nanocomposites.

As observed from Figures 9.7 and 9.8, a longitudinal orientation tends to obstruct the crack propagation process, whilst during the fracture process in a transversal direction this process is facilitated. It is of interest to analyse if this orientation problem is due to the polymer lamellas or to the clay platelets orientation or both. Figure 9.9 displays the power-law fit resistance curves for longitudinally and transversally tested compact tension specimens of polymer and polymer/clay nanocomposites. The power-law fit resistance curves for the neat polymer appear to create the upper and lower limits for the crack initiation processes and the crack propagation. This suggested that the orientation of the polymer lamellas represents a key factor in assessing the toughness of a polymer. Evaluating the slopes of the linearised regression curves for longitudinally and transversally tested CT specimens it was observed that the differences between the slopes were statistically significant, which confirmed the importance of polymer lamellas orientation. As it was previously discussed, the addition of clay obstructed the formation of

hydrogen-bonds; this resulted in a more 'consistent' fracture toughness trend. However, nylon/Clay nanocomposites created upper and lower limits for the fracture process that were orientated opposite to the ones for the neat polymer. Thus, the presence of clay, the orientation of the clay platelets and the orientation of the polymer lamellas are essential.

The brittle character of the materials facilitated the crack propagation process and obstructed the formation of a clear-cut linear domain of crack blunting.[444] In cases like this the critical initiation J-integral value (J_c) may be calculated by extrapolating the J from the J-R curve to a value corresponding to $\Delta a \approx 0$.[151, 159, 441, 445] However, as it was previously discussed in some cases C_6 was higher than 1, which would indicate an incipient brittle fracture. This aspect (as well as the small dimensions of the specimens tested) and the controversial aspect of the crack blunting line prompted the evaluation of critical crack initiation value as the minimal value used for crack growth (i.e., 0.05 mm) which represented the delimitation line according to ASTM 6068-96 (2002).[441, 443, 446, 447] The high importance of evaluating the energy necessary to produce a new crack surface has been stated by Taylor et al.[448] who described it as the "defect tolerance". The J-integral values representing the crack growth[445] at 0.05 mm in SENB specimens and CT specimens tested on the longitudinal (L) and the transversal (T) are summarised in Table 9.2.

Table 9.2. Critical fracture toughness for pristine polymer and polymer/clay nanocomposites with different exfoliation degrees obtained from two specimen geometries and tested in the longitudinal and transversal direction

Material	J_c^{SENB} / $J \cdot m^{-2}$	$J_c^{CT(L)}$ / $kJ \cdot m^{-2}$	$J_c^{CT(T)}$ / $kJ \cdot m^{-2}$
Nylon	14	46	316
Nylon/MMT	50	18	60
Nylon/Clay	41	106	13
Nylon/ADC-Clay	54	49	87

The presence of the clay platelets delayed the crack growth process in SENB specimens (Table 9.2, Column 1). During the injection moulding process the clay platelets have orientated parallel to the crack growth. Thus, in order for the crack to start to propagate, it needs to find an opening in the torturous path the clay platelets/tactoids created.

The discrepancies observed between the critical crack initiation values of the longitudinal and the transversal compact tension specimens tested (Table 9.2, Column 2 vs. Column 3) showed that the neat polymer and polymer/clay nanocomposite materials presented a strong dependence on the orientation of the polymer lamellas. This intrinsic dependence has been previously reported in literature for neat polymers.[154]

9.3.3. Structural characterisation

The type of nanostructure present in the polymer/clay nanocomposites before the toughness test was performed was analysed *via* TEM and the representative images are displayed in Figure 9.10. Analysing the cross sections of injection moulded specimens SENB specimens, the TEM images showed the presence of intercalated/exfoliated nanocomposite structures. The degree of exfoliation and the number of clay platelets per stack in a clay tactoid have been previously reported in Chapter 8. As can be observed from Figure 9.10A and 9.10B, the dispersion of MMT or Clay in nylon 6 resulted in clay platelets/tactoids orientated in the flow direction. However, by adding ADC-Clay to the nylon matrix, the decomposition of the blowing agent inside the clay gallery, led to a higher exfoliation degree, which was also observed when the blowing agent-treated organoclay was dispersed in PS or PP/PPgMA, as it was discussed in Chapter 7. The nylon/ADC-Clay nanocomposite presented clay platelets that were randomly orientate (Figure 9.10C).

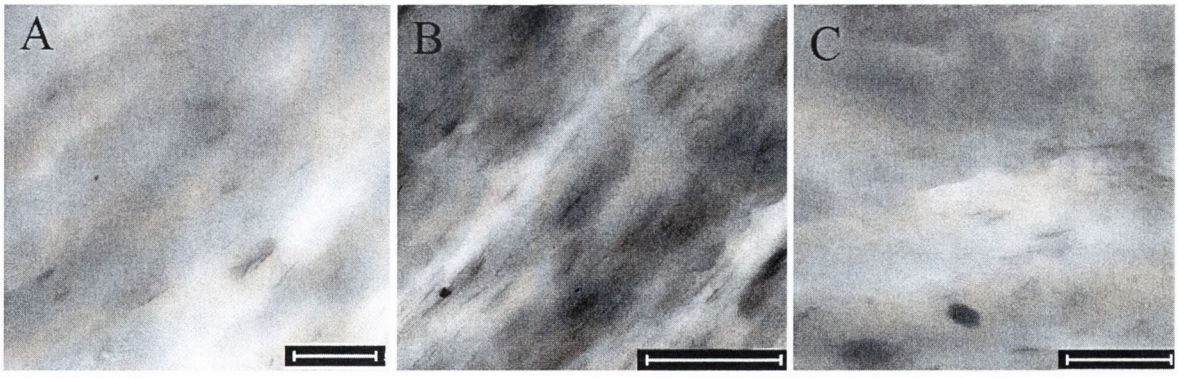

Figure 9.10. TEM images: A) Nylon/MMT, B) Nylon/Clay and C) Nylon/ADC-Clay (Scale bar: 500 nm).

During the crack propagation process the SENB specimens were subjected to three point bending, which made the tip of the natural crack act as a stress concentration area.[43]

The TEM images acquired from the crack tip area after the material was subjected to external stresses (Figure 9.4, location A) showed that the clay tactoids have splitted[17] (Figure 9.11A and Figure 9.11B). The increased exfoliation degree and the random dispersion of clay tactoids and clay platelets in nylon/ADC-Clay nanocomposite (Figure 9.10C) resulted in an area at the crack tip that exhibited (Figure 9.11C) single clay platelets, whilst the clay tactoids showed possible opening and slipping phenomena due to the random orientation. These findings are in accordance with the deformation mechanism proposed by Kim et al.[17] who stated that the orthogonal orientation of the clay tactoids to the applied force resulted in the splitting of the clay tactoids in the middle section.

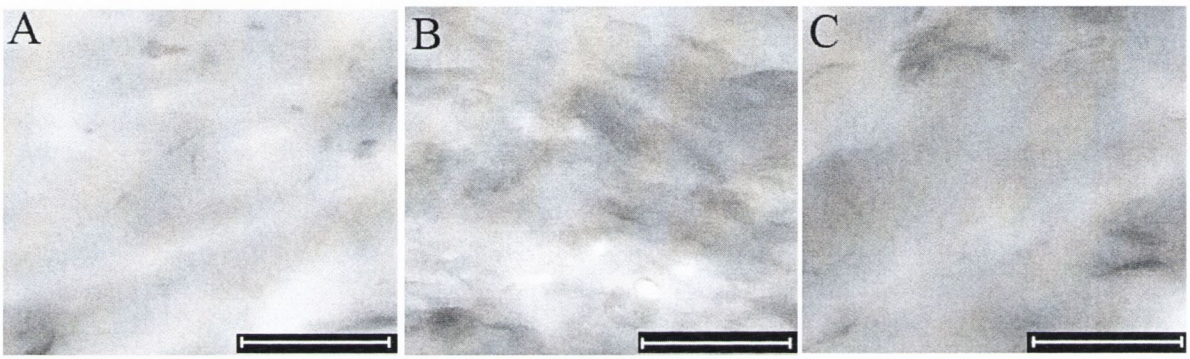

Figure 9.11. TEM images from the crack tip of SENB specimens after the fracture toughness test was performed: A) Nylon/MMT, B) Nylon/Clay and C) Nylon/ADC-Clay (Scale bar: 500 nm).

The TEM images from inside the crack fractured surface showed that the clay platelets increased their alignment after the material was subjected to external stresses (Figure 9.12 vs. Figure 9.10). Although the TEM for the polymer/clay nanocomposites presented intercalated and exfoliated nanostructures; by comparing the same area before and after the material was subjected to external stresses, it can be observed that the density of clay tactoids had increased. This again suggested a reorientation of the nanostructures which led to better visibility of some layers. The reorientation of the nanostructures can be attributed to the mobility of the clay platelets during the deformation process and also to the changes that the crystalline structure of the nylon 6 was experiencing during the deformation process, as it has been previously stated in literature.[408-411]

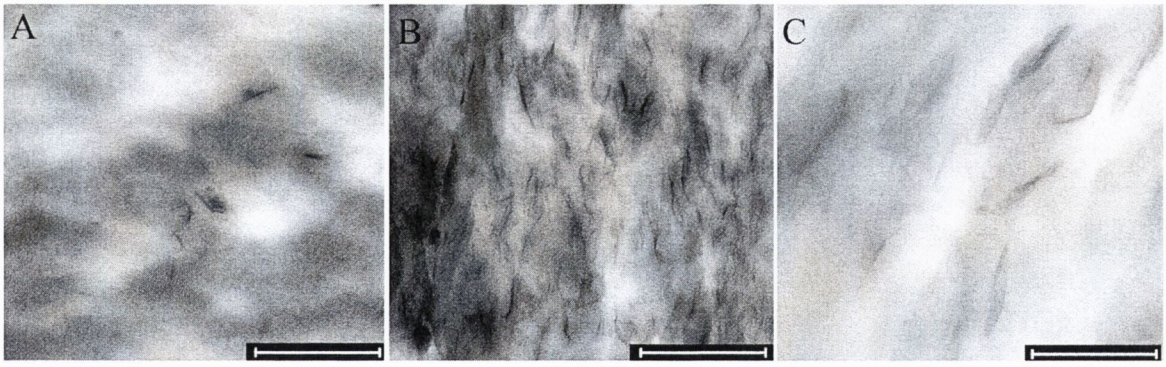

Figure 9.12. TEM images of the cracked area of SENB specimens: A) Nylon/MMT, B) Nylon/Clay and C) Nylon/ADC-Clay (Scale bar: 500 nm).

9.3.4. Fracture surface characterisation

In order to better understand the changes that undergo in the pristine polymer and polymer/clay nanocomposites with performing fracture toughness tests at high and low speeds, the surface of the broken materials was characterised *via* SEM. The study of the high speed fracture surfaces of polymer and polymer/clay nanocomposite materials with different exfoliation degrees was performed on the impact tested specimens. For the same materials, the low speed fracture surfaces of specimens tested *via* J-integral were investigated using SENB configurations. To obtain a more comprehensive evaluation of the low-speed fractured surface of polymer and polymer/clay nanocomposites, the compact tension specimens broken in the longitudinal and transversal directions were also analysed.

9.3.4.1. High speed impact tested fracture surfaces

The fracture surface of Charpy impacted neat nylon is displayed in Figure 9.13a. The impacted fracture surface presented two distinct zones: the crack initiation zone (1) and the crack propagation zone (2). The crack initiation zone (Figure 9.13b) exhibited the appearance of a ripple effect, being characterised by two areas: a relatively smooth region (1A) and a radial area (1B). The smooth region, representing the primary crack initiation site was similar to the one observed by Dasari et al.[168] The region was characterised by a diameter of 125 μm and was situated at approximately 380 μm ahead of the root of the notch. This suggested that prior to crack initiation blunting and plastic flow phenomena had occurred, which is in good agreement with the observations made by Wilbrink et al. for nylon 6/$CaCO_3$ materials.[164] The smooth area was surrounded by a radial area with "river markings" that resembled long grooves parallel to the crack grow direction (left to

right). Due to the location of the primary crack initiation point, smaller grooves that grew opposite to the crack propagation direction were observed (Figure 9.13c). The "river markings" presented brittle fracture morphology customary to fast propagation of the crack. This observations were in good agreement with the findings of Yuan et al.[131] while studying the impact surface of polypropylene/organoclay (i.e., Nanomer® I44.P) intercalated nanocomposites.

In the direction of crack propagation the brittle zone evolved into a brittle-like zone[129] (2A) due to the breakdown of the craze initiation zone.[131] This area was characterised by long grooves which presented a terraced aspect (Figure 9.13d). They emerged due to rapid dissipation of the energy induced during the impact test. The higher magnification SEM images showed that on each of these grooves there are smaller terraces assembled circularly to the crack growth with a "fish scale" aspect (Figure 9.13e). The areas between these smaller terraces presented reminiscents of the ripple effect that started the crack propagation process. The interior aspect of these areas was found to present as a smooth surface. However, the "fish scales" occurred not only on the long grooves but also in space between the long grooves (Figure 9.13f). Thus, during the crack propagation process the crack grew radial from the point of origin slowing down until it reached a temporary crack arrest area (Figure 9.13g).

The rapid crack-growing area which presented a brittle-like aspect was followed by a smoother area (Figure 9.13h). The end of the smooth area was marked by the presence of small fibrils (indicated by arrows in Figure 9.13i). The temporary crack arrest area, well visible even at low magnification (Figure 9.13a), was described by Deshmane et al.[129, 449] as a "stick-slip and stop-go" area which can be associated with dynamic crack propagation effects.

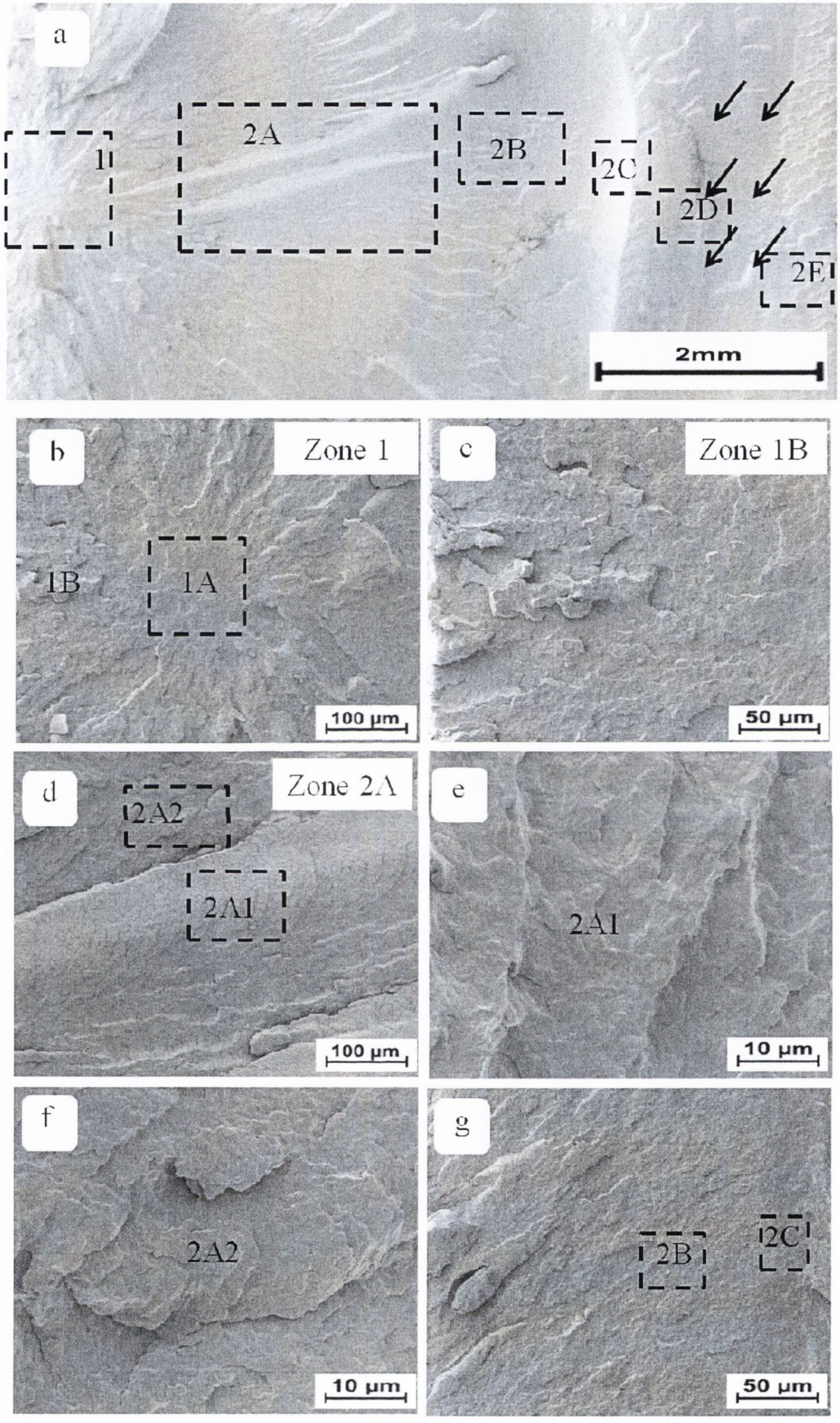

Figure 9.13. Scanning electron micrographs of the impact fracture surface of neat nylon.

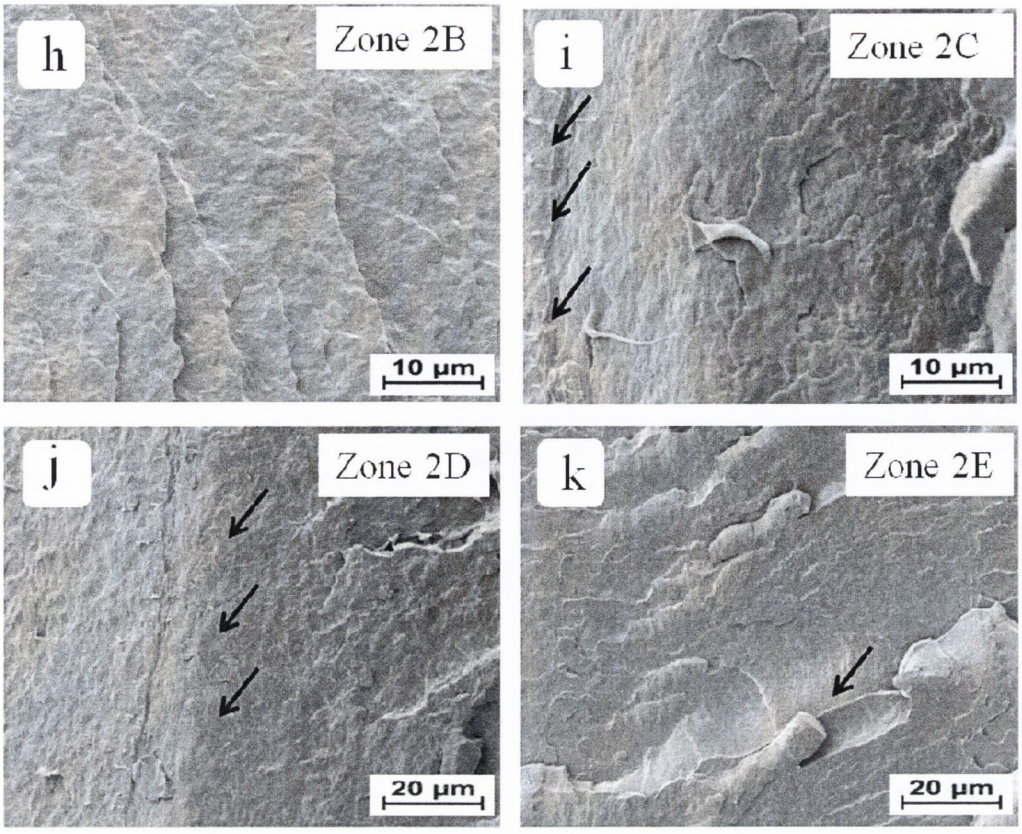

Figure 9.13. (continued)

During the crack propagation process the crack initiated and propagated due to the stress induced by the Charpy hammer. However, as the stress propagated it reduced its initial strength until it decreased under a critical value and caused the crack to arrest (stick); once the stress built-up again; the crack was reinitiated (slips). [129, 449 129, 449 129, 449 129, 448 129, 448 129, 448 129, 448 129, 448 128, 447 127, 446 127, 446 128, 447 128, 447] The re-initiation of the crack was characterised by the occurrence of structures described in literature[131] as "river markings" (indicated by arrows in Figure 9.13j). These small "river markings" made up a new area, denoted by Deshmane et al.[37] as slow shear zone (Figure 9.13j, zone 2D). Due to insufficient energy available to propagate the crack, the area was more similar to zone 2B, being characterised by demure "river markings". The slow shear zone was followed by two more stop-go fronts in which the energy built-up during the stick-slip area was quickly consumed by the crack propagation and then the energy built-up again (indicated by arrows in Figure 9.13a). As the energy increased the crack propagated once again and passed into a new area characterised by rapid shear flow (zone 2E – Figure 9.13k) that resembled the terraced aspect from the crack propagation area (zone 2A). The brittle character of the material is highly visible in the rapid shear flow zone where some breakings in the grooves (indicated by an arrow in Figure 9.13k) had formed.

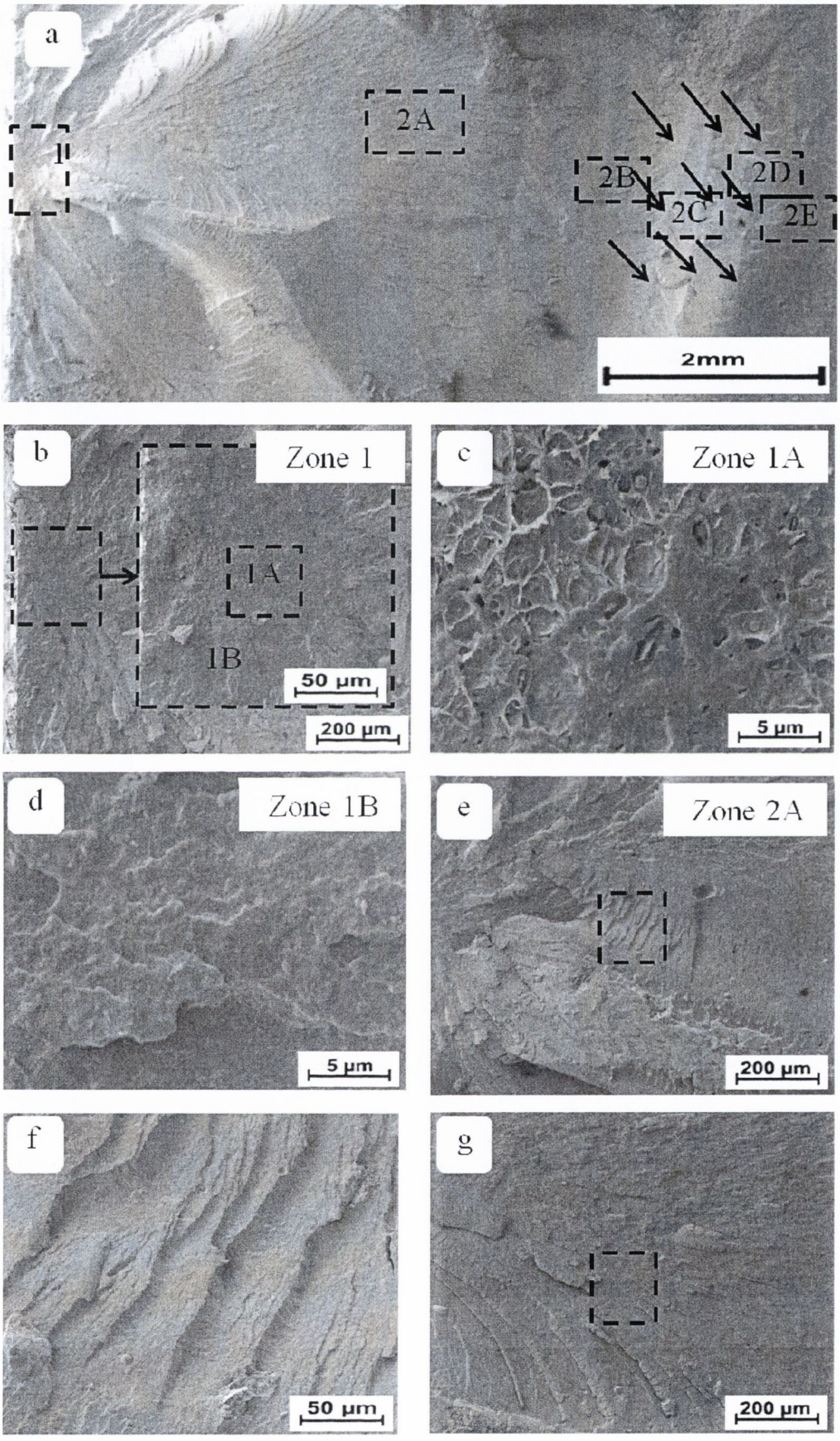

Figure 9.14. Scanning electron micrographs of the impact fracture surface of nylon/MMT nanocomposite.

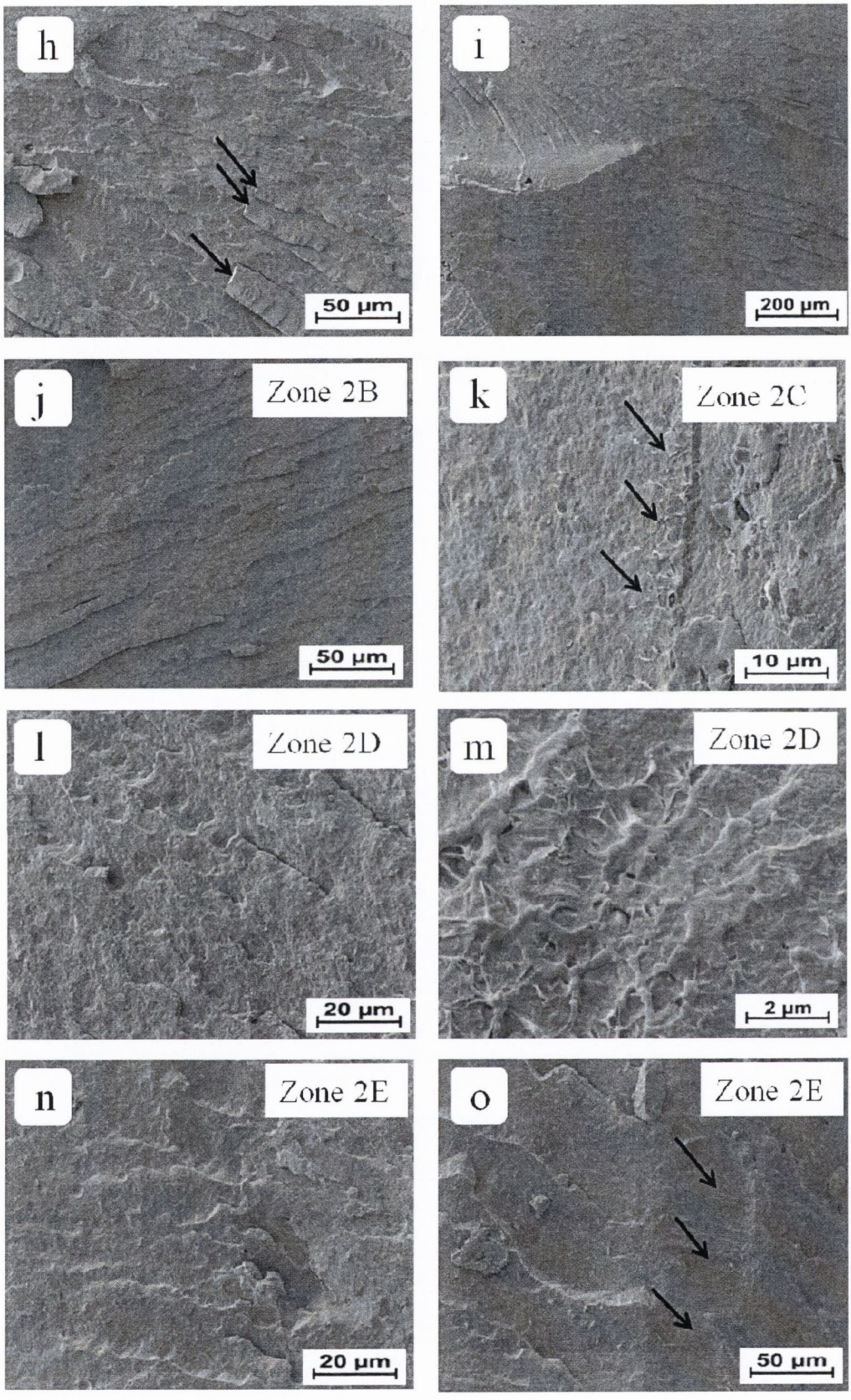

Figure 9.14. (continued)

The impacted surface of nylon 6/MMT nanocomposites (Figure 9.14a) was characterised by two main zones (Figure 9.14b): crack initiation zone (1) and crack propagation zone (2). Similarly to the pristine nylon, the nylon 6/MMT nanocomposite presented a crack initiation zone characterised by a "ripple aspect", in which the edges were made up by "river markings". The crack initiation zone presented two distinct areas: a primarily crack initiation site which was situated at approximately 86 μm from the edge and a central initiation point (Figure 9.14c) which presented a fibrillar aspect and a radius of 77 μm. The fibrils indicated that the presence of the clay attempted to prevent the crack propagation; however, the resistance of the clay was overcome and the crack was initiated. The proximity of the primarily crack initiation site (Figure 9.14d) to the edge suggested that no blunting had occurred at the crack tip.

The crack propagation area was made up by: (2A) brittle-like area, (2B) less brittle like area, (2C) stick-slip area, (2D) slow shear area and (2E) rapid shear area, which is similar to the findings of Deshmane et al.[129] The brittle-like area was characterised by a terraced aspect (Figure 9.14e). This area presented the appearance of "fish-slips" that were orientated almost perpendicular to the crack propagation direction (Figure 9.14f). The aspect of the "fish-slips" appeared to be slightly more spongious than the aspect of the same "fish-slips" observed on the brittle-like area of pristine nylon (Figure 9.13h).

During the crack propagation, the long grooves attempted to change their path from the crack propagation direction towards the edges of the impact specimen (Figure 9.14g). This emphasised the brittleness of the material through the breaking of some of the long groves (indicated by arrows in Figure 9.14h). However, the "river markings" that formed in the initiation zone propagated into the brittle-like area as chevron markings and prevented the change in the crack path (Figure 9.14i). Similar to the pristine case, the brittle-like zone passed into a smother area - zone 2B (Figure 9.14j). This area presented a very soft terraced aspect in which no breakings in the soft short grooves were observed. The end of the smooth area was marked by the occurrence of small fibrils (indicated by arrows in Figure 9.14k). Again similar to the pristine nylon fracture, the smooth area passed into a stick-slip area (2C) that was well visible at low and high magnifications. During the stick and slip area the crack propagation speed decreased under the critical crack propagation value. This resulted in local deformation; however, once the energy built-up surpassed the critical crack propagation value, the crack was re-initiated.

The stick and slip area was followed by a slow shear area (2D) in which the crack started to propagate once again (Figure 9.14l). The slow propagation speed led to the

formation of a spongious surface with very small grooves. Similar to the crack propagation in the neat polymer two more stop-go areas were observed during the slow shear area (indicated by arrows in Figure 9.14a). The last of the areas presented a vein-type pattern with very small fibrils (Figure 9.14m). When enough energy was built-up the crack passed into a rapid shear zone (2E, Figure 9.14n). The end of this area was marked by another stop-go area, in which some tearing in the crack propagation direction was observed (indicated by arrows in Figure 9.14o).

The fractography of crack initiation and propagation in impact tested nylon and nylon/MMT nanocomposites suggested, through the presence of microfibrills and stick and slip areas that the energy absorbed by the nanocomposite should have increased. However, the shift in the crack initiation area towards the root of the notch was responsible for the formation of additional stick and slip areas, as well as, the reduction in the toughness value. Since the crack initiated closer to the root of the notch, the distance that the propagating crack needed to cover increased. Thus, the intensity of the crack diminished which reflected in the higher number of stick and slip areas encountered in the nylon/MMT compared to pristine nylon.

By analysing the fracture surface of Charpy impacted nylon 6/Clay nanocomposite it was observed that the two distinctive zones previously observed for nylon and nylon/MMT nanocomposite were present in this case as well (Figure 9.15a). Similar to the previously discussed fracture surfaces, the initiation zone presented a ripple effect and the zone was divided into two areas. The improved dispersion of clay platelets and increase in the exfoliation degree resulted in the shift of the primary crack initiation site to approximately 64 μm ahead of the root of the notch and in a reduction in diameter to 31 μm (Figure 9.15b). The primary crack initiation site presented a vein-type pattern (Figure 9.15c). Compared to nylon/MMT nanocomposite, the fracture surface of the nylon/Clay nanocomposite exhibited a more fibrillar aspect which can be attributed to the better dispersion of the clay platelets and the increase in the exfoliation degree. The fibrillar aspect suggested that more energy is necessary to initiate the crack. The primary crack initiation site evolved into a radial area similar to a ripple effect represented by the formation of river markings around the initiation area (Figure 9.15d).

Similar to the previously analysed fracture surfaces the crack initiation zone developed into a crack propagation area. The river markings observed in the crack initiation area perpetuated in the brittle-like zone of the crack propagation area (2A) as long grooves (Figure 9.15e). The analysis of the long grooves at a higher magnification

revealed that the surface was characterised by a rough aspect (Figure 9.15f). Since no dislocations were observed and the TEM image revealed that the clay platelets and clay tactoids were well dispersed (Figure 9.10B) it can be hypothesised that the silicate layers are attempting to prevent the crack propagation process. As the crack propagated, a weak "ripple effect" similar to the one in the crack initiation area, was observed (indicated by arrows in Figure 9.15g). The higher magnification SEM image (Figure 9.15h) showed that this area was characterised by a rough aspect which resembled the zone observed at the beginning of the brittle-like area (Figure 9.15f).

Like the nylon/MMT nanocomposite, on the surface of the nylon/Clay nanocomposite, the brittle like area continued into a less brittle-like area (Figure 9.15i). This area was followed by a stick and slip area (zone 2C) in which the crack slowed down and then restarted its propagation (Figure 9.15j). Once enough energy was built-up, the fracture process continued with the formation of a slow shear area (zone 2D). The crack propagation from the less brittle like area to the slow shear area was depicted in Figure 9.15k. The slow shear area (Figure 9.14l) presented a very similar aspect to the less brittle like area (zone 2B). Unlike the previously analysed materials, the nylon/Clay nanocomposite presented two more stop and go areas, with the last one being characterised by a vein-type pattern with small fibrils (Figure 9.15m). This may be a consequence of the well dispersed clay platelets (Figure 9.10B), which might attempt to prevent the final break. As before, the slow shear zone transformed into a rapid shear zone (2E) represented in Figure 9.15n. This area was characterised by a terraced aspect.

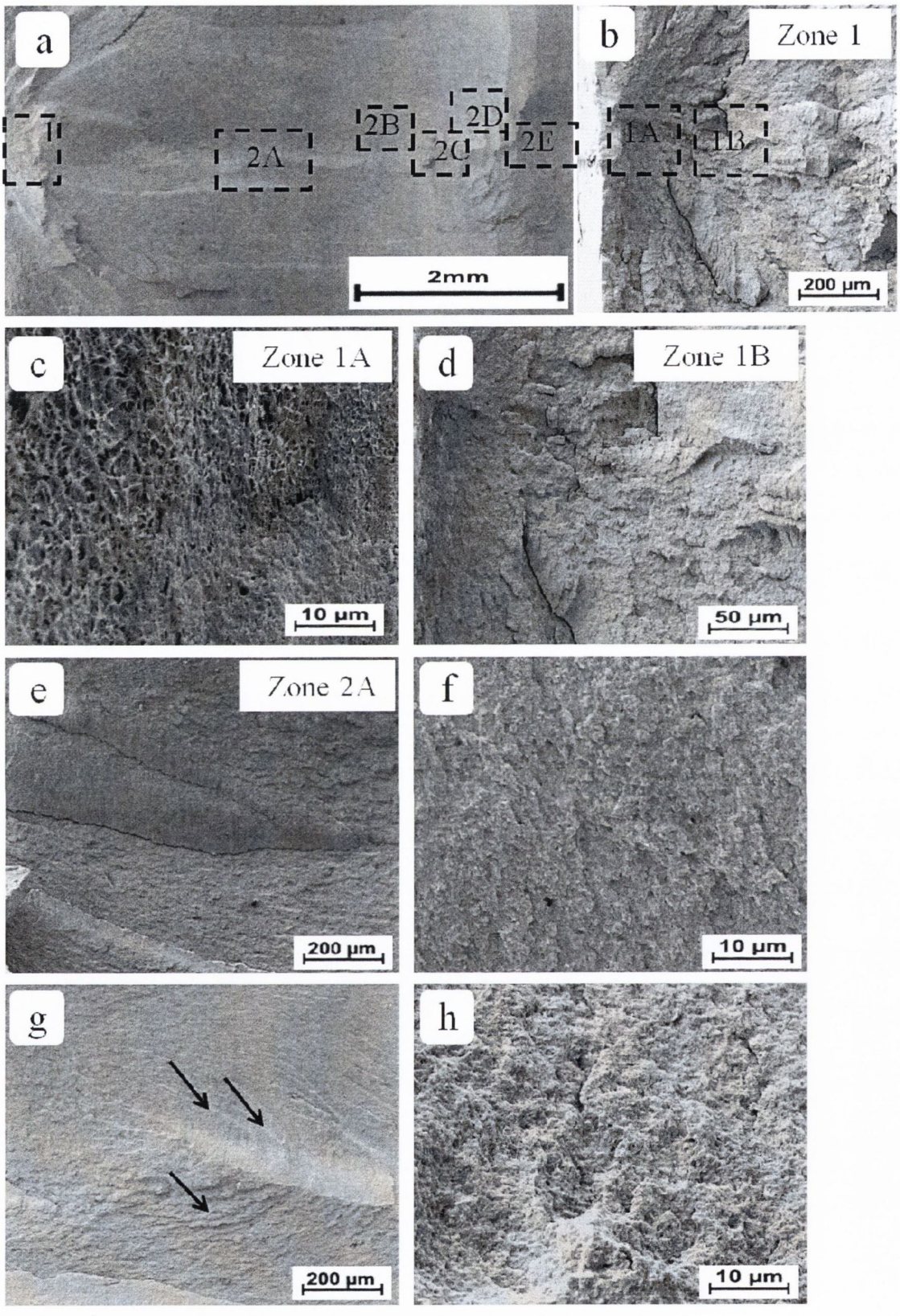

Figure 9.15. Scanning electron micrographs of the impact fracture surface of nylon/Clay nanocomposite.

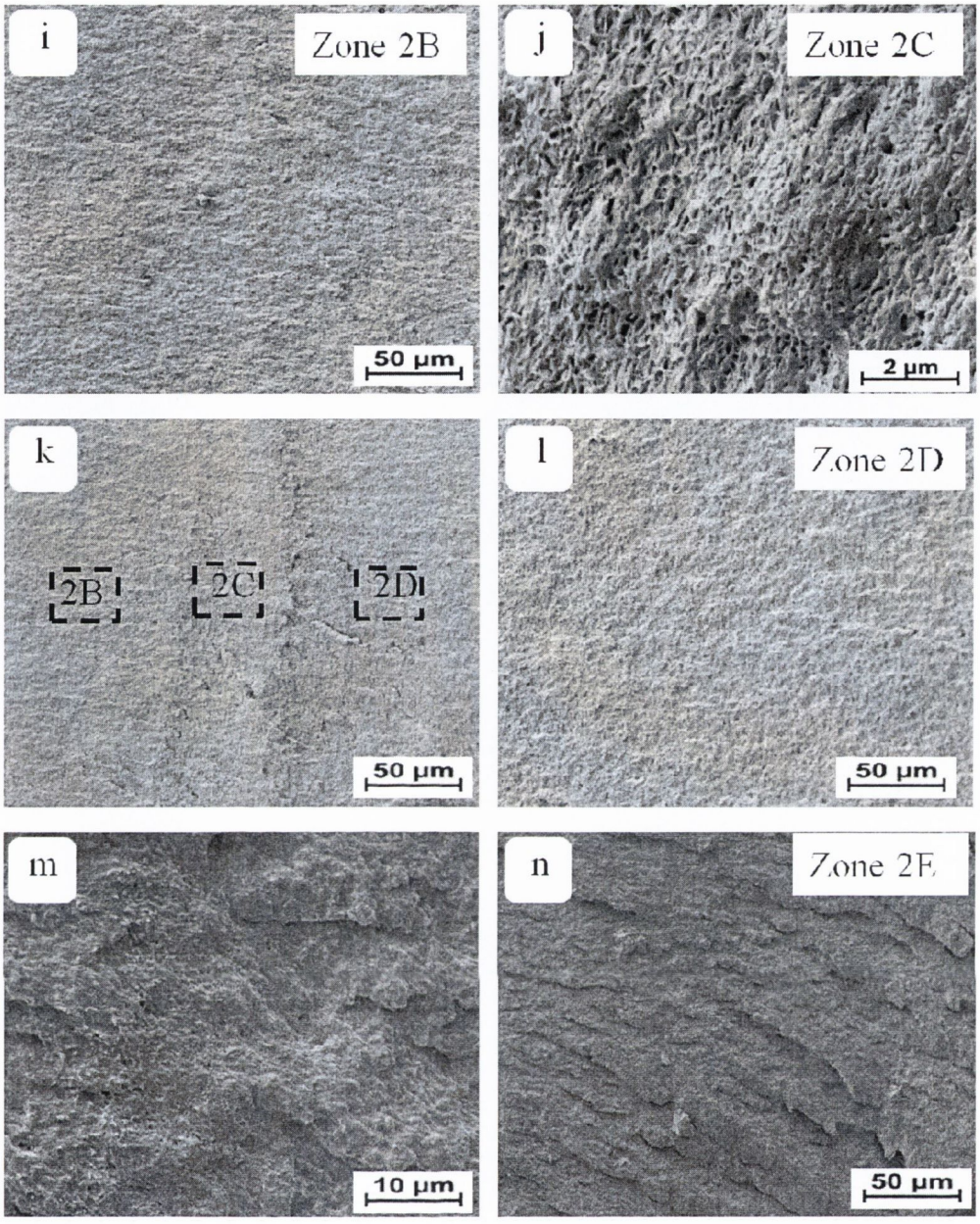

Figure 9.15. (continued)

The nylon/ADC-Clay nanocomposite Charpy impacted area, presented in Figure 9.16a, was characterised by the same two main areas previously observed for the other fractured surfaces. Unlike the cases, the dispersion of ADC-Clay shifted the crack initiation zone away from the centre of the root of the notch. This means that the highly exfoliated clay platelets had effectively prevented the crack initiation process and created a deviation path. Again, the crack initiation area (Figure 9.16b) was divided into two distinct zones a primary crack initiation site and a radial area. The primary crack initiation site was characterised by a radius of approximately 15 µm and was situated at only 41 µm ahead of the root of the notch. Similar to the primarily crack initiation site observed for nylon/Clay

nanocomposite (Figure 9.15c), the nylon/ADC-Clay nanocomposite (Figure 9.16c) presented a vein-type pattern. The initiation point was surrounded by "river markings" (Figure 9.16d). As with the previous impact fractured areas, the "river markings" from the crack initiation area evolved into short (Figure 9.16e) and long grooves (Figure 9.16f) passing into the brittle like area of the crack propagation zone. The short grooves (Figure 9.16e) were present mostly when the crack propagated away from the centre of the specimen.

The brittle-like area developed into a smooth area (Figure 9.16g) which presented a slightly rough aspect (Figure 9.16h). The distribution of highly exfoliated clay platelets may have been responsible for the premature occurrence of the smooth area, which suggested that crack propagated rapidly. The stick-slip area was very well delimitated; however, the area was no longer following a straight path (Figure 9.16i). This can be a consequence of the highly exfoliated clay platelets that were present in the nylon matrix and that attempted to modify the crack path. The stick-slip area was characterised by the occurrence of small fibrils (Figure 9.16j) which again can be attributed to the presence of well dispersed exfoliated clay platelets. A number of approximately five stick-slip areas were observed, most of them being located on different planes than the rest. Figure 9.16k presents a series of stick and slip areas in which the energy to fracture is being build-up. Once enough energy was build up a very small rapid shear area formed (Figure 9.16l). This area presented a slightly rougher aspect probably due to the presence of highly exfoliated clay platelets (Figure 9.16m).

Since the crack path was deviated from the beginning of the crack initiation process, part of the energy was eliminated fast from the system. The remaining energy continued to travel through the system and resulted in the formation of grooves; however, because of the size of the area that needed to be covered by this energy, the crack slowed down and build-up several times. The lower amount of energy available and the obstruction of the crack path led to the formation of uneven planes.

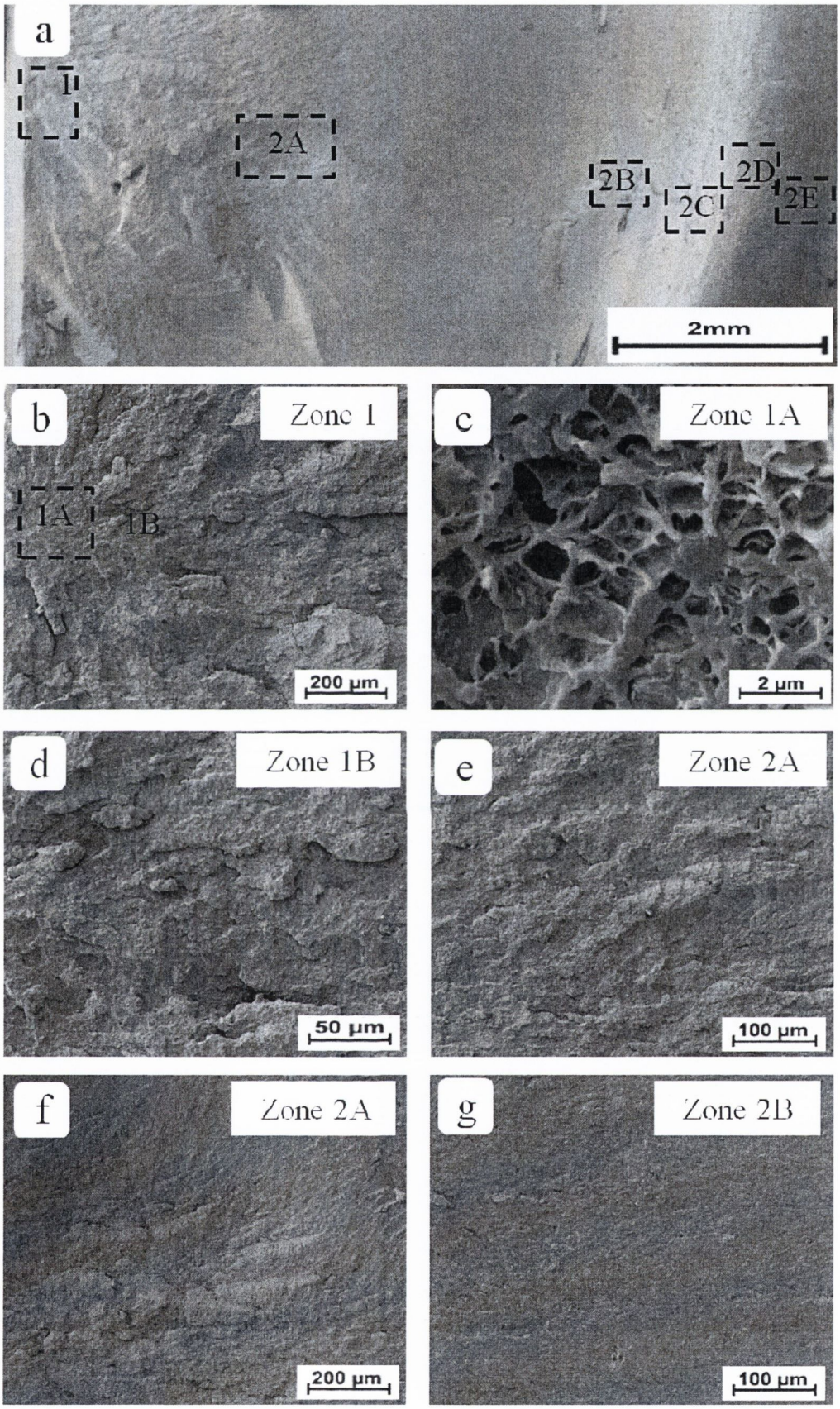

Figure 9.16. Scanning electron micrographs of the impact fracture surface of nylon/ADC-Clay nanocomposite.

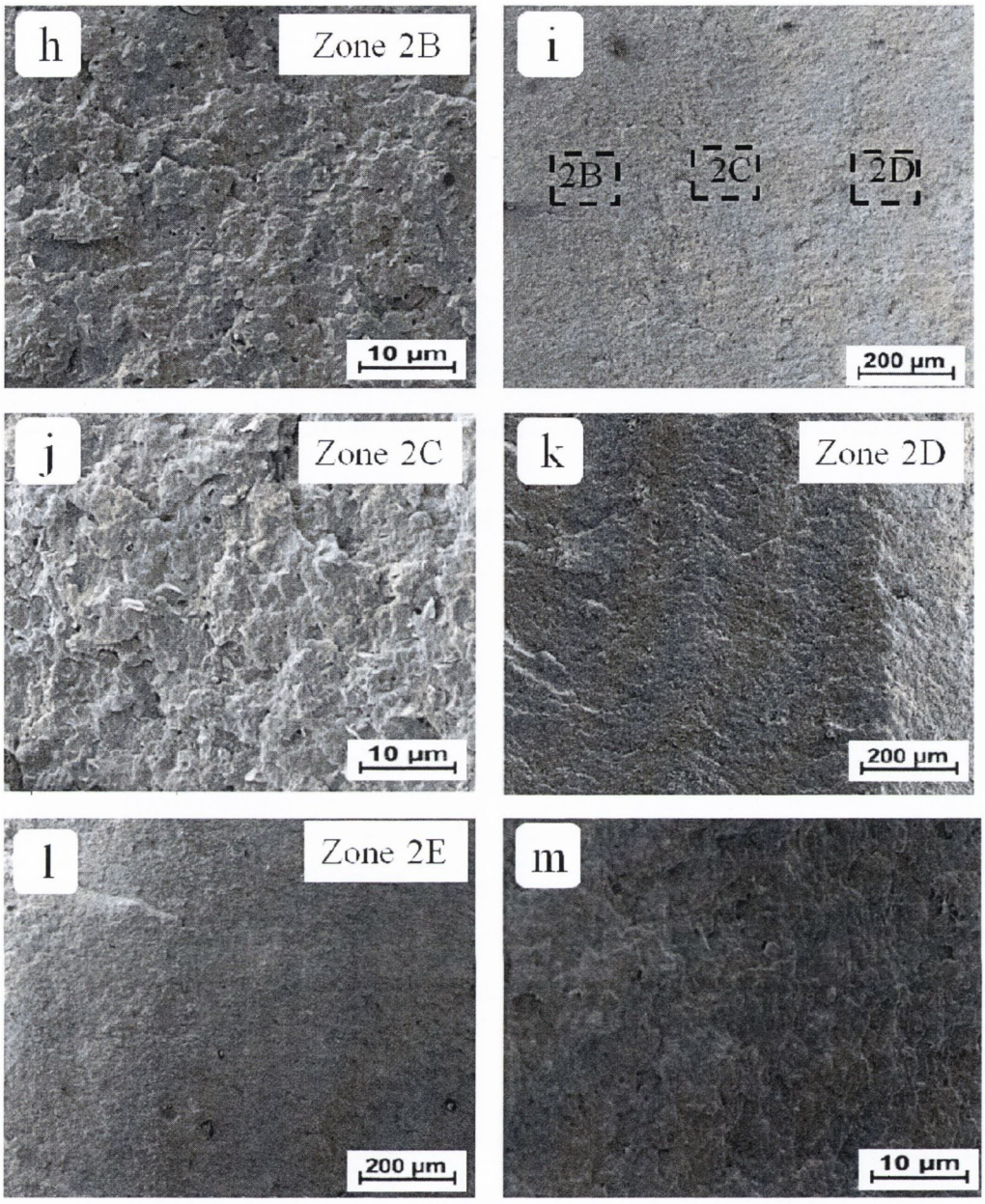

Figure 9.16. (continued)

From Figures 9.13-9.16 it was observed that the Charpy impact fractured specimens presented a blunting phenomenon that was caused by the type A notch present on the tested specimens. This type of notch is characterised according to ISO 179:1997 by a radius of 0.2 mm. The surface analysis of the impact fractured specimens revealed that with the addition of clay the blunting phenomena that took place in impact specimens had shifted towards the root of the notch, while the radius for primary crack initiation site decreased. This was in good agreement with the brittle character that the polymer/clay nanocomposites exhibited compared to the pristine polymer (Figure 9.5). However, the presence of clay transformed the primary crack initiation site from a smooth area (Figure

9.13b) to a vein-type pattern with fibrils (Figures 9.14c, 9.15b and 9.16c) which would suggest that the clay attempted to prevent the crack initiation process. These findings prompted the investigation of the changes in the impact strength, the location and structure of the primarily crack initiation zone with the degree of exfoliation of the clay platelets which reflected in the ratio of exfoliated nanocomposite, determined according to literature,[122] present in the intercalated/exfoliated nanocomposite (Figure 9.17).

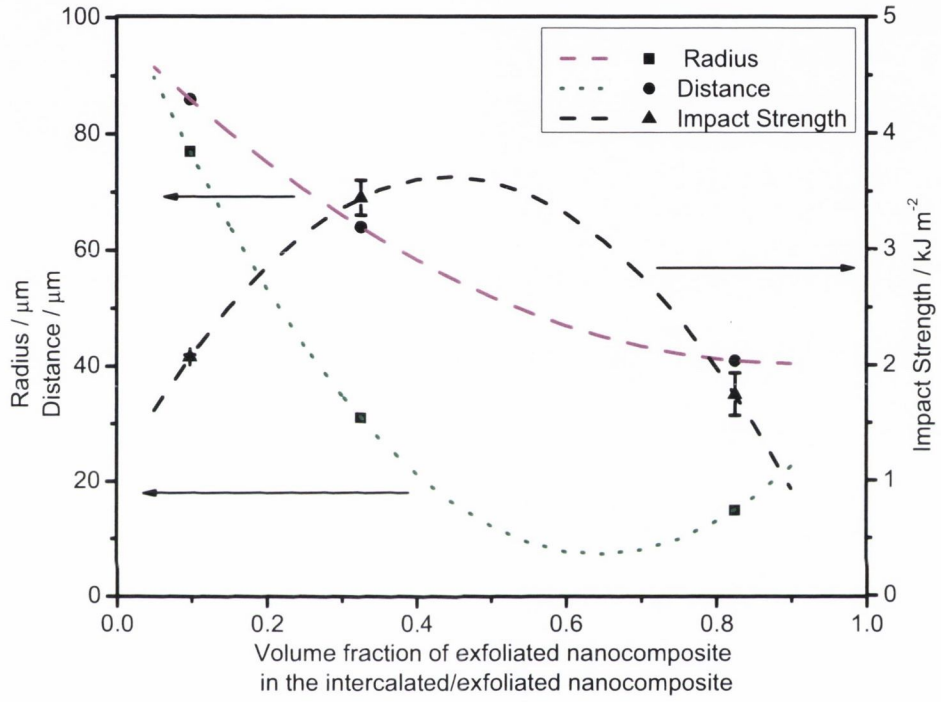

Figure 9.17. Variation of the radius of the primary crack initiation site and of the distance between the centre of the primary crack initiation site the root of the notch with the impact strength and the volume fraction of the exfoliated nanocomposite present in the intercalated/exfoliated nanocomposite

As can be observed the distance between the root of the notch and crack initiation site decreased almost linearly with the increase in the exfoliated nanocomposite. Similarly, the radius of the crack initiation site decreased with exfoliation. This suggested that a higher intercalation degree may delay the formation of the primary crack initiation site and thus accentuate the blunting phenomenon that the material exhibited.

Unlike the location and the radius of the primary crack initiation site, the impact strength exhibited an almost parabolic variation with the fraction of exfoliated nanocomposite. From Figure 9.17, it can be hypothesised that in order to obtain enhanced

impact strength, the volume fraction of the exfoliated nanocomposite has to represent approximately 0.45 of the intercalated/exfoliated polymer/clay nanocomposite, which corresponded to a degree of exfoliation of around 60%. Thus, assuming ideal dispersion of clay nanostructures, the optimal toughness for a nylon 6/clay nanocomposite was determined to be achieved when 60% of the nanostructures are represented by single clay platelets and the remaining 40% of nanostructures are represented by intercalated clay tactoids with 2.4 clay platelets per stack (Appendix IV). These factors will produce a primary crack initiation site with a radius of 20 μm, which will be located at 55 μm from the root of the notch.

9.3.4.2. Low-speed toughness tested fracture surfaces

The low speed used during the fracturing process limited the occurrence of elaborate crack surfaces and produced a fairly uniform crack propagation front. For each sample the fractography of the crack propagation path was observed in four distinct areas (Figure 9.18).

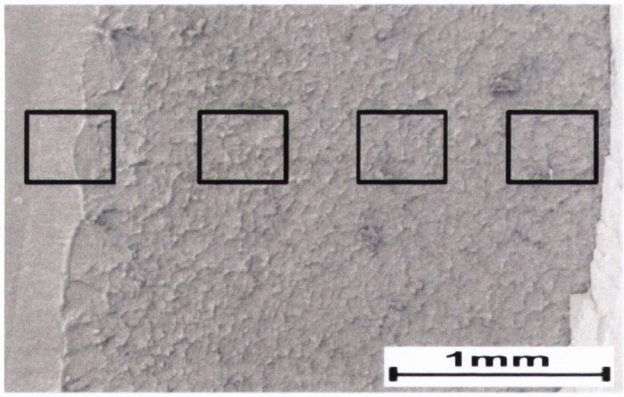

Figure 9.18. The location of the areas of interest on the crack propagation path, exemplified for a compact tension specimen.

SENB specimens

The fracture toughness test on SENB pristine nylon produced a surface that presented a smooth initiation area (Figure 9.19a). This area presented very sporadic fibrils that can be a consequence of the breaking of the amorphous polymer present in the semicrystalline polymer, as it has been previously reported in literature.[131] Between these breaking points, spherulites with very soft edges were encountered (Figure 9.19a1). As the

crack began to propagate, the crack front showed signs of brittle fracture (Figure 9.19b-9.19d). At the beginning of the process small grooves (Figure 9.19b) with very smooth areas and larger and sporadic spherulite shaped holes were observed (Figure 9.19b1). The increase in the spherulite shape may suggest a reduced opposition of the material.

The brittle character was best observed further on the crack propagation path (Figure 9.19c) where side grooves were encountered. An increase in the magnification showed breakings in the side grooves (Figure 9.19c1). As the crack continued to propagate the surface exhibited smaller side grooves (Figure 9.19d) and a reduction in size of the cleavage breakings (Figure 9.19d1).[154] By comparing the fracture toughness surface with the impacted surface, a similar pattern was observed in the slowdown area of the crack, with the surface presenting a slightly less brittle behaviour. This brittle fractography, characterised by cleavage fracture surfaces, can be attributed to the high crystallinity degree of the neat polymer (over 30%)[440] which in the presence of a defect can lead to microvoid coalescence and sharp crack propagation regardless of the testing speed. These findings are in good agreement with the observations made by Brown and Dattelbaum[154] and Lim et al.[437] for pristine PTFE and nylon 6/organoclay/elastomer systems.

The dispersion of clay platelets and clay tactoids into the nylon matrix led to the formation of a tougher material (Figure 9.20), which is in accordance with the fracture tests results (Figure 9.6). The early stages of crack propagation in nylon/MMT nanocomposite revealed the formation of a vein-type pattern (Figure 9.20a) with small fibrils on the edges of the veins (Figure 9.20a1). The vein-type pattern, described in literature[450] as "dimples", resembled a closed-cell foam structure, with the faces of the cells presenting small torn areas. As the crack propagated the vein-type pattern intensified and the dimensions of the closed-cells decreased (Figure 9.20b). However, the higher magnification view of the area showed an increase in the fibrils density on cell edges as well as enhanced tearing of the cellular faces (Figure 9.20b1). The further propagation of the fracture maintained the vein-type pattern (Figure 9.20c), whilst leading to microvoid cavitation. The increase in the defect density resulted in the formation of thick veins that were orientated perpendicular to the crack propagation direction (Figure 9.20c1). This phenomenon has been previously reported in literature[164] and attributed to the delamination of the clay tactoids (Figure 9.11B). Microvoid cavitation was still visible and as the crack propagated further the cellular density decreased (Figure 9.20d and Figure 9.20d1).

By increasing the exfoliation degree in nylon/Clay nanocomposite the vein-type pattern transformed into a more fibrillar pattern (Figure 9.21a and Figure 9.21b). The

fibrils present in the early stages of crack propagation exhibited a height of approximately 1-2 μm (Figure 9.21a1 and 9.21b1). These type of fibrils have been previously reported in literature[164] and attributed to the presence of adiabatic heating that deformed the ligaments and oriented them in the crack propagation direction.[172] Since this fibrillar aspect was not observed in the neat polymer (Figure 9.19) or nylon/MMT nanocomposite (Figure 9.20), it can be assumed that the excellent dispersion of clay platelets and clay tactoids (Figure 9.10) was responsible for the changes in the fracture surface. As the crack continued to propagate, the material showed enhanced resistance to the crack propagation process by forming "rib marks" with line separating tilted planes indicate small hesitations and deviation from the crack path (Figure 9.21c), which is in agreement with the previously reported literature.[451] A higher magnification of the area showed that smaller fibrils were present on the "rib markings" and on the terraces that formed between the "rib markings" (Figure 9.21c1).

The increase in the crack initiation in the detriment of the crack propagation observed at higher crack lengths (Figure 9.6) suggested that the clay tactoids had delaminated. This aspect was reinforced by the "rib markings" formation that was observed at high stresses. With the further propagation of the crack larger terraces were formed (Figure 9.21d). This area presented smaller and shorter fibrils which are due to the acceleration of crack speed that occurred with the increase in the damaged area. The microvoids observed in Figure 9.21d1 can be explained by the slipping of clay platelets and the rearrangement of the hydrogen bonds that formed between the polymeric lamellas.

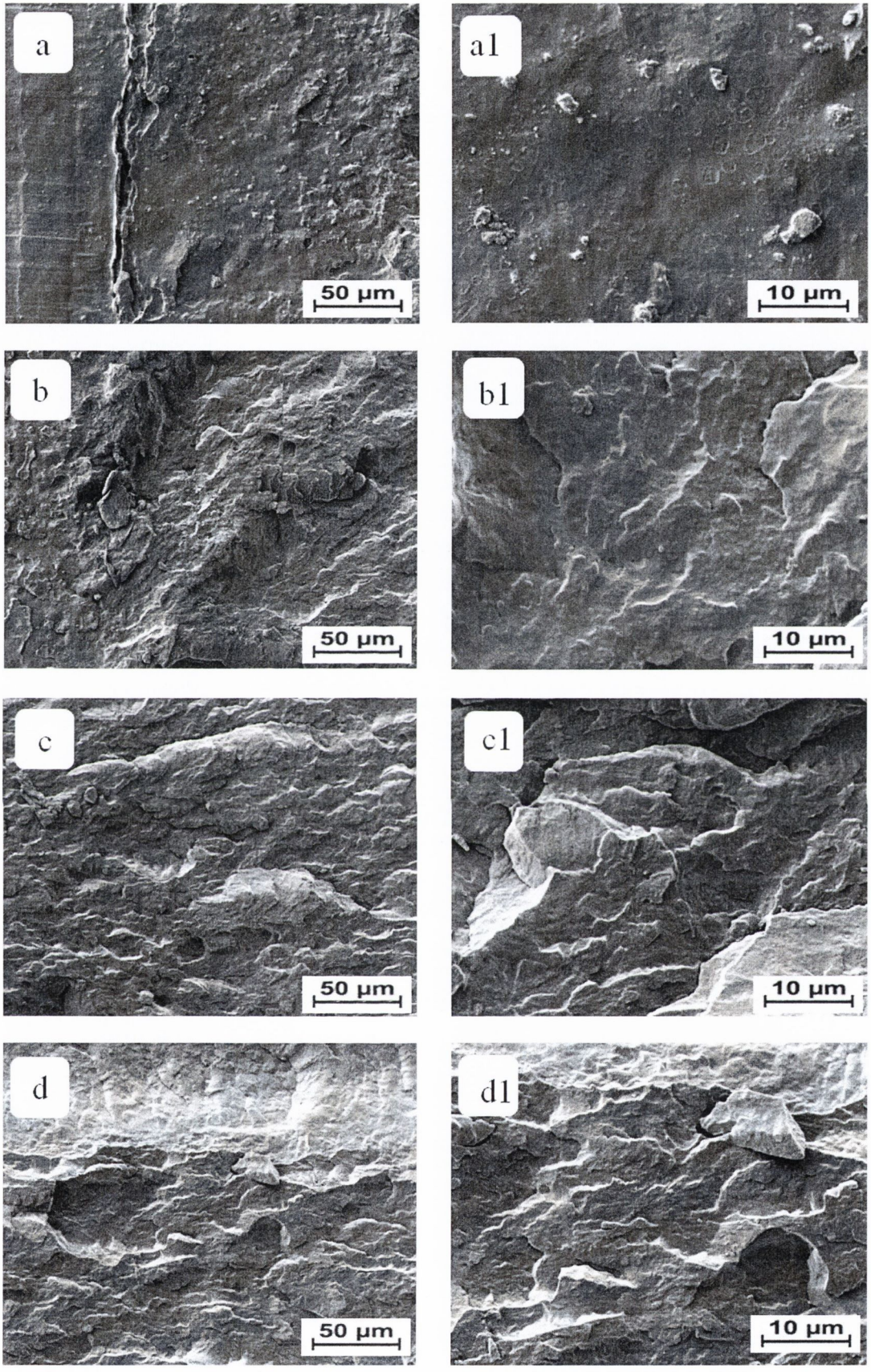

Figure 9.19. Scanning electron micrographs of the SENB fracture surface of neat nylon.

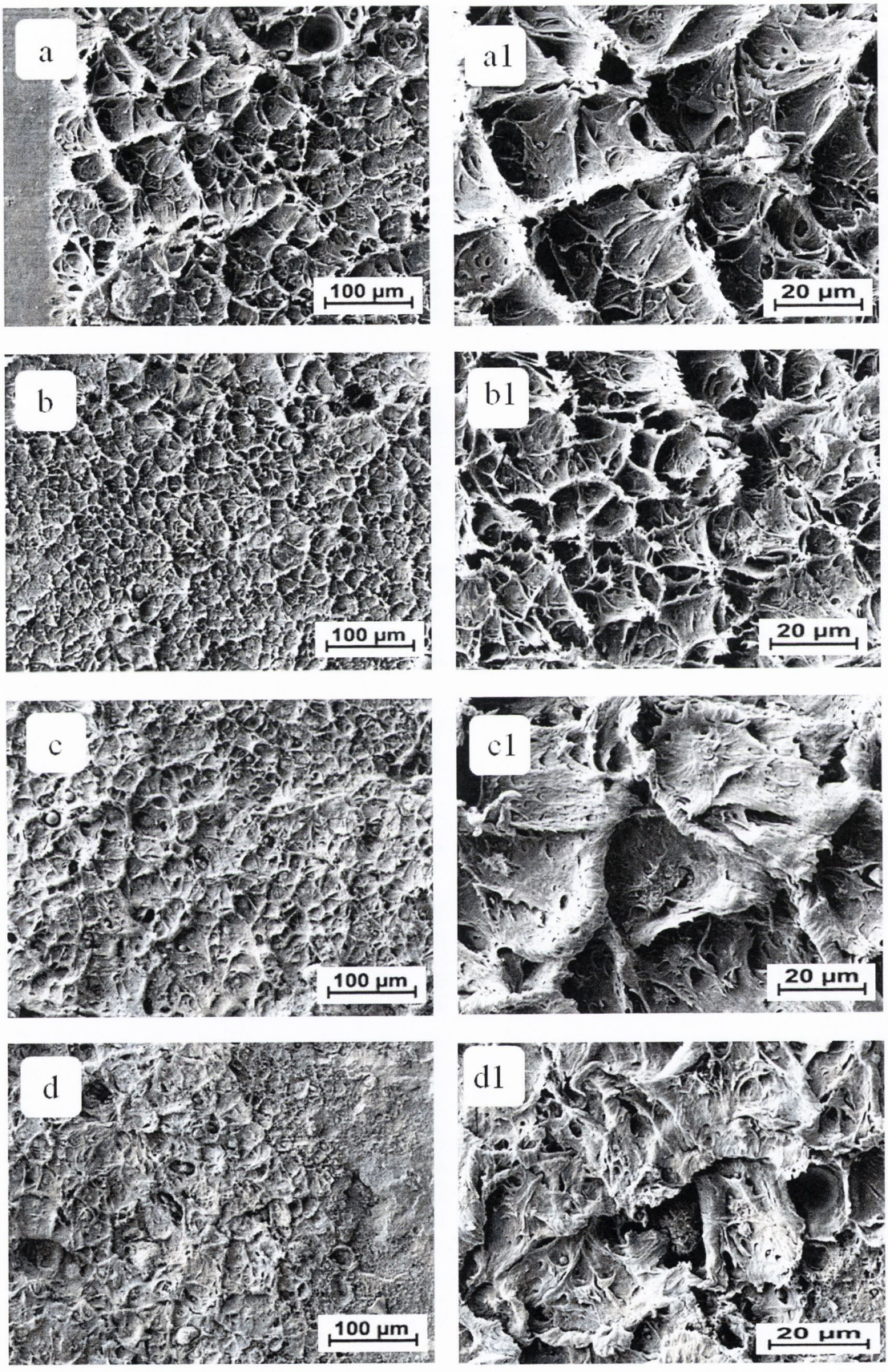

Figure 9.20. Scanning electron micrographs of the SENB fracture surface of nylon/MMT nanocomposite.

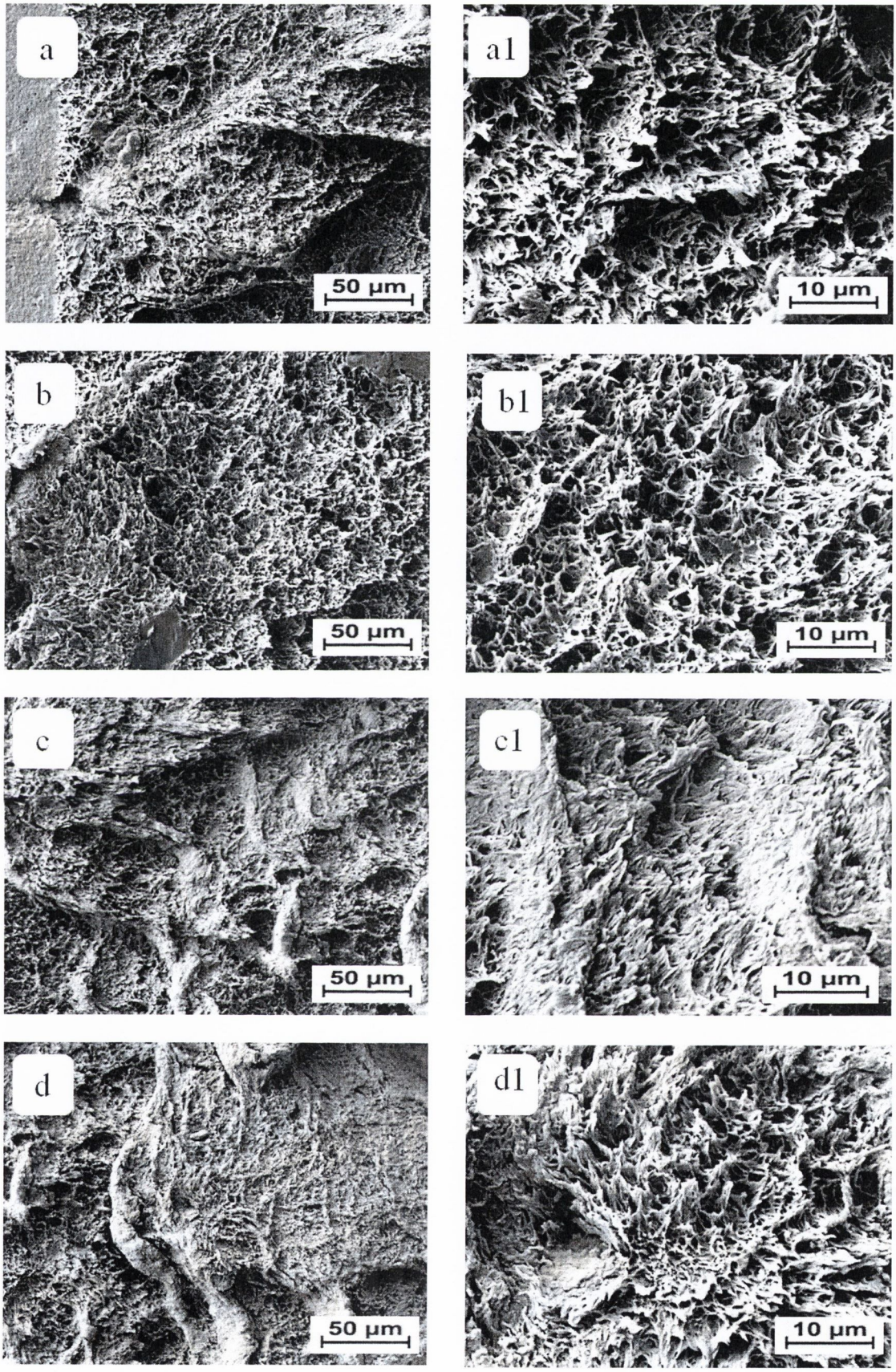

Figure 9.21. Scanning electron micrographs of the SENB fracture surface of nylon/Clay nanocomposite.

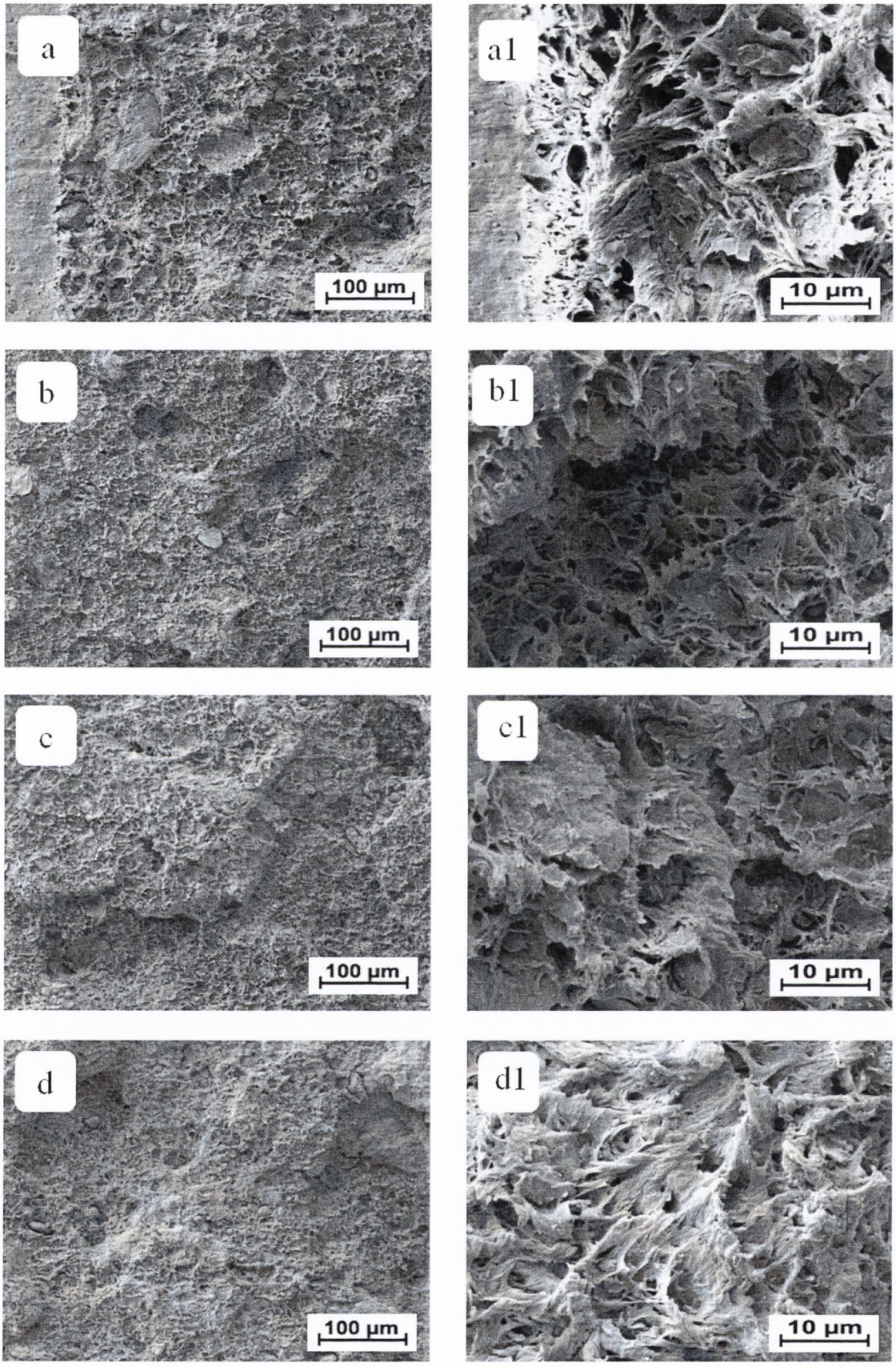

Figure 9.22. Scanning electron micrographs of the SENB fracture surface of nylon/ADC-Clay nanocomposite.

The increase in the exfoliation degree in nylon/ADC-Clay nanocomposite led to the formation of a vein-type pattern (Figure 9.22a). However, a higher magnification revealed a more fibrillar aspect (Figure 9.22a1). Unlike the early stages of crack propagation in nylon/Clay nanocomposite (Figure 9.21a1), the fibrils were orientated mostly against the crack propagation direction. As the applied stress increased, the fractured surface showed a more terraced vein-type patterned (at low magnifications - Figure 9.22b-9.22d) compared to nylon/Clay nanocomposite. The imaging of these fracture areas at higher magnification revealed a slight reorientation of the fibrils (Figure 9.22b1); followed by the occurrence of thick veins (Figure 9.22c1) and the clear reorientation of the fibrils against the crack propagation path (Figure 9.22d1). The reorientation of the fibrils implied that adiabatic heating had occurred.[172] This aspect was confirmed by SEM fractography which showed the formation of a fairly homogeneous fracture surface (at low magnification). This homogeneous surface showed little change at higher magnifications.

From the SENB specimens it can be concluded that in the pristine nylon the presence of a flaw led to direct propagation of the crack, by producing a very smooth crack surface corresponding to a sharp crack, which is in agreement with the previous findings reported in literature.[150] However, the addition of the clay, regardless of the exfoliation degree, led to surfaces that presented vein-type patterns and drawn-out polymer fibers. In this case, it can be hypothesised that the presence of clay had obstructed the crack propagation *via* delamination characterised by TEM. The delamination and the movement of the clay platelets created a sieve effect that reflected in the formation of venations and fibrils. The variation in the degree of exfoliation was best reflected by the fibrils. It was observed that the at approximately 50% exfoliation, the fibrils are individually small, whereas, in the minimum and maximum exfoliation cases, the fracture surface presented large areas with coils, indicating that in this case the sieve effect was not as strong.

Longitudinally tested CT specimens

Maintaining the same orientation of the polymer lamellas in the neat polymer, and clay tactoids and clay platelets in polymer/clay nanocomposites, compact tension specimens were tested longitudinally. The fractography of neat polymer showed a fairly uniform morphology with a vein-type pattern (Figure 9.23a-9.23d). The density of venation appeared to present accretion behaviour with crack propagation. The higher magnification imaging of the areas showed that at the beginning of the crack propagation the fibrils on the veins and the venation present inside the vein cluster were orientated

against the fracture path (Figure 9.23b1-9.23d1). This is similar to the observations made by Wilbrink et al.,[164] who studied the tensile fracture surface of nylon 6/$CaCO_3$. As the crack propagated, the fibrils start to show a small shift in the orientation (Figure 9.23c1) which may be due to an increase in the adiabatic temperature inside the polymer.[172] Towards the end of the crack propagation process, the elongated fibrils present on the veins coiled into slightly thicker veins arranged perpendicular to the path of fracture (indicated by arrows in Figure 9.23d1).

The dispersion of MMT in nylon resulted in a material that showed instant crack propagation (Figure 9.24a). As the crack grew the nylon/MMT nanocomposite presented a very rough structure (Figure 9.24a-9.24d). The early stages of crack propagation showed the presence of smooth areas with limited vein-type pattern (Figure 9.24a). This suggested that the crack was immediately initiated and that very little opposition from the polymer matrix was encountered during the process. At higher magnifications, the structure appeared to present a lacy vein-type pattern (Figure 9.24b1-9.24d1). As the crack propagated further a vein-type pattern with minimal fibrils was observed (Figure 9.24b1). Towards the end of the crack path, the material obstructed the crack propagation by forming small coiled veins, orientated almost perpendicular to the crack path (Figure 9.24d1).

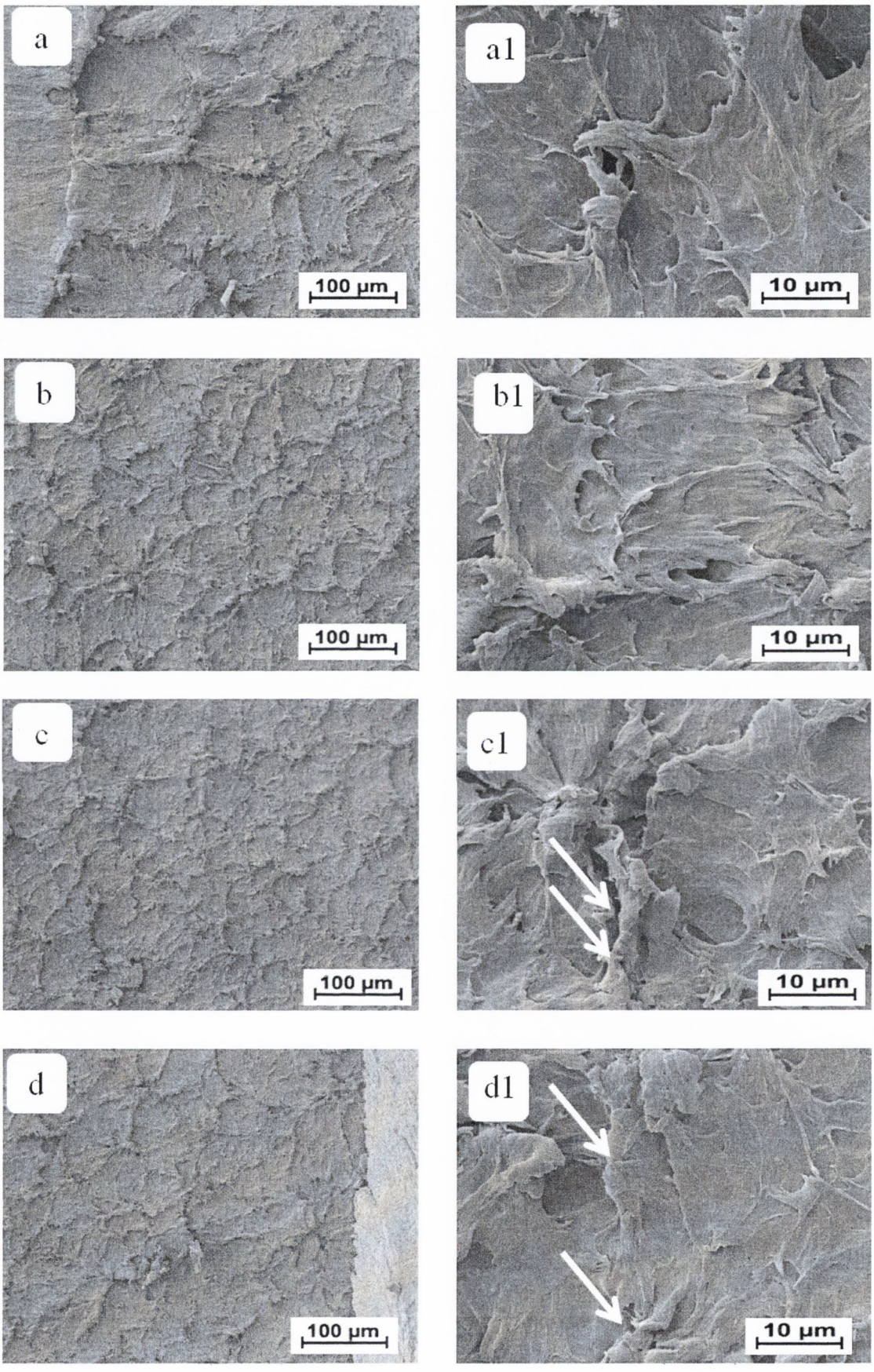

Figure 9.23. Scanning electron micrographs of the fracture surface of neat nylon in CT specimen longitudinally tested.

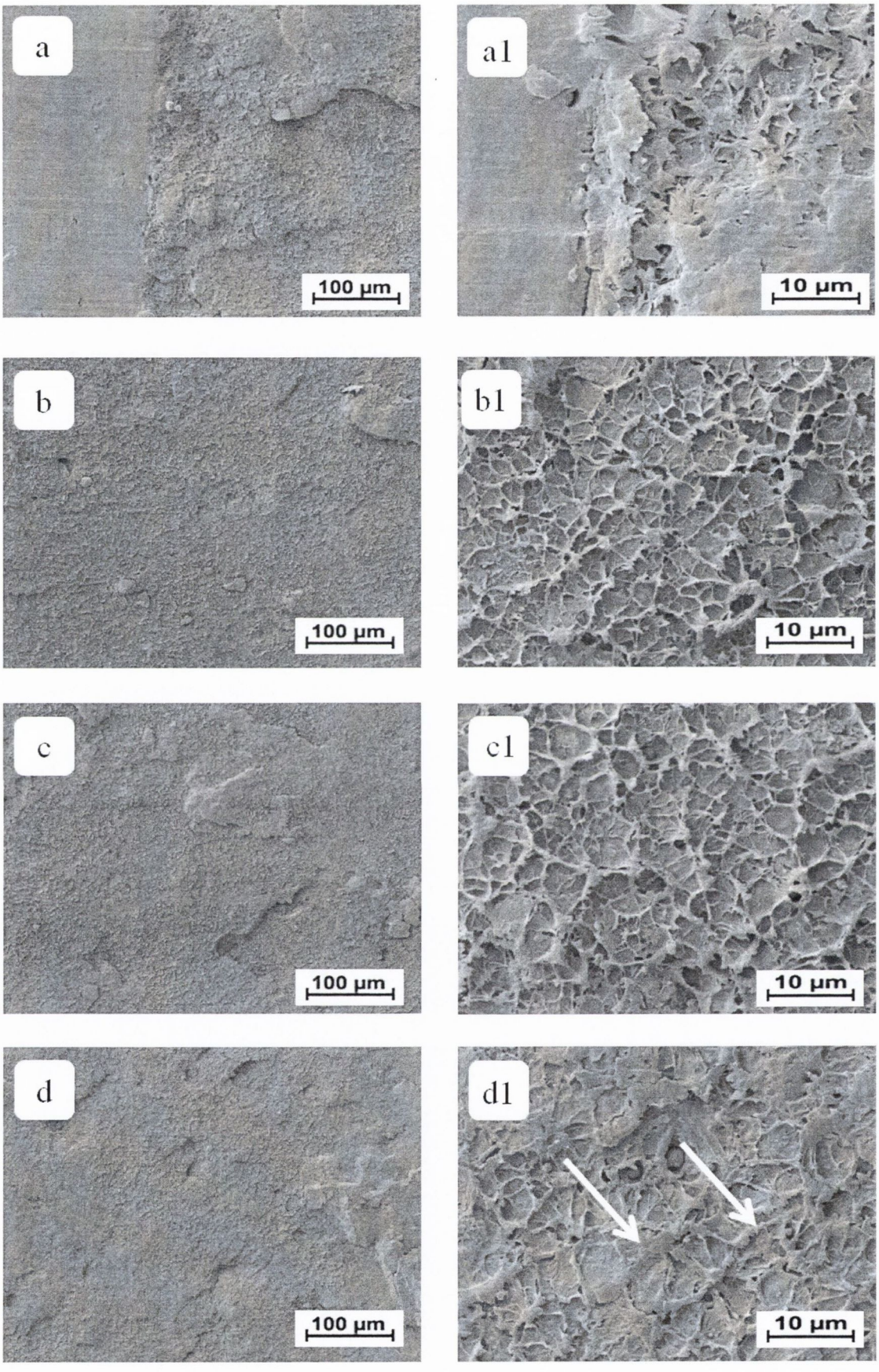

Figure 9.24. Scanning electron micrographs of the fracture surface of nylon/MMT nanocomposite in CT specimen longitudinally tested.

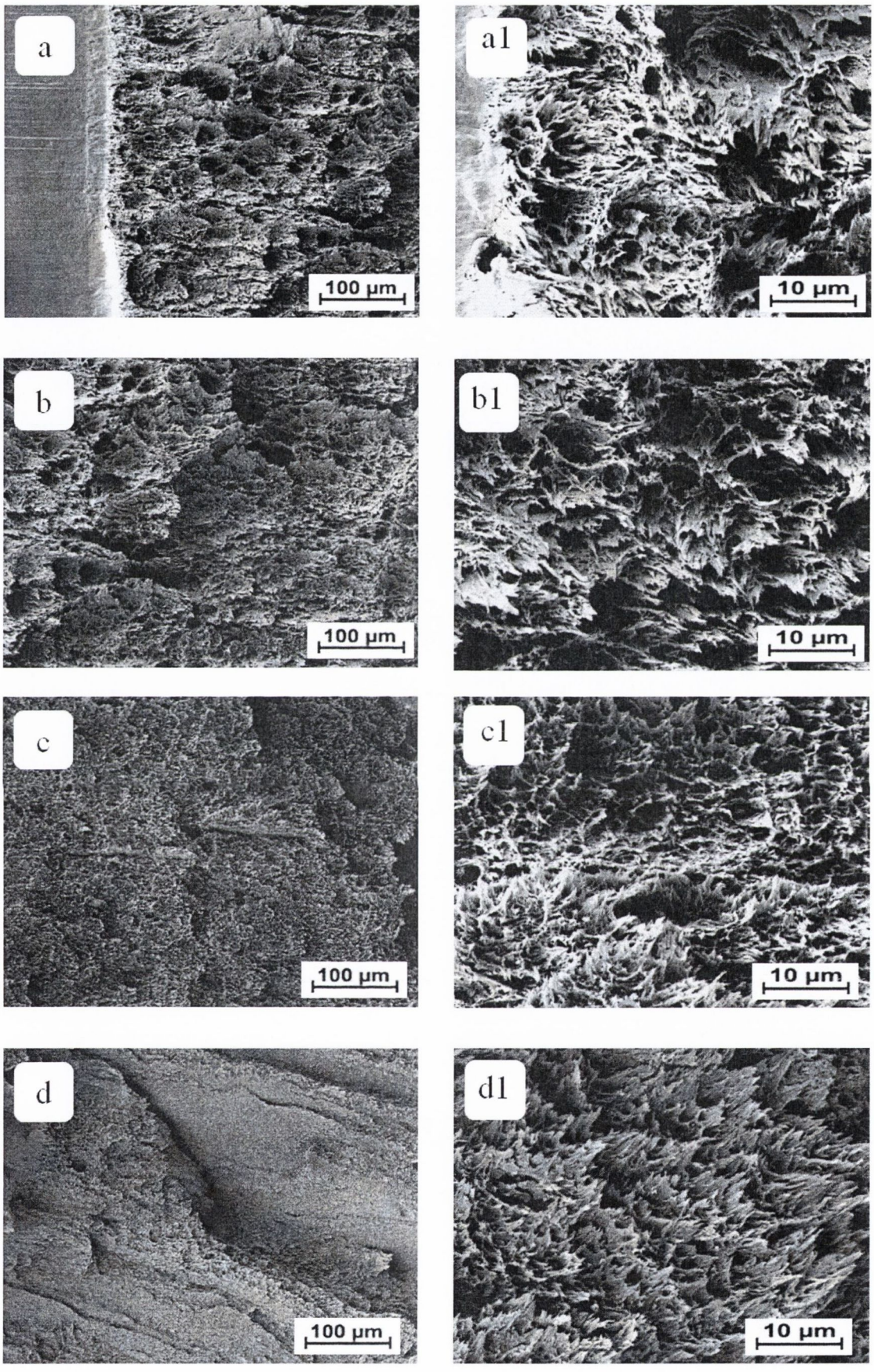

Figure 9.25. Scanning electron micrographs of the fracture surface of nylon/Clay nanocomposite in CT specimen longitudinally tested.

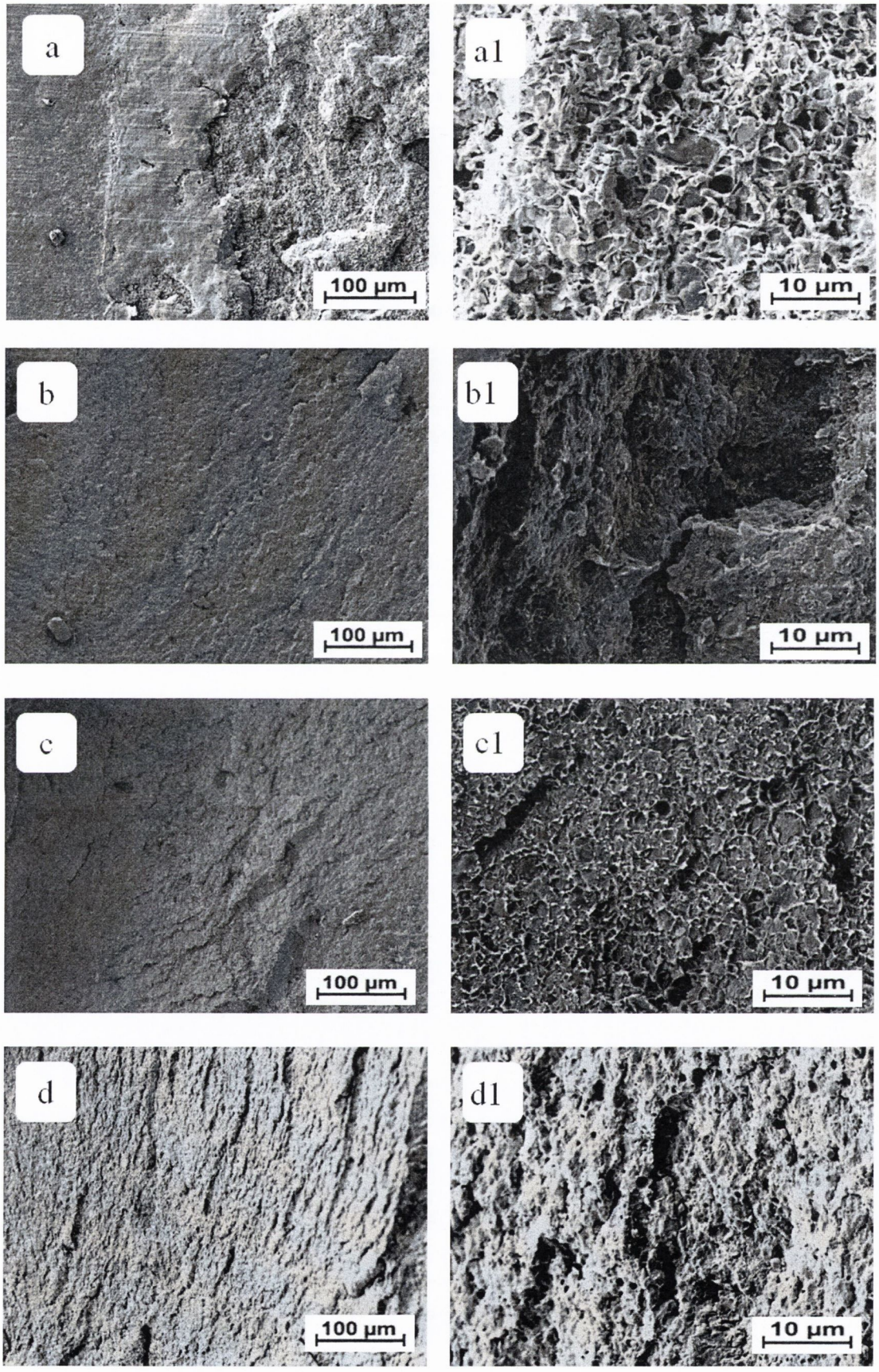

Figure 9.26. Scanning electron micrographs of the fracture surface of nylon/ADC-Clay nanocomposite in CT specimen longitudinally tested.

Nylon/Clay nanocomposite presented minimal delay in the crack propagation process (Figure 9.25a). The lower magnification images revealed a rough aspect (Figure 9.25b and Figure 9.25c). As the crack propagated tearing occurred in the fibrillar aspect and possible dislocations that led to an uneven surface (Figure 9.25d). Higher magnification images revealed that the fibrils were elongated and that the break was produced due to tearing in the elongated polymer ligaments (Figure 9.25a1-9.25d1), which was caused by the orientation of the fibrils. This structure was observed even on the terraced surface that occurred towards the end of the crack front. This pronounced fibrillation has been previously encountered and attributed to energy dissipation, by Tjong and Bao[185] who characterised the fracture toughness of HDPE/SEBS-g-MA/MMT *via* essential work of fracture. Since this kind of structure was not encountered in the pristine polymer, it may be hypothesised that the presence of well distributed, optimal exfoliated clay platelets was responsible for the increase in the toughness of the material. Thus, part of the stress that was applied to the polymer/clay nanocomposite transferred from the polymer matrix to the filler component and delayed the crack propagation process.

Further increase in the exfoliation degree led to a material that presented almost immediate crack initiation followed by a fast crack propagation process (Figure 9.26a). The propagation of the crack showed the formation of a rougher area in the early stages of crack growth followed by areas with a brittle aspect (Figure 9.26b-9.26d). Higher magnification imaging revealed that a vein-type pattern had formed. At the beginning of the crack propagation process the fibrils present on the veins were orientated against the crack propagation path (Figure 9.26a1). As the crack propagated, the fibrils began to re-orientate, facing against the crack propagation direction towards the end of the crack path (Figure 9.26b1-9.26d1).

Transversally tested CT specimens

The tensile deformation of the compact tension specimen on the transversal axis showed instant crack propagation with the polymer exhibiting "an unfolding fan" resistance (Figure 9.27a). As the fracture started to propagate, the distance between the polymer lamellas increased. Because the polymer lamellas were connected by hydrogen bonds, the increase in the crack initiation energy extended those bonds until the breaking point. By excessively stretching of the structure, microvoids may have been formed. As the crack kept growing the microvoids cavitated,[154] thus introducing large defects (Figure 9.27b), that dictated a brittle-like propagation crack path (Figure 9.27c and 9.27d). Higher

magnification imaging showed a "shish-kebab effect" (Figure 9.27a1), as it has been previously denoted in literature,[452] in the early stages of crack propagation, followed by a brittle surface (Figure 9.27b1). The brittle behaviour can be a consequence of the breaking of the hydrogen bonds which induced a tearing into the alignment of the polymer lamellas creating defects into the material (Figure 9.27c1-9.27d1).

The dispersion of MMT in the nylon matrix resulted in a crack propagation surface that presented a very brittle character. The crack appeared to be almost instantly initiated and the fractographic analysis revealed that the surface was very similar to an impact tested fracture. The early stages of crack propagation showed that the crack initiated very fast (Figure 9.28a) and it developed into a crack propagation surface with "river markings" (Figure 9.28b). Under constant loading the laminar polymer obstructed the crack path by forming a terraced aspect (Figure 9.28c). As the crack continued to propagate the SEM imaging revealed that brittle breaking had occurred (Figure 9.28d).

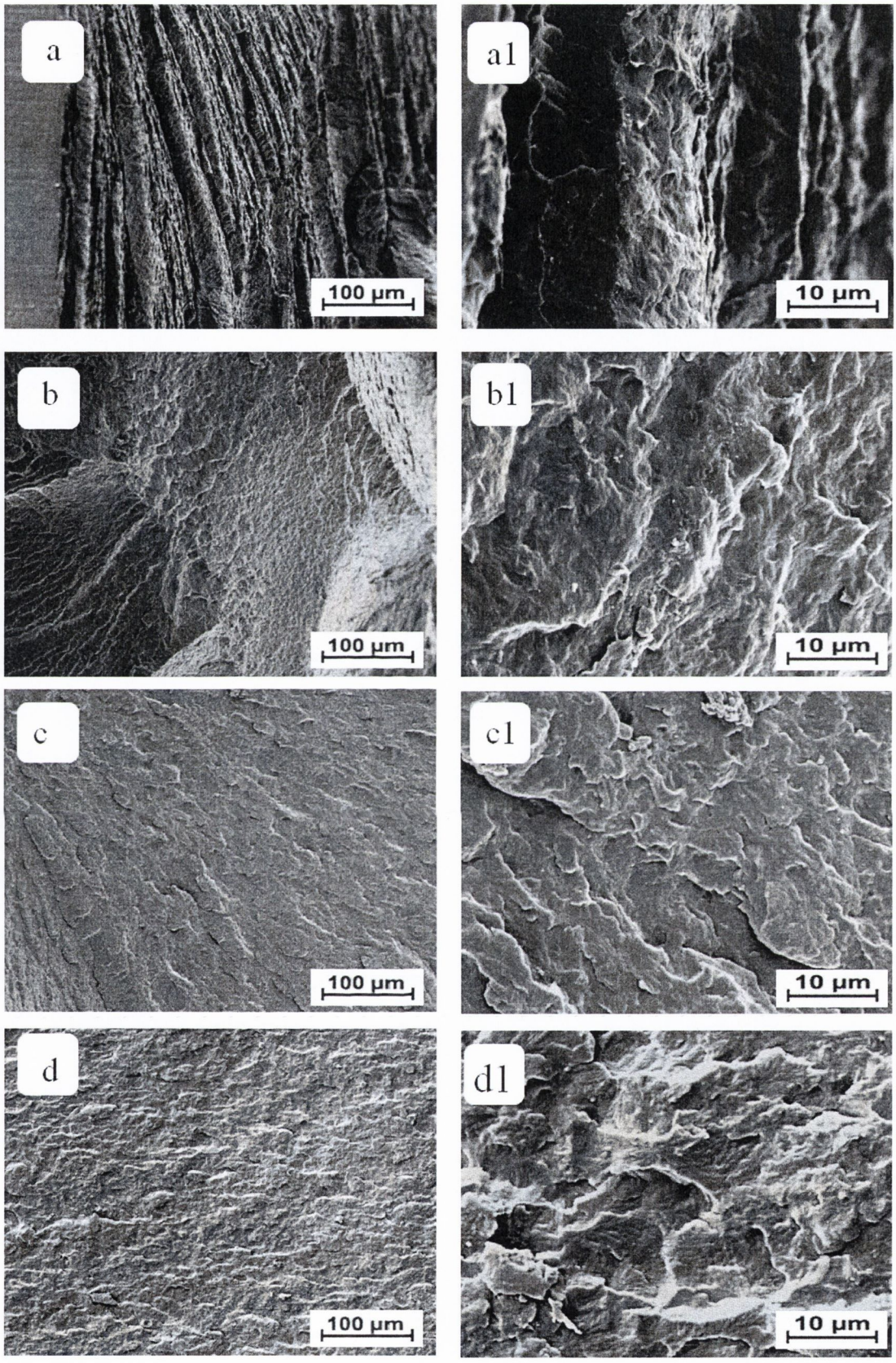

Figure 9.27. Scanning electron micrographs of the fracture surface of neat nylon in CT specimen transversally tested.

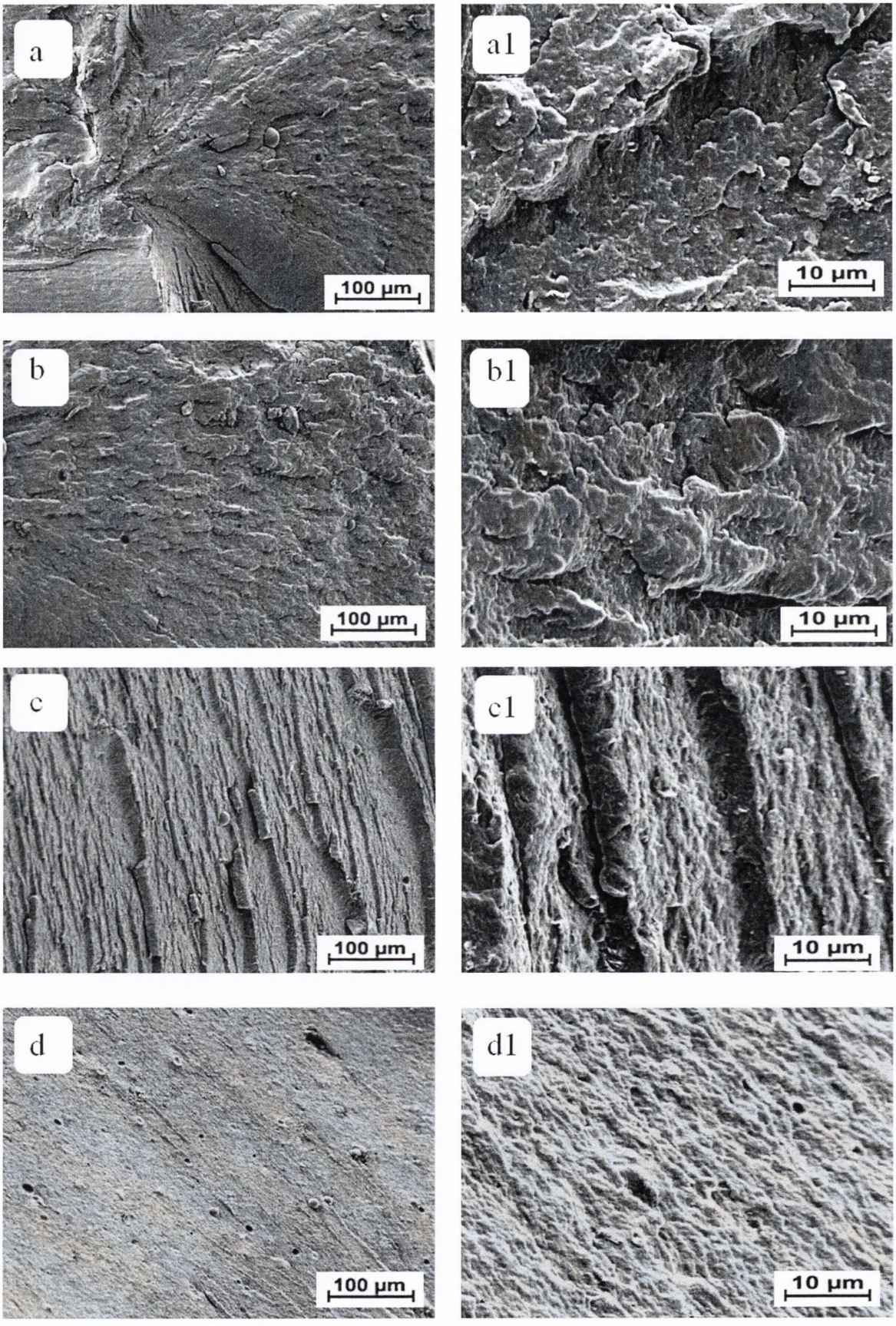

Figure 9.28. Scanning electron micrographs of the fracture surface of nylon/MMT nanocomposite in CT specimen transversally tested.

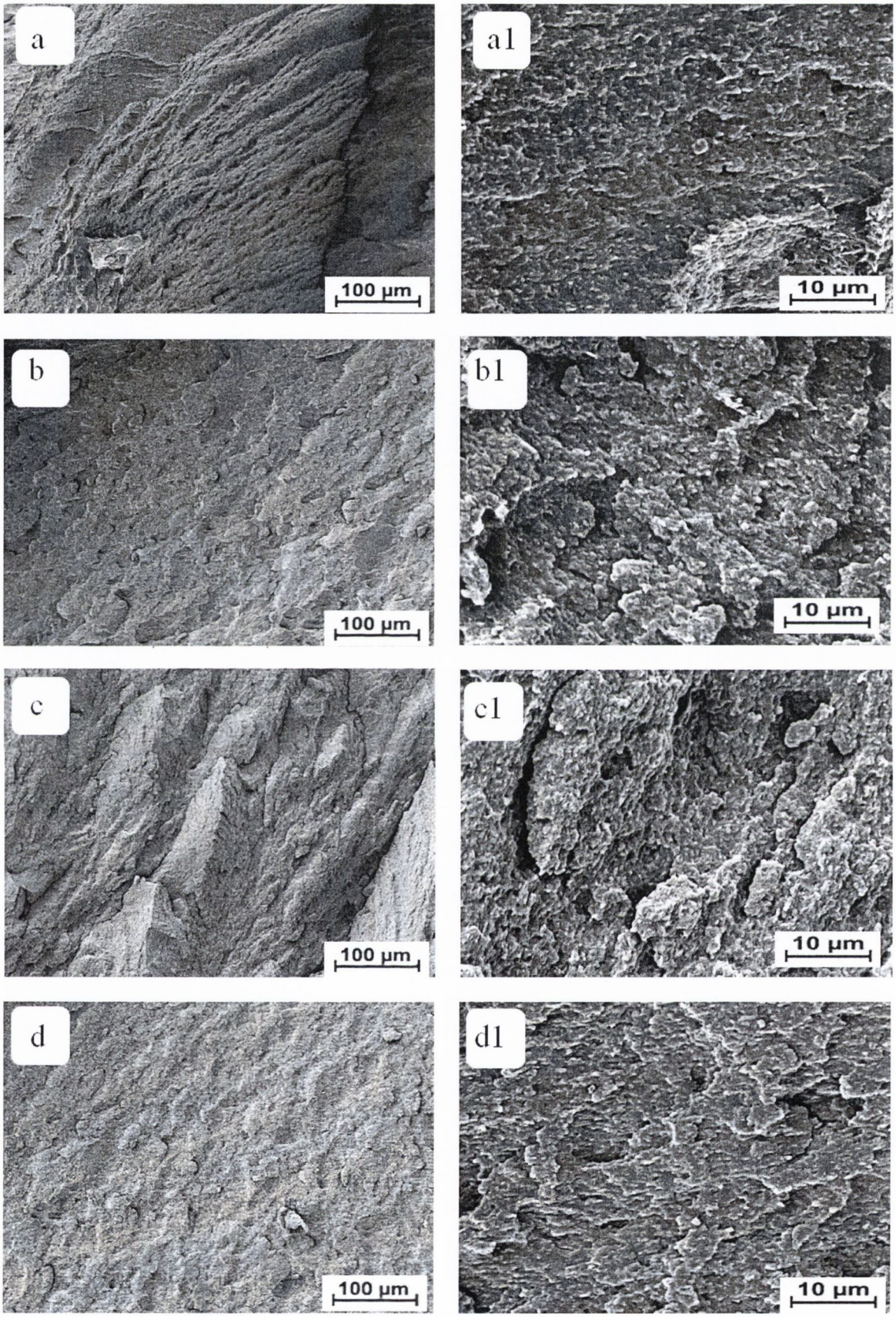

Figure 9.29. Scanning electron micrographs of the fracture surface of nylon/Clay nanocomposite in CT specimen transversally tested.

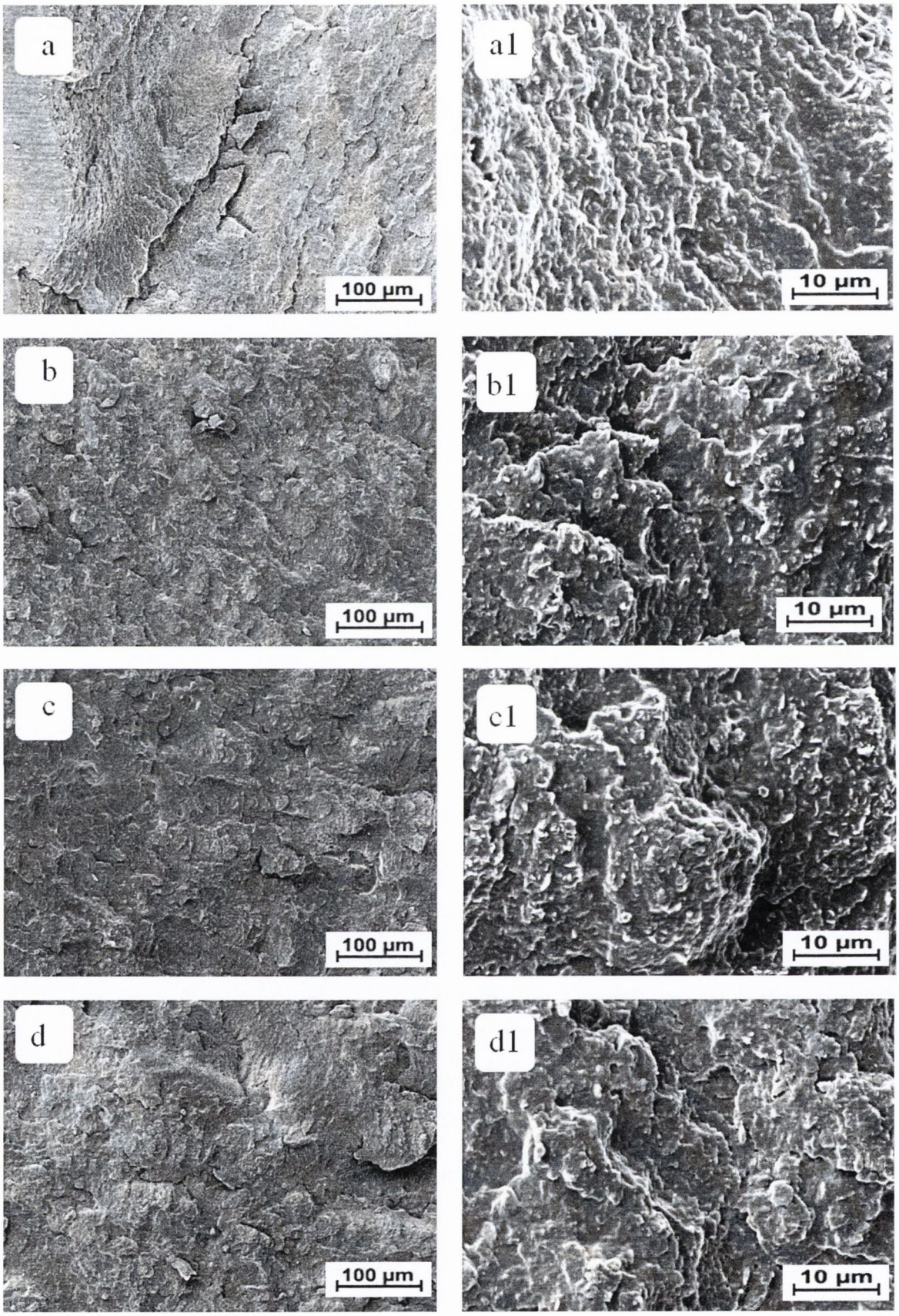

Figure 9.30. Scanning electron micrographs of the fracture surface of nylon/ADC-Clay nanocomposite in CT specimen transversally tested.

The nylon/Clay nanocomposite presented instant crack propagation behaviour (Figure 9.29a). In the early stages of crack propagation the polymer appeared to present very light "unfolding fan" resistance. This led to the breaking of the hydrogen bonds and the formation of a brittle surface (Figure 9.29b). As the specimen was subjected to the tensile test, a more brittle crack propagation surface was observed (Figure 9.29c). This surface was characterised by "rib marks" with line separating tilted planes indicating possible hesitations and deviations from the crack path, which is in agreement with the findings previously reported in literature.[451] As the crack continued to propagate a more brittle like surface was observed (Figure 9.29d). Higher magnification imaging revealed microvoids and a brittle like structure that maintained its aspect throughout the crack propagation surface (Figure 9.29a1-9.29d1).

The transversal deformation of nylon/ADC-Clay nanocomposite led to the formation of a brittle fracture surface. The crack initiation process occurred almost immediately (Figure 9.30a). As the crack grew a crack propagation surface with grooves and a slightly terraced aspect was observed (Figure 9.30b-9.30d). Higher magnification imaging revealed that the crack presented as a rough surface with sporadic small fibrils (Figure 9.30a1-9.30d1).

The brittle character exhibited by the nylon and nylon/clay nanocomposites in the SENB, and longitudinal and transversal CT was confirmed by the formation of superficial voids in the vein-type pattern observed during the fractography studies. This behaviour has been previously encountered by Yuan et al.[188] while studying the impact surface of HDPE/$CaCO_3$ nanocomposites. The presence of clay in the longitudinally tested compact tension specimens led to surfaces slightly similar to the corresponding SENB specimens. The formation of a vein-type pattern in nylon/MMT nanocomposite showed decreased density with the enhanced exfoliation degree. However, an almost equal balance between the intercalated and exfoliated nanostructures resulted in a highly fibrillar surface corresponding to the tearing of the polymer. In this case it can be hypothesised that the excellent dispersion of the clay platelets and clay tactoids obstructed the break by clay tactoid delamination and by creating a sieve effect. Unlike the longitudinal testing of the pristine nylon that resulted in a vein-type pattern, the transversal testing showed an unfolding fan resistance which developed in an almost brittle like fracture surface. With the addition of clay, brittle fracture surfaces were observed with very limited side grooves, regardless of the degree of exfoliation. As previously reported in literature,[136] the perpendicular orientation of the clay platelets facilitated the crack growth. Although the

same speed was used for the longitudinal and the transversal testing of the CT specimens, the orientation of the polymer lamellas and of the clay tactoids and clay platelets had a significant impact on the fracture surface. The testing of the CT specimens in the longitudinal direction showed a surface similar to tensile deformation, whilst the transversal testing presented a surface that resembled an impact tested surface.

The occurrence of the fibrils may indicate minimal plasticity and their reorientation can be a consequence of adiabatic heating, as suggested by Rittel[153] for glassy polymers. Thus, during the deformation process part of the mechanical work to which the samples are subjected becomes mechanical deformation whilst the rest is the heat dissipated during the process.

9.4. Conclusions

The toughness of pristine nylon and nylon/clay nanocomposites with different exfoliation degrees was investigated *via* tensile, impact and J-integral tests. These investigations were performed in order to test the hypothesis that an intercalated/exfoliated polymer/clay nanocomposite may present superior toughness than intercalated or exfoliated nanocomposites. Using injection moulded specimens, the effect of clay platelets orientation was also take into consideration. Since the study was performed on a semicrystalline polymer matrix, the lamellar orientation was also taken into account.

The energy at break and the impact strength of the intercalated/exfoliated nylon/Clay nanocomposite presented superior values compared nylon/ADC-Clay nanocomposite which showed enhanced exfoliation. Analysing the location of the primary crack initiation site in the impact tested specimens it was observed that the presence of clay created a vein-type pattern, suggesting that the clay may obstruct the initiation of the crack. In regard to the exfoliation degree, it was observed that an intercalated/exfoliated nanocomposite with nearly equal volume fractions of intercalated and exfoliated nanocomposite had the highest impact strength. The surface analysis of the crack propagation in the impact tested specimens showed that the mostly intercalated nylon/MMT nanocomposite presented a slightly spongious surface which suggested that more energy was absorbed in the area, while the increase in the exfoliation degree observed in nylon/Clay and nylon/ADC-Clay nanocomposites enhanced the number of stick-slip areas. This phenomenon indicated that a higher amount of energy had been adsorbed during the crack initiation and propagation.

Performing J-integral testing on SENB specimens it was observed that a higher exfoliation degree prevented the crack propagation process more efficiently by delaminating and increasing the surface that comes into contact with the polymer matrix. Thus, it was established that the testing speed represents a key factor in assessing the toughness of a polymer/clay nanocomposites.

During the low-speed deformation process the clay tactoids were subjected to splitting, opening and delamination phenomena. However, both clay tactoids and clay platelets showed mobility and led to a vein-type pattern in the mostly intercalated nylon/MMT nanocomposite, a sieve effect with terraced aspect in nylon/Clay nanocomposite and fibrils that changed their orientation in the highly exfoliated nylon/ADC-Clay nanocomposite. The fractography of the compact tensile specimens showed that in the presence of clay the longitudinally tested specimens presented a more tensile fracture surface, whilst the transversally tested specimens had smoother surfaces.

The comparison between the longitudinally and transversally CT specimens, revealed that the lamellar and clay platelets orientation are essential in analysing the toughness of systems. The power-law fit resistance curves for the neat polymer revealed the upper and lower limits for the crack initiation processes and the crack propagation. However, nylon/Clay nanocomposites presented upper and lower limits for the fracture process that were orientated opposite to the ones for the neat polymer. This attested to the ability of clay platelets to obstruct the crack propagation path.

From the tensile, impact and toughness tests, it was revealed that indeed, an intercalated/exfoliated polymer/clay nanocomposite has superior mechanical properties compared to a mostly intercalated or mostly exfoliated nanocomposite.

Chapter 10. Structure-property relationships of polymer blend/clay nanocomposites: compatibilised and noncompatibilised polystyrene/propylene/clay

10.1. Introduction

The interest in polymer blends is constantly increasing because they confer the manufacturers the opportunity to tailor the final properties of the materials. However, most polymer blends are classified as immiscible and the simple mixing of two polymers is likely to lead to an undesired material, characterised by weak interfacial adhesion and poor mechanical properties.[231] The process of compatibilising two immiscible polymers can be achieved by the addition of a third component or by an *in situ* chemical reaction between the two components,[453] the former being the easiest method that can be applied to obtain a compatibilised polymer blend. The role of the compatibiliser is to: reduce the interfacial tension of the two components, to stabilize the morphology of the blend and to improve the performance of the material. Typically the third component is of organic nature, e.g. copolymers.[454, 455] However, in the last few years the research into the possibility of using an inorganic material, e.g. clay, which is characterised by a large surface area[35] and high stiffness,[16] and is ubiquitous in nature and environmentally friendly, has been gaining wide interest.[231, 234, 237, 456, 457]

Previous research has shown that the addition of a compatibilising agent in a polypropylene-clay nanocomposite has to be kept under 10 wt.% for maleic anhydride grafted polypropylene in PP/PPgMA/organoclay (I.30T) nanocomposites, a higher maleated content resulting in changes in the properties or structure.[187] For polyethylene-clay nanocomposites, Yuan et al.[188] suggested that the maleic anhydride grafted polyethylene quantity had to be kept close to the quantity of filler used. By having equal amounts of compatibilising agent and nano-calcium carbonate (5 wt.%), the Young's modulus of PE increased by 25% and the elongation at break decreased by 30%, while by doubling the compatibilising agent content the elastic modulus increased additionally by only 4% and the elongation at break decreased by 85%. A similar observation was made by Kim et al.[189] who showed that the addition of equal quantities of PPgMA and organoclay (di-methyl, dihydrogenated tallow-montmorillonite) into a PP matrix gave rise to optimum mechanical and thermal properties.

Polystyrene and polypropylene are two widely used commodity polymers. By mixing them together an immiscible polymer blend, characterised by a semicrystalline phase and an amorphous one is formed.[236] Polymer blend/clay nanocomposites represent a new class of unique low density materials. The insertion of organoclay in polymer blends significantly changes the structure, typically decreasing the size of the dispersed phase.[234] The location and the degree of dispersion of clay influence the mechanical and thermal properties of polymer blend/clay nanocomposites.[458] For a polypropylene/polystyrene (PP/PS) blend (80:20), the addition of 4 wt.% organoclay (octadecyl trimethyl ammonium modified montmorillonite)[237] resulted in PS chains being intercalated inside the clay galleries. However, with the insertion of maleated polypropylene, Zhu et al.[237] observed *via* transmission electron microscopy that the clay completely migrated from the PS phase to the modified PP phase in which it was homogeneously dispersed. In a separate study,[231] TEM on a PP/PS (80:20) blend with 5 wt.% organoclay (Cloisite® 20A) revealed that the intercalated clay tactoids were located at the interface of the two components, which led to a slight increase in Young's modulus and a substantial increase in the elongation at break from 1.5 mm to 4.4 mm. By replacing the PP with PPgMA, Ray et al.[231] observed that in the PPgMA/PS (80:20) blend with 5 wt.% organoclay (Cloisite® 20A), the clay was exfoliated in the PPgMA matrix and surrounded the PS domains; this material presented a significant increase in Young's modulus and a substantial decrease in the elongation at break, compared to the neat polymer blend.

The past few years marked advances in understanding the morphology and the properties of the polymer blend/clay nanocomposites. However, there are still a number of questions that need to be answered in order to fully comprehend the impact of clay addition to a polymer blend. An issue of paramount importance is whether the clay acts as a compatibiliser in an immiscible polymer blend. If it does, where should the clay locate? Also, how to quantify the relationships between the mechanical properties and the amount of reinforcement added? What are the effects that the clay induces on the thermal and mechanical properties of an immiscible polymer blend with the amorphous phase as the major component? The aim of this project was to address these issues by using immiscible PS/PP blends that are often found in the recycled stock due to their wide range of applications in commodity products. In some cases, maleated PP was used as the organic compatibiliser in order to modify the morphology of the immiscible blend, hence providing comparisons to the noncompatibilised polymer blends.

10.2. Experimental section

10.2.1. Materials

Polypropylene (SABIC PP, Grade: 500P) from SABIC (Saudi Basic Industries Corporation), with a melt flow rate of 3 g·(10 min)$^{-1}$, and polystyrene (DOW STYRON, Grade: 634, general purpose) from DOW Plastics, with a melt flow rate of 3.5 g·(10 min)$^{-1}$, were purchased from Resinex (UK). Organoclay Nanomer® I44.P, a dimethyl dihydrogenated tallow ammonium chloride (2M2HTA) modified montmorillonite, from Nanocor Corporation was kindly supplied by Nordmann, Rassmann GmbH (Hamburg, Germany). This organoclay (Clay) had a particle size of 15-25 μm,[459] a density of 1605 kg·m^{-3}, determined using a Micromeritics AccuPyc 1330 pycnometer, and an organic content of 40%, established by performing a Loss on Ignition test, that is, heating the clay from room temperature to 600 °C at a rate of 10 °C·min^{-1} with a dwell of 600 s at 600 °C in a Eurotherm 2416CG furnace (Lenton Thermal Designs LTD). As a compatibilising agent polypropylene grafted with maleic anhydride (PPgMA) with 8-10 wt.% maleic anhydride composition, purchased from Sigma Aldrich, was used.

10.2.2. Preparation of polymer blend/clay nanocomposite batches and specimens

Melt blending of PS/PP (70:30, w/w) with 4 wt.% clay platelets and with or without 4 wt.% PPgMA was conducted by simultaneously mixing the components on a Prism twin screw extruder (UK) with 16 mm-diameter screws and a length to diameter ratio of 25. The operating temperatures of the extruder were maintained at 160, 170, 175, and 180 °C from hopper to die, while the screw speed was set at 200 rpm. After cooling in water, the extrudates were pelletized. In order to obtain the specimens for the tensile, flexural and impact testing, a bench-top injection moulder (Ray Ran model 2 Test Sample Injection Moulding Apparatus, UK) was used at a barrel temperature of 210 °C, a tool temperature of 55 °C and a pressure of 0.55 MPa.

10.2.3. Characterisation

X-ray Diffraction was carried out on a Phillips PW1720 X-Ray Diffractometer with a CuKα_1 (λ = 0.15406 nm) anode tube at the standard conditions of 40 kV and 20 mA. The

samples were tested from 2° to 10°, 2θ angle, at a step size of 0.02° and duration of 2.5 seconds per step. Powder samples were used.

TEM was performed on a TECNAI G2 20 twin electron microscope for PP/PPgMA/Clay, PS/PP/Clay and PS/PPgMA/PP/Clay and on a FEI Titan for PS/Clay nanocomposites. The first three specimens were ultrathin-sectioned using a Reichert-Jug 'Ultracut' ultra-microtome equipped with a diamond knife. The sections (~100 nm in thickness) were collected in a trough filled with water and placed on a 200 mesh copper grid. The PS/Clay sample was gold coated and cut into ~100 nm thick sections using a Zeiss Auriga Focused Ion Beam (FIB) with Cobra ion column. The transmission electron microscopes were run in bright field at 200 kV accelerating voltage.

Scanning Electron Microscopy imaging was performed on impact tested surfaces using a Zeiss Ultra Scanning Electron Microscope at a voltage of 5.0 kV. Prior to being analysed the samples were mounted on stubs and their surface was gold coated.

Polarized Light Microscopy (PLM) was carried out on an Olympus Microscope equipped with an Olympus DP 70 Lens. Samples were prepared by inserting small particles between two glass slides and pressing them at 180 °C for 35 minutes to yield thin films of thickness of approximately 6 μm.

Thermal Gravimetric Analysis measurements were performed on a Perkin Elmer Pyrus 1 TGA under nitrogen flow (20 $mL \cdot min^{-1}$), from 30 °C to 650 °C at a heating rate of 10 $°C \cdot min^{-1}$.

Differential Scanning Calorimetry was conducted on a Perkin Elmer Diamond DSC at a scan rate of 10 $°C \cdot min^{-1}$. The crystallinity of polymer blend/clay nanocomposites (χ_c) was calculated, using Equation 4.1 [251, 327] and considering the melting enthalpy of the sample from the second heat scan in order to eliminate the effects of the heating history. The melting enthalpy of 100% crystalline PP was taken from literature[460] as 146.5 $J \cdot g^{-1}$.

Tensile and four-point flexural tests were carried out on an INSTRON 1011 universal testing machine according to ISO 527:1993 and ASTM D 6272-02, respectively. The tensile tests were performed at a test speed of 1 $mm \cdot min^{-1}$ and using a load of 1 kN. Six dog bone specimens (Type 1BA) were tested for each of the materials. The four-point flexural tests were carried out at a test speed of 2 $mm \cdot min^{-1}$ and using a load of 1 kN, a load span of 15 mm and a support span of 30.5 mm. Six specimens (80 mm x 10 mm x 4 mm, length x width x thickness) of each material, i.e., PP, PP/PPgMA, PS, PP/PS, PP/PPgMA/PS, PP/Clay, PP/PPgMA/Clay PS/Clay, PP/PS/Clay or PP/PPgMA/PS/Clay, were tested. The software used was Labview 'Aquire and Log', which ran at a 20 Hz scan

rate. Impact tests were performed according to standard ISO 179:1997 at room temperature on a Charpy impact tester (JinJian XJJD-5), at a speed of 2.9 $m \cdot s^{-1}$ and using a hammer of 0.5 J. Six specimens (80 mm x 10 mm x 4 mm, length x width x thickness) were tested for each batch of materials. Prior to being tested the impact specimens were notched with a type A notch, using a 45° cutter and a milling machine. The mean and standard deviation values reported for the mechanical tests represent a confidence level of 95%. Statistical significance was assessed by a Two-tailed, Type II 't' test with a criterion that the probability of a difference in means due to chance is less than 0.05.

10.3. Results and discussion

10.3.1. Structure

As can be observed from the XRD diagrams presented in Figure 10.1 the organoclay (Curve 1) exhibited an intensive diffraction peak at a 2θ value of 3.3°, corresponding to a basal spacing, $d_{(001)}$, of 2.7 nm. When 4 wt.% clay platelets were dispersed into PP (Curve 2) the peak shifted towards a slightly higher 2θ value which suggested that in this case some impurities or surfactants might have been removed from the galleries of the clay during processing and a conventional composite was formed. In contrast, the addition of 4 wt.% clay platelets into PS (Curve 4) shifted the peak towards a lower 2θ value (~2.9°) increasing the basal spacing to 3 nm and indicating that intercalated structures were presented in the nanocomposite. These results suggested that the organoclay had a higher affinity for PS than for PP. With the incorporation of the organic compatibiliser (i.e., PPgMA) into PP, the *(001)* peak of clay (Curve 3) became significantly wider. This indicated the formation of a nanocomposite with an exfoliation degree greater than that of PS/Clay, which was confirmed from the TEM images below.

The XRD peak for PS/PP/Clay (Curve 5) appeared to locate at the same 2θ position and presented a similar peak width at the half peak height compared to those in the case of PS/Clay. This suggested that the clay was located in the PS phase in the immiscible PS/PP blend and formed an intercalated nanocomposite with the PS. The PS/PPgMA/PP/Clay (Curve 6) exhibited a *(001)* peak with the $d_{(001)}$ similar to that of both PS/Clay and PP/PPgMA/Clay, and with the peak width situated in between those of the nanocomposites (Curves 3 and 4), which might suggest a hybrid of both nanocomposites. Thus, clay was postulated to locate in both the PS and the PP phases when the compatibiliser was present.

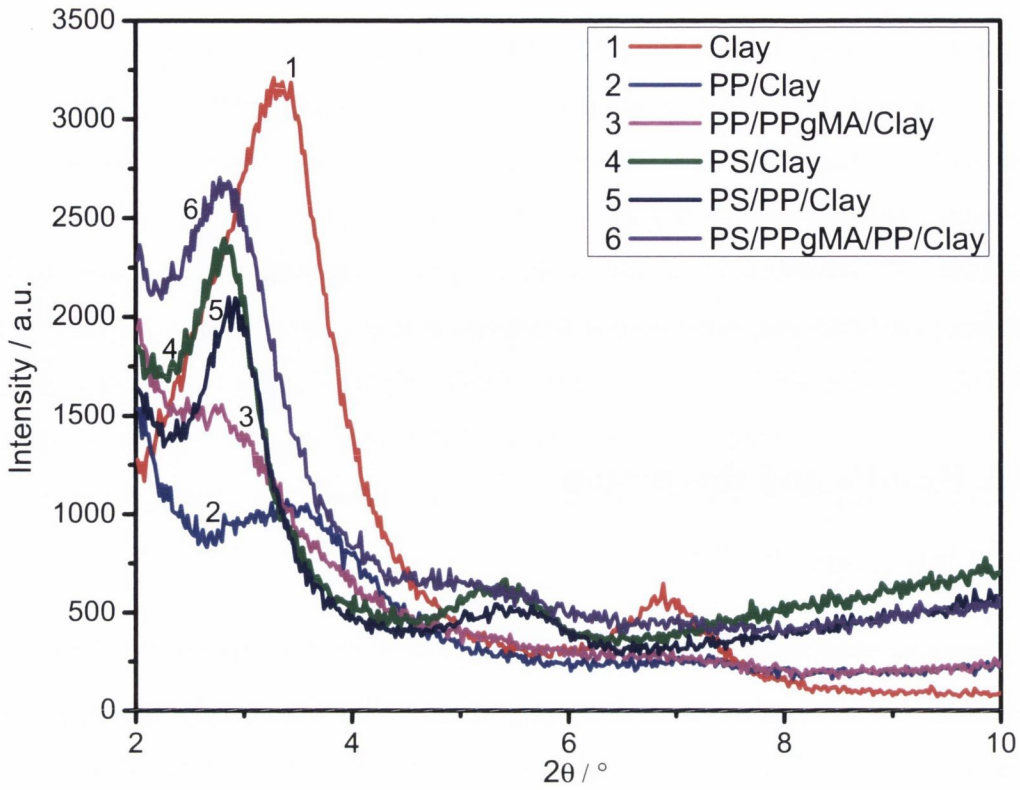

Figure 10.1. XRD profiles of organoclay and polymer/clay and polymer blend/clay composites.

The intercalated structures detected *via* XRD for PS/Clay nanocomposites were confirmed by TEM (Figure 10.2A) which showed that the number of clay platelets per stack ranged from 2 to 9 with an average of 3.0 (estimated from over 25 nanostructures observed in representative images). The existence of intercalated/exfoliated structures in PP/PPgMA/Clay was also ratified by TEM (Figure 10.2B). Twenty-five percent of the clay platelets demonstrated full exfoliation as single platelets in the matrix whereas the remaining 75% existed as intercalated tactoids with 2 - 5 clay layers per stack and an average of 2.3 layers per stack (estimated from over 35 nanostructures).

The PS/PP/Clay (Figure 10.2C) and PS/PPgMA/PP/Clay (Figure 10.2D) nanocomposites were characterised by mostly intercalated structures. In the former, the clay morphology appeared to be similar to that in the PS/Clay and presented as intercalated tactoids with an average number of 3.4 platelets per stack (estimated from over 10 nanostructures). This gave further evidence that clay was located in the PS phase. A similar observation was found previously in the literature work[237] for PS/PP with a different ratio,

i.e., PS/PP (20/80). The addition of the maleated copolymer led to a better dispersion of the clay platelets inside the polymer blend and to the reduction of the average number of clay platelets per stack to 2.6 (estimated from close to 20 nanostructures observed in over five representative images). A close observation of Figure 10.2D resulted in the finding that the compatibilised polymer blend/clay nanocomposite consisted of two types of structures, one similar to that of the PS/Clay nanocomposite with an intercalated structure and the other similar to that of the PP/PPgMA/Clay nanocomposite with fewer clay layers per stack including single layers. This validated the hypothesis from the XRD results that this material is in fact a hybrid of PP/PPgMA/Clay and PS/Clay.

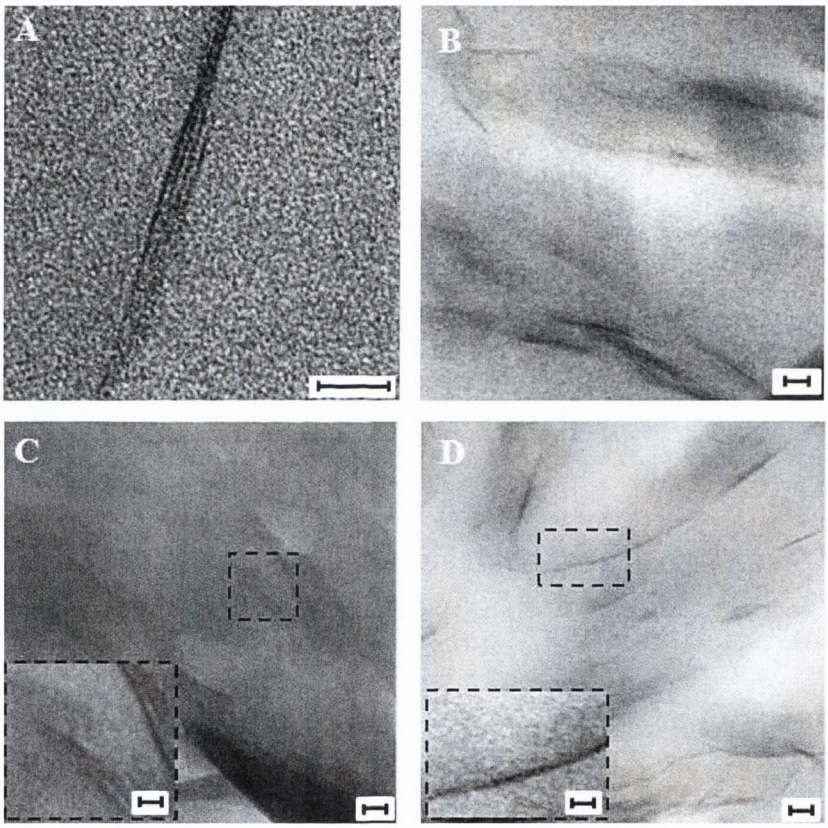

Figure 10.2. TEM images of: A) PS/Clay, B) PP/PPgMA/Clay, C) PS/PP/Clay and D) PS/PPgMA/PP/Clay (Scale bars for the main figures: 50 nm; and for the insets: 20 nm).

The typical morphologies of blends observed *via* SEM for impact fractured surfaces are presented in Figure 10.3. When PP was mixed with PS, the neat polymer blend (Figure 10.3A) was characterised by phase separation due to the high immiscibility and the large molecular weights[461] of the two components. The use of a compatibilising agent changed the interfacial energy[234, 462] between the polymers and led to a domain shift (Figure 10.3B).

The addition of clay caused a statistically significant decrease in mean domain size from 6.5 μm to 1.0 μm (measured from over 50 droplets) in the noncompatibilised blend making the semicrystalline and amorphous phases less identifiable (Figure 10.3C vs. Figure 10.3A).

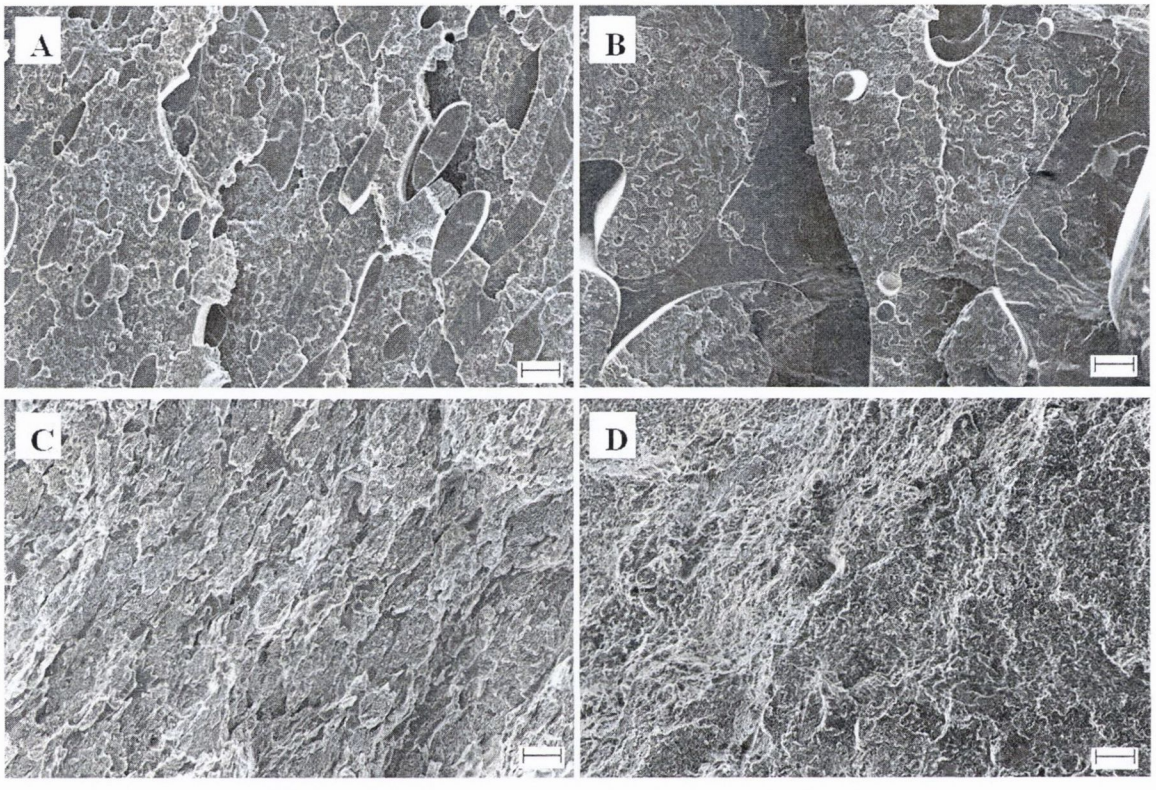

Figure 10.3. SEM images of polymer blends: A) PS/PP and B) PS/PPgMA/PP and polymer blend/clay nanocomposites: C) PS/PP/Clay and D) PS/PPgMA/PP/Clay (Scale bar: 10 μm).

When the organoclay was added to PS/PP it distributed solely inside the PS matrix due to the higher affinity that the clay exhibits for PS. The presence of intercalated PS/Clay tactoids led to an increase in the viscosity of the blend that influenced the deformability and the breakup of the droplets, as well as a barrier effect preventing coalescence.[231] Both effects accounted for the reduction in the domain size for the noncompatibilised PS/PP blend. The presence of the compatibilising agent in the PS/PP/Clay nanocomposite resulted in the formation of a nearly homogenous fracture surface, with the size of the droplets decreasing to 0.6 μm (measured from over 50 droplets) (Figure 10.3D). The further reduction in the droplet size could suggest the occurrence of an additional effect, i.e., compatibilisation, inside the PS/PPgMA/PP/Clay. The compatibilising effect of the clay

might be due to the intercalation of both PS and PP/PPgMA in the same clay gallery which generated a block copolymer effect.[231, 236] As a result, the clay platelets appeared to be distributed in both phases of the polymer blend as well as at their interfaces, as seen in the TEM image (Figure 10.2D). The clay located at the interface generated Marangoni forces and steric interactions which also prevented coalescence of the polymer droplets.[462]

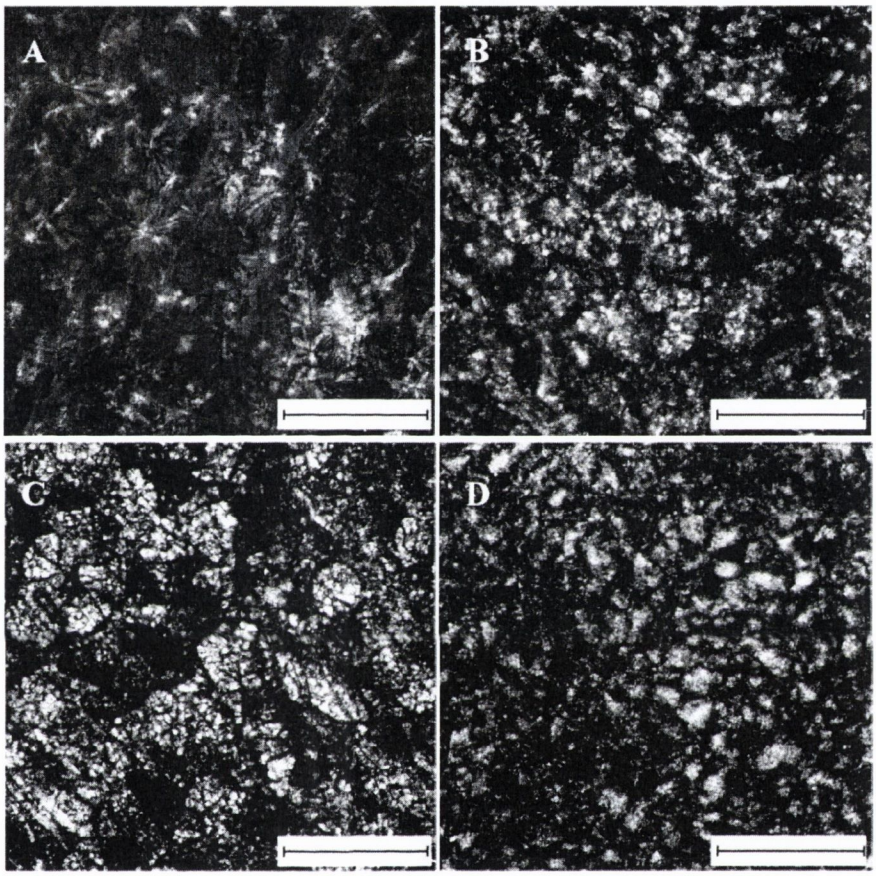

Figure 10.4. Polarized Light Microscopy images for polymer blends: A) PS/PP and B) PS/PPgMA/PP and polymer blend/clay nanocomposites: C) PS/PP/Clay and D) PS/PPgMA/PP/Clay (Scale bar: 200 μm).

Representative polarized light micrographs of the materials are given in Figure 10.4. The presence of the maleated polypropylene produced a decrease in the spherulite size from 55 μm to 33 μm (measured from at least 10 spherulites). This led to better dispersion of the semicrystalline polymer into the amorphous phase (Figure 10.4B vs. Figure 10.4A). Compared to pristine PS/PP blend the addition of clay induced a 62% reduction in the spherulite size (Figure 10.4C vs. Figure 10.4A). Yet, the presence of the clay and the maleated component decreased the spherulite size by 80% (Figure 10.4D); this polymer

blend displayed the best distribution of the semicrystalline component in the amorphous matrix. The reduction in the spherulite size with the addition of clay has been previously observed by Deshmane et al.[191] The phenomenon was attributed to the higher nucleation density that the clay induced[139] due to heterogeneous nucleation.[463]

10.3.2. Crystallinity and thermal properties

The results from DSC analysis, i.e., the glass transition temperature (T_g - measured at the mid-point of the initial slope of the heating curve),[464] the melting temperature (T_m - temperature at which the peak in the heating curve was recorded), the crystallisation temperature (T_c - determined as the peak on the cooling curve) and the degree of crystallinity (χ_c) are summarized in Table 10.1. From the second heating curve displayed in Figure 10.5A, it can be observed that the presence of clay and/or maleated compatibiliser in the polymer blend did not alter the glass transition temperature (Table 10.1, Column 1) or the melting temperature (Table 10.1, Column 3) of the materials. This is similar to the work of Zhang et al.[465] who reported insignificant changes in the glass transition temperature and the melting temperature of neat PP/PS (70/30) blends with SiO_2 nanoparticles.

From the cooling curves presented in Figure 10.5B it can be noticed that the crystallisation exotherms appeared in the 113-117 °C range (Table 10.1, Column 2) and that the crystallisation temperature (T_c) only marginally decreased with the addition of the maleated polypropylene. The cooling curves exhibited a second crystallisation exotherm at 75 °C (Figure 10.5B) which became slightly more pronounced with the addition of the compatibilising agent, due to enhanced polypropylene content. The occurrence of a second exotherm in this immiscible polymer blend has been previously reported by Santana and Muller[466] who attributed it to the good dispersion of PP inside the PS matrix which induced homogeneous nucleation. When 4 wt.% organoclay was added to the blends the second crystallisation peaks decreased their intensities due to heterogeneous nucleation.

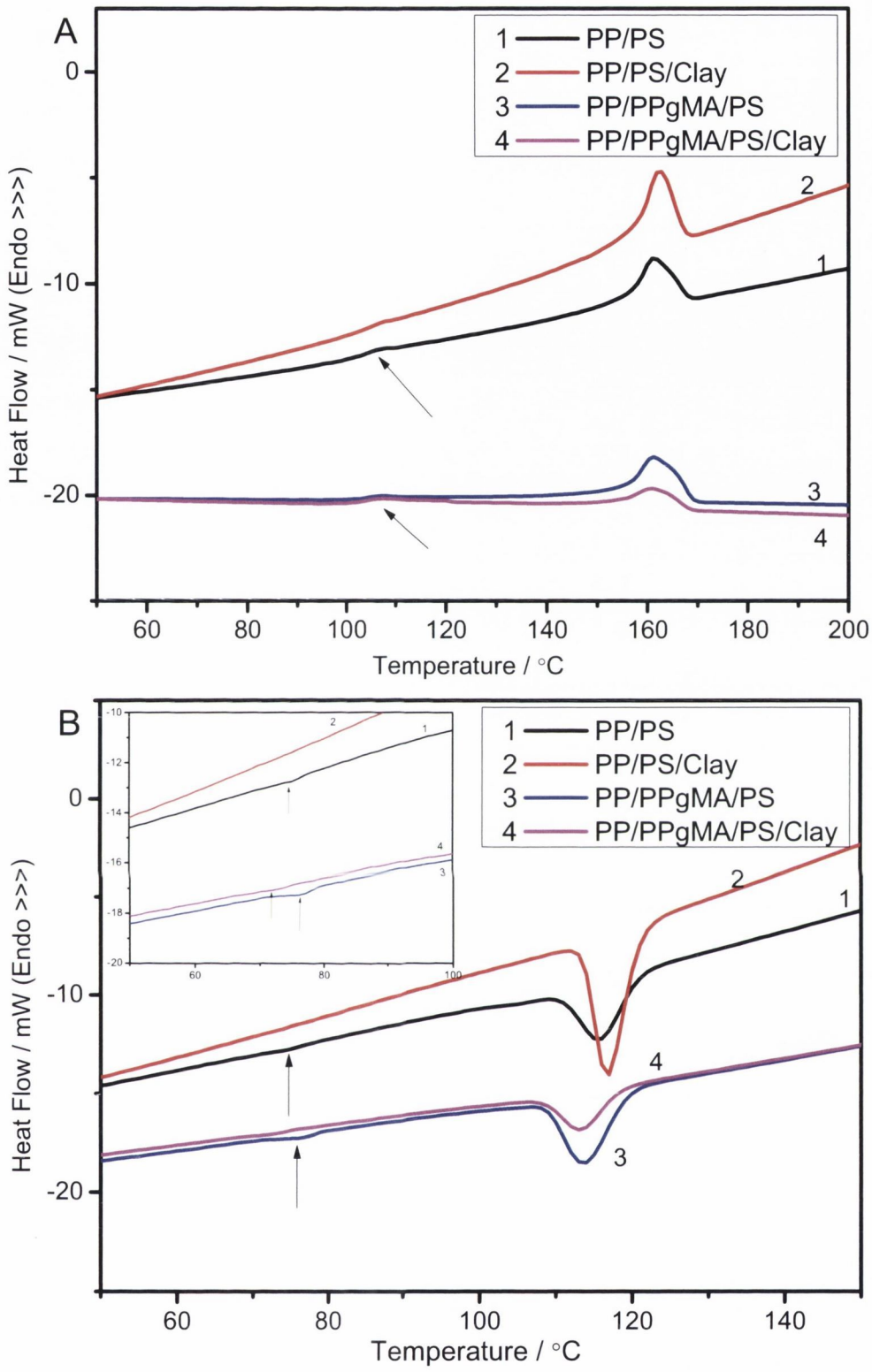

Figure 10.5. DSC second heating (A) and cooling (B) scans of polymer blend and polymer blend/clay nanocomposites.

Compatibilising the neat polymer blend with PPgMA resulted in augmentation of the crystallinity (Table 10.1, Column 4) due to the higher amount of PP inside the material.

The dispersion of clay inside the compatibilised or noncompatibilised polymer blend induces two opposing effects: nucleation and chain stiffening. The overexposure of the former over the later resulted in enhanced crystallisation, whereas a more prominent chain stiffening effect reflected in a reduction in the crystallinity degree.[467] Thus, the presence of clay in the PS/PP blend generated an increase in the crystallinity of the noncompatibilised polymer blend/clay nanocomposites from 41.5% to 68.5%. This suggested that the clay facilitated the nucleation process, whilst reducing the domain size as observed from the SEM and PLM images (Figures 10.3 and 10.4). When the clay was dispersed inside the PP/PPgMA and the PS matrices, as it was in the case of the compatibilised polymer blend, the crystallinity decreased from 59.1% to 28.4%. The reduction in crystallinity could be accounted for by the increased chain stiffness due to the strong interactions between PP/PPgMA and clay which suppressed the nucleating effect of the clay.

Table 10.1. Thermal properties of polymer blends

Sample	T_g / °C	T_c / °C	T_m / °C	χ_c / %	T^d_{peak} / °C	
					1st step	2nd step
PS/PP	102	115	161	41.5	411	456
PS/PP/Clay	102	117	162	68.5	438	447
PS/PPgMA/PP	103	114	162	59.1	429	464
PS/PPgMA/PP/Clay	103	113	161	28.4	451	-

The thermal degradation of the different systems was analysed, and the TGA and derivative thermogravimetric (DTG) curves are depicted in Figure 10.6. The thermal degradation of pristine and compatibilised polymer blends presented two clear degradation steps, summarised in Table 10.1, Columns 5 and 6. The first degradation step occurred at 411 °C for PS/PP and at 429 °C for the maleated blend, being characteristic of PS degradation (i.e., 424 °C). The second degradation step developed at 456 °C and 464 °C for neat PS/PP blend and maleated polymer blend, corresponding to the degradation of PP (i.e., 461 °C). The addition of clay into the neat polymer blend combined both degradation peaks into a sharp intensive peak at 438 °C with a shoulder at 447 °C (Figure 10.6B, Curve 2). These could be associated with the increase in the peak degradation temperature recorded on the derivative thermogravimetric curve (T^d_{peak}) of PS due to the strong bonding

with clay. In contrast, the sharp degradation peak shifted to a higher temperature (i.e., 451 °C) when the maleated PP was present because of the additional strong interactions between PP/PPgMA and clay and the slightly higher amount of PP (Figure 10.6B, Curve 4). Furthermore, the shoulder, attributed to the second degradation, almost disappeared, implying that the clay might have acted as a compatibiliser in this case, in accordance with the SEM and PLM observations.

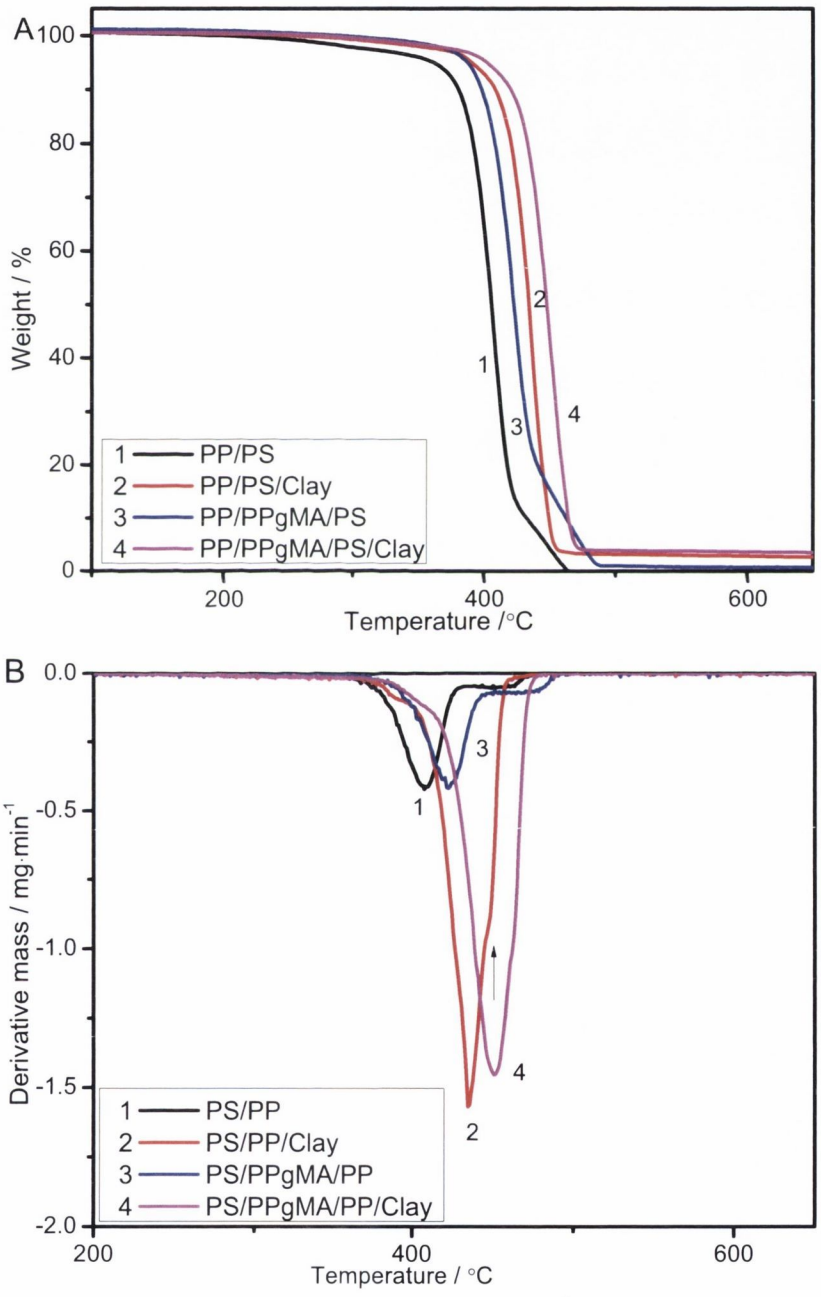

Figure 10.6. A) TGA and B) DTG curves of polymer blend/clay and maleated polymer blend/clay nanocomposites. The arrow points to the shoulder that corresponds to the second degradation.

10.3.3. Mechanical properties

The tensile and flexural modulus of PS/PP and compatibilised polymer blends with and without clay are represented in Figure 10.7. The addition of clay increased the tensile moduli by 20% for PS/PP and by 17% for PS/PPgMA/PP, while the flexural moduli were enhanced by 18% and 28%, all with statistical significance. Comparing PS/PP with the maleated polymer blend/clay nanocomposite, it was observed that the tensile and flexural moduli increased with statistical significance by 23% and by 19%, attesting to the uniform dispersion of the stiff clay.

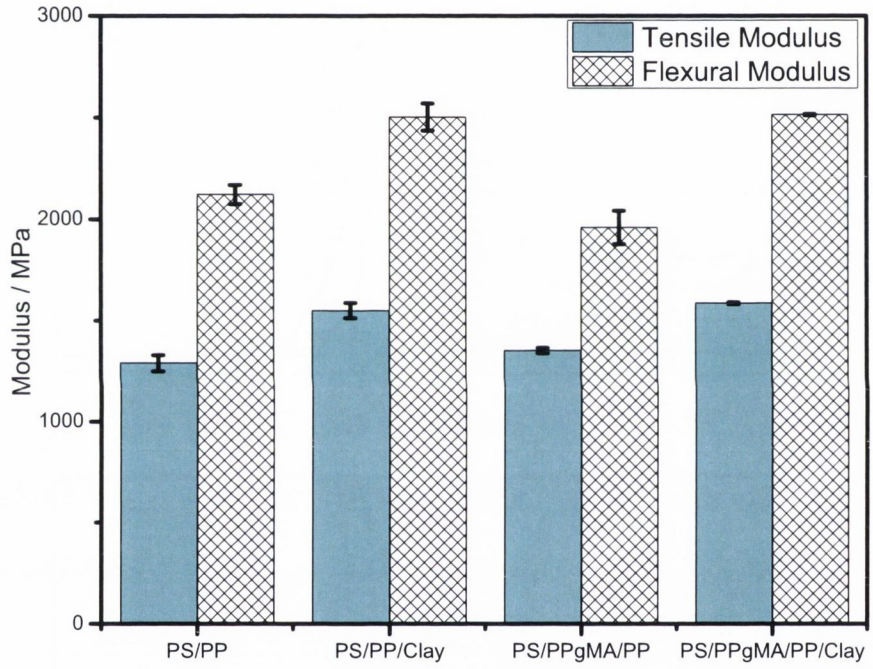

Figure 10.7. Tensile and flexural moduli of polymer blend and polymer blend/clay nanocomposites (The bars represent averages of six measurements; the error bars represent ± one standard deviation).

Figure 10.8 shows the impact strengths of the polymer blends with and without the compatibiliser and the clay. The impact strength of the polymer blend/clay nanocomposite diminished compared to that of the pristine polymer blend. Such reduction was attributed to the presence of the clay platelets which influenced the toughness directly, by the exclusive dispersion of the clay tactoids in the PS, and indirectly, by inducing a heterogeneous nucleation that led to a higher crystallinity. In contrast, the addition of clay

into the maleated polymer blend resulted in a 52% increase in the toughness of the material. This is in good agreement with the rougher fracture surface observed *via* SEM (Figure 10.3D versus Figure 10.3B) and with the droplet size decrement.

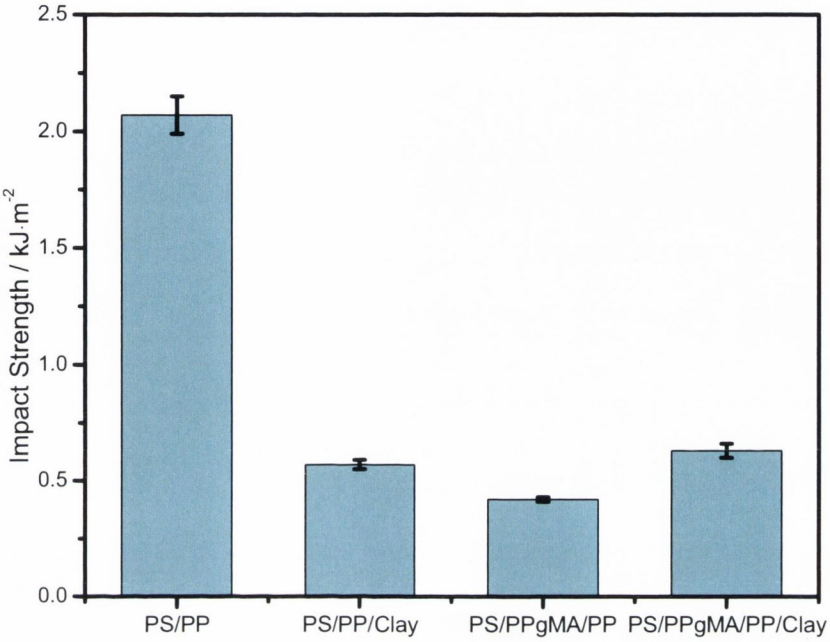

Figure 10.8. Impact strength of polymer blend and polymer blend/clay nanocomposites (The bars represent averages of six measurements; the error bars represent ± one standard deviation).

The higher toughness accomplished agreed with the previous observation that the clay platelets were well dispersed in both polymers and with the decreased crystallinity determined *via* DSC (Table 10.1, Column 4).[468] The improvement in toughness displayed by the maleated polymer blend nanocomposite inferred that the clay executed dual roles: reinforcing agent and compatibiliser. The toughness enhancement in the PS/PPgMA/PP with 4 wt.% organoclay, is different from the previously reported results[234] for a PP/PS (30:70, w/w) with PPgMA:clay = 1 (MA content 1 wt.%) and 3 wt.% organoclay (Cloisite® 20A), where the clay was located at the interface and a 65% decrease in the impact strength was observed. So, it seems appropriate to conclude that in order for clay to act as a compatibiliser it has to locate in both polymer phases, which is in agreement with the previous study by Wang et al.[236]

10.3.4. Quantitative analysis of the elastic moduli of polymer blend/clay nanocomposites

The area of polymer blend/clay nanocomposites has been extensively studied; however, thus far the elastic moduli of immiscible polymer blend/clay nanocomposites have yet to be quantitatively analysed in terms of the clay content and location. This section will discuss the elastic moduli of noncompatibilised PS/PP/Clay and compatibilised PS/PPgMA/PP/Clay nanocomposites. As found from XRD and TEM results, the PS/PP/Clay nanocomposite consisted of intercalated PS/Clay nanocomposite and PP, while the PS/PPgMA/PP/Clay nanocomposite presented a hybrid structure being made up of intercalated PS/Clay nanocomposite and intercalated/exfoliated PP/PPgMA/Clay nanocomposite. Both nanocomposites are depicted in Figure 10.9.

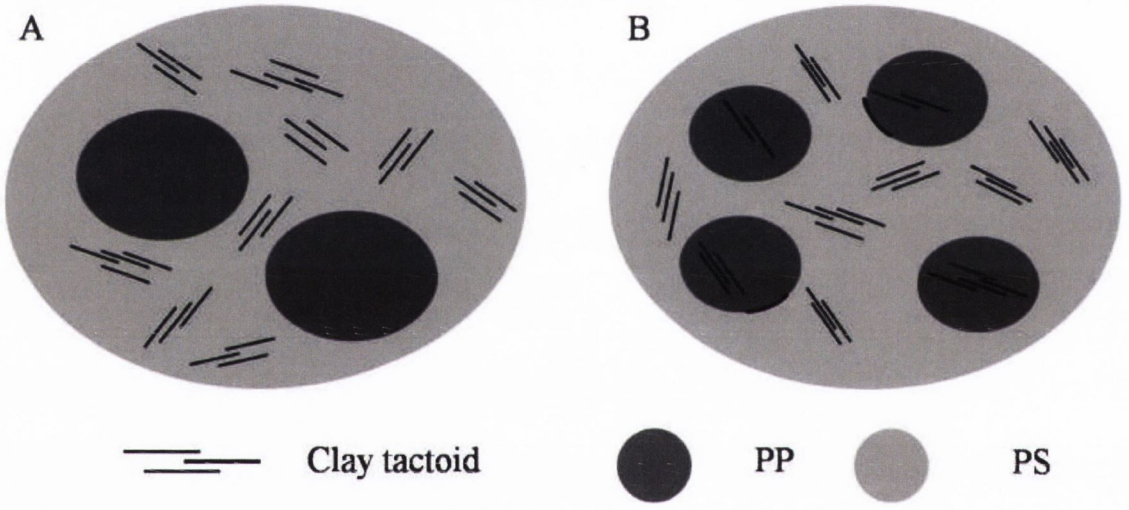

Figure 10.9. Location of reinforcement in (A) PS/PP/Clay and (B) PS/PPgMA/PP/Clay nanocomposite.

As illustrated in Figure 10.9A, the PS/PP/Clay nanocomposite can be considered as a composite material in which the PP represents the dispersed phase and PS/Clay nanocomposite the continuous phase that is further made up of a matrix (i.e., PS) and reinforcement. The reinforcement in the PS/Clay nanocomposite was represented by the intercalated clay tactoids consisting of clay platelets with the surfactant and PS molecules occupying part of the interlayer spacing. In order to calculate the elastic modulus of the reinforcement, the intercalated tactoids were considered as a sandwich-type composite in which the surfactant and PS molecules presented as a porous structure and the density and modulus of the surfactant were assumed to be the same as for PS due to the small amount

of surfactant in relation to the entire blend/clay nanocomposite. The Gibson-Ashby model for open cells (Equation 2.9)[175] was used for calculation of the modulus of the interlayer porous material. For PS, a modulus of 3066 MPa determined from flexural testing and a solid density of 1050 $kg \cdot m^{-3}$ [394] were considered. The foam density was calculated from Equation 2.10. Following the steps described in section 2.5.3.1.2. and using a Poisson's ratio 0.33 [394] for PS, the modulus of reinforcement (i.e., intercalated clay tactoids) was calculated as 94 GPa. The effective volume fraction of the reinforcement in the PS/Clay nanocomposite was determined according to Equation 2.15 [122] to be 0.07.

By inserting the above parameters into composite theories, the modulus for the PS/Clay nanocomposite was calculated as 4110 MPa using the Mori-Tanaka model for platelet-reinforced composites,[176, 177] and 4058 MPa using the Halpin-Tsai model[178, 469] for platelet-reinforced composites with the van Es correction.[15, 470] The experimental value of flexural modulus for the PS/Clay nanocomposite with 4 wt.% clay platelets was found to be 3615 MPa. Because in the PS/PP/Clay nanocomposite the clay was located entirely in the PS matrix which constituted 70% of PS/PP or 67% of PS/PP/Clay, the content of clay platelets in the PS phase was determined as 5.6 wt.%. Thus, the modulus for the PS/Clay nanocomposite in the PS/PP/Clay should be higher than 3615 MPa. The two theoretical values appeared to be very close and reasonable, both being higher than 3615 MPa. The value calculated from the Mori-Tanaka model for platelet-reinforced composites,[176, 177] i.e., 4110 MPa, was therefore used for subsequent calculation of the theoretical modulus of the PS/PP/Clay nanocomposite.

Since in the PS/PP/Clay nanocomposite the PS/Clay nanocomposite represented the continuous phase and PP represented the discontinuous phase, the theoretical modulus was estimated according to the Mori-Tanaka model[176, 177] and the Christensen model[362] for spherical inclusions. The elastic modulus for the dispersed phase, PP, was determined from flexural testing as 1410 MPa. Based on the Mori-Tanaka model,[176, 177] the modulus of the PS/PP/Clay nanocomposite was calculated as 2960 MPa. Considering a Poisson's ratio of 0.36 [393] of the dispersed phase, the modulus of the blend/clay nanocomposite was calculated from the Christensen model[362] as 2819 MPa. The theoretical values for the elastic modulus of the PS/PP/Clay nanocomposite are depicted in Figure 10.10 for comparison with the experimental datum.

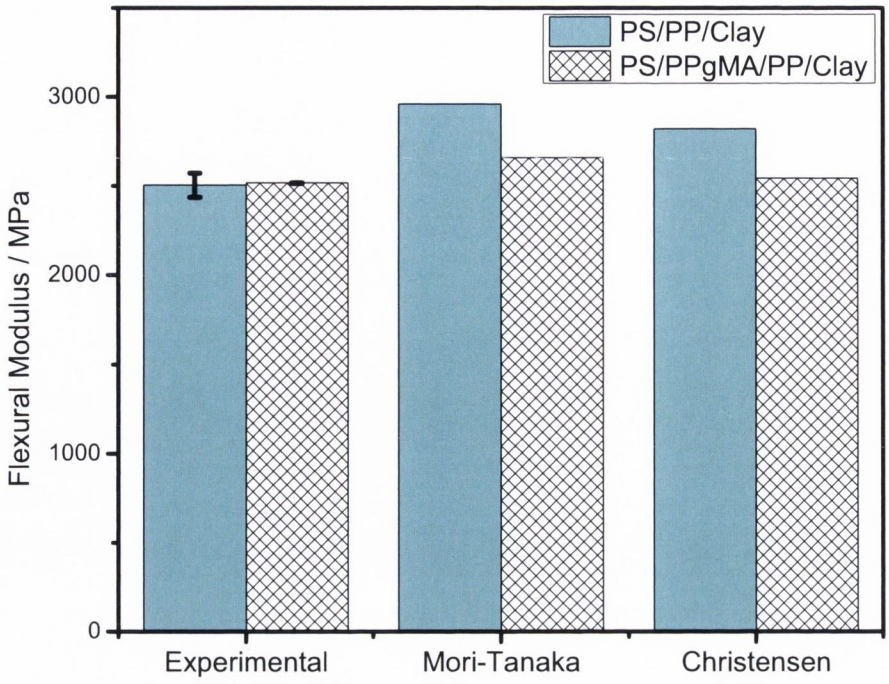

Figure 10.10. Experimental and theoretical flexural moduli of PS/PP/Clay and PS/PPgMA/PP/Clay nanocomposites.

As previously mentioned, the PS/PPgMA/PP/Clay nanocomposite can be considered as a hybrid structure in which PP/PPgMA/Clay nanocomposite represents the dispersed phase and PS/Clay nanocomposite the continuous phase (Figure 10.9B). Due to the presence of the compatibilising agent, the clay was assumed to be evenly distributed in both phases, i.e., 4 wt.% clay platelets. The flexural moduli of the PS/Clay and PP/PPgMA/Clay nanocomposites containing 4 wt.% clay platelets each were determined experimentally to be 3615 MPa and 1460 MPa respectively. Again, using the Mori-Tanaka model[176, 177] and the Christensen model[362] for spherical inclusions the theoretical moduli for PS/PPgMA/PP/Clay nanocomposite were calculated as 2657 MPa and 2543 MPa, respectively, which are presented in Figure 10.10 along with the experimental datum.

As can be observed from Figure 10.10, the elastic moduli for noncompatibilised and compatibilised polymer blend/clay nanocomposites determined *via* both models gave reasonable predictions of the experimental data. The Mori-Tanaka model[176, 177] presented an accuracy of 82% for the PS/PP/Clay nanocomposite and 94% for the PS/PPgMA/PP/Clay nanocomposite, while the Christensen's model[362] yielded slightly better predictions with accuracies of 88% and 99% for the two nanocomposites respectively. The good correlations between the theoretical values and experimental data suggested that the classical composite models can be utilised to interpret the elastic

modulus-volume fraction relationships of both compatibilised and noncompatibilised polymer blend/clay nanocomposites provided each phase of the materials is correctly considered.

10.4. Conclusions

The structure and properties of the compatibilised and noncompatibilised polymer blend (PS/PP)/clay nanocomposites, manufactured *via* melt processing, were evaluated and their relationships were investigated in detail both qualitatively and quantitatively. The presence of the compatibilising agent (PPgMA) had a profound influence on the location of clay in the immiscible polymer blend, which was subsequently reflected on the structure and thermal and mechanical properties of the materials. From the XRD and TEM results it was postulated that in the noncompatibilised polymer blend the clay was solely dispersed in PS, whilst in the compatibilised polymer blend the clay was located in both polymers due to the compatibilisation effect of PPgMA on the PP and clay.

The incorporation of clay significantly reduced the domain size of the dispersed phase in the polymer blends in both compatibilised and noncompatibilised blends, as characterised by SEM and PLM, presumably due to increased viscosity and suppressed coalescence for both blends and an additional compatibilisation effect for the compatibilised blend. The crystallinity of PP was found to be influenced by the location of clay. Thus, the crystallinity increased from 41.5% to 68.5% when the clay was distributed exclusively inside the PS, whilst, when the clay inhabited both phases, it induced a chain stiffening effect. This effect suppressed the ability of clay to induce a nucleation effect and reduced the crystallinity from 59.1% to 28.4%. The thermal degradation temperatures of PS and PP were almost merged in the presence of clay due to the strong interactions of PS in the noncompatibilised blend and also to the compatibilisation effect of clay in the compatibilised blend.

The mechanical testing results showed that the addition of clay into the compatibilised and noncompatibilised polymer blends enhanced the tensile and flexural moduli by up to 20% and 28%, respectively. Compared to the noncompatibilised neat polymer blend, the inclusion of the maleated copolymer and organoclay resulted in a 23% increase in the tensile modulus and a 19% enhancement in the flexural modulus. The addition of clay to the maleated polymer blend increased the impact strength of the material by 52%. These enhancements attest to the ability of clay to attain two significant

functions, reinforcement and compatibilisation, confirming the previous hypothesis on the compatibilisation effect.

The elastic moduli of the compatibilised and noncompatibilised polymer blend/clay nanocomposites were quantitatively analysed by considering the morphology and location of the reinforcement and the material of the dispersed phase in the blends and by using the classical composite theories. Both the Mori-Tanaka model and Christensen's model gave good predictions of the experimental values suggesting they can be used for design of the polymer blend/clay nanocomposites.

Chapter 11. Effect of clay on thermal and mechanical properties of recycled plastics

11.1. Introduction

Plastic materials are a constant part of our lives, with the polymer industry reaching new zeniths every day. The polymer industry began its development in the 19th century and it was not until the 1930s that the exponential development of plastic production commenced.[471] Less than 100 years after polymers such as polyethylene and polystyrene were discovered and the first thermoplastics were extruded[471] the polymer production culminated reaching 260 Mt per year in 2007.[272]

Today, most of the plastic production is represented by commodity polymers, e.g. polyethylene, polypropylene, polystyrene, poly(vinyl chloride), and engineering plastics, e.g. polycarbonate, polyamide, poly(ethylene terephthalate). Since these polymers are considered high-volume plastics, the waste resulted from them needs to be prevented, minimised, reused, recovered by mechanical or feedstock recycling.[274]

Lately the environmental community has focussed on the reuse, recycle and recovery of waste from electrical and electric equipment; this is represented by engineering plastics that are characterised by superior mechanical and thermal properties.[319, 472, 473] However, 38% of the world plastic production is represented by the packaging industry and only 7% by the electric and electronic industry.[272] Thus, it is imperative to reintroduce the waste from the packaging industry back on the market.

During the life cycle of a plastic material and depending on the environment in which the material is used, the polymer may undergo thermo- and/or photo-oxidative degradation, leading to irreversible changes on molecular and morphological levels.[276, 474] These changes on the structure of the polymer are typically amplified when material recovery is performed. Mechanical recycling is a suitable method of recovering polymeric materials from the recycled plastic stock,[274] due to the limited amount of energy needed to process these materials compared to the amount of energy used to manufacture new pristine polymers.[475] However, the mechanically recycled polymers are typically characterised by inferior mechanical properties, compared to the same properties displayed by the pristine material.[276] During the recovery process, the polymers tend to deteriorate by thermo-mechanical degradation.[274] This typically involves the degradation and scission of molecular chains due to shear forces applied during grinding and processing and a thermo-

oxidative degradation that occurs when the polymer, at high temperatures, is exposed to oxygen.[476] Over the years, a myriad of materials (such as: stabilisers, compatibilisers, particles and nanoparticles) have been used in order to diminish the impact of thermo-oxidative and mechano-oxidative phenomena experienced by the plastic materials.[274, 477]

The thermo- and mechanical-oxidative degradation of polymer chains and the possible presence of unwanted chemical substances make imperative the use of additives that are able to minimise the impact of these undesirable products. The well-known ability of clay to adsorb and absorb chemical substances and the beneficial improvement of thermal, mechanical and barrier properties with the dispersion of small amounts of clay in pristine polymers and polymer blends make clay an ideal candidate to aid in the recovery of plastic materials.[2, 26, 27, 66, 478, 479]

Clay is ubiquitous in nature, has the ability to absorb harmful substances that might be present in the recycled stock and each clay platelet is characterised by superior stiffness compared to any polymer matrix.[122] The effects of adding natural clay (i.e., Cloisite® Na) or organoclay (i.e., Cloisite® 25A) in recycled PET have been structurally and mechanically evaluated for different clay loads.[480] It was observed that the dispersion of organoclay resulted in intercalated clay nanostructures, whilst natural clay presented mostly as aggregates. The tensile properties showed that the modulus increased with the augmentation of the clay content and the tensile strength climaxed at 5 wt.% clay regardless of the type of clay used. The formation of intercalated and exfoliated nanostructures increases the exposure of the surface of the clay platelets and allows for the stress to which polymer matrix is subjected to transfer to the nanostructure, and thus withhold superior loads. The dispersion of organoclay (i.e., Cloisite® 30B or Cloisite® 93A) into recycled polypropylene with 30 wt.% maleated polypropylene led to the formation of well dispersed composite materials characterised by highly intercalated nanostructures (for Cloisite® 30B) and low intercalated nanostructures (for Cloisite® 93A).[481] Similar to the recycled PET case,[480] the mechanical properties showed progressive improvements with clay augmentation with the highest values for tensile strength and Charpy impact strength being encountered for a clay load of 4 wt.%.[481]

Analysing the average waste consumption of a household, it was discovered that thermoplastic waste represented 12% of the yearly household residue; from which PE made up 75% and PP, PS, PET and PVC represented 10, 8, 4 and 3%, respectively.[475] Thus, the current study analyses two major household waste thermoplastics, a highly non-polar polymer, i.e., PE, and a low-polar polymer, i.e., PS. This work examines the structure

and the thermal and the mechanical properties of recycled polymer/clay composites manufactured with an as-received organoclay and a blowing agent-treated organoclay. Since these clays have been previously used for pristine polymer matrices, they have the potential of creating intercalated and exfoliated nanostructures in the recycled polymer matrices. As it was previously stated the exposure of the surface of the clay platelets could lead to recycled polymer/clay materials with superior properties compared to the recycled polymer matrices. It is hoped that by using this procedure higher amounts of plastics will be recycled and reintroduced to the market and that the versatility of the products manufactured with recycled polymers will increase by substantially improving their properties. The dispersion of small amounts of clay platelets in recycled polymers may lead to two major outcomes: the improvement of mechanical properties and the decrease in the degradation temperature, facilitating the use of feedstock recycling.

11.2. Experimental Section

11.2.1. Materials

Recycled high-density polyethylene (R-PE) from Monnad Industries (Naas, co. Kildare), obtained from pelletising milk jugs, was generously provided by Athlone Institute of Technology (Athlone, Ireland). Recycled impact-modified polystyrene (Axpoly® PS01), denoted from here on as R-PS and representing 100% post-consumer recycled polymer recovered from refrigerators, was generously supplied by Axion Polymers (Manchester, United Kingdom). Recycled high density polyethylene and recycled impact modified polystyrene were used as polymer matrices for the manufacturing of polymer/clay composites. For recycled PE a compatibilising agent, i.e., polyethylene-grafted-maleic anhydride (PEgMA) was used. PEgMA was purchased from Sigma Aldrich (Ireland). Organoclay Nanomer® I44.P (Clay), a dimethyl dihydrogenated tallow ammonium chloride (2M2HTA) modified montmorillonite, from Nanocor Corporation (Illinois, USA) was kindly supplied by Nordmann, Rassmann GmbH (Hamburg, Germany). The organic content of the clay was determined to be 40% by performing Loss on Ignition test.[351] The Clay was treated with azodicarboxamide (ADC), a well known blowing agent, in the presence of zinc oxide (ZnO). Both materials were purchased from Sigma-Aldrich Ireland Ltd. The solvent for clay treatment was tetrahydrofuran (THF) from Hazmat (Dublin, Ireland). The clay treatment was performed according to the procedure described in Chapter 7.

11.2.2. Nanocomposite manufacturing

Compatibilised R-PE (R-PE/PEgMA=90/10, w/w), R-PE and PS with 4 wt.% clay platelets were manufactured on Prism twin screw extruder (UK) with 16 mm-diameter screws and a length to diameter ratio of 25. The materials were passed three times. Firstly the screw speed was set at 200 rpm and then at 100 rpm. For the organoclay nanocomposites the temperature was maintained at 160, 170, 175, and 180 °C from hopper to die, for all three processes. However, for the blowing agent-treated clay the temperatures were kept constant when the material was first processed, and then the temperatures were increased to 165, 175, 190, 200 °C. After cooling in water, the extrudates were pelletized. In order to obtain the specimens for the tensile and impact testing, a bench top injection moulder (Ray Ran model 2 Test Sample Injection Moulding Apparatus, UK) was used at a barrel temperature of 220 °C, a tool temperature of 55 °C and a pressure of 0.76 MPa for recycled PE (R-PE) materials and a barrel temperature of 210 °C, a tool temperature of 55 °C and a pressure of 0.76 MPa for recycled PS (R-PS) materials.

11.2.3. Characterisation

X-ray Diffraction was carried out on a Phillips PW1720 X-Ray Diffractometre with a $CuK\alpha_1$ (λ=0.15406 nm) anode tube at the standard conditions of 40 kV and 20 mA. The samples were tested from 2° to 10°, 2θ angle, at a step size of 0.02° and duration of 2.5 seconds per step. Powder samples were used for the clays. Composite materials were hot pressed into 1 mm thick samples by applying a pressure of 5.1 MPa for 10 seconds at 210 °C.

Transmission Electron Microscopy was performed on a TECNAI G2 20 Twin electron microscope at 200 kV accelerating voltage. The specimens were ultramicrotomed using a Reichert–Jug 'Ultracut' equipped with a diamond knife. The sections (~100 nm in thickness) were collected in a trough filled with water and then placed on a 200 mesh copper grid.

Scanning Electron Microscopy imaging on tensile fractured surfaces was performed using a Zeiss Ultra Scanning Electron Microscope (for recycled PE materials) or on a Tescan MIra Variable Pressure Field Emission Scanning Electron Microscope (for

recycled PS materials) at a voltage of 5.0 kV. Prior to being analysed the samples were mounted on stubs and their surface were platinum or gold coated.

Thermal Gravimetric Analysis was performed on a Perkin Elmer Pyrus 1 TGA equipped with an ultra-micro balance with a sensitivity of 0.1 μg, under nitrogen flow (20 $mL \cdot min^{-1}$), from 100 °C to 650 °C at a heating rate of 10 $°C \cdot min^{-1}$.

The tensile tests were run according to ISO 527:1996 on a Zwick Z005 machine (Germany). Five dog bone specimens (Type 1BA) were tensile tested using a 5 kN load cell and a testing speed of 20 $mm \cdot min^{-1}$ for recycled PE materials and a 2.5 kN load cell and a testing speed of 5 $mm \cdot min^{-1}$ for recycled PS materials. Impact tests were run according to standard ISO 179:1997 at room temperature on a Charpy impact tester, JinJian XJJD-5, at a speed of 2.9 $m \cdot s^{-1}$ and using a hammer of 2 J for recycled PE materials and 0.5 J for recycled PS. Seven specimens (80 mm x 10 mm x 4 mm, length x width x thickness) were tested for each batch of materials. Prior to being tested the impact specimens were notched with a type A notch, using a 45° cutter and a milling machine. The mean and standard deviation values reported for the mechanical tests represent a confidence level of 95%. Statistical significance was assessed by a Two-tailed, Type II 't' test with a criterion that the probability of a difference in means due to chance is smaller than 0.05.

11.3. Results and Discussion

11.3.1. Structure

The XRD diagrams presented in Figure 11.1 show that the untreated organoclay (Curve 1) presented a broad diffraction peak at a 2θ value of 3.3°, corresponding to a basal spacing, $d_{(001)}$, of 2.7 nm. By treating the organoclay with the organic blowing agent (ADC-Clay), the diffraction peak shifted towards a higher 2θ value. The intercalation of azodicarboxamide inside the clay gallery and the positive shift which was attributed to the removal of some surfactant molecules from the clay gallery have been previously discussed in Chapter 7.

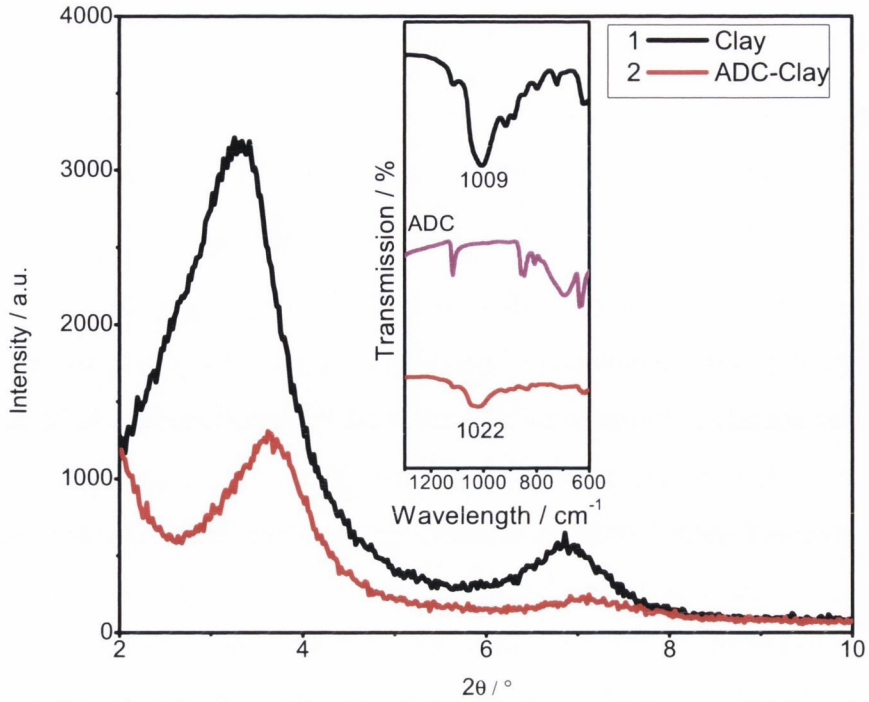

Figure 11.1. XRD profiles of clay and blowing agent-treated clay.

The dispersion of Clay (Figure 11.2A, Curve 1) into recycled PS shifted the *(001)* diffraction peak for Clay to a lower 2θ value of 2.5°, corresponding to a $d_{(001)}$ of 3.5 nm. This indicated the formation of intercalated nanostructures. However, as observed from Figure 11.2A, Curve 2, the XRD spectrum for the ADC-Clay in the recycled PS does not present any significant peaks, except for a small diffraction peak at a 2θ value of 5°. This peak represented the *(002)* diffraction peak. Thus, it was suggested that the dispersion of ADC-Clay in R-PS led to the formation of intercalated/exfoliated nanocomposites. This will be sequentially discussed from the TEM images.

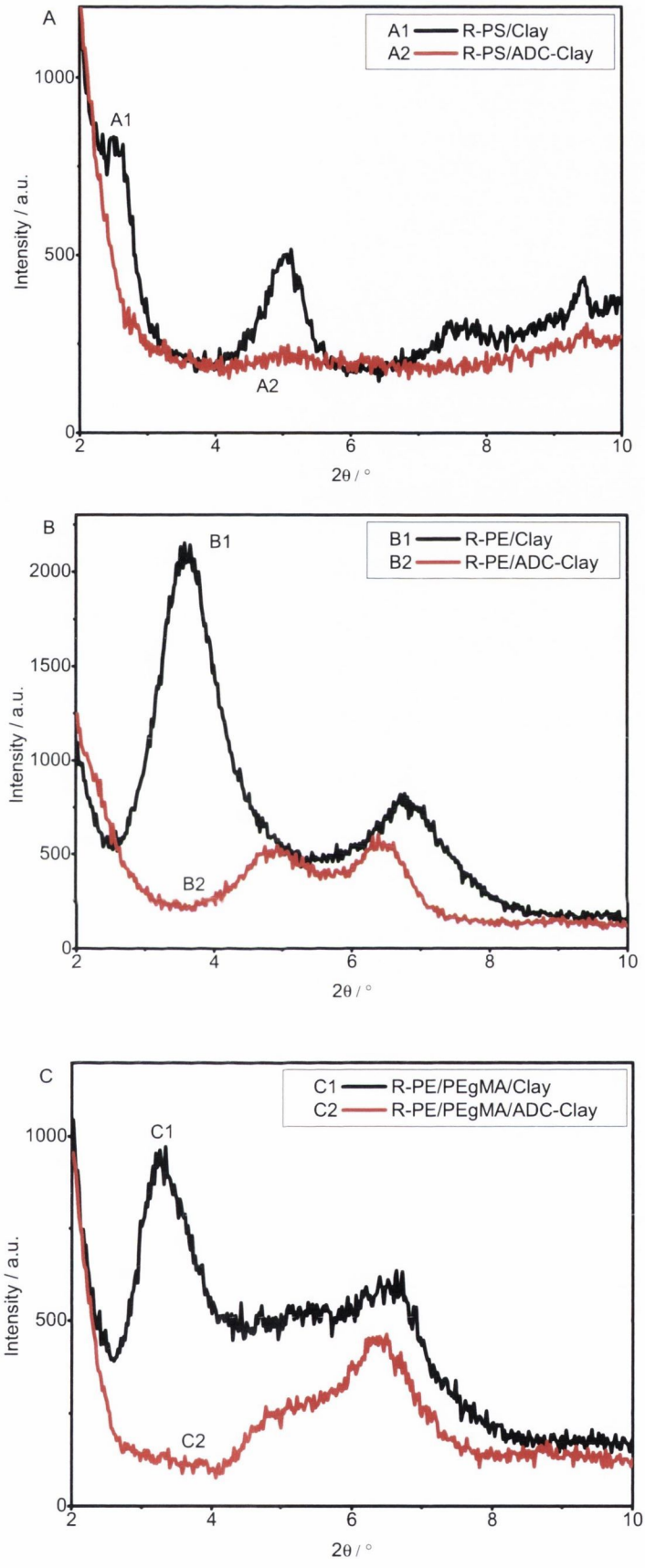

Figure 11.2. XRD profiles of A) R-PS/clay, B) R-PE/clay and C) R-PE/PEgMA/clay composites and nanocomposites.

By dispersing Clay in recycled PE the diffraction peak shifted to higher 2θ values indicating that conventional composites have formed (Figure 11.2B, Curve B1), due to the high non-polar character of the polymer matrix the clay aggregated. Replacing the Clay with ADC-Clay, the XRD spectra (Figure 11.2B, Curve B2) showed no significant *(001)* diffraction peaks between the 2θ values of 2° and 4°, where the *(001)* peaks for Clay (Figure 11.1, Curve 1), ADC-Clay (Figure 11.1, Curve 2) and R-PE/Clay (Figure 11.2B, Curve B1) were encountered. This indicated that either conventional composites or exfoliated nanostructures were present. This will be discussed from the TEM images. The dispersion of Clay into maleated ethylene compatibilised recycled PE (R-PE/PEgMA) showed no shift in the *(001)* diffraction peak (Figure 11.2C, Curve C1). Similarly to the R-PE/ADC-Clay XRD spectra (Figure 11.2B, Curve B2), the presence of blowing agent-treated organoclay in R-PE/PEgMA showed no significant *(001)* peaks between the 2θ values of 2° and 4°. The formation of composite or nanocomposite structures in R-PE/PEgMA/ADC-Clay will be discussed from the TEM images.

The intercalated nanostructures observed *via* XRD for R-PS/clay were confirmed by TEM (Figure 11.3A and 11.3B). As observed from the XRD (Figure 11.2A) the addition Clay (Curve A1) resulted in the formation of mostly intercalated clay nanostructures (Figure 11.3B). From the TEM images it was assessed that the intercalated mass fraction of nanostructures represented 87%, whilst only 13% of the nanostructures presented as exfoliated clay platelets (determined from over 80 nanostructures). The intercalated clay tactoids presented between 2 and 12 clay platelets per stack with an average of 3.9 clay platelets per stack. The absence of the *(001)* peak from the R-PS/ADC-Clay XRD trance (Figure 11.2, Curve A2) was explained by the occurrence of intercalated and exfoliated nanostructures (Figure 11.3C and 11.3D), with a higher exfoliation degree than R-PS/Clay nanocomposites. The fraction of intercalated clay tactoids was determined to be 57%, whilst 43% of the nanostructures presented as single clay platelets (determined from over 80 nanostructures). The intercalated nanostructures exhibited between 2 and 7 clay platelets per stack with an average of 3.2 clay layers per stack.

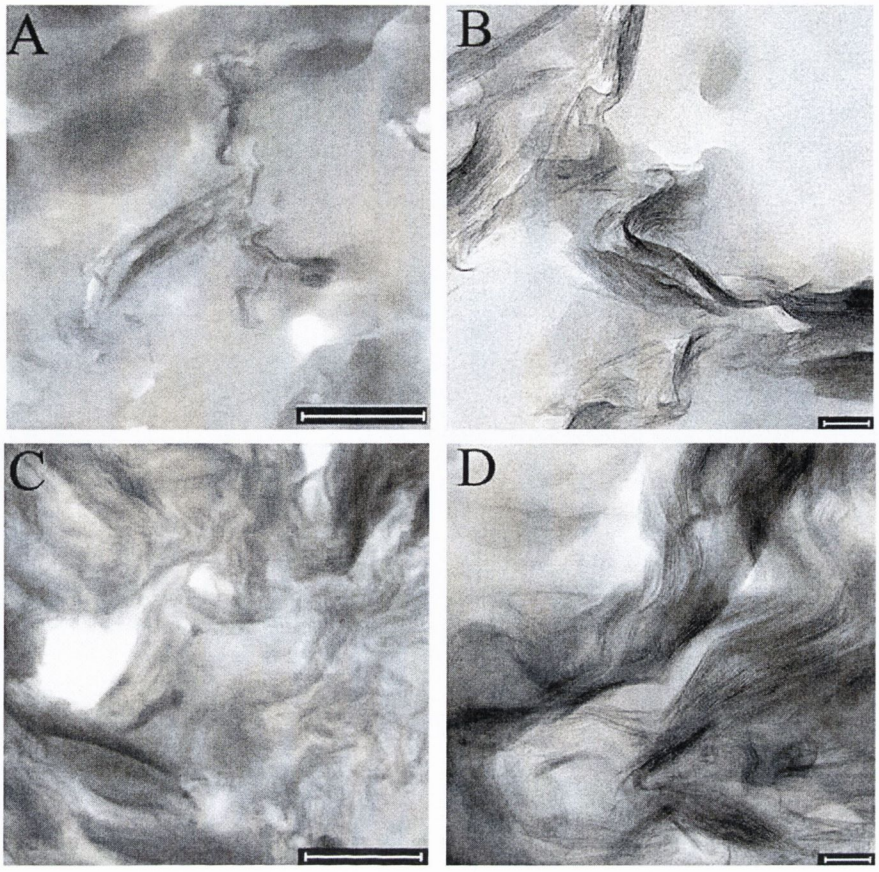

Figure 11.3. TEM images of A. R-PS/Clay (Scale bar: 500 nm), B. R-PS/Clay (Scale bar: 50 nm), C. R-PS/ADC-Clay (Scale bar: 500 nm) and D. PS/ADC-Clay (Scale bar: 50 nm).

The absence of *(001)* diffraction peaks observed *via* XRD for R-PE/ADC-Clay (Figure 11.2B, Curve 2) was explained by the formation of conventional composites (Figure 11.4A). The TEM representative images for compatibilised R-PE/PEgMA/ADC-Clay (Figure 11.4B) showed that although the clay was well dispersed in the polymer matrix, the reinforcement was made up by clay particles with intercalated clay tactoids being marginally identified. Thus, from the XRD traces and the representative TEM images it was concluded that the dispersion of organoclay and ADC-treated organoclay in compatibilised and noncompatibilised R-PE resulted in the formation of conventional composites. This was due to the non-polar character of PE, different polymer grades and impurities. The presence of the blowing agent inside the interlayer and the decomposition[371] of the azodicarboxamide between the clay layers while attempting to increase the basal spacing was observed *via* TEM (Figure 11.4C). The phenomenon was more visible in a highly noncompatible environment due to the repulsive forces that exist between the polyethylene and clay.

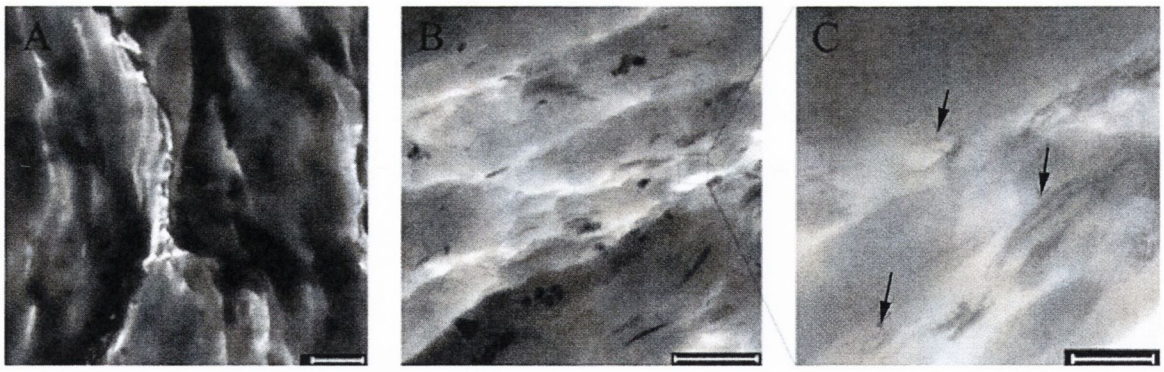

Figure 11.4. TEM images of A. R-PE/BA-Clay (Scale bar: 2 μm), B. R-PE/PEgMA/BA-Clay (Scale bar: 1 μm) and C. R-PE/PEgMA/BA-Clay (Scale bar: 200 nm; the arrows indicate the presence of gas molecules between the clay platelets).

11.3.2. Thermal properties

The maximum degradation temperature (T^{d}_{peak}, measured as the peak temperature on the differential thermogravimetric curves, Figure 11.5) showed different variations according to the type of recycled polymer matrix, the type of clay used and the presence or absence of the compatibilising agent. From Figure 11.5A it can be observed that the dispersion of clay (Curve A2 and Curve A3 vs. Curve A1) led to no change in the peak degradation temperature. This was a consequence of the presence of the surfactant which once decomposed acted as a catalyser; however, the clay platelets and clay tactoids created a barrier effect by preventing the diffusion of oxygen and delaying the volatilisation of the gases produced by the decomposition of the surfactant.[75, 227, 355, 356] These two opposite effects cancelled each other when the clay was dispersed in R-PS.

The dispersion of Clay in recycled PE resulted in a slight decrease in the peak degradation temperature (Figure 11.5B, Curve B2), whilst the presence of ADC-Clay in R-PE exhibited a prominent negative shift in the maximum degradation temperature form 491 °C in R-PE (Figure 11.5B, Curve B1) to 468 °C (Figure 11.5B, Curve B3). Since this decrease was not observed in the R-PE/PEgMA/ADC-Clay it can be hypothesised that the decreased occurred due to poor dispersion of clay particles. Compared to R-PE or R-PE/PEgMA the peak degradation temperature of R-PE/PEgMA/Clay and R-PE/PEgMA/ADC-Clay (Figure 11.5C) was found to diminish; thus, it can be concluded that the exposure of the surfactant can act as a catalyst and facilitate the degradation of the recycled material. These results are in good agreement with the findings reported in Chapter 7 for PP/clay composites.

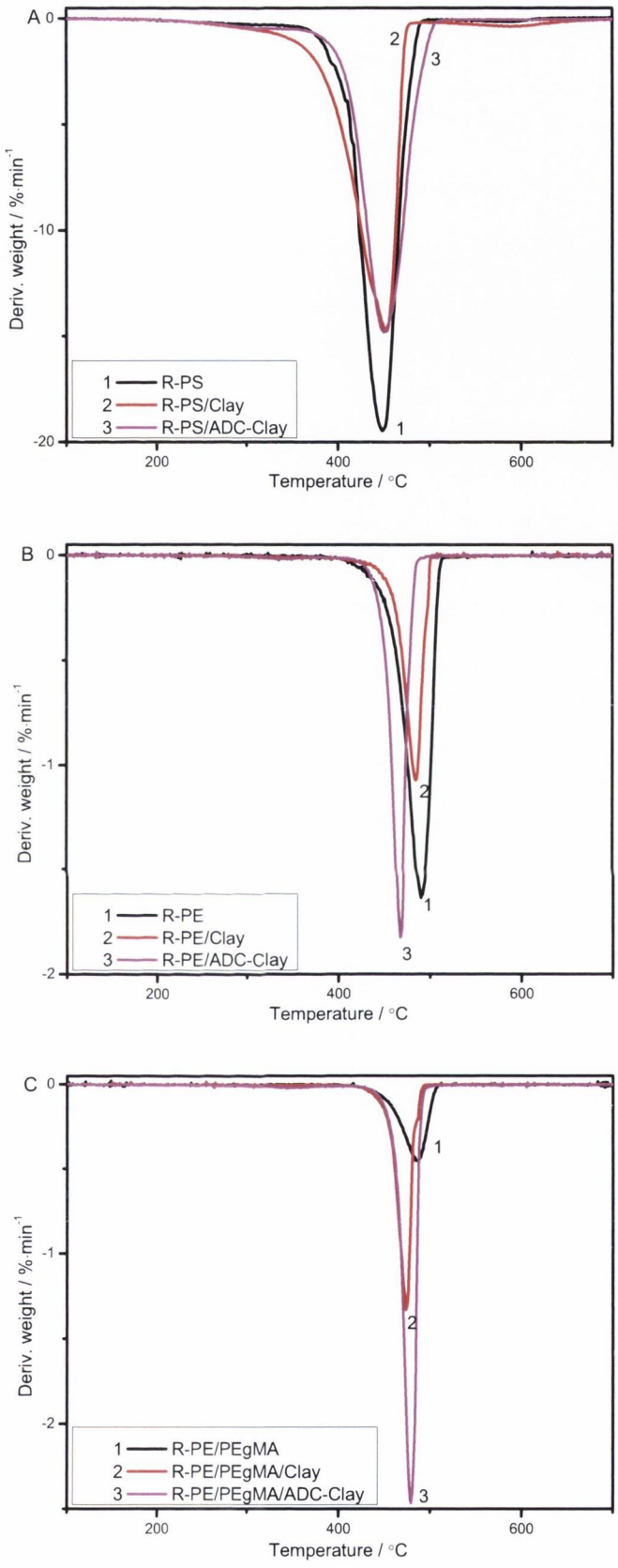

Figure 11.5. Differential thermogravimetric profiles of A) R-PS/clay, B) R-PE/clay and C) R-PE/PEgMA/clay composites and nanocomposites.

11.3.3. Mechanical properties

The dispersion of Clay and ADC-Clay in R-PS increased the Young's modulus, with statistical significance, by 41% and 35%. The delamination of the clay particles exposed the surface of the clay platelets and allowed for the load from the polymer matrix to be transferred to the clay platelets and clay tactoids, which led to materials characterised by higher moduli due to the superior stiffness of clay platelets. The addition of organoclay or ADC-treated organoclay into R-PE and R-PE/PEgMA resulted in statistically significant enhancements in the Young's modulus of up to 36% without the presence of a compatibilising agent and up to 47% in the presence of PEgMA compared to R-PE. As opposed to the stiffness of R-PE/PEgMA, the dispersion of the as-received organoclay and the blowing agent-treated organoclay led to up to 34% statistically significant improvements. In this case the reinforcement was represented by clay particles that were characterised by a superior stiffness compared to the polymer matrix.

The changes in toughness observed during tensile testing (calculated as the energy absorbed by the system before the breaking point)[136] and impact testing are depicted in Figure 11.7. Regardless of the type of clay dispersed in R-PS, the energy absorbed at break was found to decrease by 72-77%. Similarly, the amount of energy absorbed by the R-PE/clay composites reduced by 38-39% when the maleated component was incorporated and further reduced in the absence of the compatibilising agent. The reductions are due to the ability of clay to embrittle a material, as previously reported in literature.[140] The addition of the maleated component into the R-PE led to a significant decrease in the energy absorbed by the material before breaking. This reduction occurred due to the presence of the maleated anhydride which presented a more polar character compared to the non-polar character of the PE and which was grafted on pristine PE, introducing yet another PE grade into the R-PE blend. Thus, the addition of this component generated repulsive forces in the R-PE/PEgMA material. Still, compared to R-PE/PEgMA, the presence of Clay and ADC-Clay led to statistically significant enhancements in the energy absorbed of 458-463%. The spectacular increases that occurred in the compatibilised R-PE with the addition of clay indicated that during the tensile test the stress was transferred from the maleated polymer matrix to the clay particles. The clay, in the presence of the maleated component, acted as a compatibilising agent between the different polymer grades. Compared to the noncompatibilised R-PE/clay composites, the R-PE/PEgMA/clay composites presented a better dispersion of the clay particles (Figure 11.4B). Thus, the

homogeneous dispersion of clay particles in the compatibilised R-PE resulted in improved tensile properties as opposed to the noncompatibilised R-PE/clay composites.

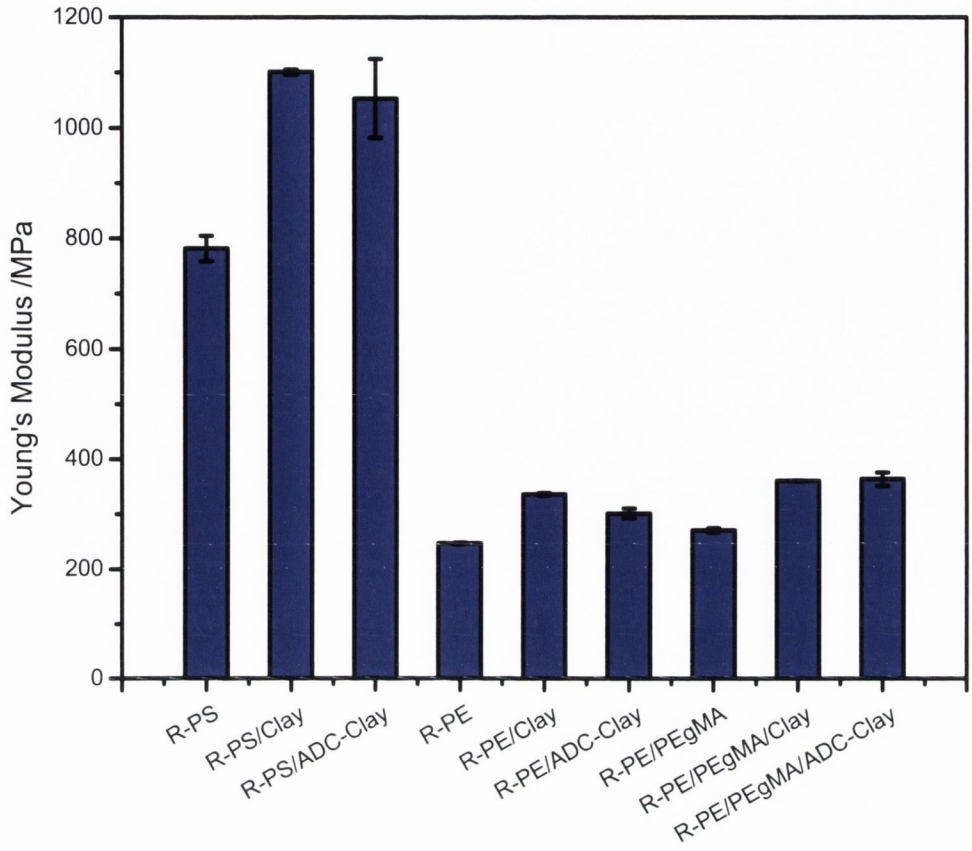

Figure 11.6. Young's modulus for R-PS/clay nanocomposites and compatibilised and noncompatibilised R-PE/clay (The bars represent averages of five measurements; the error bars represent ± one standard deviation).

Similar to the energy absorbed before breaking during the tensile test, the impact strength decreased with statistical significance, regardless of the type of clay used. However, R-PS/ADC-Clay showed a 93% statistically significant improvement in toughness compared to R-PS/Clay. This impressive enhancement can be attributed to the excellent dispersion of nanostructures and to the increase in the degree of exfoliation. These were achieved by treating the organoclay with a bowing agent that degraded inside the clay gallery, thus pushing the silicate layers apart, as it was previously discussed.

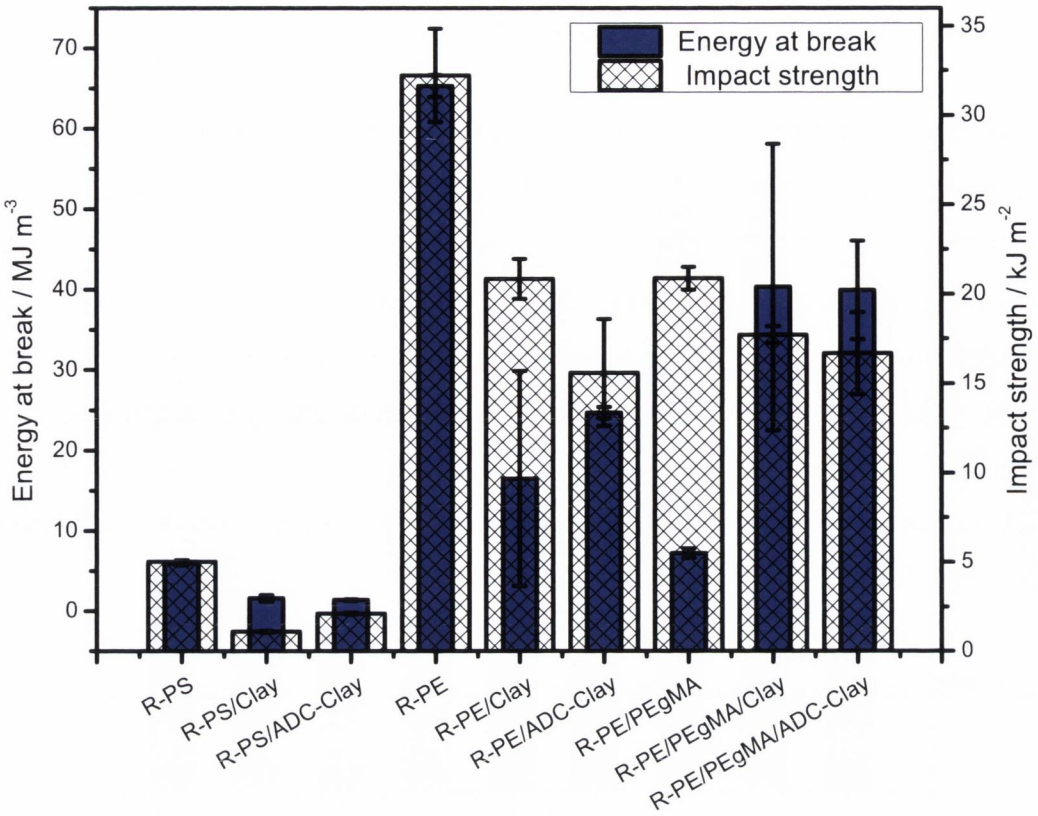

Figure 11.7. Toughness of R-PS/clay nanocomposites and compatibilised and noncompatibilised R-PE/clay composites (The bars represent averages of seven measurements; the error bars represent ± one standard deviation).

The effect of dispersing organoclay or blowing agent-treated organoclay in R-PS, R-PE or R-PE/PEgMA was investigated *via* SEM by analysing the impact fractured surfaces of the recycled polymers and polymer/clay composites and nanocomposites. The dispersion of clay in R-PS (Figure 11.8A1 and 11.8A2) led to the formation of a rougher surface compared to neat R-PS (Figure 11.8A). However, the presence of Clay resulted in a material that exhibited some smoother areas compared to R-PS/ADC-Clay nanocomposites which is in good agreement with the increase in the impact strength observed during fracture toughness testing. The R-PE (Figure 11.8B) presented a vein-type pattern with a fibrillar aspect, in which the addition of the compatibilising agent led to a change in the fibrillar and vein-type pattern density (Figure 11.8C), which is in accordance with the decrease in the toughness (estimated as the tensile energy at break during the tensile test or as the impact strength determined from the Charpy impact test). The conventional composites obtained by dispersing Clay in R-PE showed a fibrillar pattern and some smooth areas that were due to the embrittlement phenomenon that the clay

induced.[140] The dispersion of ADC-Clay in R-PE led to the formation of longer fibrils which is in good agreement with the higher energy absorbed at break that was observed *via* tensile testing for R-PE/ADC-Clay in comparison to R-PE/Clay. The presence of clay in maleated R-PE resulted in the occurrence of highly fibrillar impact surfaces which were in accordance with the improvements observed in the break energy.

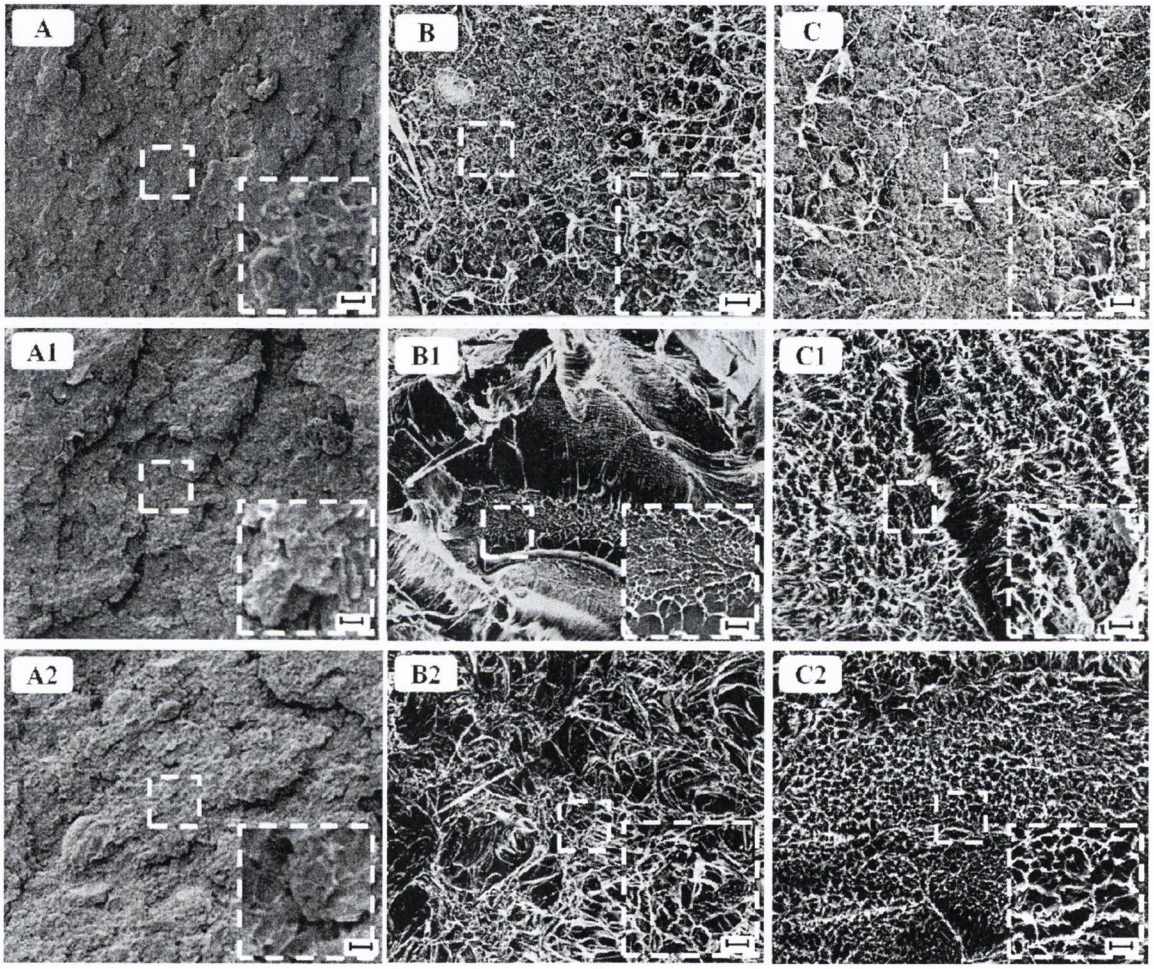

Figure 11.8. SEM images: A. R-PS, A1. R-PS/Clay and A2. R-PS/ADC-Clay; B. R-PE, B1. R-PE/Clay and B2. R-PE/ADC-Clay; C. R-PE/PEgMA, C1 R-PE/PEgMA/Clay, and C2. R-PE/PEgMA/ADC-Clay (Scale bars for the main figures: 10 μm; and for the insets: 1 μm).

The intercalated/exfoliated R-PS/ADC-Clay nanocomposites in which the ratio of the mass fraction of the intercalated clay tactoids to the mass fraction of exfoliated clay platelets was close to unity presented a substantial increase in the impact strength compared to the highly intercalated R-PS/Clay nanocomposite. However, the energy at break of the two recycled polymer/clay nanocomposites presented little variation. These

results contradict the previous findings by Dasari et al.[139] who observed that a highly intercalated nylon 6/clay nanocomposite presented a superior impact strength compared to a highly exfoliated nylon 6/clay nanocomposite. Since in this work impact modified-recycled PS was used, it can be hypothesised that the increase in the impact strength of the intercalated/exfoliated polymer/clay nanocomposite over the intercalated one represented a consequence of exfoliation and exposure of the surfactant which may interact with the impact additives and improve the toughness of the system. Still, it would be expected for the improvement in the impact strength to be accompanied by an enhancement in the tensile energy at break. However, the R-PS/clay nanocomposites present little variation in the tensile energy at break. The rougher fracture surface of R-PS/ADC-Clay nanocomposite compared to the slightly smoother fracture surfaces of R-PS/Clay nanocomposite were in good agreement with the impact strength data.

Unlike the R-PS/clay nanocomposites, R-PE/ADC-Clay microcomposite presented a reduction in the impact strength compared to R-PE/Clay microcomposite, whereas the energy at break presented the opposite variation. This can be attributed to the smaller clay aggregates that form when the ADC-Clay was dispersed in R-PE. The enhanced impact strength of R-PE/Clay over R-PE/ADC-Clay may be a consequence of those aggregates that once encountered on the crack path may force the crack to deviate and thus increase the energy absorbed by the system during the crack propagation. In this case the SEM images are better described by the tensile data. The presence of a compatibilising agent in the R-PE/clay systems led to similar variations in the impact strength and tensile energy at break.

R-PS/Clay and R-PS/ADC-Clay presented superior stiffness compared to R-PS; however, the toughness decreased regardless of the system. In these cases the addition of clay embrittled the material. The compatibilised and noncompatibilised R-PE/clay microcomposites presented higher Young's moduli compared to the R-PE and R/PE/PEgMA. However, the toughness of R-PE/clay systems decreased regardless of the testing method. Unlike R-PR/clay systems, the presence of a compatibilising agent resulted in enhanced tensile energy at break and small reductions in the impact strength. These results are similar to the result reported by Chen and Evans[135] for intercalated PS/clay nanocomposites. The superior stiffness and improved toughness attained with the dispersion of clay in a compatibilised R-PE matrix suggest the immensurable potential that the dispersion of a small amount of clay in a recycled polymer matrix has.

11.4. Conclusions

The dispersion of as-received organoclay and blowing agent-treated organoclay in recycled polystyrene led to the formation of intercalated/exfoliated polymer/clay nanocomposites. By dispersing the same clays in recycled polyethylene with or without the addition of a compatibilising agent, conventional composites were formed. The highly non-polar character of the matrix, even with the introduction of the compatibilising agent, obstructed the delamination of the clay particles.

The presence of clay in R-PS only marginally improved the peak degradation temperature of the material. However, the dispersion of the as-received organoclay or blowing agent-treated organoclay decreased the peak degradation temperatures of the compatibilised and noncompatibilised R-PE. In this case, the exposure of the surfactant acted as a catalyser for the degradation process.

By dispersing Clay or ADC-Clay in the recycled materials the stiffness improved, whether the reinforcing agent was represented by clay platelets and clay tactoids (i.e., R-PS) or clay particles (i.e., R-PE and R-PE/PEgMA). The energy at break of the R-PE/PEgMA, assessed from the tensile tests, was found to significantly increase with the addition of clay. This attested to the ability of clay to act, in the presence of a maleated component, as a compatibilising agent between different polymer grades. The superiority of the blowing agent-treated organoclay over the as-received organoclay was emphasised by a 93% increase in the impact strength of recycled polystyrene.

Thus, the presence of clay improved the mechanical properties of the recycled materials. Although the peak degradation temperature was reduced; this procedure is expected to enable the reuse of recycled materials and ease the unavoidable polymer feedstock recuperation process.

Chapter 12. General discussion and conclusion

This thesis studies the structure-property relationships of polymer/clay nanocomposite foams, polymer/clay nanocomposites and polymer blend/clay nanocomposites. It also investigates the toughness of polymer/clay nanocomposites by studying the mechanical properties of intercalated/exfoliated polymer/clay nanocomposites with different exfoliation degrees.

Although the mechanical and structural properties of polymer/clay nanocomposite foams have been widely investigated, the structure-property relationships have not been quantified. In order to study the fundamental relationship between the relative density and the relative modulus polymer/clay nanocomposite foams were developed by dispersing natural clay into a low-density thermosetting polymer foam (i.e., polyurethane). This work presented two secondary goals: to investigate the best mixing sequence of the three components (by varying the polyol, MDI and clay order) and to assess the proper clay content (i.e., 4 wt.% or 8 wt.% clay platelets). By performing this work the structure-property relationship for low-density polymer/clay nanocomposite foams was established. It was found that this fundamental relationship can be described by a normalised Gibson-Ashby model and by using established foam theories. It was also determined that the best mixing sequence was to mix the clay with the polyol followed by the addition of the diisocyanate and last but not least, it was found that a 8 wt.% clay platelets content rendered the best mechanical properties.

High density polyethylene, a commodity plastic that is typically found in the recycled stock was selected as the polymer matrix. In literature, a clay content of approximately 5 wt.% is recommended for the manufacturing of polymer/clay nanocomposites; however, according to the polyurethane/clay nanocomposite foams study, a higher clay load was found to result in better mechanical properties. The main goal of this work was to assess whether the melt compounded polymer/clay nanocomposites with 4 or 8 wt.% clay platelets would result in superior properties. The secondary aim of the work was to evaluate the necessity of adding a compatibilising agent to the non-polar polymer matrix. This study revealed that a clay content of 4 wt.% clay platelets was appropriate for manufacturing polymer/clay nanocomposites *via* melt processing. It also revealed that in order to obtain a polymer/clay nanocomposite with a non-polar matrix an organoclay and a compatibilising agent had to be used.

Polystyrene, an amorphous polymer typically found in the recycled stock, was chosen as the polymer matrix to study the most appropriate type of surfactant (i.e., cationic, anionic or non-ionic) to be used to treat the natural clay in order to achieve polymer/clay nanocomposites. The dispersion of the natural clay without a surfactant was also investigated by using a montmorillonite-gel. Again, quantities of 4 and 8 wt.% clay platelets were used. It was determined that in order for intercalated polymer/clay nanocomposite to be obtained it is ideal to apply a cationic treatment or to simultaneously mix the polymer and the un-treated montmorillonite with a non-ionic surfactant. The PS/MMT-gel materials displayed ductility which may represent a potential improvement in the toughness of the brittle PS. Similar, to the HDPE case, it was determined that a 4 wt.% clay platelets content was optimal for achieving superior mechanical properties.

Following the study of the structure-property relationships on low-density polymer/clay nanocomposite foams, high-density polymer/clay nanocomposite foams were developed. A biocompatible thermoplastic polymer (i.e., poly(ε-caprolactone)) was selected as the polymer matrix due to its packaging and biomedical applications, e.g. drug delivery systems and bioabsorbable surgical sutures, etc. The goals of this work were to establish the structure-property relationship in high-density polymer/clay nanocomposite foams and to develop novel clays by inserting the blowing agent inside the clay gallery. These new clays were used to create polymer/clay nanocomposites and by sequentially degrading the blowing agent inside the gallery porous polymer/clay nanocomposites were developed. By performing this work it was found that the normalised Gibson-Ashby model may be used only for low-density polymer/clay nanocomposite foams. For higher-density foams a cellular model, such as Mills-Zhu which was found to agree reasonably well with the experimental data, may be used to describe the structure-property relationships. It was also determined that by modifying the clay with the blowing agent enhanced and even full exfoliation of the clay platelets can be achieved, due to the gas molecules that produce inside the gallery of clay upon the degradation of the blowing agent and that push apart the clay platelets, thus improving the exfoliation degree.

The enhanced exfoliation observed in porous PCL/blowing agent-treated organoclay nanocomposites prompted the question if this procedure could be used for melt mixing polymer/clay nanocomposite manufacturing. In order to test this hypothesis 4 wt.% blowing agent-treated organoclays or as-received organoclay were dispersed in a low polarity polymer (i.e., PS) and a compatibilised non-polar polymer (i.e., PP/PPgMA). It was observed that the commercially available organoclay yielded intercalated/exfoliated

polymer/clay nanocomposites, whereas the dispersion of blowing agent-treated organoclays led to intercalated/exfoliated polymer/clay nanocomposites with higher exfoliation degrees. The improved exfoliation attained *via* this novel method shows the potential of using this technique for the future development of highly exfoliated polymer/clay nanocomposites.

As the previous study demonstrated the potential of obtaining intercalated/exfoliated polymer/clay nanocomposites with various degrees of exfoliation in amorphous and compatibilised semicrystalline polymers, a project using a semicrystalline nylon 6 polymer matrix was developed in order to investigate the effects of the exfoliation degree on the thermal and mechanical properties. Natural clay, as-received organoclay and blowing agent-treated organoclay were melt mixed with nylon 6 to obtain intercalated/exfoliated polymer/clay nanocomposites with different exfoliation degrees. The main objective of this work was to assess the changes that undergo in the crystalline structure of polymer in the presence of clay, before and after exposing the polymer to uniaxial deformation. The results showed that the presence of clay hindered the formation of the more thermodynamically stable state. Using the same nylon/clay nanocomposite systems, the toughness of polymer/clay nanocomposites was investigated from the tensile, impact and J-integral fracture mechanics tests. Toughness represents a complex property that is influenced by a number of factors and, at the moment, there are a series of theories that argue whether an intercalated polymer/clay nanocomposite is superior to an exfoliated one. The current research showed that an intercalated/exfoliated polymer/clay nanocomposite with equal mass fractions of intercalated and exfoliated nanostructures presented the best mechanical properties.

Since most of the times the recycled stock is represented by a blend of polymers with different grades, the dispersion of clay to compatibilised and noncompatibilised immiscible polymer blend (i.e., PS/PP) was investigated. The main objectives of the study were to assess the role of the clay and to develop the structure-polymer relationship for immiscible polymer blends, a fundamental relationship that was missing from literature. It was observed that the clay located in the low polarity polymer (i.e., PS) in the noncompatibilised blend and in both polymers and at the interface when the compatibilising agent was added. Thus, the clay has the role of the reinforcing agent in the noncompatibilised polymer blend; however, in the presence of a compatibilising agent the clay platelets undertake a secondary role, acting as compatibilisers. Taking into

consideration the location of clay platelets, the structure-property relationships were developed for compatibilised and noncompatibilised polymer blends.

The results obtained for pristine polymer and polymer blend/clay nanocomposites suggested that the addition of clay to recycled polymers may prove beneficial. In order to investigate this hypothesis, two polymer matrices were chosen: recycled polystyrene and recycled polyethylene. The main aim of this work was to study the impact that clay dispersion had on the recycled polymers and to establish the potential of using clays to reintroduce the plastic materials back into consumption. It was found that the addition of clay enhanced the mechanical properties and facilitated the degradation process which enabled the reuse of the recycled material. So, the dispersion of clay into recycled polymer matrices represents a viable solution for reducing the world plastic consumption.

In conclusion, this thesis demonstrated that by pre-treating the as-received organoclay with blowing agents the exfoliation degree of an intercalated/exfoliated polymer/clay nanocomposite can be enhanced. It also showed that the dispersion of clay and hence the exfoliation degree of the clay platelets influences the crystallinity and the toughness of the polymer/clay nanocomposite. Although currently there are a number of results that suggest that an intercalated or an exfoliated morphology of the clay platelets would be more beneficial for the mechanical properties of the polymer/clay nanocomposites, the current studies showed that intercalated/exfoliated polymer/clay nanocomposites with a ratio of intercalated:exfoliated nanostructures close to unity produced superior properties. The fundamental structure-property relationships for polymer/clay nanocomposite foams, for porous polymer/clay nanocomposites and for polymer blend/clay nanocomposites were developed. The ability of clay to act as a reinforcing agent in polymer/clay nanocomposites, as well as a nucleation agent in polymer/clay nanocomposite foams and as a compatibilising agent in polymer blend/clay nanocomposites indicates that clay platelets may be used to manufacture highly superior, environmentally friendly and economically feasible nanocomposite materials. It has also been shown that the addition of clay to recycled polymers can be a viable solution to excessive plastic waste.

Future work

1. Investigate the PS/MMT-gel to establish the full potential of this method;
2. Analyse the changes in temperature that may appear during the crack propagation process;
3. Develop polymer/clay nanocomposites with a desired exfoliation degree;
4. Study the kinetics of crystallisation on polymer/clay nanocomposites before and after subjecting the material to uniaxial deformation;
5. Develop structure-property relationships for the toughness of polymer/clay nanocomposites.

Publications

- O. M. Istrate and B. Chen – Relative modulus-relative density relationships in low density polymer-clay nanocomposite foams, *Soft Matter*, 2011, 7, 1840;
- O. M. Istrate and B. Chen – Porous exfoliated poly(ε-caprolactone)/clay nanocomposites: preparation, structure and properties, *Journal of Applied Polymer Science* – DOI: 10.1002/app.36336;
- O. M. Istrate, M. A. Gunning, C. L. Higginbotham and B. Chen – Structure-property relationships of polymer blend/clay nanocomposites: compatibilised and noncompatibilised polystyrene/propylene/clay, *Journal of Polymer Science Part B: Polymer Physics*, 2012, 50, 431-441;
- M. A. Gunning, O. M. Istrate, L. M. Geever, J. G. Lyons, P. Blackie, B. Chen and C. L. Higginbotham – The effect of maleic anhydride grafting efficiency on the flexural properties of polyethylene composites, *Journal of Applied Polymer Science*, 2012, 124: 4799–4808;

Papers in preparation

- O. M. Istrate and B. Chen – A facile method for improving clay exfoliation in polymer nanocomposites;
- O. M. Istrate and B. Chen – Changes in crystallinity and crystalline structure in nylon 6/clay nanocomposites;
- O. M. Istrate and B. Chen – On the toughness of polymer/clay nanocomposites;
- O. M. Istrate and B. Chen – Preparation of polystyrene/clay composites of different morphologies with cationic, anionic or non-ionic surfactants;
- O. M. Istrate and B. Chen – Effect of clay on thermal and mechanical properties of recycled plastics.

Oral Conference Presentations

- O.M. Istrate and B. Chen – Pristine and recycled polymer-clay nanocomposites, Environmental Protection Agency Post-Graduate Seminar, Dublin, Republic of Ireland, 2011
- O.M. Istrate and B. Chen – Polymer-clay nanocomposite foams: preparation, structure and mechanical properties, Second International Conference on Multifunctional, Hybrid and Nanomaterials, Strasburg, France, 2011
- O.M. Istrate and B. Chen – Structure and thermal properties of polypropylene/polystyrene blend clay nanocomposites, Materials Ireland Conference, Dublin, Republic of Ireland, 2010.
- O.M. Istrate – Polymer/clay nanocomposite foams, Young Persons Lecture Competition, Materials Ireland Conference, Dublin, Republic of Ireland, 2010.

Poster Conference Presentations (selected)

- O.M. Istrate and B. Chen – Investigation of the structural and mechanical properties of polymer blend/clay nanocomposites for sustainable development, Environmental Protection Agency Post-Graduate Seminar, Dublin, Republic of Ireland, 2010
- O.M. Istrate and B. Chen – Biodegradable poly(ε-caprolactone) – clay nanocomposite foams, Environmental Protection Agency National Research Conference, Dublin, Republic of Ireland, 2010
- O.M. Istrate and B. Chen – Preparation and characterization of polymer-clay nanocomposites, Materials Ireland Conference, Cork, Republic of Ireland, 2009
- O.M. Istrate and B. Chen – Polymer-clay nanocomposites for plastic recycling, Environmental Protection Agency Post-Graduate Seminar, Dublin, Republic of Ireland, 2009

References

(1) Bousmina, M. *Macromolecules* **2006,** 39, 4259-4263.

(2) Okada, A.; Usuki, A. *Macromol. Mater. Eng.* **2007,** 291, 1449-1476.

(3) Fornes, T. D.; Paul, D. R. *Polymer* **2003,** 44, 4993-5013.

(4) Jordan, J. W. *J. Phys. Colloid Chem.* **1950,** 53, 294–306.

(5) Jordan, J. W.; Hook, B. J.; Finlayson, C. M. *J. Polym. Sci., Part B: Polym. Phys.* **1950,** 54, 1196-1208.

(6) Duan, Z.; Sun, R. *Chem. Geology* **2003,** 193, 257-271.

(7) Pavlidou, S.; Papaspyrides, C. D. *Prog. Polym. Sci.* **2008,** 33, 1119-1198.

(8) Chen, B.; Evans, J. R. G.; Greenwell, H. C.; Boulet, P.; Coveney, P. V.; Bowden, A. A.; Whiting, A. *Chem. Soc. Rev.* **2008,** 37, 568-594.

(9) Ray, S.; Easteal, A. J. In *Advances in polymer-filler composites: Macro to nano*, International Composites Conference, Sydney, Australia, Jul 11-14, 2006; Sydney, Australia, 2006; pp 741-749.

(10) Rehab, A.; Salahuddin, N. *Mater. Sci. Eng. A* **2005,** 399, 368-376.

(11) Wang, Z.; Pinnavaia, T. J. *Chem. Mater.* **1998,** 10, 3769-+.

(12) Pinnavaia, T. J.; Beall, G. W., In *Polymer clay-nanocomposites*,Wiley: Chishester, 2000.

(13) Hassan, M. K.; Abou-Hussein, R.; Zhang, X. J.; Mark, J. E.; Noda, I. *Mol. Cryst. Liq. Cryst. Sci. Technol., Sect. A* **2006,** 447, 341-362.

(14) Vanorio, T.; Prasad, M.; Nur, A. *Geophys. J. Int.* **2003,** 155, 319-326.

(15) Kinloch, A. J.; Taylor, A. C. *J. Mater. Sci. Lett.* **2003,** 22, 1439-1441.

(16) Chen, B.; Evans, J. R. G. *Scripta Mater.* **2006,** 54, 1581-1585.

(17) Kim, G. M.; Goerlitz, S.; Michler, G. H. *J. Appl. Polym. Sci.* **2007,** 105, 38-48.

(18) Sammon, C. Clay Based Nanocomposites - An Introduction to Clay Polymer Nanocomposites. (Oct. 28, 2011),

(19) Lee, L. J.; Zeng, C.; Cao, X.; Han, X.; Shen, J.; Xu, G. *Compos. Sci. Technol.* **2005,** 65, 2344-2363.

(20) Ashby, M. F.; Bush, S. F.; Swindells, N.; Bullough, R.; Ellison, G.; Lindblom, Y.; Cahn, R. W.; Barnes, J. F. *Philos. Trans. R. Soc. London, Ser. A* **1987,** 322, 393-407.

(21) Hull, D.; Clyne, T. W., In *An introduction to composite materials* 2nd ed.;Cambridge University Press: 1996; p 32.

(22) Vaia, R. A.; Wagner, H. D. *Mater. Today* **2004,** 7, 32-37.

(23) Vu, H. N.; Vermogen, A.; Gauthier, C.; Masenelli-Varlot, K.; Cavaille, J. Y. *J. Polym. Sci., Part B: Polym. Phys.* **2008,** 46, 1820-1836.

(24) Vaia, R. A.; Jandt, K. D.; Kramer, E. J.; Giannelis, E. P. *Chem. Mater.* **1996,** 8, 2628-2635.

(25) Nathani, H.; Dasari, A.; Misra, R. D. K. *Acta Mater.* **2004,** 52, 3217-3227.

(26) Zhao, J.; Morgan, A. B.; Harris, J. D. *Polymer* **2005,** 46, 8641-8660.

(27) Katti, K. S.; Sikdar, D.; Katti, D. R.; Ghosh, P.; Verma, D. *Polymer* **2006,** 47, 403-414.

(28) Dasari, A.; Yu, Z.-Z.; Mai, Y.-W.; Hu, G.-H.; Varlet, J. *Compos. Sci. Technol.* **2005,** 65, 2314-2328.

(29) Hasegawa, N.; Okamoto, H.; Kato, M.; Usuki, A.; Sato, N. *Polymer* **2003,** 44, 2933-2937.

(30) Marquis, D. M.; Éric, G.; Chivas-Joly, C., Properties of Nanofillers in Polymer. In *Nanocomposites and Polymers with Analytical Methods*, Cuppoletti, J., Ed. InTech: 2011; pp 261-284.

(31) Caseri, W. R. *Mater. Sci.Technol.* **2006,** 22, 807-817.

(32) Tjong, S. C. *Mater. Sci. Eng. R* **2006,** 53, 73-197.

(33) Dasari, A.; Yu, Z. Z.; Mai, Y. W. *Polymer* **2005,** 46, 5986-5991.

(34) Meneghetti, P.; Qutubuddin, S. *Thermochim. Acta* **2006,** 442, 74-77.

(35) Hussain, F.; Hojjati, M.; Okamoto, M.; Gorga, R. E. *J. Compos.Mater.* **2006,** 40, 1511-1575.

(36) Ke, Y. C., Stroeve, P., , In *Polymer-Layered Silicate and Silica Nanocomposites*, Elsevier: 2005.

(37) Du, X. S.; Xiao, M.; Meng, Y. Z.; Hay, A. S. *Polym. Int.* **2004,** 53, 789-793.

(38) Li, Y. J.; Shimizu, H. *J. Polym. Sci., Part B: Polym. Phys.* **2006,** 44, 284-290.

(39) Koo, J. H., In *Polymer Nanocomposites: Processing, Characterization and Applications*, McGraw-Hill: 2006.

(40) Biron, M., In *Thermoplastics and Thermoplastic Composites, Technical Information for Plastic Users*, Elsevier: 2007; p 156.

(41) Petrie, E. M. Extreme High Temperature Thermoplastics - Gateway to the Future or the Same Old Trail? (Jan. 30, 2012),

(42) Moczo, J.; Pukanszky, B. *J. Ind. Eng. Chem.* **2008,** 14, 535-563.

(43) Zuiderduin, W. C. J.; Westzaan, C.; Huetink, J.; Gaymans, R. J. *Polymer* **2003,** 44, 261-275.

(44) Kalendova, A.; Pospisil, M.; Kovarova, L.; Merinska, D.; Valaskova, M.; Vlkova, H.; Simonik, J.; Capkova, P. *Plast. Rubber Compos.* **2004,** 33, 279-285.

(45) Lepoittevin, B.; Pantoustier, N.; Devalckenaere, M.; Alexandre, M.; Calberg, C.; Jerome, R.; Henrist, C.; Rulmont, A.; Dubois, P. *Polymer* **2003,** 44, 2033-2040.

(46) Fu, J.; Naguib, H. E. *J. Cell. Plast.* **2006,** 42, 325-342.

(47) Kuronuma, Y.; Shindo, Y.; Takeda, T.; Narita, F. *Fatigue Fract. Eng. M.* **2010,** 33, 87-93.

(48) Zanetti, M.; Lomakin, S.; Camino, G. *Macromolec. Mater. Eng.* **2000,** 279, 1-9.

(49) Wakabayashi, K.; Pierre, C.; Dikin, D. A.; Ruoff, R. S.; Ramanathan, T.; Brinson, L. C.; Torkelson, J. M. *Macromolecules* **2008,** 41, 1905-1908.

(50) Kim, G. M.; Lee, D. H.; Hoffmann, B.; Kressler, J.; Stoppelmann, G. *Polymer* **2001,** 42, 1095-1100.

(51) Morgan, A. B.; Chu, L. L.; Harris, J. D. *Fire Mat.* **2005,** 29, 213-229.

(52) Grim, R. E., In *Clay mineralogy*,Second edition ed.;McGraw-Hill Book Company: 1968.

(53) Murray, H. H., Clays. In *Clays. Ullmann's Encyclopedia of Industrial Chemistry*, 2006.

(54) Murray, H. H., In *Applied Clay Mineralogy – Occurrences, Processing and Application of Kaolins, Bentonites, Palygorskite-Sepiolite, and Common Clays. Developments in clay mineralogy; 2*, Elsevier: Amsterdam; Oxford 2007.

(55) Liu, J.; Boo, W. J.; Clearfield, A.; Sue, H. J. *Mater. Manuf. Processes* **2006,** 21, 143-151.

(56) Panwar, A.; Choudhary, V.; Sharma, D. K. *J. Reinf. Plast. Compos.* **2011,** 30, 446-459.

(57) Auerbach, S. M.; Carrado, K. A.; Dutta, P. K., In *Handbook of Layered Materials*,Marcel Deeker, Inc.: New York, 2004.

(58) Ogata, N.; Jimenez, G.; Kawai, H.; Ogihara, T. *J. Polym. Sci. B* **1997,** 35, 389-396.

(59) Marras, S. I.; Tsimpliaraki, A.; Zuburtikudis, I.; Panayiotou, C. *J. Colloid Interface Sci.* **2007,** 315, 520-527.

(60) Manias, E.; Touny, A.; Wu, L.; Strawhecker, K.; Lu, B.; Chung, T. C. *Chem. Mater.* **2001,** 13, 3516-3523.

(61) Zulfiqar, S.; Ishaq, M.; Sarwar, M. I. *Surf. Interface Anal.* **2008,** 40, 1195-1201.

(62) Chen, B.; Evans, J. R. G. *J. Phys. Chem. B* **2004,** 108, 14986-14990.

(63) Luo, J.-J.; Daniel, I. M. *Compos. Sci. Technol.* **2003,** 63, 1607-1616.

(64) Kozak, M.; Domka, L. In *Adsorption of the quaternary ammonium salts on montmorillonite*, 12th International Symposium on Intercalation Compounds, Poznan, Poland, Jun 01-05, 2003; Poznan, Poland, 2003; pp 441-445.

(65) Jordan, J. W.; Williams, F. J. *Kolloid-Zeitschrift and Zeitschrift Fur Polymere* **1954,** 137, 40-48.

(66) Chaiko, D. J.; Leyva, A. A. *Chem. Mater.* **2005,** 17, 13-19.

(67) Liu, X. H.; Wu, Q. J. *Polymer* **2001,** 42, 10013-10019.

(68) Zhang, J. G.; Manias, E.; Wilkie, C. A. *J. Nanosci. Nanotechno.* **2008,** 8, 1597-1615.

(69) Shmuel Yariv, H. C., In *Organo-clay complexes and interactions*,CRC Press: 2002.

(70) Krishnamoorti, R.; Vaia, R. A., In *ACS symposium series*,Krishnamoorti, R.; Vaia, R. A.; American Chemical Society Washington, D.C., 2002; Vol. 804.

(71) Sharma, S. K.; Nayak, S. K. *Polym. Degrad. Stab.* **2009,** 94, 132-138.

(72) de Paiva, L. B.; Morales, A. R.; Diaz, F. R. V. *Appl. Clay Sci.* **2008,** 42, 8-24.

(73) Choudalakis, G.; Gotsis, A. D. *Eur. Polym. J.* **2009,** 45, 967-984.

(74) Fischer, H. *Mater. Sci. Eng. C* **2003,** 23, 763-772.

(75) Araujo, E. M.; Barbosa, R.; Rodrigues, A. W. B.; Melo, T. J. A.; Ito, E. N. *Mater. Sci. Eng. A* **2007,** 445, 141-147.

(76) Daniel, I. M.; Miyagawa, H.; Gdoutos, E. E.; Luo, J. J. *Experim. Mech.* **2003,** 43, 348-354.

(77) Chen, B.; Bowden, A. A.; Greenwell, H. C.; Boulet, P.; Coveney, P. V.; Whiting, A.; Evans, J. R. G. *J. Polym. Sci. B* **2005,** 43, 1785-1793.

(78) Mariott, W. R.; Escude, N. C.; Chen, E. Y. X. *J. Polym. Sci. B* **2007,** 45, 2581-2592.

(79) Bergaya, F.; Theng, B. K. G.; Lagaly, G., In *Handbook of clay science*,Elsevier: 2006.

(80) Liu, P. *Appl. Clay Sci.* **2007,** 38, 64-76.

(81) Breen, C. *Appl. Clay Sci.* **1999,** 15, 187-219.

(82) Öztekin, N.; Alemdar, A.; Güngör, N.; Erim, F. B. *Mater. Lett.* **2002,** 55, 73-76.

(83) Song, K.; Sandi, G. *Clays Clay Miner.* **2001,** 49, 119-125.

(84) Ko, C. H.; Fan, C.; Chiang, P. N.; Wang, M. K.; Lin, K. C. *J. Hazard. Mater.* **2007,** 149, 275-282.

(85) Han, B.; Ji, G. D.; Wu, S. S.; Shen, J. *Eur. Polym. J.* **2003,** 39, 1641-1646.

(86) LeBaron, P. C.; Pinnavaia, T. J. *Chem. Mater.* **2001,** 13, 3760-3765.

(87) Sinha Ray, S.; Okamoto, M. *Prog. Polym. Sci.* **2003,** 28, 1539-1641.

(88) Alexandre, M.; Dubois, P. *Mater. Sci. Eng. R* **2000,** 28, 1-63.

(89) Chu, C. C.; Chiang, M. L.; Tsai, C. M.; Lin, J. J. *Macromolecules* **2005,** 38, 6240-6243.

(90) Saha, M. C.; Kabir, M. E.; Jeelani, S. *Mat. Sci. Eng. A* **2008,** 479, 213-222.

(91) Park, J. H.; Jana, S. C. *Macromolecules* **2003,** 36, 2758-2768.

(92) Horsch, S.; Serhatkulu, G.; Gulari, E.; Kannan, R. M. *Polymer* **2006,** 47, 7485-7496.

(93) Bharadwaj, R. K.; Mehrabi, A. R.; Hamilton, C.; Trujillo, C.; Murga, M.; Fan, R.; Chavira, A.; Thompson, A. K. *Polymer* **2002,** 43, 3699-3705.

(94) Liu, L. M.; Qi, Z. N.; Zhu, X. G. *J. Appl. Polym. Sci.* **1999,** 71, 1133-1138.

(95) Arunvisut, S.; Phummanee, S.; Somwangthanaroj, A. *J. Appl. Polym. Sci.* **2007,** 106, 2210-2217.

(96) Wang, K. H.; Choi, M. H.; Koo, C. M.; Choi, Y. S.; Chung, I. J. *Polymer* **2001,** 42, 9819-9826.

(97) Mittal, V. *J. Thermoplast. Compos. Mater.* **2008,** 21, 9-26.

(98) Zhong, Y.; Janes, D.; Zheng, Y.; Hetzer, M.; De Kee, D. *Polym. Eng. Sci.* **2007,** 47, 1101-1107.

(99) Morawiec, J.; Pawlak, A.; Slouf, M.; Galeski, A.; Piorkowska, E.; Krasnikowa, N. *Eur. Polym. J.* **2005,** 41, 1115-1122.

(100) Garcia-Lopez, D.; Picazo, O.; Merino, J. C.; Pastor, J. M. *Eur. Polym. J.* **2003,** 39, 945-950.

(101) Nikolaidis, A. K.; Achilias, D. S.; Karayannidis, G. P. *Ind. Eng. Chem. Res.* **2010,** 50, 571-579.

(102) Akat, H.; Tasdelen, M. A.; Du Prez, F.; Yagci, Y. *Eur. Polym. J.* **2008,** 44, 1949-1954.

(103) Monticelli, O.; Musina, Z.; Ghigliotti, F.; Russo, S.; Causin, V. *E-Polymers* **2007**.

(104) Baniasadi, H.; Ramazani S.A, A.; Javan Nikkhah, S. *Mater. & Design* **2010,** 31, 76-84.

(105) Wang, D.; Wilkie, C. A. *Polym. Degrad. Stab.* **2003,** 80, 171-182.

(106) Yin, M.; Li, C. C.; Guan, G. H.; Zhang, D.; Xiao, Y. N. *J. Appl. Polym. Sci.* **2009,** 114, 2327-2338.

(107) Filippi, S.; Marazzato, C.; Magagnini, P.; Famulari, A.; Arosio, P.; Meille, S. V. *Eur. Polym. J.* **2008,** 44, 987-1002.

(108) Chen, B.; Evans, J. R. G.; Holding, S. *J. Appl. Polym. Sci.* **2004,** 94, 548-552.

(109) Rai, U. S.; Singh, R. K. *Mater. Lett.* **2004,** 58, 235-240.

(110) Vaia, R. A.; Giannelis, E. P. *Macromolecules* **1997,** 30, 7990-7999.

(111) Aranda, P.; Ruizhitzky, E. *Chem. Mater.* **1992,** 4, 1395-1403.

(112) Jimenez, G.; Ogata, N.; Kawai, H.; Ogihara, T. *J. Appl. Polym. Sci.* **1997,** 64, 2211-2220.

(113) Jeon, H. G.; Jung, H. T.; Lee, S. W.; Hudson, S. D. *Polym. Bull.* **1998,** 41, 107-113.

(114) Lee, Y. H.; Park, C. B.; Sain, M.; Kontopoulou, M.; Zheng, W. *J. Appl. Polym. Sci.* **2007,** 105, 1993-1999.

(115) Alexandre, B.; Langevin, D.; Médéric, P.; Aubry, T.; Couderc, H.; Nguyen, Q. T.; Saiter, A.; Marais, S. *J. Membrane Sci.* **2009,** 328, 186-204.

(116) Park, J. H.; Jana, S. C. *Polymer* **2003,** 44, 2091-2100.

(117) Paul, D. R.; Robeson, L. M. *Polymer* **2008,** 49, 3187-3204.

(118) Chen, B.; Evans, J. R. G. *Philos. Mag.* **2005,** 85, 1519 - 1538.

(119) Chrissopoulou, K.; Altintzi, I.; Anastasiadis, S. H.; Giannelis, E. P.; Pitsikalis, M.; Hadjichristidis, N.; Theophilou, N. *Polymer* **2005,** 46, 12440-12451.

(120) Fu, X.; Qutubuddin, S. *Polymer* **2001,** 42, 807-813.

(121) Barus, S.; Zanetti, M.; Lazzari, M.; Costa, L. *Polymer* **2009,** 50, 2595-2600.

(122) Chen, B.; Evans, J. R. G. *Macromolecules* **2006,** 39, 1790-1796.

(123) Chenggang, C.; Tia Benson, T. *J. Polym. Sci. B* **2004,** 42, 3981-3986.

(124) Osman, M. A.; Mittal, V.; Morbidelli, M.; Suter, U. W. *Macromolecules* **2004,** 37, 7250-7257.

(125) Djouani, F.; Herbst, F.; Chehimi, M. M.; Benzarti, K. *Constr. Build. Mater.* **2011,** 25, 424-431.

(126) Swain, S. K.; Isayev, A. I. *Polymer* **2007,** 48, 281-289.

(127) Palza, H.; Yazdani-Pedram, M. *Macromol. Mater. Eng.* **2010,** 295, 48-57.

(128) Tanaka, G.; Goettler, L. A. *Polymer* **2002,** 43, 541-553.

(129) Deshmane, C.; Yuan, Q.; Misra, R. D. K. *Mater .Sci. Eng. A* **2007,** 460-461, 277-287.

(130) Chen, B.; Evans, J. R. G. *Polym. Int.* **2005,** 54, 807-813.

(131) Yuan, Q.; Misra, R. D. K. *Polymer* **2006,** 47, 4421-4433.

(132) Osman, M. A.; Rupp, J. E. P.; Suter, U. W. *Polymer* **2005,** 46, 1653-1660.

(133) Castrillo, P. D.; Olmos, D.; Gonzalez-Benito, J. *J. Appl. Polym. Sci.* **2009,** 111, 2062-2070.

(134) Moore, D. R., In *ESIS Publication*,Moore, D. R.; Elsevier: 2004; Vol. 33, p 201-226.

(135) Chen, B.; Evans, J. R. G. *Polymer* **2008,** 49, 5113-5118.

(136) Chen, B.; Evans, J. R. G. *Soft Matter* **2009,** 5, 3572 - 3584.

(137) Yao, K. J.; Song, M.; Hourston, D. J.; Luo, D. Z. *Polymer* **2002,** 43, 1017-1020.

(138) Ahn, Y. C.; Paul, D. R. *Polymer* **2006,** 47, 2830-2838.

(139) Dasari, A.; Yu, Z.-Z.; Mai, Y.-W. *Macromolecules* **2007,** 40, 123-130.

(140) Cotterell, B.; Chia, J. Y. H.; Hbaieb, K. *Eng. Fract. Mech.* **2007,** 74, 1054-1078.

(141) Lim, S. H.; Dasari, A.; Wang, G. T.; Yu, Z. Z.; Mai, Y. W.; Yuan, Q.; Liu, S. L.; Yong, M. S. *Composites Part B* **2010,** 41, 67-75.

(142) Karger-Kocsis, J., In *ESIS Publication*,Moore, D. R.; Elsevier: 2004; Vol. 33, p 25.

(143) Hosford , W. F., In Cambridge University Press: 2005; p 210-220, 231.

(144) Chen, X.-h.; Mai, Y.-W.; Tong, P.; Zhang, L.-c., Numerical simulation of the essential fracture work method. In *European Structural Integrity Society*, Williams, J. G.; Pavan, A., Eds. Elsevier: 2000; Vol. Volume 27, pp 175-186.

(145) Rice, J. R. *Int. J. Fract. Mech.* **1966,** 2, 369-369.

(146) Rice, J. R. *J. Appl.Mech.* **1968,** 35, 379-&.

(147) Hale, G. E.; Ramsteiner, F., In *ESIS Publication*,Moore, D. R.; Pavan, A.; Williams, J. G.; Elsevier: 2001; Vol. 28, p 123-156.

(148) Williams, J. G., In *ESIS Publication*,Moore, D. R.; Pavan, A.; Williams, J. G.; Elsevier: 2001; Vol. 28, p 119.

(149) Zhou, Z.; Landes, J. D.; Huang, D. D. *Polym. Eng. Sci.* **1994,** 34, 128-134.

(150) Griffith, A. A. *Philos. Trans. R. Soc. London, Ser. A* **1921,** 221, 163-198.

(151) Swei, H.; Crist, B.; Carr, S. H. *Polymer* **1991,** 32, 1440-1446.

(152) Bjerke, T.; Li, Z. H.; Lambros, J. *Int. J. Plast.* **2002,** 18, 549-567.

(153) Rittel, D. *Mech. Mater.* **1999,** 31, 131-139.

(154) Brown, E. N.; Dattelbaum, D. M. *Polymer* **2005,** 46, 3056-3068.

(155) Taylor, G. I.; Quinney, H. *Proc. R. Soc. A* **1934,** 143, 307-326.

(156) Farren, W. S.; Taylor, G. I. *Proc. R. Soc. A* **1925,** 107, 422-451.

(157) Adams, G. W.; Farris, R. J. *J. Polym. Sci. B* **1988,** 26, 433-445.

(158) Wainstein, J.; Fasce, L. A.; Cassanelli, A.; Frontini, P. M. *Eng. Fract. Mech.* **2007,** 74, 2070-2083.

(159) International, A. S. M., In ASM International: Materials Park, OH, 2003; p 212.

(160) Wegner, L. D.; Gibson, L. J. *Int. J. Mech. Sci.* **2001,** 43, 1771-1791.

(161) Tielking, J. T. *Polym. Test.* **1993,** 12, 207-220.

(162) Wu, S. *Polymer* **1985,** 26, 1855-1863.

(163) Muratoglu, O. K.; Argon, A. S.; Cohen, R. E.; Weinberg, M. *Polymer* **1995,** 36, 921-930.

(164) Wilbrink, M. W. L.; Argon, A. S.; Cohen, R. E.; Weinberg, M. *Polymer* **2001,** 42, 10155-10180.

(165) Thio, Y. S.; Argon, A. S.; Cohen, R. E.; Weinberg, M. *Polymer* **2002,** 43, 3661-3674.

(166) Qi, B.; Zhang, Q. X.; Bannister, M.; Mai, Y. W. *Compos. Struct.* **2006,** 75, 514-519.

(167) Yoo, Y.; Cui, L.; Yoon, P. J.; Paul, D. R. *Macromolecules* **2010,** 43, 615-624.

(168) Dasari, A.; Yu, Z. Z.; Yang, M. S.; Zhang, Q. X.; Xie, X. L.; Mai, Y. W. *Compos. Sci. Technol.* **2006,** 66, 3097-3114.

(169) Hashin, Z. *J. Mech. Phys. Solid* **1996,** 44, 1129-1145.

(170) Anderson, T. L., In *Fracture mechanics: fundamentals and applications*,2nd ed.;1995; p 31-.

(171) Bartczak, Z.; Argon, A. S.; Cohen, R. E.; Weinberg, M. *Polymer* **1999,** 40, 2331-2346.

(172) Bartczak, Z.; Argon, A. S.; Cohen, R. E.; Weinberg, M. *Polymer* **1999,** 40, 2347-2365.

(173) Bafna, A.; Beaucage, G.; Mirabella, F.; Mehta, S. *Polymer* **2003,** 44, 1103-1115.

(174) Christensen, R. M. *J. Eng. Mater. Technol.* **1979,** 101, 299-303.

(175) Gibson, L. J.; Ashby, M. F., In *Cellular solids: structure and properties* Cambridge University Press: Cambridge, 1997; p 36.

(176) Mori, T.; Tanaka, K. *Acta Metall.* **1973,** 21, 571-574.

(177) Tandon, G. P.; Weng, G. J. *Polym. Compos.* **1984,** 5, 327-333.

(178) Halpin, J. C.; Kardos, J. L. *Polym. Eng. Sci.* **1976,** 16, 344-352.

(179) Wang, J.; Pyrz, R. *Compos. Sci. Technol.* **2004,** 64, 935-944.

(180) Chen, B.; Evans, J. R. G. *Macromolecules* **2006,** 39, 747-754.

(181) Wang, J.; Pyrz, R. *Compos. Sci. Technol.* **2004,** 64, 925-934.

(182) La Mantia, F. P.; Lo Verso, S.; Dintcheva, N. T. *Macromolec. Mater. Eng.* **2002,** 287, 909-914.

(183) Zhang, Y. C.; Pan, E. L. *J. Appl. Polym. Sci.* **2003,** 87, 2120-2129.

(184) Zhang, J.; Gupta, R. K.; Wilkie, C. A. *Polymer* **2006,** 47, 4537-4543.

(185) Tjong, S. C.; Bao, S. P. *Compos. Sci. Technol.* **2007,** 67, 314-323.

(186) Tanniru, M.; Yuan, Q.; Misra, R. D. K. *Polymer* **2006,** 47, 2133-2146.

(187) García-López, D.; Gobernado-Mitre, I.; Merino, J. C.; Pastor, J. M. *Polym. Bull.* **2007,** 59, 667-676.

(188) Yuan, Q.; Shah, J. S.; Bertrand, K. J.; Misra, R. D. K. *Macromol. Mater. Eng.* **2009,** 294, 141-151.

(189) Kim, D. H.; Fasulo, P. D.; Rodgers, W. R.; Paul, D. R. *Polymer* **2007,** 48, 5308-5323.

(190) Zhao, C. G.; Qin, H. L.; Gong, F. L.; Feng, M.; Zhang, S. M.; Yang, M. S. *Polym. Degrad. Stab.* **2005,** 87, 183-189.

(191) Deshmane, C.; Yuan, Q.; Perkins, R. S.; Misra, R. D. K. *Mater .Sci. Eng. A* **2007,** 458, 150-157.

(192) Fornes, T. D.; Yoon, P. J.; Hunter, D. L.; Keskkula, H.; Paul, D. R. *Polymer* **2002,** 43, 5915-5933.

(193) Sinha Ray, S.; Yamada, K.; Okamoto, M.; Fujimoto, Y.; Ogami, A.; Ueda, K. *Polymer* **2003,** 44, 6633-6646.

(194) Sinha Ray, S.; Yamada, K.; Okamoto, M.; Ogami, A.; Ueda, K. *Chemistry of Materials* **2003,** 15, 1456-1465.

(195) Ludueña, L. N.; Alvarez, V. A.; Vazquez, A. *Mater. Sci. Eng. A* **2007,** 460-461, 121-129.

(196) Saha, M. C.; Kabir, M. E.; Jeelani, S. *Mater. Sci. Eng., A* **2008,** 479, 213-222.

(197) Triantafyllidis, K. S.; LeBaron, P. C.; Pinnavaia, T. J. *J. Solid State Chem.* **2002,** 167, 354-362.

(198) Patro, T. U.; Harikrishnan, G.; Misra, A.; Khakhar, D. V. *Polym. Eng. Sci.* **2008,** 48, 1778-1784.

(199) Zilg, C.; Mülhaupt, R.; Finter, J. *Macromol. Chem. Phys.* **1999,** 200, 661-670.

(200) Yu, Z.-Z.; Yan, C.; Yang, M.; Mai, Y.-W. *Polym. Int.* **2004,** 53, 1093-1098.

(201) Dasari, A.; Lim, S.-H.; Yu, Z.-Z.; Mai, Y.-W. In *Some Issues on Structure-Properties of Polymer Nanocomposites*, International Conference onNanoscience and Nanotechnology, 3-7 July, 2006; 2006.

(202) González, I.; Eguiazábal, J. I.; Nazábal, J. *Compos. Sci.Technol.* **2006,** 66, 1833-1843.

(203) Zhu, Z. K.; Yang, Y.; Yin, J.; Wang, X. Y.; Ke, Y. C.; Qi, Z. N. *J. Appl. Polym. Sci.* **1999,** 73, 2063-2068.

(204) Sinha Ray, S.; Yamada, K.; Okamoto, M.; Ogami, A.; Ueda, K. *Chem. Mater.* **2003,** 15, 1456-1465.

(205) Pannirselvam, M.; Genovese, A.; Jollands, M. C.; Bhattacharya, S. N.; Shanks, R. A. *Express Polym. Lett.* **2008,** 2, 429-439.

(206) Sun, L.; Boo, W. J.; Clearfield, A.; Sue, H. J.; Pham, H. Q. *J. Membrane Sci.* **2008,** 318, 129-136.

(207) Gardebien, F.; Bredas, J.-L.; Lazzaroni, R. *J. Phys. Chem. B* **2005,** 109, 12287-12296.

(208) Wang, Z. F.; Wang, B.; Qi, N.; Zhang, H. F.; Zhang, L. Q. *Polymer* **2005,** 46, 719-724.

(209) Jiang, T.; Wang, Y.-h.; Yeh, J.-t.; Fan, Z.-q. *Eur. Polym. J.* **2005,** 41, 459-466.

(210) Mehrabzadeh, M.; Kamal, M. R. In *Melt processing of PA-66/clay, HDPE/clay and HDPE/PA-66/clay nanocomposites*, 2nd International Symposium on Polymeric Nanocomposites, Boucherville, Canada, Oct 06-08, 2003; John Wiley & Sons Inc: Boucherville, CANADA, 2003; pp 1152-1161.

(211) Tang, Y.; Hu, Y.; Song, L.; Zong, R.; Gui, Z.; Chen, Z.; Fan, W. *Polym. Degrad. Stab.* **2003,** 82, 127-131.

(212) Chen, K.; Wilkie, C. A.; Vyazovkin, S. *J Phys. Chem. B* **2007,** 111, 12685-12692.

(213) Xie, W.; Gao, Z.; Pan, W.-P.; Hunter, D.; Singh, A.; Vaia, R. *Chem. Mater.* **2001,** 13, 2979-2990.

(214) Jang, B. N.; Wilkie, C. A. *Polymer* **2005,** 46, 2933-2942.

(215) Rabek, J. F.; Ranby, B. *Polym. Eng. Sci.* **1975,** 15, 40-43.

(216) Su, S.; Wilkie, C. A. *Polym. Degrad. Stabil.* **2004,** 83, 347-362.

(217) Cui, L.; Khramov, D. M.; Bielawski, C. W.; Hunter, D. L.; Yoon, P. J.; Paul, D. R. *Polymer* **2008,** 49, 3751-3761.

(218) Huaili, Q.; Zhenguang, Z.; Meng, F.; Fangling, G.; Shimin, Z.; Mingshu, Y. *J. Polym. Sci. B* **2004,** 42, 3006-3012.

(219) Zanetti, M.; Camino, G.; Thomann, R.; Mülhaupt, R. *Polymer* **2001,** 42, 4501-4507.

(220) Samal, S. K.; Nayak, S. K.; Mohanty, S. *J. Thermoplast. Compos. Mater.* **2008,** 21, 243-263.

(221) Costache, M. C.; Wang, D.; Heidecker, M. J.; Manias, E.; Wilkie, C. A. *Polym. Adv.Technol.* **2006,** 17, 272-280.

(222) Kiliaris, P.; Papaspyrides, C. D.; Pfaendner, R. *Polym. Degrad. Stab.* **2009,** 94, 389-396.

(223) Cho, J. W.; Paul, D. R. *Polymer* **2001,** 42, 1083-1094.

(224) Modesti, M.; Lorenzetti, A. *Polym. Degrad. Stabil.* **2002,** 78, 341-347.

(225) Chattopadhyay, D. K.; Webster, D. C. *Prog. Polym. Sci.* **2009,** 34, 1068-1133.

(226) Cai, Y. B.; Hu, Y.; Song, L.; Tang, Y.; Yang, R.; Zhang, Y. P.; Chen, Z. Y.; Fan, W. C. *J. Appl. Polym. Sci.* **2006,** 99, 1320-1327.

(227) Gilman, J. W.; Jackson, C. L.; Morgan, A. B.; Harris, R.; Manias, E.; Giannelis, E. P.; Wuthenow, M.; Hilton, D.; Phillips, S. H. *Chem. Mater.* **2000,** 12, 1866-1873.

(228) Modesti, M.; Lorenzetti, A.; Besco, S.; Hreja, D.; Semenzato, S.; Bertani, R.; Michelin, R. A. *Polym. Degrad. Stab.* **2008,** 93, 2166-2171.

(229) Filippone, G.; Dintcheva, N. T.; Acierno, D.; La Mantia, F. P. *Polymer* **2008,** 49, 1312-1322.

(230) Ou, B.; Li, D.; Liu, Y. *Compos. Sci. Technol.* **2009,** 69, 421-426.

(231) Sinha Ray, S.; Pouliot, S.; Bousmina, M.; Utracki, L. A. *Polymer* **2004,** 45, 8403-8413.

(232) Lipatov, Y. S., In *Polymer reinforcement*,ChemTec Publishing Toronto, 1995; p 314.

(233) Utracki, L. A., In *Polymer blends handbook*, Springer: 2002; Vol. 1.

(234) Tiwari, R. R.; Paul, D. R. *Polymer* **2011,** 52, 1141-1154.

(235) Hua, W.; Changchun, Z.; Mark, E.; Lee, L. J.; Kurt, W. K. *Polym. Eng. Sci.* **2001,** 41, 2036-2046.

(236) Wang, Y.; Zhang, Q.; Fu, Q. *Macromol. Rapid Comm.* **2003,** 24, 231-235.

(237) Zhu, Y.; Xu, Y.; Tong, L.; Xu, Z.; Fang, Z. *J. Appl. Polym. Sci.* **2008,** 110, 3130-3139.

(238) Chen, G.-X.; Kim, H.-S.; Kim, E.-S.; Yoon, J.-S. *Polymer* **2005,** 46, 11829-11836.

(239) Torres-Sanchez, C.; Corney, J. R. *Ultrasonics Sonochemistry* **2008,** 15, 408-415.

(240) Gibson, L. J.; Ashby, M. F., Cellular solids: structure and properties In *Cellular solids: structure and properties* 2nd ed.; Cambridge University Press: Cambridge, 1997; pp 38-197.

(241) Gibson, L. J.; Ashby, M. F. *Proc. R. Soci. A* **1982,** 382, 43-59.

(242) Mills, N. J., In *Polymer Foams Handbook - Engineering and Biomechanics Applications and Design Guide*,Elsevier: Oxford, 2007.

(243) Gibson, L. J.; Ashby, M. F., In *Cellular solids: structure and properties* 2nd ed.;Cambridge University Press: Cambridge, 1997.

(244) Barsema, J. N.; Bostoen, C. L.; Jansen, R. H. S.; Mulder, M. H. V.; Nauta, W. J.; Steeman, P. A. M.; Wessling, M. *Macromolecules* **2003,** 36, 6817-6823.

(245) Mori, T.; Hayashi, H.; Okamoto, M.; Yamasaki, S.; Hayami, H. *Compos. Part A* **2009,** 40, 1708-1716.

(246) Nam, P. H.; Maiti, P.; Okamoto, M.; Kotaka, T.; Nakayama, T.; Takada, M.; Ohshima, M.; Usuki, A.; Hasegawa, N.; Okamoto, H. *Polym. Eng. Sci.* **2002,** 42, 1907-1918.

(247) Arora, K. A.; Lesser, A. J.; McCarthy, T. J. *Macromolecules* **1998,** 31, 4614-4620.

(248) Diaz, C. A.; Matuana, L. M. *J. Vinyl Addit.Technol.* **2009,** 15, 211-218.

(249) Zhang, Q.; Xanthos, M.; Dey, S. K. *J. Cell. Plast.* **2001,** 37, 284-292.

(250) DiMaio, E.; Mensitieri, G.; Iannace, S.; Nicolais, L.; Li, W.; Flumerfelt, R. W. *Polym. Eng. Sci.* **2005,** 45, 432-441.

(251) Liu, H.; Han, C.; Dong, L. *J. Appl. Polym. Sci.* **2010,** 115, 3120-3129.

(252) Lee, S. T.; Kareko, L.; Jun, J. *J. Cell. Plast.* **2008,** 44, 293-305.

(253) Sims, G. L. A.; O'Connor, C., Modification of azodicarbonamide decomposition characteristics: interface with base polymer and process parameters. In *Blowing Agent Systems: Formulations and Processing*, Limited, R. T., Ed. iSmithers Rapra Publishing: Shawbury, Shrewsbury, UK, 1998; pp 1-7.

(254) Sims, G. L. A.; Sirithongtaworn, W. *Cell. Polym.* **1997,** 16, 271-283.

(255) Quinn, S. *Plast. Add. Compound.* **2001,** 3, 16-21.

(256) Sorrentino, L.; Aurilia, M.; Iannace, S. *Polym. Test.* **2007,** 26, 878-885.

(257) Jo, C.; Naguib, H. E. *Polymer* **2007,** 48, 3349-3360.

(258) Han, X. M.; Zeng, C. C.; Lee, L. J.; Koelling, K. W.; Tomasko, D. L. *Polym. Eng. Sci.* **2003,** 43, 1261-1275.

(259) Masaki, M.; Yasuhito, I.; Suprakas Sinha, R.; Masami, O.; Katsuhiko, H. *Macromol. Mater. Eng.* **2003,** 288, 543-548.

(260) Cao, X.; Lee, L. J.; Widya, T.; Macosko, C. *Polymer* **2005,** 46, 775-783.

(261) Harikrishnan, G.; Patro, T. U.; Khakhar, D. V. *Ind. Eng. Chem. Res.* **2006,** 45, 7126-7134.

(262) Thirumal, M.; Khastgir, D.; Singha, N. K.; Manjunath, B. S.; Naik, Y. P. *J. Macromol. Sci. Part A* **2009,** 46, 704-712.

(263) Tu, Z. H.; Shim, V. P. W.; Lim, C. T. *Int. J. Solid Struct.* **2001,** 38, 9267-9279.

(264) Di, Y. W.; Iannace, S.; Di Maio, E.; Nicolais, L. *J. Polym. Sci. B* **2005,** 43, 689-698.

(265) Hao, L.; Changyu, H.; Lisong, D. *J. Appl. Polym. Sci.* **2009,** 115, 3120-3129.

(266) Lee, S. T.; Lee, K. *Adv. Polym. Techol.* **2000,** 19, 87-96.

(267) Okamoto, M.; Nam, P. H.; Maiti, P.; Kotaka, T.; Nakayama, T.; Takada, M.; Ohshima, M.; Usuki, A.; Hasegawa, N.; Okamoto, H. *Nano Letters* **2001,** 1, 503-505.

(268) Hilyard, N. C.; Young, J., Introduction. In *Mechanics of cellular plastics* Hilyard, N. C., Ed. Appiled Science Publishers Ltd. : London, 1982; p 21.

(269) Brezny, R.; Green, D. J. *Acta Metallurgica et Materialia* **1990,** 38, 2517-2526.

(270) Roberts, A. P.; Garboczi, E. J. *J. Mech. Phys. Solid* **2002,** 50, 33-55.

(271) Diebles, S., Micropolar mixture models on the basis of the Theory of Porous Media. In *Porous Media: Theory, Experiments and Numerical Applications*, Ehlers, W.; Bluhm, J., Eds. Springer: Berlin, 2002; p 121.

(272) PEMRG *The Compelling Facts About Plastics - An analysis of European plastics production, demand and recovery for 2008*; Plastics Europe: Brussels, 2009.

(273) Sinha Ray, S.; Bousmina, M. *Progr. Mater. Sci.* **2005,** 50, 962-1079.

(274) Vilaplana, F.; Karlsson, S. *Macromolec. Mater. Eng.* **2008,** 293, 274-297.

(275) PlasticsEurope.com Applied Markets information. http://www.plasteurope.com/news/PLASTICS_MARKETS_t214609 (October 28),

(276) Kartalis, C. N.; Papaspyrides, C. D.; Pfaendner, R.; Hoffmann, K.; Herbst, H. *Polym. Eng. Sci.* **2001,** 41, 771-781.

(277) Hamaya, S. *Conservation & Recycling* **1981,** 4, 185-192.

(278) Xu, X.; Ding, Y.; Qian, Z.; Wang, F.; Wen, B.; Zhou, H.; Zhang, S.; Yang, M. *Polym. Degrad. Stab.* **2009,** 94, 113-123.

(279) Sánchez-Soto, M.; Rossa, A.; Sánchez, A. J.; Gámez-Pérez, J. *Waste Manag.* **2008,** 28, 2565-2573.

(280) Alexandre, M.; Dubois, P. *Mat. Sci. Eng. R* **2000,** 28, 1-63.

(281) Esposito Corcione, C.; Manera, M. G.; Maffezzoli, A.; Rella, R. *Mater. Sci. Eng., C* **2009,** 29, 1798-1802.

(282) Hassan, M. K.; Abou-Hussein, R.; Zhang, X. J.; Mark, J. E.; Noda, I. *Mol. Cryst. Liq. Cryst.* **2006,** 447, 341-362.

(283) Chen, T. K.; Tien, Y. I.; Wei, K. H. *Polymer* **2000,** 41, 1345-1353.

(284) Liu, Z.; Scanlon, M. G. *J. Mater. Sci. Lett.* **2004,** 22, 547-548.

(285) Hilyard, N. C.; Cunninghan, A., Physical behaviour of polymeric foams – an overview. In *Low density cellular plastics: physical basis of behaviour*, Hilyard, N. C.; Cunninghan, A., Eds. Chapman & Hall: London, 1994; p 13.

(286) Mills, N. J., Polymer Foams Handbook - Engineering and Biomechanics Applications and Design Guide. In *Polymer Foams Handbook - Engineering and Biomechanics Applications and Design Guide*, Elsevier: Oxford, 2007; pp 153-270.

(287) Gent, A. N.; Thomas, A. G. *Rubber Chem. Technol.* **1963,** 36, 597-610.

(288) Renz, R.; Ehrenstein, G. W. *Cell. Polym.* **1982,** 1, 5-13.

(289) Mills, N. J.; Zhu, H. X. *J. Mech. Phys. Solid* **1999,** 47, 669-695.

(290) McCullough, K. Y. G.; Fleck, N. A.; Ashby, M. F. *Acta Mater.* **1999,** 47, 2323-2330.

(291) Liu, Z.; Chuah, C. S. L.; Scanlon, M. G. *Acta Mater.* **2003,** 51, 365-371.

(292) Roberts, A. P.; Garboczi, E. J. *Acta Mater.* **2001,** 49, 189-197.

(293) Christensen, R. M. *J. Mech. Phys. Solid* **1986,** 34, 563-578.

(294) Choi, J. B.; Lakes, R. S. *Int. J. Mech. Sci.* **1995,** 37, 51-59.

(295) Hagiwara, H.; Green, D. J. *J. Am. Cer. Soc.* **1987,** 70, 811-815.

(296) Dement'ev, A. G.; Tarakanov, O. G. *Mech. Compos. Mater.* **1970,** 6, 744-749.

(297) Kraynik, A. M.; Warren, W. E., The elastic behaviour of low density cellular plastics In *Low density cellular plastics: physical basis of behaviour*, Hilyard, N. C.; Cunninghan, A., Eds. Chapman & Hall: London, 1994; p 188.

(298) Mondal, P.; Khakhar, D. V. *J. Appl. Polym. Sci.* **2007,** 103, 2802-2809.

(299) Günister, E.; Çobanoglu, I.; Isçi, S. *Prog. Org. Coat.* **2009,** 65, 357-361.

(300) Chavarria, F.; Paul, D. R. *Polymer* **2006,** 47, 7760-7773.

(301) Chen, B.; Evans, J. R. G. *Carbohydr. Polym.* **2005,** 61, 455-463.

(302) Reinholdt, M. X.; Kirkpatrick, R. J.; Pinnavaia, T. J. *J. Phys. Chem. B* **2005,** 109, 16296-16303.

(303) Greenwell, H. C.; Bowden, A. A.; Chen, B. Q.; Boulet, P.; Evans, J. R. G.; Coveney, P. V.; Whiting, A. *J. Mater. Chem.* **2006,** 16, 1082-1094.

(304) Theng, B. K. G., Formation and properties of clay-polymer complexes In *Formation and properties of clay-polymer complexes* Elsevier Scientific Publishing Company: Amsterdam, 1979; Vol. 9, p 84.

(305) Vaia, R. A.; Jandt, K. D.; Kramer, E. J.; Giannelis, E. P. *Chem. Mater.* **1996,** 8, 2628-2635.

(306) Manias, E.; Touny, A.; Wu, L.; Strawhecker, K.; Lu, B.; Chung, T. C. *Chem. Mater* **2001,** 13, 3516-3523.

(307) Greenwell, H. C.; Bowden, A. A.; Chen, B. Q.; Boulet, P.; Evans, J. R. G.; Coveney, P. V.; Whiting, A. *J. Membrane Sci.* **2006,** 16, 1082-1094.

(308) Greenwell, H. C.; Harvey, M. J.; Boulet, P.; Bowden, A. A.; Coveney, P. V.; Whiting, A. *Macromolecules* **2005,** 38, 6189-6200.

(309) Boulet, P.; Bowden, A. A.; Coveney, P. V.; Whiting, A. *J. Mater. Chem.* **2003,** 13, 2540-2550.

(310) Widya, T.; Macosko, C. W. *J. Macromol. Sci., Phys.* **2005,** B44, 897-908.

(311) Xu, Z. B.; Tang, X. L.; Gu, A. J.; Fang, Z. P. *J. Appl. Polym. Sci.* **2007,** 106, 439-447.

(312) Ashby, M. F. *Metall. Trans. A* **1983,** 14, 1755-1769.

(313) Gibson, L. J.; Ashby, M. F. *Proc. Royal Soc. London. Series A* **1982,** 382, 43-59.

(314) Patro, T. U.; Harikrishnan, G.; Misra, A.; Khakhar, D. V. *Polym. Eng. Sci.* **2008,** 48, 1778-1784.

(315) Saint-Michel, F.; Chazeau, L.; Cavaillé, J.-Y.; Chabert, E. *Compos. Sci. Technol.* **2006,** 66, 2700-2708.

(316) Frydrych, M.; Wan, C.; Stengler, R.; O'Kelly, K. U.; Chen, B. *J. Mater. Chem.* **2011,** 21, 9103-9111.

(317) Liu, S.; Jeannes, S.; Chen, B. *J Biomat Tissue Eng* **2011,** 1, 60-67.

(318) Federle, T. W.; Barlaz, M. A.; Pettigrew, C. A.; Kerr, K. M.; Kemper, J. J.; Nuck, B. A.; Schechtman, L. A. *Biomacromolecules* **2002,** 3, 813-822.

(319) Queiruga, D.; Walther, G.; González-Benito, J.; Spengler, T. *Waste Manage.* **2008,** 28, 181-190.

(320) Wei, M.; Shuai, X.; Tonelli, A. E. *Biomacromolecules* **2003,** 4, 783-792.

(321) Sangwan, P.; Way, C.; Wu, D.-Y. *Macromol. Biosci.* **2009,** 9, 677-686.

(322) Mangiacapra, P.; Raimondo, M.; Tammaro, L.; Vittoria; Malinconico, M.; Laurienzo, P. *Biomacromolecules* **2007,** 8, 773-779.

(323) Ozkoc, G.; Kemaloglu, S.; Quaedflieg, M. *Polym. Compos.* **2010,** 31, 674-683.

(324) Marrazzo, C.; Di Maio, E.; Iannace, S. *J. Cell. Plast.* **2007,** 43, 123-133.

(325) Ding, M.; Li, J.; Fu, X.; Zhou, J.; Tan, H.; Gu, Q.; Fu, Q. *Biomacromolecules* **2009,** 10, 2857-2865.

(326) Robledo-Ortiz, J. R.; Zepeda, C.; Gomez, C.; Rodrigue, D.; González-Núñez, R. *Polym. Test.* **2008,** 27, 730-735.

(327) Kiziltas, A.; Gardner, D. J.; Han, Y.; Yang, H.-S. *Thermochim. Acta* **2011,** 519, 38-43.

(328) De Kesel, C.; Lefèvre, C.; Nagy, J. B.; David, C. *Polymer* **1999,** 40, 1969-1978.

(329) Kuila, B. K.; Nandi, A. K. *Macromolecules* **2004,** 37, 8577-8584.

(330) Singhal, R.; Datta, M. *Polym. Compos.* **2009,** 30, 887-890.

(331) Socrates, G., In Wiley: Chichester, 2001; p 35.

(332) Chen, G. M.; Liu, S. H.; Chen, S. J.; Qi, Z. N. *Macromol. Chem. Phys.* **2001,** 202, 1189-1193.

(333) Dodds, W. S.; Stutzman, L. F.; Sollami, B. J. *Ind. Eng. Chem. Chem. Eng. Data Series* **1956,** 1, 92-95.

(334) Lu, C.; Mai, Y.-W. *Phys. Rev. Lett.* **2005,** 95, 088303.

(335) Kawasumi, M.; Hasegawa, N.; Kato, M.; Usuki, A.; Okada, A. *Macromolecules* **1997,** 30, 6333-6338.

(336) Mills, N. J., In *Polymer Foams Handbook - Engineering and Biomechanics Applications and Design Guide*,Elsevier: Oxford, 2007; p 153-270.

(337) Baker, S. C.; Rohman, G.; Southgate, J.; Cameron, N. R. *Biomaterials* **2009,** 30, 1321-1328.

(338) Liufu, S.-C.; Xiao, H.-N.; Li, Y.-P. *Polym. Degrad. Stab.* **2005,** 87, 103-110.

(339) Feyz, E.; Jahani, Y.; Esfandeh, M. *Macromolec.Symp.* **2011,** 298, 130-137.

(340) Chen, B. Polymer-clay nanocomposites. PhD thesis, The University of London, 2005.

(341) Andrews, E.; Sanders, W.; Gibson, L. J. *Mater. Sci. Eng., A* **1999,** 270, 113-124.

(342) Simone, A. E.; Gibson, L. J. *Acta Mater.* **1998,** 46, 2139-2150.

(343) Weaire, D.; Phelan, R. *J. Phys.-Condens. Mat.* **1996,** 8, 9519-9524.

(344) Clutton, E. Q.; Rice, G. N. *Cell. polym.* **1992,** 11, 429-449.

(345) Istrate, O. M.; Chen, B. *Soft Matter* **2011,** 7, 1840-1848.

(346) Ruike, M.; Kasu, T.; Setoyama, N.; Suzuki, T.; Kaneko, K. *J. Phys. Chem.* **1994,** 98, 9594-9600.

(347) Mignoni, M. L.; Silva, J. V. M.; de Souza, M. O.; Mauler, R. d. S.; de Souza, R. F.; Bernardo-Gusmão, K. *J. Appl. Polym. Sci.* **2011,** 122, 2159-2165.

(348) Maneshi, A.; Soares, J. B. P.; Simon, L. C. *Macromol. Chem. Phys.* **2011,** 212, 2017-2028.

(349) Sivalingam, G.; Natarajan, V.; Sarma, K. R.; Parasuveera, U. *Ind. Eng. Chem. Res.* **2008,** 47, 8940-8946.

(350) Beijer, J. G. J.; Spoormaker, J. L. *Polymer* **2000,** 41, 5443-5449.

(351) Istrate, O. M.; Gunning, M. A.; Higginbotham, C. L.; Chen, B. *J. Polym. Sci. B* **2012,** 50, 431-441.

(352) Shi, H.; Lan, T.; Pinnavaia, T. J. *Chem. Mat.* **1996,** 8, 1584-1587.

(353) Lee, Y. H.; Park, C. B.; Sain, M.; Kontopoulou, M.; Zheng, W. *J. Appl. Polym. Sci.* **2007,** 105, 1993-1999.

(354) Minkova, L.; Peneva, Y.; Tashev, E.; Filippi, S.; Pracella, M.; Magagnini, P. *Polym. Test.* **2009,** 28, 528-533.

(355) Xu, X.; Ding, Y.; Wang, F.; Wen, B.; Zhang, J.; Zhang, S.; Yang, M. *Polym. Compos.* **2010,** 31, 825-834.

(356) Gilman, J. W. *Appl. Clay Sci.* **1999,** 15, 31-49.

(357) Turhan, Y.; Dogan, M.; Alkan, M. *Ind. Eng. Chem. Res.* 49, 1503-1513.

(358) Sahebian, S.; Zebarjad, S. M.; Khaki, J. V.; Sajjadi, S. A. *J. Mater. Process. Technol.* **2009,** 209, 1310-1317.

(359) Hashin, Z.; Shtrikman, S. *J. Mech.Phys.Solid* **1963,** 11, 127-140.

(360) Altun, S.; Yasar, F.; Oner, C. *Int. J. Eng. Res. Develop.* **2010,** 2, 2-5.

(361) Nightingale, K.; McAleavey, S.; Trahey, G. *Ultras. Med. Bio.* **2003,** 29, 1715-1723.

(362) Christensen, R. M., In *Mechanics of composite materials*, John Wiley: New York, 1979; p 41-47.

(363) Ishihara, N.; Seimiya, T.; Kuramoto, M.; Uoi, M. *Macromolecules* **1986,** 19, 2464-2465.

(364) Sepehr, M.; Utracki, L. A.; Zheng, X.; Wilkie, C. A. *Polymer* **2005,** 46, 11557-11568.

(365) Zhu, Y.; Ma, H. Y.; Tong, L. F.; Fang, Z. P. *J. Zhejiang Univ.-Sc. A* **2008,** 9, 1614-1620.

(366) Manitiu, M.; Bellair, R. J.; Horsch, S.; Gulari, E.; Kannan, R. M. *Macromolecules* **2008,** 41, 8038-8046.

(367) Zhu, J.; Morgan, A. B.; Lamelas, F. J.; Wilkie, C. A. *Chem. Mat.* **2001,** 13, 3774-3780.

(368) Kuila, B. K.; Nandi, A. K. *Macromolecules* **2004,** 37, 8577-8584.

(369) Macêdo-Fonsêca, J. C.; Silva, I. S.; Souto-Maior, R. M. *Synth. Met.* **2009,** 159, 2215-2218.

(370) Singhal, R.; Datta, M. *Polym. Compos.* **2009,** 30, 887-890.

(371) Istrate, O. M.; Chen, B. *J. Appl. Polym. Sci.* **2012,** DOI: 10.1002/app.36336.

(372) Zanetti, M.; Camino, G.; Reichert, P.; Mülhaupt, R. *Macromol. Rapid Commun.* **2001,** 22, 176-180.

(373) Lyons, J. G.; Holehonnur, H.; Devine, D. M.; Kennedy, J. E.; Geever, L. M.; Blackie, P.; Higginbotham, C. L. *Mat. Chem. Phys.* **2007,** 103, 419-426.

(374) Cui, L.; Tarte, N. H.; Woo, S. I. *Macromolecules* **2008,** 41, 4268-4274.

(375) Wang, X.; Tao, F.; Xue, G.; Zhu, J.; Chen, T.; Sun, P.; Winter, H. H.; Shi, A.-C. *Macromol. Mater. Eng.* **2009,** 294, 190-195.

(376) Tseng, C.-R.; Wu, J.-Y.; Lee, H.-Y.; Chang, F.-C. *J. Appl. Polym. Sci.* **2002,** 85, 1370-1377.

(377) Strawhecker, K. E.; Manias, E. *Chem. Mat.* **2000,** 12, 2943-2949.

(378) Pack, S.; Kashiwagi, T.; Cao, C.; Korach, C. S.; Lewin, M.; Rafailovich, M. H. *Macromolecules* **2010,** 43, 5338-5351.

(379) Basara, C.; Yilmazer, U.; Bayram, G. *J. Appl. Polym. Sci.* **2005,** 98, 1081-1086.

(380) Shi, Y.; Peterson, S.; Sogah, D. Y. *Chem. Mat.* **2007,** 19, 1552-1564.

(381) Chen, G.-X.; Choi, J. B.; Yoon, J. S. *Macromol. Rapid Commun.* **2005,** 26, 183-187.

(382) Chen, G.-X.; Kim, H.-S.; Shim, J.-H.; Yoon, J.-S. *Macromolecules* **2005,** 38, 3738-3744.

(383) Prasad, M.; Kopycinska, M.; Rabe, U.; Arnold, W. *Geophys. Res. Lett.* **2002,** 29.

(384) Wang, H.-W.; Chang, K.-C.; Yeh, J.-M.; Liou, S.-J. *J. Appl. Polym. Sci.* **2004,** 91, 1368-1373.

(385) Gilman, J. W.; Awad, W. H.; Davis, R. D.; Shields, J.; Harris, R. H.; Davis, C.; Morgan, A. B.; Sutto, T. E.; Callahan, J.; Trulove, P. C.; DeLong, H. C. *Chem. Mat.* **2002,** 14, 3776-3785.

(386) Quinn, S. *Plast. Addit. Compound.* **2001,** 3, 16-21.

(387) Dai, X.; Xu, J.; Guo, X.; Lu, Y.; Shen, D.; Zhao, N.; Luo, X.; Zhang, X. *Macromolecules* **2004,** 37, 5615-5623.

(388) Lu, H.; Nutt, S. *Macromolecules* **2003,** 36, 4010-4016.

(389) Park, J.; Jana, S. C. *Macromolecules* **2003,** 36, 8391-8397.

(390) Zhang, X.; Loo, L. S. *Macromolecules* **2009,** 42, 5196-5207.

(391) Meng, J.; Hu, X. *Polymer* **2004,** 45, 9011-9018.

(392) van Es, M.; Feng, X. Q.; van Turnhout, J.; van der Giessen, E., Comparing polymer-clay nanocomposites with conventional composites using composite modelling. In *Specialty Polymer Additives - Principles and Applications* Al-Malaika, S.; Golovoy, A.; Wilkie, C. A., Eds. Blackwell Science: Oxford, 2001; pp 391-413.

(393) Li, H.; Jia, Y.; Mamtimin, G.; Jiang, W.; An, L. *Mater. Sci. Eng. A* **2006,** 425, 178-184.

(394) Thomas, S. P.; Thomas, S.; Bandyopadhyay, S. *Composites Part A* **2009,** 40, 36-44.

(395) Wallace, W. E.; Fischer, D. A.; Efimenko, K.; Wu, W. L.; Genzer, J. *Macromolecules* **2001,** 34, 5081-5082.

(396) Sakaguchi, R. L.; Wiltbank, B. D.; Murchison, C. F. *Dent. Mater.* **2004,** 20, 397-401.

(397) Wong, C. P.; Bollampally, R. S. *J. Appl. Polym. Sci.* **1999,** 74, 3396-3403.

(398) Bower, D. I., In *An introduction to polymer physics*,Cambridge University Press: Cambridge, 2002.

(399) Christensen, R. M. *J. Mech. Phys. Solid* **1990,** 38, 379-404.

(400) Qiu, Y. P.; Weng, G. J. *Int. J. Eng. Sci.* **1990,** 28, 1121-1137.

(401) Lielens, G.; Pirotte, P.; Couniot, A.; Dupret, F.; Keunings, R. *Compos.A:* **1998,** 29, 63-70.

(402) Tandon, G. P.; Weng, G. J. *Compos. Sci. Technol.* **1986,** 27, 111-132.

(403) Feynman, R. P. *Eng. Sci.* **1960,** 23, 22-36.

(404) Hasan, M. M.; Zhou, Y.; Mahfuz, H.; Jeelani, S. *Mat. Sci. Eng. A* **2006,** 429, 181-188.

(405) Zhao, X.-y. *Polym. Inter.* **2009,** 58, 469-474.

(406) Hatfield, G. R.; Glans, J. H.; Hammond, W. B. *Macromolecules* **1990,** 23, 1654-1658.

(407) Wu, T.-M.; Liao, C.-S. *Macromol. Chem. Phys.* **2000,** 201, 2820-2825.

(408) Li, Y.; Goddard, W. A. *Macromolecules* **2002,** 35, 8440-8455.

(409) Zhang, Y.; Zhang, Y.; Liu, S.; Huang, A.; Chi, Z.; Xu, J.; Economy, J. *J. Appl. Polym. Sci.* **2011,** 120, 1885-1891.

(410) Fornes, T. D.; Paul, D. R. *Polymer* **2003,** 44, 3945-3961.

(411) Ramesh, C. *Macromolecules* **1999,** 32, 3721-3726.

(412) Yebra-Rodriguez, A.; Alvarez-Lloret, P.; Rodriguez-Navarro, A. B.; Martin-Ramos, J. D.; Cardell, C. *Mater. Lett.* **2009,** 63, 1159-1161.

(413) Geddem, U. W., Crystallization kinetics. In *Polymer physics*, Chapman & Hall: London, 1995; pp 169-197.

(414) Lin, C. C. *Polym. Eng. Sci.* **1983,** 23, 113-116.

(415) Di Lorenzo, M. L.; Cimmino, S.; Silvestre, C. *Macromolecules* **2000,** 33, 3828-3832.

(416) Lauritze.J; Hoffman, J. D. *J. Appl. Phys.* **1973,** 44, 4340-4352.

(417) Jiang, T.; Liu, M.; Fu, P.; Wang, Y.; Fang, Y.; Zhao, Q. *Polym. Eng. Sci.* **2009,** 49, 1366-1374.

(418) Patki, R.; Mezghani, K.; Phililips, P. J., Crystallization kinetics of polymers. In *Physical properties of polymers handbook*, 2nd ed.; Mark, J. E., Ed. Springer: 2007; p 626.

(419) Zhang, Q.; Zhang, Z.; Zhang, H.; Mo, Z. *J. Polym. Sci. B* **2002,** 40, 1784-1793.

(420) Zhong, Z.; Guo, Q. *J. Polym. Sci. B* **1999,** 37, 2726-2736.

(421) Williams, M. L.; Landel, R. F.; Ferry, J. D. *J. Am. Chem. Soc.* **1955,** 77, 3701-3707.

(422) Geddem, U. W., Crystalline polymers. In *Polymer physics*, Chapman&Hall: London, 1995; pp 131-165.

(423) Hoffman, J. D.; Weeks, J. J. *J. Chem. Phys.* **1962,** 37, 1723-&.

(424) Fornes, T. D.; Paul, D. R. *Polímeros* **2003,** 13, 212-217.

(425) Ginzburg, V. V.; Weinhold, J. D.; Jog, P. K.; Srivastava, R. *Macromolecules* **2009,** 42, 9089-9095.

(426) Fornes, T. D.; Hunter, D. L.; Paul, D. R. *Macromolecules* **2004,** 37, 1793-1798.

(427) Marco, C.; Collar, E. P.; Areso, S.; García-Martínez, J. M. *J. Polym. Sci., Part B: Polym. Phys.* **2002,** 40, 1307-1315.

(428) Ho, J.-C.; Wei, K.-H. *Macromolecules* **2000,** 33, 5181-5186.

(429) Gurato, G.; Fichera, A.; Grandi, F. Z.; Zannetti, R.; Canal, P. *Makromol. Chem.* **1974,** 175, 953-975.

(430) Zheng, J.; Siegel, R. W.; Toney, C. G. *J. Polym. Sci. B* **2003,** 41, 1033-1050.

(431) Zhang, Q.; Wang, Y.; Fu, Q. *J. Polym. Sci. B* **2003,** 41, 1-10.

(432) Katoh, Y.; Okamoto, M. *Polymer* **2009,** 50, 4718-4726.

(433) Geddem, U. W., The rubber elastic state. In *Polymer physics*, Chapman & Hall: London, 1995; pp 39-53.

(434) Lincoln, D. M.; Vaia, R. A.; Wang, Z. G.; Hsiao, B. S. *Polymer* **2001,** 42, 1621-1631.

(435) Jackson, C. L.; McKenna, G. B. *Chem. Mat.* **1996,** 8, 2128-2137.

(436) Xu, W.; Lv, R.; Na, B.; Tian, N.; Li, Z.; Fu, Q. *J. Phys. Chem. B* **2009,** 113, 9664-9668.

(437) Lim, S. H.; Dasari, A.; Yu, Z. Z.; Mai, Y. W.; Liu, S. L.; Yong, M. S. *Compos. Sci. Technol.* **2007,** 67, 2914-2923.

(438) Atkins, A. G.; Chen, Z.; Cotterell, B. *Proc. R. Soc. London, Ser. A* **1998,** 454, 815-833.

(439) Gere, J. M.; Goodno, B. J., Axially Loaded Members. In *Mechanics of materials* 7th ed.; Thomson: London, 2009; pp 140-141.

(440) Perkins, W. G. *Polym. Eng. Sci.* **1999,** 39, 2445-2460.

(441) Ouederni, M.; Phillips, P. J. *J. Polym. Sci., Part B: Polym. Phys.* **1995,** 33, 1313-1322.

(442) Bernal, C. R.; Frontini, P. M.; Herrera, R. *Polym. Test.* **1992,** 11, 271-288.

(443) Narisawa, I.; Takemori, M. T. *Polym. Eng. Sci.* **1989,** 29, 671-678.

(444) Labour, T.; Gauthier, C.; Séguéla, R.; Vigier, G.; Bomal, Y.; Orange, G. *Polymer* **2001,** 42, 7127-7135.

(445) Mai, Y.-W.; Powell, P. *J. Polym. Sci. B: Polym. Phys.* **1991,** 29, 785-793.

(446) Huang, D. D.; Williams, J. G. *J. Mater. Sci.* **1987,** 22, 2503-2508.

(447) Lu, M.-L.; Chiou, K.-C.; Chang, F.-C. *Polymer* **1996,** 37, 4289-4297.

(448) Taylor, D.; O'Mara, N.; Ryan, E.; Takaza, M.; Simms, C. *JMBBM* **2012,** doi:10.1016/j.jmbbm.2011.09.018.

(449) Deshmane, C.; Yuan, Q.; Misra, R. D. K. *Mater. Sci. Eng.* **2007,** 452-453, 592-601.

(450) Mills, K.; Davis, J. R., ASM Handbook, Volume 12 - Fractography. In ASM International.

(451) Kulander, B. R.; Dean, S. L., Observations on fractography with laboratory experiments for geologists. In *Fractography: fracture topography as a tool in fracture mechanics and stress analysis*, Ameen, M. S., Ed. The Geological Society: London, 1995.

(452) Zwijnenburg, A.; Pennings, A. J. *J. Polym. Sci.: Letters* **1976,** 14, 339-346.

(453) Chow, W. S.; Mohd Ishak, Z. A.; Karger-Kocsis, J.; Apostolov, A. A.; Ishiaku, U. S. *Polymer* **2003,** 44, 7427-7440.

(454) Agrawal, P.; Araújo, E.; Mélo, T. *J. Mater. Sci.* **2008,** 43, 4443-4449.

(455) Cho, S.; Hong, J. S.; Lee, S. J.; Ahn, K. H.; Covas, J. A.; Maia, J. M. *Macromol. Mater. Eng.* **2011,** 296, 341-348.

(456) Ruiz-Hitzky, E.; Aranda, P.; Darder, M.; Rytwo, G. *J. Mater. Chem.* **2010,** 20, 9306-9321.

(457) Tiwari, R. R.; Natarajan, U. *Polym. Eng. Sci.* **2011,** 51, 979-991.

(458) Zhu, Y.; Ma, H. Y.; Tong, L. F.; Fang, Z. P. *Chin. J. Polym. Sci.* **2008,** 26, 783-792.

(459) Rohlmann, C. O.; Horst, M. F.; Quinzani, L. M.; Failla, M. D. *Eur. Polym. J.* **2008,** 44, 2749-2760.

(460) Zhang, D.; Bhat, G.; Malkan, S.; Wadsworth, L. *J. Therm. Anal. Calorim.* **1997,** 49, 161-167.

(461) Denesyuk, N. A.; Gompper, G. *Macromolecules* **2006,** 39, 5497-5511.

(462) Hong, J. S.; Namkung, H.; Ahn, K. H.; Lee, S. J.; Kim, C. *Polymer* **2006,** 47, 3967-3975.

(463) Yuan, Q.; Deshmane, C.; Pesacreta, T. C.; Misra, R. D. K. *Mater. Sci. Eng. A* **2008,** 480, 181-188.

(464) Sakurai, K.; Maegawa, T.; Takahashi, T. *Polymer* **2000,** 41, 7051-7056.

(465) Zhang, Q.; Yang, H.; Fu, Q. *Polymer* **2004,** 45, 1913-1922.

(466) Santana, O. O.; Muller, A. J. *Polym. Bull.* **1994,** 32, 471-477.

(467) Zheng, W.; Lu, X.; Ling Toh, C.; Hua Zheng, T.; He, C. *J. Polym. Sci., Part B: Polym. Phys.* **2004,** 42, 1810-1816.

(468) Vo, L. T.; Giannelis, E. P. *Macromolecules* **2007,** 40, 8271-8276.

(469) Ramakrishna, S.; Lim, T. C.; Inai, R.; Fujihara, K. *Mech. Adv. Mater. Struc.* **2006,** 13, 77 - 81.

(470) Brune, D. A.; Bicerano, J. *Polymer* **2002,** 43, 369-387.

(471) Utracki, L. A. *Polym. Eng. Sci.* **1995,** 35, 2-17.

(472) Tarantili, P. A.; Mitsakaki, A. N.; Petoussi, M. A. *Polym. Degrad. Stabil.* **2010,** 95, 405-410.

(473) Brennan, L. B.; Isaac, D. H.; Arnold, J. C. *J. Appl. Polym. Sci.* **2002,** 86, 572-578.

(474) Pospíšil, J.; Sitek, F. A.; Pfaendner, R. *Polym. Degrad. Stab.* **1995,** 48, 351-358.

(475) Finnveden, G.; Johansson, J.; Lind, P.; Moberg, A. *J. Clean Prod.* **2005,** 13, 213-229.

(476) Strömberg, E.; Karlsson, S. *J. Appl. Polym. Sci.* **2009,** 112, 1835-1844.

(477) Fortelný, I.; Michálková, D.; Kruliš, Z. *Polym. Degrad. Stab.* **2004,** 85, 975-979.

(478) Lee, J. H.; Song, D. I.; Jeon, Y. W. *Sep. Sci. Technol.* **1997,** 32, 1975-1992.

(479) Liu, W.; Gan, J.; Papiernik, S. K.; Yates, S. R. *J. Agric. Food Chem.* **2000,** 48, 1935-1940.

(480) Pegoretti, A.; Kolarik, J.; Peroni, C.; Migliaresi, C. *Polymer* **2004,** 45, 2751-2759.

(481) Tri Phuong, N.; Gilbert, V.; Chuong, B. *J. Reinf. Plast. Compos.* **2008,** 27, 1983-2000.

Appendix

Appendix I

The Mori-Tanaka coefficients used to calculate the modulus of a composite material are:[176, 177]

$$A_1 = D_1(B_4 + B_5) - 2B_2 \quad (A1)$$

$$A_2 = (1 + D_1)B_2 - (B_4 + B_5) \quad (A2)$$

$$A_3 = B_1 - D_1 B_3 \quad (A3)$$

$$A_4 = (1 + D_1)B_1 - B_3 \quad (A4)$$

$$A_5 = (1 - D_1)/(B_4 - B_5) \quad (A5)$$

$$A = 2B_2B_3 - B_1(B_4 + B_5) \quad (A6)$$

where

$$B_1 = \phi_r D_1 + D_2 + (1 - \phi_r)(D_1S_{1111} + 2S_{2211}) \quad (A7)$$

$$B_2 = \phi_r + D_3 + (1 - \phi_r)(D_1S_{1122} + S_{2222} + S_{2233}) \quad (A8)$$

$$B_3 = \phi_r + D_3 + (1 - \phi_r)(S_{1111} + (1 + D_1)S_{2211}) \quad (A9)$$

$$B_4 = \phi_r D_1 + D_2 + (1 - \phi_r)(S_{1122} + D_1S_{2222} + S_{2233}) \quad (A10)$$

$$B_5 = \phi_r + D_3 + (1 - \phi_r)(S_{1122} + S_{2222} + D_1S_{2233}) \quad (A11)$$

and ϕ_r represents the volume fraction of reinforcement and

$$D_1 = 1 + 2\frac{\mu_r - \mu_p}{\lambda_r - \lambda_p} \quad (A12)$$

$$D_2 = \frac{\lambda_p + 2\mu_p}{\lambda_r - \lambda_p} \quad (A13)$$

$$D_3 = \frac{\lambda_p}{\lambda_r - \lambda_p} \quad (A14)$$

where μ and λ are the Lamé constants for which the subscript p and r refer to the polymer matrix and to the reinforcement.

In order to calculate the Mori-Tanaka coefficients that the model uses, the Eshelby tensors need to be calculated. The Eshelby tensors for the Mori-Tanaka model for spheroidal inclusions are given by:

$$S_{1111} = \frac{1}{2(1-\nu_p)}\left\{1 - 2\nu_p + \frac{3\alpha^2-1}{\alpha^2-1} - \left[1 - 2\nu_p + \frac{3\alpha^2}{\alpha^2-1}\right] g\right\} \quad (A15)$$

$$S_{2222} = S_{3333} = \frac{3}{8(1-\nu_p)}\frac{\alpha^2}{\alpha^2-1} + \frac{1}{4(1-\nu_p)}\left[1 - 2\nu_p + \frac{9}{4(\alpha^2-1)}\right] g \quad (A16)$$

$$S_{2233} = S_{3322} = \frac{1}{4(1-\nu_p)}\left\{\frac{\alpha^2}{2(\alpha^2-1)} - \left[1 - 2\nu_p + \frac{3}{4(\alpha^2-1)}\right] g\right\} \quad (A17)$$

$$S_{2211} = S_{3311} = \frac{1}{2(1-\nu_p)}\frac{\alpha^2}{\alpha^2-1} + \frac{1}{4(1-\nu_p)}\left[\frac{3\alpha^2}{\alpha^2-1} - (1 - 2\nu_p)\right] g \quad (A18)$$

$$S_{1122} = S_{1133} = \frac{1}{2(1-\nu_p)}\left[1 - 2\nu_p + \frac{1}{\alpha^2-1}\right] + \frac{1}{2(1-\nu_p)}\left[1 - 2\nu_p + \frac{3}{2(\alpha^2-1)}\right] g \quad (A19)$$

$$S_{2323} = S_{3232} = \frac{1}{4(1-\nu_p)}\left\{\frac{\alpha^2}{2(\alpha^2-1)} + \left[1 - 2\nu_p - \frac{3}{4(\alpha^2-1)}\right] g\right\} \quad (A20)$$

$$S_{1212} = S_{1313} = \frac{1}{4(1-\nu_p)}\left\{1 - 2\nu_p - \frac{\alpha^2+1}{\alpha^2-1} - \frac{1}{2}\left[1 - 2\nu_p - \frac{3(\alpha^2-1)}{\alpha^2-1}\right] g\right\} \quad (A21)$$

where ν_p is the Poisson ratio of the polymer matrix and

$$g = \frac{\alpha}{(\alpha^2-1)^{3/2}}\left[cos^{-1}\alpha - \alpha(1-\alpha^2)^{1/2}\right] \quad (A22)$$

and α is the aspect ratio of inclusions (i.e., t/w).

Appendix II

AII.1. Calculation of mass fraction of clay platelets in porous polymer/clay nanocomposites

Mass of blowing agent-treated clay (m_c)

$$m_c = \frac{m_p \mu_c}{1 - \mu_c} \tag{A1}$$

where μ_c represents the mass fraction of blowing agent-treated organoclay in polymer/clay nanocomposites and m_p represents the mass of polymer.

Mass of clay platelets (m_c^0)

$$m_c^0 = \frac{m_c^2 \mu_c^0}{m_c + \mu_b m_p} \tag{A2}$$

where μ_b and $\mu_c{}^0$ represent the mass fractions of blowing agent and of clay platelets in organoclay.

Mass of polymer/clay nanocomposite solid (m_s)

$$m_s = m_p + m_c - \frac{m_c m_p \mu_b \mu_g}{m_c + \mu_b m_p} \tag{A3}$$

where μ_g depicts the mass fraction of gas released by the blowing agent determined by TGA as 0.37 for SB and 0.99 for ADC.

Mass fraction of clay platelets in porous polymer/blowing agent-treated clay nanocomposites

$$\mu_c^0 = \frac{m_c^0}{m_s} \tag{A4}$$

AII.2. Calculation of the density of the solid nanocomposite that constructs the cell struts in the porous nanocomposite

Volume of the fully exfoliated solid nanocomposite (V_s^e)

$$V_s^e = \frac{m_c^0}{\rho_c^0} + \frac{m_p}{\rho_p} \tag{A5}$$

where ρ represents the density, ρ_c^0 represents the density of the clay platelets and ρ_p represents the density of the polymer.

Volume of the intercalated-exfoliated solid nanocomposite (V_s^{ie})

$$V_s^{ie} = \frac{m_c^0(1-f_i)}{\rho_c^0} + \frac{\mu_c m_c f_i}{\rho_c} + \frac{m_p}{\rho_p} \tag{A6}$$

where ρ_c represents the density of the clay, while f_i depicts the fraction of intercalated clay platelets.

Density of the solid nanocomposite (ρ_s)

$$\rho_s = \frac{m_s}{V_s} \tag{A7}$$

where m_s and V_s represent the mass and volume of the solid nanocomposite

AII.3. Calculation volume fraction of clay reinforcement located in the cell struts of the porous nanocomposite[122]

Radius of gyration (R_g)

$$R_g = \sqrt{\frac{\left(\frac{\overline{M_n}}{M_m}\right) \cdot l^2}{6}} \tag{A8}$$

where $\overline{M_n}$ represents the number average molecular weight of the polymer, i.e., 80,000, M_m is the molecular weight of the monomer and l is the end-to-end length of the monomer taking the bond lengths of C–C and C–O as 0.154 nm and 0.143 nm.[398]

The effective volume fraction of the reinforcement (ϕ_r) in an exfoliated nanocomposite:

$$\phi_r = \frac{\mu_c \mu_c^0 \rho_s}{\rho_c^0}(1 + kR_g A_T \rho_c^0) \tag{A9}$$

where A_T is the total specific surface area of the clay platelets (i.e., A_T = 658 $m^2 \cdot g^{-1}$) and k is the fraction of absorbed polymer on the clay layer that behaves like clay (i.e., 0.2 for Clay(SB)).

The volume fraction of exfoliated clay platelets (ϕ_e) present in the intercalated-exfoliated nanocomposites:

$$\phi_e = \frac{\mu_c \mu_c^0 \rho_s (1 - f_i)}{\rho_c^0}(1 + kR_g A_T \rho_c^0) \tag{A10}$$

Appendix III

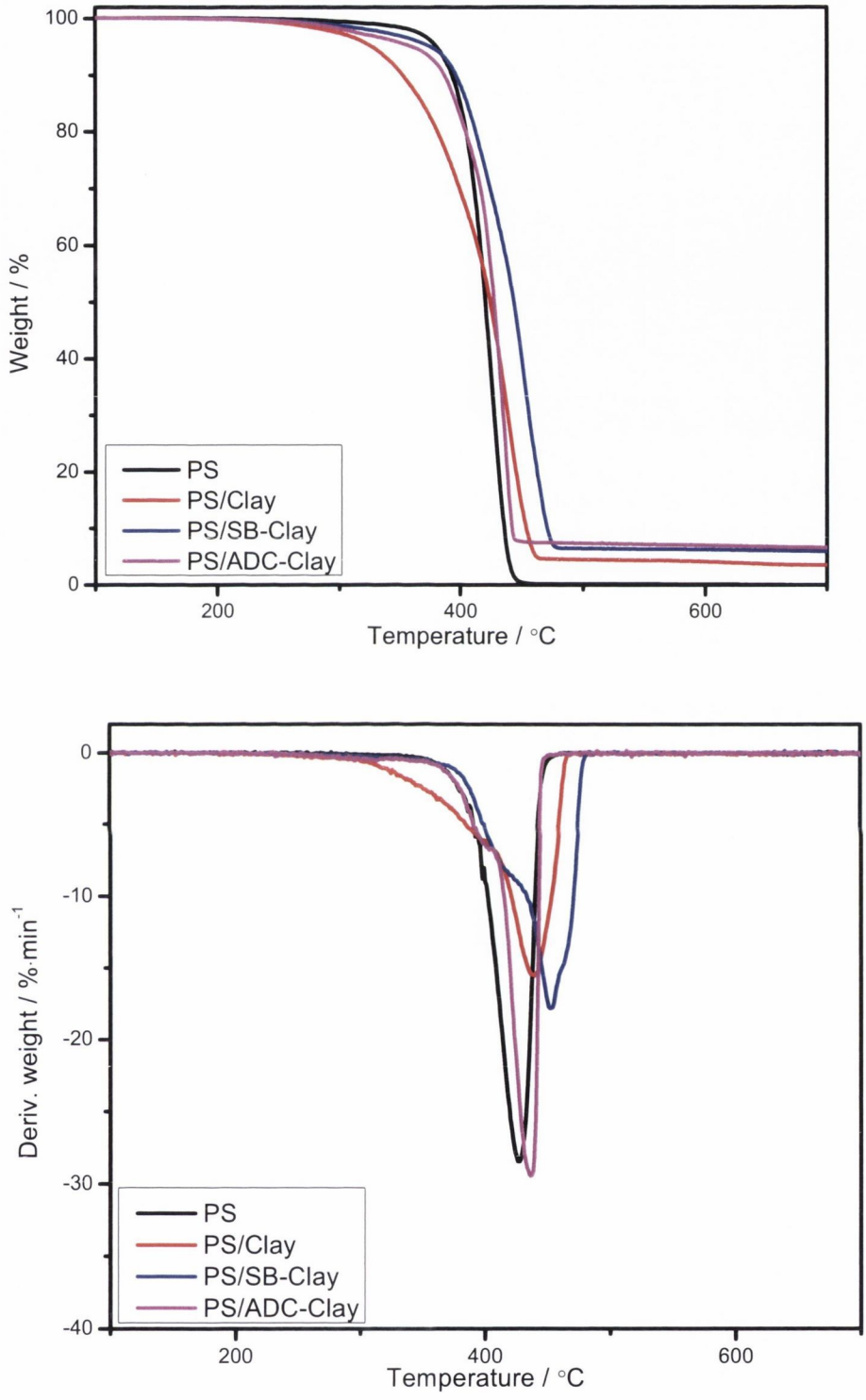

Figure A1. TGA and DTG curves for PS and PS/clay nanocomposites

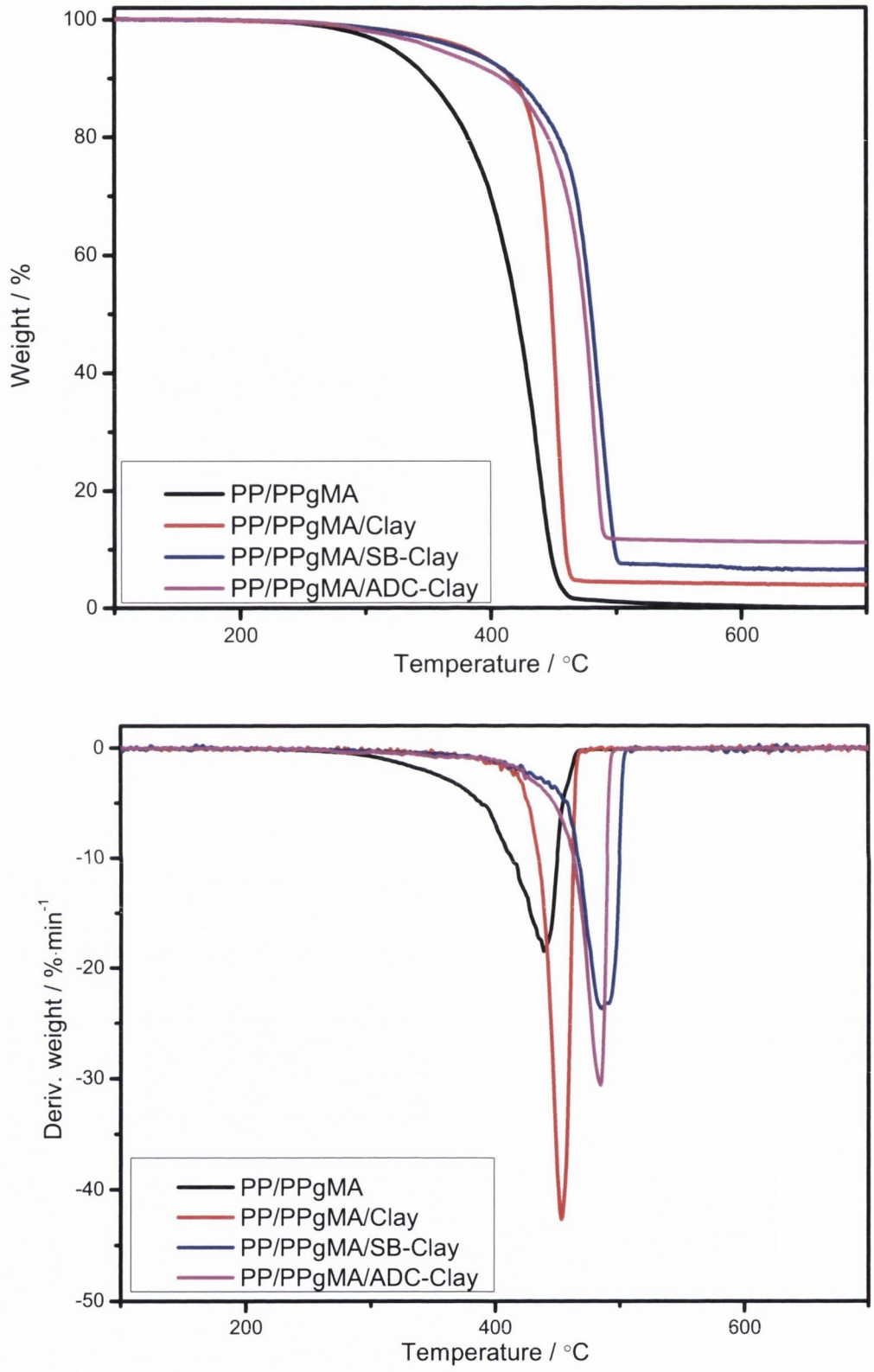

Figure A2. TGA and DTG curves for PP/PPgMA and PP/PPgMA/clay nanocomposites

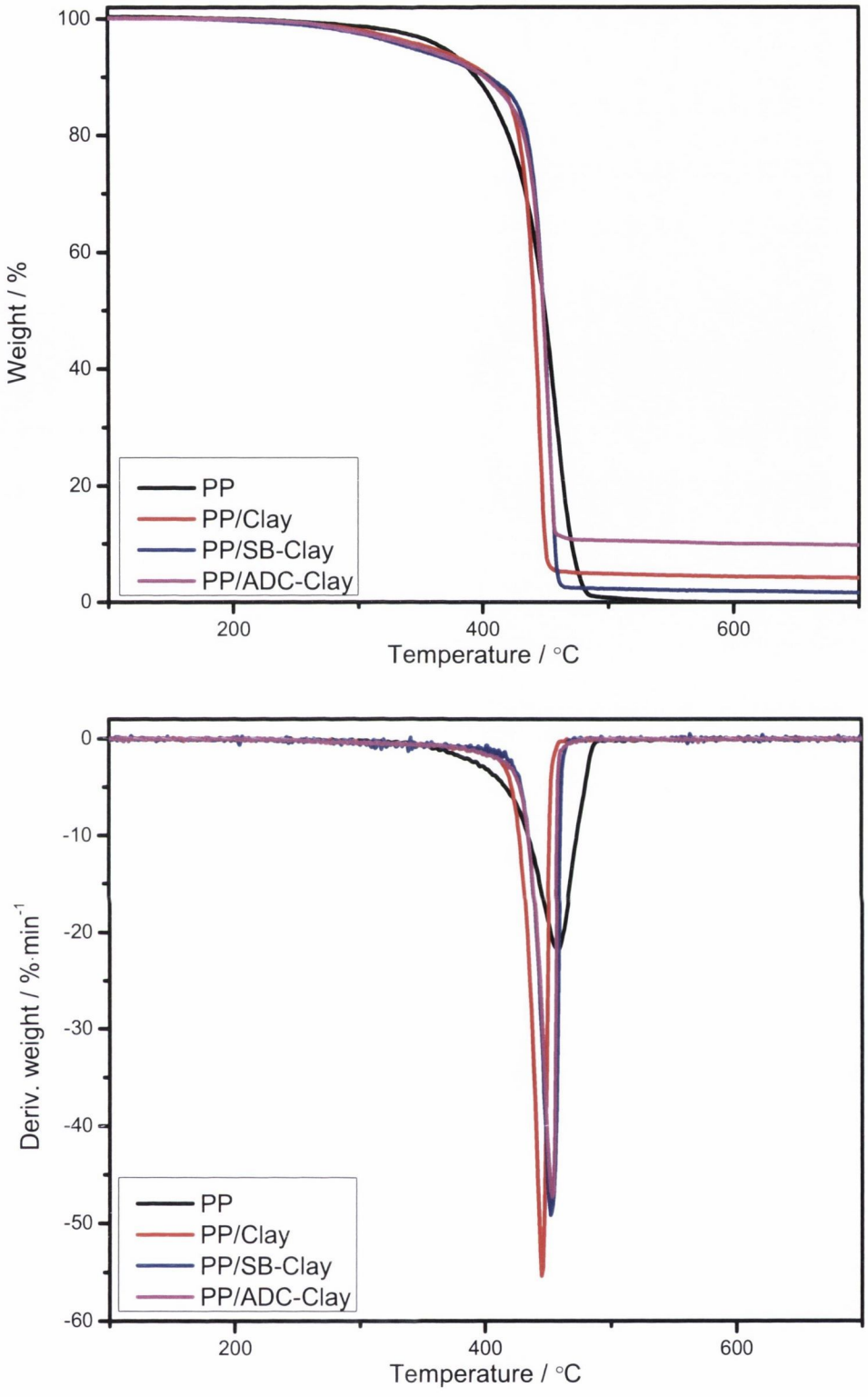

Figure A3. TGA and DTG curves for PP and PP/clay composites

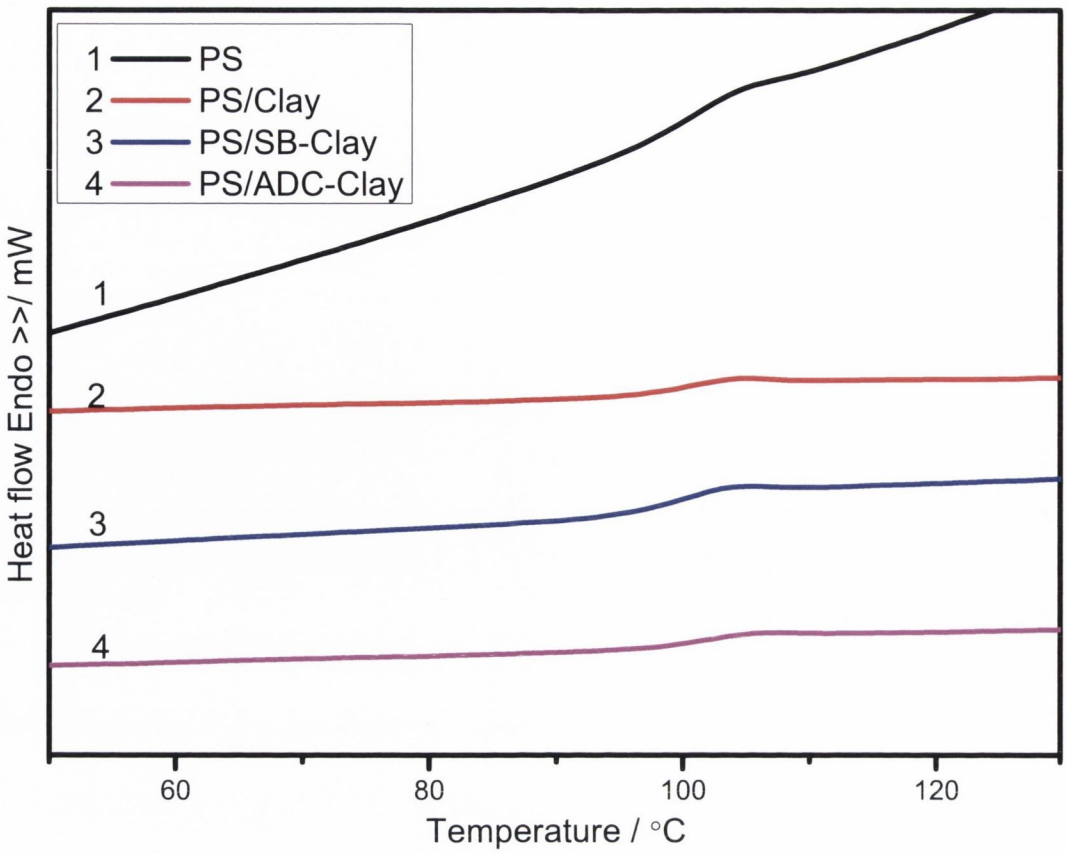

Figure A4. DSC heating curves for PS and PS/clay nanocomposites

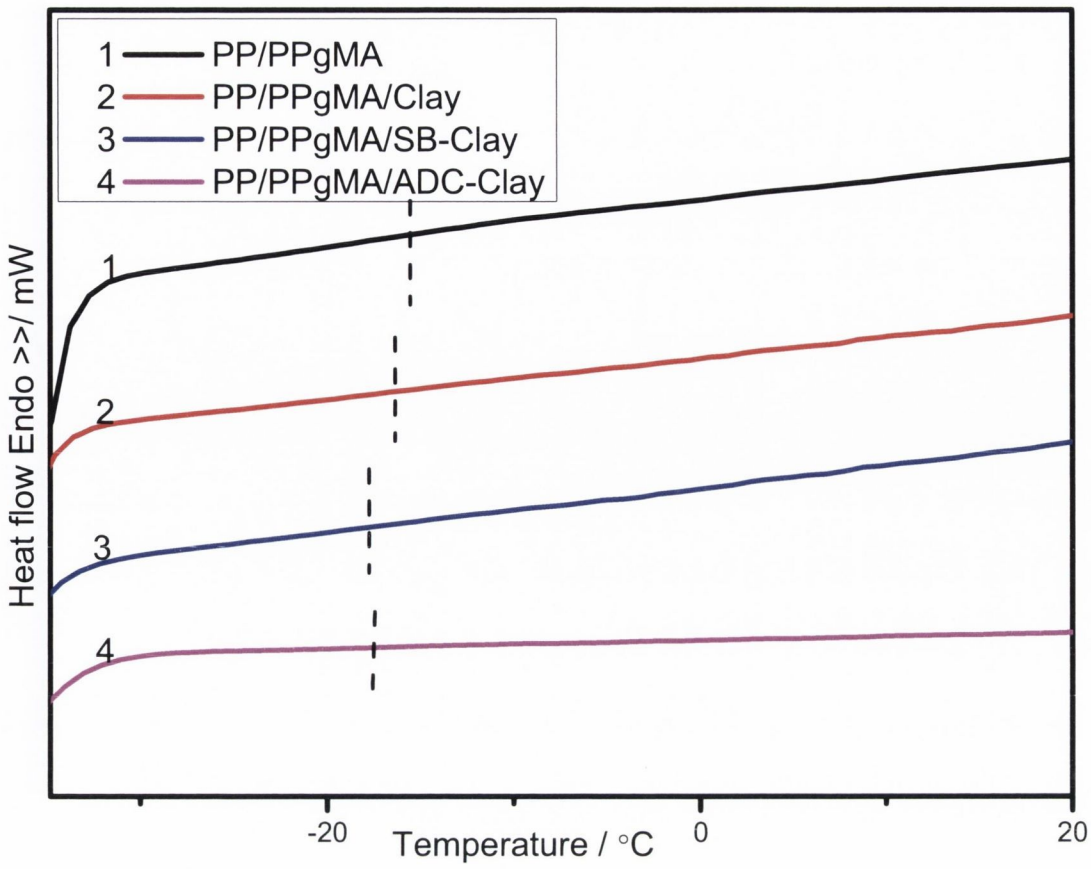

Figure A5. DSC heating curves for PP/PPgMA and PP/PPgMA /clay nanocomposites

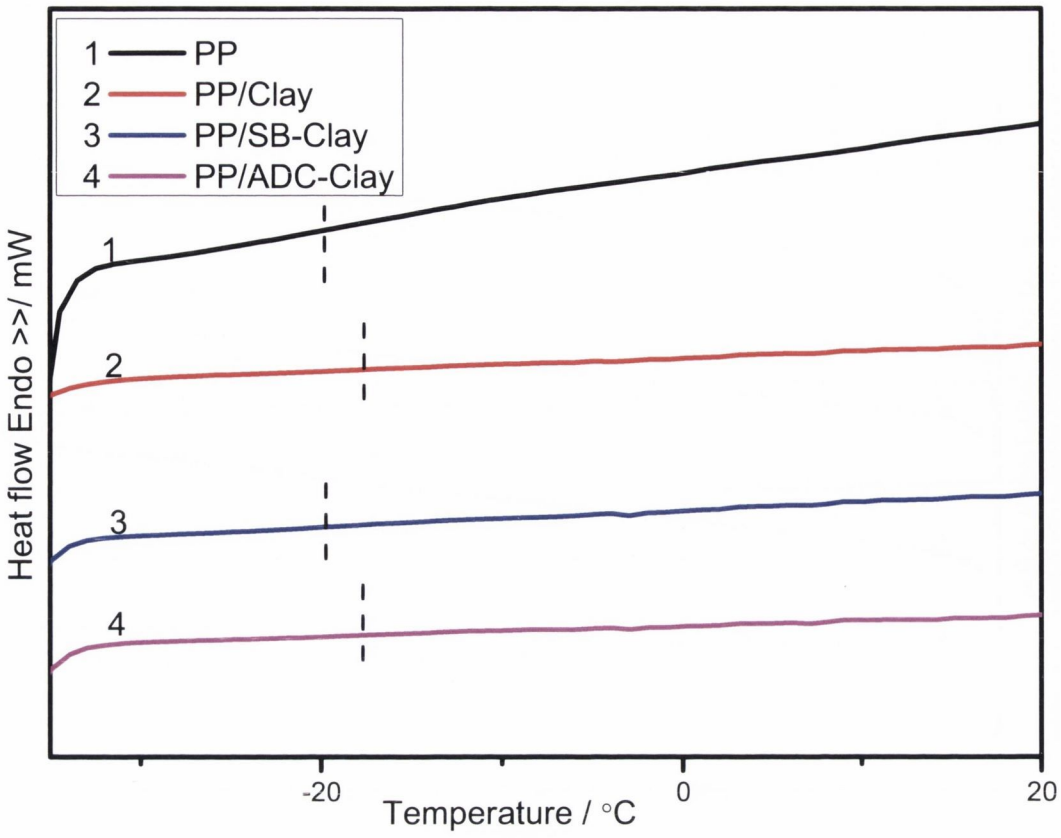

Figure A6. DSC heating curves for PP and PP /clay composites

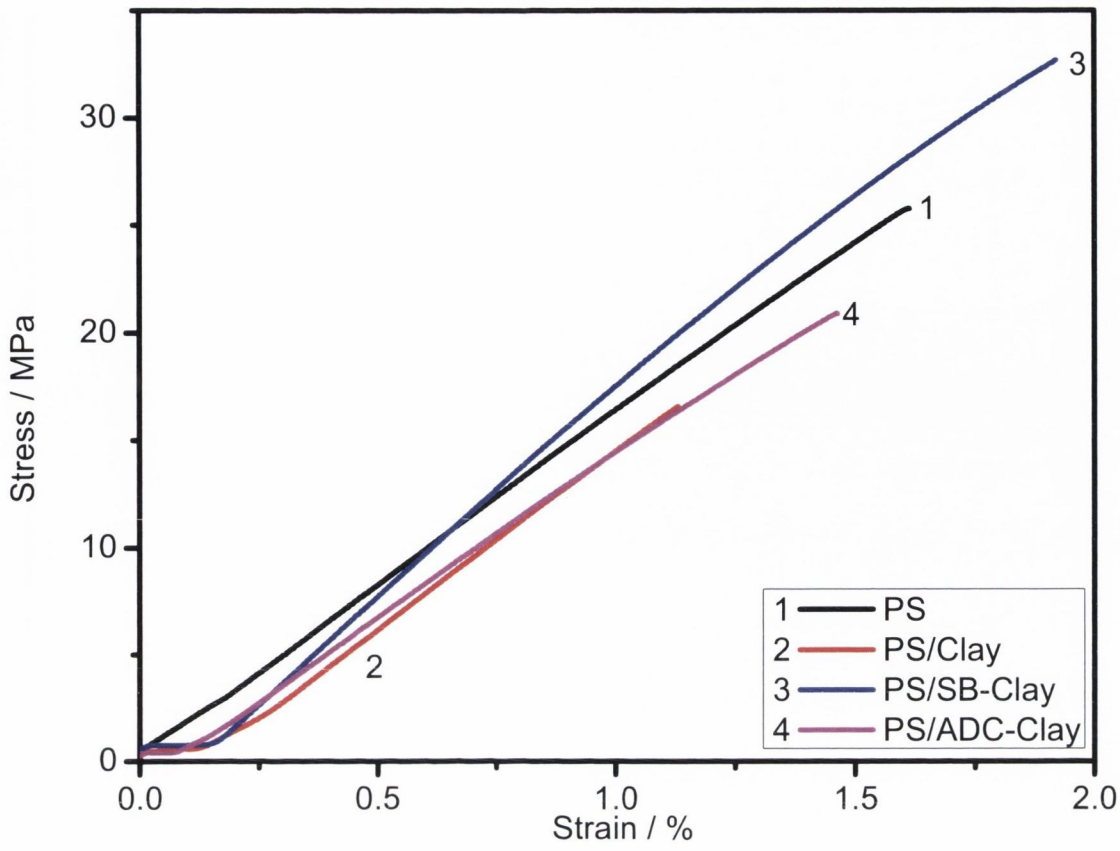

Figure A7. Tensile curves for PS and PS/clay nanocomposites

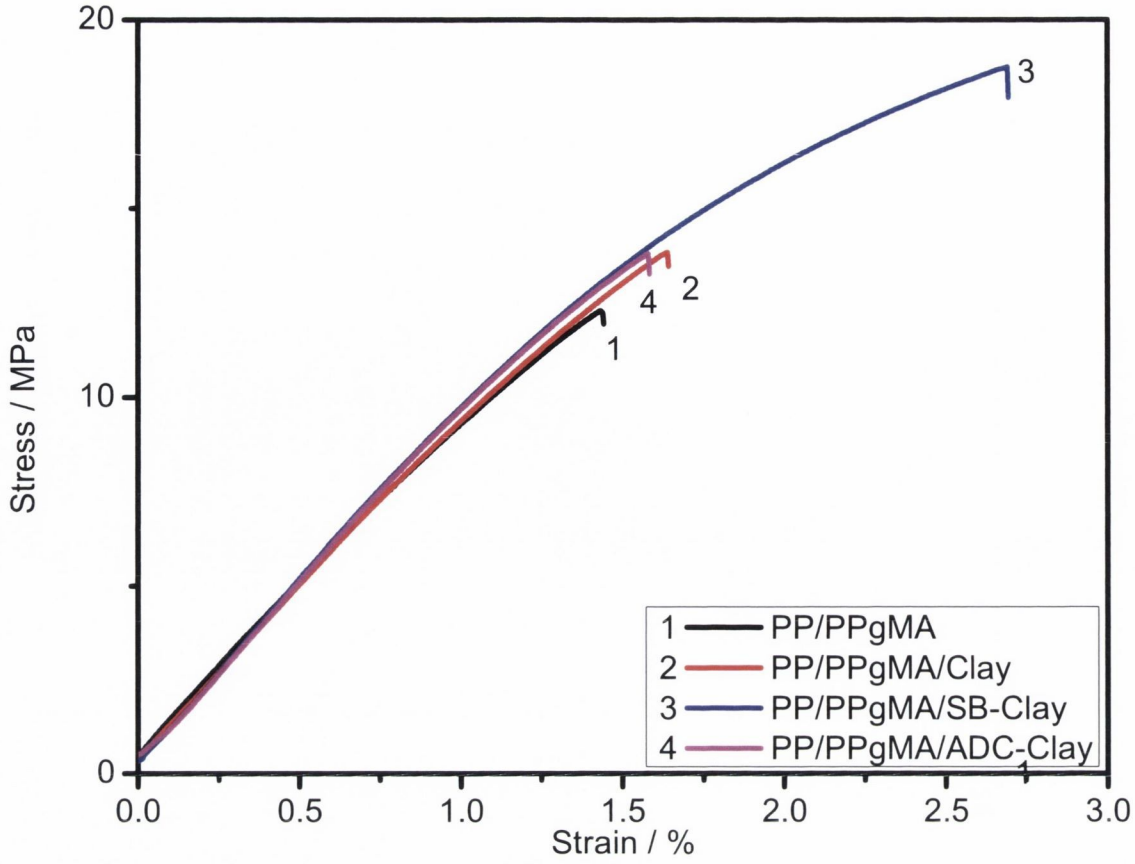

Figure A8. Tensile curves for PP/PPgMA and PP/PPgMA/clay nanocomposites

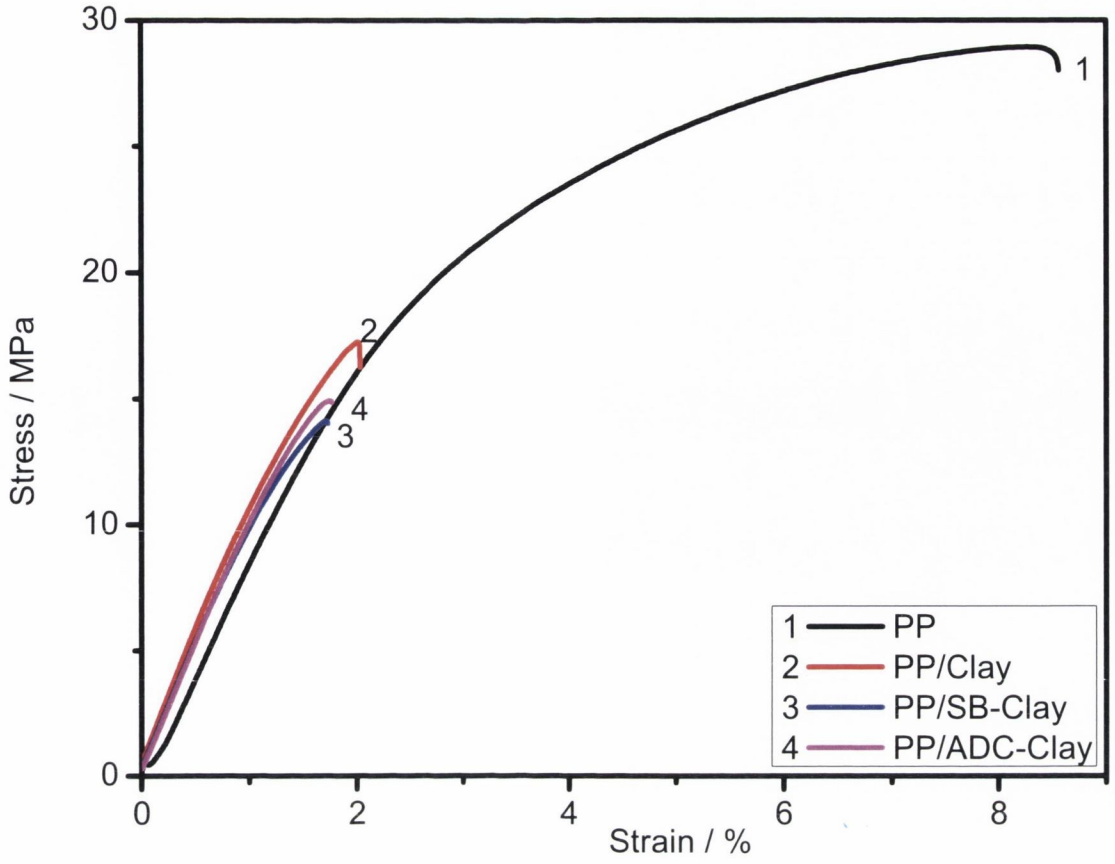

Figure A9. Tensile curves for PP and PP/clay composites

Appendix IV

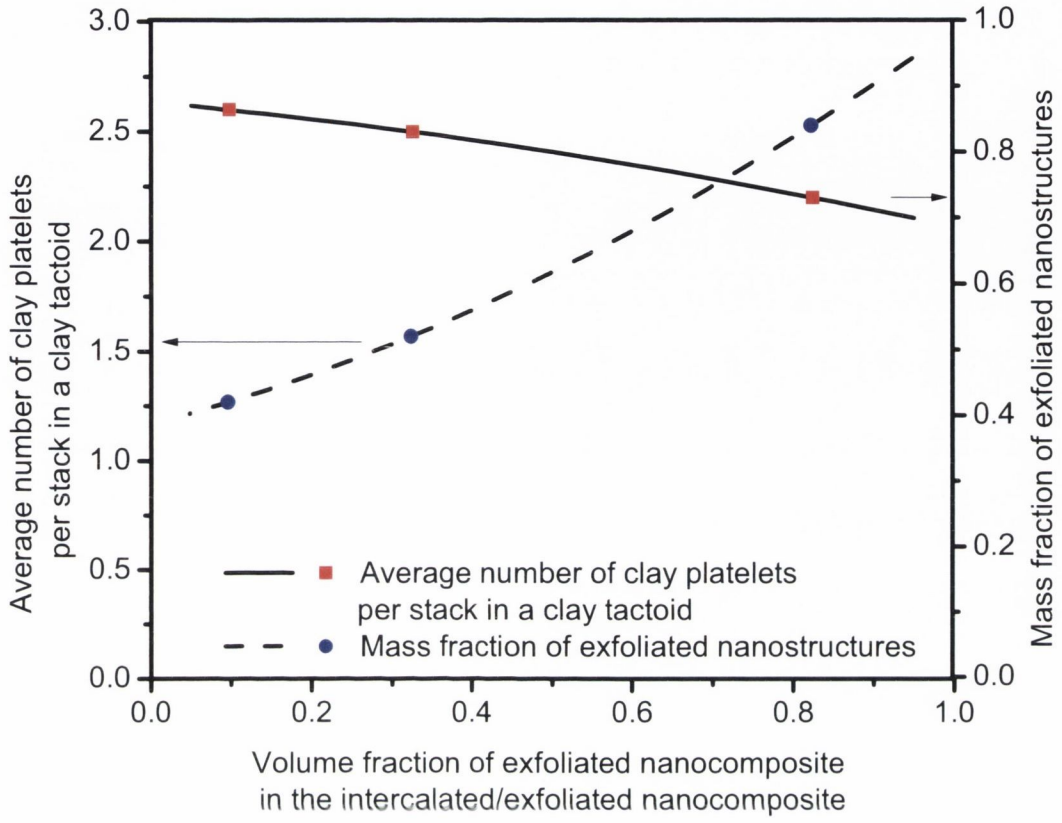

Figure A1. Variations of the mass fraction and average number clay platelets per stack with the volume fraction of exfoliated nanocomposites